SYNTHESIS AND EVALUATION OF NOVEL PYRIDINE-, PYRIMIDINE- AND TRIAZINE-BASED DERIVATIVES AS POTENTIAL HIV-1 NON-NUCLEOSIDE REVERSE TRANSCRIPTASE INHIBITORS (NNRTIs)

Charles Reuben K. Changunda

A Dissertation submitted to the Faculty of Science, University of the Witwatersrand, in fulfilment of the requirements of the Doctor of Philosophy

Johannesburg, 2018

DECLARATION

I declare that this Thesis is my own, original work which was produced under the supervision of **Dr**. **Moira Bode** and **Dr**. **Amanda Rousseau** in the School of Chemistry. It is submitted for the Degree of Doctor of Philosophy at the University of the Witwatersrand, Johannesburg. It has not been submitted before for any degree or examination at any other University.

Signature

March 2018

ABSTRACT

As part of our goal to identify heterocyclic-based analogues that could act as allosteric inhibitors of the HIV-1 reverse transcriptase (RT) enzyme, small libraries of novel molecules containing pyridine, pyrimidine and triazine central cores were designed and synthesized for a preliminary *in vitro* assay against the wild-type RT virus. To achieve this goal, in the first instance we explored a scaffold-hopping approach as a possible strategy for identifying promising molecules. This scaffold-hopping approach primarily involved the "dismantlement" of an imidazo[1,2-*a*]pyridine central core of a potent anti-HIV novel compound previously identified in our research laboratory to generate 2,6-disubstituted pyridines. As discussed in chapter 2, we utilized the 2,6-disubstituted pyridine core as a platform for accessing a more conformationally flexible set of analogues in which the central pyridine core was connected to the chloro-substituted aromatic ring via an amido, amino or sulfonamido hetero-linker to generate the pyridyl-benzamide, pyridyl-benzylamine and pyridyl-sulfonamides scaffolds, respectively. The scaffolds were cross-coupled with selected nitrogen-, oxygen- and sulfur-containing nucleophiles via a palladium-mediated methodology to generate a small library of novel analogues for testing against the wild-type virus. One novel pyridyl-benzamide, 2-chloro-*N*-(6-(piperidin-1-yl)pyridin-2-yl)benzamide, showing excellent antiviral activity (IC_{50}=0.7μM), was identified from whole-cell antiviral screening.

The second approach, which is covered in chapter 3, used molecular modelling in the design of potential heterocyclic NNRTI compounds that resembled a DAPY-type horse-shoe framework. The approach involved *in silico* docking of di-functionalized pyridine- and tri-functionalized pyridine-, pyrimidine-, and triazine-based virtual analogues into the allosteric site of the reverse transcriptase enzyme crystal structure (pdb: 3MEG RT). The tri-functionalized pyridine-core containing amides emerged as top modelling hits with superior ligand-receptor interaction energies. In addition, these analogues also displayed a favourable binding conformation that targeted key hydrophobic (Tyr181, Tyr188, Phe227, Trp229, Leu234, Pro236, Tyr318) and hydrophilic interactions in the allosteric site of the 3MEG RT crystal structure and were synthesized via our already developed palladium-catalyzed methodology as candidates for a primary screen against the wild-type HI virus. Moreover, biocatalysis was also successfully applied for the selective hydrolysis of a pyridyl nitrile group to access one of the top modelling hit compounds, 6-(4-chlorophenoxy)-2-((2-cyano-5-methylphenyl)amino)nicotinamide as a key target for the antiviral screening.

The scaffold hopping approach proved more rewarding as it led to the identification of a novel pyridyl-benzamide novel compound with excellent antiviral activity against the wild-type RT virus. This is the first such compound to be identified as displaying activity against RT. As

discussed in chapter 4, novel pyridyl-benzamide and pyridyl-sulfonamide compounds that displayed reasonable antimicrobial activity (39 μg/ml) against two gram-positive bacteria, *S. aureus* and *B. cereus*, were also identified from an antimicrobial screen.

DEDICATION

To my dear wife and companion, **Nester**, and our sons - **Farai** and **Tinashe**, who endured my absence, sacrificed themselves and continuously supported me throughout the course of this research project.

ACKNOWLEDGEMENTS

The research outputs contained in this thesis were achieved via a collective investment of both personal and institutional resources. In that regard, I would like to sincerely thank my supervisors, **Dr. Moira L. Bode** and **Dr. Amanda L. Rousseau**, for their guidance, advice, encouragement and support during the course of the research work. As I see it, their mentorship has adequately prepared me to serve the world better through chemistry.

Secondly, this project would also not have been accomplished without the following contributions;

- **Wits University** and the **School of Chemistry** for giving me the opportunity, workspace, resources and an enabling research environment.
- **Prof Dean Brady**, **Prof Charles de Koning** and **Prof Jo Michael** for providing the much-needed leadership and research expertise within the **Organic Chemistry group**
- **Dr**. **Izak Kortz** and **Dr**. **Myron Johnson** for ensuring continuous access to the NMR suite
- My research colleagues, **Memory Zimuwandeyi, Peter Wanyama**, **Kennedy Ngwira**, **Jean Dam**, **Donald Seanego**, **Jimmy Sumani and Hendrik Henning** for their continuous support and encouragement.
- **Dr**. **Carthlyn Slabbert** for providing me with a prompt IR spectral data service

Thirdly, I would like thank **Dr**. **Adriaan Basson** for performing the *in vitro* antiviral assays. Similarly, the collaborative effort from **Prof**. **Sandy van Vuuren** is also greatly appreciated.

I truly appreciate the financial contributions from the following institutions; The **National Research Foundation** (NRF), **South African Medical Research Council** (MRC), **Wits Biocatalysis Research Initiative (funded by DST)**, and the **Wits Post-graduate Merit Award** (PMA) and the School of Chemistry.

I would like to express my gratitude to my dear cousins **Kenneth** and **Fungai Nyandoro** family as well as **Moses** and **Christina Marimira** for all the support sacrifices you made to make this research possible.

Let me also express, my sincere thanks to my brother **Bright Munongwa** and his wife, **Erica Munongwa** for the support and hospitality.

Allow me to also thank my brothers **Herry Changunda**, **Owen Changunda**, **Garainashe Changunda**, **Leonard Changunda** and their families for their encouragement and support. To my sisters, **Fortunate Tanyanyiwa**, **Julia Matanga** and **Helen Mukushwa** and their families – Thank you.

In the chemical stores section, David Moloto and Elias Valoyi – thank so much for all the help.

And above all, I am thankfully of God Almighty's grace.

CONTENTS

CHAPTER ONE - INTRODUCTION

1.0 HIV: A global perspective

The Human Immunodeficiency Virus type 1 (HIV-1) infection, which eventually progresses to the acquired immunodeficiency syndrome (AIDS), is arguably one of the most tenacious[1] and costly public health challenges[2] facing mankind on a global scale today. Inarguably, the HIV-AIDS pandemic has left an indelible footprint on the history of humanity as millions of people have succumbed to the disease whilst a significant proportion of the global populace is living with the virus.

Although the current antiretroviral regimens have played a pivotal role in improving the quality of life of HIV patients, the latest WHO[3] report highlighted that global antiretroviral coverage of only 46% is rather low and needs scaling up to achieve an effective 73% coverage target set by WHO for 2020. The challenges associated therewith shall be covered in the following sections.

Nonetheless, under the stewardship of WHO over the last decade, the global community effort has laid a firm foundation for spearheading regional HIV management efforts, saving lives and giving hope that the HIV-AIDS challenge may be contained. The global effort has not only highlighted HIV-AIDS as a global threat, but more importantly, tapped into the much-needed political will to stimulate the requisite partial domestic funding and facilitate the institutionalization of efficient ARV roll out programs. These efforts have impacted positively on many economies by improving the productive life[4] of people living with HIV globally and also bring hope for the future containment of the scourge, although a lot of work lies ahead before AIDS is brought under control.

Our motivation in this research stems from the fact that in sub-Saharan Africa[5] (SSA), HIV-AIDS has socioeconomically decimated family structures as young children have been forced into social vices to fend for their siblings. Against this background, it is quite refreshing to note that countries like South Africa[6] are playing a leading role in the fight against HIV-AIDS by developing supportive policy frameworks that allocate financial resources for creating operational structures necessary for maintaining efficient antiviral roll-out programs that have benefited approximately 3 million people countrywide.

Another success story involves Kenya,[3] where a country-wide systematic assessment of the high AIDS prevalence done in 2014 showed that only 9 of the 47 counties contributed a staggering 65% of new infections country wide. This prompted the Kenya Health Ministry to roll

out a responsive structural intervention five-year program with the target of lowering new infections by 75% by 2020.

However, other SSA countries like Malawi, Mozambique, Zambia and Zimbabwe, which lack the stewardship approach displayed by South Africa, continue to battle with the ravages of HIV-AIDS since most programs remain entirely donor-funded, whilst the requisite domestic financing, especially raised through AIDS levies in Zimbabwe, is misappropriated.

1.1 HIV-AIDS Global Trends and Challenges

The latest UNAIDS Global report 2016[3] shows that, as of December 2015, an estimated 78 million people have become infected with HIV globally (160 countries) since the onset of the epidemic, about four decades[7] ago. Regrettably, approximately 35 million people are reported[3] to have succumbed to the disease, whilst around 37 million are living with HIV world-wide. As shown in Fig. 1.1, roughly 17 million people are accessing antiretroviral medication, which translates to 46% treatment coverage globally, across all age groups.

This latest global achievement is highly commendable as it represents more than double the 22% global treatment coverage achieved in 2010. However, a lot of work still needs to be done to eventually scale-up this treatment coverage and achieve the newly revised 90-90-90 targets for 2020 (See section 1.2 below) as announced by the World Health Organization during their 21st International AIDS Conference held in RSA in July 2016.

Although new infections have apparently dropped by 6% since 2010, with AIDS-related deaths also plummeting significantly by 45% since 2005, other incidental diseases remain the leading causes of death among HIV infected persons, with tuberculosis accounting for at least 30% of AIDS-related deaths. This implies that, going into the future, global HIV-AIDS management programs and financial investments will have to be more responsive and financially inclusive to holistically maintain the current baseline achievements as well as proactively manage any impact arising from such incidental diseases.

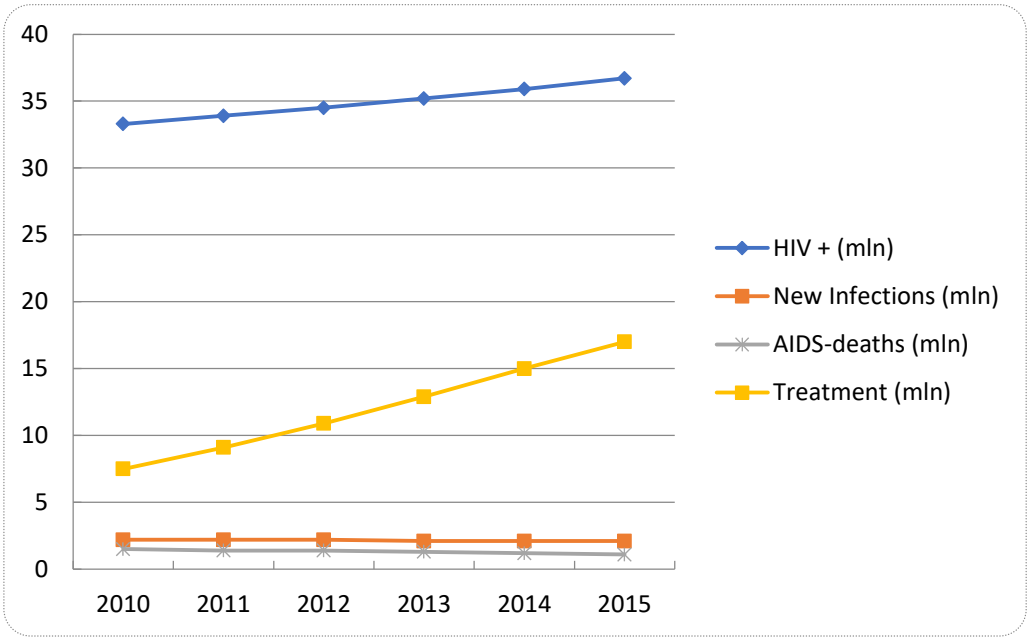

Figure 1.1: Global HIV Trends (people in millions – y-axis) for the period 2010 to 2015 (*Raw Data adapted from UNAIDS Global Report 2016*)

In line with the aforementioned data, the global fiscal space has not been spared either. In his keynote address at the 21st International AIDS Conference, Charles Wysonge (Professor of Clinical Medicine, Stellenbosch University, RSA) aptly highlighted that an estimated US$109 billion had reportedly been spent globally on anti-HIV and AIDS initiatives up to year 2014. The tranche was inclusive of domestic contributions through infrastructure, skills, partial funding, facilities and levies and had been useful in championing and streamlining general efficient and highly responsive HIV-AIDS management programs in low- to medium-income countries, thus culminating in the global achievements highlighted above.

1.2 New HIV Treatment Targets

UNAIDS' recently promulgated world vision of ending the AIDS pandemic by 2030 as announced at the 21st International AIDS Conference, though noble, sounds rather audacious from a practical perspective. The summary objective of meeting the 90-90-90 target by 2020 whereby 90% of people living with HIV will know their status, 90% of people who know their HIV+ status will access treatment and 90% of people on treatment will achieve viral suppression, mathematically implies that at least three million more people per annum will have to be added to the treatment roster globally. Simply put, the 90-90 target implies 81% should be accessing antiviral therapy between 2016 and 2020, whilst the 90-90-90 target translates to at least 70% viral suppression during the intervening period. Unfortunately, the aggregated 2015

global treatment coverage of 46% represents a 36% performance gap against the global target of 81%. The big question really is; what gap closing strategies will be in place to ensure that country-specific targets are properly aligned and dovetail into such highly ambitious global targets?

The other issue relates to the budgetary requirements. WHO reportedly estimates an initial financial outlay approximating US$27 billion by 2020 to increase by between 30 – 50% yearly the number of people on antiretroviral therapy and leap-frog the momentous achievements of 2015 with a further tranche of US$24 billion also being required by 2030 to tie up any loose ends.

Agreed, UNAIDS' fiscal space is obviously limited in as much as we may not be privy to the financial modelling employed to arrive at such a budget. Nonetheless, our tentative view is that the current UNAIDS budgetary projection could, arguably, represent a baseline estimate that falls far short of the actual capital requirements needed to cover both direct and indirect obligations.

The chief reason is that more money will obviously be required to train more health care workers and care givers inclusive of incentivising. Secondly, other critical parallel initiatives like drug research and development programs will need scaling up to ensure continued access to new, potent and affordable antiviral medication in line with the future demands of the global AIDS management programs. Thirdly, the very countries carrying the highest HIV burdens happen to be severely resource-limited economies lacking the financial accommodation to even maintain, let alone expand, their current AIDS programs to achieve the revised 90% target without external funding. So, who is going to finance the budgetary shortfall?

Although Africa and Asia carry the largest burden of HIV (32.33 million) accounting for a combined 88% of people living with HIV globally, the WHO Global Health Sector Response to HIV (2000 – 2015) report shows that all hope is not lost as significant inroads have been made, especially in SSA, where innovative ways have been used to reverse the trend of the HIV epidemic.

1.3 Regional HIV-AIDS Trends

The latest regional HIV trends (Fig. 1.2) also show that, although SSA accounts for the highest infection rate globally, it has, nonetheless, made tremendous progress in HIV-AIDS management through setting up efficient health care systems that enabled an estimated 10.3

million people to access antiretroviral treatment by 2015. This translates to 54% treatment coverage for the region, which is 17% higher than the global coverage for 2015.

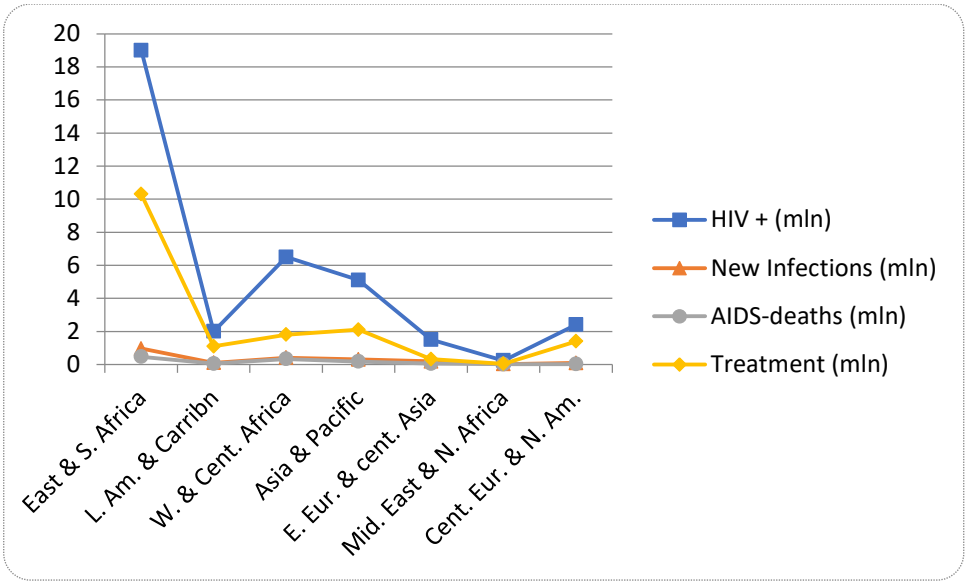

Figure 1.2: Regional HIV Trends (million people: y-axis) for year 2015 (*Raw Data adapted from UNAIDS Global Report 2016*)

It is crucial to point out that the African success story which was achieved against the backdrop of a limited fiscal space contributed greatly towards achieving the 2015 global treatment coverage of 41% in 2014, with a year to spare. Again, we foresee several challenges going into the future. The obvious big question being; how much more will Africa sacrifice to achieve the 90% targets set by UNAIDS for 2020?

1.4 Key Challenges

Given the above background, it becomes imperative that going forward, five fundamental questions should, *inter alia*, be addressed and these are; (a) What type of a global strategy, technically or otherwise, would be required to collectively sustain the momentous achievements up to 2015 and even scale up programs to achieve the 90% treatment target set by UNAIDS for 2020?; (b) How will the key drivers relating to ARV availability and affordability be addressed in such a short space of time to, in the main, sustain the current aggregate demand for antiretroviral medication as well as anticipate and accommodate the expected increased ARV uptake when more patients come on stream?; (c) How will country- and region-specific AIDS programs be fine-tuned to dovetail into the 90% global target set for 2020, let alone 2030?; (d)

How will the drug research and development value chain be re-engineered to primarily sustain current and future requirements and, most importantly, ensure new, more potent and affordable antiviral agents are supplied in such a short space of time?; and lastly, e) Given that the speed-to-market interval for novel antiviral agents is rather long, what is bound to happen once drug resistance among the current HIV patients reaches its critical mass?

All these questions are obviously difficult to answer given the complex nature of the problem at hand and the fact that huge sacrifices have already been made, at country level, to achieve the current 46% global treatment coverage envisaged in 2015.

However, our research gap primarily stems from the last question whereby the high mutation rate of the HI virus makes it a moving target as it rapidly generates mutant species that have a high genetic resistance barrier towards the current antiviral drugs in use.

Despite the several inroads that have been made to systematically manage the HIV burden globally, Africa remains worst hit as it contributed 66% new infections as well as 71% of AIDS-related mortalities in 2015.

1.5 HIV Treatment Strategies

HIV-1 is a retrovirus[8] where the overall life cycle is controlled by three viral-encoded enzymes, namely; reverse transcriptase (RT), integrase (IN) and protease (PR), which are vital for its replication, genome integration and viral maturation, respectively.

RT controls the viral replication by transcribing the single stranded ribonucleic acid (ssRNA) into the double stranded deoxyribonucleic acid (dsDNA) in the host cell cytoplasm. The IN enzyme facilitates the integration-insertion[8a] of proviral DNA into the host cell genome.

The PR enzyme is equally important in the viral life cycle[9] by cleaving the viral precursor proteins to afford mature virions which are packaged and exported to infect other host cells. As such RT, IN and PR enzymes have become key pharmacological targets[10] for novel anti-AIDS drug research and development strategies as will be explained in the next section.

Technological advances in both crystallographic studies and computational chemistry enabled scientists to resolve the three-dimensional structure and life cycle of the virus to provide vital information that championed the rational design and development of novel drug candidates that target various stages of the viral life (Fig. 1.3).

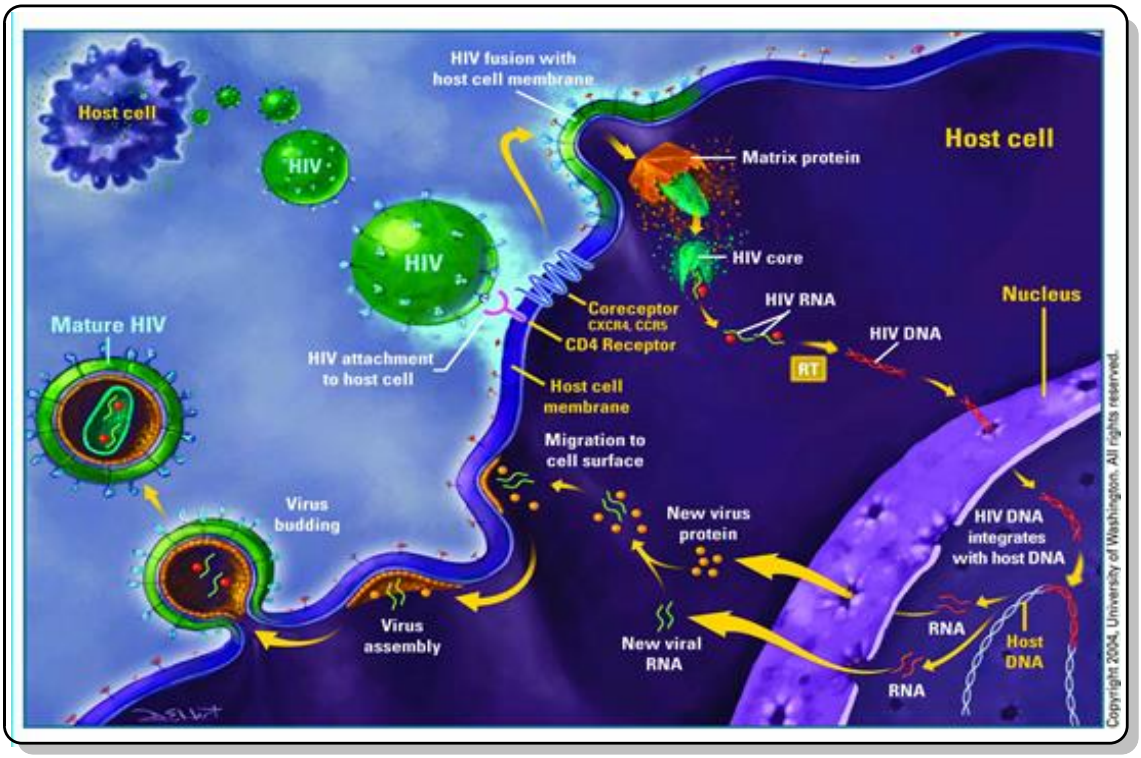

Figure 1.3: HIV Life Cycle (University of *Washington, 2004*).

1.5.1 Highly Active Antiretroviral Therapy

The highly active antiretroviral therapy (HAART) concept[12] currently being used for treating AIDS patients, employs a cocktail of drugs that are specifically designed to optimally suppress HIV replication and boost the body's immune function.[13-14] These drug classes include a) nucleoside reverse transcriptase inhibitors (NRTIs); b) non-nucleoside reverse transcriptase inhibitors (NNRTIs); c) protease inhibitors (PIs); d) integrase inhibitors (INIs); e) entry inhibitors (EIs)[15] and f) fusion inhibitors (FIs).

Most first and second line treatment regimens are based on the inhibition of two key viral enzymes namely, reverse transcriptase (RT) and protease (PR). Inhibition of RT prevents viral replication and presents an attractive choice for the structure-based design and development of NRTI and NNRTI drugs. These drug classes are discussed in detail in the following section. The protease inhibitors, typified by saquinavir **1** and indinavir **2** (Fig. 1.4), act as transition-state analogues[16] which competitively bind in the viral protease catalytic site to prevent cleavage of precursor proteins, which is a crucial process for viral maturation.[17]

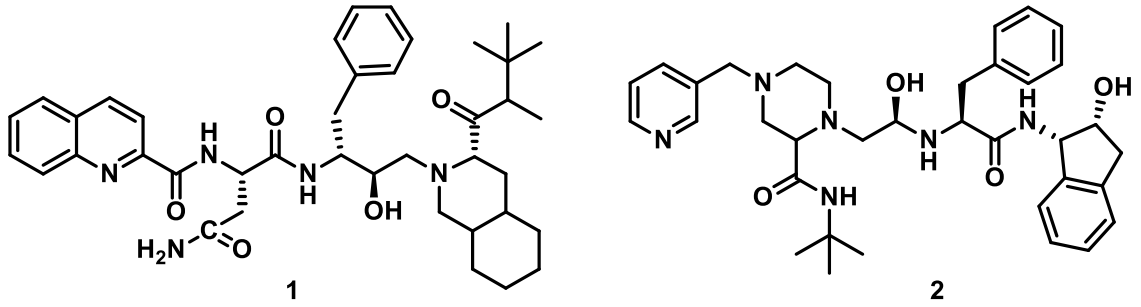

Figure 1.4: FDA-approved protease inhibitor drugs, saquinavir **1** and indinavir **2.**

Despite the significant benefits associated with antiretroviral therapy, the development of mutant viral strains resistant to drugs currently being used in HIV treatment presents a major stumbling block towards the long-term treatment of HIV & AIDS. In addition, antiviral therapy is associated with undesirable side effects which may include diarrhoea, nausea, dizziness, headaches and sleeping disorders. Hence there is on-going interest in the design and development of novel antiviral agents[18] with desirable safety profiles as alternative treatment options.

1.5.2 The RT Enzyme as a Drug Target

The RT enzyme is a highly flexible heterodimer[9] consisting of the p66 subunit comprising 560 amino acids and a relatively smaller p51 subunit with 440 amino acids. These subunits form a stable dimer which is essential for catalytic activity. The RT enzyme is error-prone and lacks proof-reading capability during the viral replication cycle, causing selection of resistance mutations under drug pressure.[11]

The larger p66 subunit contains two catalytic sites namely, the polymerase and RNase H domains. In addition, the RT enzyme also possesses a highly flexible hydrophobic allosteric binding site which is situated about 10Å from the polymerase site.

X-ray crystallographic data has revealed that the RT enzyme structure resembles that of a human right hand[10-12] possessing the palm, thumb and fingers subdomains (Fig. 1.5). The polymerase active site and hydrophobic allosteric site are both situated on the palm subdomain whilst the RNase H active site is situated 18 base-pairs from the catalytic site.

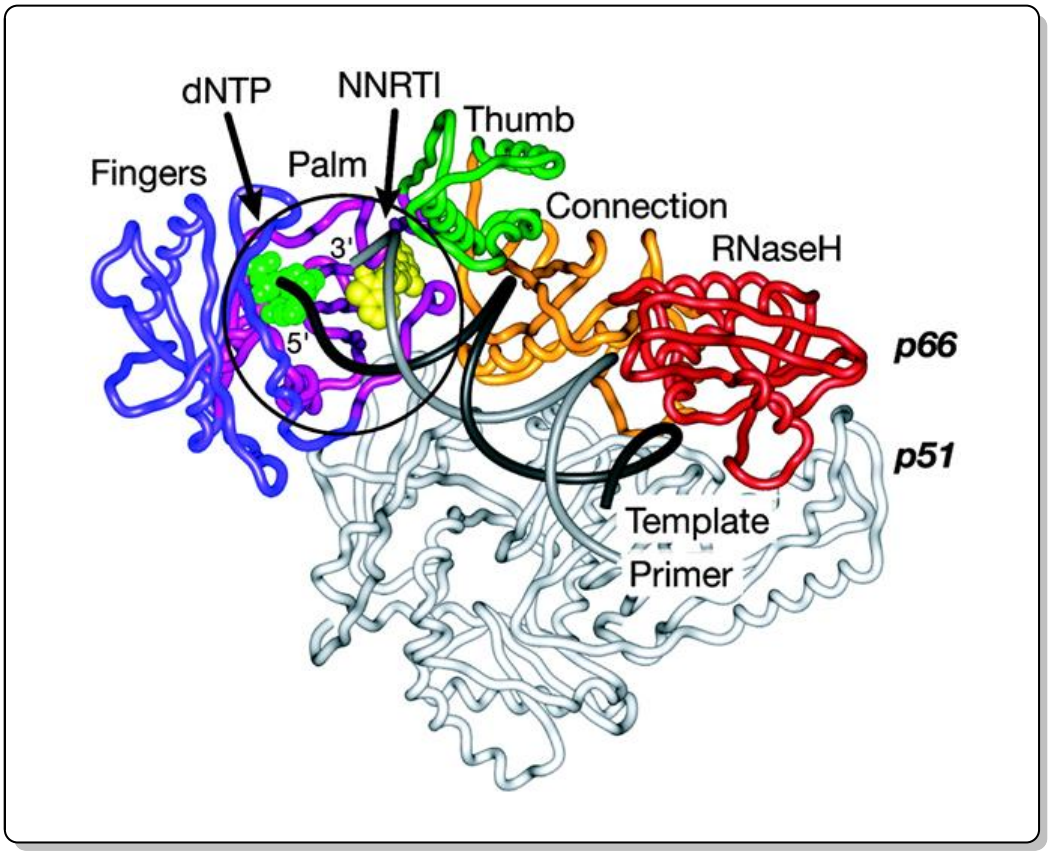

Figure 1.5: Ribbon structure of HIV-1 RT Enzyme

The RT enzyme presents an excellent target for anti-AIDS drug research and development by medicinal chemists given its utility in the retrovirus' replication cycle.[19] The commercially available drugs that target RT inhibition fall into two groups; the nucleoside (NRTIs) and the non-nucleoside inhibitors (NNRTIs) as will be elaborated below.

1.5.2.1 NRTIs

The NRTIs, exemplified by the FDA-approved azidothymidine **3**, stavudine **4** and tenofovir **5** (Fig. 1.6), essentially comprise of nucleos(t)ide analogues that undergo prior phosphorylation by host cell kinases before competitively binding in the conserved RT aspartate catalytic site.

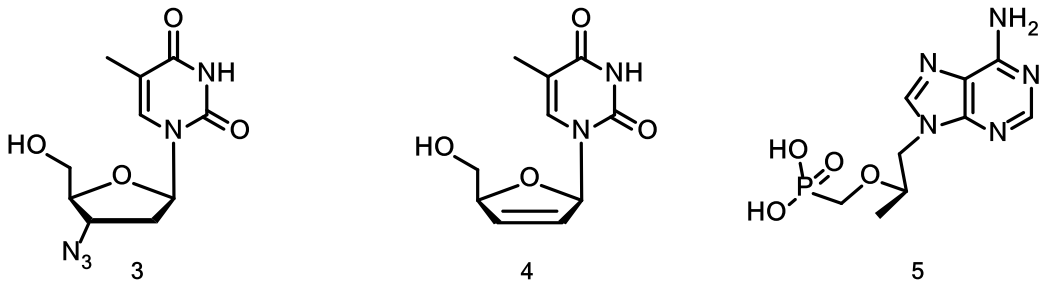

Figure 1.6: Some commercially available FDA-approved NRTI drugs

Thereafter, these substrate decoys, lacking a 3-OH group, become incorporated into the DNA primer strand as chain terminators[20] that slow down the overall viral replication process. It is important to emphasize that the incorporation of the NRTI does not affect the binding of the natural substrate in the catalytic site but prevents its incorporation into the pro-viral DNA strand.

1.5.2.2 Non-nucleoside reverse transcriptase inhibitors (NNRTIs)

The NNRTI drugs form the second drug class targeting the RT enzyme. This class includes a diverse range[21] of small molecules but, unlike NRTIs, they do not require any prior activation to selectively bind in the hydrophobic allosteric site of the enzyme. These drugs, exemplified by nevirapine **6**, delavirdine **7** and efavirenz **8** (Fig. 1.7), are non-competitive inhibitors which bind to a lipophilic, non-substrate binding pocket (NSBP) located approximately 10Å from the polymerase active site to allosterically[22] induce conformational changes that eventually distort the catalytic site to retard catalytic activity.[18-19]

Nevirapine **6** and delavirdine **7** represent the first generation of NNRTI drugs which are highly susceptible to most single point and virtually all multipoint amino acid mutations occurring in the lining of the non-nucleoside inhibitor binding pocket of the RT enzyme. Efavirenz **8** is regarded as a second generation NNRTI which is able to maintain activity against most viral mutants with single point mutations and some strains with double point amino acid mutations.

Etravirine **9** and rilpivirine **10** (Fig. 1.7) are diaryl pyrimidines (DAPYs), and constitute the latest generation of torsionally flexible and highly potent drugs which are efficacious towards all clinically relevant mutant viral strains which are resistant to the first and second generation NNRTIs.

The continued evolution of drug resistant mutations in HIV treatment-experienced patients presents imminent scientific and global challenges which mandate further research into more

potent NNRTI drug leads with better solubility and safety profiles. Thus, the ongoing preclinical studies being carried out by Merck to assess the suitability of doravirine **11** as an NNRTI drug candidate brings some hope to the NNRTI drug research field given that 6 years have elapsed since rilpivirine **10** was approved by the FDA.

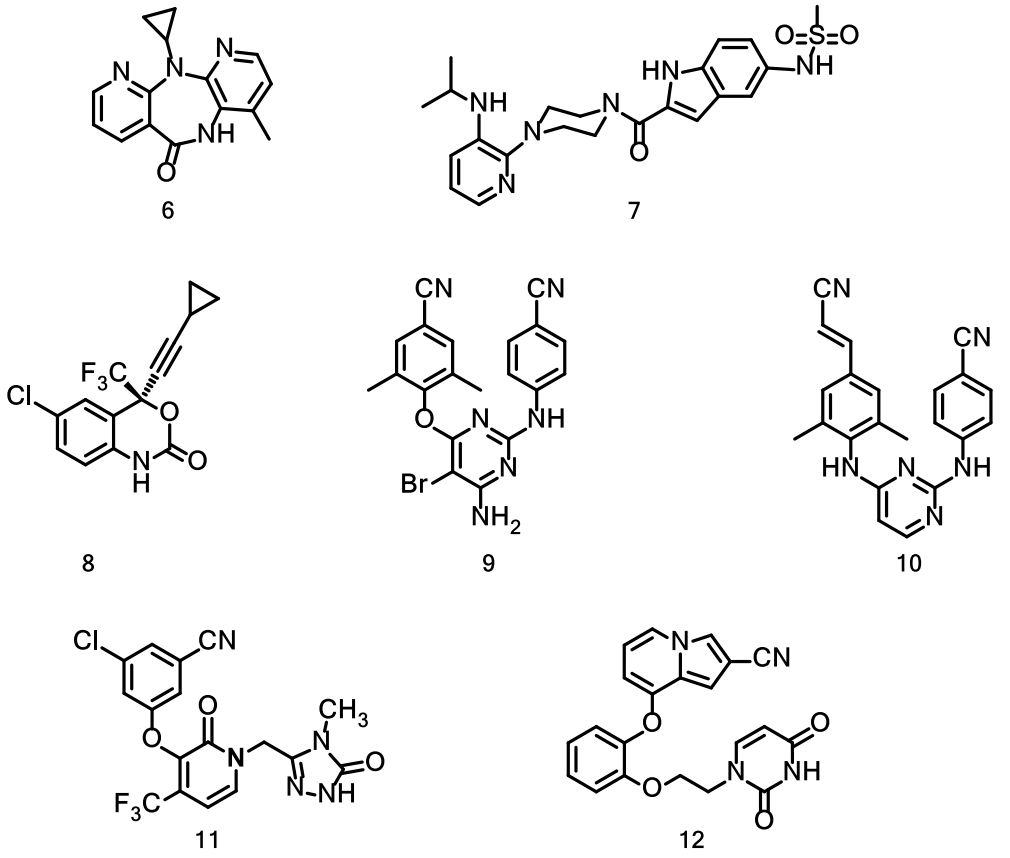

Figure 1.7: FDA-approved NNRTI drugs **6** – **10**, clinical candidate **11** and NNRTI lead **12**

On another note, Jorgensen's[23b] identification of catechol diethers, represented by compound **12** (Fig. 1.7) as potent NNRTI leads potentially presents the research fraternity with an attractive option for pursuing further novel NNRTI drug development based on the catechol diether scaffold.

1.5.2.2.1 NNRTI Mode of Action

The significant technological developments characterizing the fields of molecular and structural biology as well as X-ray crystallography that occurred in early1990s enabled several

researchers to determine both molecular and 3-D structures of the unbound HIV-RT enzyme as well as its corresponding NNRTI[25] and DNA[26] complexes. Thus, the observed different conformational states in those complexes provided salient information with regard to the structural and functional plasticity of the enzyme as well as highlighting the mechanistic model underlying drug resistance which were utilized by Tibotec Pharmaceuticals to access the DAPY series of potent NNRTIs such as etravirine **9** and rilpivirine **10** (Fig. 1.7).

Furthermore, the above-mentioned studies also showed that even though the allosteric site (NNIBP) was conserved in the unbound RT enzyme, it adopted unique conformations when complexed with different substrate/ligands/inhibitors as determined by chemistry, size and conformational flexibility of the ligands.

The NNIBP site is proximally flanked by aromatic (Y181, Y188, F227, W229), hydrophilic (K101, K103, E138) and hydrophobic (L100, V106, V179, L234, P236) side chain residues,[23a] with the hydropilic residues K101 and K103 (p66 sub unit) and E138 (p51 sub unit) occupying a putative entrance[24] to the binding pocket.

Das[27] credits the utility of the above-mentioned scientific discoveries as having provided essential structural information which showed that RT-NNRTI binding affinities were largely reliant on the extent of the π-π stacking (aromatic), hydrophobic (alkyl) and electrostatic (hydrogen bonding) interactions between the enzyme and inhibitor, with the first generation inhibitors nevirapine and delavirdine preferring a 'butterfly-like' conformation.[28]

Although NNRTIs are used together with NRTIs and protease inhibitors as drug cocktails[27] to achieve optimal viral suppression and boost the body's immune function,[13,29] the rapid emergence of drug-resistant RT variants[30] mandates the continuous search for alternative efficacious chemotherapeutic drug candidates.

1.5.2.2.2 NNRTI Structure

Despite the prevailing chemical and structural variations within the first generation NNRTI category, such compounds generally possess rigid 'butterfly-like' structures. As a suitable representative, nevirapine **6** possesses a central hydrophilic core which is sandwiched between two aromatic outskirts (wings).

Contrastingly, the latest generation compounds **9** and **10** possess a much more evolved scaffold resembling a horse-shoe conformation. These compounds possess a central hydrophobic core which may be functionalized to enhance interaction with hydrophilic amino acid residues in the NNIBP. Unlike in first generation NNRTIs where the two outskirts may be fused to the central core, in compounds **9** and **10**, the central core is connected to the hydrophobic outskirts (aromatic) via easily rotatable hetero-linkers to enhance the latter compounds' torsional freedom.

1.5.2.2.3 Development of Drug Resistance

A significant drawback of continually using the first generation NNRTIs like nevirapine **6** and delavirdine **7** is their high susceptibility to single and multipoint mutations of amino acids in the allosteric site which disrupts the favourable binding interactions between protein and inhibitor leading to drug resistance.[15]

Although nevirapine is still being administered for prevention of mother-to-child HIV transmission, it is highly susceptible to single-point viral escape mutations like Y181C and Y188L/H which are rapidly selected under drug pressure. The RT's inherent preferred selection for the K103N mutation as a drug escape route could be explained from Hsiou's[24, 25e] crystallographic studies of RT-K103N/HBY 097 (quinoxaline-based NNRTI) complexes. The structural information derived from these complexes seems to indicate that the K103N plays the role of a 'gate-keeper' mutation that 'zips up' the pocket through an electrostatic interaction (hydrogen bonding) with the phenoxy group of the Y188 side chain thereby restricting NNRTI access to the pocket of the apoenzyme (Fig. 1.8).

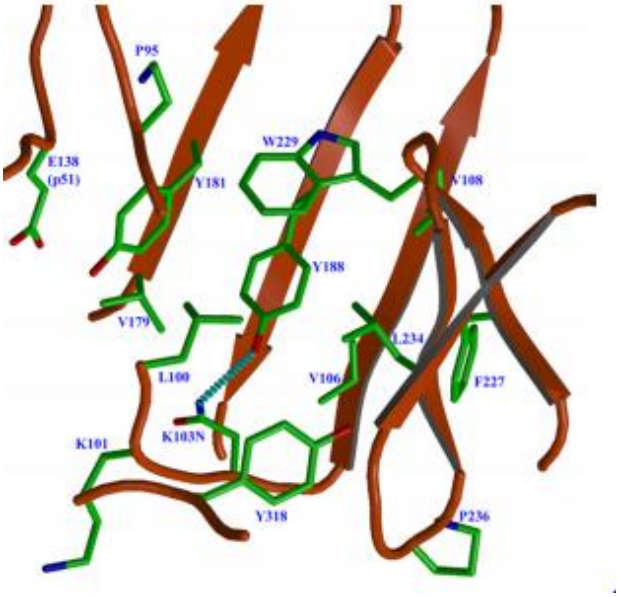

Figure 1.8: Unliganded K103N mutant RT s showing an H-bonding interaction between Y188 and Asn103 (Hsiou[24])

Other mutations like L100I, Y181C and Y188L/P reportedly[23] possess varied resistance mechanisms which uniquely affect the chemistry and topological space in the binding pocket and hence RT-inhibitor interactions. The L100I and G190A mutations have been shown to cause steric clashes with bound inhibitors due to the extra alkyl side chain branches emanating from such mutations.

Whilst efavirenz is highly effective against most clinically relevant single point mutations, it rapidly loses potency against most double-point mutations chief among which are, Y181C/K103N and G190A/K103N. The K103N, G190A and Y181C mutations have emerged as highly prevalent clinically relevant mutants with K103N conspicuously displaying general cross-resistance across all the NNRTI categories.

The rapid emergence of drug-resistant mutations even under the HAART multi-drug approach prompted Janssen[1,8] to identify tetrahydroimidazo[4,5,1,*jk*][1,4]benzodiazepin-2(1*H*)-one (TIBO) (e.g. tivirapine **13**) and α-anilinophenylacetamido (α-APA) (e.g. loviride **14**) (Fig. 1.9) derivatives as alternative NNRTI leads during high throughput screening (HTS) of a large compound library against the MT4 cell-line. These leads were very potent against the wild type virus but, unfortunately, were less effective against strains bearing the Y181C, Y188L, K103N and G190A mutations.

Janssen and his collaborators[8] then employed a comprehensive multidisciplinary approach which involved molecular modelling, structural biology (crystallography) and traditional medicinal chemistry protocols to access potent NNRTI hit compounds that are based on the 'horse-shoe'

type DAPY and diaryl triazine (DATA) pharmacophores. Through a lead optimization strategy spanning almost two decades, the highly potent latest generation NNRTIs, etravirine **9** and rilpivirine **10** (Fig. 1.7), were developed.

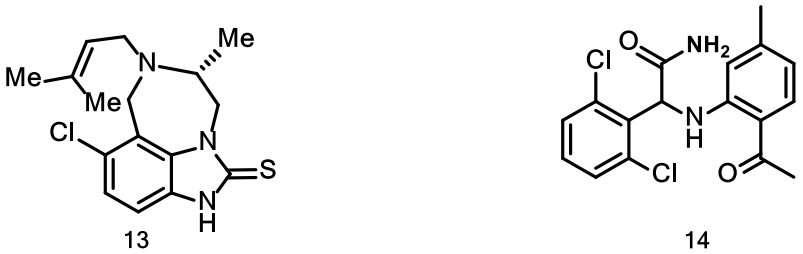

Figure 1.9: TIBO derivative – tivirapine **13** and α-APA derivative – loviride **14**.

Crystallographic and molecular modelling data have attributed the high antiviral potencies exhibited by these drugs to their inherently high torsionally flexibility.[19,31] This enables them to adopt multiple binding conformations without significant loss in binding affinity, even in the presence of the clinically relevant mutations.

Despite the generally high potencies displayed by the latest generation NNRTIs across all RT mutants, K103N and Y181C as well as E138K/P and K101P are slowly emerging as moderate-level resistance mutations in the clinical isolates of etravirine and rilpivirine treatment-experienced patients. Thus, research work aimed at rationally optimizing etravirine and rilpivirine as drug leads for accessing more potent NNRTIs has already commenced. Unfortunately, analogues generated so far exhibit inferior barriers to the development of viral resistance than their respective progenitors.[1,23b]

Given the above challenges associated with emerging drug resistance mutations against the highly potent second generation NNRTIs, more research is needed to explore new scaffolds as possible leads towards the discovery of alternative NNRTI drug candidates.

Thus, our research project aims to access nitrogen-based heterocyclic derivatives as potential NNRTIs on the basis of a scaffold-hopping approach and a molecular modelling initiative. The objective will be to produce analogues that target binding interactions with the amino acids lining the putative entrance to the NNIB pocket.

As such, metal-catalyzed cross-coupling reactions and *in silico* modelling will play a crucial role towards accessing these compounds as discussed in the following sections.

1.6 Transition metal-catalyzed cross-coupling reactions

The successful development and adaptation of selective and highly efficient transition-metal catalyzed cross-coupling protocols over the past three and a half decades has enabled synthetic chemists to access a broad and unique array of antibiotics,[32] hormones[33] antagonists,[34] biologically active molecules,[35] industrial chemicals[36] and aniline derivatives[37] which are otherwise inaccessible conventionally.

Whilst several other transition metals like iron,[38] nickel[39] and platinum,[40] to mention just a few, continue to play crucial catalytic roles that support both academia and various industrial applications, this section will primarily focus on the historical perspective behind catalysis with special emphasis on both copper and palladium-based protocols as evolutionary, versatile and complementary synthetic approaches that are easily adaptable towards accessing novel target compounds in the 21st century and far beyond.

1.6.1 Historical perspective

The first cross-coupling reactions were pioneered by Glaser[41] in 1869 when he reported the successful copper-assisted oxidative dimerization of phenyl acetylene **15** to form diphenyl di-acetylene **16** (Scheme 1.1). The major beneficiary of this novel carbon-carbon bond formation was Baeyer, who successfully commercialized this copper catalyzed technology to access indigo[41] **17** from 3-phenylpropiolic acid **18** (Scheme 1.2) - which led to the birth of the lucrative dye industry.

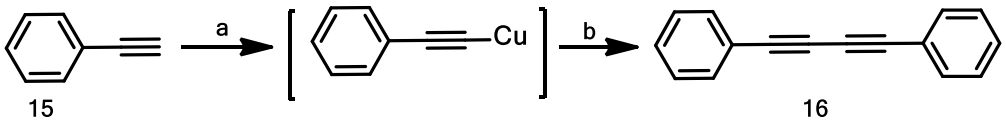

Scheme1.1: *Reagents and conditions*; (a) CuI, NH_4OH, EtOH; (b) O_2, NH_4OH, EtOH.

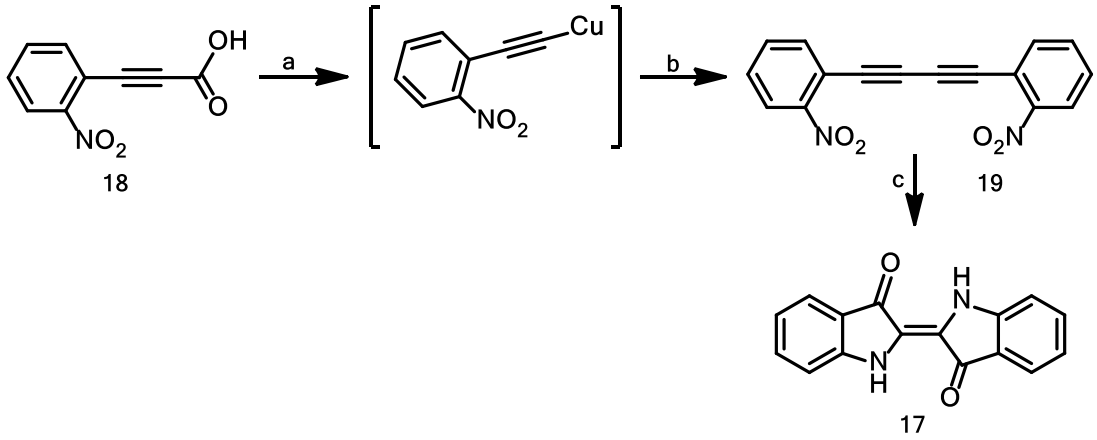

Scheme1.2: *Reagents and conditions*; (a) H_2O, heat, CuCl, EtOH; (b) $K_3[Fe(CN)]_6$, H_2O; NH_4OH, EtOH; (c) H_2SO_4, $(NH_4)_2S$.

Thereafter, in 1901, Fritz Ullmann[42] also reported the successful homocoupling of 2-halo-nitrobenzene **20** using stoichiometric amounts of copper to produce symmetrical biaryl ring systems **21** (Scheme 1.3) through what is now referred to as the classical Ullmann reaction.

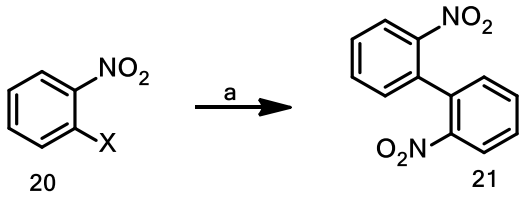

Scheme 1.3: *Reagents and conditions*; (a) Cu; 200°C.

1.6.2 Classical Ullman Chemistry

Although copper-assisted cross-coupling reactions generally appear to be taking a back seat, with most researchers preferring the more facile and more costly palladium-mediated protocols, it is important, at this juncture, to emphasize that copper catalysis pioneered the traditional C-N metathesis from which the contemporary and highly selective palladium-catalyzed reactions were later developed. The evolution of palladium-mediated chemistry will be covered in section 1.6.4.

Beletskaya[43] generally defines classical Ullman chemistry as all those aromatic nucleophilic substitution reactions which occur in the presence of either metallic copper or copper salts

under very high temperatures ranging from 150 – 200ºC, utilizing haloarene-based substrates to access C-N, C-O and C-S containing synthetic targets.

In the same vein, Hartwig[44] also supports the pioneering role of traditional copper-mediated chemistry in the small scale production of arylamines that were used as key intermediates for accessing conducting polymers and layers of organic light-emitting diodes. Hartwig and other researchers[45] further concur that the increasing global demand for aryl amine substrates, the associated small scale production bottlenecks and the harsh reaction conditions that limited product scope were major contributing factors which led to the development of cost-effective palladium-catalyzed coupling technologies.

Such factors, coupled with the high cost of palladium, could also have played a large part in spearheading the parallel development of more robust supporting ligands which provided a more efficient alternative route for cross-coupling aryl halides and amines to improve the economies of scale and provide variety in the much-needed aryl amine building blocks that were crucial in developing the pharmaceutical and material science fields.

Furthermore, any continued or unrestricted and stoichiometric usage of copper beyond the 1970s proved unattractive as its high water persistency led to waste handling challenges[36, 46] amid environmental concerns and tightening environmental regulations. Scientific logic dictates that these challenges left researchers with two choices: to modify the traditional Ullmann protocol and make it catalytic and/or to develop other cost-effective metal-catalyzed cross-coupling reactions.

1.6.3 Improved Ullman protocol

The optimization of the stoichiometric copper-based reactions into more cost-effective and milder copper-catalyzed protocols occurred rather sluggishly, unlike palladium catalysis, primarily due to a lack of mechanistic understanding[47] surrounding copper-mediated chemistry. On the other hand, the exploration and development of successful palladium-catalyzed cross-coupling reactions was gathering momentum in the 1970s as typified by the emergence of more versatile protocols like the Heck-Mizoroki, Stille and Sonogashira coupling reactions, as will be explained later under palladium catalysis.

Thus, the “softening” of the traditional Ullman protocol only started to bear fruit when researchers explored the use of complexing ligands as a parallel strategy to what was happening on the palladium catalysis front. Hence the availability of cheap nitrogen-based[48a] and oxygen-containing[48b] ‘implicit’ chelating compounds **22** and **23** (Schemes 1.4 and 1.5)

contributed greatly to ushering in a new era where milder carbon-nitrogen[49] bond formation could be carried out at comparatively lower catalyst loadings and reaction temperatures.

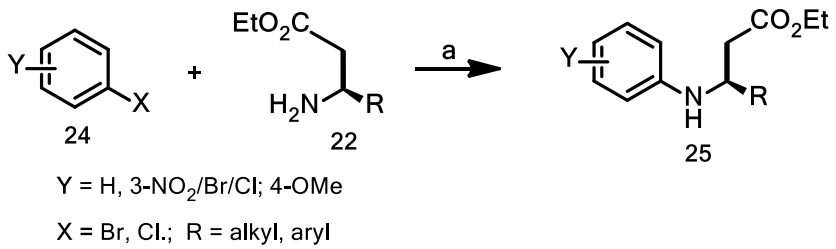

Scheme 1.4: *Reagents and conditions*; (a) CuI, K_2CO_3, DMF, H_2O, 100°C, 24 h.

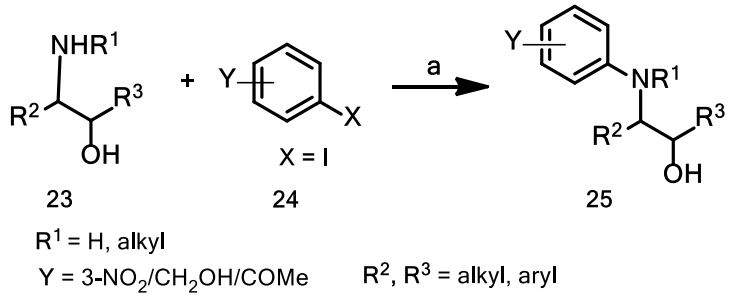

Scheme 1.5: *Reagents and conditions*; (a) CuI, K_3PO_4, $HO(CH_2)_2OH$, ^{i}PrOH, N_2 atm. 75-80°C, 20 h.

In this regard, the modified Ullman protocol, once again, restored the utility of copper-mediated reactions as a complementary and relatively cheaper synthetic approach which could equally be used to broaden the scope of carbon-carbon formations and more importantly, even be extended towards carbon-nitrogen bond formation chiefly involving the *N*-arylation of a variety of anilines,[50] amides,[51] and other heterocyclic nucleophiles.[52]

Thus, even today, copper-catalyzed carbon-carbon bond forming reactions are very useful for accessing symmetrical and unsymmetrical biaryl compounds and novel heterocyclic biaryl substrates which are used to prepare prototypes for scintillators. As such, literature is now endowed with mild, efficient and selective copper-catalyzed protocols that employ accessible ligands like 1,10-phenanthroline, aliphatic amines, phosphine-based bidentate dppp[43] **26** (Fig. 1.10), *N,N*-diethylsalicylamide,[52] and ethylene glycol[53] to aminate aryl iodo and bromo derivatives, and most recently, a few selected chloro arenes.

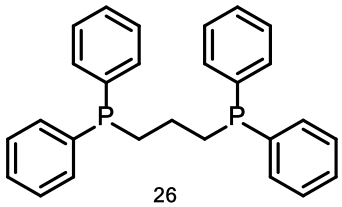

26

Figure 1.10: 1,3-Bis(diphenylphosphino)propane, dppp **26**

In addition the developments of air-stable soluble copper(I) complexes[54] has duly provided another dimension that allows convenient cross-coupling using organic solvents and basic media, thereby broadening substrate scope.

On a comparative platform, Enguehard[53] successfully aminated a substituted imidazo[1,2-*a*]pyridine core **27** (a fused imidazole ring system that forms a critical component of p38 MAP kinase inhibitors) using independent copper-based and palladium-catalyzed protocols employing glycerol and *rac*-BINAP as respective ancillary ligands (Scheme 1.6), once again, showing the complementary utility of the two catalyst systems.

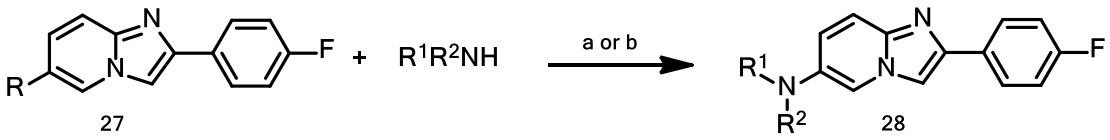

27 28

R^1 = H, alkyl; R^2 = alkyl, aryl

Scheme 1.6: *Reagents and conditions*; (a) Cu catalysis: R = I; CuI, K_3PO_4, $HO(CH_2)_2OH$, ^{i}PrOH, N_2 atm. 85 - 112°C, 24 h; (b) Pd catalysis: R = Br; Pd_2dba_3/*rac*-BINAP, NaO^{t}Bu, PhMe, N_2 atm. 85 - 112°C, 24 h.

Thus Enguehard's[53] achievements help to bring copper-mediated protocols into the limelight as cheap and versatile methodologies that help complement palladium-catalyzed reactions in the realm of total synthesis.

1.6.4 Palladium-based catalysis for carbon-carbon bond formation

Although palladium was discovered by Wollaston in 1805,[55] its industrial importance lagged far behind that of its close relatives, platinum and nickel, until almost 150 years later, in 1959. Then, a research team at Wacker-Chemie[56] central research institute, led by chief chemist, Walter Hafner, serendipitously discovered palladium's catalytic potential which eventually led to the

historic commercialization of the palladium-catalyzed (copper-supported) oxidation of ethylene **29** to form acetaldehyde **30**, that was later coined the Wacker process[56] (Scheme 1.7).

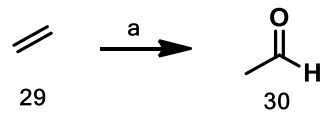

Scheme 1.7: *Reagents and conditions*; cat. $PdCl_2$, $CuCl_2$; HCl/H_2O.

This discovery proved to be the turning point in the chemistry of palladium[57] as subsequent mechanistic studies by Hafner, showing that palladium underwent 'carbopalladation' forming stable palladium π-allyl complexes as essential transition state species, not only validated observations earlier made by Tsuji[58] in 1965, but also enlightened the scientific community as to the mechanistic utility of palladium in these carbon-carbon transformations.

Thus, the subsequent commercialization of the Wacker process as a reliable source of cheap chemicals that were in great demand for making plastics, bulk chemicals and construction materials to support the rebuilding and industrialization[56] efforts in Europe after the Second World War, eventually put palladium chemistry in the limelight of many scientific research frontiers.

The ability of palladium to activate carbon-hydrogen bonds, as observed in the Wacker process, further opened other research windows as chemists broadened substrate scope by incorporating functionalized olefinic derivatives as coupling partners. Such variations eventually gave birth to some of the most universally applied palladium-catalyzed carbon-carbon bond construction protocols, namely the Heck-Mizoroki reaction, Suzuki-Miyaura coupling, Sonogashira reaction, Tsuji-Frost and Negishi[59] reactions.

Beletskaya[43] argues that whilst the utility of copper-based protocols primarily depends on the optimization of the whole catalytic system (nature of palladium precursor, base, solvent, ligands), palladium catalysis, on the other hand, is more reliant on the nature of the ligand system. We are of the opinion that the above realization, coupled with a clear mechanistic understanding of palladium catalysis, led to the rapid development of more evolved ancillary ligand systems which helped in tuning the palladium coordination sphere to achieve better

selectivity, more substrate scope and high reaction rates for palladium-catalyzed protocols in comparison to copper-mediated reactions.

Whilst we acknowledge the importance of other carbon-carbon bond forming protocols as exemplified by the Grignard, Diels Alder and Wittig reactions[60] in the construction of novel and highly complex carbon compounds, this section will be restricted to the Heck-Mizoroki, Suzuki-Miyaura and Sonogashira reactions as foundational palladium-catalyzed platforms whose invaluable contribution towards total organic synthesis inevitably led to the development of complementary carbon-heteronuclear coupling technologies. The latter palladium-mediated heteronuclear technologies will be covered much later in section 1.6.5 covering the Buchwald-Hartwig C-N protocol.

1.6.4.1 The Heck-Mizoroki reaction

The Heck-Mizoroki reaction essentially involves a palladium catalyzed carbon-carbon bond formation between an olefin-based substrate **31** and aryl halides or triflates **32** (Scheme 1.8) to give unique olefinated targets of general structure **33** which could not be accessed conventionally. Besides extending the substrate scope as explained above, Heck[61] and Mizoroki[62] also made some of the most remarkable contributions towards the palladium-catalyzed protocols by studying the reaction kinetics and elucidating the key mechanistic steps leading to carbon-carbon bond formation.

Thus, the key steps involved were identified as comprising oxidative addition, complexation/substrate insertion, β-hydride elimination and reductive elimination which eventually led to a palladium catalyzed catalytic model which is explained later in section 1.6.5.1.

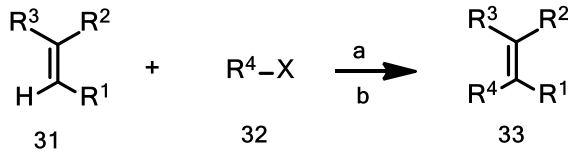

31 32 33

Scheme 1.8: Heck-Mizoroki Reaction; (a) cat [Pd^0L_n], (b) base; R^4 = aryl, benzyl, vinyl; X = Cl, Br, I, OTf

Among the notable applications of the Heck-Mizoroki reaction has been the intramolecular cyclization step used by Rawal[60,63] in 1993 to access a complex alkaloid named dehydrotubifoline **34** (Scheme 1.9).

The reaction employed a palladium-catalyzed carbon-carbon bond metathesis involving an initial 6-*exo*-palladation step of substrate **35** that is followed by β-hydride elimination and tautomerization to form the expected enamine polycyclic structure **34.**

Surprisingly, the corresponding *N*-methoxylated substrate **36** underwent an unexpected **7**-*endo*-cyclopalladation reaction to produce a completely unexpected product **37**, with inversion of configuration of the exocyclic double bond.

Intrigued, Rawal performed mechanistic studies under modified Heck-Mizoroki reaction conditions which showed that the σ-alkyl-palladium species **38** initially formed was stabilized through a carbonyl complexation step (Scheme 1.9).

This stabilization obviated the expected *syn*-β-hydride elimination route in favour of the second cyclo-palladation reaction to form another intermediate **39**, which due to steric strain, underwent 120° rotation, followed by the exocyclic double-bond rotation and rearrangement to give intermediate **40**, and eventually β-hydride elimination to give the product **37**.

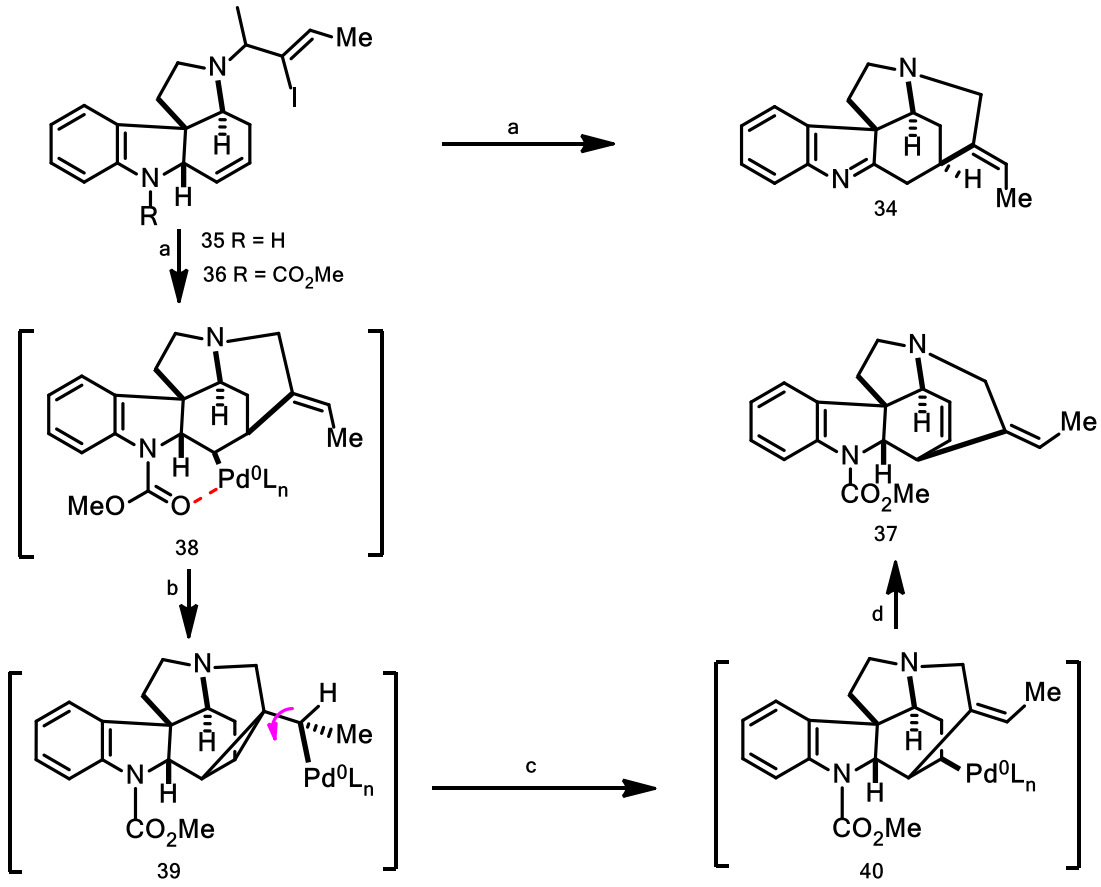

Scheme 1.9: *Reagents and conditions* (a) cat $Pd(OAc)_2$, K_2CO_3, $^nBu_4NCl$, DMF, 60°C; (b) second 1,2- insertion; (c) bond rotation, rearrangement; (d) β-hydride elimination.

This protocol validates the significance of what Beletskaya[43] calls 'intramolecular assistance' which is commonly used in synthetic chemistry to 'actuate' or 'tune' the mechanistic pathway towards accessing specific synthetic targets. The same concept has also been successfully applied for aminating *o*-halobenzoic acids[64] to produce *N*-aryl anthranilic acids under mild copper catalysis.

The second example relates to the industrial synthesis of an anti-asthma drug, Singulair **41**, which was developed by Merck in 1993 (Scheme 1.10).[65]

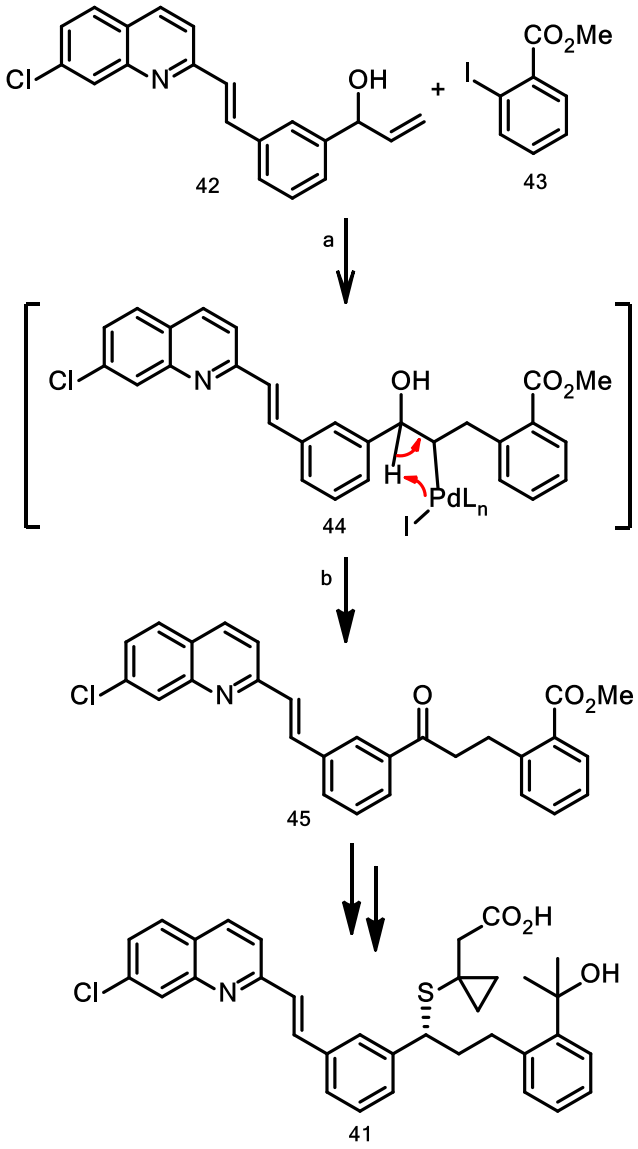

Scheme 1.10: *Reagents and conditions*: (a) cat $Pd(OAc)_2$, Et_3N, MeCN, 85°C, intermolecular Heck-Mizoroki reaction; (b) β-hydride elimination, tautomerism.

In this industrial protocol, a palladium-catalyzed intermolecular carbon-carbon metathesis (Heck-Mizoroki reaction) was used to couple an allylic alcohol **42** and an ester-functionalized aryl iodide **43** forming an alkyl-palladium enol intermediate **44**. Tautomerization to form ketone **45** allowed for eventual conversion to the target product **41** (Scheme 1.10).

1.6.4.2 Suzuki-Miyaura reaction

This carbon-carbon bond forming transformation involves palladium-catalyzed coupling of aryl-, or alkenyl halides or triflates **46** using organoboronic acids **47** as coupling partners (Scheme 1.11).

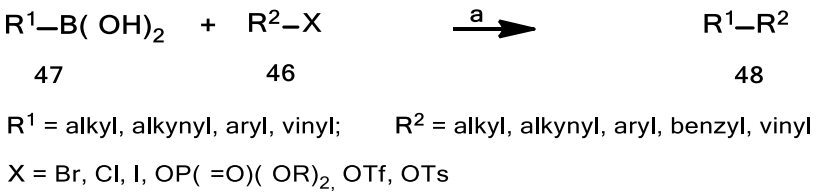

Scheme 1.11: *Reagents and conditions*; (a) Pd catalyst, base, solvent.

Nicolaou[60] points out that the Suzuki-Miyaura coupling is a vital synthetic tool for accessing conjugated dienes, polyenes, and biaryl ring systems. In a way, this protocol complements the traditional Ullmann homo-coupling chemistry. As such, the Suzuki-Miyaura reaction was used by Rossi and co-workers[66] to couple vinyl bromide **49** and vinyl borane **50** to access an insect pheromone (*E*)-9, 11-dodecadien-1-yl acetate **51** using $Pd(PPh_3)_4$ as catalyst (Scheme 1.12).

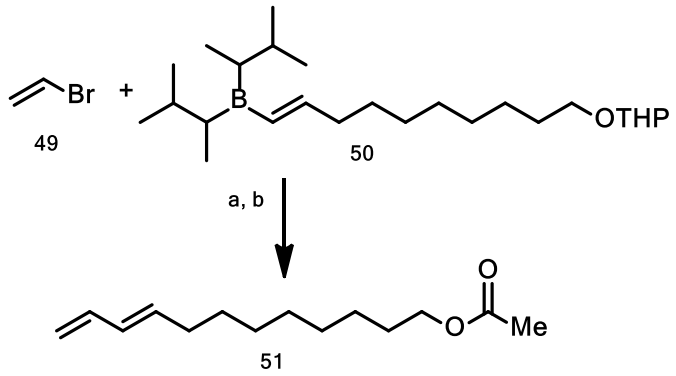

Scheme 1.12: *Reagents and conditions*; (a) cat [$Pd(PPh_3)_4$], NaOH, THF/H_2O, 50°C; (b) Ac_2O/AcOH, 80°C.

It is important to point out that $Pd(PPh_3)_4$ appears to be the catalyst of choice for Suzuki-Miyaura coupling reactions since vinylic systems are activated substrates that are predominantly reactive.

However, another interesting example involves Ishikura's[67] application of a three-component, carbonylative Suzuki-Miyaura cross-coupling as a key step in the total synthesis of a bisindole alkaloid yuehchukene **52** via a 2-indolyl ketone **53** (Scheme 1.13).

Boc-protected indole **54** was *ortho*-lithiated and reacted with triethylborane to give a lithiated complex **55** *in situ*, which was carbonylated with a triflate **56**, under palladium catalysis, to generate the 2-indolyl ketone intermediate **53**, for eventual conversion to the target product **52.**

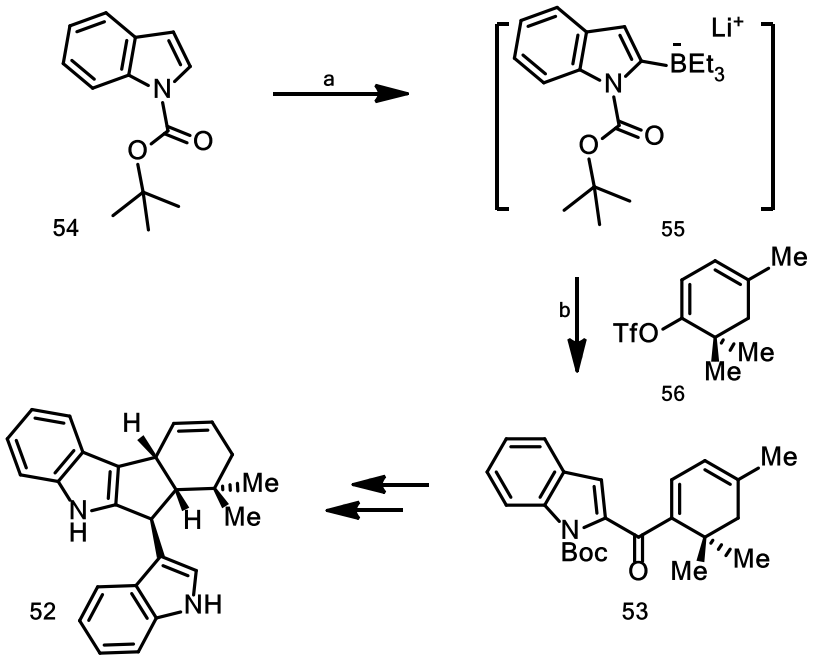

Scheme 1.13: *Reagents and conditions*; (a) ^{t}BuLi, THF, BEt_3; (b) cat $[PdCl_2(PPh_3)_2]$, CO (10 atm), THF, 60°C.

1.6.4.3 Sonogashira reaction

The Sonogashira reaction is a valuable synthetic protocol for making conjugated acetylenic systems[68] which find use as sensitizers and/or scintillators in material science research. This approach provides a more cost-effective route for accessing polyene systems than the Suzuki-Miyaura reaction. The Sonogashira protocol is a carbon-carbon bond forming reaction which employs palladium catalysis for coupling acetylenes **57** with organic electrophiles **58** to generate functionalized alkynes **59** (Scheme 14). In most protocols, co-catalytic amounts of cuprous salts are also added to the reaction mixture to improve the yield of target products.

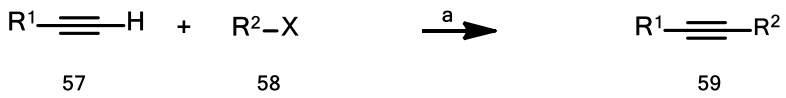

R^1 = alkyl, aryl, vinyl; R^2 = aryl, benzyl, vinyl; X = Br, Cl, I, OTf

Scheme 1.14: *Reagents and conditions*; (a) cat [Pd^0L_n], base.

The Sonogashira protocol provides an essential synthetic approach for the stereoselective construction of polyene systems. An exemplary application of this approach involves the pioneering synthesis of the biologically active eicosanoid **60** by Nicolau and Webber[69] in 1984. The research group developed a stereospecific synthetic construction of the target compound **60** (Scheme 1.15) in such a way that targeted the generation of the *Z*-configuration of the alkene systems.

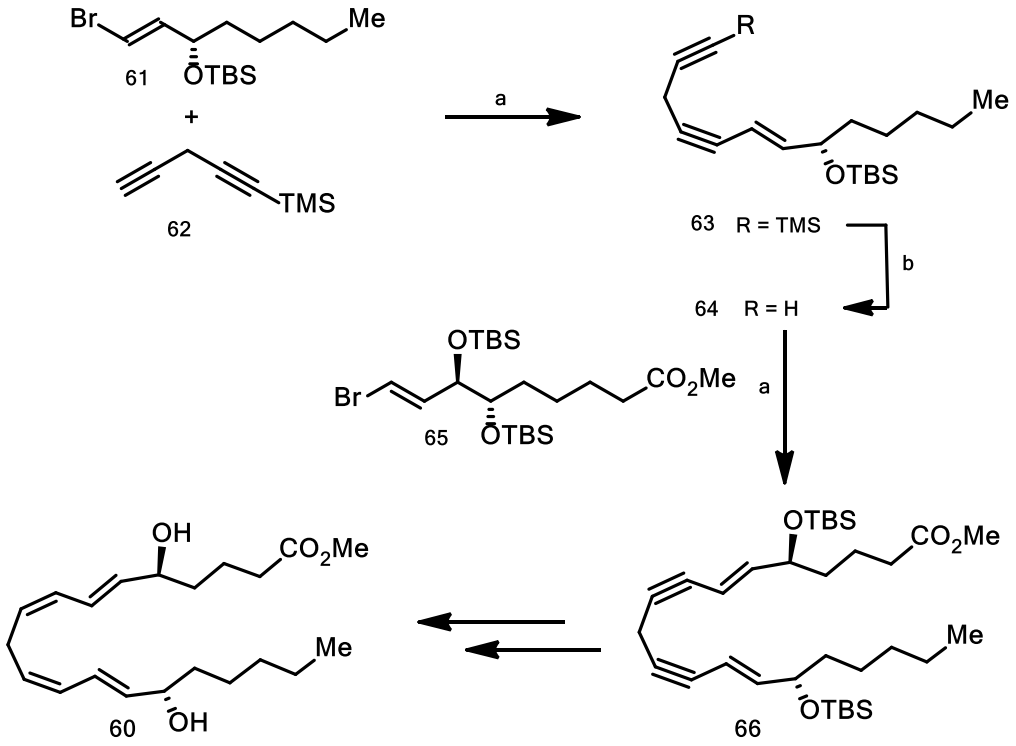

Scheme 1.15: *Reagents and conditions*; (a) cat. 4 mol% [$Pd(PPh_3)_4$], 16 mol% CuI, $^nPrNH_2$, benzene, 25°C; (b) $AgNO_3$, KCN.

This was achieved by coupling a vinyl bromide **61** to a terminal alkyne **62** using $Pd(PPh_3)_4$ in the presence of co-catalytic amounts of Cu(I)I to afford the enediyne (*E*)-isomer **63**. Removal of the terminal alkyne group gave an intermediate **64** which was further coupled with another vinyl bromide **65** using similar catalytic conditions to generate the bis(enyne) isomer **66**. Subsequent selective hydrogenation of the two alkyne groups followed by cleavage of the TBS protecting groups gave the target product **60** in good yield.

A second application of the Sonogashira coupling involves the industrial synthesis of eniluracil **67** (Scheme 1.16), a chemotoxic agent for the treatment of both breast and colorectal cancers.

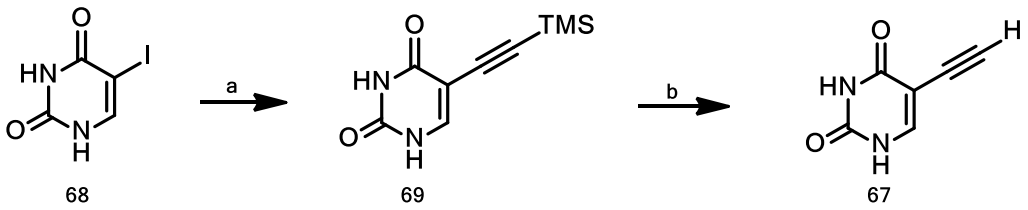

68 69 67

Scheme 1.16: *Reagents and conditions*; (a) cat. 0.5 mol% $[Pd(PPh_3)_4]$, 0.5 mol% CuI, (trimethylsilyl)acetylene, EtOAc, Et_3N, 25°C; (b) NaOH.

Developed by GlaxoSmithKline[70] in 2001, the synthetic pathway involves usage of low transition metal catalyst loadings for coupling iodouracil **68** with (trimethylsilyl)acetylene (Scheme 1.16) to give a TMS-protected compound **69**. Subsequent base-promoted TMS deprotection afforded the target product **67** in good yield.

1.6.5 Palladium catalysis for C-N bond formation

Although Migita and coworkers[71] pioneered the successful palladium-catalyzed C-N coupling reaction between an aryl bromide **70** and stoichiometric amounts of tin amide **71**, using tris(*o*-tolyl)phosphine as ancillary ligand (Scheme 1.17) to access aryl amines **72**, some credit should also go to a Russian scientist named Yagupol'skii'.[59a]

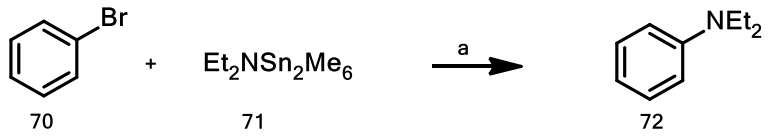

Scheme 1.17: *Reagents and conditions*; (a) cat [$Pd(P(o\text{-tolyl})_3)_4$], PhMe, 100°C, 3 h.

In 1986, Yagupol'skii' showed that sodamides **73** could also be successfully coupled with aryl halides **74** (Scheme 1.18) to give aminated products **75**, thus obviating the exclusive use of toxic tin amides as coupling partners in future palladium-assisted amination protocols. Unfortunately, this work seems to have been published in a non-peer reviewed Russian journal that failed to reach the interested research groups at the time.

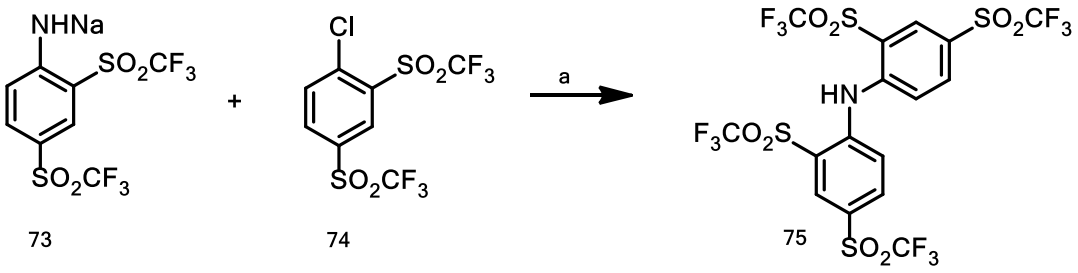

Scheme 1.18: *Reagents and conditions*; (a) cat [$PhPd(PPh_3)_2$], MeCN, reflux, 6 h.

At this point, it becomes instructive to point out that whilst the Migita protocol gave excellent yields (Table 1.1) for bromobenzene (entry i, 81%), 3-methyl- (ii, 61%) and 4-methyl bromobenzene (iii, 79%) using $PdCl_2(o\text{-tolyl}_3P)$ as catalyst, unfortunately, poor conversions[69] were realized for 2-methoxy- (iv), 4-methoxy- (v), 4-acetyl- (vi) and 4-nitrobromobenzene (vii). Regrettably, no conversions were realized for similar reactions with chloro- and iodobromobenzene (entries viii – ix) (Table 1.1).

Table 1.1: Migita's Pd-catalyzed aminations using tin amides

	Aryl halide	Product	Yield
i)	Bromobenzene	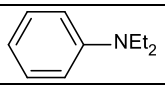	81%
ii)	3-Methylbromobenzene	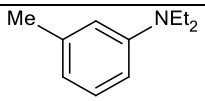	61%
iii)	4-Methylbromobenzene	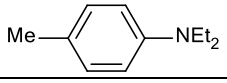	79%
iv)	2-Methoxybromobenzene	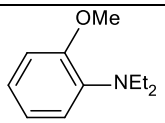	33%
v)	4-Methoxybromobenzene	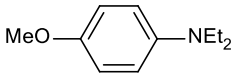	39%
vi)	4-Bromoacetophenone	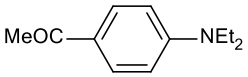	16%
vii)	4-Nitrobromobenzene	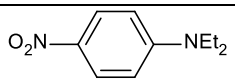	24%
viii)	Chlorobenzene	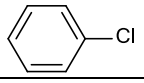	0%
ix)	Iodobenzene	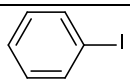	0%

In an attempt to investigate the mechanistic steps underlying this unique palladium-catalyzed amination which was very different from the usual aromatic nucleophilic aminations that proceeded via the aryne and $S_{NR}1$ mechanism, Migita reacted *para*-chlorobromobenzene **76** with potassium *N,N*-diethylamide **77** (Scheme 1.19).[71]

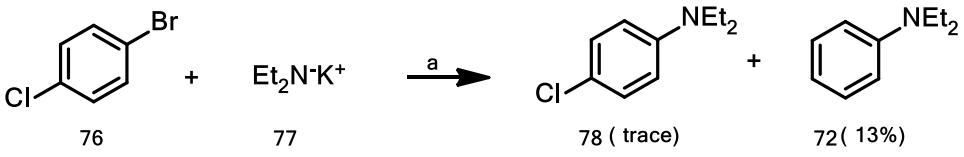

Scheme 1.19: *Reagents and conditions*; (a) $NHEt_2$, RT.

The identification of an unexpected major product **72** prompted Migita to propose the possible involvement of a free radical mechanism involving diethyl aminophenyl radical species. Migita

then suggested that oxidative-addition, transmetallation and reductive elimination were key steps in the palladium catalyzed amination reactions. This was the starting point for investigating the mechanistic detail surrounding palladium-catalyzed C-N bond forming reactions which, ten years later, attracted the interest and involvement of the Buchwald and Hartwig independent research groups.

1.6.5.1 Mechanistic Model - Transition metal catalytic cycle

The successful palladium catalyzed aminations of aryl bromides with tin amides achieved by Migita and coworkers generated renewed enthusiasm and research interest in the field of palladium catalyzed amination chemistry. Guram and Buchwald[72] noted that the Migita protocol had challenges associated with limited product scope, long reaction times, tedious work-up and residual toxicity which obviated its suitability in the preparation of amines targeted for downstream use, especially in the pharmaceutical industry. On that basis, the duo eventually developed an efficient amination protocol (Scheme 1.20) that employed $[Pd(dba)_2]/2P(o\text{-tolyl})_3$ or $[PdCl_2(P(o\text{-tolyl})_3)_2]$ catalyst and NaO^{t}Bu (base) as a general route for accessing a variety of arylamines **79**.

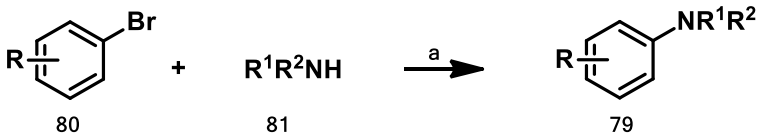

Scheme 1.20: *Reagents and conditions*; (a) $[Pd(dba)_2]/2P(o\text{-tolyl})_3$ or $[PdCl_2(P(o\text{-tolyl})_3)_2]$, NaO^{t}Bu, PhMe, 65 -100°C.

One interesting observation was the presence of an unexpected arene side product – the reduced form of the aryl halide substrate – whose quantities were determined by both electronic and steric features of the aryl halide and amine in use.

Given the above observation, Guram and Buchwald[72] proposed that Pd-mediated reactions occurred via a preliminary oxidative addition of the aryl halide substrate **82** to the Pd^0-centre of the catalytic species **83** (Fig. 1.11). The Pd^0 gets oxidized (to the divalent state - Pd^{II}) as the oxidative addition complex **84** is formed, which further reacts with the amine **85** to give the palladium-amido complex **86**.

Depending on electronic and steric circumstances, the complex **86** can either undergo reductive elimination to give the target amine **87** and regenerate the active catalytic species **83** or pursue a β-hydride elimination process to produce species **88** which further undergoes reductive elimination to form the arene side product **89,** whilst regenerating **83** into the catalytic loop.

When another experimental run was conducted using *N*-methylbenzylamine **90** (Fig 1.12), the expected arene side product - *N*-methylbenzylidene of general structure **91**, was detected in the product stream thereby giving credence to the proposed catalytic cycle (Fig. 1.11).

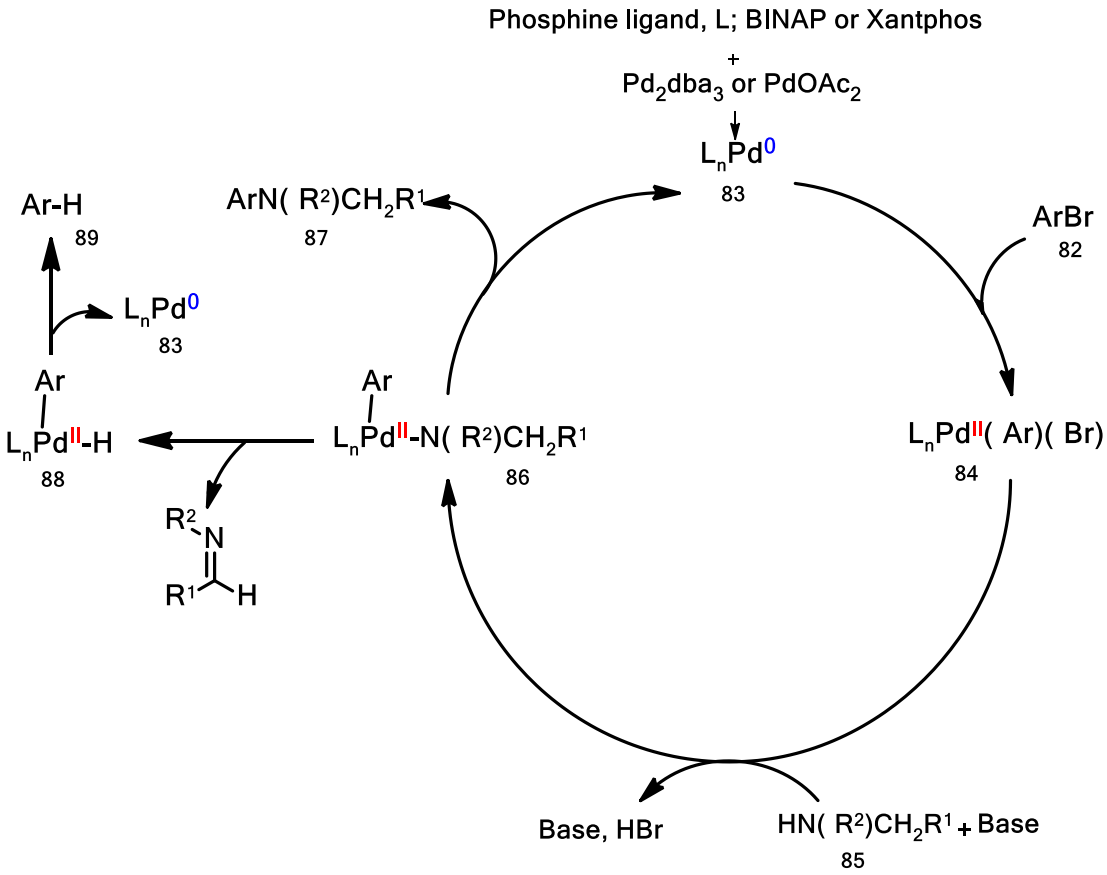

Figure 1.11: Generalized Mechanism for Pd-catalyzed amination cycle (Guram[72] and Buchwald, 1995).

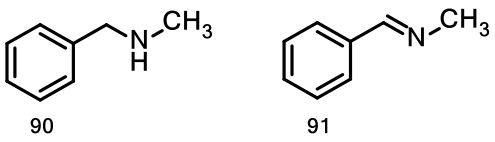

90 91

Figure 1.12: *N*-methylbenzylamine **90** and *N*-methylbenzylidene **91**

The above catalytic model (Fig. 1.11) was also verified by Louie and Hartwig[73] who were independently working on establishing the mechanistic detail underlying the Pd-catalyzed amination of aryl bromides in the presence of the [$PdCl_2(P(o\text{-tolyl})_3)_2$] catalyst system.

1.6.5.2 Ligand Effects

The mono-phosphine (mono-dentate) and diphosphine ligands (Fig. 1.13) constitute the two major classes of ligands which are normally used for supporting transition metal-mediated carbon-carbon and carbon-heteroatom bond formations. The mono-phosphine ligands, typified by tri(*ortho*-tolyl)phosphine **92** and triphenylphosphine **93** (Fig. 1.13), contain one phosphorus atom which coordinates to the metal centre through a phosphorus atom via a σ-bond, whilst the diphosphine counterparts, exemplified by **94**–**99** (Fig. 1.13) are, due to the chelate effect, bound more tightly via two bonds with the metal centre.

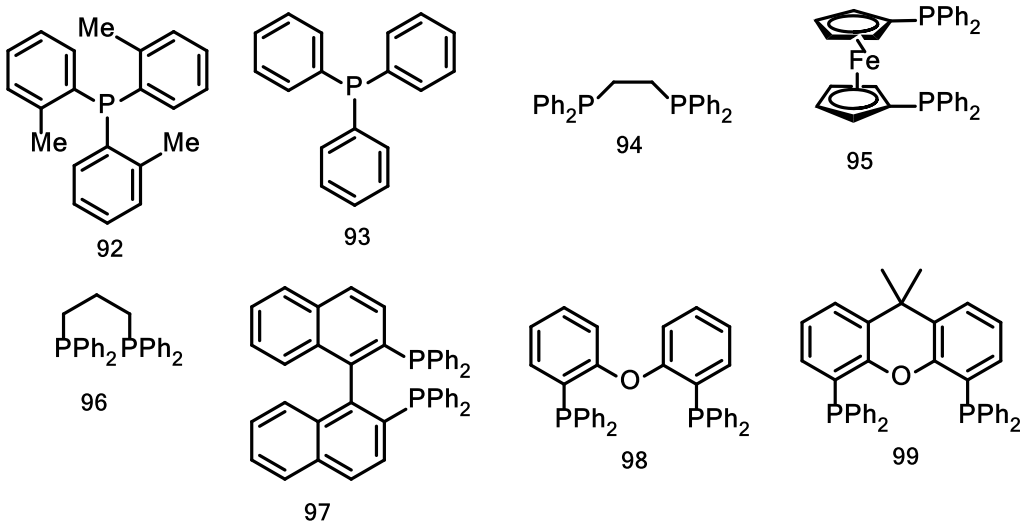

Figure 1.13: Commonly used monodentate (**92**-**93**) and bidentate (**94**–**99**) phosphine-based ligands.

The diphosphine ligands contain bulky electron-donating alkyl and/or aryl substituents that are strategically placed around a rigid to semi-rigid backbone. These features enable the electron-rich second generation ligands to bind more tightly to the metal centre and stabilize the active catalyst species whilst accommodating various conformational preferences that may be sterically crucial in facilitating the oxidative addition of the aryl halide and ligation of the amine nucleophile to the palladium centre. Their steric properties also allow them to superintend the coordination sphere surrounding the active palladium centre, thereby suppressing β-hydride elimination to facilitate reductive elimination and target product formation.

Pre-catalysts are palladium-based complexes or salts that act as primary sources of palladium in most homogeneous catalysis reactions. Whilst most traditional palladium sources are unstable on exposure to aerial oxygen, tris(dibenzylidene)dipalladium(0), Pd_2dba_3, represents the most cost-effective air stable palladium source although more advanced precatalysts are now commercially available on the market.

In most C-N bond forming reactions, prior catalyst activation to generate and release the active Pd^0 species into solution forms a key step that demands a high level of practical expertise. The active palladium species is normally generated via the preliminary reaction of an air stable palladium precursor (Pd_2dba_3 or $Pd(OAc)_2$) with an appropriate phosphine-based supporting ligand (*rac*-BINAP **97** or Xantphos **99**) under inert conditions.

Migita demonstrated the superior performance of P(*o*-tolyl)$_3$ **92** over PPh_3 **93** (Fig. 1.13) as a ligand for supporting the aminostannane-based amination reactions under palladium catalysis.[71] Although both are monophosphine-based ligands, the superior performance achieved using **92** as ligand was attributed to its better electronic and steric properties as compared to **93**.

Having been impressed by the excellent catalytic efficiency of both [Pd(dba)$_2$)P(*o*-tolyl)$_3$)$_2$] and [$PdCl_2$(P(*o*-tolyl)$_3$)$_2$], Guram and Buchwald[72] used a standard amination protocol (Scheme 1.21) to assess the utility of PPh_3 **93**, dppf **95** and dppp **96** as supporting ligands against P(o-tolyl)$_3$ **92** as yardstick.

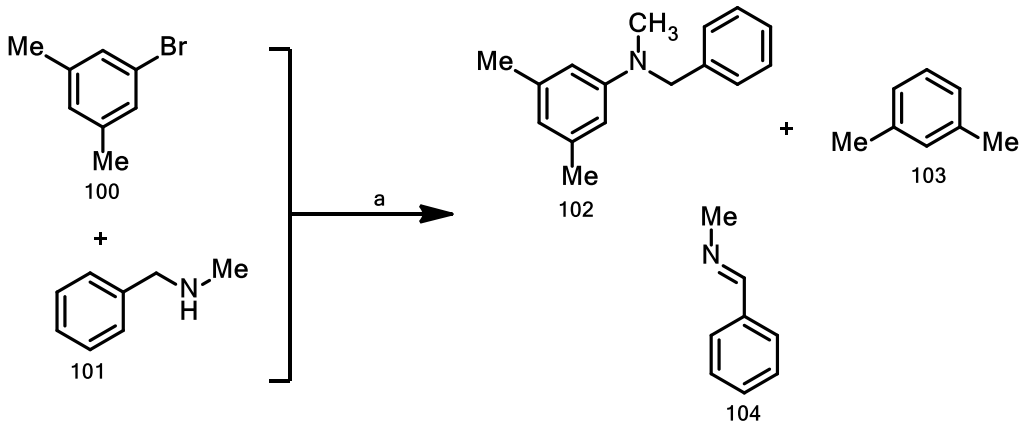

Scheme 1.21: *Reagents and conditions*;(a) cat [Pd(dba)$_2$)P(*o*-tolyl)$_3$)$_2$] or [$PdCl_2$(P(*o*-tolyl)$_3$)$_2$], NaO^{t}Bu, PhMe, 65-100°C.

The amination protocol involved palladium-catalyzed C-N coupling of an aryl halide **100** with a secondary amine nucleophile **101** to generate the target product **102** (Scheme 1.21). Whilst use of ligand **92** gave an excellent yield for target product **102** (84%), a *meta*-xylene side product **103** (10%) was also observed in the reaction mixture. Unfortunately, reactions supported by ligands **93** and **95** proved inefficient as they mainly contained the reduced side product **104** and the unreacted amine **101**, whilst for reaction with ligand **96**, only traces of **102** were observed in a reaction mixture that essentially contained unreacted starting material.

Despite Guram and Buchwald's initial failure at aminating aryl iodides using $PdCl_2$ as a palladium source, Wolfe and Buchwald[74] eventually made a breakthrough after developing a modified protocol (Scheme 1.22) that employed Pd_2dba_3 as a palladium precursor. The amination protocol provided a general route for accessing a variety of aryl amines **79** from functionalized aryl iodides **105** and primary and secondary amines **81**.

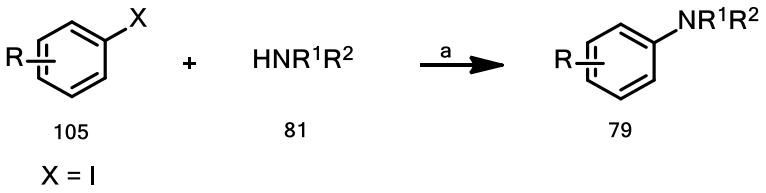

Scheme 1.22: *Reagents and conditions*; (a) cat [$Pd_2(dba)_3$)P(*o*-tolyl)$_3$)], NaO^{t}Bu, 1.4-dioxane/PhMe/THF, 65-100°C.

Contrary to the inefficiencies reportedly associated with use of dppf ligand as earlier reported by Buchwald,[72] Driver and Hartwig[75] developed an optimized protocol (Scheme 1.23) which, unlike before, efficiently utilized the second generation ligand dppf **95** to access aryl amines **79** from aryl iodides **105** and aryl amines **81**. In addition, the protocol was also extended to cross-coupling functionalized aryl bromides using both primary and secondary amines as coupling partners.

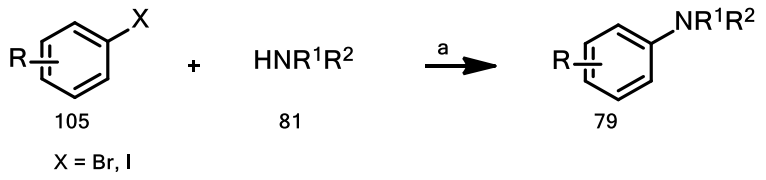

Scheme 1.23: *Reagents and conditions*; (a) cat [$PdCl_2$/dppf], NaO^{t}Bu, THF, 100°C, 3 h.

These achievements are demonstrative of two critical learning points that are paramount towards achieving meaningful cross-coupling reactions. The first point relates to the fact that small changes in reaction conditions (e.g. nature of solvent, temperature) can have a strong influence on the reaction kinetics and equilibrium position. In this regard, by simply replacing PhMe with THF as solvent – the researchers managed to provide a conducive environment for accessing the desired aminated product(s) **79**.

The second observation is that even though efficient aminations had been achieved on aryl bromide substrates using P(o-tolyl)$_3$ **92** as supporting ligand, the product scope was strictly confined to use of secondary amines as coupling partners. Regrettably, use of primary amines encouraged inherent degradation through β-hydride elimination to form the imine (benzylidene) **91** as explained earlier. Contrastingly, use of the second generation ligand dppf **95** achieved much better conversions (80–96% yield) in the presence of both primary and secondary amine substrates, thereby broadening the product scope.

The functional superiority manifested by dppf could be attributed to its better binding affinity (bidentate) which enables it to electronically control and stabilize the palladium coordination sphere in the palladium-amido complex **86** to suppress β-hydride elimination in favor of reductive elimination and target product **87** formation (Fig. 1.11).

The utility of second generation ligands is further augmented by similar research work done by Wolfe and Buchwald[76,77] using BINAP **97** (bidentate ligand, Fig. 1.13) as supporting ligand. As already highlighted above,[72] these investigations, just like the case with Driver and Hartwig,[75] were motivated by the need to explore alternative supporting ligands given the inefficient conversions previously realized when cross-coupling primary amines using **92** as supporting ligand.

In addition, the major problem of β-hydride elimination which facilitated arene side product formation, and also led to low product yields, implied that P(*o*-tolyl)$_3$ **92** supported technology could be of no productive use in the pharmaceutical industry. Thus, the researchers developed an efficient amination protocol that employed Pd_2dba_3 and BINAP **97** (racemic and non-racemic) as catalyst system (Scheme 1.24). Using this protocol, a variety of arylamines **107** were

accessed in high yield (61–98%) by reacting substituted aryl halides **105** with various primary (**106**) and secondary amines.

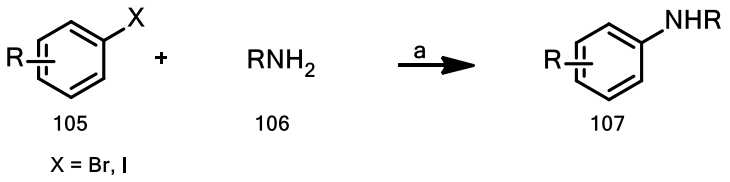

Scheme 1.24: *Reagents and conditions*; (a) cat Pd_2dba_3/BINAP, NaO^tBu, PhMe, 80°C.

In accord with the above observations, Beletskaya[78] also supports the notion that the viability of the Pd-diphosphine complexes in C-N transformations is determined by the ligand's ability to electronically and sterically tune the transition metal coordination sphere to influence reductive amination and product formation. The corollary of this is that monophosphine-based ligands typified by P(*o*-tolyl)$_3$ **92** exert poor electronic control over the relatively acidic palladium-amido transition state complex **86** (Fig. 1.11), leading to β-hydride elimination and arene and imine side product generation – a phenomenon more pronounced with primary amines as coupling partners.

Thus, in our view, whilst monophosphine-based ligands (and their associated cost-advantage) are mainly confined to efficiently support aminations involving electron-rich substrates and more nucleophilic (amine) coupling partners (as evident with the Migita protocol), diphosphine ligands have the capacity to accommodate a wide range of substrates from neutral aryl halides to highly electron deficient heteroaryl halides and amine coupling partners. Despite the development of more evolved phosphine- and nitrogen-based ligand systems dedicated to support Pd-catalyzed C-N bond formations in electron deficient heterocyclic substrates, the latest review article[79] by Ruiz-Castillo and Buchwald shows that monophosphine-based ligand systems still have a big role to play in the construction of target compounds in synthetic organic chemistry.

On the other hand, the attractiveness of second generation ligands as viable support systems in metal-catalyzed carbon-heteroatom bond transformations can also be appreciated by briefly looking at the investigative work done by van Leeuwen and co-workers.[80] After *in silico* docking

and studying Pd-Xantphos complexes, the group concluded that ligand chelational preferences could be ascertained via the magnitude of the ligand's bite angle (β_n).

Kamer[80] defines β_n as 'the preferred chelation angle determined by the ligand backbone only and not by metal valence angles.' They also deduced that ligands possessing large β_n (and hence flexible backbones) could be excellent support systems in metal-catalyzed reactions since they could 'stretch' or reposition in space to facilitate the migration of the metal centre towards the energetically unstable transition state (e.g. Pd-amido complex **86**) (Fig. 1.11).

This could explain why diphosphine ligands like BINAP **97** (β_n = 93˚), dppf **95** (β_n = 99˚), DPEphos **98** (β_n = 104˚) and Xantphos **99** (β_n = 108˚) (Fig. 1.13) efficiently catalyze similar reactions and at best, even complement one another. Thus ligands with small bite angles would be expected to possess rigid backbones whose conformations can affect the reaction path in many ways.

Although other higher order ligands are available on the market, our tentative view is that the second generation ligands will remain a viable and cost-effective option for the targeted synthesis of heterocycles, natural products and pharmaceuticals as highlighted in Ruiz-Castillo and Buchwald's latest review article.[79]

1.6.5.3 N-containing Heterocyclic Substrates

As shown in the previous section, palladium-catalyzed carbon-carbon and carbon-heteroatom coupling reactions play key roles in the total synthesis of natural products, veterinary and pharmaceutical drugs. Nonetheless, extending similar palladium-catalyzed concepts towards C-N cross-coupling of heteroaryl halides is still plagued with several challenges.

Firstly, several research publications tend to primarily focus on metal-catalyzed C-N conversions that employ unhindered and relatively more reactive aryl bromide and iodide substrates with limited coverage of the more electron-deficient aryl chloride systems.

Secondly, unlike the case with most simple and moderately electron-rich aryl halide substrates, there is no general methodology for carrying out the transition-metal catalyzed C-N cross-coupling of heteroaryl halide substrates. As already discussed, the independent development of

more efficient amination protocols by the Buchwald and Hartwig research groups using second generation ligands dppf **95** and *rac*-BINAP **97** (Fig. 1.13), provided the much-needed general routes for aminating aryl bromides with primary amines.[75-77] Unfortunately, extending similar protocols towards cross-coupling heteroaryl halides – especially those bearing a heterocyclic core like the halopyridine nucleus – proved difficult. We will expand on this point later in this section.

Although Buchwald and co-workers[82] demonstrated the general utility of more evolved ligand systems – BrettPhos (1) **108** and RuPhos (2) **109** (Fig. 1.14) – unfortunately, the substrate scope for C-N conversions was primarily limited to monosubstituted aryl and heteroaryl halide substrates. One major drawback associated with the above two ligands and other higher generation ligands available on the market today, is the high cost barrier they impose on research efforts, which logically disqualifies their selection as likely candidates for supporting research in academic institutions and industry. Latest prices from Sigma-Aldrich show that the more evolved ligand systems - Brettphos (1) **108** and RuPhos (2) **109** - are much more expensive than the competitively priced second generation ligands, *rac*-BINAP and Xantphos.

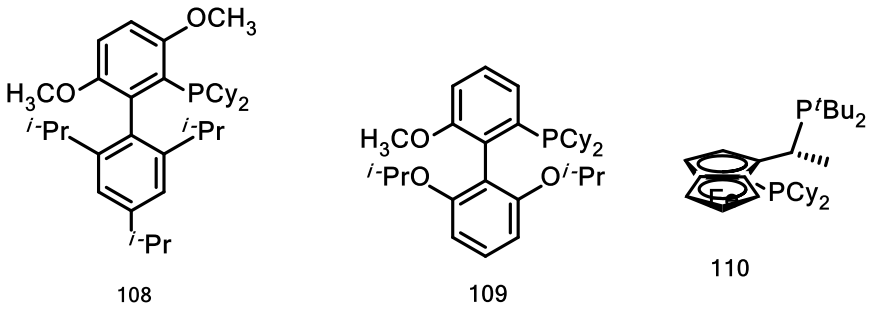

Fig 1.14: BrettPhos **108**, RuPhos **109** and Josiphos **110** ligands

Although commonplace in synthetic organic chemistry literature, neither hindered di-halogenated heteroaryl halides nor sterically hindered amine nucleophiles were considered as potential candidates in the above-mentioned investigations. Why? Our opinion is that various research groups prefer working with unhindered and mono-halogenated heteroaryl halide substrates – especially heteroaryl bromides – whilst the cheaper, sterically hindered, more

electron deficient di-halogenated substrates (like di-chlorinated substrates), which are relatively less reactive, are omitted.

In addition, the selected nucleophile ranges, even though it may be heteroaryl-based in some cases, contain strategically positioned activating groups to enhance reactivity. As such, there exists a huge research gap for pursuing the development of cross-coupling concepts that exploit the readily available and cheaper heteroaryl chloride substrates as they offer unique structural motifs that could be useful in creating novel scaffolds in medicinal chemistry.

Last but not least, the functional group tolerance displayed by most documented C-N amination protocols is relatively narrow as most procedures heavily depend on the use of aggressive reaction conditions that employ high temperatures and strong bases like KO^{t}Bu and NaO^{t}Bu. Such high temperatures and/or strong bases may not be compatible with heteroaryl halide substrates bearing base-sensitive functionalities like enolizable ketones, hydroxyl, primary amide, and ester and carboxylic acid groups. Whilst Hartwig employed a Josiphos-type ligand **110** (Fig. 1.14) to successfully cross-couple functionalized aryl **111** and selected heteroaryl **113** halides[83] (Schemes 1.25a-b) with rugged amine nucleophiles **106** under basic reaction conditions, unfortunately, selected base-stable and unhindered heteroaryl substrates were used in the first set of compounds investigated during that research.

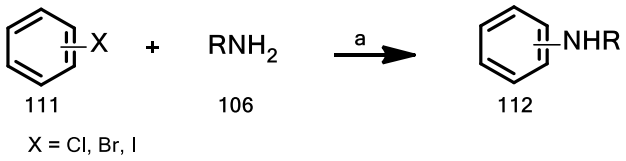

Scheme 1.25a: *Reagents and conditions;* (a) cat. 10ppm-2 mol% $LPdCl_2$ (L = ligand **111**), NaO^{t}Bu, dimethoxyethane (DME), 80-110℃.

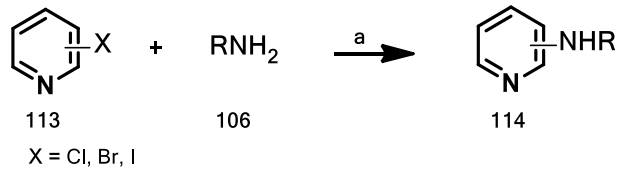

Scheme 1.25b: *Reagents and conditions;* (a) cat. 10ppm-2 mol% $LPdCl_2$ (L = ligand **110**), NaO^{t}Bu, dimethoxyethane (DME), 80-110℃.

Agreeably, the protocol helped in broadening the substrate scope from the usual aryl halides to include pyridyl chlorides and isoquinoline-based halide substrates even though the coupling partners remained restricted to the unhindered primary amine nucleophiles. Nevertheless, what we found interesting was the researchers' ability to extend the same protocol towards aminating functionalized aryl halides **115** with primary alkylamine coupling partners **106** (Scheme 1.26) to give products **116**.

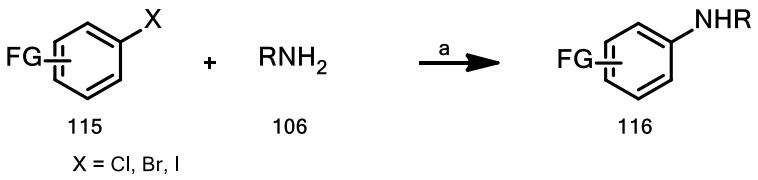

115 106 116

X = Cl, Br, I

FG = COPh, $CONH_2$, $COCH_3$, $CHCH_3OH$, CH_2OH, CO_2H, CO_2Et, phenolic OH, NO_2

Scheme 1.26: *Reagents and conditions*; (a) cat. 0.05–0.5 mol% $LPdCl_2$ (L = **110**), LiHMDS, DME, 100°C

As expected, replacement of the more reactive NaO*t*Bu base with the milder and non-nucleophilic LiHMDS assisted greatly in preserving the base-sensitive functional groups indicated above. Although the protocol was mainly confined to aminating functionalized aryl halide substrates, the change of base evidently broadened the substrate scope for such transformations. What remains to be seen is whether similar protocols could be extended towards aminating highly functionalized and sterically hindered heteroaryl halide substrates which are increasingly becoming key motifs for pharmaceutical leads in synthetic chemistry.

Despite the availability of evolved ligand systems developed by the Buchwald and Hartwig research groups over the years to improve the viability of palladium-catalyzed cross-coupling transformations, most synthetic chemists still prefer using the cheaper PPh_3, $P(o\text{-tolyl})_3$, *rac*-BINAP and Xantphos ligands to support the amination of various aryl and heteroaryl halide substrates.

In addition, synthetic organic chemistry literature contains very few publications that focus on use of palladium-catalyzed cross-coupling protocols as key steps for the regioselective amination of functionalized heteroaryl halides in the synthesis of lead compounds, especially those targeting activity against HIV. On the other hand, numerous research publications are available where conventional protocols involving nucleophilic aromatic substitution reactions are used towards the research and development of NNRTI lead compounds.

In this vein, Buchwald and Castillo's review article[79] on the application of palladium-catalyzed C-N bond forming reactions over the past 20 years shows that such reactions have been aptly customized to mainly service access to kinase inhibitors, anticancer compounds, antiarrhythmic agents, specialized material science products, antagonists and nitrogen-based heterocyclic carbene ligands, to mention a few.

Interestingly, only three publications out of more than five hundred referred to in the manuscript are devoted towards the research and development of compounds that are active against HIV. Of the said three publications, only one article focuses on a regioselective large scale synthesis of a potent NNRTI compound MK-6186 **117** (Scheme 1.27) by Goodyear and co-workers (Merck).[84]

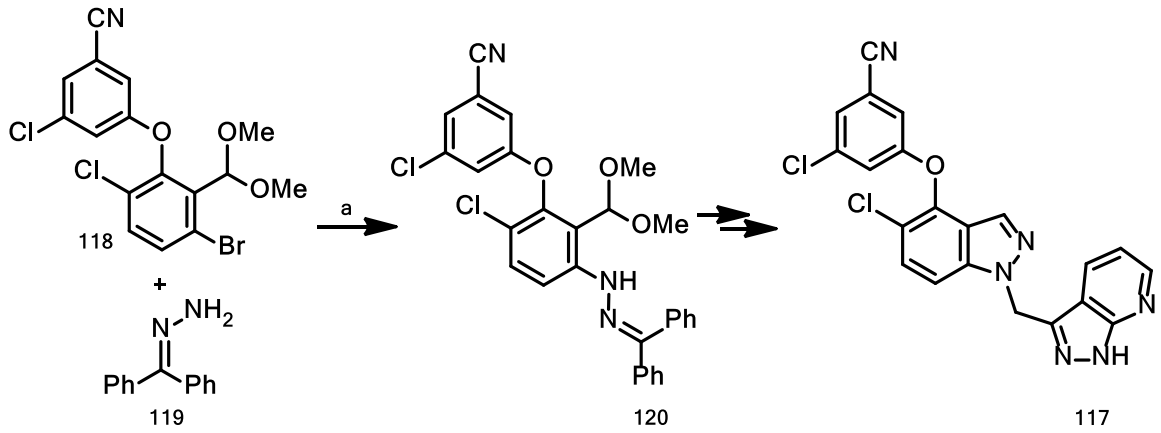

Scheme 1.27: *Reagents and conditions;* (a) cat $PdCl_2(dppf).CH_2Cl_2$, K_3PO_4, PhMe, 90°C, 35%.

The target compound **117**, containing a core indazole ring, was made via a regioselective Pd-catalyzed arylation of benzophenone hydrazone **119** to generate an intermediate **120** which was allowed to undergo a selective N1-alkylation. Further deprotection and subsequent cyclization gave the target compound **117** in better yield (Scheme 1.27) than previously reported.

Although the target product had previously been made using hydrazine hydrate as a nitrogen source, the toxicity associated with the latter as well as the low yield (5%) obtained when using *rac*-BINAP and NaO^{t}Bu base in the coupling step, negatively affected the large scale production of compound **117**. Thus, faced with such challenges, Goodyear and co-workers developed an alternative and scalable Pd-catalyzed regioselective arylation protocol (Scheme 1.27) that used benzophenone hydrazone **119** as the nitrogen source, and replaced *rac*-BINAP with dppf **95**

and NaO^{t}Bu with the much milder K_3PO_4. The overall yield significantly improved from 5% to a scalable 35% over the entire process.

Maes and co-workers[85] also provide another excellent example involving the tandem application of Pd-catalyzed cross-coupling of 2,4-dichloro-5-fluoropyrimidine **121** with selected amine nucleophiles to generate novel DAPY-type NNRTI leads (Scheme 1.28).

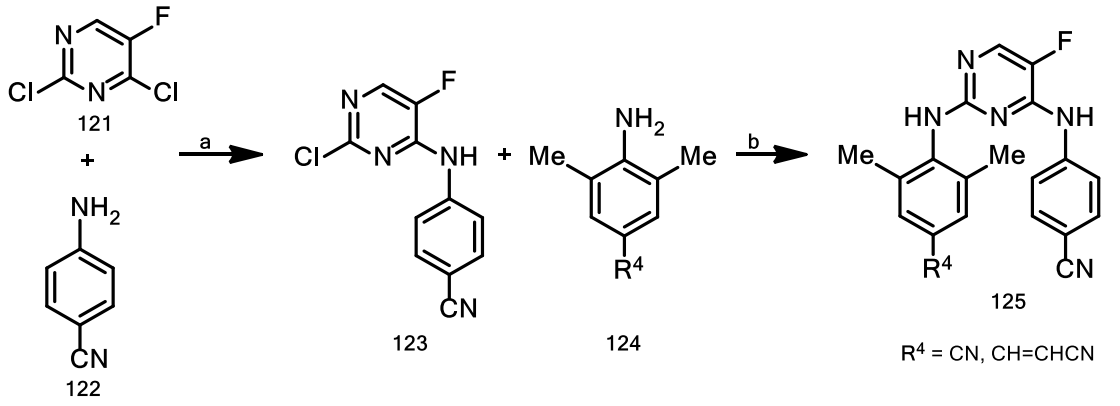

Scheme 1.28: *Reagents and conditions*; (a) Pd_2dba_3, Xantphos, Cs_2CO_3, 1,4-dioxane, 110°C, 16 h; (b) $Pd(OAc)_2$, Xphos, Cs_2CO_3, 1.4-dioxane, 110°C, 16 h.

As a first step, the researchers were able to regioselectively aminate position 4 on the heteroaryl halide core **121** by reaction with **122** to generate the intermediate **123** (Scheme 1.28). Further Pd-catalyzed cross-coupling of **123** with another amine nucleophile **124** using Xphos **126** (Fig. 1.15) as supporting ligand, afforded the desired compounds of general structure **125** (Scheme 1.28) from which NNRTI leads with nanomolar activity against wild type HIV were identified.

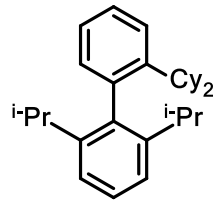

Figure 1.15: Xphos ligand **126**

Although the tandem usage of Pd-catalyzed protocols were mainly confined to cross-coupling base-stable tri-halogenated heteroaryl halide substrates, similar protocols could also be

extended towards investigating the reactions of di-halogenated heteroaryl substrates bearing protic functional groups.

1.7 Molecular Modelling

One of the aspects of computational chemistry (molecular modelling) entails the *in silico* docking of virtual analogues into the binding site of the target protein crystal structure. It uses flexible docking perturbations to ensure the potential analogues (ligands) interact effectively with key side chain amino acids lining the targeted chemical space in the binding site (receptor).

Historically, the utility of molecular modelling in medicinal chemistry has been rather academic since the paradigm underpinning earlier drug design and development strategies were primarily centred on enhancing activity against one genetic species of the HI-1 virus, the wild-type variant. The rapid emergence of clinically relevant mutations, even under HAART, informed researchers that the HI virus was a moving target which could only be managed by continuously developing and providing efficacious antiviral agents that target both the wild type and mutant HIV strains.

Although the first anti-HIV drug, AZT, targeting RT polymerase active site inhibition was first used in 1985 when both the structure and life-cycle of the retrovirus were not fully understood, the opposite is true in the case of NNRTIs. The development of this latter drug class benefitted immensely from advances in technology, particularly X-ray crystallography, which enabled scientists to unveil the retrovirus' unique structural features[27] and also explore the molecular basis surrounding NNRTI binding and drug resistance mechanisms.

As explained earlier in section 1.5.2.2.3, the major clinical significance of NNRTI drug-induced mutations[11,86,87] like L100I, K103N, K101P, E138K, Y181C and G190A is that current HIV treatment regimens will need to be replaced in future. The K103N mutation is also known as a gate-keeper mutation which stabilizes[88] the unbound N103 RT enzyme by 'zipping-up' the non-nucleoside inhibitor binding pocket (Fig. 1.8) via an electrostatic contact with the Y188 phenoxy group. This slows down the rate of inhibitor entry into the pocket and could be one of the reasons why the K103N mutation is the most prevalent mutation across all NNRTI drug classes that are used for HIV treatment.

The Y181C mutation[89] causes loss of π-π aromatic stacking interactions with aryl ring containing inhibitors and contributes towards loss of potency among first generation NNRTIs like

nevirapine **6** and delavirdine **7** (Fig. 1.17). The G190A alkyl side chain mutation also causes steric clashes when bulky inhibitor motifs are bound close enough and is one of the reasons for the loss of potency by HBY097 **127**, (Fig. 1.16) a first generation NNRTI.

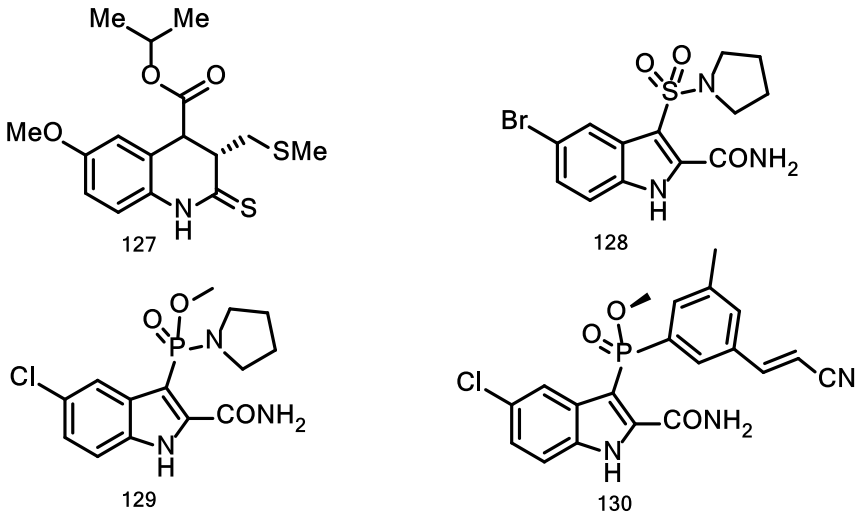

Figure 1.16: HBY 097 **127** and indole-based NNRTIs **128**, **129** and fosdevirine **130**

More importantly, K101P, K101H, K101E and E138K mutations[90] are increasingly becoming evident in etravirine **9** and rilpivirine **10** treatment-experienced patients. K101P has been reported to confer high level resistance on efavirenz and etravirine which are respectively contained in the current Atripla[90] and Comprela[90] NNRTI regimens. Thus, the emerging drug resistance trends, especially against the latest NNRTI drugs, coupled with associated severe side-effects, leave HIV patients with very limited treatment options.

Over the past three decades, molecular modelling has made significant contributions towards anti-HIV drug research and development as highlighted in part by the identification of potent NNRTI leads possessing the indole nucleus[91] like the sulfonamide **128,** phosphoindole **129** and fosdevirine **130** (Fig. 1.16). These NNRTI leads were developed by targeting interactions with K101 as well as optimizing the indole occupation of the hydrophobic cavity flanked by aromatic Tyr181/188 and alkyl Val179 side chains.

In addition, the computer-aided discovery of the latest generation DAPY-based drugs dapivirine **133**, etravirine **9** and rilpivirine **10** by the late Janssen,[8,92] as well as the development of the latest NNRTI clinical candidate doravirine **11** by Merck, (Fig. 1.17) signify the utility of this technology in the NNRTI drug development process.

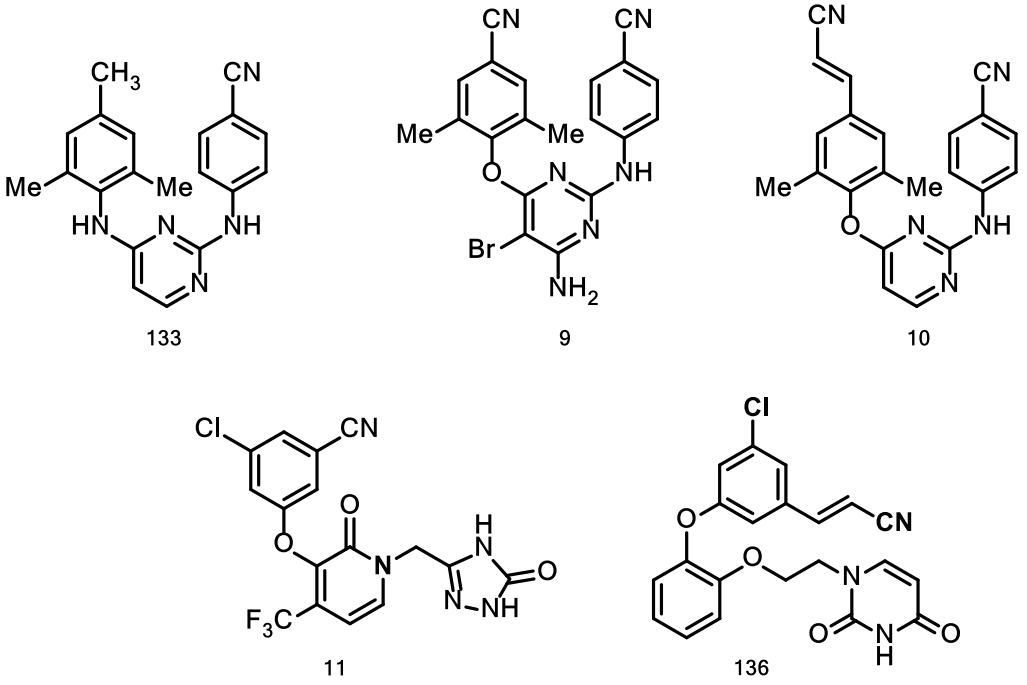

Figure 1.17: DAPY-based NNRTIs dapivirine **133**, etravirine **9** and rilpivirine **10**; fosdevirine **11** and a catechol diether lead compound **136**.

In our view, Jorgensen's[93] development and identification of a potent series of catechol diethers could represent a viable source of the next generation NNRTIs in the not too distant future. These catechol diethers were developed and optimized using Free Energy Perturbations (FEP) which led to the identification of a lead chemotype **136** (Fig. 1.17) that displays picomolar potency against HIV. The major target features being (1) the halogen bond (3.6Å) between the 5-Cl of the cyanovinyl phenyl ring and Cα of Pro95 residue, (2) the electrostatic interactions between the 3-(2-aryloxyethyl) uracil and Lys102/103 and Pro236 residues. We will cover this novel NNRTI class in more detail later.

Today, most lead identification and drug development protocols in both academia and industry incorporate some form of 'due-diligence' routine where a preliminary computational screening is

done to identify potential drug leads before further resources are unnecessarily wasted on trial and error experimentation.

In the following sections, we shall concisely highlight the fundamental concepts underpinning the drug development paradigm in the 21st century with particular emphasis on the utility of computational chemistry as a rational tool for identifying novel drug leads in the NNRTI domain. Two specific examples relating to the development of latest generation DAPY-type NNRTIs etravirine **9** and rilpivirine **10** as well as the unique catechol diether chemotype NNRTI lead **136** will be discussed in detail later.

The current drug design initiatives fall under two categories namely; the ligand-based strategy and the target-based[94] strategy, which will be explained shortly.

1.7.1 Ligand-based and target-based NNRTI drug design strategies

The prevailing computer-assisted 3-D NNRTI drug design initiatives fall under two categories namely; ligand- and target-based approaches. The ligand-based strategy is a traditional approach mostly applied in situations where the 3-D structure of the target protein is unknown. Ligands with known structures are then used to build a pharmacophore[95,96] with favourable molecular fingerprints for filtering and screening potential ligands from virtual databases. The ligands can be purchased or synthesized, assayed and modified as necessary until a suitable potential lead candidate is identified.

On the other hand, the structure-based NNRTI lead identification concept primarily relies on the availability of 3-D structural information[94,97] of the receptor or ligand-receptor complexes. The significant technological advances characterizing the latter part of the 20th century has enabled scientists to obtain detailed and reliable 3-D structures and generate virtual databases for a wide range of proteins and ligand-protein complexes. An exemplary beneficiary of this development has been the field of antiviral research and development targeted at the identification of novel anti-HIV lead candidates.

Caffarena and co-workers[98] reported that more than 100 RT-inhibitor complexes are stored in the virtual Protein Data Bank (PDB). These crystal structures, albeit presenting snapshots of the

underlying topographies on the receptor binding sites, have provided researchers with various insights about binding affinities, key binding groups, favourable binding conformations and more importantly, shed more light on the molecular mechanisms underlying drug resistance. These outcomes have assisted researchers in designing and developing novel drug scaffolds that take cognisance of increasing trends in drug resistance as explained in the following section.

1.7.1.1 Development of etravirine 9 and rilpivirine 10

Although Jorgensen and co-workers[99] have made tremendous inroads towards developing alternative NNRTI lead candidates as will be covered later, Janssen and co-workers pioneered a multidisciplinary approach towards designing, developing and accessing the latest generation of potent NNRTIs (etravirine **9** and rilpivirine **10**, Fig. 1.17) that are currently being used in HIV treatment. In the same vein, our research attempts to extend the same paradigm towards accessing potential NNRTI lead candidates.

Whilst efavirenz, unlike nevirapine and delavirdine, displayed better potency against most single point mutations, its clinical utility remained threatened by the emergence of drug resistant single and multipoint mutations. Nonetheless, as the K103N/Y181C panel emerged into a potent mutation negating the efficacy of first generation NNRTIs - more so - even conferring high level resistance towards the second generation NNRTI, efavirenz, it became mandatory to research for more novel NNRTIs.

Thus, faced with potential long term clinical failure from the current drug regimens, Janssen and co-workers[27] embarked on a rational multidisciplinary project that culminated in the development of potent antiviral compounds namely dapivirine **133**, etravirine **9** and rilpivirine **10** as summarized in Fig. 1.18. These latest generation of highly potent NNRTIs bearing a 'horse-shoe' shaped diaryl pyrimidine (DAPY) pharmacophore were designed and developed by a multidisciplinary team of researchers. From the onset, high throughput screening of Janssen library of compounds gave tivirapine **13** as a potent NNRTI lead.

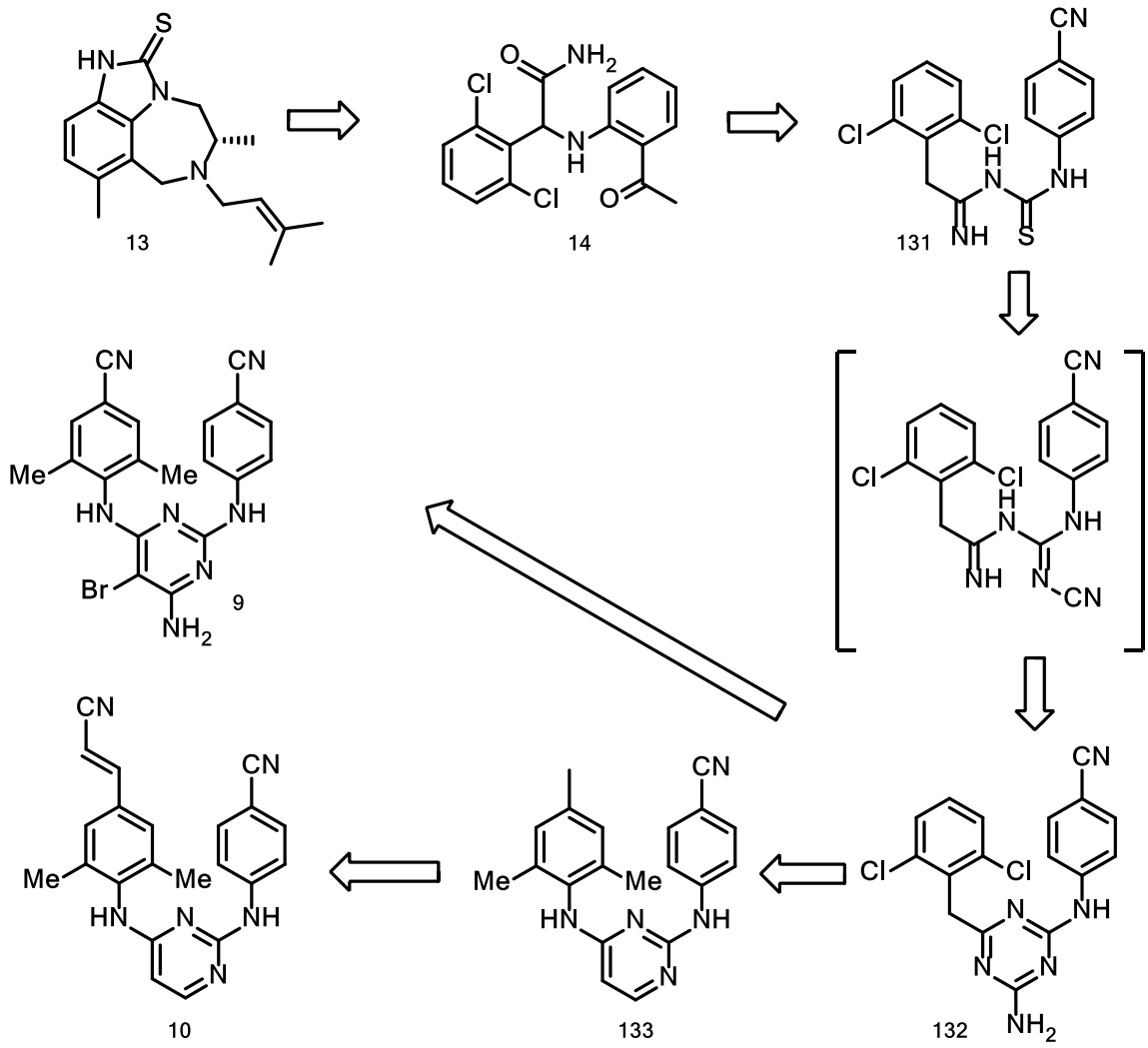

Figure 1.18: Janssen's optimization pathway from TIBO **131** to rilpivirine **10**

Further screening led to the identification of loviride **14**, an α-APA derivative. Using a combination of structural biology, computational and synthetic chemistry compound **14** was rationally modified via **131** to generate a diaryl triazine based derivative **132** (Fig. 1.18). Compound **132** was further modified to generate dapivirine **133**, and the highly potent and latest generation NNRTIs etravirine **9** and rilpivirine **10**, which gained FDA-approval in 2008 and 2011, respectively.

At each stage, the emphasis was on improving the binding conformation, conformational flexibility, ligand-receptor binding interactions as well as creating a refined pharmacophore

possessing enhanced activity against the HIV-1 wild type virus. This lead optimization strategy applied on **13** which resulted in the discovery of rilpivirine **10**, has afforded the medicinal drug research fraternity with a bench mark procedure for designing and developing novel antiviral drug candidates.

1.7.1.2 Catechol diethers as alternative NNRTI drug leads

The development of catechol diethers as alternative NNRTI leads was motivated by the quest for more potent antiviral agents with better solubility and safety profiles[23b] than the latest generation NNRTIs, etravirine and rilpivirine. Given the current drug resistant K103N, Y181C mutants and the newly emerging rilpivirine-induced E138K and K101P mutations, Jorgensen and co-workers modified a docking hit compound **139** to generate a series of potent catechol diethers of structures **135**, **136** and **12** (Fig. 1.19).[100]

Using three docking hits[100] TNK-651 **137**, R221239 **138** and **134** (Fig. 1.19) that had been identified by docking nine compounds in composite RT crystal structures, Jorgensen[100] employed an *in silico*-led modification and various synthetic protocols to access the catechol diethers. Successive *in silico* modification of compound **134** including 'expropriation' of the ubiquitous cyanovinyl motif from rilpivirine **10** led to further identification of more potent analogues **139**, **136** and **135**. Compounds **136** (EC_{50} = 5 nM) and **135** (EC_{50} = 2 nM) were found to be more potent than efavirenz **8** (EC_{50} = 15 nM) and rilpivirine **10** (EC_{50} = 13 nM) against RT wild type enzyme and the K101P mutation.

Although the cyanovinyl group had been incorporated in compounds **139**, **136** and **135** as a privileged motif for enhancing interaction in the hydrophobic cavity surrounded by Trp229, Phe227, Leu234 and Y188, it was eventually replaced on safety grounds. The replacement was motivated by the cyanovinyl functionality's potential liability towards Michael addition reactions with cysteine amino acid residues biological systems. This had led to the prior abandonment of Phase IIb trials for fosdevirine,[101] **11** (Fig. 1.17) another potent NNRTI candidate bearing the cyanovinyl group.

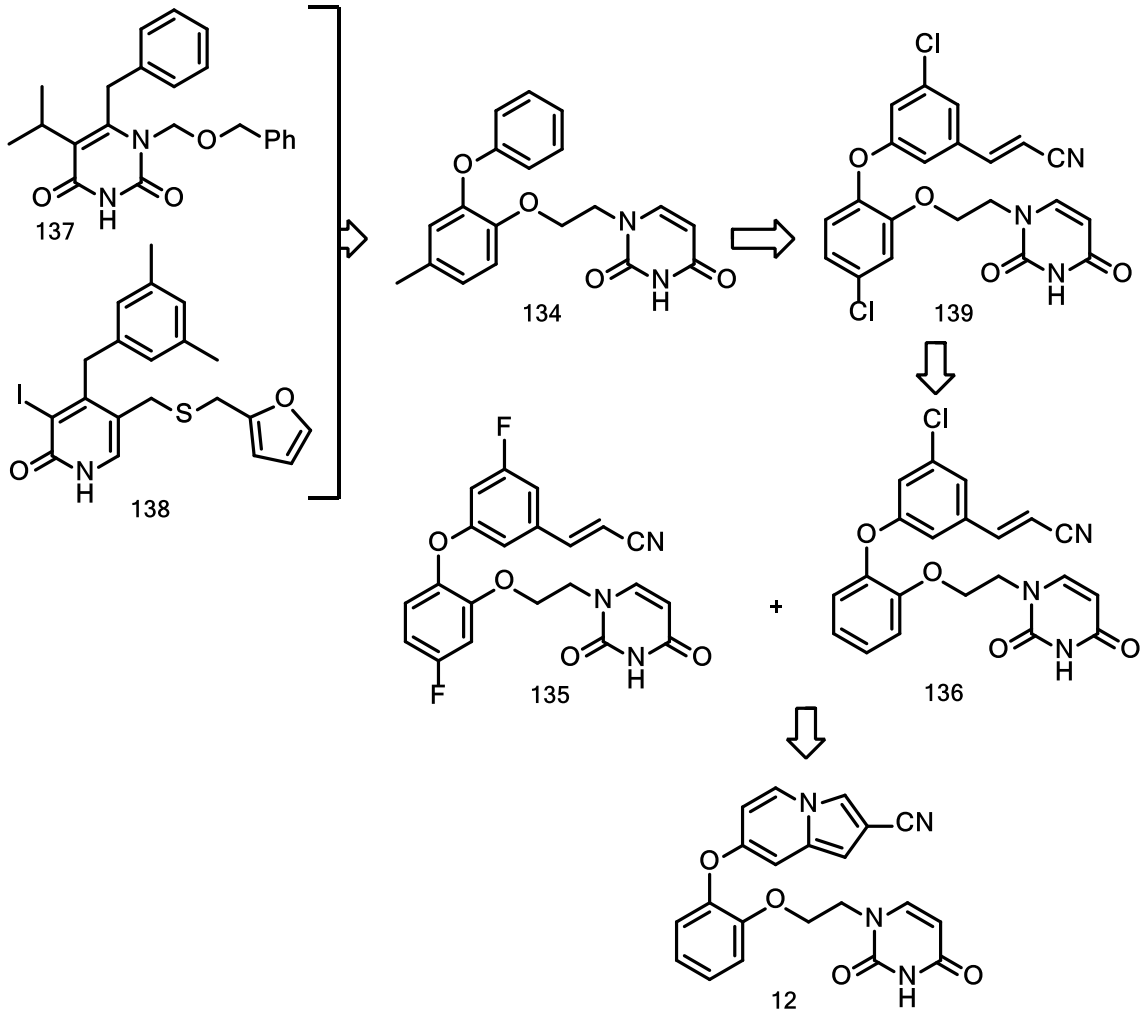

Figure 1.19: Jorgensen's potent catechol diether NNRT inhibitors **135**, **136** and **12**

After obtaining favourable results from *in silico* modelling, the cyanovinyl group was eventually replaced by a bicyclic motif to yield a non-toxic but more potent analogue **12** (Fig. 1.19) possessing superior antiviral activity profiles against wild type RT (EC_{50} = 1 nM), K101P (EC_{50} = 1 nM), K103N (EC_{50} = 1 nM) and Y181C (EC_{50} = 2 nM) and better solubility when compared to efavirenz **8** and rilpivirine **10**.

Analysis of the crystal structures (Fig. 1.20) of efavirenz **8** (A), rilpivirine **10** (B) and **12** (C) bound conformations in the wild type RT enzyme showed that the binding hypothesis of the first two NNRTIs depended on the presence of a salt bridge between K101 and E138 residues. The

salt bridge facilitated the formation of electrostatic contacts between the inhibitors and the K101 side chain. On the other hand, the absence of the salt bridge in the K101P mutant (due to charge repulsion with E138K) prevented any electrostatic interactions between the NNRTIs and K101 side chain which led to poor binding affinities and loss of potency.

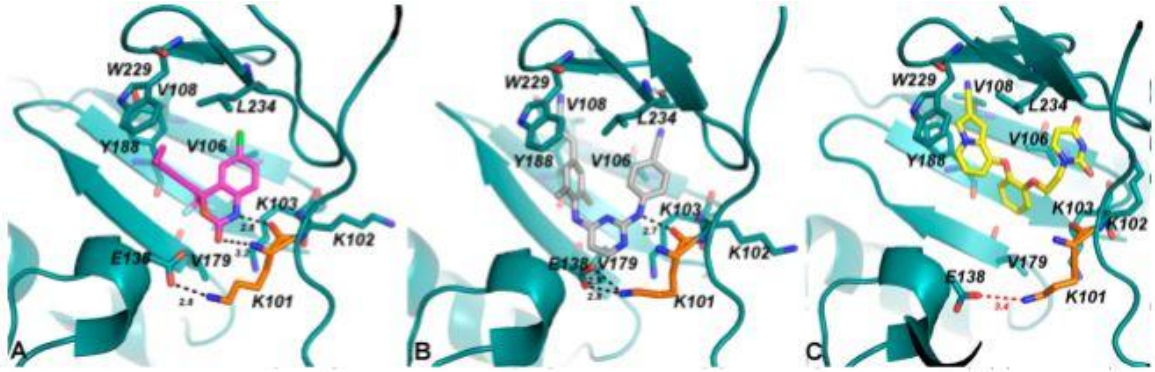

Figure 1.20: Comparison of efavirenz (A)-, rilpivirine (B)- and compound 12 (C)-RT (wt.) complexes[90]

In contrast, the catechol diether **12** maintains the same binding conformation in both wild type and K101P mutation. It is bound deeper in the NNIBP without making use of any electrostatic contacts with K101 side chain to maintain the high potency.

1.8 Research Background

As part of ongoing efforts in our laboratory to identify compounds which could provide potential leads that show activity against HIV, a small library of imidazopyridines[11] was previously generated for a primary screen against HIV RT and *N*-cyclohexyl-2-isopropylimidazo[1,2-*a*]pyridin-3-amine **140** was identified as a potential NNRTI (Fig. 1.21).

140 141

Figure 1.21: Structures of hit compound **140** and lead compound **141**

Using hit compound **140** as a guide, a larger library of analogues was generated and screened against wild type RT. Compound **141** was identified as a lead compound with a whole cell anti-HIV IC_{50} of 0.18 μM which was comparable to that of nevirapine (0.09 μM) in the same assay.

1.8.1 Research aims and objectives

The aim of this project was to design and synthesize novel pyridine, pyrimidine and triazine-based derivatives as potential HIV-1 NNRTIs using two approaches. The first approach involved a rational virtual "ring-opening" of an imidazo[1,2-*a*]pyridine[11] lead compound **141** which identified pyridinyl-benzamide, -benzylamine and –sulfonamide scaffolds as targets for synthesis and testing. The second approach involved an attempt at using molecular modeling in the design and synthesis of torsionally flexible NNRTI analogues resembling the DAPY pharmacophore with bound conformations that could enhance activity against the wild type-and selected RT mutant strains. This was achieved through the following objectives;

1) Our starting point involved the adoption of the scaffold hopping approach, using the virtual ring-opening of the imidazo[1,2-*a*]pyridine compound **141** in the design and synthesis of libraries of pyridinyl-benzamides, -sulfonamides and the torsionally flexible pyridinyl-benzylamines (Fig. 1.22) in order to identify novel scaffolds with possible activity against HIV-1 RT.

2) The second approach tested to identify novel scaffolds with anti-HIV activity using molecular modelling in the design and synthesis of torsionally flexible analogues bearing the DAPY NNRTI pharmacophore and a favourable binding pose which could enhance activity against the wild-type and mutant RT strains using the pyridine, pyrimidine and triazine motifs as central cores (Fig. 1.23).

3) Primary screening of synthesized derivatives against the wild-type virus was used to identify the potentially active NNRTI analogues from both approaches for further mutant screening.

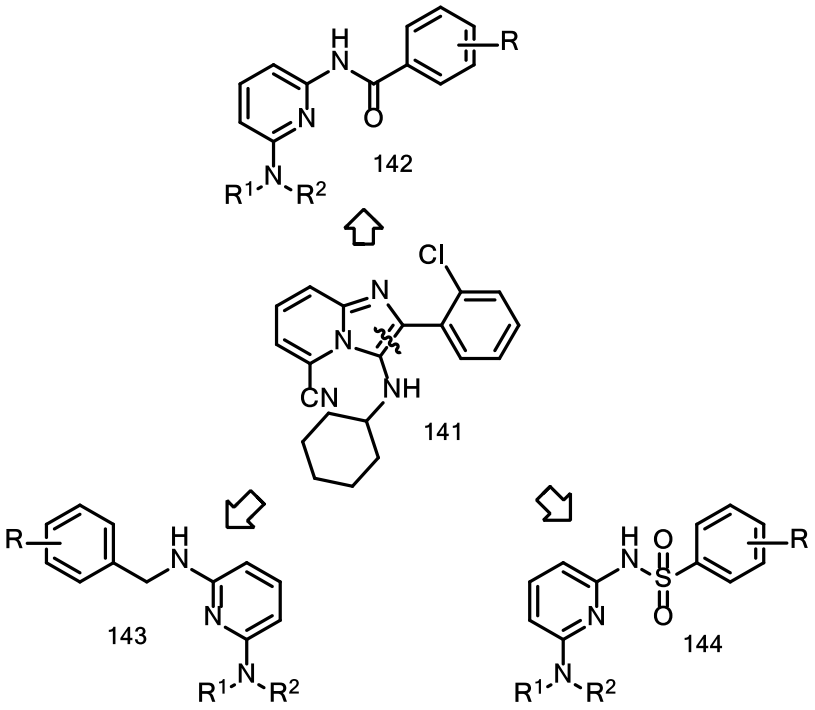

Figure 1.22: Schematic virtual ring-opening of **141** to produce scaffolds **142**, **143** and **144**

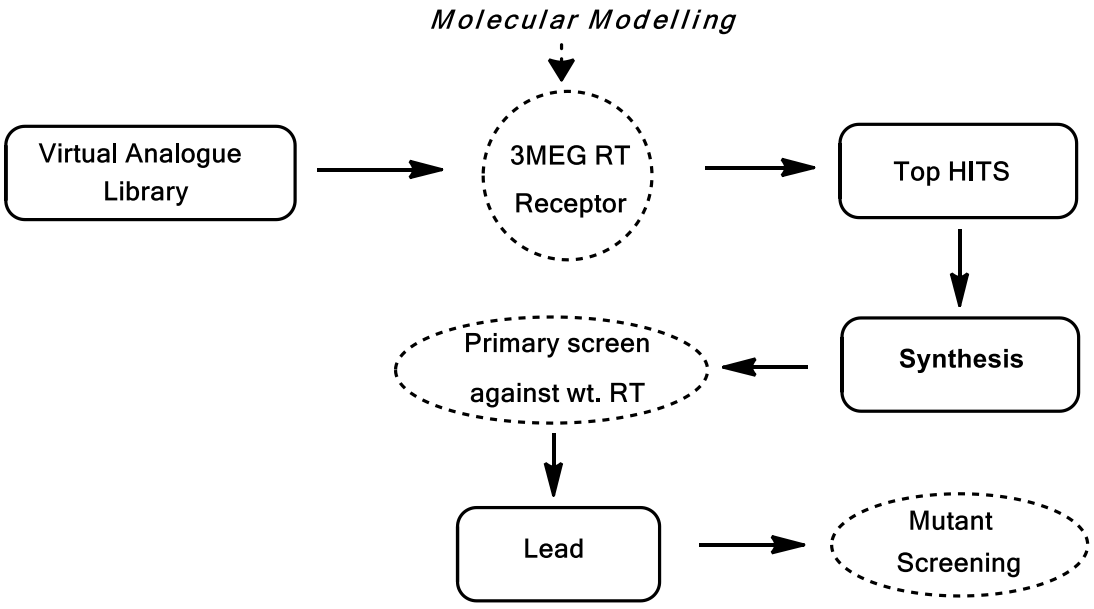

Figure 1.23: Schematic representation of the molecular modelling approach in the development of potential NNRTI leads.

1.9 References

1. Zhan, P.; Chen, X.; Li, D.; Fang, Z.; de Clercq, E. and Liu, X., *Med. Res. Rev*. **2013**, 33 (S1) E1 - E72.
2. Demberg, T. and Robert-Guroff, M., *Front. Immunol.* **2012**, 3, 1 – 16.
3. UNAIDS 2016 Global Report; www.unaids.org/Global_Report_2016_pdf
4. Mislak, A. C.; Frey, K. M.; Bollini, M.; Jogensen, W. L. and Anderson, K. S. *Biochim. Biophys. Acta*, **2014**, 1840, 2203 – 2211.
5. Hassam, M; Basson, A. E.; Liotta, D. C.; Morris, L.; van Otterlo, W. A. L and Pelly, S. C. *ACS Med. Chem. Lett.* **2012**, 3, 470 – 475.
6. Nizami, B; Sydow, D.; Wolber, G. and Honarparvar, B. *Mol. BoiSyst*., **2016**, 12, 3385 – 3395.
7. Das, K. and Arnold, E. *Curr. Opin. Virol*., **2013**, 3, 111 – 118
8. (a) Janssen, P. A.; Lewi, P. J.; Arnold, E.; Daeyaert, F.; de Jonge, M.; Heeres, J.; Koymans, L.; Vinkers, M.; Guillemont, J.; Pasquier, E.; Kukla M.; Ludovici, D.; Andries, K.; de Béthune, M.P.; Pauwels, R.; Das, K.; Clark, A. D. Jr.; Frenkel, Y. V.; Hughes, S. H.; Medaer, B.; De Knaep, F.; Bohets, H.; De Clerck, F.; Lampo, A.; Williams, P. and Stoffels, P. *J. Med. Chem*. **2005**, 48, 1901 – 1909. (b) Wielens, J.; Headey, S. J.; Jeevarajah, D.; Rhodes, D. I.; Deadman, J.; Charmers, D. K.; Scanlon, M. J. and Parker, M.W. *FEBS Letters*, **2010**, 584, 1455 – 1462.
9. Sharaf, G. N., Ishima, R. and Gronenborn, A. M. *Biochem*., **2016**, 55, 3864 – 3873.
10. Chen, L.; Ao, Z.; Jayappa, K. D.; Kobinger, G.; Liu, S.; Wu, G.; Weinberg, M. A. and Yao, X., *Antimicrob. Ag. Chemother.* **2013**, 1 – 27.
11. Bode, M. L.; Gravestock, D.; Moleele, S. S., van der Westhuyzen, C. W.; Pelly, S. C.; Steenkamp, P. A.; Hoppe, H. C.; Khan, T. and Nkabinde, L. A*., Bioorg. Med. Chem.* **2011**, 19, 4227 – 4237.
12. Ren, J.; Milton, J.; Weaver, K. L.; Short, S. A.; Stuart, D. I. and Stammers, D. K., *Structure,* **2000**, 8, 1089 – 1094.
13. Asahchop, E. L.; Wainberg, M. A.; Sloan, R. D. and Tremblay, C. L., *Antimicrob. Ag. Chemother*. **2012**, 56, 5000 – 5008.
14. de Clercq, E., *Antiv. Res.* **2005**, 67, 56 – 75.
15. Tsamis, F.; Gavrilov, S.; Kajumo, F.; Seibert, C.; Kuhmann, S.; Ketas, T.; Trkola, A.; Palani, A.; Clader, J. W.; Tagat, J. R.; McCombie, S.; Baroudy, B.; Moore, J. P.; Sakmar, T. P. and Dragic, T., *J. Virol.* **2003,** 77, 5201 – 5208.
16. Wlodawer, A. and Vondrasek, J. *Ann. Rev. Biophys. Biomol. Struct*. **1998**, 27, 249 – 284.
17. Pauwels, R. *Curr. Opin. Pharmacol.* **2004**, 4, 437 – 446.
18. Reynolds, C.; de Koning, C. B.; Pelly, S. C.; van Otterlo, W. A. L. and Bode, M. L. *Chem. Soc. Rev*. **2012**, 41, 4657 – 4670.

19. Kang, D.; Fang, Z.; Li, Z.; Huang, B.; Zhang, H.; Lu, X.; Xu, H.; Zhou, Z.; Ding, X.; Daelemans, D.; de Clercq, E.; Pannecouque, C.; Zhan, P. and Liu, X. *J. Med. Chem*. **2016**, 59, 7991 – 8007.

20. Tian, X.; Qin, B.; Wu, Z.; Wang, X.; Lu, H.; M-Natschke, S. L.; Chen, C. H.; Jiang, S.; Lee, K-H. and Xie, L. *J. Med. Chem*. **2010**, 53, 8287 – 8297.

21. Gu, S-H.; Qiao, H.; Zhu, Y-Y.; Shu, Q-C.; Liu, H.; Ju, X-H.; De Clercq.; Balzarini, J. and Pannecouque, C. *Bioorg. Med. Chem*. **2015**, 23, 6587 – 6593.

22. Xu, H-T.; Oliveira, M.; Asahchop, E. L.; McCallum, M.; Quashie, P. K.; Han, Y.; Quan, Y. and Wainberg, M. *J. Virol*. **2012**, 86, 12983 – 12990.

23. (a) Das, K.; Lewi, P. J.; Hughes, S. H. and Arnold, E. *Biophys. Mol. Biol*. **2005**, 88, 209 – 231.; (b) Lee, W.-G.; Chan, A. H.; Spasov, K. A.; Anderson, K. S. and Jorgensen, W. L. *ACS Med. Chem. Lett*. **2016**, 7, 1156 – 1160.

24. Hsiou, Y.; Ding, J.; Das, K.; Clark Jr, A. D.; Boyer, P. L.; Lewi, P.; Janssen, P. A. J.; Kleim, J.-P.; Rosner, M.; Hughes, S. H. and Arnold, E. *J. Mol. Biol.* **2001**, 309, 437 – 445.

25. (a) Kohlstaedt, L. A.; Wang, J.; Friedman, J. M.; Rice, P. A. and Steitz, T. A. *Science*, **1992**, 256, 1783 – 1790; (b) Ren, J.; Esnouf, R.; Garman, E.; Somers, D. and Ross, C. *Nat. Struct, Biol*. **1995**, 2, 293 – 302; (c) Esnouf, R. M.; Ren, J.; Hopkins, A. L.; Ross, C. K. and Jones, E. Y. *Proc. Natl. Acad. Sci. U.S.A* **1997**, 94, 3984 – 3989; (d) Lindberg, J.; Sigurdsson, S.; Lowgren, S.; Andersson, H. O. and Sahlberg, C. *Eur. J. Biochem*. **2002**, 269, 1670 – 1677; (e) Hsiou, Y.; Das, K.; Ding, J.; Clark, A. D., Jr. and Kleim J. P. *J. Mol. Biol*. **1998**, 284, 313 – 323.

26. Sarafinos, S. G.; Das, K.; Tantillo, C.; Clark, A. D., Jr. and Ding, J. *EMBO J*. **2001**, 20, 1449 – 1461.

27. Das, K.; Clark, A, D., Jr.; Lewi, P. J.; Heeres, J.; de Jonge, M. R.; Koymans, L. M. H.; Vinkers, H. M.; Daeyaert, F.; Ludovici, D. W.; Kukla, M. J.; de Corte, B.; Kavash, R. W.; Ho, C. H.; Ye, H.; Lichstenstein, M. A.; Andries, K.; Pawels, R.; de Bethune, M.-P.; Boyer, P. L.; Clark, P. Hughes, S. H.; Janssen, P. A. J. and Arnold, E. *J. Med. Chem*. **2004**, 47, 2550 – 2560.

28. Ding, J.; Das, K.; Moereels, H.; Koymanns, L.; Andries, K.; Janssen, P. A.; Hughes, S. H. and Arnold, E. *Nat. Struct. Biol*. **1995**, 2, 407 – 415.

29. de Clercq, E., *Antiv. Res.* **2005**, 67, 56 – 75.

30. Liu, Z.; Chen, W.; Zhan, P.; De Clercq, E.; Pannecouque, C. and Liu, X. *Eur. J. Med. Chem*. **2014**, 87, 52 – 62.

31. Wainberg, M. A., *Scientifica*, **2012**, Article ID 238278, http://dx.doi.org/10.6064/2012/238278-

32. Shair, M.D.; Yoon, T.-Y.; Mosny, K. K.; Chou, T. C. and Danishefsky, S. J. *J. Am. Chem. Soc*. **1996**, 118, 9509 – 9525.

33. Tietze, L. F.; Nobel, T. and Spescha, M. *J. Am. Chem. Soc*. **1998**, 120, 8971 – 8977.
34. Hu, C. H.; Qiao, J. X.; Han, Y.; Wang, T.; Rehfuss, R.; Wexler, R. R. and Lam, P. Y. S. *Bioorg. Med. Chem. Lett*. **2014**, 24, 2481- 2485.
35. Kotha, S.; Lahiri, K. and Kishnath, D. *Tetrahedron*, **2002**, 58, 9633 – 9695.
36. Zhou, Q.-L. *Angew. Chem. Int. Ed*. **2016**, 55, 5352 – 5353.
37. Wolfe, J. P. and Buchwald, S. L. *J. Org. Chem*. 2000, 65, 1144 – 1157.
38. Mamane *et. al*, *Min. Rev. Org. Chem.*, **2008**, 5, 303 – 312.
39. (a) Chen, X.; Ke, H. and Zou, G. *ACS Catal*. **2014**, 4, 379−385; (b) E. B. Corcoran *et al*., Science 10.1126/science.aag0209 (2016).
40. Kang, D.; Kim, J.; Oh, S. and Lee, P. H. *Org. Lett*. **2012**, 14, 5636–5639.
41. Siemsen, P.; Livingston, R. C. and Diederich, F. *Angew. Chem. Int. Ed*. **2000**, 39, 2632 – 2657.
42. Sperotto, E.; van Klink, G. P. M.; van Koten, G. and de Vries, J. G. *Dalton Trans*. **2010**, 39, 10338 – 10351; (b) Ma, D.; Cai, Q. and Zhang, H. *Org. Lett*. **2003**, 5 (14), 2453 – 2455; (c) Ullmann, F., *Ber. Dtsch. Chem. Ges*., **1903**, 36, 2382 – 2384.
43. Beletskaya, I. P. and Chaprakov, A. V., *Coord. Chem. Rev*. **2004**, 248, 2337 – 2364.
44. Hartwig, J. P. *Acc. Chem. Res*., **2008**, 41, 1 – 11.
45. (a) Kwong, F. Y. and Buchwald, S. L. *Org. Lett*. **2003**, 5, 793 – 796; (b) Bolliger, J. L. and Frech, C. M. *Tetrahedron*, **2009**, 65, 1180 – 1187.
46. (a) Lindley J. *Tetrahedron*, **1984**, 40, 1433 – 1456; (b) Hassan, J., Sevignon, M.; Gozzi, C.; Schulz, E. and Lennaire, M.; *Chem. Rev*.; **2002**; 102, 1359 – 1470.
47. Paul, F.; Patt, J. and Hartwig, J. F. *J. Am. Chem. Soc*. **1994**, 116, 5969 – 5970.
48. (a) Ma, D. and Xia, C. *Org. Lett*. **2001**, 3, 2583 – 2586; (b) Job, G. and Buchwald, S. L. *Org. Lett*. **2002**, 4, 3703 – 3706.
49. (a) Goodbrand, H. B. and Hu, N. X. *J. Org. Chem*. **1999**, 64, 670; (b) Klapars, A.; Antilla, J. C.; Huang, X. H. and Buchwald, S. L. *Tetrahedron*, 2001, 123, 7727.
50. Ma, D.; Qian, C. and Zhang, H. *Org. Lett*. **2003**, 5, 2453 – 2455.
51. Klapars, A.; Huang, X. and Buchwald, S. L. *J. Am. Chem. Soc*. **2002**, 124, 7421 – 7428.
52. Kwong, F. Y. and Buchwald, S. L.; *Org. Lett.*, **2003**, 5, 793 – 796.
53. Enguehard, C.; Allouchi, H.; Gueiffer, A. and Buchwald, S. L. *J. Org. Chem*. **2003**, 68, 4367 – 4370.
54. Gujadhur, R. K.; Bates, C. G. and Venkataraman, D. *Org. Lett*. **2001**, 3, 4315.
55. Cottington, I. E. *Platinum Metal Rev*. **1991**, 35, 141 – 151.
56. Jira, R. *Angew. Chem. Ind. Ed*. **2009**, 48, 9034 – 9037.
57. Smidt, J. and Hafner, W. *Angew. Chem*. **1959**, 71, 284 – 284.
58. Tsuji, J. *Pure Appl. Chem*. **1999**, 71, 1539 – 1547.

59. (a) Kondratenko, N. V.; Kolomeitsev, A. A.; Mogilevskaya, V. O.; Varlamova, N. M. and Yagupol'skii L. M. *Zh. Org. Khim*. **1986**, 22, 1721 -1729; (b) Seechurn, J. C. C. C.; Kitching, M. O.; Colacot, T. J. and Snieckus, V. *Angew. Chem. Int. Ed.* **2012**, 51, 5062 – 5085.

60. Nicolaou, K. C.; Bulger, P. G. and Sarlar, D. *Angew. Chem. Int. Ed*. **2005**, 4447 – 4489.

61. Dieck, H. A. and Heck, R. F. *J. Am. Chem. Soc*. **1974**, 96, 1133 – 1136.

62. Mizoroki, T. Mori, K. and Ozaki, A. *Bull. Chem. Soc. Jpn*. **1973**, 46, 1505 – 1508.

63. Rawal, V. H., Michound, C. and Monestel, R. F. *J. Am. Chem. Soc*. **1993**, 115, 3030 – 3031.

64. Palacios, M. L. D. and Comdom, R. F. P. *Synth. Commun.* **2003**, 33, 1771-1771.

65. King, A. O.; Corley, E. G.; Anderson, .; Larsen, R. D.; Verhoeven, T. R.; Reider, P. J.; Xiang, Y. B.; Belley, M.; Leblanc, Y.; Labelle, M.; Prasit, P. and Zamboni R. J. *J. Org. Chem*. **1993**, 58, 3731 – 3735.

66. Rossi, R.; Carpita, A. and Quirici, M. G. *Tetrahedron* **1981**, 37, 2617 – 2673.

67. Suh, E. M. and Kishi, Y. *J. Am. Chem. Soc*. **1994**, 116, 11205 – 11206.

68. E. Negishi, E. and Anastasia, L. *Chem. Rev*. **2003**, 103, 1979 – 2017.

69. Nicolaou, K. C. and Webber, S. E. *J. Am. Chem. Soc.* **1984**, 106, 5734 – 5736.

70. Cooke, J. W. B.; Bright, R.; Coleman, M. J. and Jenkins, K. P. *Org. Process Res. Dev.* **2001**, 5, 383 – 386.

71. Kosugi, M.; Kameyama, M. and Migita, T. *Org. Lett*. **1983**, 927 – 928.

72. Guram, A. S., Rennels, R. A. and Buchwald, S. L. *Angew, Chem. Int. Ed. Engl*. **1995**, 34, 1348 – 1350.

73. Louie, J. and Hartwig, J. F. *Tetrahedron Letters*, **1995**, 36, 3609 – 3612.

74. Wolfe, J. P. and Buchwald, S. L. *J. Org. Chem*. **1996**, 61, 1133 – 1135.

75. (a) Driver, M. S. and Hartwig, J. F. *J. Am. Chem. Soc*. **1996**, 118, 7217 – 7218; (b) Driver, M. S. and Hartwig, J. F. *J. Am. Chem. Soc*. **1995**, 117, 4708 - 4709.

76. Wolfe, J. P.; Wagaw, S. and Buchwald, S. L. *J. Am. Chem. Soc*. **1996**, 118, 7215 – 7216.

77. Wolfe, J. P. and Buchwald, S. L. *J. Org. Chem.* **2000**, 65, 1144 - 1157.

78. Beletskaya, I. P. and Chaprakov, A. V., *Organometallics*, **2012**, 31, 7753 – 7808.

79. Ruiz-Castillo, P. and Buchwald, S. L. *Chem. Rev.* **2016**, 116, 12564 – 12649.

80. Kamer, P. C. J.; van Leeuwen, P. W. N. M. and Reek, J. N. H. *Acc. Chem. Res*. **2001**, 34, 895 – 904.

81. Klingesmith, L. M.; Strieter, E. R.; Barder, T. E. and Buchwald, S. L. *Organometallics*, **2006**, 25, 82 – 91.

82. Maiti, D.; Fors, B. P.; Henderson, J. L.; Nakamura, Y. and Buchwald, S. L. *Chem Sci*. **2011**, 2, 57 – 68.

83. (a) Shen, Q; Ogata, T. and Hartwig, J. F. *J. Am. Chem. Soc.* **2008**, 130, 6586 – 6596; (b) Shen, Q. and Hartwig, J. F. *Org. Lett*. **2008**, 130, 6586 – 6596; (c) Hartwig, J. F. *Acc. Chem.*

Res. **2008**, 41, 1534 – 1544; (d) Shen, Q; Shekhar, S.; Stambuli, J. P. and Hartwig, J. F. *Ang. Chem. Int. Ed.* **2005**, 44, 1371 – 1375.

84. Goodyear, A.; Linghu, X.; Stewart, J. W.; Xu, Y. and Yin J. *Org. Process Res. Dev*. **2012**, 16, 605 – 611.
85. Sergyev, S; Yadav, A. K.; Franck, P.; Michiels, J.; Lewi, P.; Velde, C. M. L. V.; Winter, H. D. and Maes, B. U. W. *J. Med. Chem.* **2016**, 59, 1854 – 1868.
86. Ji, J. and Loeb, L. A. *Biochemistry*, **1992**, 31, 954 – 958.
87. Das, K.; Sarafinos, S. G.; Clark, A. D.-Jnr.; Boyer, P. L.; Hughes, S. H. and Arnold, E. *J. Mol. Biol.* **2007**, 365, 77 – 89.
88. Ren, J. and Stammers, D. K. *Virus Research*, **2008**, 134, 157 – 170.
89. Greitmann, M.; Unge, T. and Danielson, U. H. *J. Med. Chem*. **2006**, 49, 2375- 2387.
90. Gray, W. T.; Frey, K. M.; Laskey, S. B.; Mislak, A. C.; Spasov, K. A.; Lee, W.-G.; Bollini, M.; Siliciano, R. F.; Jorgensen, W. L. and Anderson, K. S. *ACS Med. Chem. Lett*. **2015**, 6, 1075 -1079.
91. Hassam, M.; Basson, A. E.; Liotta, D. C.; Morris, L.; van Otterlo, W. A. L. and Pelly, S. C. *ACS Med. Chem. Lett*. **2012**, 3, 470 – 475.
92. Li, D.; Zhan, P.; de Clercq, E. and Liu, X. *J. Med. Chem*. **2012**, 55, 3595 – 3613.
93. Frey, K. M.; Puleo, D. E.; Spasov, K. A.; Bollini, Jorgensen, W. L. and Anderson, K. S. *J. Med. Chem.* **2015**, 58, 2737 - 2745.
94. Sliwoski, G.; Kothiwale, S.; Meiler, J. and Lowe, E. W-Jnr. *Pharmacol. Rev*. **2014**, 66, 334 – 395.
95. Ekins, S.; Mestres, J. and Testa, B. *Brit. J. Pharmacol*. **2007**, 152, 21 – 37.
96. Mo, M.; Rivara, S.; Lodola, A.; Lorenzi, S.; Bordi, F.; Plazzi, Vi. P.; Spadoni, G.; Bedini, A.; Deranti, A.; Tontini, A. and Tarzia, G. *Chem. Biodivers.* **2005**, 2, 1438 – 1450.
97. (a) Kubinyi, H. *DDT* **1997**, 2, 457 – 467; (b) Klebe, G. *DDT* **2006**, 11, 580 – 594.
98. Santos, L. H.; Ferreira, R. F. and Caffarena, E. R. *Mem. I. Ostwaldo Cruz* **2015**, 110, 847 – 864.
99. Jorgensen, W. L. *Acc. Chem. Res*. **2009**, 17, 724 – 733.
100. Bollini, M.; Domaoal, R. A.; Thakur, V. V.; Gallardo-Macias, R.; Spasov, K. A.; Anderson, K. S. and Jorgensen, W. L . *J. Med. Chem*. **2011**, 54, 8582 – 8591.
101. Gray, W. T.; Frey, K. M.; Laskey, S. B.; Mislak, A. C.; Spasov, K. A.; Lee, W.-G.; Bollini, M.; Siliciano, R. F.; Jorgensen, W. L. and Anderson, K. S. *ACS Med. Chem. Lett.* **2016**, 7, 1075 – 1079.

CHAPTER TWO – VIRTUAL RING OPENING APPROACH

2.0 Introduction

This chapter covers our first approach to developing novel NNRTIs. Scaffold hopping is a well-known drug design and development concept which relies on the structural modification of lead compounds to generate analogues that possess better pharmacokinetic profiles. Zhan defines scaffold hopping as the "dismantlement or simplification" of the pharmacophore of a lead compound to "produce alternative scaffolds with improved efficiency and unexpected side effects."[1]

Using the same approach, the central imidazopyridine core of a previously identified imidazo[1,2-*a*]pyridine[2] lead compound **141** was virtually disconnected or "ring-opened'' as indicated in Fig. 2.1 to generate 2,6-disubstuted pyridine derivatives. These pyridines were attached to the chloro-substituted aromatic ring by means of an amido-, amino- or sulfonamide linkage, giving rise to the pyridyl-benzamide **142**, pyridyl-benzylamine **143** and pyridyl-sulfonamide **144** scaffolds, respectively. The rationale behind designing such compounds was to create a more flexible set of novel analogues that could possess better binding affinity and more potent anti-HIV activity than their progenitor, compound **141** (Fig. 2.1). We thought it necessary to prepare compounds possessing good hydrogen bond accepting (**142** and **144**) or hydrogen bond donating (**143**) capacity to facilitate such interactions in the RT allosteric site.

At this juncture it also becomes noteworthy to point out that the concept of increased conformational flexibility needs to be pursued cautiously to maintain an optimal balance between the merits that could be derived from both improved torsional freedom as well as reduced restricted rotation. More specifically, the downside could be that sacrificing restricted rotation in favour of increasing torsional freedom may give the ligand too much entropic energy (free rotation) which could offset the intended benefits of improving ligand binding affinity as the ligand might fail to 'lock' itself in position within the enzyme's binding site.

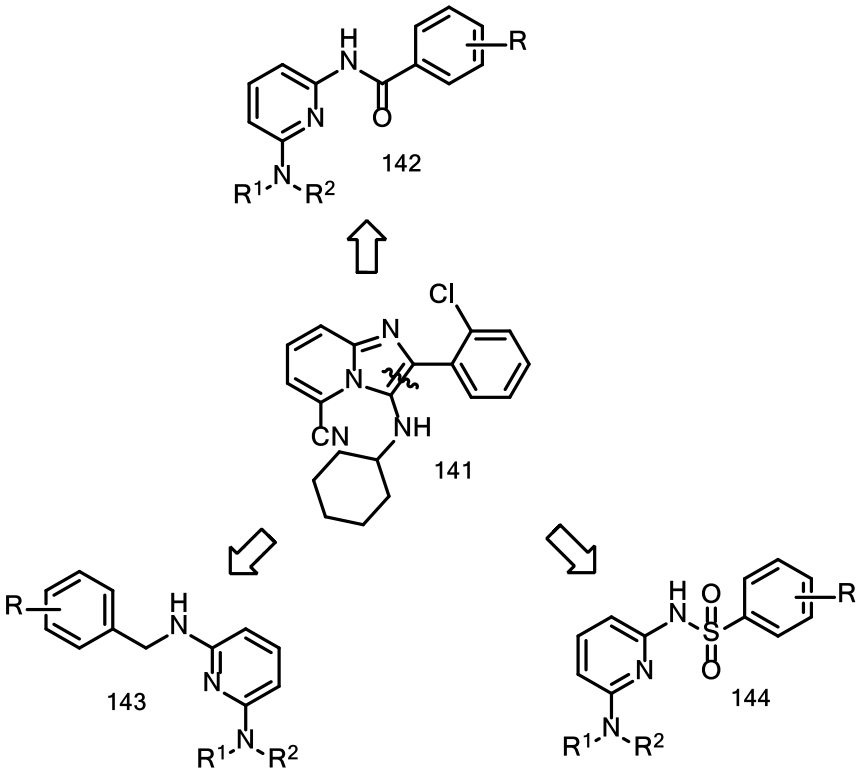

Figure 2.1: Virtual ring-opening of the imidazopyridine **141** to generate; (a) Pyridyl-benzamide **142**; (b) Pyridyl-benzylamine **143** and (c) Pyridyl-sulfonamide **144** scaffolds.

The pyridyl-benzylamine scaffold **143**, in addition to providing hydrogen bond donor capacity, was selected as a comparatively more flexible derivative or "reduced form" of the amide-bearing pyridyl-benzamide **142**. As explained above, the expectation was that such a framework could provide access to compounds possessing superior conformational freedom and a better binding hypothesis in the RT allosteric site. The downside being that increased torsional freedom may cause too much rotation which could lead to loss of binding affinity as the target molecule fails to firmly 'lock' itself in the binding site of the receptor.

Lastly, given the inherent biological activities associated with sulfonamide-containing compounds in synthetic chemistry, replacement of the amide link in scaffold **142** with the hydrogen bond accepting sulfonamide bridge appeared an attractive proposition for targeting another series of analogues that could be based on the pyridyl-sulfonamide framework **144** (Fig. 2.1).

2.1 Synthesis of pyridyl-benzamides

A retrosynthetic analysis of **142** indicated that such a compound could be constructed from commercially available 2-amino-6-bromopyridine **145** and an aromatic carboxylic acid **146** via intermediate **147** (Scheme 2.1).

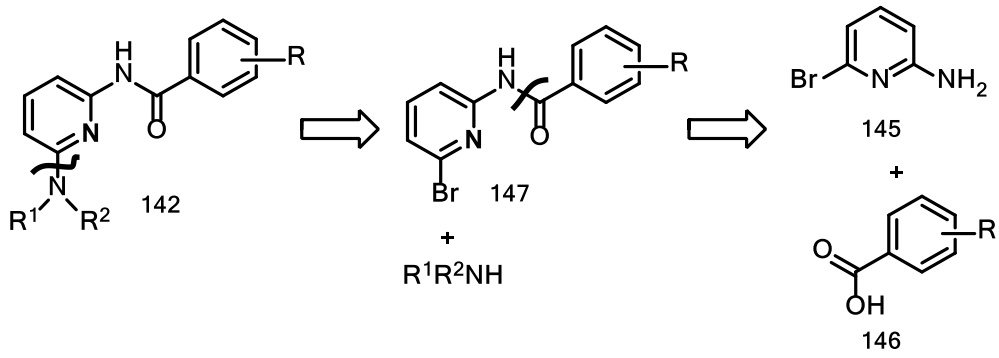

Scheme 2.1: Retrosynthetic analysis of pyridyl-benzamide target **142**

2.1.1 Synthesis of intermediate compound 147

In order to access scaffold **147**, the practicality of two approaches was assessed as possible conduits for activating the carboxylic acid substrate **146** in preparation for amination with the di-substituted amine **145** to form scaffold **147** (Scheme 2.1). The two approaches included the use of carbonyldiimidazole (CDI) or thionyl chloride in the reaction, as explained in the following sections.

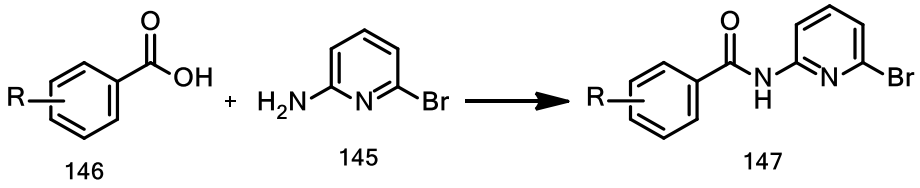

Scheme 2.2: Proposed synthetic route to intermediate scaffold **147**.

2.1.1.1 Carbonyldiimidazole route

Carbonyldiimidazole is used extensively in protein synthesis[3] for activating aliphatic carboxylic acid groups in preparation for amination with selected amino acids during the preparation of peptides and peptoids. In this research, an attempt was made to extend the utility of CDI by using it to activate aromatic carboxylic acid substrates **146** as a key step towards amide bond formation and access to target scaffold **147**.

During the initial routine, CDI **148** was reacted with 2-chlorobenzoic acid **146a** to generate an electrophilic imidazolide intermediate **149** for subsequent amination with amine **145** to afford target **147a** (Scheme 2.3).

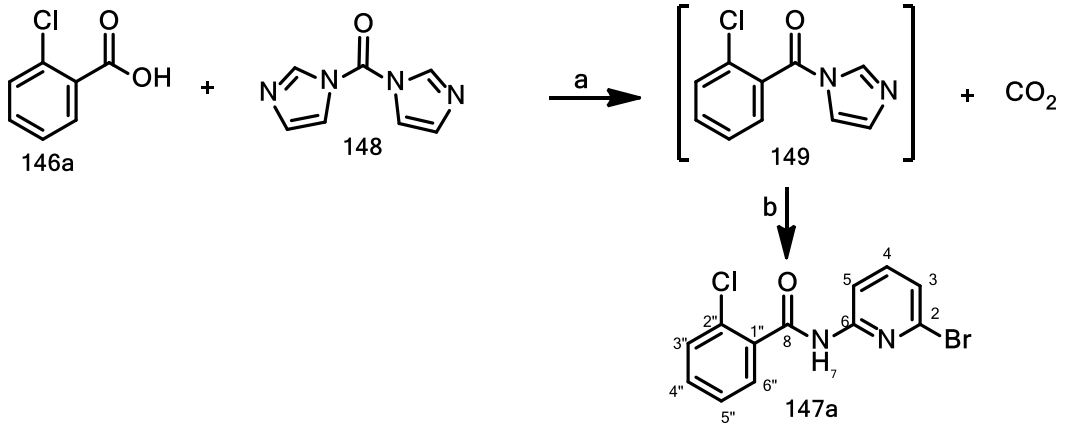

Scheme 2.3*: Reagents and conditions*; (a) 1.4-dioxane or THF, RT, 20 min; (b) amine **145**.

The coupling activation reaction was done at room temperature with step-wise addition of CDI as a precautionary measure for managing the rapid evolution of CO_2 gas as the formation of the imidazolide intermediate **149** occurred. Reaction progress was monitored visually (TLC) with the organic acid **146a** being consumed within 20 minutes as evidenced by its depletion and corresponding enlargement of the target imidazolide **149** spot.

Thereafter, attempts to initiate the required amination reaction, under room temperature conditions, proved ineffective as the unreacted amine **145** and imidazole intermediate **149** were observed by TLC 20 h after mixing the reactants.

Furthermore, attempts to catalyze the amination reaction via addition of acetic acid (3 equiv.) and prolonged stirring of the reaction mixture at room temperature, unfortunately, appeared to favour the hydrolysis and depletion of the intermediate **149** as TLC showed the presence of 2-chlorobenzoic acid **146a** in the reaction mixture.

However, the first breakthrough in the amination reaction was achieved when Montmorillonite K-10 clay was added to the reaction mixture followed by conventional heating at 80°C. ^{1}H NMR spectroscopic data showed that novel compound **147a** contained seven aromatic protons and an amide proton H-7 that gave a deshielded broad singlet signal at 8.58 ppm. Pyridyl protons H-3, H-4 and H-5 appeared as a doublet at 7.27 ppm (d, J = 7.5 Hz, partly obscured by the $CDCl_3$ solvent signal), followed by a triplet 7.63 ppm (d, J = 8.0 Hz) and another doublet at 8.34 ppm (d, J = 8.2 Hz), respectively. HMBC showed strong heteronuclear coupling between the amide

proton at 8.58 ppm and the C-5 signal at 112.64 ppm, which also confirmed the position of the H-5 signal at 8.34 ppm as being more deshielded than the H-3 signal at 7.27 ppm. This trend was also consistently observed in other pyridyl-benzamide substrates **147b-f**. For **147a**, COSY analysis also showed that H-3 coupled with H-4 to form a doublet, whilst H-4 coupled to both H-3 and H-5 to give a triplet signal. Chlorophenyl proton H-3" showed a multiplet in the region 7.74–7.64 ppm, whilst H-4"–H-6" overlapped and gave another multiplet in the range 7.54–7.50 ppm. The IR spectrum also confirmed the presence of an amide NH stretch at 3177 cm^{-1}, a carbonyl C=O stretch at 1683 cm^{-1} as well as the pyridinyl nucleus C=N stretch at 1564 cm^{-1}.

^{13}C NMR spectroscopy showed eleven carbon signals in the aromatic region and one carbonyl carbon signal at 164.8 ppm. DEPT analysis showed seven CH signals, four quaternary carbon signals in the aromatic region and one carbonyl signal. As expected, the amide carbonyl at 164.8 ppm confirmed the absence of the carboxylic acid C (≥ 168 ppm) whilst the NMR 2-D spectra also confirmed the identity of the different proton and carbon environments. HRMS data showed ($[M+H]^+$: 310.9576) corresponding to the expected molecular weight of the compound containing ^{79}Br and ^{35}Cl isotopes.

Given that the target compound **147a** was obtained in low yield (11%) during the first attempt, efforts were then made to optimize the synthetic methodology. Increasing the reaction temperature from 80 - 100℃, fortunately, doubled the yield of the target compound from 11% to 25%. Unfortunately, further increasing the reaction temperature to 120℃ only slightly improved the yield by an insignificant 4%.

As a result of the poor yields achieved under conventional heating, an attempt was made to alternatively facilitate the amination reaction via microwave irradiation. Disappointingly, low yields (10–15%) were obtained after heating the reaction mixture via intermittent 10 min ramping cycles from 100-150℃ at 150W.

2.1.1.2 Thionyl chloride route

Thionyl chloride was explored as an alternative reagent for activating carboxyl groups due to its high reactivity as well as versatility towards activating carboxyl functionalities in aliphatic and aromatic-based substrates.

Refluxing 2-chlorobenzoic acid **146a** with thionyl chloride resulted in the quantitative formation of a highly reactive acyl halide intermediate **150** (Scheme 2.4).

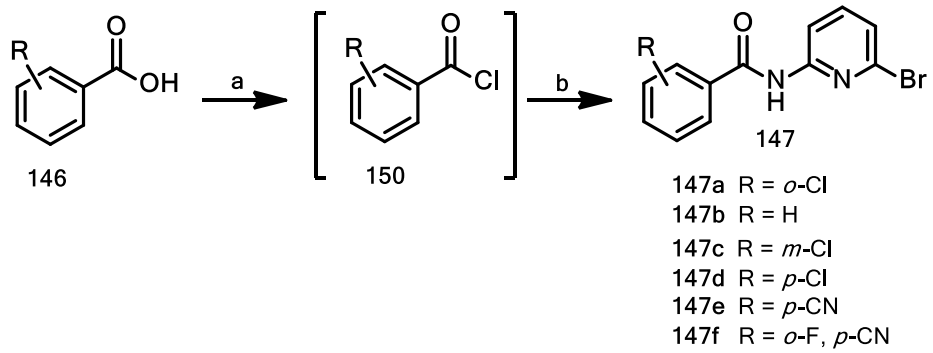

Scheme 2.4: *Reagents and conditions*: (a) $SOCl_2$, 80°C, 24 h; (b) i) **145**, PhMe, pyridine, 10% aq. NaOH, RT, 2 h; or ii) **145**, CH_3CN, pyridine, 5°C-RT, 4 h.

Thereafter, the efficiencies of two amination approaches were assessed as suitable reaction paths for accessing target scaffold **147**. The first option, based on the Schotten-Bauman concept, involved reacting the acyl halide **150** and amine **145** in a biphasic mixture containing toluene and 10% aqueous sodium hydroxide under the conditions shown in Scheme 4 (b) i). Fortunately, the target product **147a** was obtained in modest yield (55%) as compared to the CDI route (29%). Unfortunately, a similar attempt to improve the product yield by using DCM as solvent was ineffective.

As such, the second approach, which involved reacting the acid chloride **150** with amine **145** in acetonitrile, under sub-ambient conditions (5°C), using pyridine as an acyl transfer catalyst, was tested. Pleasingly, the target scaffold was afforded in excellent yield (86%). Correspondingly, the identity of compound **147a** was verified using NMR and IR spectroscopy and HRMS characterization techniques.

The high product yield achieved using the second approach could be attributed to the exclusion of water in the reaction mixture during the amination process. On the contrary, the poorer yield (55%) obtained in the first approach (Schotten-Bauman) may have been largely influenced by the miscibility and premature transfer of the pyridine 'catalyst' into the aqueous phase. This phenomenon may have negatively affected the optimal formation of the highly electrophilic acyl pyridinium reactive intermediate pending nucleophilic attack by the amine **145**, thus suppressing formation of target product **147a**.

Thus, the development of an efficient methodology for accessing scaffold **147a** enabled us to successfully extend the methodology to other target pyridyl-benzamide scaffolds **147b-f** in excellent yields that ranged from 92–98% (Fig 2.2).

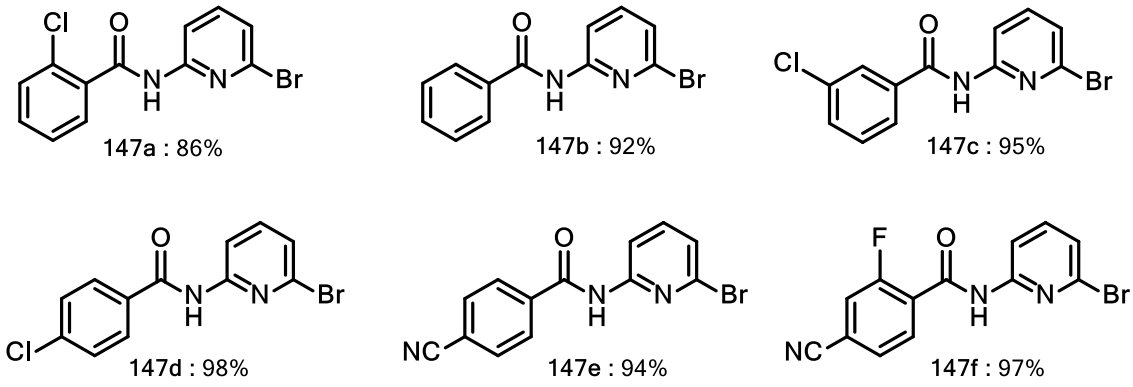

Figure 2.2: Target pyridyl-benzamide scaffolds **147a-f** accessed via the thionyl chloride route.

The ^{1}H NMR spectral data showed that whilst the amide protons for compounds **147a-e** were observed in the region 8.55–8.61 ppm, the amide proton for 2-fluoro-4-cyano substituted compound **147f** was the most deshielded at 9.00 ppm and appeared as a doublet (J = 12.2 Hz) possibly due to coupling with fluorine.

Similarly, the ^{13}C NMR spectra for compounds **147a-e** were superimposable whilst that for compound **147f** showed seven C-F couplings that are attributable to fluorine coupling 6 aryl carbon atoms plus the neighbouring amide carbon atom. Furthermore, the carbon atom carrying fluorine appeared slightly more deshielded at 160.620 ppm (d, $J_{C\text{-}F}$ = 250 Hz) than the amide carbon atom at 159.617 ppm which appeared as a doublet (d, $J_{C\text{-}F}$ = 3 Hz).

2.1.2 Synthesis of novel target compounds 142

Having successfully synthesized the required series of pyridyl-benzamide scaffolds **147a-f** in excellent yield (Fig. 2.2), our next objective was to develop synthetic methodologies for cross-coupling the scaffolds with selected primary and secondary amine nucleophiles. To this end, copper-based and palladium-mediated protocols were independently assessed as possible routes for accessing the desired aminated targets of general structure **142** (Scheme 2.5).

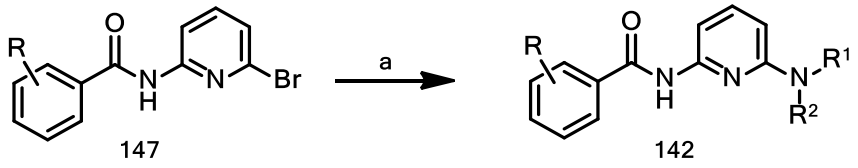

Scheme 2.5: *Reagents and conditions*; (a) amine, Cu or Pd catalysis.

2.1.2.1 Copper-mediated catalysis

Over the past one and a half centuries, Ullman copper-based catalysis has sluggishly emerged as a complementary synthetic concept, behind palladium, for cross-coupling aryl and heterocyclic halide substrates with amine nucleophiles.[4] Today, modified Ullman protocols employ a plethora of ligand systems that have transformed the utility of copper-mediated technologies into versatile cross-coupling agents that closely match the practicality realized using palladium-based catalysts.

In this vein, Enguehard and Buchwald employed a copper-based C-N bond-forming protocol, that used ethylene glycol as ligand, to successfully cross-couple a substituted imidazo[1,2-*a*]pyridine halide substrate with selected primary and secondary amine nucleophiles.[5]

Thus, we based our first attempt at cross-coupling scaffold **147a** with primary amine nucleophiles on the reaction conditions described by Enguehard and Buchwald.[4] These conditions employed a cuprous salt [CuI] as catalyst precursor and ethylene glycol as a supporting ligand to facilitate the displacement of iodine from a 6-iodo-imidazo[1,2-*a*]pyridine substrate with various amine nucleophiles in the presence of K_3PO_4 as base. Our objective was to extend the copper-based protocol towards displacing bromine from the pyridyl-benzamide scaffold **147a** with primary amine nucleophiles (cyclohexylamine, benzylamine and aniline) to access the aminated novel target compounds **142a-c** (Scheme 2. 6).

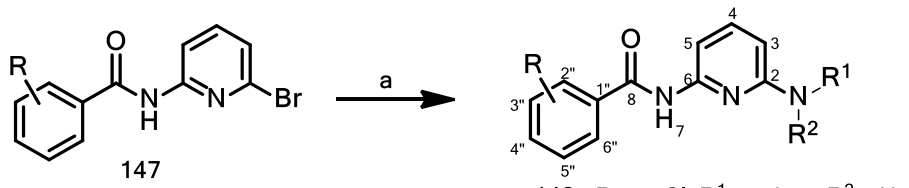

142a R = *o*-Cl, R^1 = *c*-hex, R^2 = H
142b R = *o*-Cl, R^1 = Ch_2Ph, R^2 = H
142c R = *o*-Cl, R^1 = Ph, R^2 = H

Scheme 2.6: *Reagents and conditions*; (a) CuI, $HO(CH_2)_2OH$, 1.4-dioxane, R^1R^2NH, K_3PO_4, N_2 atm., 120°C, 24 h

Fortunately, copper-catalyzed cross-coupling of cyclohexylamine with pyridyl-benzamide scaffold **147a** gave the target product **142a** in excellent yield (79%) using conventional heating

at temperatures ranging from 120–130℃. On the other hand, attempting similar cross-coupling reactions in the absence of CuI proved ineffective.

^{1}H NMR spectroscopic analysis showed a total of twenty protons in novel target **142a**, comprised of seven aromatic, eleven aliphatic protons and two NH protons. Amide proton H-7 gave a downfield broad singlet at 8.27 ppm whilst the amino proton appeared upfield as a doublet (d, J = 6.9 Hz) at 4.35 ppm. Pyridyl H-3 and H-5 showed doublet signals at 7.56 ppm (d, J = 7.7 Hz) and 6.15 ppm (d, J = 8.1 Hz), respectively, whereas H-4 overlapped with H-4”–H-6” to give a multiplet in the region 7.51–7.29 ppm (4H). H-3” was observed as a doublet of doublets at 7.66 ppm (dd, J = 7.4, 1.9 Hz) with the cyclohexyl proton signals appearing as multiplets in the regions 3.60–3.33 ppm (1H), 2.18–1.92 ppm (m, 2H) 1.81–1.56 (3H) and 1.45–0.78 ppm (5H).

The ^{13}C NMR spectrum showed the presence of eleven signals in the aromatic region and one carbonyl signal at 164.5 ppm, as well as four carbon signals belonging to the cyclohexyl motif in the aliphatic region. DEPT analysis showed seven CH signals and four quaternary aromatic carbon signals, one carbonyl signal as well as one CH and three CH_2 signals in the aliphatic region. Furthermore, the aminated quaternary carbon C-2 appeared more deshielded at 149.5 ppm as compared to that of substrate **147a** (C-Br) at 140.7 ppm. HRMS ($[M+H]^+$: 330.1374) analysis also confirmed the disappearance of Br isotopes as a result of successful copper-catalyzed amination.

Excited by the above achievement, copper-catalysis was extended to cross-couple benzylamine with the heteroaryl substrate **147a**. Unfortunately, a poor yield (25%) of the target product **142b** was obtained. ^{13}C NMR spectroscopic analysis confirmed a similar deshielding pattern (149.5 ppm) of the aminated quaternary carbon C-2 relative to the starting material, whilst HRMS data ([M+H]+: 338.064) confirmed the displacement of the bromine. IR spectral analysis showed increased intensity for the C=C stretch at 1432 cm^{-1}, confirming the presence of the extra phenyl ring. Interestingly, in the ^{1}H NMR spectrum, the benzylamine NH proton (H-7) appeared as a triplet at 4.76 ppm (t, J = 5.8 Hz) due to coupling with the benzylic protons (CH_2), which were also observed as a doublet at 4.45 ppm (d, J = 5.8 Hz).

Copper-catalyzed amination of **147a** with aniline gave target product **142c** in modest yield (43%). Interestingly, the respective amide proton H-7 was highly deshielded at 9.30 ppm whilst the amino proton appeared at 8.56 ppm in the ^{1}H NMR spectrum. The observed downfield resonance by the amino proton could be attributed to the better deshielding effect exerted by the closely situated anilino phenyl ring as compared to the benzylamine analogue where the phenyl ring is separated from the amino proton by a methylene bridge (CH_2). In addition, the ^{13}C NMR spectrum also showed that the amide carbon signal (C-8) was relatively more downfield (167.7 ppm) as compared to that in analogues **142a** and **142b** (164.5 ppm).

Disappointingly, attempts to extend the copper-mediated amination towards coupling scaffold **147a** with secondary amines – morpholine, piperidine and imidazole – proved ineffectual (Scheme 2.7).

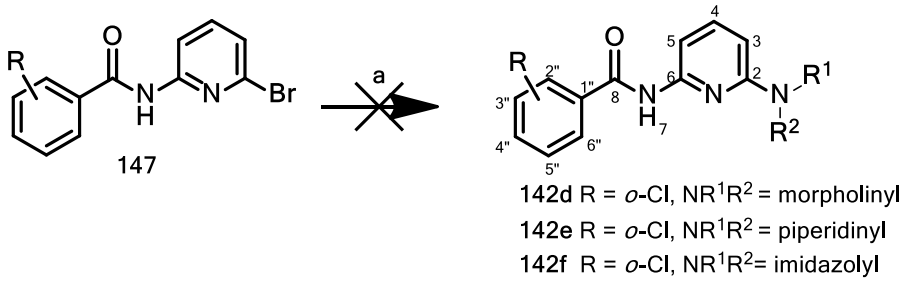

Scheme 2.7: *Reagents and conditions*; (a) CuI, $HO(CH_2)_2OH$, 1.4-dioxane, secondary amine, K_3PO_4, N_2 atm.,120℃, h.

Efforts made to optimize such reactions via prolonged heating of reaction mixtures at temperatures ranging from 120–130℃ were equally ineffective. Similarly, a three-fold increase in catalyst loadings from 5 mol% to 15 mol% also failed to facilitate the desired conversions. The change of base from K_3PO_4 to KO^{t}Bu or K_2CO_3 also failed to provide access to the target products. Regrettably, several attempts to optimize the amination reactions via change of solvent from toluene to DMF or THF proved unsuccessful, as 90% of the starting material was recovered from the reaction mixtures. No conversions were realized when aminations were attempted without copper-mediation.

The excellent yield of 79% obtained for target product **142a** under copper mediated cross-coupling of **147a** with cyclohexylamine is consistent with the analysis made by Beletskaya who observed that copper-catalyzed systems were less influenced by the degree of NH nucleophilicity but were *adversely* affected by the steric bulk of the nucleophile.[6] In line with the excellent yield obtained for **142a**, logic dictates that favourable yields could be obtained when C-N coupling is carried out using unhindered NH nucleophiles as bulky nucleophiles could be excluded from accessing the coordination sphere of the copper-based catalytic species. Similarly, the modest yield of 43% obtained for novel product **142c** also portrays aniline as a poor nucleophile in copper-based C-N bond forming reactions. As such, the lack of C-N conversion observed when the more nucleophilic secondary amines (morpholine, piperidine and imidazole) were used as coupling partners evidently shows that the steric bulk of the NH nucleophile has a tremendous impact on the viability of copper-based amination reactions.

The failure to cross-couple secondary amines could also be attributed to the fact that copper-based catalysis, unlike palladium, does not have a well-developed general C-N bond forming methodology which could be extended successfully towards cross-coupling different heteroaryl halide substrates with a variety of nucleophiles. More so, the dearth of a generalized copper-based technology in today's organic chemistry literature could be related to the highly complex copper chemistry which makes it difficult for researchers to avail a clear mechanistic understanding[6,7] that elucidates the role of copper in the catalytic system.

Thus, as long as the mechanistic detail remains elusive, it shall always be challenging for researchers to identify versatile ligand systems that can be generally employed to "tune" the catalytic copper species and fully exploit the efficiencies associated with such technologies.

Given the complementary nature of copper- and palladium-catalyzed reactions, a palladium-based system was tested as an alternative C-N bond forming protocol.

2.1.2.2 Palladium-mediated cross-coupling

Although palladium is comparatively pricier than copper, the attractiveness associated with palladium-based C-N bond-forming technologies primarily emanate from their proven practicality and general cost-effectiveness as independently documented by the Buchwald,[8] Hartwig,[9] Leeuwen,[10] and Beletskaya[11] research groups.

As already explained in Chapter 1, the Pd_2dba_3/*rac*-BINAP system represents one of the most viable and cost-effective protocols that were developed to articulate challenges associated with unfavourable β-hydride elimination and arene side product formation. Such challenges had become endemic in palladium-catalyzed amination protocols of the early 1980s which were traditionally supported by the first generation ligand tris(*ortho*-toluene)phosphine [P(*o*-tolyl)$_3$], as pioneered by Migita and co-workers.[12,13]

In this research, the Pd_2dba_3/*rac*-BINAP catalyst system was employed as a general methodology to initially cross-couple cyclohexylamine, benzylamine and aniline with the pyridyl-benzamide substrate **147a** using reaction conditions described by Enguehard and Buchwald.[5] Their reaction conditions employed Pd_2dba_3 as a palladium precursor with *rac*-BINAP as supporting ligand for cross-coupling a 6-iodoimidazo[1,2-*a*]pyridine with various primary and secondary amine nucleophiles in the presence of NaO^{t}Bu base. Our synthetic protocols employed 1,4-dioxane as solvent and KO^{t}Bu as base since these reagents were readily available in our laboratory (Scheme 2.8) as an attempt to access target products **142a-c**.

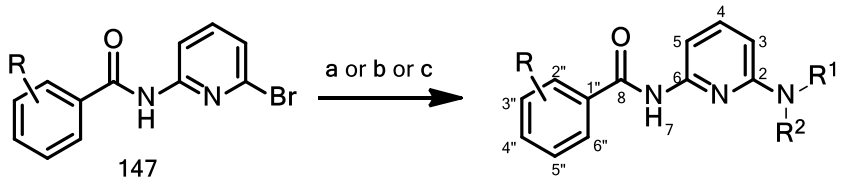

142a R = *o*-Cl, R^1 = *c*-hex, R^2 = H
142b R = *o*-Cl, R^1 = Ch_2Ph, R^2 = H
142c R = *o*-Cl, R^1 = Ph, R^2 = H
142d R = *o*-Cl, NR^1R^2 = morpholinyl
142e R = *o*-Cl, NR^1R^2 = piperidinyl
142f R = *o*-Cl, NR^1R^2= imidazolyl

Scheme 2.8: *Reagents and conditions*; (a) 2 mol% Pd_2dba_3, 6 mol% *rac*-BINAP, 1.4-dioxane, amine, KO^{t}Bu, N_2 atm., 80-150℃, MW 120–150W; 2 h; (b) 2 mol% Pd_2dba_3, 6 mol% *rac*-BINAP, 1.4-dioxane, amine, KO^{t}Bu, N_2, 120–125℃, 24 h; (c) for **142d-f**, same catalyst system, 1.4-dioxane, base; secondary amine, 130-135℃, 24 h.

Initial attempts to access the target products using microwave irradiation (120–150W) at temperatures ranging from 80-150℃, unfortunately, gave low yields of products. Furthermore, continuous irradiation at temperatures in excess of 140℃ appeared to degrade substrate **147a**.

Alternatively, the coupling reaction was repeated under conventional heating at temperatures of 100-120℃ using milder bases like K_3PO_4 or K_2CO_3 or Cs_2CO_3 but unfortunately, low product

yields were obtained. The C-N conversions remained very poor even after subjecting such reactions to long run times (48 h).

However, reasonable product yields of 75%, 52% and 65% were obtained for target products **142a, 142b** and **142c**, respectively, when the aminations were done using KO^{t}Bu as base under conventional heating at temperatures ranging from 120-125℃ (Scheme 2.8, conditions b).

As a result of the efficient yields achieved when scaffold **147a** was cross-coupled with primary amine nucleophiles, a palladium-catalyzed protocol was extended towards facilitating bromine substitution from scaffold **147a** using secondary amine nucleophiles (morpholine, piperidine and imidazole) as coupling partners. Initial efforts to cross-couple scaffold **147a** with morpholine at temperatures averaging 120℃ gave low yields (20-25%) for the target compound **142d**. Nonetheless, a modest conversion (56%) for target compound **142d** was obtained at temperatures around 130℃, whilst reaction temperatures beyond 135℃ adversely affected product yield.

The identity of compound **142d** was confirmed using ^{1}H NMR spectroscopic data which showed the presence of seven aromatic protons and one amide proton with chemical shift patterns that closely resembled earlier observations in substrate scaffold **147a**. Furthermore, the morpholinyl multiplets appearing at 3.85–3.71 ppm (4H) and 3.52–3.33 ppm (4H), were consistent with the formation of the C-N bond, as was the corresponding shift of the quaternary C-2 in the ^{13}C NMR spectrum to 149.4 ppm from 140.7 ppm in the substrate (C-Br). The IR spectrum also confirmed the presence of the morpholinyl protons due to increased intensity in CH stretches whilst the HRMS data, which did not contain any Br isotope peaks ($[M+H]^+$: 318.1006), also supported successful C-N bond formation.

In a similar fashion, target compound **142e** was synthesized in a reasonable yield of 68% using slightly higher reaction temperatures of 130-135℃ for the palladium-catalyzed reaction. The product identity was confirmed by ^{13}C NMR spectroscopic analysis which showed a downfield shift of the quaternary carbon C-2 coupled to the amine-N (C-N), from the original 140.0 ppm in substrate **147a** (C-Br) to 149.5 ppm (C-N) in target product **142e**.

Disappointingly, efforts to aminate scaffold **147a** with imidazole via copper- or palladium-mediated methodologies failed to give the desired target product **142f** (Fig. 2.3) as only starting material was recovered. This could be attributed to the low reactivity of imidazole as a nucleophile.

The comparative yields for the copper-mediated and palladium-catalyzed aminations of scaffold **147a** with various primary and secondary amine nucleophiles to afford target compounds **142a-f** are shown in Figure 2.3.

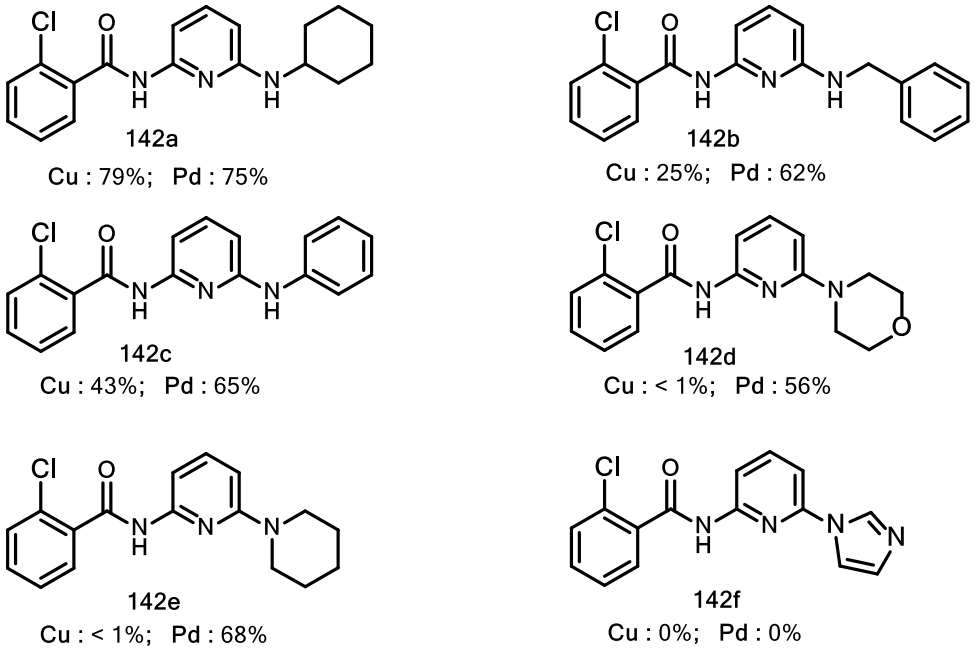

Figure 2.3: Copper-mediated and palladium-catalyzed aminations for target compounds **142a-f.**

With the exception of cyclohexylamine coupling, palladium-catalyzed reactions afforded more efficient aminations for both primary and secondary amine nucleophiles than those obtained using copper-mediation (Figure 2.3). This could be largely attributed to *rac*-BINAP's superior steric and electronic properties which stabilize and "control" the palladium-based catalytic cycle to facilitate target product formation. These results also mirror Beletskaya's observation that palladium-based systems were greatly influenced by the degree of NH nucleophilicity as compared to the steric bulkiness of the nucleophile.[6,11] This could explain the reasonable to excellent target product yields obtained for the primary amine and secondary amine nucleophiles, except for the imidazole target **142f**. The low yield of 20% obtained for target molecule **142f** also confirms the negative influence imposed by the bulkiness of the NH nucleophile on the success of the palladium-catalyzed C-N coupling reactions.

Unlike palladium, copper-based catalysis could be more sensitive to the general chemistry of the reaction mixture at hand. Thus, copper-mediated protocols cannot be easily extended to a

variety of substrates and/or nucleophiles since the dominating catalytic species or redox reaction, which may logically be unique in different reaction mixtures, remains largely unknown. This could tentatively explain why optimization of copper-based protocols started sluggishly and still lags far behind its unrivalled competitor, palladium. More so, even those optimized copper-assisted protocols that are commonplace in synthetic organic literature today, remain largely confined to a very narrow substrate scope.

It is noteworthy to also mention that no C-N bond formation was observed in control experiments where the Pd_2dba_3/*rac*-BINAP catalyst system was excluded. Similarly, attempts to use triphenylphosphine (PPh_3) as supporting ligand in similar reactions proved ineffective as only starting material was recovered. The failure to achieve the desired C-N coupling in the presence of PPh_3 as supporting ligand could be attributed to two reasons. Firstly, the less electron-rich PPh_3 monodentate ligand could have failed to dislodge the tightly-bound[11] dibenzylideneacetone ligand from the palladium coordination sphere of the highly stable palladium source - Pd_2dba_3. This could have suppressed the optimal formation of the active Pd^0 catalytic species, which is critical for the subsequent oxidative addition process in the catalytic cycle. The second reason could be attributed to premature catalyst deactivation by the pyridinyl-based halide substrate **147a** via competitive displacement of the PPh_3 from the activated catalytic complex. Nonetheless, these C-N conversions, once again, validate the functional superiority of *rac*-BINAP as a more viable candidate than PPh_3 for cross-coupling electron deficient heteroaryl substrates with amine nucleophiles.

More importantly, it was also noted that systematic catalyst preparation was crucial towards achieving efficient and reproducible palladium-catalyzed aminations. The catalyst pre-activation step involved premixing of the palladium precursor (Pd_2dba_3) with *rac*-BINAP at 80 °C and allowing sufficient time (≥ 5 min) for the optimal formation of the active Pd^0 catalytic species. Thereafter, the heterocyclic substrate **147**, amine and nucleophile could be added sequentially to the reaction mixture under N_2 purge. Situations in which reagents were added haphazardly were characterized by poor conversions and low product yields whilst the bulk of the starting material was recovered.

Following the successful amination of **147a** with selected primary and secondary amine nucleophiles, the already developed palladium-mediated protocol was successfully extended towards aminating other pyridyl-benzamide scaffolds **147b–e** with piperidine. A comprehensive review article by Castillo and Buchwald showed that piperidine has become one of the most preferred heterocycles in FDA approved drugs.[14] On that basis, novel target molecules **142g–j**

containing the piperidyl moiety, were accessed by aminating a small range of pyridyl-benzamide scaffolds **147b-e** to obtain the target products in reasonable yield (Table 2.1).

Table 2.1: Other target pyridyl-benzamide products **142g-j** obtained via palladium-catalyzed cross-coupling with piperidine.

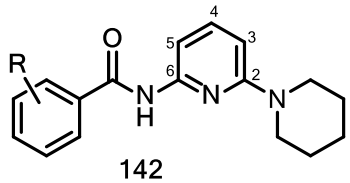

142

Compound	R	**Pd** (Yield)
142g	H	55%
142h	*m*-Cl	52%
142i	*p*-Cl	64%
142j	*p*-CN	48%

Despite the variations in functional group substitutions on the phenyl ring adjacent to the amide link among substrates **147b-e**, the electronic impact appeared minimal on amide protons in the ^{1}H NMR spectra of the corresponding aminated targets **142g-j**, which were deshielded to a similar extent (8.20–8.30 ppm). Similarly, ^{13}C NMR spectra equally confirmed successful C-N substitution with the quaternary aminated carbon (C-2) signals appearing in a narrow range of 158.43–158.37 ppm.

Substrate **147f** proved to be an interesting example as it appeared to give the highest yield of product. However, HRMS data ($[M+H]^{+}$: 385.0655) showed the presence of Br isotopes, ruling out the product being the expected **142k** (Scheme 2.9). In addition, HRMS also confirmed the absence of fluorine and pointed towards unexpected displacement of fluorine giving a different product **142g**. ^{13}C NMR spectroscopic analysis showed the absence of any C-F coupling in the aminated product, unlike what was previously evidenced with substrate **147f**.

In the ^{1}H NMR spectrum, the amide proton H-7 appeared more deshielded at 12.92 ppm as a broad singlet in contrast to the more upfield doublet at 9.00 ppm observed in substrate **147f**.

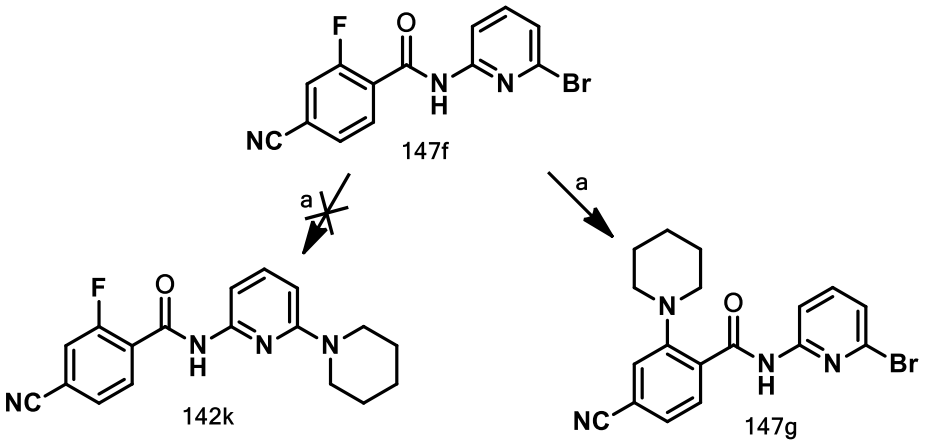

Scheme 2.9: *Reagents and conditions*; (a) (i) 2 mol% Pd_2dba_3, 6 mol% *rac*-BINAP, piperidine, 2 eq. KO^{t}Bu, 1.4-dioxane, reflux, 125℃, 24 h, 85% yield; or (ii) piperidine, 2 eq. KO^{t}Bu or KHMDS, dioxane, reflux, 100℃, 2 h, 99% yield.

In an effort to investigate this result further, a catalyst-free cross-coupling protocol of substrate **147f** with piperidine was attempted with KHMDS or KO^{t}Bu as base. Fortunately, the C-N conversion occurred rapidly as the starting material **147f** was quantitatively consumed in a much shorter time to generate compound **147g**.

Similar conversions were achieved when the same reaction was repeated in the absence of the palladium catalyst or KO^{t}Bu or KHMDS base, using excess piperidine only. Although the formation of **147g** proceeded slowly, this showed that piperidine (pK_a = 11.22) could act as both a base and nucleophile to facilitate the amination reaction.

Due to the consistent facile displacement of fluorine either in the presence or absence of palladium catalysis, it was proposed that this reaction occurred via an addition-elimination reaction (S_NAr) in which the *ortho*-amide functionality electronically stabilized the transition state intermediate **147h** (Scheme 2.10).

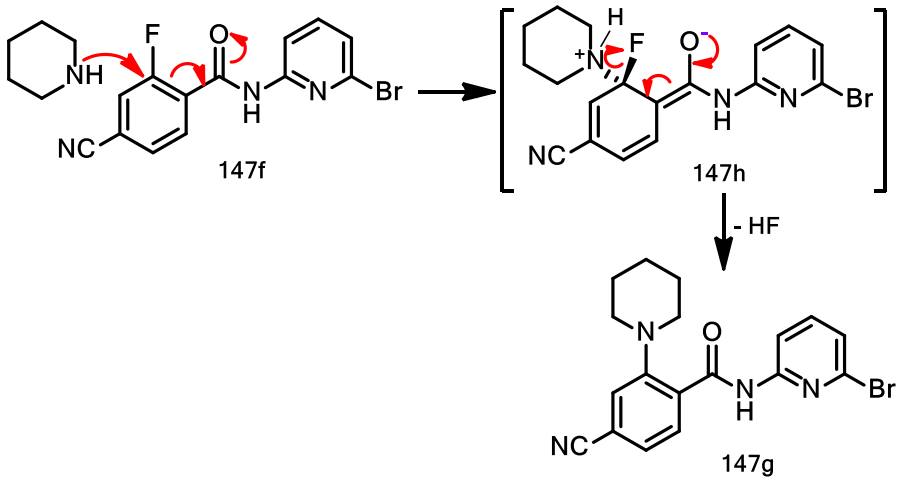

Scheme 2.10: Proposed fluorine displacement mechanism for reaction between compound **147f** and piperidine to form **147g.**

In an attempt to confirm the facile displacement of fluorine in these substrates the reaction between compound **147f** and a different nucleophile, benzyl alcohol, was investigated. Pleasingly, the reaction gave the benzyl alkoxy-substituted product **147i** (Fig 2.4) in 70% yield.

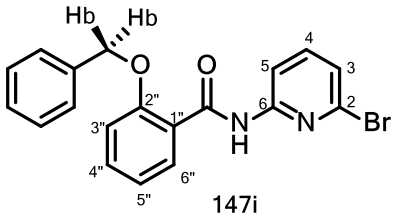

Figure 2.4: Structure of benzyl alkoxy-substituted product **147i**

The ^{1}H NMR spectrum showed the presence of twelve aromatic protons and a much deshielded amide singlet at 10.29 ppm. In addition, two benzylic protons (H-b) appeared upfield as a singlet at 5.39 ppm. ^{13}C NMR spectroscopy also showed fifteen carbon signals in the aromatic region, one signal in the carbonyl region of 161.7 ppm and one carbon signal in the aliphatic region at 72.4 ppm. DEPT analysis showed ten CH signals, five quaternary aromatic carbon signals and one slightly deshielded carbonyl at 161.7 ppm. One CH_2 signal was observed in the aliphatic region.

HMBC experiments showed significant heteronuclear long-range coupling between the benzylic protons H-b and the C-O coupled quaternary carbon C-2" (at 156.5 ppm), whilst H-6" (8.36 ppm) also coupled with both C-2" and the carbonyl carbon signal at 161.7 ppm. Moreover, the presence of the quaternary carbon C-2 signal at 140.0 ppm showed that the C-Br bond was still intact and also confirmed that product **147i** had been formed exclusively via displacement of the fluorine at the C-2" position as previously postulated in Scheme 2.10.

Thus, such facile fluorine displacement reactions warrant further investigation as key steps towards accessing novel scaffolds that could provide platforms for the synthesis of compounds that are active against HIV. Nevertheless, bromine displacement was eventually achieved when compound **147g** was cross-coupled with piperidine, under palladium catalysis, to give compound **142l** in a high yield of 85% (Scheme 2.11).

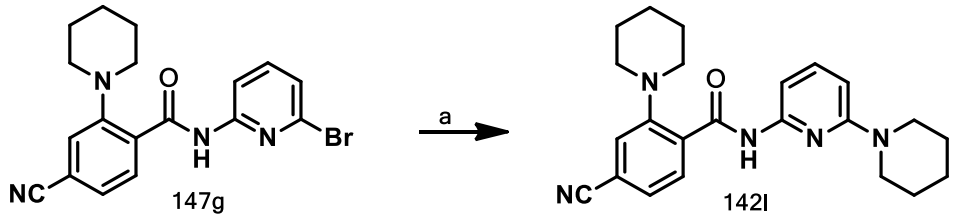

Scheme 2.11: *Reagents and conditions*; (a) 2 mol% Pd_2dba_3, 6 mol% *rac*-BINAP, piperidine, 2 eq. KO^{t}Bu, 1.4-dioxane, reflux, 125℃, 24 h, 85% yield.

2.1.2.3 Extension to oxygen- and sulfur-containing nucleophiles

As a way to broaden the range of novel target molecules for antiviral screening, selected oxygen- and sulfur-bearing nucleophiles were also considered as potential candidates for cross-coupling with scaffold **147a**. We also wanted to ascertain whether the previously developed transition metal-catalyzed methodologies that had been useful in achieving efficient C-N bond formations (Fig. 2.3) could be extended towards accessing novel target analogues that could be constructed via C-O and C-S cross-coupling.

The selected oxygen-containing nucleophiles were *n*-butyl alcohol, phenol and benzyl alcohol with thiophenol and benzylthiol making up the sulfur-bearing candidates. These nucleophiles were selected for exploratory purposes to verify whether such hetero-linkers (in addition to nitrogen nucleophiles already covered) could enhance binding (hydrophobic) interactions

between the alkyl and aryl motifs of the target molecules and the side chain amino acids lining the RT allosteric site.

A copper-based protocol employing ethylene glycol as a supporting ligand was tested using *n*-butyl alcohol, phenol, and thiophenol and benzylthiol nucleophiles as coupling partners for scaffold **147a**. Unfortunately, insignificant yields (≤ 5%) of target products **151a-b** and **151e** and a low yield of 15% for product **151d** were obtained (Fig. 2.5).

Fortunately, *n*-butyl alcohol, phenol, benzyl alcohol, thiophenol and benzylthiol were successfully cross-coupled with scaffold **147a**, under palladium catalysis, to afford novel target molecules **151a-151e** in modest to reasonable yields (Fig. 2.5).

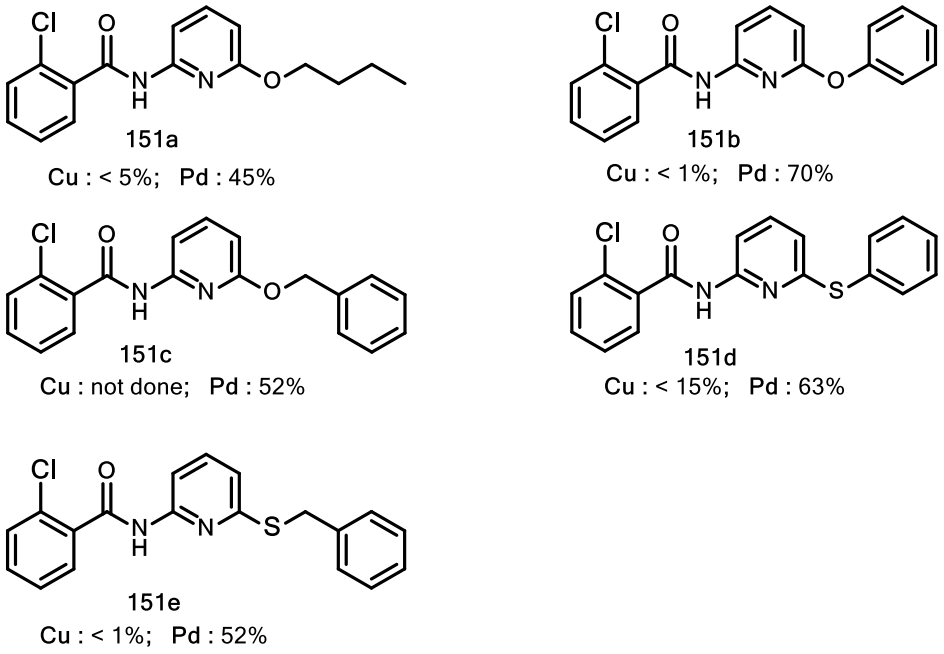

Figure 2.5: Target compounds **151a**-**151e** accessed via palladium-catalyzed cross-coupling of **147a** with selected oxygen- and sulfur-containing nucleophiles.

It is important to point out that whilst C-N conversions were efficiently carried out at 125-130℃, C-O cross-coupling reactions required higher temperatures averaging 140℃ to achieve meaningful yields. When reactions were done at temperatures below 130℃, poor yields (10–23%) of target products were obtained.

The ^{1}H NMR spectrum for target molecule **151a** integrated for seven aromatic protons and an amide proton which appeared at 8.30 ppm as a broad singlet. In addition, nine protons belonging to the coupled butoxy motif were observed in the aliphatic region distributed as a triplet at 4.18 ppm (t, J = 6.6 Hz, 2H); a multiplet in the range 1.77–1.67 ppm (2H), another upfield multiplet in the range 1.53–1.37 ppm (2H), and another triplet at 0.96 ppm (t, J = 7.4 Hz, 3H). The ^{13}C NMR spectrum contained eleven aromatic carbon signals, a carbonyl carbon signal at 164.6 ppm and four carbon signals in the aliphatic region, which belonged to the butoxy motif. The DEPT experiment showed the presence of seven CH signals, four aromatic quaternary carbon signals, a carbonyl signal at 164.5 ppm and three CH_2 and one CH_3 signal belonging to the butoxy group upfield in the aliphatic range. The C-O coupled C-2 was more deshielded at 162.86 ppm as compared to the C-Br at 140.7 ppm in substrate **147a**. Furthermore, the HRMS data ($[M+H]^+$: 305.1047) confirmed the target molecule's expected molecular weight whilst also supporting successful bromine displacement at the C-2 position of compound **147a**.

^{1}H NMR spectroscopic analysis showed that the amide protons for target molecules **151a** and **151c** were more shielded at 8.30 ppm than that of substrate **147a** (8.58 ppm) whilst that for **151b** was unchanged (8.60 ppm). The ^{13}C NMR spectra showed that the quaternary C-O (C-2) signals for targets **151a–c** were more deshielded in the range 162.86–155.63 ppm than the corresponding C-Br signal (140.7 ppm) confirming that bromine substitution had occurred successfully. The corresponding IR data for the target compounds **151a–c** also showed that the integrity of the pyridyl benzamide scaffold was still intact as the amide NH stretches (3275, 3176 and 3411 cm^{-1}) and C=O stretches (1676, 1684 and 1669 cm^{-1}) remained similar to that of substrate **147a** at 3177 (NH) and 1683 cm^{-1} (C=O).

Following the successful C-N and C-O conversions achieved using the Pd_2dba_3/*rac*-BINAP catalyst system; a similar synthetic protocol was used for cross-coupling substrate **147a** with thiophenol and benzylthiol nucleophiles. Unlike the moderately high reaction temperatures required to efficiently achieve C-N and C-O bond formations for compounds **142a-l**, C-S conversions were easily facilitated using moderate heating conditions (110-120℃). This could be due to the fact that the less electronegative sulfur is more nucleophilic than both nitrogen- and oxygen-based nucleophiles. Novel target compounds **151d** (63%) and **151e** (52%) were obtained in modest yields (Fig. 2.5).

As a representative of the C-S coupled target molecules, the ^{1}H NMR spectrum for target compound **151d** confirmed successful formation of such analogues by showing twelve aromatic protons and an amide proton signal that was much more deshielded at 8.49 ppm than for target O-containing analogues **151a** and **151c**. ^{13}C NMR spectroscopic data showed fifteen carbon

signals and one carbonyl signal at 164.8 ppm. As expected, DEPT analysis confirmed the presence of twelve CH signals and five quaternary carbon signals in the aromatic region. The C-S coupled quaternary C-2 was more deshielded at 159.80 ppm than the C-Br at 140.7 ppm in substrate **147a**. Interestingly, the quaternary C-2 for target compound **151d** appeared more deshielded than for the phenoxy-substituted analogue **151b** (155.63 ppm). HRMS data ($[M+H]^+$: 341.0506) also confirmed the absence of bromine isotopes by providing a molecular weight that was consistent with successful C-S cross-coupling and formation of novel target **151d**.

Target product yields for cross-coupling primary and secondary amine nucleophiles for the preparation of pyridyl benzamides were modest to excellent ranging from 44-75% for palladium-catalyzed protocols. Modest yields were mainly observed when cross-coupling secondary amines whose inherent steric bulk could have adversely influenced the yields achieved. On the other hand, C-O and C-S coupled reactions for novel targets **151a-e** were generally reasonable ranging from 45-70% for the O-nucleophiles and 52-63% for S-nucleophiles with the highest yield being achieved for phenol (70%) and thiophenol (63%) nucleophiles.

2.2 Synthesis of pyridyl-benzylamines

Given the restricted conformations inherent in the pyridyl-benzamide scaffold **142** due to the presence of the amide link, the pyridyl-benzylamine **143** scaffold (Scheme 2.12) was conceived as a more conformationally flexible platform for accessing torsionally flexible analogues. Such analogues were expected to possess greater torsional freedom which could enhance their binding affinities in the RT allosteric site of mutant HIV strains.

Since the pyridyl-benzylamine **143** represents a 'reduced' form of the pyridyl-benzamide scaffold **142**, an amide reduction strategy was considered as the first option towards accessing compounds bearing the benzylamine platform **143**. Our successful development of an efficient methodology for accessing a target pyridyl-benzamide **147a** inspired us to attempt the amide reduction of **147a** as a possible source of the pyridyl-benzylamine **143** (Scheme 2.12).

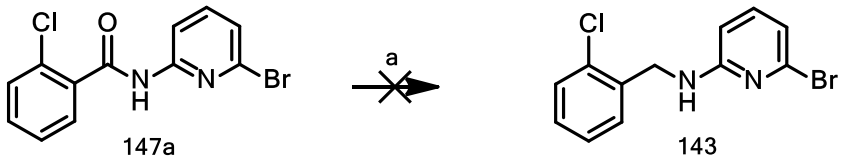

147a 143

Scheme 2.12: Amide reduction; *Reagents and conditions*: (a) $LiAlH_4$, PhMe or DMF or THF, reflux, 24 h.

Our initial attempt at reducing the amide bond using commercially available $LiAlH_4$ in refluxing toluene proved unsuccessful. Similar efforts to facilitate the reduction process by change of solvent from PhMe to DMF or THF and even refluxing for longer periods (24 h) were equally ineffective as the starting material was recovered in each case. A similar result was also encountered when we attempted to reduce one of the pyridyl-benzamide products **142d** as a direct route towards accessing corresponding benzylamine targets.

Discouraged by these results, we considered a second option as represented by the retrosynthetic analysis of scaffold **143** shown in Scheme 2.13. As shown in Scheme 2.13, target compound **143** could be obtained via C-N cross-coupling of intermediate **152**.

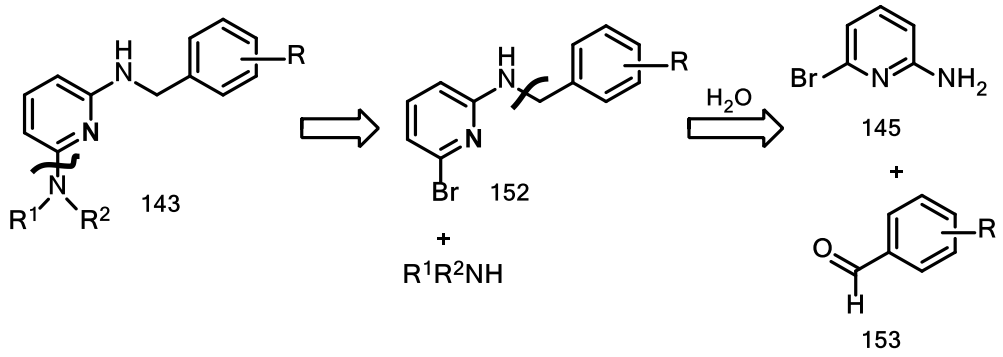

Scheme 2.13: Retrosynthetic analysis of pyridyl-benzylamine target scaffold **143**.

2.2.1 Synthesis of intermediate 152

A reductive amination strategy was explored as a possible synthetic route for accessing **152**. Our initial attempt at reacting commercially available 2-chlorobezaldehyde **153** with 2-amino-6-bromopyridine **145** under neutral conditions at room temperature proceeded very sluggishly as large amounts of starting material were observed by TLC analysis of the reaction mixture 4 h after mixing the reactants.

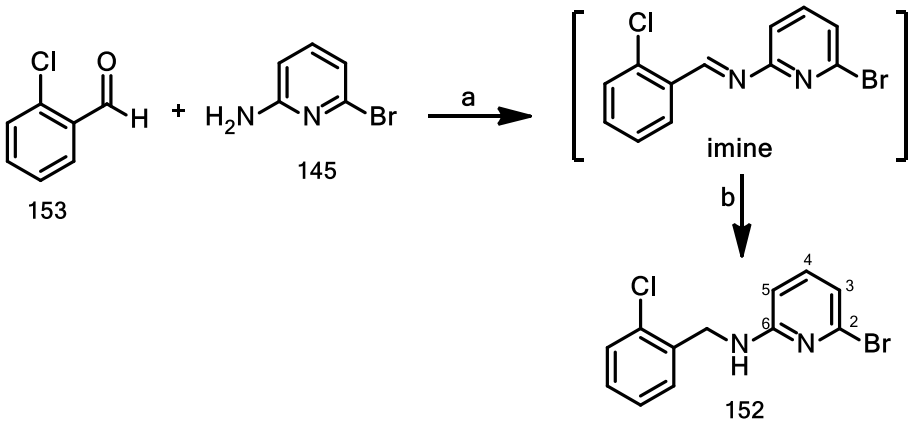

Scheme 2.14: *Reagents and conditions*: (a), 4Å MS, MeOH, pH 5-6, reflux, 24 h; (b) $NaCNBH_3$, RT , 2 h.

However, when 4Å molecular sieve and catalytic amounts of concentrated HCl were added to the reaction mixture, the reaction proceeded considerably faster as evidenced by the enlarging imine spot and gradual consumption of the starting materials. We observed that imine formation was adversely influenced by the addition of either too little (pH > 6.0) or too much (pH < 4.0) acid to the reaction mixture. Furthermore, it was also noted that imine formation, under room temperature conditions, stagnated around 40-50% conversion even after prolonged stirring of the reaction mixture (pH 5-6) for 24 h.

Nevertheless, it was refreshing to note that imine formation could be greatly facilitated by using dried solvents, 1.2 equivalents of aldehyde **153** and refluxing the reaction mixture for 12-24 h under slightly acidic conditions (pH 5-6). After cooling to room temperature, the imine was reduced *in situ* via cautious addition of $NaCNBH_3$ over a 2 h period to mitigate the evolution of toxic HCN gas (Scheme 2.14).

Target compound **152** was obtained in an excellent yield of 88%. ^1H NMR spectroscopic analysis showed the presence of seven aromatic protons, and two protons in the aliphatic region. The amino proton and benzylic protons appeared as a triplet (t, J = 6.0 Hz) and a doublet (d, J = 6.2 Hz) at 5.21 ppm and 4.57 ppm, respectively. ^{13}C NMR spectroscopic analysis showed eleven aromatic carbon signals as well as the expected benzylic carbon signal in the aliphatic region at 44.0 ppm. DEPT experiments showed seven CH signals and four aromatic quaternary carbon signals inclusive of a deshielded quaternary C-Br (C-2) in compound **152**, which appeared at 140.3 ppm. Furthermore, the IR spectrum of **152** also validated the disappearance of the carbonyl stretch supporting that reductive amination had occurred.

2.2.2 Synthesis of novel target scaffold 143

Initial attempts at accessing the novel target molecule **143a** via cross-coupling of **152** with cyclohexylamine, under palladium mediation (Scheme 2.15), proved very challenging as an unexpected product **154** appeared to have been formed. For clarification purposes corresponding ^{1}H and ^{13}C NMR spectra are shown in Figures 2.6a-b.

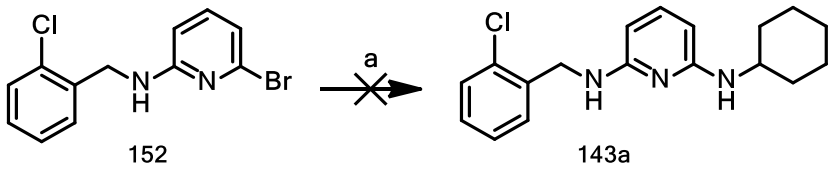

152 143a

Scheme 2.15: *Reagents and conditions*: (a) 2 mol% Pd_2dba_3, 6 mol% *rac*-BINAP, 1.3 eq. cyclohexylamine,1.2 eq. KO^{t}Bu, 1.4-dioxane, 120-130℃, 24 h.

Figure 2.6a: ^{1}HNMR spectrum for unexpected product **154**.

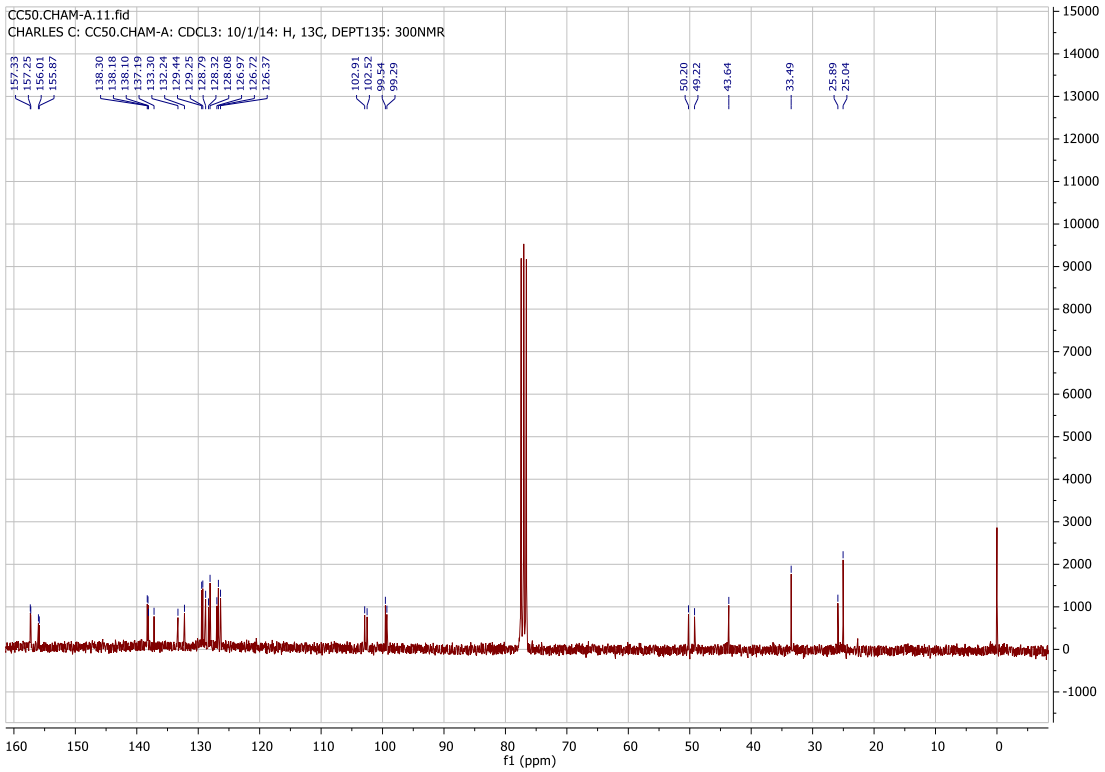

Figure 2.6b: ^{13}C NMR spectrum for unexpected product **154**.

^{1}H NMR spectroscopy of the unexpected product **154** showed the presence of thirty protons, of which fourteen were aromatic signals whilst seventeen were aliphatic proton signals. Two sets of benzylic protons were observed as one singlet at 5.41 ppm and an upfield doublet at 4.47 ppm (d, J = 4.0 Hz, 2H). In addition, an amino proton H-m was also observed at 4.78 ppm whilst the eleven upfield protons matched those expected from the cyclohexyl motif. On the other hand, successful C-N coupling of **152** and cyclohexylamine was expected to give a target product containing a total of twenty protons.

The corresponding ^{13}C NMR spectrum showed twenty-two aromatic carbon signals and six carbon signals in the aliphatic region. DEPT analysis showed fourteen CH signals and eight aromatic quaternary carbon signals, whilst two CH_2 (benzylic carbon) signals, one CH (cyclohexyl) signal and three CH_2 (cyclohexyl) signals appeared in the aliphatic region. Using the NMR spectroscopic data as a basis, we proposed **154** (Fig. 2.7) as the structure of the compound that was formed in Scheme 2.15.

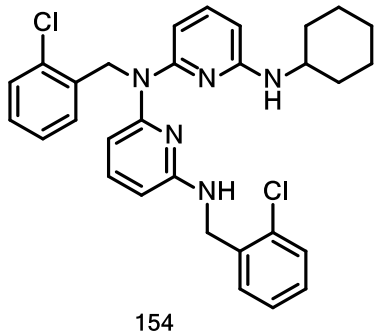

154

Figure 2.7: Proposed structure of unexpected product **154**

The proposed structure **154** (Fig. 2.7) suggests nucleophilic interference from the benzylamine nitrogen of substrate **152**. This is consistent with observations made by Hartwig and co-workers[9] when benzylamine or pyridine were noted to displace the basic and hindered alkyl monophosphine ligand (e.g. P(*o*-tolyl)$_3$) from the oxidative-addition complex during attempted C-N cross-coupling with an aryl bromide.

To prevent this from occurring, the benzylamine nitrogen in **152** was protected by reaction with Boc_2O in the presence of catalytic amounts of dimethylaminopyridine (DMAP) (Scheme 2.16). The target product **155** was obtained in quantitative yield with the ^{1}H NMR spectrum confirming displacement of the benzylamine proton by the Boc group which appeared upfield at 1.38 ppm, integrating for nine protons.

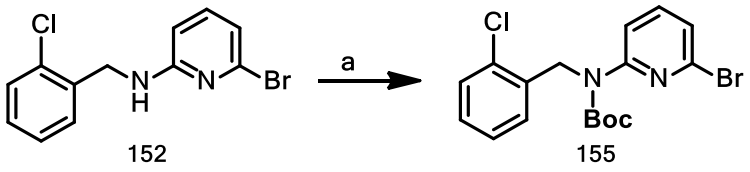

152 155

Scheme 2.16: *Reagents and conditions*: (a) $(Boc)_2O$, 0.1–0.2 eq. DMAP, CH_3CN, RT, 4 h.

Thereafter, an attempt to cross-couple **155** with cyclohexylamine proved successful in the presence of the milder Cs_2CO_3 base as the target product **143a** was obtained in a reasonable yield of 60% (Scheme 2.16) at temperatures not exceeding 120°C. On the other hand, reaction temperatures exceeding 120°C were found to be unfavourable towards C-N bond-formation, possibly due to Boc-deprotection which could facilitate competition from the benzylamine N nucleophile.

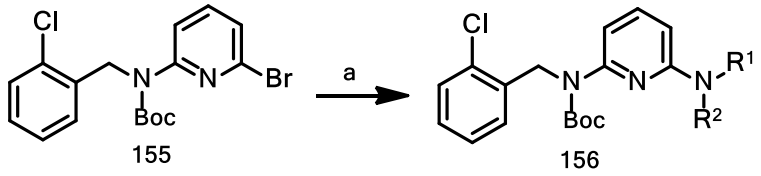

Scheme 2.16: *Reagents and conditions*: (a) 2 mol% Pd_2dba_3, 6 mol% *rac*-BINAP, R^1R^2NH, Cs_2CO_3, 1.4-dioxane, 120°C, 24 h.

Fortunately, the same palladium-catalyzed cross-coupling protocol (Scheme 2.16) could be extended towards coupling **155** with other primary (benzylamine and aniline) and secondary amine (morpholine and piperidine) nucleophiles. The Boc-protected products **156** were characterized by ^{1}H NMR spectroscopy only and treated as intermediates. Thereafter, acid-catalyzed deprotection (Scheme 2.17) afforded the novel targets **143a-e** in reasonable overall yield (Fig. 2.8).

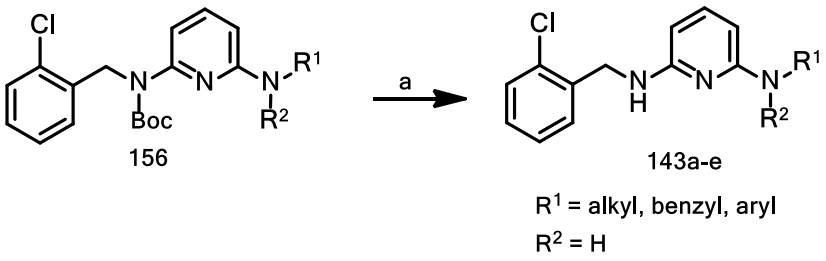

Scheme 2.17: *Reagents and conditions*: (a) 10% aq. HCl, CH_3Cl_3, reflux, 2 h.

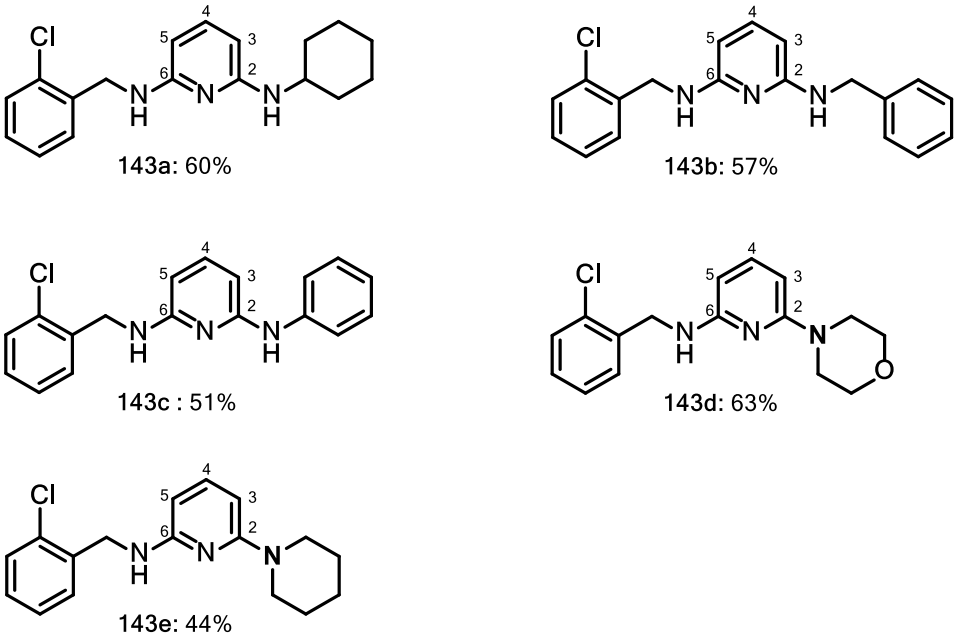

Figure 2.8: Target compounds **143a-e** accessed via palladium-catalyzed cross-coupling of **156** with selected primary and secondary amine nucleophiles

The ^{1}H NMR spectrum for target compound **143a** showed seven aromatic protons, and two amino proton signals at 5.80 ppm and 5.58 ppm. Two benzylic protons gave a doublet signal at 4.51 ppm (d, J = 5.9 Hz) whilst further upfield, multiplets belonging to the eleven protons from the coupled cyclohexyl motif were observed. ^{13}C NMR spectroscopy showed eleven aromatic carbon signals and five carbon signals in the aliphatic region. DEPT experiments showed seven CH signals, four quaternary aromatic carbons including a deshielded C-N coupled quaternary carbon signal (C-2) at 152.28 ppm. One CH_2 signal for the benzylic carbon atom was observed at 51.5 ppm followed by one CH signal and three CH_2 signals for the cyclohexyl motif, also in the aliphatic region. HRMS ($[M+H]^+$: 316.1599) also confirmed successful C-N coupling as evidenced by the expected molecular weight of the target molecule, which showed the absence of bromine isotopes.

Given that novel targets **143a-e** share common ^{1}H and ^{13}C NMR spectroscopic fingerprints as evidenced by the spectroscopic data contained in this report, a brief summary of salient NMR spectroscopic data for this series of C-N coupled derivatives is listed in Table 2.2.

As shown in Table 2.2, the benzylic proton H-b signal for compound **143a** appeared as a doublet at 4.51 ppm, whilst target **143b** contained two doublet signals at 4.53 ppm and 4.43

ppm arising from the benzylic protons in the scaffold as well as the C-N coupled benzyl amine nucleophile. Benzylic proton signals for products **143d-e** resulting from coupling reactions morpholine and piperidine, also appeared in the same range as observed for C-N coupled primary amine targets **143a-c**. Whilst the amino proton signals appeared as multiplets in this series of compounds, it was interesting to observe that compound **143a** contained the most deshielded signals with one such multiplet being observed in the range 7.81–7.79 ppm of the aromatic region.

Table 2.2: Key NMR spectroscopic signals for target pyridyl-benzylamines **143a-e**.

Compound	δ: ppm		
	Benzylic H	**Amino H**	**C-2**
143a	4.51 (d, J = 5.9 Hz)	Only one deshielded amino H signal : 7.81–7.79 (m)	152.3
143b	4.53 (d, J = 5.9 Hz)	Two multiplets: 4.82–4.70 (m, 1H) and 4.69–4.59 (m,1H)	158.0
143c	4.58 (d, J = 6.2 Hz)	Only one multiplet signal: 4.92–4.79 (m, 2H)	157.8
143d	4.79 (d, J = 5.9 Hz)	A broad singlet at 4.79 (s)	158.8
143e	4.81–4.63 (m)	4.87–4.63 (m, 2H)	158.9

The ^{13}C NMR spectra confirmed successful bromine displacement in all analogues **143a-e** as evidenced by the presence of the more deshielded aminated quaternary C-2 signal in the range 158.9–152.3 ppm for the compounds **143a–e** in comparison with the previously shielded quaternary C-Br chemical shift at 140.3 ppm.

2.2.3 Extension to oxygen- and sulfur-containing nucleophiles

Using a similar palladium-catalyzed protocol shown in Scheme 2.17, scaffold **155** was further cross-coupled with selected oxygen-containing (*n*-butanol, phenol and benzyl alcohol) and sulfur bearing (thiophenol and benzyl thiol) nucleophiles, and then Boc-deprotected under reaction conditions shown in Scheme 2.18 to afford novel target molecules **157a-e** in reasonable yield over the coupling and deprotection steps (Fig. 2.9).

As displayed in Figure 2.9, product yields of target compounds **157b-e** were better than the modest yield for target compound **157a**. Table 2.3 summarizes the benzylic, amino proton and C-2 NMR spectroscopic signals from compounds **157a-e**.

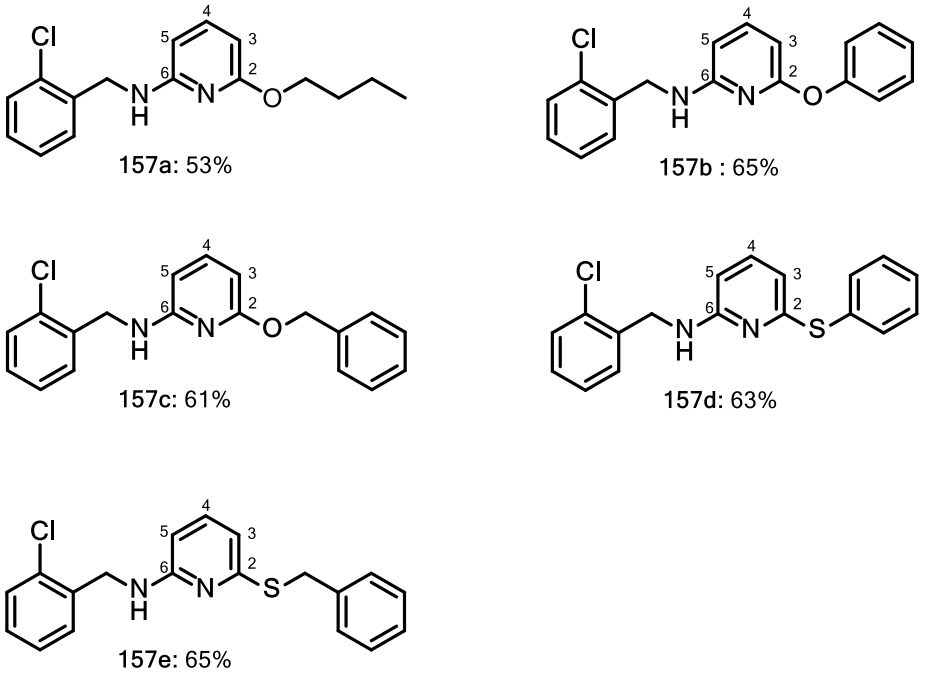

Figure 2.9: Novel C-O and C-S cross--coupled targets **157a-e**

Table 2.3: Selected NMR spectroscopic signals from the C-O and C-S coupled pyridyl-benzylamine derivatives **157a-e**.

Compound	δ: ppm		
	Benzylic H	**Amino proton**	**C-2**
157a	4.58 (d, *J* = 6.2 Hz)	4.84 (t, *J* = 5.5 Hz)	163.5
157b	4.57 (d, *J* = 6.2 Hz)	5.16 (t, *J* = 5.5 Hz)	160.8
157c	4.58 (d, *J* = 6.2 Hz)	4.87–4.81 (m)	162.9
157d	4.79 (s) (d, *J* = 5.9 Hz)	5.35 (t, *J* = 6.3 Hz)	160.1
157e	4.81 - 4.63 (m)	4.95 (t, *J* = 5.9 Hz)	156.6

Whilst the ^{1}H NMR spectrum for target molecule **157a**, made from cross-coupling an aliphatic nucleophile, appeared fairly resolved in the aromatic region, spectra for compounds made by coupling aromatic nucleophiles (**157b-e**) showed increasingly overlapping proton signals in the aromatic region (^{1}H NMR spectra). Compounds **157b-e** also showed enhanced C-H and C=C stretches around 3000 and 1400 cm^{-1} in their IR spectra.

As shown in Table 2.3, the C-2 carbon signals from the C-O coupled compounds **157a** and **157c** were more shielded at 163.5 and 162.9 ppm, respectively, the C-2 signals from the phenoxy- (**157b**) and thiophenol-coupled (**157d**) derivatives were around 160 ppm. Interestingly, the benzylthiol-coupled target **157e** displayed the most shielded C-2 signal at 156.6 ppm in this series of novel targets.

In summary, the product yields for C-N coupled novel compounds **143a-e**, just like for the pyridyl-benzamide target molecules **142**, were generally reasonable ranging from 44–63%. Similarly, the C-O and C-S coupling reactions for novel target molecules **157a-c** and **157d-e** also achieved reasonable yields in the ranges 53–65% and 63–65%, respectively, showing the versatility of palladium catalysis across the whole nucleophile range.

2.3 Synthesis of pyridyl-sulfonamides

The pyridyl-sulfonamide scaffold **144** was designed as a synthetic target given the high antiviral activities associated with NNRTI compounds that contain sulfonamide functionalities as exemplified by potent first generation NNRTI drug delavirdine **7** and NNRTI lead compounds **VRX-480773**[1] and **K-5a2**[15] (Fig. 2.10)

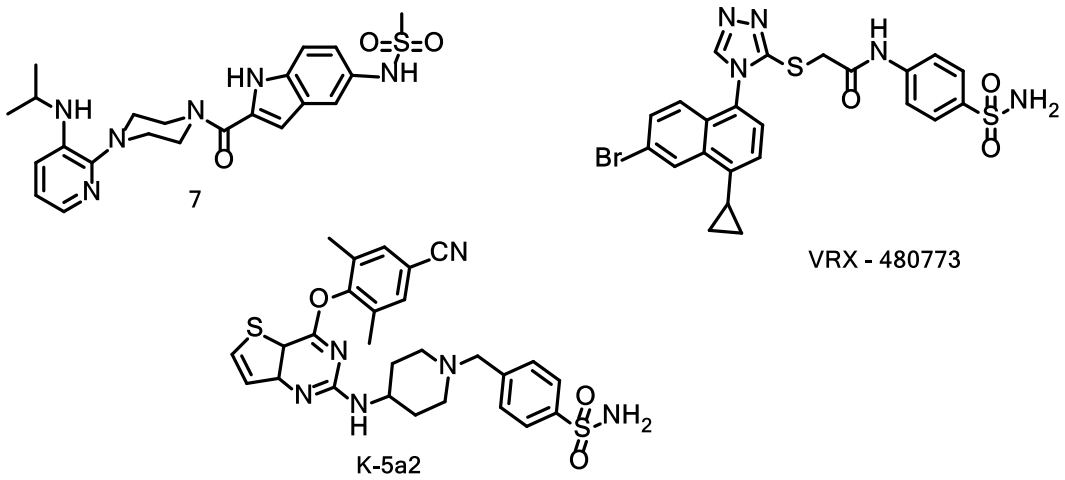

Figure 2.10: Sulfonamide-containing NNRTI delavirdine **7**, NNRTI leads **VRX-480773** and **K-5a2**

Retrosynthetic analysis of the pyridyl-sulfonamide scaffold **144** showed that it could be synthesized from 2-amino-6-bromopyridine **145** and an aromatic sulfonyl chloride **158** (Scheme 2.19).

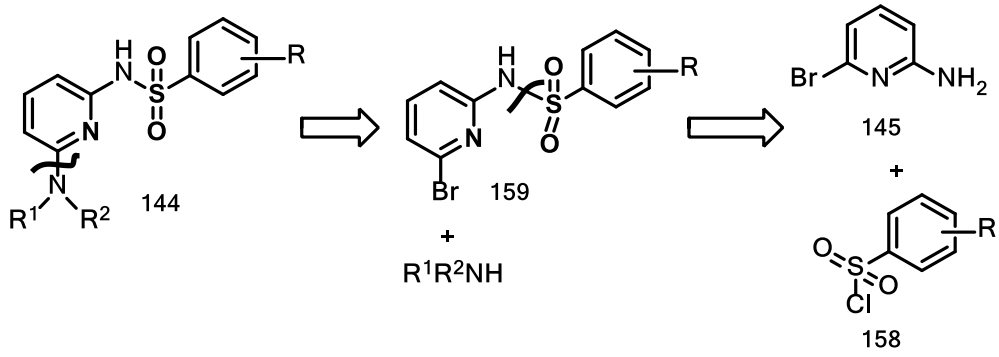

Scheme 2.19: Retrosynthetic analysis of pyridyl-sulfonamide target scaffold **144**

Target compounds **144** could be accessed via the initial construction of an intermediate scaffold **159** (Scheme 2.20), followed by palladium-catalyzed cross-coupling to obtain the desired compounds.

2.3.1 Synthesis of novel scaffold 159

Scaffold **159** was constructed by reacting commercially available aryl sulfonyl chloride **158a** or **158b** with 2-amino-6-bromopyridine **145** in the presence of pyridine as base, to afford the novel target pyridyl-sulfonamide **159a** or **159b** in a high yield of 98% (Scheme 2.20).

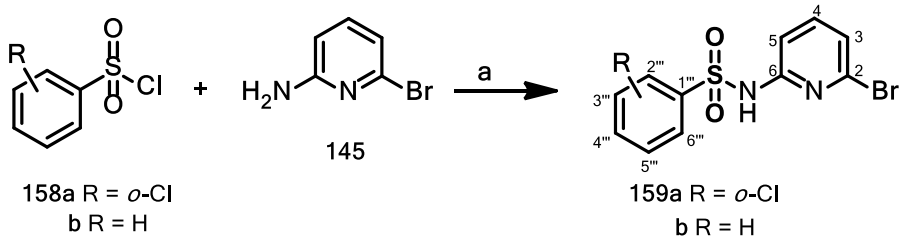

Scheme 2.20: *Reagents and conditions*: (a) CH_3CN, pyridine, 0°C-RT, 4 h.

^1H NMR spectroscopy revealed that scaffold **159a** contained the expected seven aromatic protons and an amide proton H's which gave a broad singlet at 7.82 ppm. ^{13}C NMR spectroscopic analysis showed eleven aromatic carbon signals whilst the DEPT spectrum showed seven CH signals, four quaternary carbons including C-Br (C-2) that was deshielded at 140.4 ppm. Pyridyl protons H-3 and H-5 each appeared as a doublet of doublets at 7.14 ppm

(dd, J = 7.7, 0.6 Hz) and 7.20 ppm (dd, J = 8.2, 0.6 Hz), respectively, whilst H-4 appeared as a multiplet in the region 7.46–7.37 ppm. Proton H-6''' appeared as a much deshielded multiplet in the region 8.21 – 8.16 ppm. The other protons H-3'''–H-5''' appeared as multiplets in the region 7.56–7.49 ppm and 7.46–7.37 ppm. HRMS ([M+H]$^+$: 346.9246) for ^{79}Br confirmed the expected molecular weight of the novel sulfonamide target molecule. The typical Br isotopic pattern; two M$^+$ peaks separated by two mass units, was observed.

Similarly, the identity of target **159b** was also confirmed by its ^{1}H NMR spectrum which showed the presence of eight aromatic protons and a broad amide proton singlet at 7.71 ppm. The ^{13}C NMR spectrum showed eleven aromatic carbon signals, whilst DEPT analysis showed the presence of six CH signals and three quaternary carbon signals, including C-2 that was deshielded at 140.5 ppm. HRMS ([M+H]+: 346.9246) also provided the expected molecular weight thereby confirming that the desired novel target molecule **159b** had been formed.

2.3.2 Synthesis of novel target molecules 144

Using our already developed palladium-catalyzed methodology, scaffold **159** was cross-coupled with selected primary and secondary amine nucleophiles (Scheme 2.21) to give target compounds **144a-h** in modest to excellent yields in the range 50–79% (Figure 2.10). The key proton and carbon signals from novel targets **144a-h** are contained in Table 2.4.

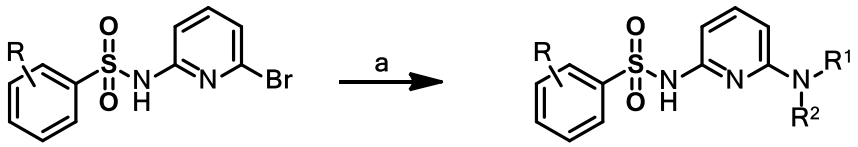

159a R = *o*-Cl
159b R = H

144a-h

Scheme 2.21: *Reagents and conditions*: (a) Pd_2dba_3, 6 mol% *rac*-BINAP, R^1R^2NH, KO^{t}Bu, 1.4-dioxane, 120-130°C, 24 h.

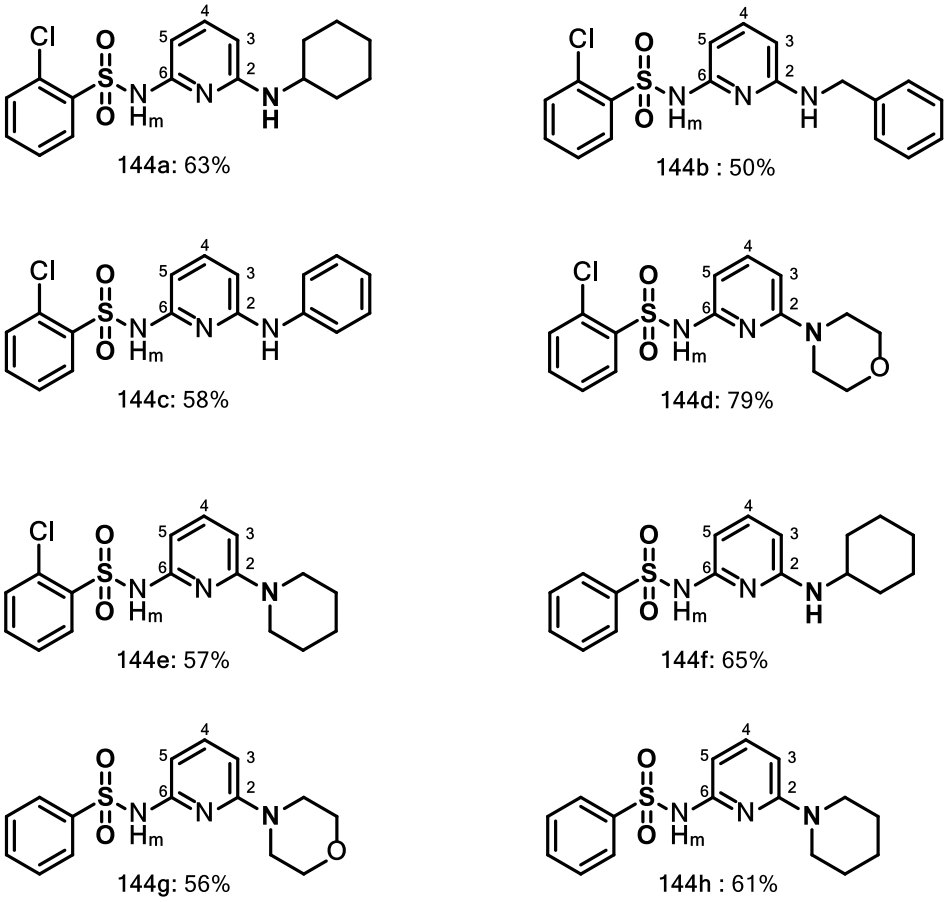

Figure 2.10: Target pyridyl-sulfonamide analogues **144a-h**

Table 2.4: Summary of key NMR spectroscopic data for target compounds **144a-h**

	δ: ppm				
Compd	NH & benzylic H	C-2	Pyridyl H-3	H-4	H-5
159a	NH: 7.82 (br, s)	140.4	7.14 (dt, *J* = 7.6, 0.6 Hz)	Overlaps with multiplet in the region 7.46–7.37	7.20(dt, *J* = 7.6, 0.6 Hz)
144a	Protons overlapped with aromatic proton signals	152.3	5.85 (d, *J* = 8.3 Hz).	Overlaps with multiplet in the region 7.43–7.28	6.62 (d, *J* = 8.0 Hz).
144b	Only one NH broad singlet at 7.70 (br, s); Benzylic protons gave a doublet at 4.39 (d, *J* = 5.4 Hz)	153.8	5.81 (d, *J* = 8.4 Hz)	Overlaps with an aromatic proton in the region 7.44–7.38	6.69 (d, *J* = 8.4 Hz)
144c	One NH at 9.01 (br, s), another NH proton overlaps with multiplet signal in the range 7.53–7.20 ppm.	152.8	6.41 – 6.34 (m)	7.16–7.07 (m)	6.89–6.81 (m)
144d	NH proton overlaps with aromatic proton multiplet in the range 7.63–7.50	158.3	6.24 (d, *J* = 8.3 Hz).	Overlaps with multiplet in the range 7.42–7.31.	6.47 (d, *J* = 7.8 Hz)
144e	Similar to **144d**	157.6	6.21 (d, *J* = 8.4 Hz).	7.30 (dd, *J* = 8.4, 7.8 Hz).	6.34 (d, *J* = 7.7 Hz).
144f	One broad NH singlet at 7.58 ppm.	154.4	5.83 (d, *J* = 8.3 Hz).	7.34 (t, *J* = 8.4 Hz).	6.59 (d, *J* = 8.1 Hz).
144g	NH proton overlapped with aromatic proton signals	158.4	6.25 (d, *J* = 8.3 Hz).	Overlaps in the region 7.73–7.35	6.57 (d, *J* = 7.8 Hz).
144h	Same pattern as **144g**	158.1	6.22 (d, *J* = 8.4 Hz).	7.32 (t, *J* = 8.4 Hz).	6.43 (d, *J* = 7.7 Hz)

Table 2.4 shows that C-N coupled C-2 signals from the target products **144a**– **144h** were more deshielded in the region 158.4–152.3 ppm than observed for substrate **159a** or **159b** (140.4 ppm). Interestingly, the secondary amine nucleophiles generally exerted the greatest

deshielding effect on the C-2 signals (158.4–157.6 ppm) than primary amines (154.4–152.3 ppm). In contrast, the corresponding pyridyl proton signal trends were indistinguishable for the primary and secondary *N*-coupled nucleophiles.

2.3.3 Extension to oxygen- and sulfur-containing nucleophiles

The palladium-catalyzed protocol was also successfully extended towards cross-coupling scaffold **159** with selected oxygen- and sulfur-containing nucleophiles (Scheme 2.21A) to afford novel target products **160a-f** in good to excellent yields (59–88%) (Fig. 2.11)

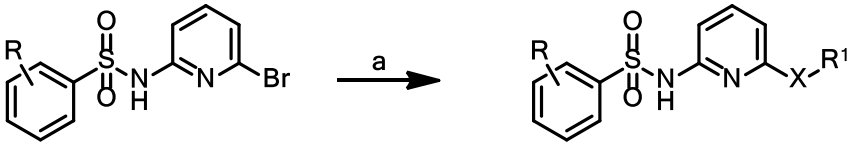

159a R = *o*-Cl
159b R = H

160a-f

Scheme 2.21A: *Reagents and conditions*: (a) Pd_2dba_3, 6 mol% *rac*-BINAP, O- or S-nucleophiles, KO^{t}Bu, 1.4-dioxane, 120-140℃, 24 h.

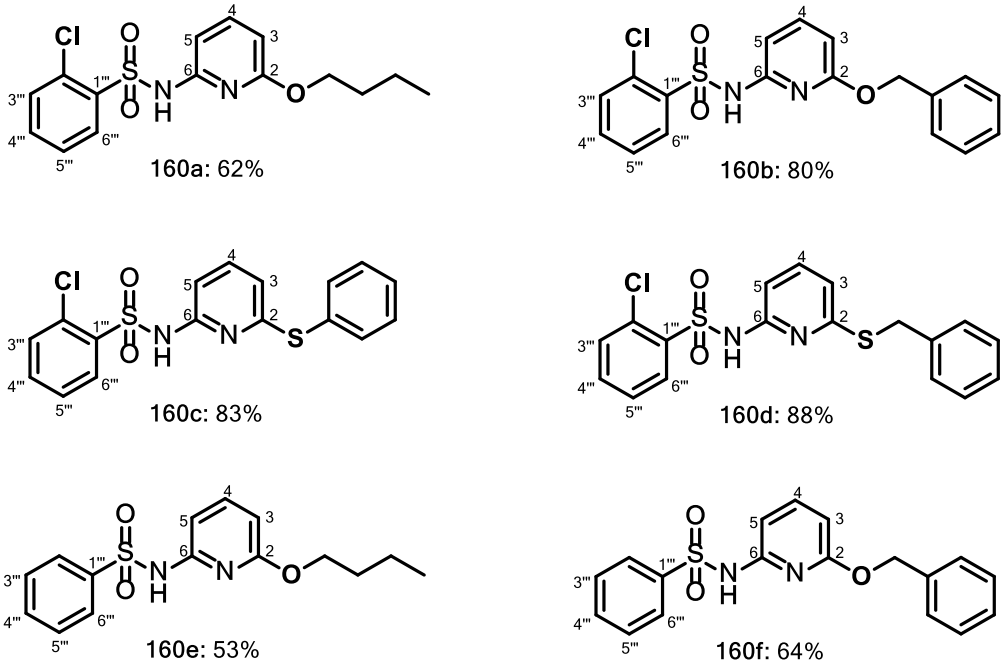

Figure 2.11: Novel O- and S-coupled pyridyl-sulfonamide targets **160a-f.**

IR spectra for target compounds **160e** and **160f** identified the expected functional groups as shown by the amide NH stretches at 3237 and 3246 cm^{-1}, respectively; CH stretches at 2962 and 2931, respectively; and 2877 cm^{-1}, and aromatic C=C stretches at 1441 cm^{-1}. HRMS spectroscopic data also confirmed successful C-O coupling in novel target products **160e** and **160f** as the expected molecular weights were obtained.

Table 2.5 Selected ^{1}H and ^{13}C NMR spectroscopic data for novel target molecules **160a-g**

	δ: ppm				
Compd	NH & benzylic H	C-2	Pyridyl H-3	H-4	H-5
160a	One NH at 7.54; the other overlaps with aromatic proton signals	163.2	6.36 (d, *J* = 8.2 Hz).	Overlaps with multiplet in the region 7.40–7.35	6.69 (d, *J* = 7.7 Hz)
160b	Benzylic proton singlet at 5.16 ppm	162.7	6.45 (d, *J* = 8.1 Hz)	7.44 (t, *J* = 8.0, Hz)	6.74 (d, *J* = 7.7 Hz)
160c	Broad amide singlet at 7.58 ppm	138.9	6.54 (d, *J* = 7.8 Hz).	7.31 (t, *J* = 7.5 Hz)	6.92 (d, *J* = 8.1 Hz).
160d	Benzylic multiplet signal in the region 4.29 – 419 ppm.	137.7	6.80 (dd, *J* = 7.8, 0.6 Hz).	Overlaps with multiplet in the range 7.35–7.22	6.89 (dd, *J* = 8.0, 0.6 Hz).
160e	Broad NH singlet; 7.31 ppm	163.3	6.36 (d, *J* = 8.2 Hz).	Overlaps with multiplet in the range 7.50–7.43.	6.77 (d, *J* = 7.7 Hz).
160f	Doublet from benzylic protons at 5.12 ppm.	162.7	6.43 (dd, *J* = 8.1, 0.6 Hz).	Overlaps with multiplet at 7.37–7.28.	6.78 (dd, *J* = 7.8, 0.7 Hz).

The C-N coupling reactions for novel target products **144a-h** were generally efficient ranging in yield from 50 to 79% with the highest yield being obtained for the piperidine analogue (**144d**). The C-O coupling reactions were efficient to excellent ranging from 59–83% for O-coupled targets **160a-b** and **160e-f**. The C-S coupling reactions were excellent with product yields ranging between 83 and 88%.

The O- and S-coupled targets **160a-f** (Table 2.5) generally displayed a more shielding effect on the pyridyl protons H-3 (6.80–6.36 ppm) and H-5 (6.92–6.74 ppm) signals as compared with the primary and secondary amine coupled targets **144a-h** discussed earlier. It was quite interesting to note that the sulfur-coupled targets **160c** and **160d** exerted the highest deshielding effect on the H-3 signal at 6.54 and 6.80 ppm, respectively, among the C-N (**144a-h**) and C-O and C-S coupled (**160a-h**) novel targets.

Table 2.5 shows that the C-2 carbon signals from the C-O coupled targets **160a-b** and **160e-f** were more deshielded than corresponding C-2 signals from the C-S coupled analogues **160c-d**. Another interesting observation was that the C-2 signals in the C-S coupled sulfonamides **160c-d** were shielded to the same extent.

2.4 Antiviral Assay

The novel target pyridyl-benzamides **142a-l**, **151a-e** and **147a-f**; pyridyl-benzylamines **143a-e**, **157a-e** and pyridyl-sulfonamides **144a-h**, **160a-f** and **159a-b** were screened against wild-type HIV using an already established antiviral assay protocol with nevirapine (NVP) as a control drug by Dr. Adriaan Basson at the National Institute of Communicable Diseases, Sandringham, South Africa. Details of the protocol can be found in the Appendix.

The antiviral assay results obtained for the pyridyl-benzamides, pyridyl-benzylamines and pyridyl-sulfonamides are listed in Tables 2.6, 2.7 and 2.8, respectively. The results display the concentration of compound that was required to inhibit 50% of viral activity (IC_{50}). Compound toxicity was measured as CC_{50}, the concentration of compound leading to 50% cell death. The selectivity index (S.I.=CC_{50}/IC_{50}) was included as an indicator of the relative toxicity of the compound to the virus versus to the normal cell. The higher this value, the better the compound as a possible lead.

The IC_{50} and CC_{50} determinations were done in triplicate with the standard deviation (SD) providing the degree of reproducibility for each determination.

2.4.1 Antiviral and toxicity results against wild-type virus

As shown in Tables 2.6–2.8, the novel pyridyl-benzamide targets **142e**, **142g**, **151a**, **151c** and **151e** as well as pyridyl-benzylamine targets **143b** and **143e** were found to be active against wild-type HIV (Fig. 2.11). Unfortunately, all the pyridyl-sulfonamide target molecules were inactive against the virus.

Table 2.6: *In vitro* anti-HIV assay for novel pyridyl-benzamide compounds **142a-l**, **147a-f** and **151a-e**

Compd	Activity		Toxicity		S. Index
	IC_{50} (μM)	S. D.	CC_{50} (μM)	S. D.	
Lead cpd 141	0.261	0.012	28.4	2.6	108.9
142a	30.8	-	31.1	-	1.0
142b	14.4	-	10.0	-	0.7
142c	66.2	-	48.2	-	0.7
142d	36.0	-	37.0	-	1.0
142e	0.689	0.005	28.3	0.07	41.0
142g	5.4	0.4	64.0	9.7	11.8
142h	9.9	0.3	40.5	14.0	4.1
142i	>19	-	46.5	16.9	-
142j	>14.9	-	34.6	3.9	-
142l	>0.7	-	3.2	0.2	-
151a	4.0	0.634	22.9	2.2	5.7
151b	-	-	>100	-	-
151c	9.5	0.2	45.9	1.4	4.8
151d	20.6	-	34.6	-	1.7
151e	8.7	0.4	38.6	1.6	4.4
147a	>100	-	96.7	-	-
147b	>50.8	-	94.3	8.1	-
147c	>28.5	-	73.5	5.5	-
147d	>34.0	-	83.5	5.2	-
147e	>21.2	-	80.2	8.7	-
147f	17.0	3.0	100.0	100.0	5.9
NVP	0.1302	-	-	-	-

Table 2.7: *In vitro* anti-HIV assay for novel pyridyl-benzylamine targets **143a-e** and **157a-e**.

Compd	Activity		Toxicity		S. Index
	IC_{50} (μM)	S. D.	CC_{50} (μM)	S. D.	
143a	inactive	-	78.31	10.1	-
143b	26.17	1.10	83.94	4.35	3.0
143c	inactive	-	41.78	9.00	-
143d	inactive	-	33.25	4.05	-
143e	18.84	2.21	18.84	4.79	3.0
157a	inactive	-	84.14	7.06	-
157b	inactive	-	44.23	12.03	-
157c	inactive	-	>100	-	-
157d	inactive	-	50.72	8.79	-
157e	inactive	-	72.22	13.07	-

Table 2.8: *In vitro* anti-HIV assay for novel pyridyl-sulfonamides targets **144a-h, 160a-f** and **159a-b**.

Compd	Activity		Toxicity		S. Index
	IC_{50} (μM)	S. D.	CC_{50} (μM)	S. D.	
144a	inactive	-	>100	-	-
144b	inactive	-	52.67	13.09	-
144c	inactive	-	>100	-	-
144d	inactive	-	>100	-	-
144e	inactive	-	74.36	0.39	-
144f	inactive	-	66.77	11.22	-
144g	inactive	-	>100	-	-
144h	inactive	-	85.76	6.04	-
160a	inactive	-	78.54	10.79	-
160b	inactive	-	77.15	19.38	-
160c	inactive	-	>100	-	-
160d	inactive	-	85.43	6.46	-
160e	inactive	-	91.66	10.36	-
160f	inactive	-	88.09	8.27	-
159a	inactive	-	>100	-	-
159b	inactive	-	>100	-	-

To our delight, one of the pyridyl-benzamides **142e** (Fig. 2.11) exhibited activity (IC_{50} = 0.689 μM) almost equaling that of our lead compound – imidazo[1,2-*a*]pyridine **141** which was also in the same range as the FDA-approved nevirapine. We also observed that the removal of the chlorine atom from the phenyl ring on moving from **142e** to **142g** resulted in a ten-fold decrease in activity against the wild-type virus. In addition, positional changes of the chlorine atom to the *meta*- or *para*-positions resulted in the total loss of activity as displayed by analogues **147c** (IC_{50} > 28.5 μM) and **147d** (IC_{50} > 34.0 μM), respectively. These observations could be supportive of the synergistic role played by the *ortho*-situated chlorine towards conferring antiviral activity as displayed by compound **142e**.

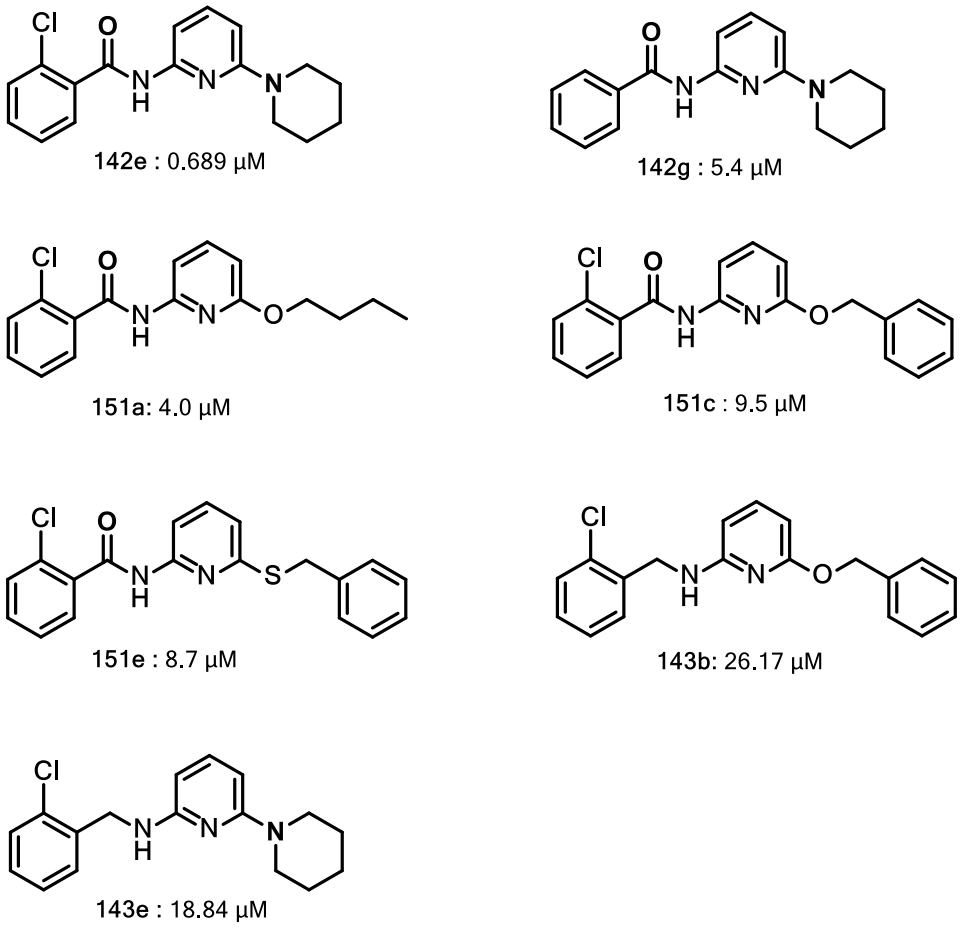

Figure 2.11: Pyridyl-benzamide and –benzylamine analogues that displayed antiviral activity against wild-type RT

More interestingly, Figure 2.11 shows that our original object to benefit from the perceived torsional freedom afforded by reducing **142e** to **143e** was, unfortunately, offset by a thirty-fold loss in original activity. This observation could be indicative of the crucial role played by the

amide link as a possible source of hydrogen bonding interactions between compound **142e** and the receptor binding site. Thus the replacement of the more rigid amide linker by a more flexible methylene group in the benzylamine analogue **143e** may have afforded the chlorophenyl group with too much torsional freedom around the methylene linker. In as much as the concept of increased torsional flexibility has been used beneficially in the design and development of highly potent latest generation antiviral drugs like etravirine **9** and rilpivirine **10**, the conception of compound **143e** shows why increased conformational flexibility may always not be the best possible approach for improving the binding affinity of desired drug-like targets.

Despite the comparatively lower anti-HIV activities (than **142e** and **142g**) displayed by the other pyridyl-benzamide analogues **151a**, **151e** and **151c**, this series of novel compounds generally displayed better activity profiles than observed for the pyridyl-benzylamine and –sulfonamide analogues. Moreover, the lack of activity displayed by the sulfonamides was quite surprising especially given the potential for inducing hydrogen bonding interactions in the binding site via the sulfonamide link. Nevertheless, the better activity profiles shown by the majority of the pyridyl-benzamides could be attributed to the amide functionality's capacity for enhancing the binding affinity of these compounds in RT allosteric site, possibly via hydrogen bonding interactions.

Thirdly, the low antiviral activity displayed by the pyridyl-benzylamine analogues as well as the lack of activity shown by the pyridyl-sulfonamide targets seem to indicate that future modifications aimed at enhancing the anti-HIV activity should focus on other areas rather than replacement of the amide link. In this vein, our opinion is that the crossover from the amide **142** to the benzylamine platform **143** led to an inherent loss of the much-needed hydrogen bonding interactions as the benzylamine analogues **143** became highly flexible and could not be 'locked' in the enzyme's binding site. More specifically, one major drawback associated with increased torsional flexibility arises from the fact that a more structurally flexible ligand naturally has access to many rotational, translational and conformational energy states which gives it high entropic freedom. Logically, the same entropic energy has to be given up if binding into the receptor is to occur as torsional freedom becomes restricted. As such, the energetic cost[16] that has to be paid if successful binding by a more conformationally flexible ligand is to occur becomes unfavorable as the ligand loses access to more degrees of torsional freedom during ligand-receptor binding. This appears to be one of the main reasons why increasing the torsional flexibility of ligands may not always be the best solution for modifying and developing potential drug leads.

We also want to highlight that halogens (F, Cl, Br and I) are normally incorporated in some drug targets primarily to improve their metabolic stability and lipophilicity so that they may easily cross the blood-brain barrier. In some cases, halogens are also incorporated in drug-like molecules to facilitate the repositioning of halogen-carrying motifs into specific hydrophobic pockets via halogen bonding. The latter approach was successfully employed by Jorgensen[17] for designing a small library of catechol diethers that are potent against the wild-type HI virus. Thus, following the virtual ring opening of the lead compound **141**, we retained the chlorophenyl motif as a key substituent that was also expected to be crucial towards repositioning and enhancing the binding affinity of subsequent 2-aminopyridine derivatives of general structures **142**-**144**.

2.4.2 Antiviral results against mutant HIV strains

The lead compound was further screened against selected clinically mutant HIV strains that included E138Q, K101P, K103N, Gl190A, M230I, V106M, Y181C, Y181I and Y188C. The results are shown in Table 2.9

Although novel target molecule **142e** was observed to be potent against wild-type HIV (Table 2.6), the mutant screen results listed in Table 2.9 show that only the V106M mutation with an 8.9 fold lower resistance relative to wild-type was somewhat susceptible to the presence of compound **142e** in the *in vitro* mutant assay. On the other hand, the Y181C mutation displayed borderline susceptibility characterized by a 10.2 decrease in activity relative to wild-type whilst the rest of the mutations were resistant against compound **142e** which lost almost 14 times the original activity displayed against the wild-type virus.

Table 2.9: Antiviral mutant screen results for the new hit compound 142e								
	IC_{50} (μM)		F.C.* (times)		IC_{50} (μM)		F.C. (times)	
Mutant								
	1	2	1	2	Average	S.D.	Average	S.D.
K103N	10.0000	10.000	13.6	13.6	10.000	-	13.6	-
V106M	6.6359	6.4501	9.0	8.8	6.5430	0.1314	8.9	0.2
Y181C	10.0000	10.000	13.6	13.6	10.000	-	13.6	-
Y188C	7.1631	7.8037	9.8	10.6	7.4834	0.4530	10.2	0.6
G190A	10.0000	10.000	13.6	13.6	10.000	-	13.6	0.5
M230I	10.0000	10.000	13.6	13.6	10.000	-	13.6	2.6
K101P	10.0000	10.000	13.6	13.6	10.000	-	13.6	2.2
E138Q	10.0000	10.000	13.6	13.6	10.000	-	13.6	4.9
Y181I	10.0000	10.000	13.6	13.6	10.000	-	13.6	-
Wt. control Average:	0.7472 0.7334	0.7197						

*Fold change with respect to wild type activity

2.5 Molecular Modelling

After a preliminary ligand minimization step, compound **142e** was *in silico*-docked into the allosteric sites of both the wild-type (pdb: 3MEE) and mutant (pdb: 3MEG) HIV-1 RT crystal structure[18] with the top ten poses being ranked on the basis of the magnitude of the ligand-receptor binding (interaction) energies. In addition, lead compound **141** was also docked into the RT allosteric site together with etravirine **9** as a benchmark compound for assessing the binding pose of compound **142e**. Due to similarities between docked ligand poses in both wild-type and mutant crystal structures, only ligand poses and bound conformations obtained for mutant crystal structures were considered in this discussion.

We are cognisant of the traditional *modus operandi* which emphasizes the importance of carrying out molecular modelling prior to the synthesis of target compounds. In our case, the

synthesis of target molecules preceded the molecular modelling exercise given that resources to carry out the latter only became available well after the project had commenced.

2.5.1 Molecular modelling results

As shown in Fig. 2.12, compound **142e** was linearly bound across the NNIB pocket in such a way that the piperidinyl motif was pushed into the hydrophobic cavity flanked by Y181 and Y188 and also displayed 'edge-face' interactions with the Trp229 aromatic side chain.

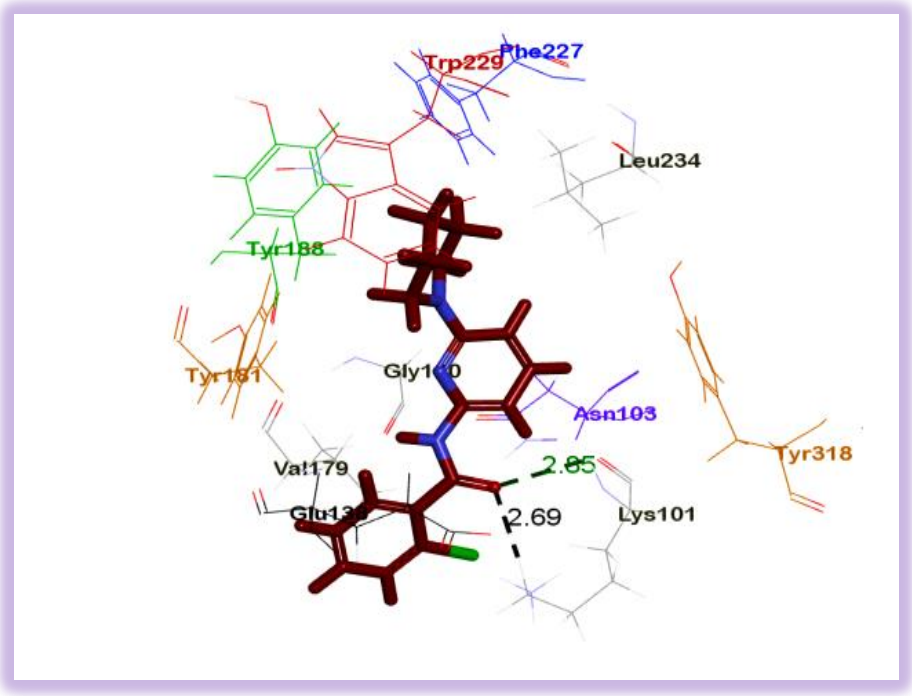

Figure 2.12: Bound conformation of compound **142e** in the NNIBP of HIV-1 RT crystal structure

The central pyridine core appeared sandwiched between Gly190 and Asn103 amino acid residues whilst the hydrophobic 2-chlorophenyl motif occupied the mostly hydrophilic putative entrance to the RT allosteric site. Interestingly, two moderately strong electrostatic contacts (H-bonds: 2.67Å, 2.85Å) were also observed between the amide (carbonyl) functionality of compound **142e** and Lys101 amide-H. The binding hypothesis of compound **142e** appeared to be more reliant on the amide linker's structural rigidity which restricted the top ten poses to similar conformations that basically occupied the same chemical space in the RT allosteric site.

However, the apparent lack of interaction between hit compound **142e** and Glu138 (p51 subunit), Gly190 and the Asn103 side chains – which are some key clinically relevant mutations – could explain low antiviral activity profiles displayed by compound **142e** against these mutations in the *in vitro* mutant HIV screening (Table 2.6).

Contrastingly, compound **141** displayed a "butterfly-like" bound conformation[19] (Fig. 2.13) with the compound **141** deeply pushed into the allosteric site as compared to compound **142e** as shown in the overlaid bound conformations (Fig. 2.14). Lead compound **141** displayed a binding hypothesis that showed hydrophobic interactions between its chlorophenyl motif and RT's Trp229 indole ring as well as some alkyl-alkyl interactions between the amino cyclohexyl outskirt and Leu234 alkyl side chain (Fig. 2.13). The imidazo[1,2-*a*]pyridine core appeared sandwiched in the cavity formed by Val179, Glu138, Asn103 and Lys101 alkyl side chains.

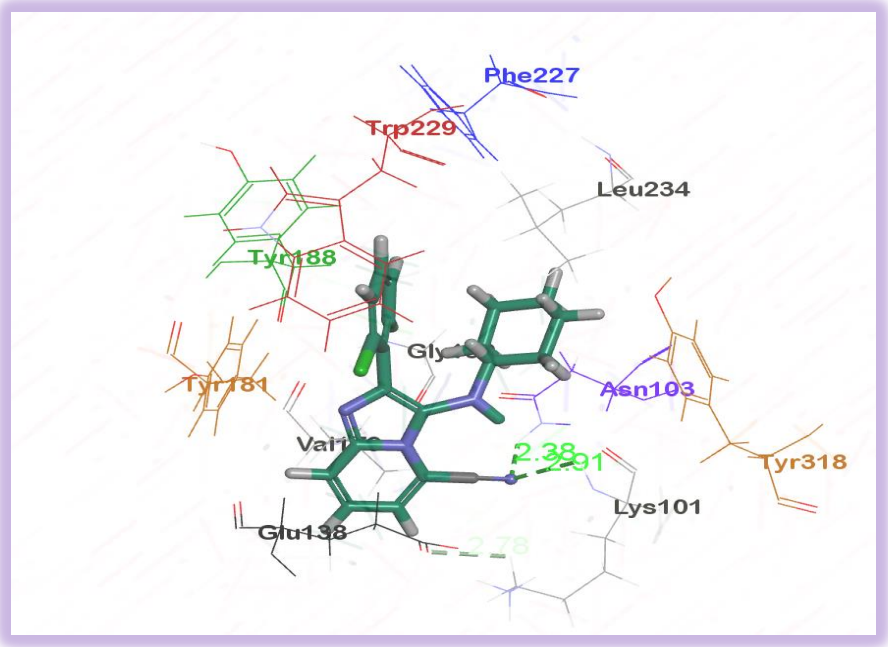

Figure 2.13: Lead compound **141** bound conformation in 3MEG RT NNIBP crystal structure

Another interesting feature relates to the presence of electrostatic interactions (H-bonds) between the CN group of compound **141** and the amide NH functionalities on Asn103 (2.38Å) and Lys101 (2.91Å). Thus, the lead compound's adoption of the ''butterfly-like'' conformation

together with the fact that it was bound more deeply in the allosteric pocket (Fig. 2.14) could have significantly contributed towards achieving a better *in vitro* anti-HIV activity than observed for compound **142e**.

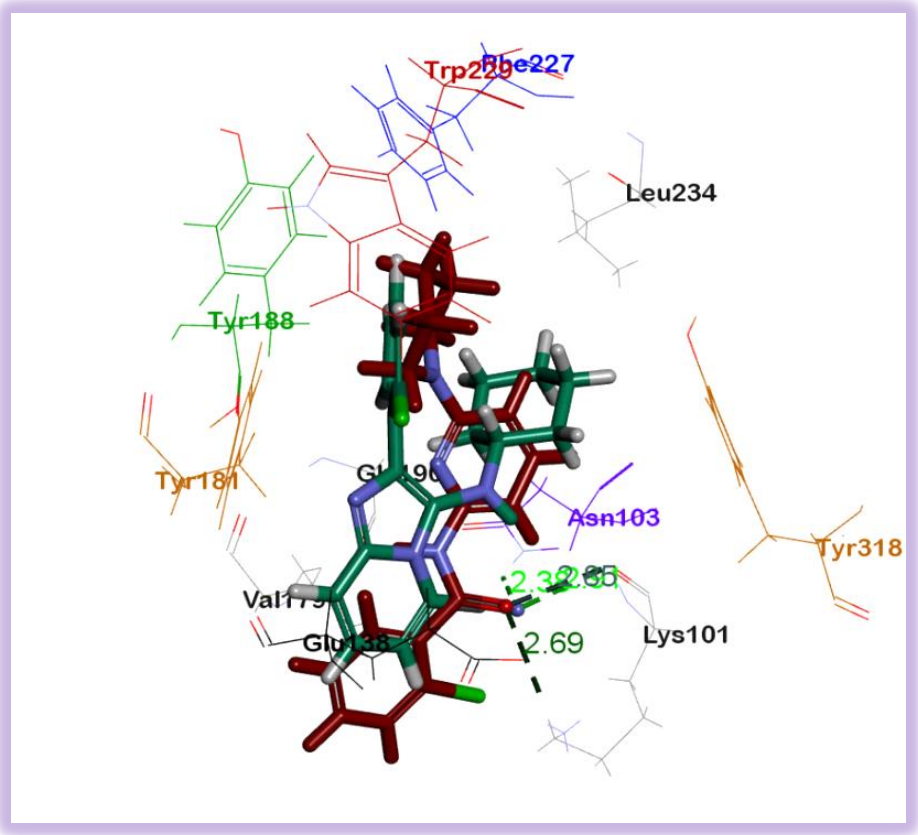

Figure 2.14: Overlaid bound conformation for **141** and **142e** in the RT allosteric site

As expected, the latest generation DAPY-type NNRTI drug etravirine **9** exhibited a favourable "horse-shoe" binding hypothesis in which the compound was docked much deeper in the RT allosteric site whilst the two para-cyano functionalities on the right and left aromatic outskirts appeared buried deeply in the hydrophobic tunnels created by Y181, Phe227 and Trp229 on the left side, and Leu234 and Y318 on the right side (Fig. 2.15).

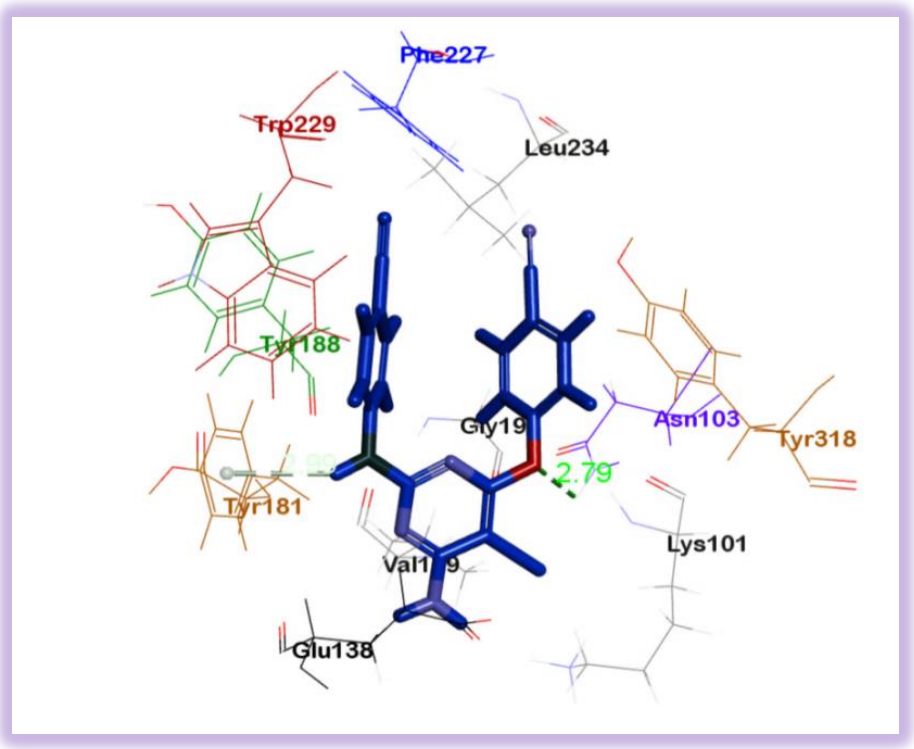

Figure 2.15: Bound conformation of etravirine **9** in the allosteric site of 3MEG crystal structure

Although compounds **141**, **142e** and etravirine **9** appeared to occupy almost the similar chemical space in the allosteric site (Fig. 2.16), the lower activity displayed by compound **142e** against mutant pseudoviruses could be attributed to its linear binding pose and lack of torsional freedom (Fig. 2.12) as opposed to the more flexible and near 'butter fly'-like conformation (Figs 2.13 and 2.14).and horse shoe conformation (Fig. 2.15) exhibited by compound **141** and etravirine respectively.

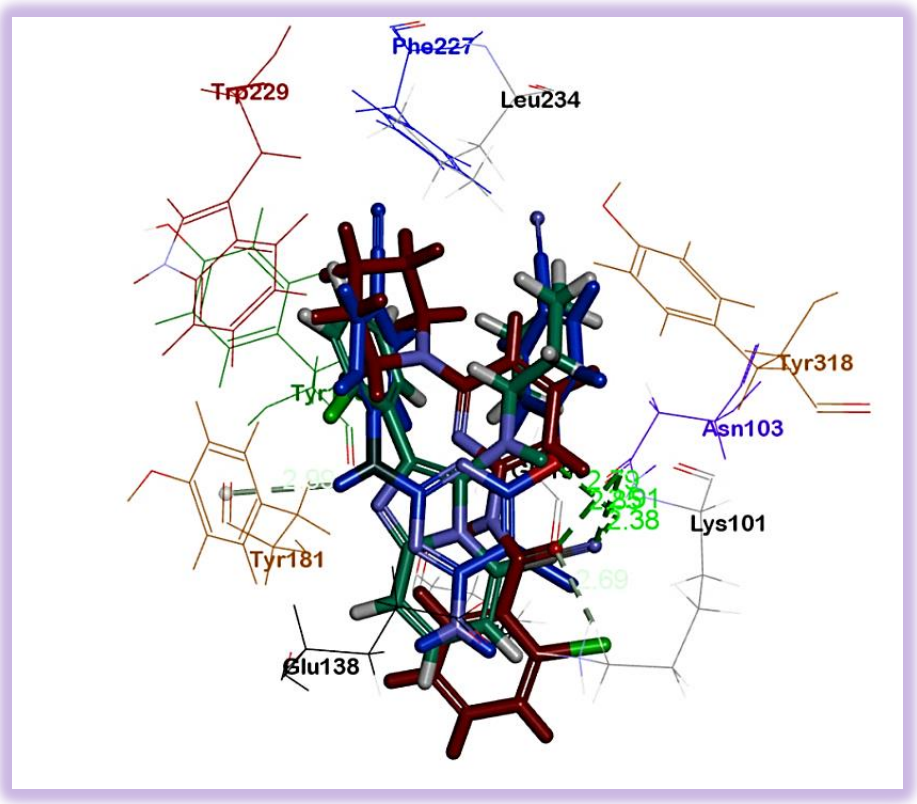

Figure 2.16: Overlaid conformations for compounds **142e** (maroon), **141** (green) and etravirine 9 (blue) docked in allosteric site of 3MEG RT crystal structure.

2.6 Conclusion

A generally versatile palladium-based protocol that employed a Pd_2dba_3/*rac*-BINAP catalyst system was successfully used to cross-couple pyridyl-benzamide, -benzylamine and –sulfonamide scaffolds with selected nitrogen-, oxygen- and sulfur-containing nucleophiles. The *rac*-BINAP ancillary ligand offered the most efficient option due to its suitable steric, electronic and chelation properties which stabilized the active palladium species to suppress β-hydride elimination in favour of reductive elimination and product formation. After screening the target compounds against wild-type RT, a novel pyridyl-benzamide hit compound **142e** was identified as a potential NNRTI lead candidate. The activity of this compound was found to be 0.689 μM in a whole-cell pseudo-virus assay. In the same way, the FDA-approved NNRTI nevirapine had an activity of 0.130 μM. *In silico* docking results showed that compound **142e** displayed a linear binding conformation in which the piperidinyl motif occupied the hydrophobic cavity flanked by Y181, Y188 and Trp229 whilst the *ortho*-chlorophenyl outskirt protruded outside the NNIB

pocket entrance lined by E138 and K101 hydrophilic residues. Such interactions together with two electrostatic contacts (H-bonds) between compound **142e**'s amide-O and K101 amide-H could explain compound **142e**'s potent activity against the wild-type pseudo virus. On the other hand, the absence of electrostatic contacts between analogue **142e** and Gl190A, E138 and K103N hydrophilic residues lining the pocket entrance could also explain the lower activity of novel compound **142e** displayed against the mutant HIV strains.

2.7 References

1. Zhan, P.; Chen, X.; Li, D.; Fang, Z.; de Clercq, E. and Liu, X., *Med. Res. Rev.* **2013**, 33 (S1) E1 - E72.
2. Bode, M. L.; Gravestock, D.; Moleele, S. S.; van der Westhuysen, C. W.; Pelly, S. C.; Steenkamp, P. A.; Hoppe, H. C.; Khan, T. and Nkabinde, L. A. *Bioorg. Med. Chem*. **2011**, 19, 4227 – 4237.
3. Montalbetti, C. A. G. N. and Falque, V. *Tetrahedron*, **2005**, 61, 10827 – 10852.
4. Sambiagio, C.; Marsden, S. P.; Blacker, A. J. and McGowan, P. C. *Chem. Soc. Rev.*, 2014, 43, 3525 – 3550.
5. Enguehard, C.; Allouchi, H.; Gueiffer, A. and Buchwald, S. L. *J. Org. Chem*. **2003**, 68, 4367 – 4370.
6. Beletskaya, I. P. and Chaprakov, A. V., *Coord. Chem. Rev.* **2004**, 248, 2337 – 2364.
7. Paul, F.; Patt, J. and Hartwig, J. F. *J. Am. Chem. Soc*. **1994**, 116, 5969 – 5970.
8. Wolfe, J. P. and Buchwald, S. L. *J. Org. Chem*. **2000**, 65, 1144 – 1157.
9. Shen, Q.; Ogata, T. and Hartwig, J. F. *J. Am. Chem. Soc*. **2008**, 44, 1371 – 1375.
10. Kamer, P. C. J.; van Leeuwen, P. W. N. M. and Reek, J. N. H. *Acc. Chem. Res*. **2001**, 34, 895.
11. Beletskaya, I. P. and Chaprakov, A. V. *Organometallics*, **2012**, 31, 7753 – 7808.
12. Kosugi, M.; Kameyama, M. and Migita, T. *Org. Lett*. **1983**, 927 – 928.
13. Shen, Q.; Shekhar, S.; Stambuli, J. P. and Hartwig, J. F. *Angew. Chem. Int. Ed*. **2005**, 44, 1371 – 1375.
14. Castillo-R., P. and Buchwald, S. L. *Chem. Rev*. **2016**, 116, 12564 – 12649.
15. Kang, D.; Ding, X.; Wu, G.; Huo, Z.; Zhou, Z.; Zhao, T.; Fang, D.; Wang, Z.; Tian, Y.; Daelemans, D.; De Clercq, E.; Pannecouque, C.; Zhan, P. and Liu, X. *ACS Med. Chem. Lett.* **2017**, 8, 1188 – 1193.
16. Mobley, D. L. and Dill, K. A. *Structure* **2009**, 17, 489 – 498.
17. Frey, K. M.; Bollini, M; Mislak, A. C.; Cisneros, J. A.; Gallardo-Macias, R.; Jorgensen, W. L. and Anderson, K. S. *J. Am. Chem. Soc*. **2012**, 134, 19501 -19503.
18. Landson, E. B.; Brendza, K. M.; Hung, M.; Wang, R.; Mukund, S.; Jin, D.; Birkus, G.; Kutty, N. and Liu, X. *J. Med. Chem*. **2009**, 17, 5744.
19. Janssen, P. A.; Lewi, P. J.; Arnold, E.; Daeyaert, F.; de Jonge, M.; Heeres, J.; Koymans, L.; Vinkers, M.; Guillemont, J.; Pasquier, E.; Kukla M.; Ludovici, D.; Andries, K.; de Béthune, M.P.; Pauwels, R.; Das, K.; Clark, A. D. Jr.; Frenkel, Y. V.; Hughes, S. H.; Medaer, B.; De Knaep, F.; Bohets, H.; De Clerck, F.; Lampo, A.; Williams, P. and Stoffels, P. *J. Med. Chem*. **2005**, 48, 1901 – 1909.

3.0 Introduction

The research findings discussed in this chapter complement our research efforts detailed in Chapter 2 in which we developed transition metal-catalyzed protocols as key steps towards constructing the desired novel target molecules. Our second approach, described here, involved the use of molecular modelling in the virtual design of potential NNRTI compounds that contain pyridine, pyrimidine and triazine central cores. Top modelling hits that displayed a favourable conformational pose in the RT allosteric site (pdb: 3MEG RT)[1] (Fig. 3.1) were synthesized as candidates for a primary screen against the wild-type HI virus.

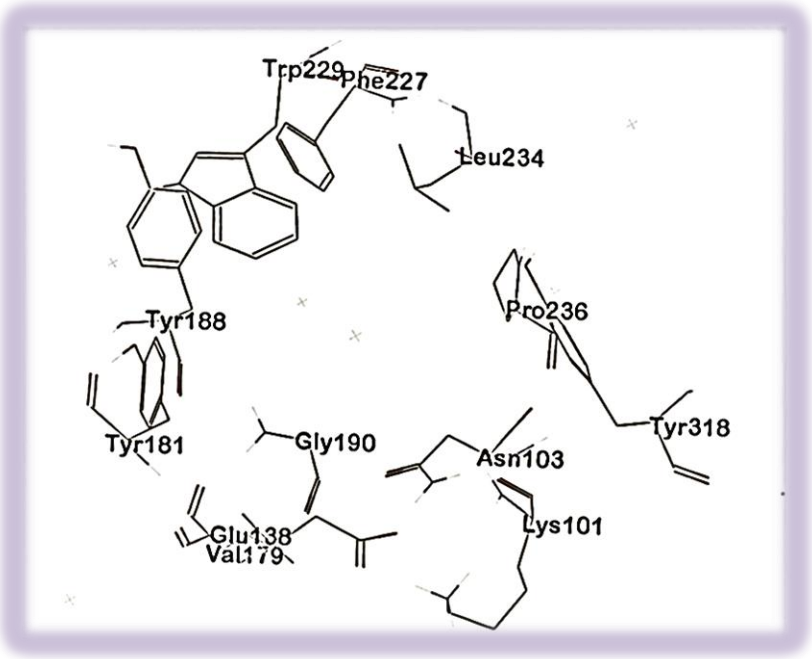

Figure 3.1: Schematic representation of key amino acid side chains in the NNIBP of 3MEG RT

Inspired by the high potency displayed by etravirine **9** against the wild-type and most drug-resistant RT mutants, we wanted to develop novel target molecules bearing flexible O- and N(H)-linked aromatic substituents. These motifs were expected to be crucial in exploring the hydrophobic spaces surrounded by Try181, Tyr188, Phe227 and Trp229 aromatic side chains on the top left side of the RT allosteric site, as well as Leu234, Pro236 and Tyr318 on the top right side (Fig. 3.1). Thus, our first challenge was to identify suitable aromatic groups which

could fulfill such a function. More importantly, the rationale was that the torsional freedom afforded by the hetero-linkers (O- and N(H)) could also enable the target molecules to avoid steric clashes in the RT allosteric site by reorienting and repositioning to adopt conformations which could enhance hydrophobic binding. Secondly, the hetero-linkers also offered potential hydrogen bond donors and acceptors via which electrostatic interactions with hydrophilic residues could enhance the binding affinities of the target molecules in the RT NNIBP.

In this regard, 4-chlorophenol, 2-amino-4-methylbenzonitrile and piperidine were selected as possible candidates for coupling onto the 2- and 6-positions of the central heterocyclic cores. Firstly, 4-chlorophenol presented an interesting variation from the usual *para*-substituted anilines that have become synonymous with the construction of potent NNRTIs like the benzo-fused efavirenz and multi-cyclic tivirapine and rilpivirine.[2] Secondly, 2-amino-4-methylbenzonitrile also provided an unexplored candidate as an NH-attached substituent whose methyl and nitrile substituents were viewed as an interesting combination for probing the chemical spaces in the NNIBP. Lastly, we selected piperidine on the basis that our piperidine-substituted pyridyl-benzamide hit compound **142e**, previously identified in Chapter 2, had displayed excellent *in vitro* activity against the wild-type HI virus.

Our second challenge was to identify potential functional groups which could be tethered onto the central heterocyclic cores to initiate electrostatic contacts with hydrophilic amino acid residues (K101, N103, E138) lining the NNIBP entrance (Fig. 3.1). The 3-position and 4-position of the pyridine nucleus provided possible sites for tethering such handles whilst, for practical reasons, the 4-position was selected for the pyrimidine nucleus. As such, carbonitrile (CN), carboxamide and cyclopropylamide groups were selected as synthetic handles for the pyridine nucleus, whilst in addition to the aforementioned groups, chloride was also chosen for functionalizing the pyrimidine core as will be explained in subsequent sections.

In this vein, our first approach involved designing the first set of novel target molecules containing di-functionalized pyridine cores resembling the conformationally flexible Janssen-type topology[1] as will be discussed in the next section.

3.1 Molecular Modelling Phase 1 – 2, 6-di-substituted pyridines

We used molecular modelling as a guide to select potential target compounds for synthesis. Our first set of virtual analogues were based on a 2,6-disubstituted pyridine platform as a torsionally flexible template onto which any combination of 4-chlorophenoxy- or 2-amino-4-methylbenzonitrile or piperidinyl motifs were coupled (Fig 3.2). After an *in situ* ligand

minimization step, the low energy conformations from the virtual ligands **161**, **162** and **163** (Fig. 3.2) were docked into the allosteric site of the **3MEG RT** crystal structure[2] (Fig. 3.1).

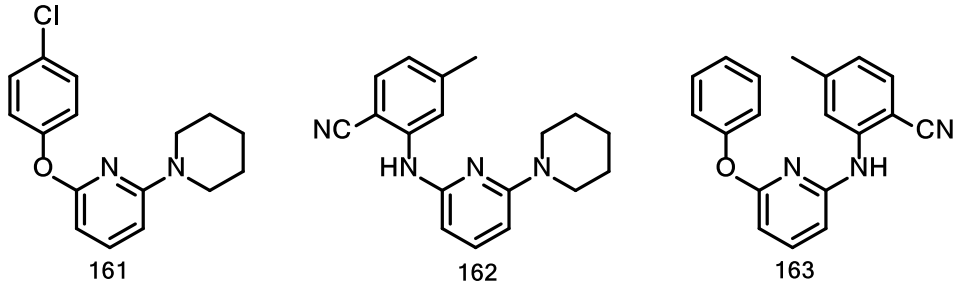

Figure 3.2: Structures of pyridine-based virtual compounds **161**, **162** and **163**

To our delight, the three virtual analogues **161-163** displayed a favourable bound conformation in which the piperidinyl or 4-chlorophenoxy or 2-amino-4-methylbenzonitrile motifs showed preference for hydrophobic interactions with Tyr181, Tyr188, Phe227 and Trp229 (top left side) as well as Leu234, Pro236 and Tyr318 side chains (top right hand side) surrounding the 3MEG-RT binding site. Unfortunately, the lack of hydrogen bonding groups on the central pyridine cores appeared to be a limitation which prevented any hydrogen bond formation between the central core and the hydrophilic residues (K101, K103N, E138) lining the putative entrance to the RT NNIBP. Nonetheless, the three virtual analogues were synthesized as the first set of novel target molecules for a preliminary screen against the wild-type virus.

3.2 Synthesis of novel targets 161, 162 and 163

Retrosynthetic analysis of **164** as a representative scaffold for target molecules **161** and **162**, showed that these compounds could be accessed from intermediate scaffold **165** via palladium-catalyzed C-N or C-O cross-coupling[3] of **165**, which could be derived from commercially available 2,6-dibromopyridine **168** (Scheme 3.1).

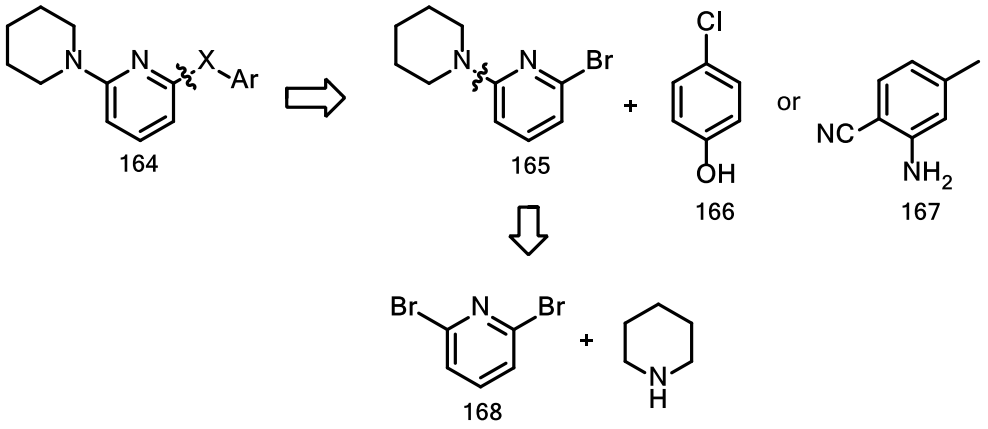

Scheme 3.1: Retrosynthetic analysis of target scaffold **164**

3.2.1 Synthesis of intermediate scaffold 165

Scaffold **165** was accessed via a palladium-catalyzed amination of commercially available 2,6-dibromopyridine **168** with piperidine (Scheme 3.2).

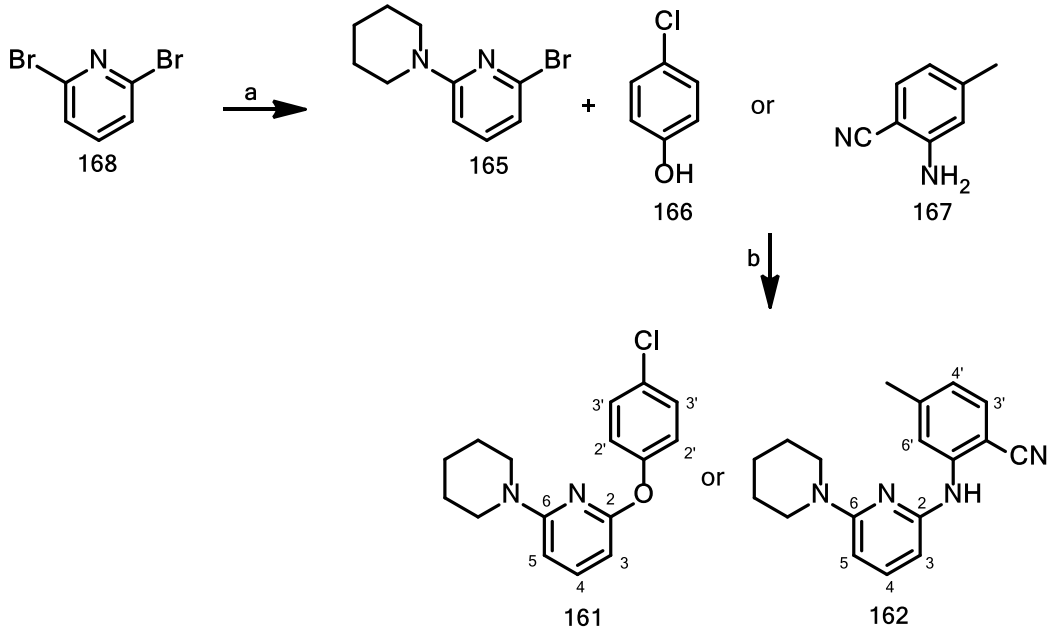

Scheme 3.2: *Reagents and conditions:* (a) cat. 2 mol% Pd_2dba_3/*rac*-BINAP, DMF, 1.3 eq. piperidine, 1.2 eq. KO^{t}Bu, 125 -130°C, 24 h, 89%; (b) i) same catalyst system as in (a), 1.3 eq. **166**, 1.2 eq. KO^{t}Bu, 135-140°C, 24 h; 65% or ii) same catalyst system as in (a), 1.5 eq. **167**, 1.2 eq. KO^{t}Bu, 125-130°C, 24 h, 65%.

Intermediate **165** was obtained in good yield (89%) and confirmed by ^{1}H NMR spectroscopy which showed the presence of three aromatic proton signals and ten piperidyl proton signals in

the aliphatic region. The pyridyl H-3 appeared as a doublet at 6.66 ppm (J = 7.4 Hz) and coupled with H-4 which gave a doublet of doublets at 7.23 ppm (J = 8.4, 7.4 Hz), whilst H-5 was observed as another doublet at 6.49 ppm (J = 8.4 Hz). Piperidyl protons gave two groups of multiplets in the regions 3.52–3.49 ppm (4H) and 1.62–1.60 ppm (6H) in the aliphatic region. The ^{13}C NMR spectral data showed five carbon signals comprising two quaternary and three CH signals, as well as three CH_2 signals in the aliphatic region. The C-2 signal, which appeared much deshielded at 159.3 ppm, confirmed successful bromine substitution.

3.2.2 Synthesis of novel target 161 and 162

Target molecules **161** and **162** were finally obtained in 65% and 79% yield, respectively, by cross-coupling **165** with 4-chlorophenol **166** or 2-amino-4-methylbenzonitrile **167** (Scheme 3.2 b).

^{1}H NMR spectroscopy for target molecule **161** showed successful C-O bond formation as evidenced by the presence of an additional four protons which appeared as two sets of multiplets in the range 7.30–7.27 ppm (H-2'', 2H) and 7.09–7.07 ppm (H-3'', 2H). On the other hand, novel target **162** gave four additional proton signals (H-3', H-4', H-6' and an amino proton) in the aromatic region and an aliphatic signal for three protons at 2.35 ppm arising from the C-N coupled 2-amino-4-methylbenzonitrile motif. Proton H-3' overlapped with the H-4 triplet at 7.37 ppm, whereas H-4' also overlapped with amino proton (NH) at 6.74 ppm, whilst H-6' gave a singlet signal at 8.14 ppm. ^{13}C NMR spectroscopic analysis of target **161** showed nine aromatic carbon signals and three aliphatic carbon signals from the piperidinyl motif. Novel target **162** displayed twelve carbon signals in the aromatic region including the CN signal and four aliphatic carbon signals. 2D NMR spectroscopy confirmed successful C-O coupling at C-2 by showing a quaternary carbon signal at 162.1 ppm for compound **161** whilst HRMS data analysis ($[M+H]^+$: 336.0898) confirmed successful formation of target product **162**.

3.2.3 Synthesis of target molecule 163

Retrosynthetic analysis showed that target compound **163** could be accessed from scaffold **168** via a tandem palladium-catalyzed C-N and C-O cross-coupling of 2-amino-4-methylbenzonitrile **167** and 4-chlorophenol **166.**

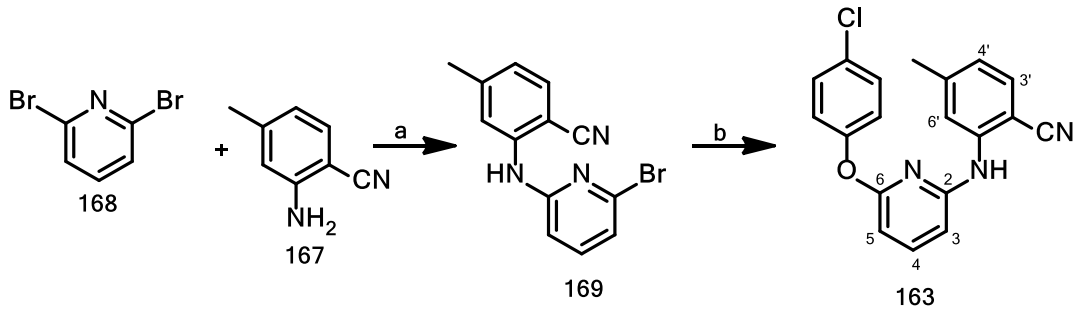

Scheme 3.3: *Reagents and conditions:* (a) cat. 2 mol% Pd_2dba_3/*rac*-BINAP, DMF, 1.3 eq. **167**, 1.2 eq. KO^{t}Bu, 67%; (b) cat.[2 mol% Pd_2dba_3/*rac*-BINAP], DMF, 1.3 eq. 4-chlorophenol **166**, 1.2 eq. KO^{t}Bu, 74%;

Intermediate scaffold **169** was prepared by cross-coupling 2-amino-4-methylbenzonitrile **167** with substrate **168** and the intermediate was confirmed by ^{1}H NMR spectroscopy (Scheme 3.3). Palladium-catalyzed amination of intermediate **169** with phenol **166** afforded target product **163** in reasonable yield. NMR spectroscopic and HRMS analysis confirmed successful C-O and C-N bond formation in the target product.

3.2.4 Antiviral Assay

Novel target molecules **161**, **162** and **163** were screened against the wild-type HI virus by our collaborators at National Institute of Communicable Diseases, Sandringham, South Africa, using nevirapine (NVP) as a control drug (Table 3.1). The IC_{50} and CC_{50} assays were done in triplicate with standard deviation measuring the degree of reproducibility for each set of results.

Table 3.1: *In vitro* anti-HIV assay results for novel targets **161**, **162** and **163**

Entry	Activity		Toxicity	
	IC_{50} (μM)	S. D.	CC_{50} (μM)	S. D.
161	>26.8	-	81.7	1.9
162	>24.8	-	79.5	3.8
163	>28.1	-	82.4	8.4
NVP	0.111	0.111	-	-

Although the novel compounds **161** – **163** were non-cytotoxic against the pseudovirus, they were inactive against the wild-type HI virus (Table 3.1). The lack of antiviral activity could be attributed to the absence of any hydrogen bonding interaction between the central pyridine core and the hydrophilic residues (K101, N103, E138) surrounding the entrance channel to the NNIBP, as previously observed during the molecular modelling exercise.

3.3 Molecular Modelling Phase 2 – Tri-functionalized virtual analogues

As a way to encourage hydrogen bonding interactions between the functionalized pyridine, pyrimidine and triazine central cores and hydrophilic groups in the RT allosteric site, we designed a further set of virtual molecules with tri-functionalized central cores as an improvement from the di-functionalized analogues (Fig. 3.2) by tethering synthetic handles (CN, carboxamide, cyclopropylamide and Cl) to generate the tri-functionalized library shown in Figure 3.3. The small library of compounds **170**–**180** was minimized and *in silico* docked into the allosteric site of 3MEG-RT crystal structure (Fig. 3.1), using etravirine **9** as a benchmark compound.

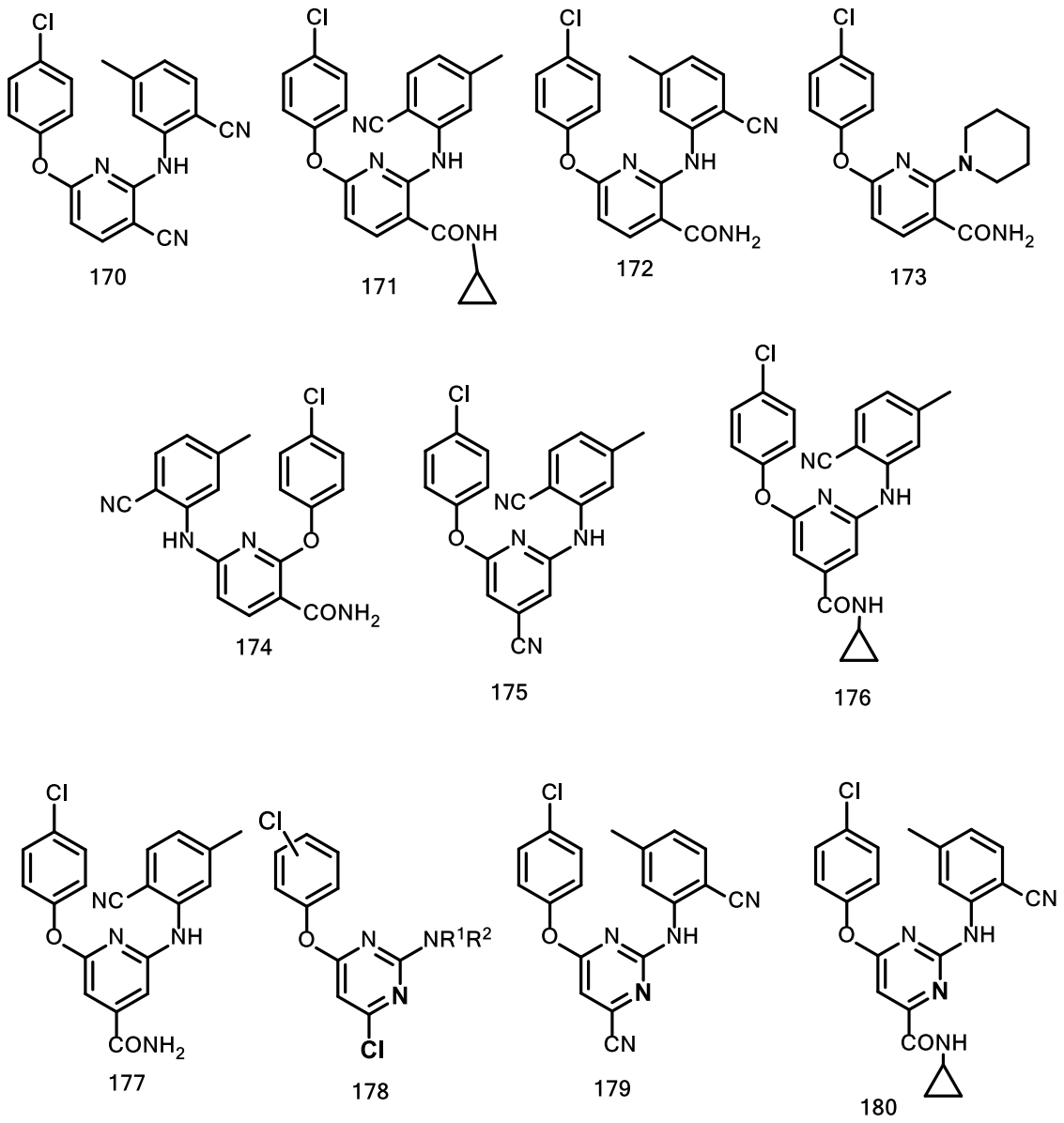

Figure 3.3: Virtual library of tri-functionalized pyridine-, pyrimidine-, and triazine-based analogues

The top hits were ranked on the basis of the magnitude of ligand-receptor interaction energies and also selected based on their tendency towards displaying a favourable bound pose that targeted key hydrophobic and hydrogen bonding groups in the allosteric site.

3.3.1 Molecular Modelling Results

Virtual analogue **174** bearing a carboxamide functionality *ortho* to the 4-chlorophenoxy substituent (Fig. 3.4) and analogue **172** with an amide group situated *ortho* to the 2-amino-4-

methylbenzonitrile motif (Fig. 3.5) emerged as the top hits from the molecular modelling protocol.

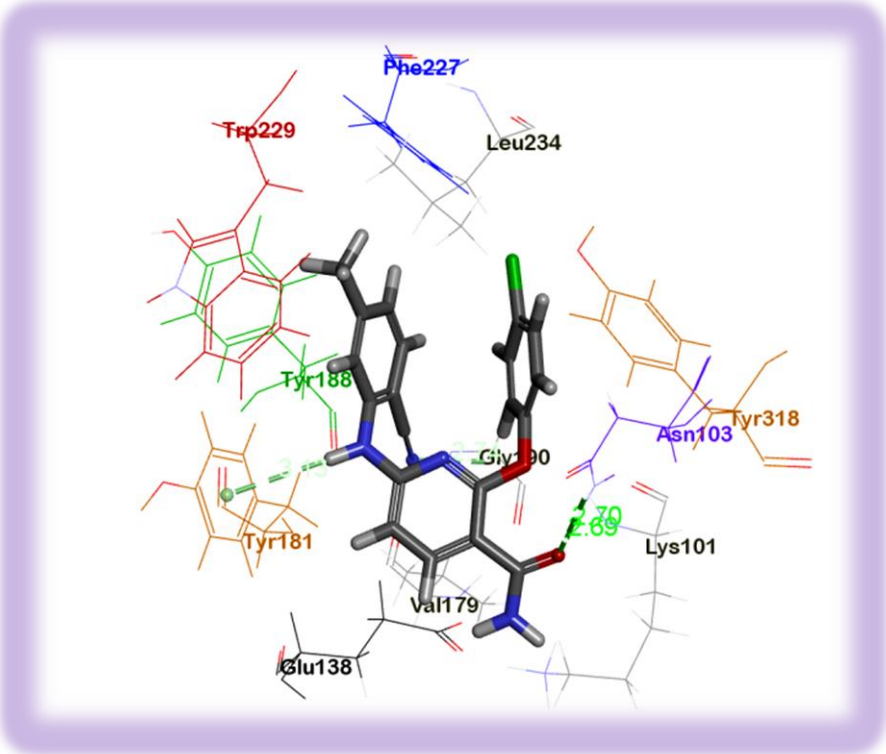

Figure 3.4: Bound conformation of analogue **174** in the allosteric site of 3MEG RT

As shown in Fig. 3.4, a nicotinic acid-derived carboxamide derivative **174** displayed promising hydrophobic interactions characterized by the sandwiching of the 2-amino-4-methylbenzonitrile motif within the hydrophobic cavity created by side chain residues from Trp229, Tyr188 and Leu234. In addition, analogue **174** also showed π-π stacking interactions between the 4-chlorophenoxy motif and the Tyr318 side chain as well as the 'edge-face' interactions between benzonitrile amino (NH) proton and the Tyr181 phenyl group. Furthermore, two electrostatic contacts were also observed between the carbonyl-O on the analogue's amide functionality and NH groups of the Asn103 and Ly101 side chain residues (RT).

Another interesting observation was that **174** also appeared to occupy the same chemical space as etravirine as shown by the overlaid poses in Fig. 3.5. Thus, in our view, accessing such torsionally flexible compounds appeared worthwhile as they could have antiviral activity profiles comparable with etravirine.

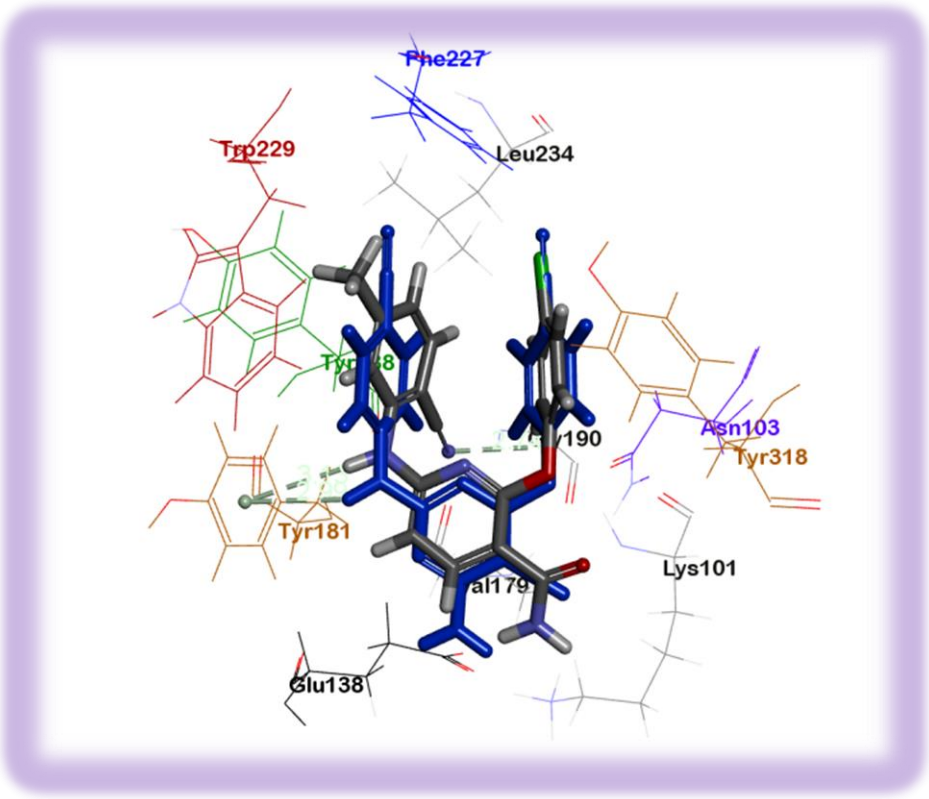

Figure 3.5: Overlaid conformations of **174** and etravirine poses in 3MEG RT allosteric site

Analogue **174** displayed a similar binding hypothesis to that of **172**, which was characterized by hydrophobic interactions between the 4-chlorophenoxy group and Tyr 181, Tyr188 and Trp229 as well as that between 2-amino-4-methylbenzonitrile motif and Leu234 and Tyr318 side chains. Interestingly, three electrostatic interactions were observed between Gly190 and the CN group; amino proton and carbonyl-O on K101 as well as carboxamide-O and N103 residue.

The binding conformations displayed by analogues **172** and **174** were considered as favourable towards enhancing inhibitor binding affinity in the RT allosteric site in comparison with the docked poses of the isonicotinic acid-derived carboxamide **177** (Fig. 3.6). Although analogue **177** formed electrostatic contacts with K101 and N103 via the O-linker, an additional interaction between the carbonyl-O on the carboxamide group and K101 appeared to pull **177** downwards towards the RT pocket entrance (Fig. 3.6). This reduced overall interactions of the hydrophobic outskirts with Trp229 or Tyr181 or Tyr318.

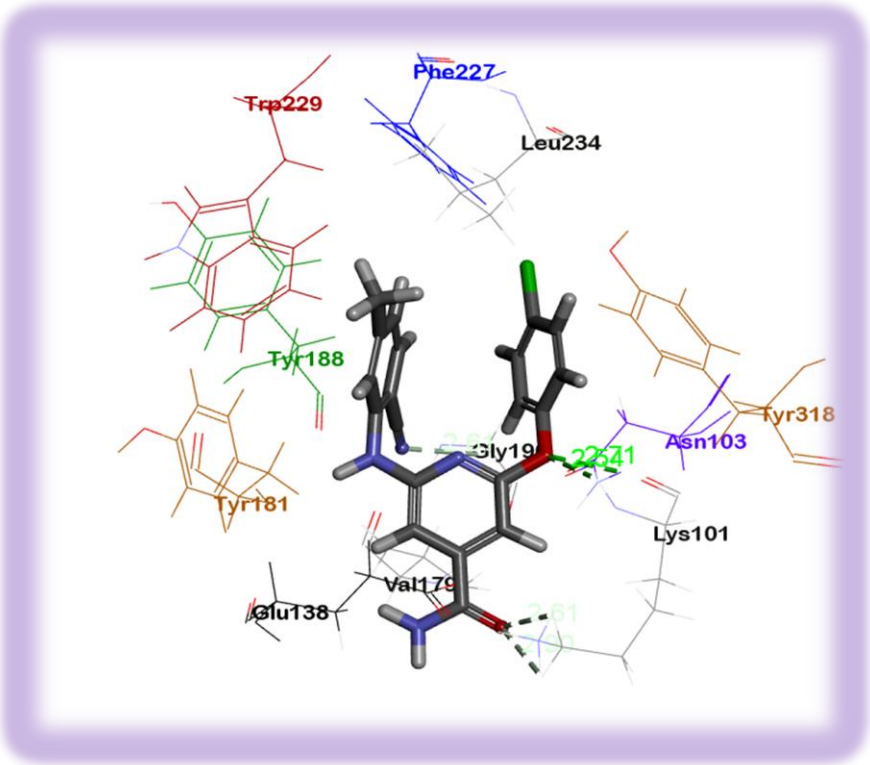

Figure 3.6: Bound conformation of isonicotinic acid-based carboxamide **177** in the allosteric site 3MEG RT

In the same vein, cyclopropylamide-based derivatives **171** (Fig. 3.7) and **176** (Fig. 3.8) also showed promising binding conformations, albeit with inferior binding energies to both **172** and **174**. Docking results showed poses in which the analogues **171** and **176** were pulled towards the pocket entrance with the cyclopropyl motif of **176** being sandwiched between the hydrophilic space flanked by E138 and K101 residues.

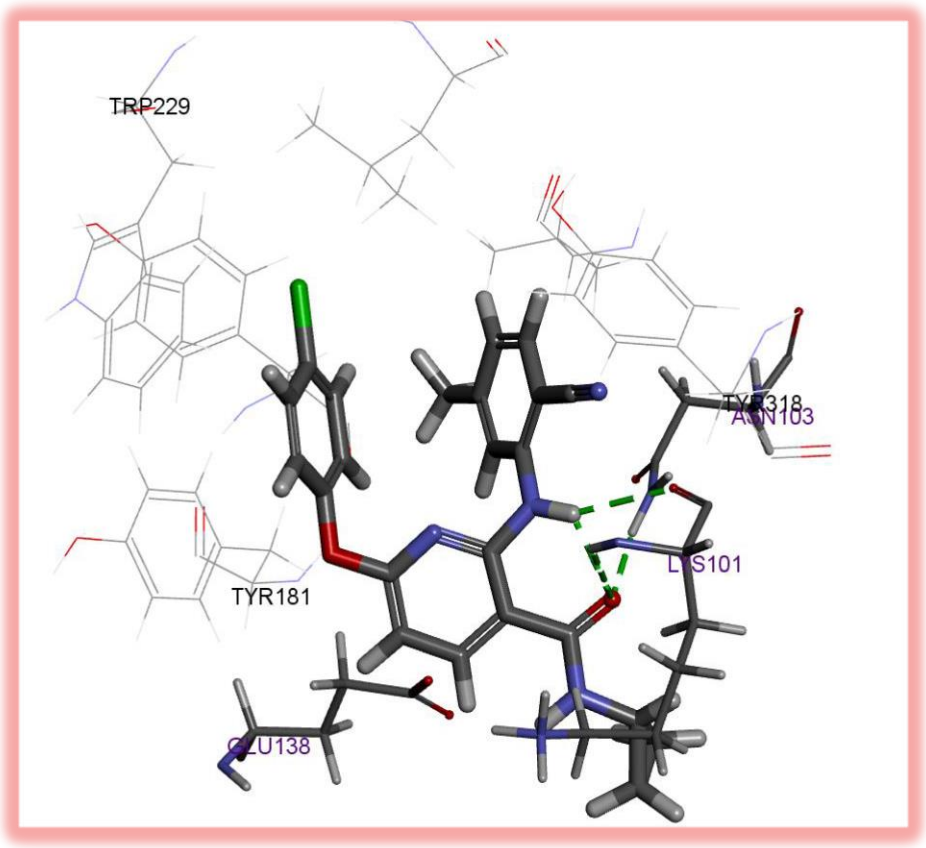

Fig.3 7: Bound conformation of nicotinic acid-based analogue **171** in 3MEG RT allosteric site

Although such binding conformations were also observed for methoxy- and ethoxy-ester and pyrimidine-based cyclopropyl amide **180**, during the *in silico* docking routine, analogues **171**, **176** and pyrimidine derivative **180** were included as synthetic targets given their binding hypothesis which was superimposable with etravirine. Similarly, nitrile-based derivatives **170**, **175** and **179** were also synthesized for exploratory purposes.

We also considered synthesizing **173** and the pyrimidine-based analogues bearing general structure **178** in order to broaden the analogue library for a primary screen against the wild-type RT. In addition, triazine derivatives of general structure **181** were synthesized following an interesting binding poses (in the RT allosteric site) in which the triazine-linked Cl group preferentially occupied the hydrophilic cavity flanked by K101, E138 and N103 residues. Although the ligand-receptor interaction energies of the triazine analogues were inferior to those observed for analogues **171-2**, **174** and **176**, we also wanted to assess the biological significance, if any, of such unique halogen bonds via an in vitro assay.

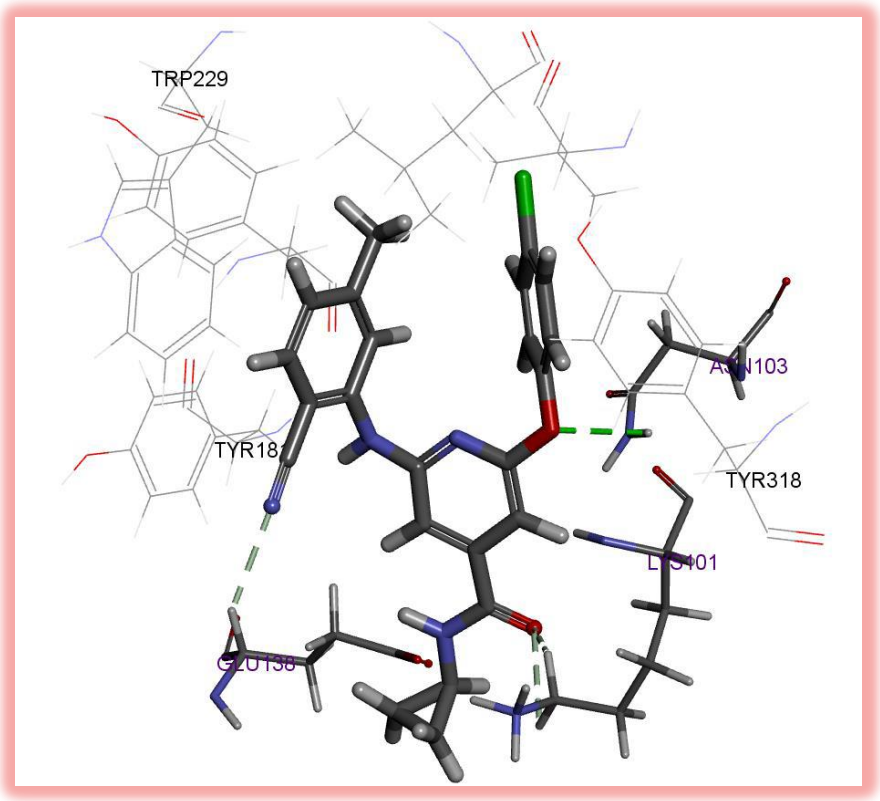

Figure 3.8: Bound conformation of cyclopropylisonicotinamide analogue **176** in 3MEG RT NNIBP

3.4 Chemistry

3.4.1 Synthesis of pyridine-based amide and nitrile derivatives

A general retrosynthetic analysis was utilized to plan the synthesis of novel pyridine-based amide and nitrile derivatives of general structure **182** (Scheme 3.4).

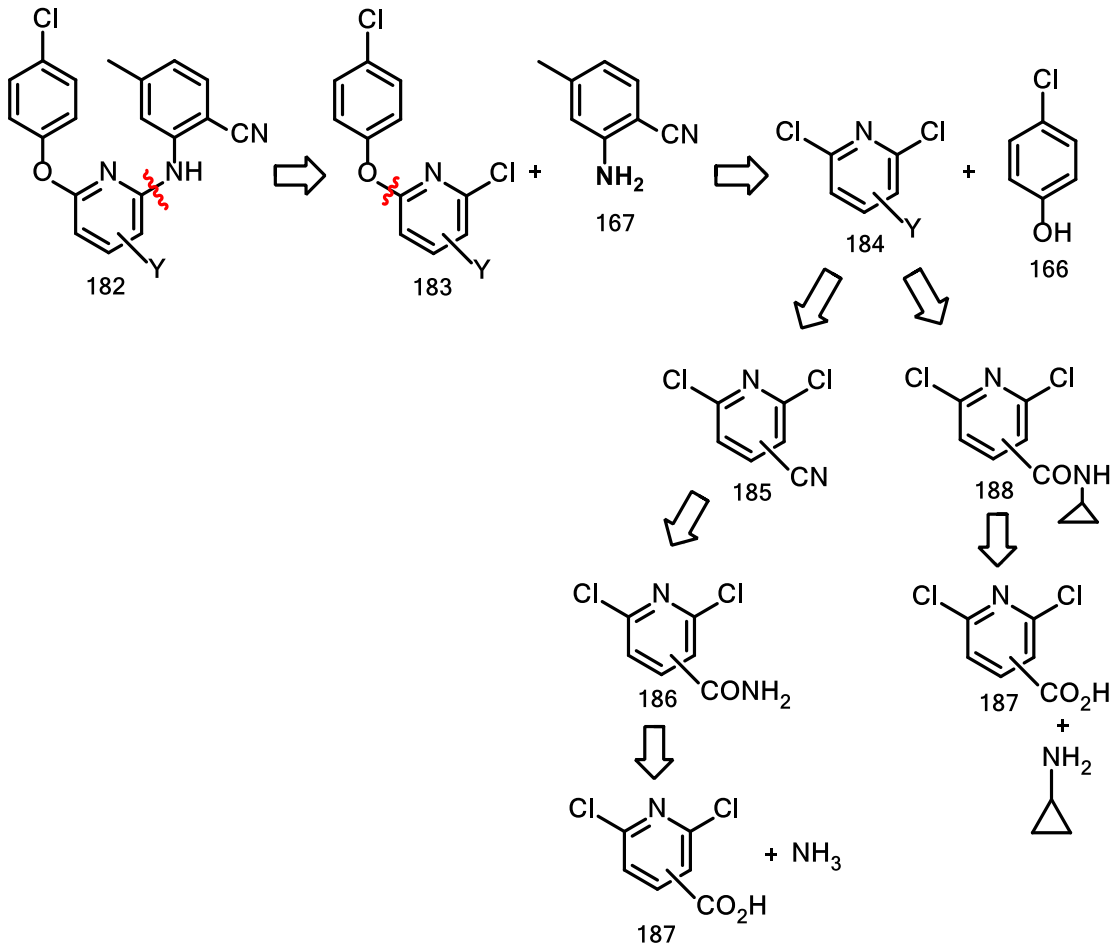

Scheme 3.4: Retrosynthetic analysis of general scaffold **182**

Target compounds **170** and **175**, **171** and **176** as well as **172** and **177** were accessed via the initial synthesis of intermediate scaffolds **185**, **187** and **188**, respectively (Scheme 3.4).

3.4.1.1 Synthesis of novel nitrile-based derivative 170

Target carbonitrile derivative **170** was constructed via intermediate compound **185** which was synthesized using the thionyl chloride activation of commercially available 2,6-dichloronicotinic acid **187a**. The resulting acyl halide was reacted with aqueous ammonia to generate the carboxamide intermediate **186a** in quantitative yield (Scheme 3.5).

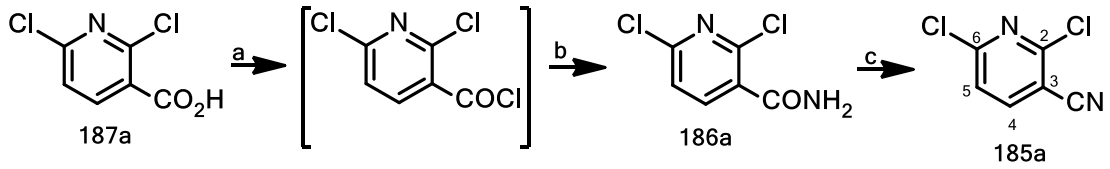

Scheme 3.5: *Reagents and conditions*; (a) $SOCl_2$, 80°C, 24 h; 99%; (b) 25% aq. NH_3, 0°C-RT, 4 h; 100%; (c) $POCl_3$, 80-100°C, 4 h; 96%.

As expected, ^1H NMR spectroscopic analysis showed the presence of a broad singlet proton signal at 7.50 ppm signifying the presence of the two amide protons in compound **186a**[4]. In addition, the ^{13}C NMR spectrum showed that the amide carbonyl signal had shifted upfield to 165.9 ppm as compared to the more deshielded range ≥168 ppm in substrate **187a**. The NMR spectroscopic data is consistent with that already found in literature.[4]

Dehydration of 2,6-dichloronicotinamide **186a** via the conventional $POCl_3$-mediated methodology obtained from literature[5] afforded the carbonitrile **185a**[6] (96%). ^1H NMR spectroscopy showed pyridyl protons H-4 and H-5 as coupled doublets at 7.95 (d, J = 8.1 Hz) and 7.43 ppm (d, J = 8.1 Hz), respectively. The ^{13}C NMR spectrum showed the expected five aromatic carbon signals and the CN signal at 114.7 ppm (CN) which was in agreement with the literature data produced by Bach and coworkers.[6]

As an initial step towards accessing novel target **170**, we employed our already developed palladium-catalyzed protocol[3] for coupling compound **185a** with 4-chlorophenol **166** (Scheme 3.6).

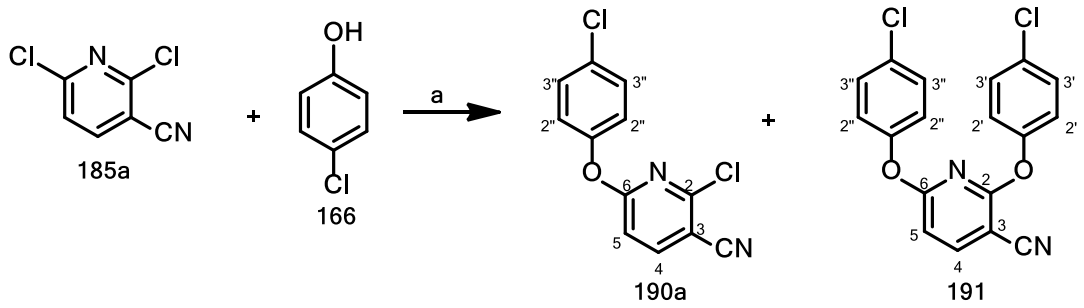

Scheme 3.6: *Reagents and conditions*: (a) cat. 2 mol% Pd_2dba_3, 6 mol% (*rac*)-BINAP, 2.0 eq. 4-chlorophenol, NaO^{t}Bu, THF, 100-110°C, 24 h.

Although the intended target product **190a** was produced in low yield (17%), a bis-(4-chlorophenoxy)-substituted product **191** was also formed (Scheme 3.6) in high yield (78%). The formation of compound **191** could be due to the high reactivity of intermediate **185a** in the

presence of an excess of 4-chlorophenol as evidenced by the facile substitution of halogens at both 2- and 6- positions which gave product **191** in high yield.

^{1}H NMR spectroscopic analysis for compound **191** showed the presence of ten aromatic protons with the H-4 doublet (J = 8.3 Hz) appearing unchanged at 7.94 ppm, whilst H-5 appeared more shielded at 6.63 ppm due to successful C-O coupling. Eight protons from the two 4-chlorophenoxy motifs appeared as three multiplets in the ranges 7.25–7.20 ppm (4H); 6.98–6.93 ppm (2H) and 6.90–6.86 ppm (2H). The HRMS data ([M+]$^+$: 357.0173) also supported the identity of the bis-substituted product **191**.

Nonetheless, when the reaction was repeated with 0.5 equivalents of 4-chlorophenol, the monosubstituted intermediate **190a** was formed in excellent yield (87%) relative to the limiting reagent (4-chlorophenol). The identity of the regioselectively C-O coupled 6-(4-chlorophenoxy)-substituted intermediate **190a** was confirmed via ^{1}H NMR spectroscopic analysis which showed the presence of the expected six aromatic protons. Pyridyl protons H-4 and H-5 were observed as coupled doublets (J = 8.3 Hz) at 7.94 and 6.63 ppm, respectively, whilst protons from the C-O coupled 4-chlorophenoxy substituent were observed as multiplets in the ranges 7.26–7.21 ppm (2H), 6.98–6.94 ppm (1H) and 6.91–6.86 (1H) ppm. Regioselectivity for the C-6 position in product **190a** was confirmed by a NOESY experiment which showed long range coupling between H-2" (m, 7.26–7.21 ppm) and H-5 (6.63 ppm). Furthermore, ^{1}H NMR spectroscopy also showed that the H-5 signal at 6.63 ppm for intermediate **190a** was more shielded than the 7.43 ppm observed in the precursor (**185**), whilst the H-4 signals for both **190a** and **185** remained unchanged at 7.94 ppm. Nonetheless, we cannot rule out the possible formation of an alternative C-O coupled isomer via replacement of chlorine at the C-2 position.

Target molecule **170** was obtained by aminating intermediate **190** with 2-amino-4-methylbenzonitrile **167**, under palladium catalysis conditions as shown in Scheme 3.7.

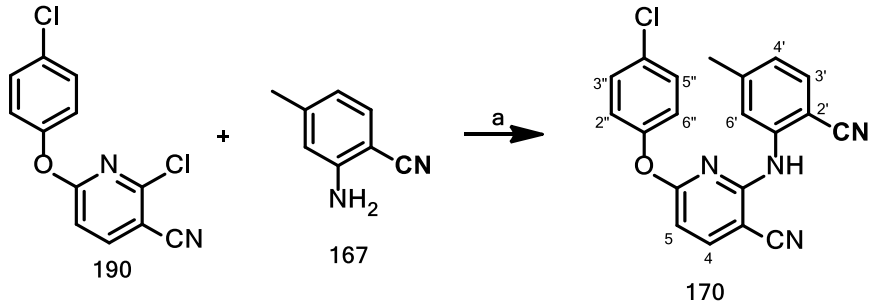

Scheme 3.7: *Reagents and conditions*: (a) cat. 2 mol% Pd_2dba_3, 6 mol% *ra*c-BINAP, 2-amino-4-methylbenzonitrile **167**, NaO^{t}Bu, THF, 110-120°C, 24 h; 71%.

The ^{1}H NMR spectrum for novel target **170** showed signals which integrated for nine aromatic protons and one signal which integrated for three protons was present in the aliphatic region. The amino proton was observed as a broad singlet at 8.40 ppm. Meanwhile, protons H-3', H-4' and H-6' were observed as a doublet (J = 8.1 Hz) at 7.39 ppm, another doublet at 6.65 ppm and a singlet at 6.85 ppm, respectively. The 4-chlorophenoxy protons appeared as multiplets in the ranges 7.26–7.21 ppm (2H) and 6.98–6.94 ppm (2H). ^{13}C NMR spectroscopic analysis showed the presence of fifteen aromatic carbon signals and one aliphatic carbon signal, with DEPT showing seven CH signals, eight quaternary aromatic carbon signals, two quaternary signals (CN) and one CH_3 signal in the aliphatic region. 2D NMR spectroscopy also confirmed successful amination at the C-2 position as evidenced by the more shielded carbon signal which appeared at 154 ppm.

3.4.1.2 Synthesis of novel nitrile-based derivatives 175

Our retrosynthetic assessment showed that novel compound **175** could be constructed by cross-coupling 2,6-dichloroisonicotinonitrile **185b** with 4-chlorophenol **166** and 2-amino-4-methylbenzonitrile **167**. Using a similar procedure employed in section 3.4.1.1, substrate **186b** could be obtained from 2,6-dichloroisonicotinic acid **187b**.

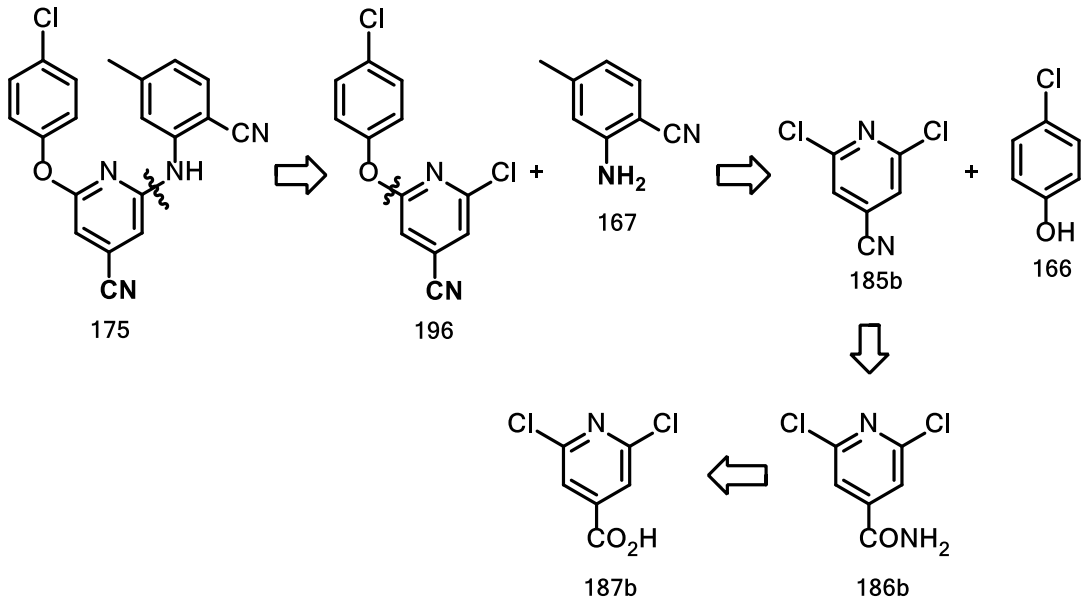

Scheme 3.8: Retrosynthetic analysis of novel target molecule **175**

Although substrate **187b** is available commercially, we welcomed the opportunity of developing a synthetic methodology for accessing this feedstock to meet our in-house requirements. As shown in Scheme 3.9, further virtual disconnection of **187b** indicated that **187b** could be

assembled via 2,6-dihydroisonicotinic acid **192** from cheaply available citric acid **193** and biuret **194** as respective carbon and nitrogen sources.

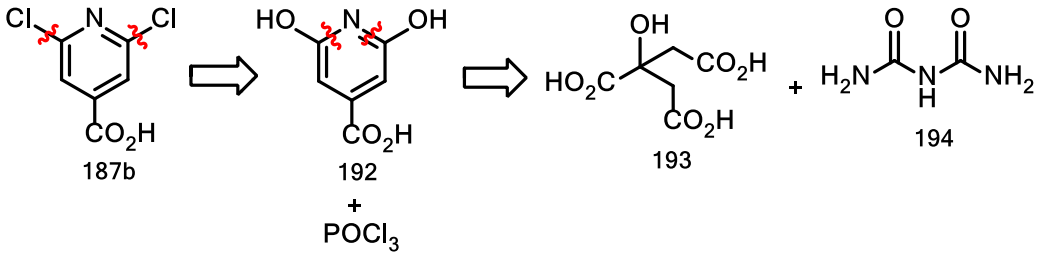

Scheme 3.9: Retrosynthetic analysis of substrate **187b**

3.4.1.2.1 Synthesis of 2,6-dihydroxyisonicotinic acid 192

Target molecule **192** was accessed via the citric acid trimethyl ester intermediate **195**[7] (Scheme 3.10). The ester **195** was prepared using thionyl chloride-activated condensation of citric acid **193** with methanol to give the ester as a crystalline solid in quantitative yield.

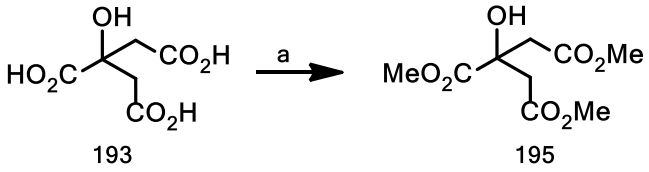

Scheme 3.10: *Reagents and conditions*; (a) $SOCl_2$, MeOH, 0℃-RT, 24 h; 99%.

^{1}H NMR spectroscopic analysis showed the trimethyl ester **195**[7] had been successfully formed due to the presence of a signal for three methoxy groups at 3.67 ppm and a signal due to the four methylene protons at 3.78 ppm. The NMR spectroscopic data matched that already available in literature.[7]

After a thorough mixing of the trimethyl triester **195** with urea, the reaction mixture was gently triturated with water (20 ml) at 130–145℃ in a well-ventilated reactor to allow ammonia to escape. When all the ammonia gas had been released, the reaction mixture was cooled to 100℃, diluted with hot water, basified with NaOH pellets to pH 9.0 and filtered to remove unreacted suspended material. The golden-brown and syrupy filtrate was then acidified (pH 3-5) and chilled overnight to precipitate the title compound **192**[8] as a tan solid (Scheme 3.11).

We observed that when the trimethyl ester **195** was reacted with a single mole equivalent of biuret **194**, low product yields (27–31%) were generally obtained. To our delight, the yield for the target product **192** improved significantly (73% overall) when the reaction was repeated whilst adding biuret **194** intermittently, in three separate portions.

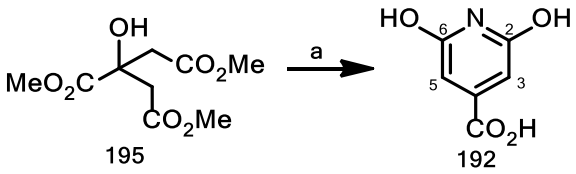

195 192

Scheme 3.11: *Reagents and conditions*; (a) 3 eq. biuret **194**, 130–140°C, 2 h; H_2O, 80°C, 30min; NaOH, pH 9.5; conc. HCl; 73%.

^{1}H NMR spectroscopic analysis showed the expected singlet signal in the aromatic region at 6.12 ppm (H-3 and H-5). Two other downfield broad singlet signals were also observed at 7.45 ppm and 7.92 ppm corresponding to possible keto-enol tautomeric forms of the two hydroxyl groups attached to the C-2 and C-6 positions of the pyridine nucleus. ^{13}C NMR spectroscopy showed one CH signal at 96.6 ppm, two quaternary carbon signals at 148.0 ppm (C-4) and 161.5 ppm (C-2) and a deshielded carbonyl signal at 166.8 ppm in line with NMR spectroscopic information found in literature.[8]

We transformed substrate **192** into the more reactive derivative 2,6-dichloroisonicotinic acid **187b** via a $POCl_3$-mediated methodology obtained from literature[5] to afford the target compound in an excellent 88% yield (Scheme 3.12).

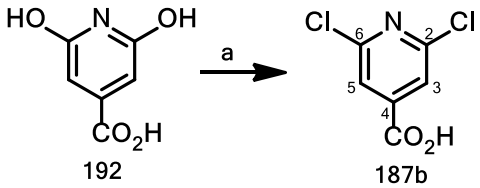

192 187b

Scheme 3.12: *Reagents and conditions*; (a) $POCl_3$, Et_4NCl, 130–145°C, 24 h, 88%.

The ^{1}H NMR spectrum for product **187b** showed a deshielded singlet signal at 7.86 ppm (H-3 and H-5). ^{13}C NMR spectroscopic analysis showed a carbon signal from C-2 and C-6 at 150.6 ppm whilst another carbon signal from C-3 and C-5 was observed at 126.5 ppm. These results are consistent with the NMR spectroscopic data already available in literature.[9]

3.4.1.2.2 Synthesis of isonicotinonitrile scaffold 185b

We accessed the isonicotinonitrile core **185b** via a thionyl chloride-mediated[3] amination of 2,6-dichloroisonicotinic acid **187b** with aqueous ammonia to generate 2,6-dichloroisonicotinamide **186b**,[10a] which was further dehydrated to afford product **185b**[10b] (Scheme 3.13).

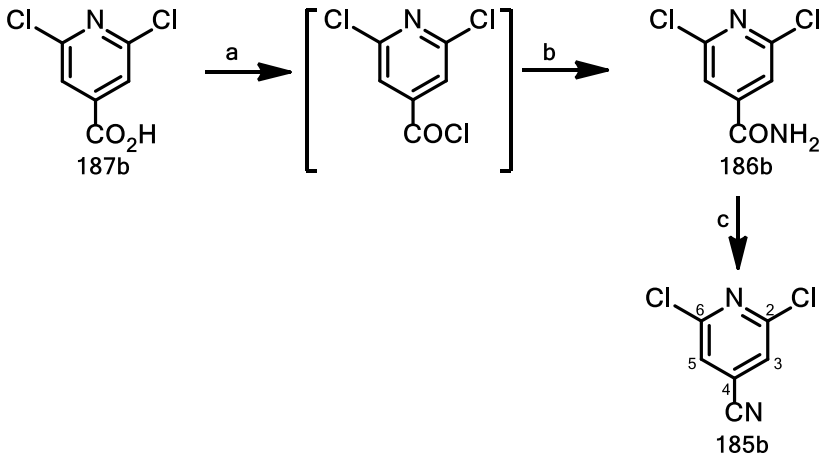

Scheme 3.13: *Reagents and conditions*; (a) $SOCl_2$, 80°C, 24 h; (b) 25% aq. NH_3, 0°C–RT, 4 h; (c) $POCl_3$, 80–100°C, 4 h.

^1H NMR spectroscopy showed that the aromatic proton singlet signal from H-3 and H-5 was more deshielded at 8.23 ppm than at 7.86 ppm previously observed in **186b**. In the ^{13}C NMR spectrum, the most deshielded quaternary carbon atoms were C-2 and C-6 at 150.7 ppm, followed by C-3 and C-5 at 126.5 ppm, C-4 at 125.3 ppm and CN at 115.2 ppm. The NMR spectral data agrees with that already found in literature.[10]

3.4.1.2.3 Synthesis of novel target 175

In order to access novel target compound **175**, our already developed palladium-catalyzed protocol[3] was employed to cross-couple 2,6-dichloroisoicotinonitrile **185b** with 1.5 equivalents of 4-chlorophenol **166** (Scheme 3.14) using similar conditions as already explained in section 3.4.1.1.

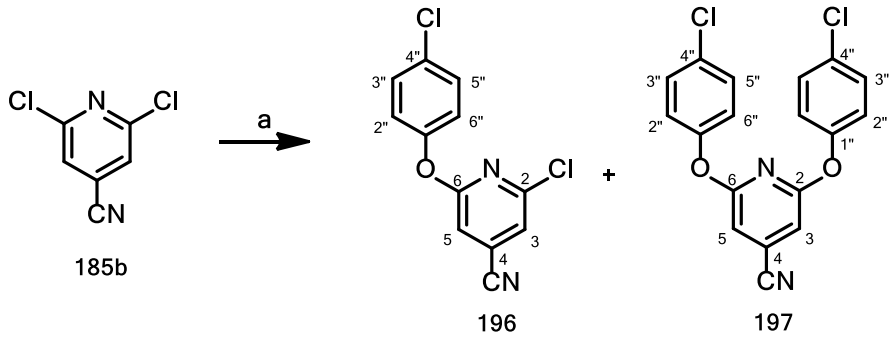

Scheme 3.14: *Reagents and conditions*; (a) i) cat. 2 mol% Pd_2dba_3, 6 mol% *rac*-BINAP, 1.5 eq. 4-chlorophenol **166**, THF, KO^{t}Bu, 100-110°C, **196** (4%); **197** (71%); or ii) cat. 2 mol% Pd_2dba_3, 6 mol% *rac*-BINAP, 0.5 eq. 4-chlorophenol **166**, THF, KO^{t}Bu, 100-110°C, **196** (99%).

Although our intention was to optimize the formation of a monosubstituted 6-(4-chlorophenoxy)-substituted intermediate **196** *en route* to **175**, an unexpected bis-(4-chlorophenoxy)-substituted novel molecule **197** was formed in higher yield (71%) than the expected 2-chloro-6-(-4-chlorophenoxy)isonicotinonitrile **196** (4%, Scheme 3.14).

The ^{1}H NMR spectrum for **197** showed signals integrating for ten aromatic protons. Interestingly, pyridyl protons H-3 and H-5, which previously appeared as a singlet in compound **185b**, were observed as separate *meta*-coupled doublets (J = 0.9 Hz) at 7.25 and 7.06 ppm, possibly due to the non-symmetric conformation adopted by this compound at room temperature. Similarly, the 4-chlorophenoxy protons were observed as four pairs of multiplets in the ranges 7.43–7.37 ppm (2H), 7.29–7.26 ppm (2H), 7.11–7.07 ppm (2H) and 6.96–6.93 ppm (2H). ^{13}C NMR spectroscopy showed eighteen carbon signals in the aromatic region signifying the fact that the carbon atoms on the apparently symmetric pyridine core as well as those on two 4-chlorophenoxy substituents all occupied non-equivalent carbon environments. The DEPT experiments showed ten CH signals and eight quaternary carbon signals with the C-O coupled C-6 and C-2 appearing deshielded at 162.9 and 162.5 ppm.

When the C-O cross-coupling reaction was repeated using 0.5 equivalents of 4-chlorophenol **166**, the expected 6-(4-chloropenoxy)-substituted intermediate **196** was formed in quantitative yield relative to the phenol (Scheme 3.14).

^{1}H NMR spectroscopy showed six aromatic proton signals in the ^{1}H NMR spectrum of **196**. The pyridyl H-3 doublet (J = 1.0 Hz) was deshielded and overlapped with the $CDCl_3$ solvent signal whilst the H-5 doublet overlapped with the multiplet signal from two 4-chlorophenoxy protons in

the range 7.12–7.06 ppm. The other two chlorophenoxy protons gave a downfield multiplet in the region 7.42–7.36 ppm.

Product **175** was made via C-N coupling of **196** with amine **167** (Scheme 3.15). ^{1}H NMR spectroscopy showed nine aromatic protons, one amino and three aliphatic protons. Pyridyl H-3 and H-5 appeared as meta-coupled doublets (J = 1.0 Hz) at 8.14 and 7.86 ppm, respectively. H-3' gave a doublet at 7.67 ppm (d, J = 8.4 Hz), with H-6' appearing as a singlet at 7.76 ppm whilst the H-4' and amino protons overlapped with the H-2" multiplet signal from 4-chlorophenoxy in the region 7.41–7.35 ppm.

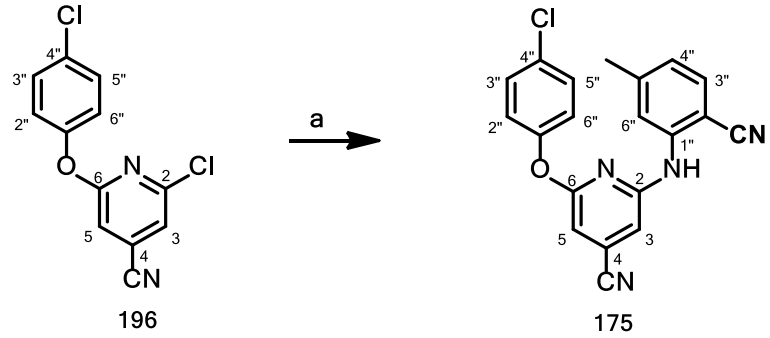

Scheme 3.15: *Reagents and conditions*; (a) i) 2 mol% Pd_2dba_3, 6 mol% *rac*-BINAP, 1.2 eq. 2-amino-4-methylbenzonitrile **167**, THF, KO^{t}Bu, 110-120°C, 84%.

3.4.1.3 Synthesis of novel cyclopropylamide-based derivatives 171 and 176

The cyclopropylamide-based derivatives **171** and **176** (Fig. 3.9) were accessed via intermediate scaffolds **188a** and **188b**, respectively, as previously shown during the retrosynthetic analysis of general scaffold **182** in Scheme 3.4.

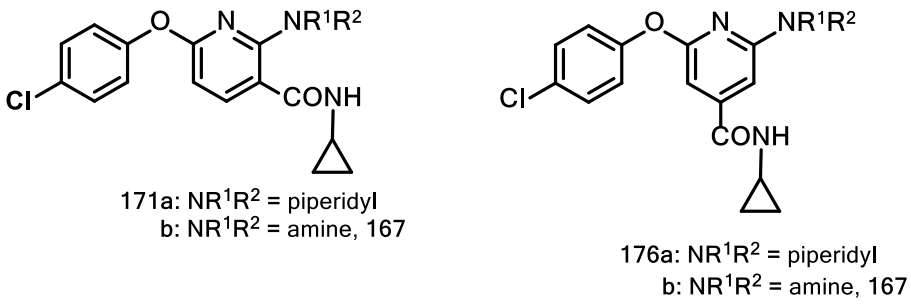

Figure 3.9: Novel target cyclopropylamide compounds **171** and **176**

3.4.1.3.1 Synthesis of intermediate scaffolds 188a and 188b

Intermediate scaffolds **188a** and **188b** were constructed from 2,6-dichloronicotinic acid **187a** and 2,6-dichloroisonicotinic acid **187b**, respectively, via a thionyl chloride activation route[3] already discussed in section 3.4.1.2.2. The resulting acyl halides were reacted *in situ* with cyclopropylamine to give the corresponding intermediate scaffolds **188a** and **188b** in quantitative yields (Scheme 3.16).

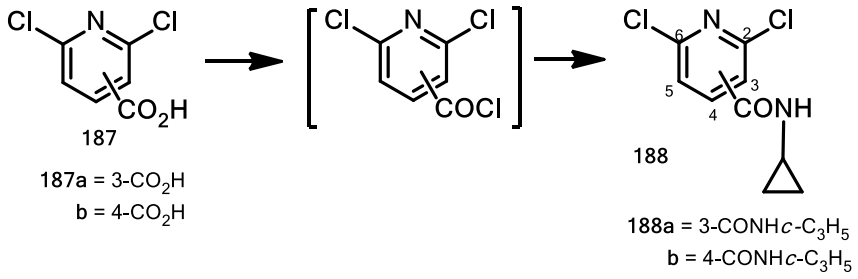

Scheme 3.16: *Reagents and conditions*; (a) $SOCl_2$, 80°C, 24 h; 99%; (b) DCM, cyclopropylamine, Et_3N, 0°C–RT, 4 h; 99%.

The ^1H NMR spectra for targets **188a** and **188b** showed signals that integrated for two aromatic protons with H-4 and H-5 for **188a** appearing as doublets at 8.11 ppm and 7.37 ppm (J = 8.1 Hz), respectively. In contrast, the pyridyl H-3 and H-5 from **188b** were observed as a singlet signal at 7.55 ppm. Successful amination in **188a** and **188b** was confirmed by the presence of a broad amide proton singlet at 6.60 ppm and 6.43 ppm, respectively. Cyclopropyl protons were observed as three multiplets in the ranges 2.97–2.86 ppm (1H), 0.95–0.87 ppm (2H) and 0.70–0.62 ppm (2H) of the aliphatic region for both products. ^{13}C NMR spectroscopic data showed the presence of five aromatic carbon signals and one carbonyl signal in both intermediates. Furthermore, two cyclopropyl carbon signals were also observed at 23.4 ppm and 6.9 ppm in the aliphatic region.

The appropriate cyclopropylamide substrate (**188a** or **188b**) was cross-coupled with 4-chlorophenol **166**, using a Pd/*rac*-BINAP catalyst system,[3] to generate the 4-chlorophenoxy-substituted intermediates **198a** and **198b** in 68% and 71% yield, respectively (Scheme 3.17).

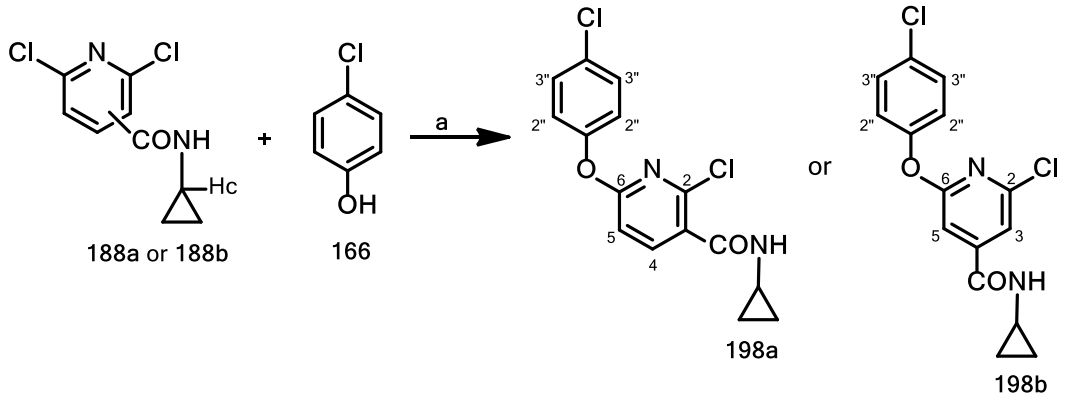

Scheme 3.17: *Reagents and conditions*: (a) (i) cat. 2 mol% Pd_2dba_3, 6 mol% (*rac*)-BINAP, 4-chlorophenol, NaO^{t}Bu, THF, 100-110°C, 24 h; **198a** (68%); **198b** (71%); or (ii) cat. 2 mol% Pd_2dba_3, 3 mol% Xantphos, 4-chlorophenol, NaO^{t}Bu, THF, 100-110°C, 24 h; **198a** (73%); **198b** (86%).

^{1}H NMR spectroscopy confirmed successful chlorine substitution and C-O bond formation at the C-6 position of the central pyridine nucleus in **198a** as evidenced by the upfield movement of the H-5 doublet to 7.16 ppm from 8.11 ppm previously observed in **188a**. Although there is an alternative isomeric possibility for substituting the C-2 chlorine, the replacement of the C-6 chlorine as a predominant reaction was confirmed by the NOESY experiment which showed long-range coupling (J = 0.6 Hz) between the H-2" and H-5 protons. On the other hand, protons H-3 and H-5 from **198b** gave meta-coupled doublets (J = 1.1 Hz) with H-3 appearing downfield at 7.28 ppm whilst H-5 overlapped with the H-3'' multiplet signal (on 4-chlorophenoxy group) in the region 7.09–7.06 ppm. In addition, 2D NMR spectroscopic analysis also showed that the quaternary C-6 signal previously observed at 151.2 ppm in substrate **188a** had shifted downfield to 158 ppm in product **198a**, whilst the quaternary C-6 signal for **198b** appeared more deshielded at 163.2 ppm.

3.4.1.3.2 Synthesis of novel targets 171 and 176

When we attempted to access target molecules **171a** and **176a** via palladium-catalyzed amination of **198a** and **198b** with piperidine using the reaction conditions given in Scheme 3.18 a) i), only product **176a** was formed in 55% yield. To our surprise, target product **171a** was not formed and only starting material was recovered.

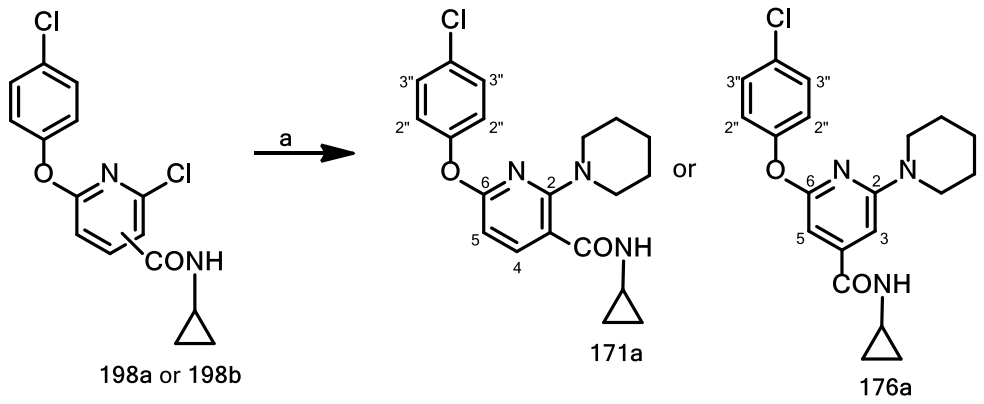

Scheme 3.18: *Reagents and conditions*: (a) (i) 2 mol% Pd_2dba_3, 6 mol% *rac*-BINAP, 1.5 eq. piperidine, NaO^tBu, THF, 100-110°C, 24 h; **171a** (0%), **176a** (53%); or (ii) 2 mol% Pd_2dba_3, 3 mol% Xantphos, 1.5 eq. piperidine, NaO^tBu, THF, 100-110°C, 24 h; **171a** (54%), **176a** (67%).

In an effort to facilitate the amination of **198a** with piperidine, we replaced *rac*-BINAP with Xantphos as ancillary ligand for the palladium-catalyzed amination, given Xantphos' more flexible backbone and larger bite angle (108°) relative to *rac*-BINAP (93°). Fortunately, novel target **171a** was formed in a reasonable yield of 54% using these modified conditions (Scheme 3.18 (a) ii)). The formation of novel target **171a** in the presence of Xantphos as supporting ligand is consistent with Klingesmith,[11] van Leeuwen,[12] and Nicolaou and Webber's[13] observations that ligands possessing large bite angles make excellent support systems in cross-coupling reactions. The large bite angles enable such ligand systems to "stretch" or reposition in space to facilitate the migration of the metal centre towards the energetically unstable transition state involving the Pd-amido complex in the palladium-catalyzed aminations.

^{1}H NMR spectroscopy confirmed successful C-N coupling of the piperidinyl motif at the C-2 position in product **171a** as evidenced by three additional alkyl proton multiplet signals in the ranges 3.38–3.31 ppm (4H), 1.67–1.59 ppm (3H) and 1.50–1.45 ppm (3H). Similarly, alkyl proton multiplets from product **176a** appeared in the regions 3.67–3.33 ppm (4H) and 1.60–1.50 ppm (6H). Furthermore, signals due to the six aromatic protons were observed in the two analogues. Amide protons were observed as broad singlets at 7.58 ppm and 6.87 ppm in targets **171a** and **176a**, respectively. ^{13}C NMR spectroscopic analysis showed nine aromatic carbon signals in both products and the carbonyl signals at 165.7 ppm (**171a**) and 167.0 ppm (**176a**). Similarly, DEPT showed the presence of four CH signals, six quaternary carbon signals including the C-N coupled C-2 at 158.2 ppm (**171a**) and 162.7 ppm (**176a**). In addition, three CH_2 signals belonging to the C-N coupled piperidinyl motif as well as one CH signal and two CH_2 signals from the cyclopropyl group were observed in the aliphatic region.

3.4.1.3.3 Synthesis of novel targets 171b and 176b

In a similar fashion to **171a** and **176a**, target molecules **171b** and **176b** were accessed via palladium-catalyzed cross-coupling[2] of **198a** and **198b** with 2-amino-4-methylbenzonitrile **167** to afford **171b** and **176b** in good yield (Fig. 3.10)

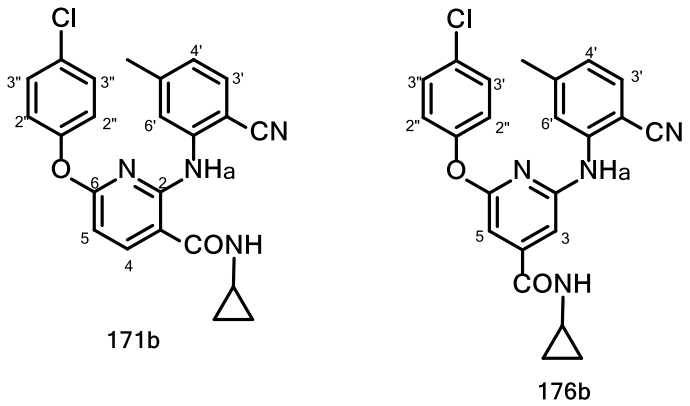

Figure 3.10: Novel targets **171b** and **176b**

The ^{1}H NMR spectra for both **171b** and **176b** showed signals integrating for nineteen protons. These included three additional aromatic proton signals, one anilino proton Ha signal as well as three alkyl proton signals from the C-2 coupled 2-amino-4-methylbenzonitrile motif. Proton H-6' and neighbouring protons H-3' and H-4' on **171b** appeared as a singlet signal at 7.57 ppm followed by two doublets (J = 7.9 Hz) at 7.37 ppm and 6.78 ppm, respectively, whereas H-3', H-4' and H-6' on compound **176b** gave doublets (J = 7.9 Hz) at 7.46 ppm and 6.92 ppm and a singlet signal at 7.94 ppm, respectively. ^{13}C NMR spectroscopic analysis for the two analogues showed the presence of seventeen carbon signals in the aromatic region and three carbon signals in the aliphatic region. 2D NMR spectroscopy displayed seven CH signals and nine quaternary carbon signals, including the aminated C-2 signal at 154.0 ppm for **171b**, which appeared more deshielded than 146.3 ppm observed for target product **176b**. The CN signal was observed at 117.2 ppm in both products.

3.4.1.4 Synthesis of carboxamide derivatives

Although virtual analogues **172** and **174** (Fig. 3.11) showed similar ligand-receptor interaction energies and displayed promising ligand-receptor binding conformations in the allosteric site of the 3MEG-RT crystal structure during the molecular modelling exercise, we pursued the synthesis of virtual target **172**. Our preference for the latter compound was motivated by the

presence of an already established synthetic route since the development of a new synthetic approach for accessing compound **174** could have taken more time.

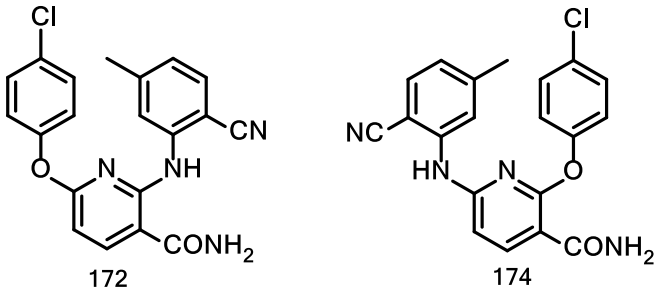

Figure 3.11: Virtual carboxamide targets **172** and **174**

Retrosynthetic analysis of general scaffold **182**, as already highlighted in Scheme 3.4, showed that novel molecule **172** could be made from 2,6-dichloronicotinamide **186a**. Synthesis of **186a** has already been described (Scheme 3.5).

Our successful application of the palladium-based catalysis for cross-coupling cyclopropylamide-based scaffolds **198** (Scheme 3.18) with selected nitrogen- and oxygen-containing nucleophiles prompted us to extend the same protocol towards accessing target **172**. Our initial attempt involved cross-coupling 2,6-dichloronicotinamide **186a** with 4-chlorophenol **166** as shown below (Scheme 3.19).

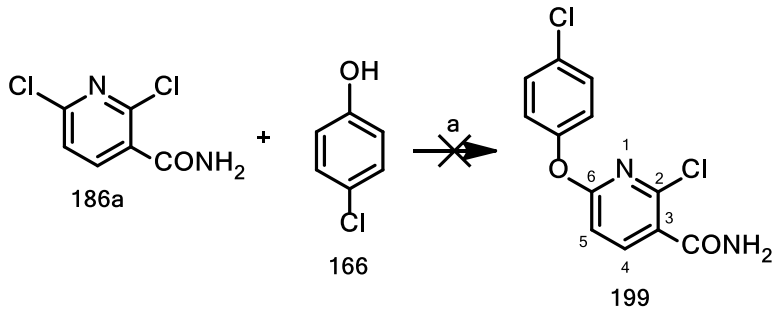

Scheme 3.19: *Reagents and conditions*: (a) cat. [2 mol% Pd_2dba_3, 6 mol% *rac*-BINAP (or 3 mol% Xantphos)], 4-chlorophenol, NaO^{t}Bu (Cs_2CO_3 or K_2CO_3 or K_3PO_4 or KHMDS), THF (or 1.4-dioxane or DMF or DME), 100-110°C, 24 h; No conversion.

Unfortunately, the expected 6-(4-chlorophenoxy)-substituted intermediate **199** was not formed. Several efforts that included changing of solvent from THF to 1.4-dioxane, DMF or DME) proved equally ineffective. Neither did the change of supporting ligand from *rac*-BINAP to Xantphos

improve the situation. Similarly, replacement of KO^{t}Bu with Cs_2CO_3 or K_2CO_3 or K_3PO_4 or KHMDS failed to initiate the C-O coupling, as the starting material was recovered in each case. However, an attempt was then made to indirectly access the novel target **172** from the nitrile-based derivative **170** using biocatalysis as a key step for selectively hydrolysing the nitrile group.

3.4.1.5 Biocatalysis as a key step for nitrile hydrolysis

Biocatalysis is one of the most cost-effective approaches for accessing amides and carboxylic acids via enzyme-based hydrolysis of nitriles. Over the past two decades use of enzymes has rapidly grown as an efficient green technology for catalysing transformations of various substrates to access both stereo- and regio-specific industrial products. In our quest to access novel pyridine- and pyrimidine-based potential HIV-1 NNRTIs, we have successfully synthesized key nitrile-based intermediates (Scheme 3.20) for subsequent conversion to the requisite carboxamide target products.

3.4.1.5.1 Synthesis of carboxamide target 200

Prior to accessing novel target product **172** via biocatalysis, we tested the utility of the nitrilase enzyme in converting the already made bis-(4-chlorophenoxy)-substituted isonicotinonitrile substrate **197** into the corresponding carboxamide **200** using the reaction conditions shown in Scheme 3.20.

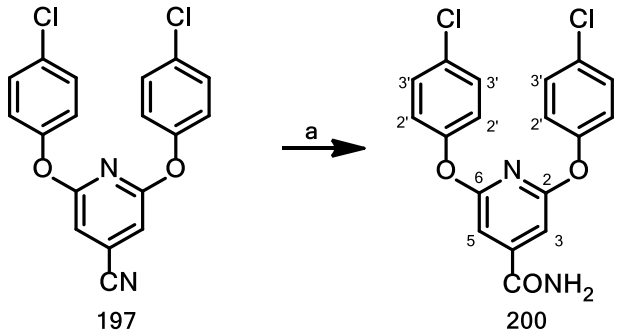

Scheme 3.20: Reagents and conditions: (a) substrate **197**, nitrile hydratase, 10% MeOH, phosphate buffer, 30–37 °C, 72 h

In this research, we used the purified nitrile hydratase enzyme that had been expressed by the bacterial species *Rhodococcus Rhodocrous* ATCC BAA-870 by our collaborators at the Centre for Scientific and Industrial Research[14] in an attempt to hydrolyse the pyridyl nitrile group into

novel product **200**. We employed the methodology that we had previously developed for the hydrolysis of β-aminonitriles.[14]

An initial attempt was made to facilitate the nitrile hydrolysis using 5–10 mg scale quantities of substrate **197** and 2.5–5 mg of enzyme catalyst at 37℃, whilst monitoring reaction progress visually using TLC over a 24 h period. Although a new highly polar spot was observed at the base of the TLC plate within 12–24 h, it became evident that recoveries were too low to conclusively confirm product identity via NMR spectroscopic analysis. However, when substrate **197** and enzyme quantities were scaled up to 20 mg and 15 mg, respectively, whilst allowing the reaction to progress for 12–26 hours, ensured meaningful hydrolysis of the pyridyl nitrile substrate **197** to generate the carboxamide product **200**.

The ^{1}H NMR spectrum for product **200** showed signals that integrated for twelve protons in the aromatic region. The presence of two amide protons as a broad singlet at 9.62 ppm confirmed the successful hydrolysis of the nitrile group. Protons H-3 and H-5 were observed as a singlet at 7.88 ppm whilst two doublets from H-2' and H-3' on the 4-chlorophenoxy motifs appeared at 7.17 ppm (J = 8.4 Hz, 4H) and 6.75 ppm (J = 8.37 Hz, 4H), respectively. ^{13}C NMR spectroscopy showed seven aromatic signals and one carbonyl signal at 162.7 ppm.

3.4.1.5.2 Synthesis of novel target molecule 172

Following the successful enzymatic conversion of the bis-(4-chlorophenoxy)-substituted nitrile derivative **197** to the corresponding carboxamide derivative **200**, we extended the same method towards converting **170** to the hydrolysed product **172** (Scheme 3.21). As a way forward, a biocatalysis approach that used nitrile hydratase enzyme was explored as a potential key step for achieving hydrolysis of the CN group (Scheme 3.21).

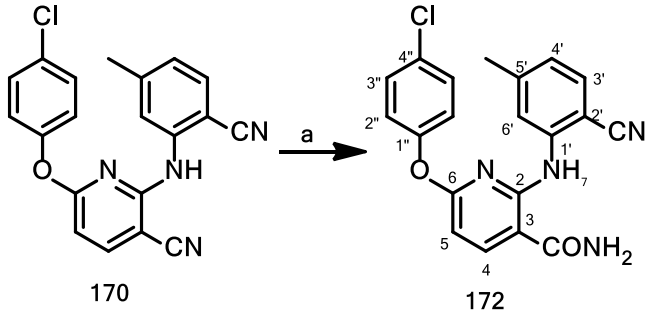

Scheme 3.21: Reagents and conditions: (a) substrate 197, nitrile hydratase, 10% MeOH, phosphate buffer, 30–37 ℃, 72 h.

We also wanted to ascertain whether such a reaction could be selective towards either the CN group attached onto the central pyridine core or the second nitrile functionality on the benzonitrile substituent. In this vein, equivalent amounts of substrate **170** and nitrile hydratase enzyme were dissolved in methanol. After addition of phosphate buffer, the reaction mixture was stirred and incubated at 37°C whilst the reaction progress was monitored at 4 hourly intervals over 96 hours. The title compound **172** was extracted with ethyl acetate, purified by column chromatography and characterized by NMR and IR spectroscopy. This boicatalytic step was completely selective for the hydrolysis of the pyridyl nitrile, with no evidence seen of hydrolysis of the benzonitrile as will be explained below.

The ^{1}H NMR spectrum showed that compound **172** contained twelve protons in the aromatic region and three aliphatic protons. As expected, two amide protons were observed as a broad singlet which overlapped with the H-3' doublet signal at 7.49 ppm (J = 8.0 Hz). H-3' also coupled with H-4' at 6.91 ppm (d, J = 7.9 Hz) whilst H-6' and H-7 singlet signals appeared at 7.31 ppm and 9.40 ppm, respectively. Neighbouring pyridyl protons H-4 and H-5 gave corresponding doublet signals (J = 8.4 Hz) at 8.18 ppm and 6.77 ppm whereas H-2" and H-3" multiplet signals from the 4-chlorophenoxy motif appeared in the ranges 7.43–7.40 ppm and 7.26–7.21 ppm, respectively. ^{13}C NMR spectroscopy showed fifteen aromatic signals as well as one carbonyl signal, one CN signal and one aliphatic carbon signal at 165.3 ppm, 117.9 ppm and 21.8 ppm, respectively. More importantly, 2D NMR spectroscopic analysis (HMBC) confirmed the presence of an intact CN group on the 2-amino-4-methylbenzyl motif as evidenced by the strong heteronuclear coupling between H-6' (7.31 ppm) and a quaternary carbon signal at 117.9 ppm (CN). In addition, heteronuclear coupling was also observed between H-3' (7.49 ppm) and a CN signal at 117.9 ppm, whilst H-4 also coupled with a quaternary carbon signal at 165.3 ppm (amide carbonyl) thus validating that selective hydrolysis of the CN group attached to the central pyridine core had occurred.

IR spectroscopy showed strong N-H, C-H, CN (nitrile) and C=O stretches at 3633, 2950, 2216 and 1662 cm^{-1}, respectively, which confirmed the presence of amide and carbonitrile functionality in target product **172**. HRMS ([M+H]+ : 379.0952) confirmed the formation of the target product as the expected molecular weight was obtained.

3.4.2 Antiviral Assay for novel pyridine-based compounds

The novel target pyridine-based compounds **171a**, **171b**, **172**, **175**, **176a**, **176b**, **191** and **197** were screened against wild-type HIV using nevirapine as a bench mark drug. The antiviral assay results are listed in Table 3.1

Table 3.1: *In vitro* anti-HIV assay for novel pyridine-based target compounds.

Compd	Toxicity		Activity		S. Index
	CC_{50} (μM)	S. D.	IC_{50} (μM)	S. D.	
171a	81.75	11.40	60.21	3.28	1.4
171b	>100	-	>100	-	-
172	83.9	14.5	>21.34	-	
175	>100	-	>100	-	
176a	1.52	0.63	7.61	0.19	0.2
176b	8.34	1.24	27.20	2.92	0.3
191	30.78	1.79	28.09	1.23	1.1
197	54.42	13.25	53.40	1.29	1.0
142e	54.25	9.76	1.07	0.03	50.7
Toxicity Control DMSO	>1%	>1%	-	-	-
Activity Control NVP	-	-	0.12	0.0	-

NB: DMSO – dimethyl sulfoxide, NVP – nevirapine.

As shown in Table 3.1, the nicotinic acid-based (**171a**, **171b**, **172**, **191**) and isonicotinic acid-derived (**175**, **176a**, **176b 197**) analogues (Fig. 3.12) were inactive against the wild-type RT. Refreshingly, all the nicotinic acid-derived analogues (carbonitrile, carboxamide, and cyclopropylamide) displayed modest (CC_{50} = 30.78 μM for **191**) to excellent (**171a**, **171b**, **172**) cytotoxic profiles during the *in vitro* assay. By comparison, the isonicotinic-acid based novel targets (**176a**: CC_{50} = 1.52 μM; **176b**: CC_{50} = 8.34 μM) (Fig 3.13c-d) were highly toxic and adversely affected cell viability, with the exception of compound **197** (CC_{50} = 54.42 μM), whilst almost promoting the replication of the wild-type virus (Fig. 3.13c-d). Contrastingly, our pyridyl benzamide hit compound **142e** displayed a higher selectivity for the virus at reasonable cytotoxic levels (Fig. 3.13e).

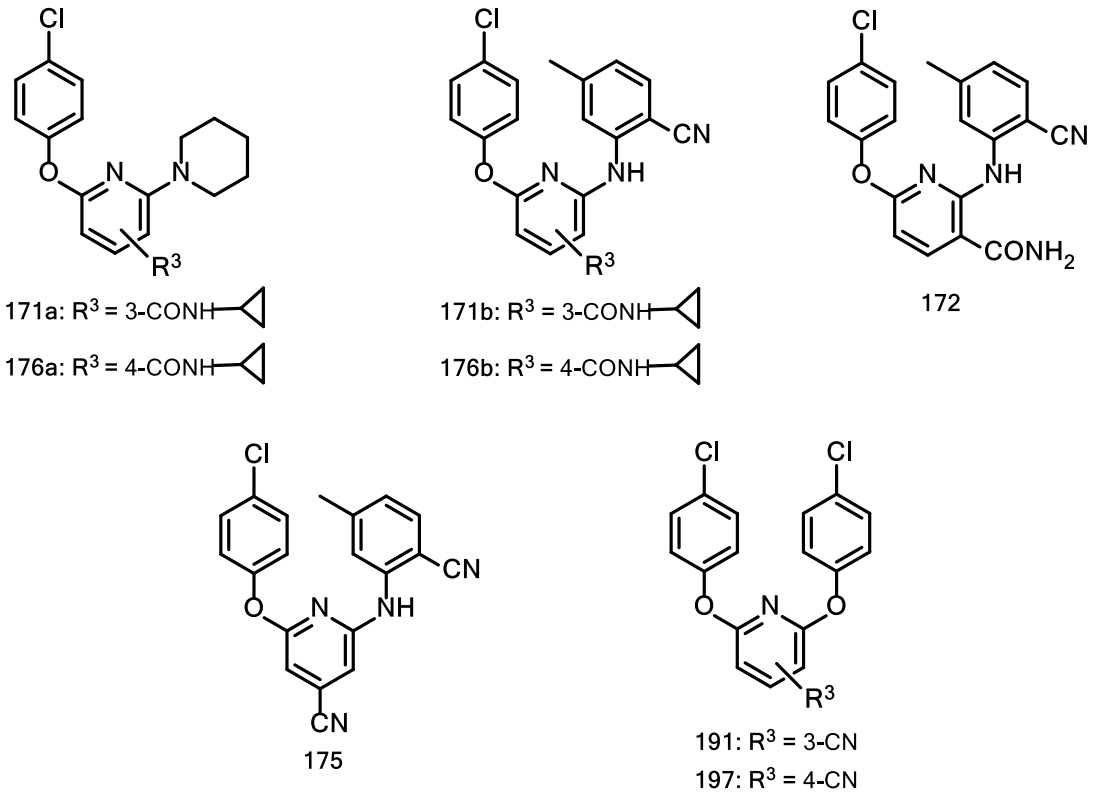

Figure 3.12: Nicotinic acid- and isonicotinic acid derived target molecules.

Although the promising bound conformation displayed by modelling hit compound **172** did not directly translate into superior antiviral activity against the wild-type virus, the less favorably bound nicotinic acid-derived analogues (**171a** and **171b**, Fig. 3.13a-b) displayed excellent cytotoxic profiles as shown in Table 3.1. This seems to suggest that molecular modelling results are not *always* a good predictor of the potential *in vitro* and/or *in vivo* activity that could be displayed by a target compound.

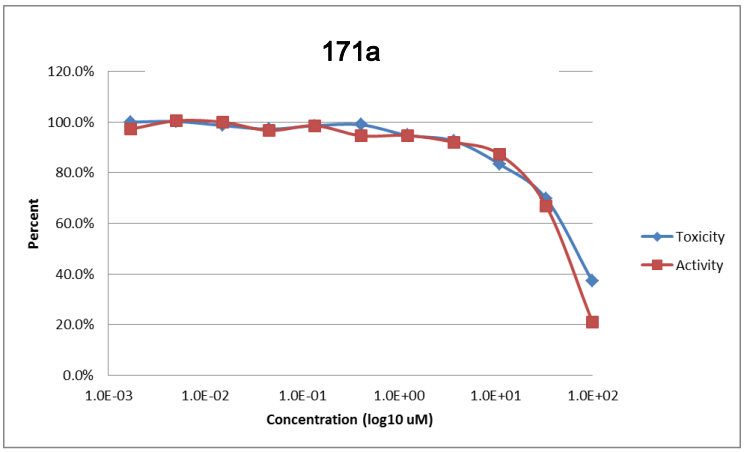

Figure 3.13a: Cytotoxic (blue) and antiviral activity (red) profiles of novel target **171a**

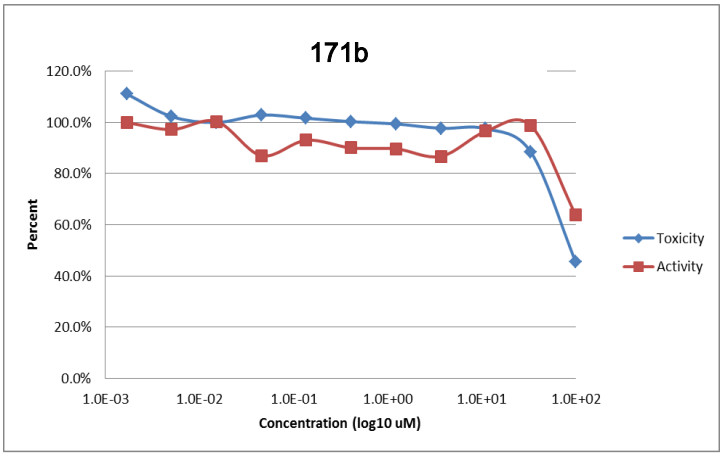

Figure 3.13b: Cytotoxic (blue) and antiviral activity (red) profiles of novel target **171b**

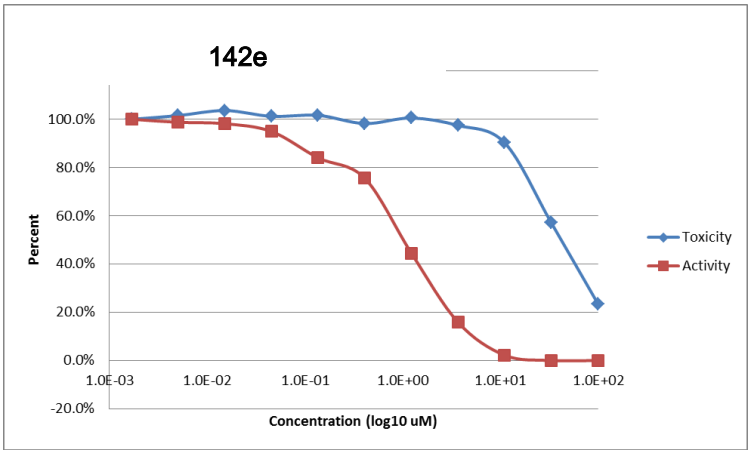

Figure 3.13c: Cytotoxic (blue) and antiviral activity (red) profiles of novel target **142e**

Contrary to observations made for compounds **171a** (Fig. 3.13a) and **171b** (Fig. 3.13b), the lead compound **142e** shows a clear therapeutic window (Fig. 3.13c) with a clear separation between the toxicity and efficacy profiles as reflected in the selectivity index quoted in Table 3.1.

3.5 Synthesis of pyrimidine based derivatives

The pyrimidine-based compounds that will be discussed in this section resemble the DAPY-type framework and contain a tri-functionalized pyrimidine core with two attached hydrophobic substituents for enhancing hydrophobic interactions in the RT NNIBP. This section will cover the synthesis and *in vitro* assay of pyrimidine-based compounds of general structures **178**, **179**, **180a** and **180b** (Fig. 3.14).

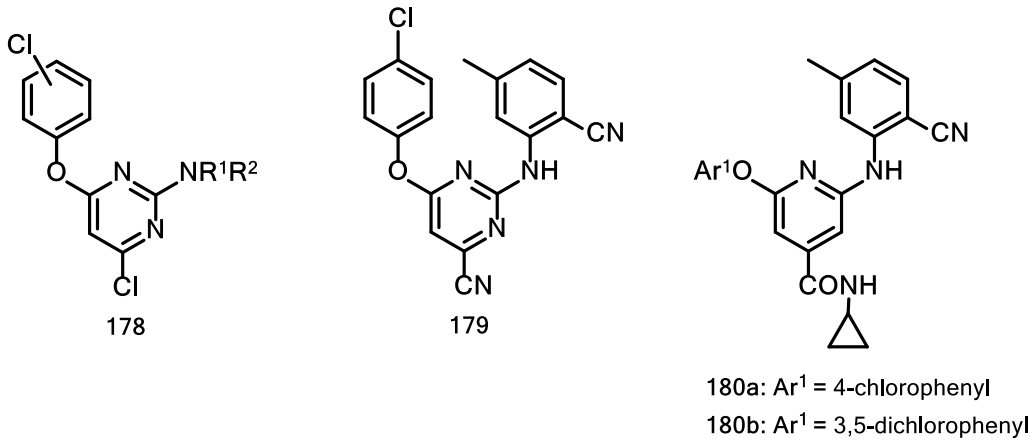

Figure 3.14: Structures for chloride-, carbonitrile- and amide-based pyrimidine derivatives

3.5.1 Synthesis of chlorine substituted pyrimidine-based analogues 178

The general structure **178** is representative of a small library of novel compounds that were made using a central pyrimidine nucleus which had a chlorine atom attached at the C-4 position. Our objective was to explore whether halogen bonds could function as suitable pendants for initiating electrostatic contacts with hydrophilic amino acid residues lining the putative entrance to the RT allosteric site. Among the pyrimidine-based series of target molecules (Fig. 3.14), we started by constructing compounds of general structure **178** as they were easily accessible. These compounds (**207**–**220**) were accessed via a tandem palladium-mediated cross-coupling of an appropriate substituted phenol and an appropriately substituted amine with 2,4,6-trichloropymidine **204** (Scheme 3.22).

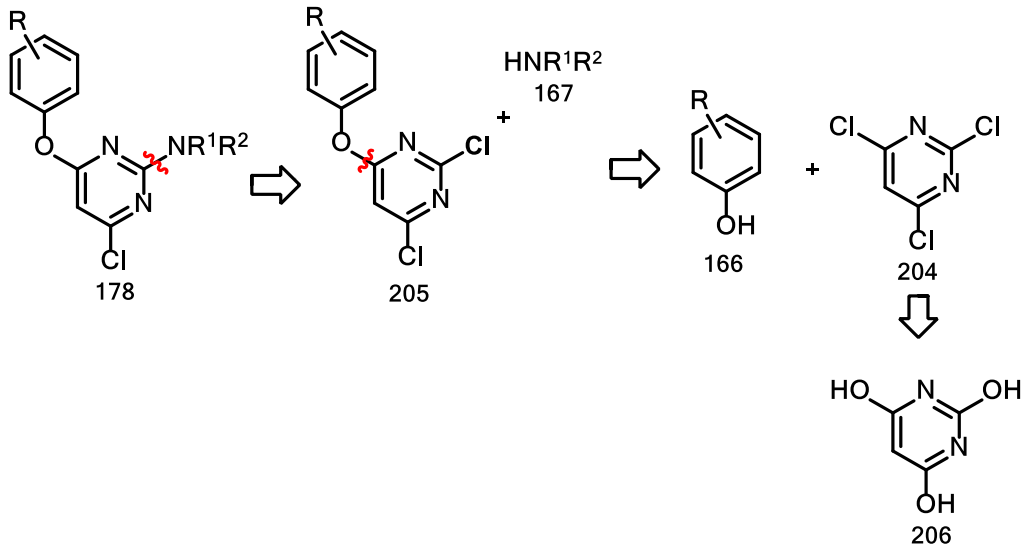

Scheme 3.22: Retrosynthetic analysis of general target molecule **178**

3.5.1.1 Synthesis of intermediate compound 204

We extended the $POCl_3$/quaternary ammonium salt-activated protocol obtained from literature[4-5a] towards halogenating commercially available barbituric acid **206** *en route* to forming the highly reactive substrate, 2,4,6-trichloropyrimidine **204**[5b] (Scheme 3.23). Fortunately, the target substrate **204** was obtained in excellent yield (86%). Aside from the tedious, documented traditional halogenation protocols which utilize secondary amines and $POCl_3$, to the best of our knowledge, this represents the first time that a protocol which uses a quaternary ammonium salt and $POCl_3$ has been successfully employed for halogenating barbituric acid.

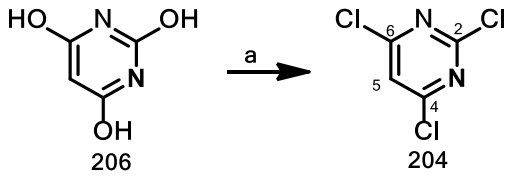

Scheme 3.23: *Reagents and conditions*; (a) $POCl_3$, Et_4NCl, 120°C, 4 h; 86%.

The ^1H NMR spectrum for compound **204** showed the presence of the expected H-5 pyrimidyl proton singlet signal at 7.39 ppm. ^{13}C NMR spectroscopic data showed three aromatic carbon signals with DEPT showing one C-H and two quaternary carbon signals. C-4 and C-6 appeared as a deshielded singlet at 163.1 ppm, followed by C-2 at 160.2 ppm, whilst C-5 was shielded at 120.2 ppm. This data was consistent with the spectroscopic data already contained in literature.[5b]

3.5.1.2 Synthesis of novel targets 207, 208, 209 and 210

Due to the highly electrophilic nature of 2,4,6-trichloropyrimidine **204**, target molecules **207-210** were accessed via a general addition-elimination methodology reported by Delia and co-workers.[15] A 6-phenoxy-subtituted regioisomer **222a** was made via the slow addition of aqueous sodium phenoxide **166a** to an ice-cold acetone solution of substrate **204** (Scheme 3.24).

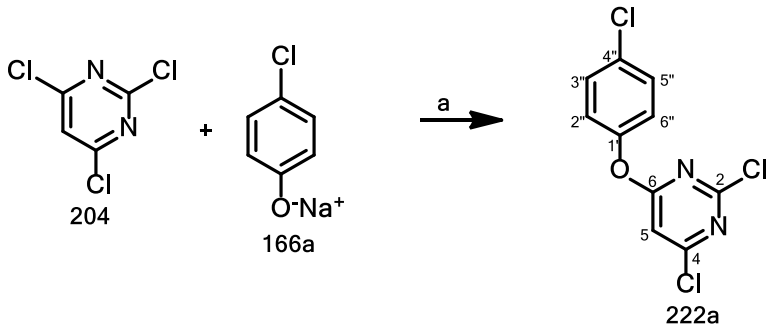

Scheme 3.24: *Reagents and conditions*; (a) aq. sodium phenoxide **166a**, acetone, 0°C-RT, 2 h, 90%.

^{1}H NMR spectroscopy showed the presence of three aromatic proton signals with H-5 appearing upfield at 6.70 ppm whilst the 4-chlorophenoxy protons appeared as multiplets in the ranges 7.43–7.39 ppm (2H) and 7.21–7.17 ppm (2H). DEPT analysis showed three CH signals and five quaternary carbon signals in the aromatic region. The C-O coupled C-6 signal was the most deshielded at 170.7 ppm as compared to 163.1 ppm observed in substrate **204** (Scheme 3.24).

Although there is a 2:1 statistical chance of nucleophilic displacement of chlorine at the C-4/C-6 or C-2 positions in substrate **204**, the 6-substituted regioisomer **222a** was the predominant species with a 90% minimum yield. We attribute this observation to the prolonged ice-cold chilling which could have imposed some kinetic control on the reaction by lowering entropic energy. This is consistent with the observation made by Delia[15] which demonstrated that nucleophilic substitution predominantly occurred at the C-4/C-6 position as it promoted the formation of a thermodynamically favourable *para*-quinoid[15] transition state that appeared better stabilized than the *ortho*-quinoid[15] transition state arising from C-2 substitution (Scheme 3.25).

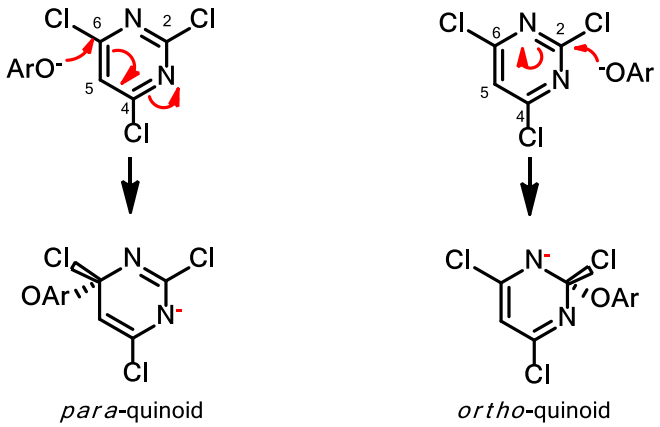

Scheme 3.25: *para*-quinoid vs *ortho*-quinoid structure transition states

The preference for the *para*-quinoid intermediate was confirmed via NOESY 2D-NMR spectroscopy, which showed weak through-space coupling (J = 0.6 Hz) between H-5 and H-2'' protons (Fig. 3.15) for intermediate **222a** – an interaction which could not be detected via COSY ($J \geq 1.5$ Hz).

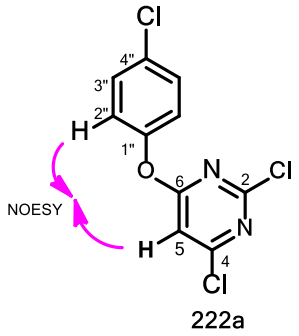

Figure 3.15: H-5 and H-2" through space coupling in *para*-quinoid derived product **222a**

With intermediate **222a** on hand, we proceeded to aminate its C-2 position using 5-methylpyridin-2-amine **167a** via the slow addition of KO^{t}Bu (over 4 h) to produce the target molecule **207** in good yield (Scheme 3.26).

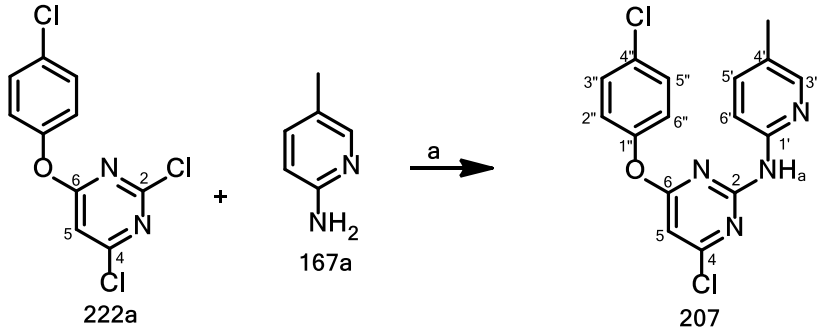

Scheme 3.26: *Reagents and conditions*; (a) R_2NH_2, KO^{t}Bu, THF, RT, 4 h, 73%.

We extended the same protocol (Scheme 3.27) towards aminating intermediate **222a** with 2-amino-4-methylbenzonitrile **167**, 3-chloro-4-methylamine **167b** and 3-methyl-4-bromoaniline **167c** to afford target molecules **208**, **209** and **210** in 68%, 51% and 47% yield, respectively (Fig. 3.16).

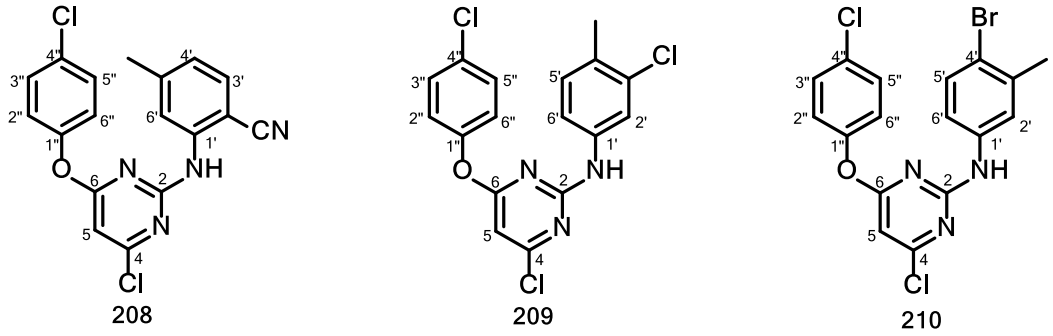

Figure 3.16: Structures for novel targets **208**, **209** and **210**

The ^{1}H NMR spectra for novel targets **208**, **209** and **210** (Fig. 3.16) showed signals that integrated for eight aromatic protons, one amino proton and three aliphatic protons. The pyrimidyl H-5 signals for the four analogues appeared in a similar range of 6.41–5.99 ppm. The amino proton for **207** gave a more deshielded broad singlet signal which overlapped with the H-3' singlet at 8.06 ppm whilst amino protons from targets **208–210** appeared upfield in the region 7.64–7.40 ppm. The H-5' signal overlapped with the $CDCl_3$ solvent signal whereas the H-6' doublet signal appeared at 7.63 ppm (J = 8.1 Hz) for target product **207**. H-3' overlapped with the multiplet from 4-chlorophenoxy protons in the region 7.42–7.38 ppm, whilst H-4' appeared as a doublet at 6.83 ppm (J = 7.9 Hz) followed by the H-6' singlet signal at 7.79 ppm for compound **208**. For product **209**, the H-2' singlet was observed at 6.93 ppm but H-5' and H-6' overlapped into a multiplet signal in the 7.07–6.99 ppm region. Lastly, H-5' and H-6' signals from **210** appeared as a doublet at 7.48 ppm and a multiplet signal in the range 7.00–7.98 ppm, respectively. ^{13}C NMR spectroscopic analysis showed fourteen aromatic carbon signals and one aliphatic carbon signal whilst DEPT analysis showed six CH signals, seven quaternary carbon signals and one carbon atom in the aliphatic region from target molecule **207**. For compound **207**, an HMBC experiment showed heteronuclear coupling between H-5 (6.41 ppm) and C-4 (157.4 ppm) and between H-5 (6.41 ppm) and C-6 (170.1 ppm), whilst no such coupling was observed between the H-5 proton and the protons belonging to the amine nucleophile. This suggested that the amine nucleophile was not coupled to the C-4 position but to a remote C-2 carbon atom. Thus structure **207** was considered as the most likely product that could be formed from aminating **222a** using the amine **167a**. However, there is also a possibility that the amination of **222a** could replace the C-4 chlorine and give the C-4 aminated isomer. For the same reasons, the most likely products that could be formed by aminating intermediates **222b–f** were proposed as structures **208–220**.

In this vein, novel targets **208–210** gave similar ^{13}C NMR spectroscopic trends but contained an extra quaternary carbon signal than **207**. The C-O and C-N coupled quaternary carbon signals were observed in the same ranges of 170.8–170.6 ppm and 164.3–162.2 ppm, respectively, for all compounds.

3.5.1.3 Synthesis of novel targets 211 and 212

In a similar fashion, target molecule **211** was accessed via intermediate scaffold **222b** which was made by reacting substrate **204** with 2,4-dichlophenoxide **166b** under transition metal-free reaction conditions (Scheme 3.27).

^{1}H NMR spectroscopic analysis showed four aromatic protons with the H-5 signal appearing at 6.95 ppm. On the other hand, H-3" coupled with H-5" and was observed as a doublet (J = 2.4 Hz) at 7.51 ppm whilst H-5" coupled to both H-3" and H-6" and appeared as a doublet of doublets (J = 8.7, 2.4 Hz) at 7.33 ppm, with H-6" being observed as a second doublet at 7.15 ppm.

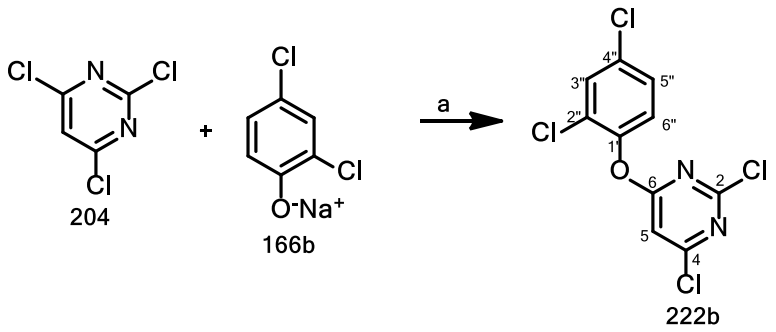

Scheme 3.27: *Reagents and conditions*; (a) aq. sodium 2,4-dichlorophenoxide **166b**, acetone, 0°C-RT, 2 h, 90%.

Reaction of intermediate **222b** with amine **167a** in the presence of KO^{t}Bu as previously described for novel target **207**, afforded novel compound **211** in a reasonable yield of 78% (Scheme 3.28).

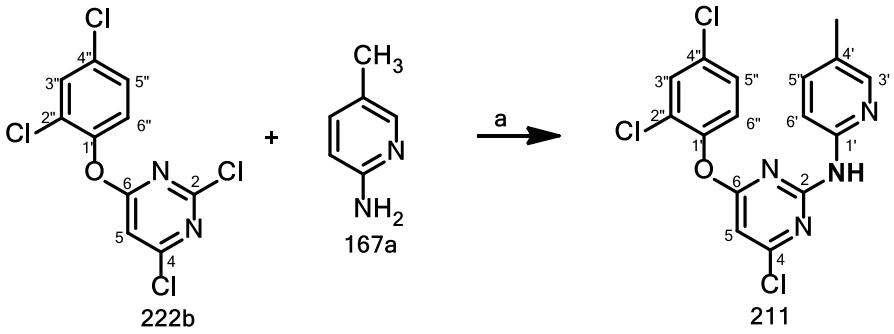

Scheme 3.28: *Reagents and conditions*; (a) Amine **167a**, THF, 0°C - RT, KO^{t}Bu, 2 h, 78%.

Similarly, novel target **212** (Fig. 3.17) was generated by reacting **222b** with 2-amino-4-methylbenzonitrile **167**.

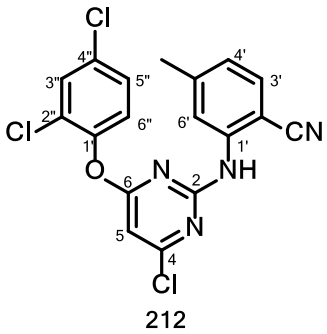

Figure 3.17: Structure for novel target **212**

^{1}H NMR spectroscopic data for novel molecules **211** and **212** showed seven aromatic proton signals, one amino proton signal and three aliphatic protons. The pyrimidyl protons H-5 for products **211** and **212** appeared in the same region at 6.50 ppm and 6.60 ppm, respectively. Amino protons for **211** and **212** showed broad singlets at 8.05 and 7.51 ppm, respectively. H-3', H-5' and H-6' signals from **211** were observed as a singlet at 8.10 ppm and two coupled doublets (J = 8.6 Hz) at 7.33 ppm and 7.17 ppm, respectively. For compound **212**, H-3' and H-4' showed coupling doublets (J = 7.9 Hz) at 7.39 ppm and 6.84 ppm, respectively whilst H-6' appeared as a singlet at 7.73 ppm. ^{13}C NMR spectroscopy for targets **211** and **212** contained fifteen and sixteen aromatic carbon signals, respectively, and one aliphatic carbon signal apiece. DEPT analysis for compound **211** showed seven CH signals, eight quaternary carbon signals and one aliphatic carbon signal whereas product **212** contained two extra quaternary carbon signals. HRMS analysis confirmed successful C-O and C-N coupling as the expected molecular weight of the target products was obtained in each case.

3.5.2 Synthesis of novel target 213

Using a similar base-promoted C-O coupling protocol already described above, target molecule **213** was synthesized via intermediate **222c**. Intermediate **222c** was formed from the nucleophilic displacement of chlorine by piperidine. Further base-catalyzed amination of **222c** with amine **167a** afforded target product **213** in good yield (Scheme 3.29).

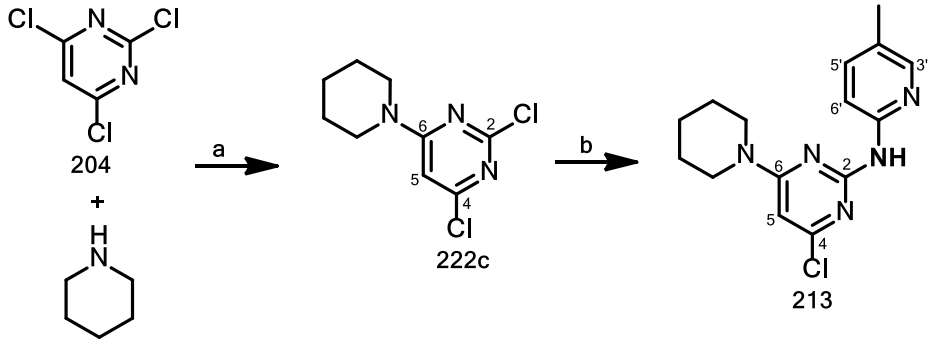

Scheme 3.29: *Reagents and conditions*; (a) aq. NaOH, piperidine, acetone, 0°C-RT, 2 h, 83%; (b) Amine **167a**, THF, KO^{t}Bu, RT, 2 h, 60%.

^{1}H NMR spectroscopic analysis of **222c** showed the expected one aromatic proton signal and ten aliphatic protons belonging to the C-N coupled piperidinyl motif. The pyrimidyl H-5 appeared at 6.46 ppm whilst piperidyl protons were observed as multiplets in the ranges 3.79–3.75 ppm (4H) and 1.68–1.58 ppm (6H) of the aliphatic region. ^{13}C NMR spectroscopy showed the presence of four aromatic carbon signals and three aliphatic carbon signals. DEPT analysis showed one C-H signal, three quaternary aromatic carbon signals and five CH_2 signals in the aliphatic region.

^{1}H NMR spectroscopy for novel compound **213** showed four aromatic proton signals and signals integrating for thirteen protons in the aliphatic region. The H-5 singlet was the most shielded at 6.08 ppm whilst the H-3' doublet overlapped with the H-6' doublet to appear as multiplets in the range 8.18–8.10 ppm. In addition, H-5' was observed as a doublet of doublets (J = 8.5, 2.3 Hz) at 7.48 ppm with the amino proton appearing as a broad singlet at 7.83 ppm. The methyl protons were observed at 2.27 ppm. ^{13}C NMR spectroscopy showed nine aromatic carbon signals and four aliphatic carbon signals. 2D NMR spectroscopic analysis confirmed successful C-N coupling at the quaternary C-2 position which gave a corresponding carbon signal at 159.9 ppm.

3.5.3 Synthesis of novel targets 214 and 215

Target compounds **214** and **215** were synthesized via intermediate **222d**. Intermediate **222d** was prepared by reacting substrate **204** with 3,5-dichlorophenoxide **166d** to form the 6-(3,5-dichlorophenoxy)-substituted regioisomer **222d** in a high yield of 92% (Scheme 3.30). Further independent amination of **222d** with amines **167a** and **167** gave novel targets **214** and **215** in reasonable yield (Scheme 3.31).

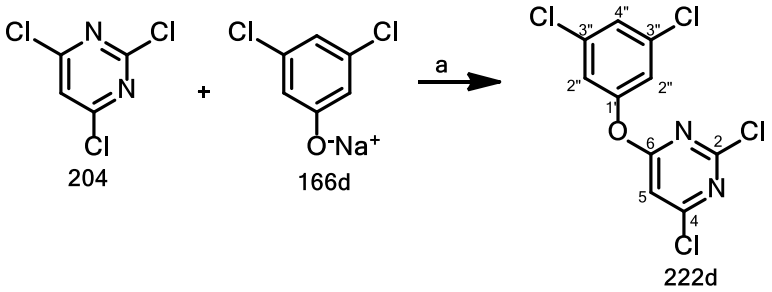

Scheme 3.30: *Reagents and conditions*; (a) acetone, 0°C-RT, 2 h, 92%.

Formation of intermediate compound **222d** was confirmed by ^{1}H NMR analysis which showed the presence of 3 proton signals in the aromatic region. The H-5 signal appeared unchanged at 6.90 ppm with NOESY showing weak through-space coupling (J = 0.6 Hz) with H-2" protons. Protons H-2" were observed as a doublet (J = 1.8 Hz) at 7.09 ppm, whilst H-4" appeared as a triplet (J = 1.8, 1.8 Hz) at 7.32 ppm. ^{13}C NMR spectroscopy showed the presence of eight aromatic carbon signals whilst DEPT analysis showed three CH signals and six quaternary carbon signals, with the C-O coupled C-6 being deshielded at 170.0 ppm.

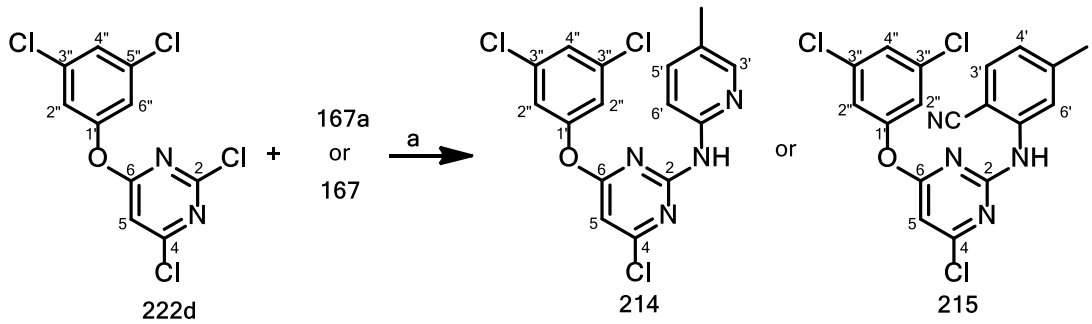

Scheme 3.31: *Reagents and conditions*; (a) amine **167a** or **167**, THF, KO^{t}Bu, RT, 2 h, 74% (**214**); 61% (**215**).

The ^{1}H NMR spectra for novel products **214** and **215** contained seven aromatic proton signals, one amino proton signal and three methyl protons in the aliphatic region. Protons H-3', H-5' and H-6' from the C-2 coupled amine on product **214** gave a multiplet in the region 8.17–8.13 ppm followed by a doublet of doublets (J = 8.4, 2.3 Hz) at 7.50 ppm and a doublet (J = 8.6 Hz) at

7.05 ppm, respectively. On the other hand, H-3', H-4' and H-6' proton signals from **215** showed a doublet (J = 8.0 Hz) at 7.57 ppm, a multiplet that overlapped with H-4' in the range 7.15–7.07 ppm and another multiplet in the region 7.79–7.72 ppm, respectively. ^{13}C NMR spectroscopic analysis for compound **214** showed thirteen aromatic carbon signals and one carbon signal in the aliphatic region whereas product **215** contained fourteen carbon signals in the aromatic region, one CN signal and one carbon signal in the aliphatic region.

3.5.3.1 Synthesis of novel targets 216 and 217

Novel compounds **216** and **217** were synthesized via intermediate **222e**. Intermediate **222e** was accessed by reacting **204** with 4-fluorophenoxide **166e** to form the 6-(4-flourophenoxy)-substituted regioisomer **222e** in a similar fashion to that discussed previously (Scheme 3.32). Thereafter, aminating **222e** with **167a** and **167** afforded the target products **216** and **217**, respectively (Fig. 3.18).

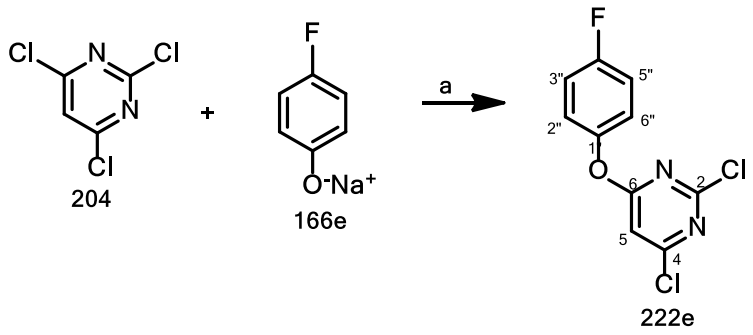

Scheme 3.32: *Reagents and conditions*; (a) acetone, 0°C-RT, 2 h, 94%.

Synthesis of intermediate **222e** was confirmed by ^{1}H NMR spectroscopic analysis which showed signals that integrated for five aromatic protons. The pyrimidyl H-5 appeared at 6.40 ppm, whilst the H-2" as well as H-3" signals were observed as a doublet (J = 5.4 Hz, 4H) at 7.14 ppm. ^{13}C NMR spectroscopy showed eight aromatic carbon signals whilst the DEPT experiment showed three CH signals and five quaternary carbon signals with the C-O coupled C-6 being highly deshielded at 170.8 ppm.

Substrate **222e** was separately aminated with amine **167a** and **167** to give target molecules **216** and **217** at reasonable yield (Fig. 3.18).

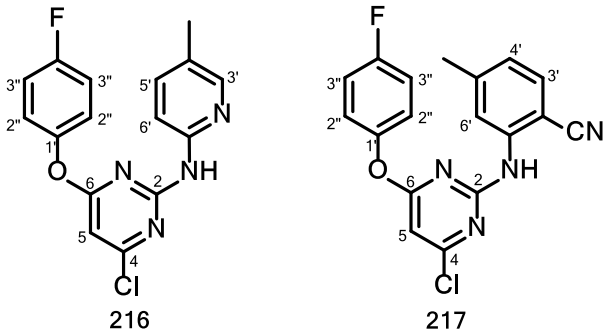

Figure 3.18: Target compounds **216** (61%) and **217** (54%).

^{1}H NMR spectroscopic analysis for compounds **216** and **217** showed the presence of eight and nine proton signals in the aromatic region, respectively, plus a signal for three aliphatic protons. The amino proton gave a broad singlet at 7.88 ppm whilst H-3', H-5' and H-6' on novel target **216** showed a singlet at 8.07 ppm, a doublet at 7.66 ppm (J = 5.6 Hz), and another doublet which overlapped with the H-2" doublet at 7.14 ppm, respectively. The proton signals from Ha, H-3', H-4' and H-6' on the C-2 coupled amine motif on product **217** gave a broad singlet at 7.51 ppm, a doublet at 7.39 ppm (J = 7.9 Hz), another doublet at 6.84 ppm (J = 7.9 Hz), and a further broad singlet at 7.81 ppm, respectively. ^{13}C NMR spectroscopy showed that compound **216** has thirteen aromatic carbon signals and one carbon signal in the aliphatic region whilst novel target **217** contained fifteen carbon signals in the aromatic region and one aliphatic carbon signal as well. 2D NMR spectroscopic analysis showed six CH signals for both **216** and **217**, seven quaternary carbon signals for **216**, nine quaternary carbon signals from **217** and one aliphatic carbon signal apiece.

3.5.4 Synthesis of novel targets 218 – 220

As the first member of the series, target molecule **218** was synthesized via the reaction of substrate **204** with 3-(trifluoromethyl)phenoxide **166f** to generate intermediate **222f** which was subsequently aminated using 5-chloropyrimidine-2-amine **167e** to generate product **218** in good yield (Scheme 3.33). In the same vein, target products **219** and **220** were also made via the amination of intermediate **222f** with amines **167a** and **167** to access product **219** and **220**, respectively (Fig. 3.19).

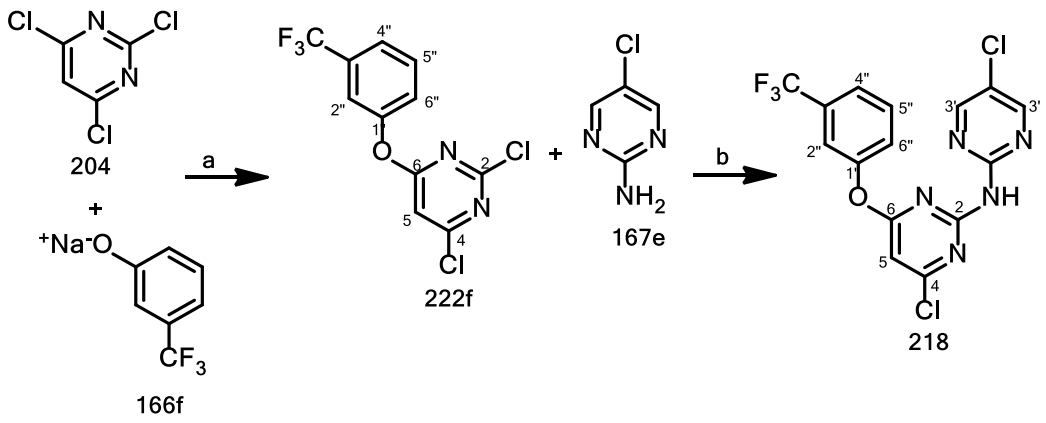

Scheme 3.33: *Reagents and conditions*; (a) acetone, 0°C-RT, 2 h, 91%; (b) amine **167e**, THF, KO^{t}Bu, RT, 2 h, 61%.

The ^{1}H NMR spectrum for intermediate compound **222f** contained five aromatic proton signals with the H-2" singlet appearing at 8.25 ppm whilst H-4", H-5" and H-6" signals overlapped to give a multiplet in the 7.63–7.46 ppm range. The H-5 signal was observed as a singlet at 6.54 ppm. ^{13}C NMR spectroscopy showed eleven carbon signals in the aromatic region with the C-O coupled C-6 appearing deshielded at 170.1 ppm.

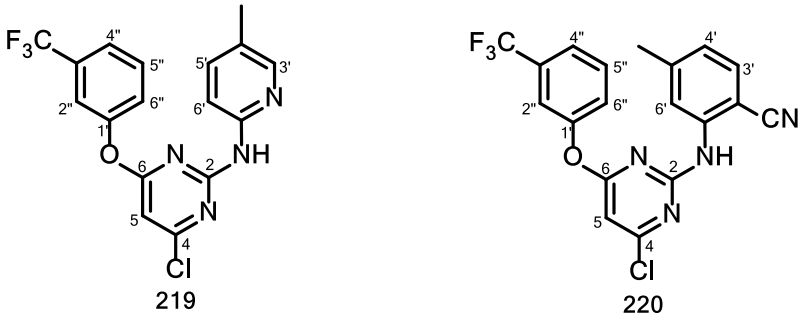

Figure 3.19: Novel target molecules **219** (78%) and **220** (73%).

The ^{1}H NMR spectra for novel products **218**, **219** and **220** showed amino proton signals at 8.77 ppm (d, J = 4.7 Hz) , 8.60 ppm (singlet) and 7.51 ppm (singlet), respectively, whilst the pyrimidyl H-5 signals from the trio were observed in the range 6.54–6.46 ppm. Protons H-3' and H-5' on compound **218** appeared as a singlet at 8.49 ppm. For novel target **219**, the H-3', H-5' and H-6' signals were observed as; one singlet at 8.19 ppm followed by two doublets 7.19 ppm (J = 7.9 Hz) and 7.37 ppm (J = 7.1 Hz) in that order. H-3', H-4' and H-6' signals from **220** appeared as a doublet that overlapped with H-4" in the 7.39–7.37 ppm region followed by a second doublet at 6.83 ppm (J = 7.9 Hz) and a singlet at 7.73 ppm, respectively. ^{13}C NMR spectroscopic analysis showed fourteen, sixteen and eighteen carbon signals in the aromatic region for compounds

218, **219** and **220**, respectively with an additional aliphatic carbon signal being observed from both **219** and **220**.

3.6.5 Antiviral Assay

The novel target pyrimidine-based compounds **207–220** were screened against the wild-type HI virus by our collaborators at the National Institute of Communicable Diseases, Sandringham, South Africa. As always, our pyridyl-benzamide lead compound **142e** and nevirapine (NVP) were also included in the *in vitro* assay, for quality control purposes.

3.6.5.1 Antiviral and toxicity results against wild-type virus

As shown in Table 3.2, the results display the concentrations of compounds that were required to inhibit 50% of cellular activity (IC_{50}) as well as achieve 50% cell viability (CC_{50}). The selectivity index (S.I. = CC_{50}/IC_{50}) was included as an indicator of the degree to which each tested compound was selective towards the wild-type virus.

The antiviral screening results show that all the 2,4,6-trichloropyrimidine-derived novel molecules **207** to **220** were essentially non-cytotoxic towards the viability of the pseudovirus. Regrettably, all the compounds were not active against the HI wild-type virus. Although such compounds are torsionally flexible, the general lack of activity against the wild-type RT displayed by this series of analogues could be attributed to the inefficiency of the 4-Cl group to make meaningful electrostatic contacts through halogen bonding with key hydrophilic amino acid side chains (K101, N103, and E138) that line the putative entrance to the RT allosteric site.

Table 3.2: In vitro anti-HIV assay for novel pyrimidine-based target compounds **207-220**

Compd	Toxicity		Activity		S. Index
	CC_{50} (μM)	S. D.	IC_{50} (μM)	S. D.	
207	>100	-	>49.4	-	-
208	>100	-	>60.7	-	-
209	71.4	21.4	>17.1	-	-
210	19.0	0.5	> 6.4	-	-
211	53.0	26.5	> 4.6	-	-
212	>100	-	>23.4	-	-
213	>100	-	>86.5	-	-
214	>100	-	>86.3	-	-
215	97.4	1.7	>27.8	-	-
216	>100	-	>67.2	-	-
217	>100	-	>52.1	-	-
218	41.5	1.3	> 8.6	-	-
219	>100	-	>100	-	-
220	36.4	3.1	>15.1	-	-
142e	37.1	7.0	1.07	0.03	34.7
NVP	-	-	0.111	-	-

3.6 Synthesis of pyrimidine-based nitrile 179 and cyclopropylamide 180 derivatives

The general retrosynthetic analysis for pyridine and pyrimidine-based derivatives given earlier in section 3.5 showed that pyrimidine-based nitrile **179** and cyclopropylamide derivatives could be accessed via intermediate scaffolds **223** and **224** (Fig. 3.20).

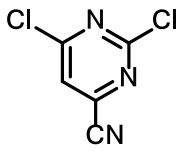

223

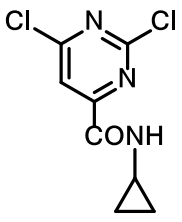

224

Figure 3.20: Intermediate pyrimidine-based scaffolds **223** and **224**

3.6.1 Synthesis of scaffold 223[5e]

Intermediate scaffold **223** was synthesized via the $POCl_3$-catalyzed halogenation[5a] of commercially available orotic acid **225** to generate 2,6-dichloroprimidine-4-carboxylic acid **226**[5c] (Scheme 3.34).

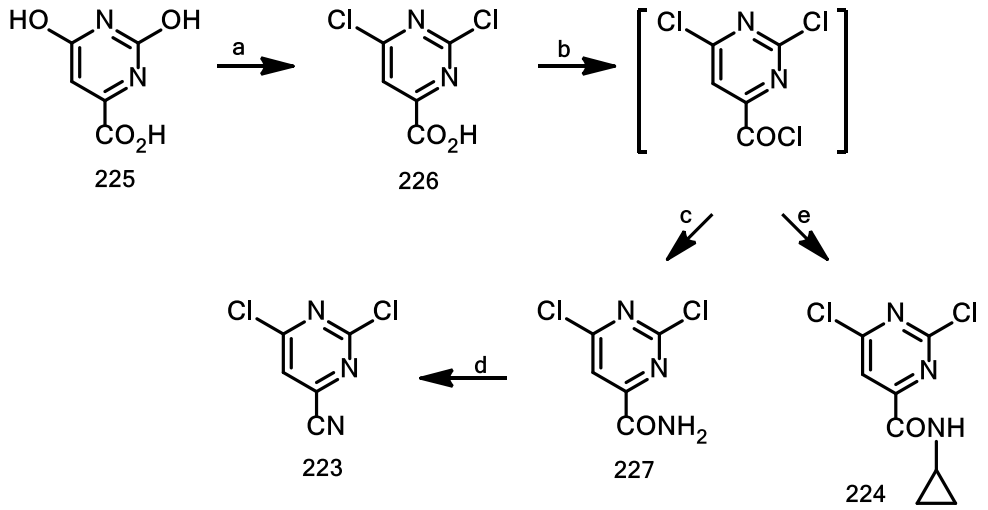

Scheme 3.34: *Reagents and conditions*: (a) $POCl_3$, Et_4NCl, 130-145°C, 24 h, 88%; (b) $SOCl_2$, 80°C, 24 h; (c) 25% aq. NH_3, 0°C-RT, 4 h; 99%; (d) $POCl_3$, 80-100°C, 4 h, 75%: (e) DCM, cyclopropylamine, Et_3N, 0°C-RT, 4 h, 99%.

Compound **226** was reacted with thionyl chloride to produce a reactive acyl halide that was aminated *in situ* with aqueous ammonia to form 2,6-dichloropyrimidine-4-carboxamide **227**.[5d] The amide **227** was dehydrated with $POCl_3$[5] at moderate temperatures to afford 2,6-dichloropyrimidine-4-carbonitrile **223**[5e] in good yield (Scheme 3.34). The intermediate compounds **226** and **227**, as well as the target compound **223**, were characterized using NMR spectroscopy as outlined below.

The ^1H NMR spectrum for compound **226** showed the pyrimidyl H-5 singlet at 8.12 ppm. ^{13}C NMR spectroscopic analysis showed that the carbonyl carbon atom was the most deshielded signal at 164.0 ppm, followed by C-6 at 163.1 ppm whilst C-2, C-4 and C-5 signals were observed at 160.3, 160.0 and 121.2 ppm, respectively.

^1H NMR spectroscopic data for amide **227** showed H-5 appearing at 6.77 ppm whilst a broad singlet signal for the two amide protons was observed at 7.27 ppm. ^{13}C NMR spectroscopic analysis showed five carbon signals in the aromatic region. The carbonyl carbon, C-6 and C-4 signals from **227** were more deshielded at 167.0 ppm, 166.7 ppm and 165.3 ppm, respectively than the carbonyl carbon signal of compound **226** at 164.0 ppm.

One proton singlet signal at 8.61 ppm was observed in the ^{1}H NMR spectrum of the carbonitrile intermediate **223**. ^{13}C NMR spectroscopy confirmed successful formation of the carbonitrile as shown by the presence of the CN signal at 115.1 ppm. C-6 was the most deshielded signal at 163.7 ppm whilst the C-4 signal observed at 138.3 ppm was more upfield than observed in product **227** (166.7 ppm).

3.6.2 Synthesis of novel pyrimidine-based nitrile 179

Novel target molecule **179** was synthesized via intermediate **228**. Intermediate **228** was accessed via the nucleophilic displacement of the 6-chloro substituent of **223** by 4-chlorophenoxide **166a** to form the 6-(4-chlorophenoxy))-substituted isomer **228** in 95% yield (Scheme 3.35).

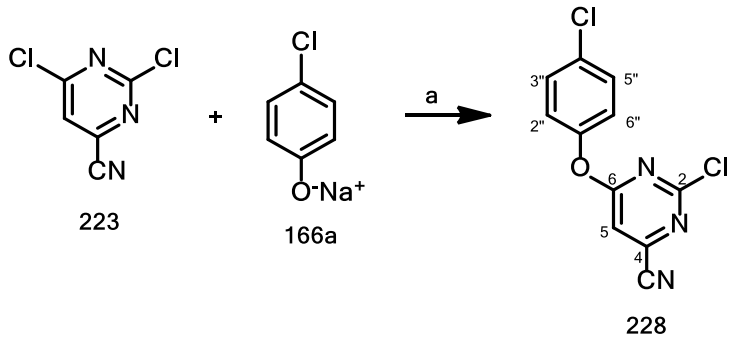

Scheme 3.35: *Reagents and conditions*; (a) acetone, 0°C-RT, 2 h, 95%.

^{1}H NMR spectroscopic analysis for intermediate **228** showed the presence of H-5 singlet at 7.21 ppm as well two sets of multiplets from proton signals on the 4-chlorophenoxy group in the region 7.43–7.37 ppm (2H) and 7.14–7.10 ppm (2H).

Intermediate **228** was cross-coupled with 2-amino-4-methylbenzonitrile **167a** under Pd catalysis to afford novel target compound **179** in good yield (Scheme 3.36).

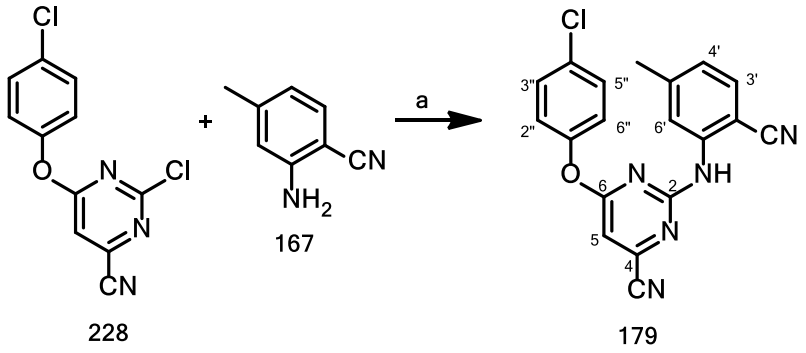

Scheme 3.36 *Reagents and conditions*; (a) amine **167**, THF, KO^{t}Bu, RT, 2 h, 76%.

^{1}H NMR spectroscopic analysis of the target molecule showed eight aromatic protons, one amine proton signal and three proton signals in the aliphatic region. ^{13}C NMR spectroscopy showed fourteen aromatic carbon signals and one aliphatic carbon signal, whilst from the DEPT experiments, six CH signals, ten quaternary carbon signals and one aliphatic carbon signal were observed.

3.7 Synthesis of novel cyclopropylamide-based targets 180a and 180b

Retrosynthetic analysis of novel target molecule **180a** showed that the compound could be accessed via intermediate scaffold **224** (Scheme 3.37).

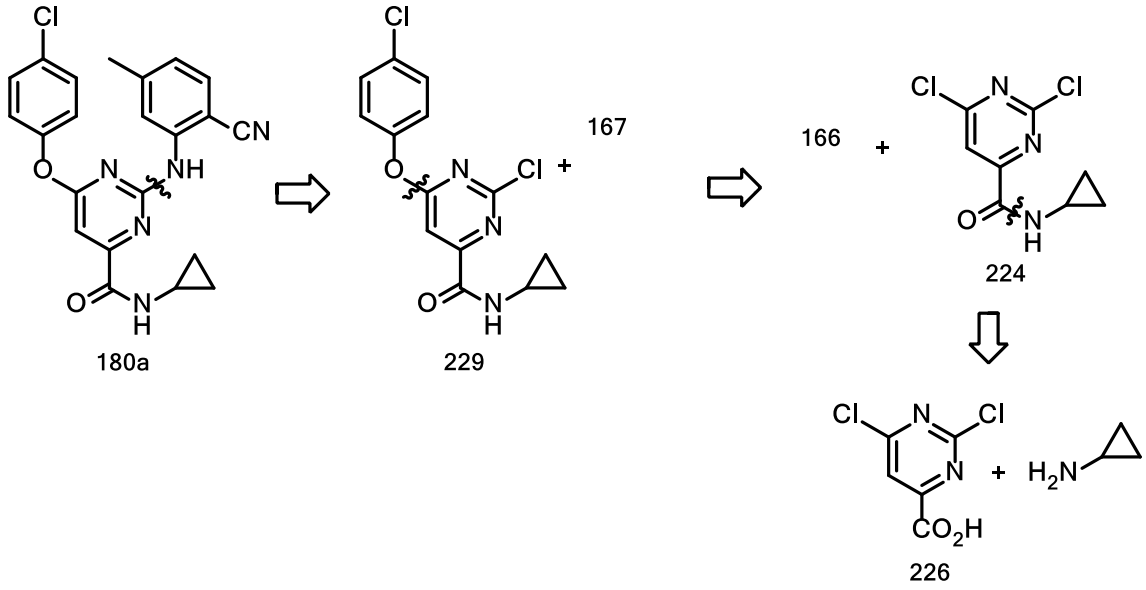

Scheme 3.37: Retrosynthetic analysis of novel target molecule **180a**

3.7.1 Synthesis of intermediate 224

The cyclopropylamide-based scaffold **224** was accessed via thionyl chloride-activated[3] amination of 2,6-dichloropyrimidine-4-carboxylic acid **225** with cyclopropylamine to generate the cyclopropylamide intermediate **224** in quantitative yield as shown in Scheme 3.38.

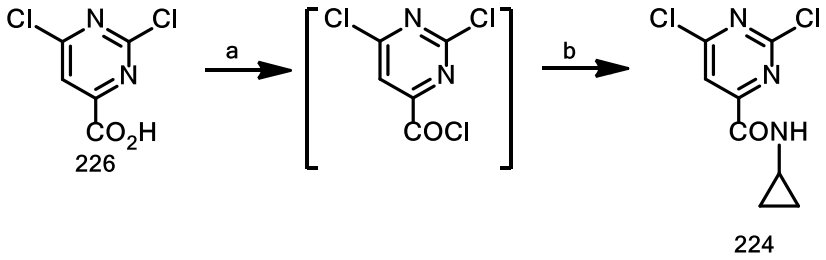

Scheme 3.38: *Reagents and conditions*: (a) $SOCl_2$, 80°C, 24 h; (b) DCM, cyclopropylamine, Et_3N, 0°C-RT, 4 h, 99%.

The formation of intermediate compound **224** was confirmed by ^1H NMR spectroscopy which showed the presence of an expected aromatic proton at 8.08 ppm, an amide proton singlet at 7.80 ppm and five proton signals in the aliphatic region.

Fortunately, substrate **224** was readily C-O coupled with 4-chlorophenoxide **166a**, using base-catalyzed conditions, to afford 6-(4-chlorophenoxy)-substituted pyrimidine **229a** in 89% yield (Scheme 3.39).

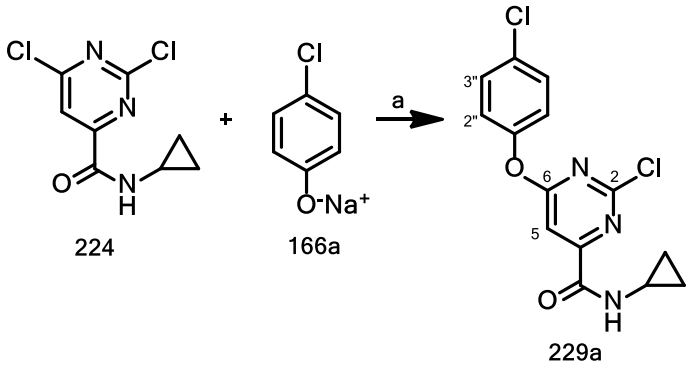

Scheme 3.39: *Reagents and conditions*; (a) 1.2 equiv. aq. 4-chlorophenoxide **166a**, acetone, 0°C-RT, 2 h, 89%.

The ^1H NMR spectrum for intermediate compound **229a** showed signals for five aromatic protons, an amide proton and five protons in the aliphatic region. Consistent with chlorine substitution at the C-6 position, the NOESY experiment for **229a** showed weak through space coupling between the pyrimidyl H-5 proton and the H-2" protons belonging to the 4-chlorophenoxy substituent. Furthermore, the pyrimidyl H-5 singlet appeared more shielded at

7.59 ppm as compared to a previous position of 8.08 ppm observed for **224**. The amide proton gave rise to a broad singlet at 7.77 ppm whilst the four protons from the 4-chlorophenoxy group showed two groups of multiplets in the regions 7.43–7.38 (2H) and 7.13–7.07 ppm (2H).

Our initial attempt to extend a similar base-catalyzed reaction for the nucleophilic displacement of the 2-chloro substituent of **229a** by 2-amino-4-methylbenzonitrile **167**, as previously done during the C-N coupling of chloride-based pyrimidine substrates, proved unsuccessful. However, the novel target molecule **180a** was successfully prepared by the palladium-catalyzed cross-coupling of intermediate compound **229a** with 2-amino-4-methylbenzonitrile **167** (Scheme 3.40).

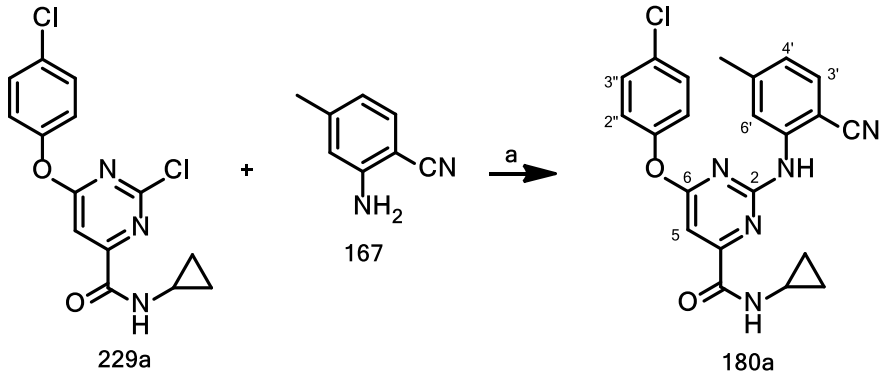

Scheme 3.40: *Reagents and conditions*; (a) 2 mol% Pd_2dba_3, 3mol% Xantphos, THF, K_3PO_4, 100-110°C; 64%.

^{1}H NMR spectroscopic analysis of novel compound **179a** showed eight aromatic proton signals, one amino proton signal, an amide proton signal and signals integrating for five protons in the aliphatic region. The amide proton appeared as a broad singlet that overlapped with H-6' in the region 7.76–7.74 ppm, whilst a second broad singlet from the amino proton was observed at 7.52 ppm. The H-2" multiplet overlapped with the H-3' doublet in the region 7.43–7.40 ppm. An H-5 singlet was observed at 7.29 ppm whilst H-3" and H-5" were as observed in the range 7.15–7.12 ppm and H-4' gave a multiplet in the 6.84–6.81 ppm region. An expected cyclopropyl proton multiplet appeared in the range 2.99–2.94 ppm whilst the other four cyclopropyl proton multiplets were observed in the regions 0.94–0.91 ppm (2H) and 0.74–0.71 ppm (2H). ^{13}C NMR spectroscopic data showed fourteen aromatic carbon signals and three carbon signals in the aliphatic region. The DEPT experiment showed six CH signals, ten quaternary aromatic carbon signals and one CH_3, one CH and one CH_2 signal in the aliphatic region. 2D NMR spectroscopy experiments showed that the carbonyl carbon signal was the most deshielded at 171.8 ppm followed by the C-O and C-N coupled C-6 and C-2 signals which appeared at 163.5 and 160.0 ppm, respectively.

Similarly, novel target molecule **180b** was accessed via intermediate **229b**. Intermediate **229b** was synthesized by nucleophilic displacement of 6-chloro substituent of **224** chlorine using 3,5-dichlorophenoxide **166b** to afford the compound **229b** (Scheme 3.41).

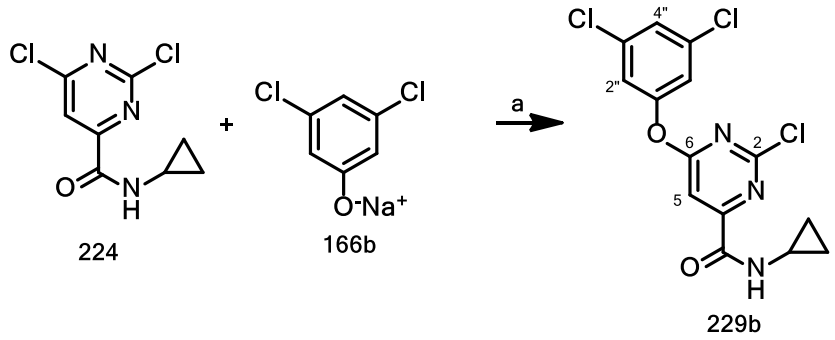

Scheme 3.41: *Reagents and conditions*; (a) 3,5-dichlorophenoxide **166b**, acetone, 0℃-RT, 2 h, 95%.

^{1}H NMR spectroscopic data showed four aromatic protons and a deshielded amide proton that appeared as a doublet (J = 5.0 Hz) at 8.94 ppm. A triplet signal (J = 1.8, 1.8 Hz) for H-4'' was observed at 7.64 ppm, whilst H-2" gave a doublet at 7.56 ppm (J = 1.8 Hz, 2H). As expected, the cyclopropyl proton signals were observed in the aliphatic region. ^{13}C NMR spectroscopy showed eight aromatic carbons, a carbonyl carbon and two aliphatic carbon signals with DEPT showing three CH (aromatic signals), and one CH and one CH_2 in the aliphatic region. The amide carbonyl was deshielded at 170.8 ppm whilst the C-O coupled C-6 signal was observed at 162.1 ppm.

Using a similar approach employed to access product **180a**, the novel target molecule **180b** was synthesized via a palladium-catalyzed coupling of intermediate **229b** with 2-amino-4-methylbenzonitrile **166b** to generate the target molecule **180b** (61%, Scheme 3.42).

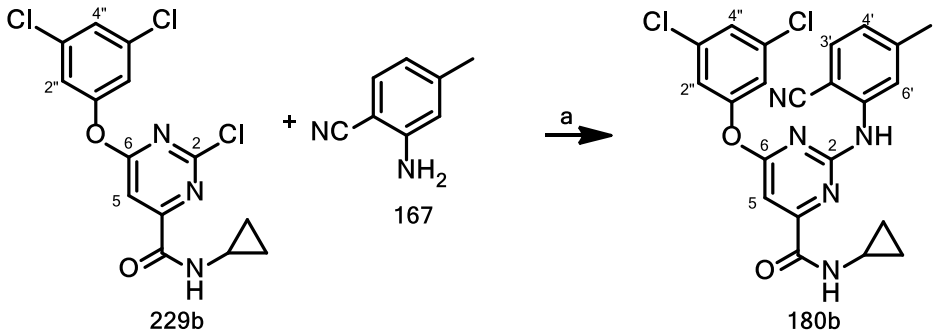

Scheme 3.42: *Reagents and conditions*; (a) 2 mol% Pd_2dba_3, Xantphos, THF, K_3PO_4; 61%.

Signals due to six aromatic and eight aliphatic protons were observed in the ^{1}H NMR spectrum of novel compound **180b**. The pyrimidyl H-5 proton was observed as a singlet at 7.51 ppm. The benzonitrile H-3' and H-4' were observed as coupling doublets (J = 8.0 Hz) at 7.49 ppm and 7.10 ppm, respectively, whilst H-6' appeared as singlet at 7.62 ppm. In addition, the amide and amino protons showed broad singlets at 8.47 ppm and 8.04 ppm, respectively. Lastly, the H-2" and H-4" protons on the 3,5-dichlorophenoxy motif appeared as a doublet (J = 1.8 Hz, 2H) at 7.14 ppm and a triplet (J = 1.8 Hz, 1H) at 7.26 ppm, respectively, whilst the cyclopropyl and methyl protons were observed in the aliphatic region, as expected. The ^{13}C NMR spectrum was similar to that obtained from product **180a**. Successful C-N coupling at the C-2 position of target **180b** was confirmed via 2D NMR spectroscopy experiments which showed a deshielded C-2 signal 162.4 ppm.

3.8 Synthesis of chlorine substituted triazine-based analogues 181

The chlorine-substituted triazine analogues **181**, just like the chloride-substitutes pyrimidine derivatives **207**-**220** discussed earlier, were also synthesized for exploratory purposes. We wanted to test whether halogen bonds could function as suitable pendants for initiating interactions with hydrophilic amino acid residues lining the putative entrance to the RT allosteric site.

The triazine-based analogues **181a** and **181b** of general structure **181** were accessed via intermediate scaffold **230** as shown in the retrosynthetic scheme below. (Scheme 3.44)

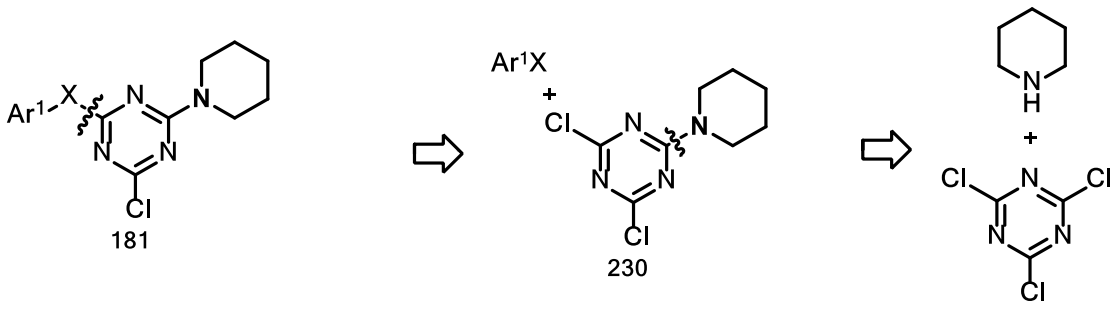

181a: X = O; Ar^1 = 4-ClPh

181b: X = NH; Ar^1 = 4-MePhCN

Scheme 3.44: Retrosynthetic analysis of triazine-based target molecule of general structure **181**

3.8.1 Synthesis of intermediate compound 230

Scaffold **230** was synthesized via a base-catalyzed amination of commercially available cyanuric chloride **231** with piperidine under ice-cold conditions[16] (Scheme 3.44).

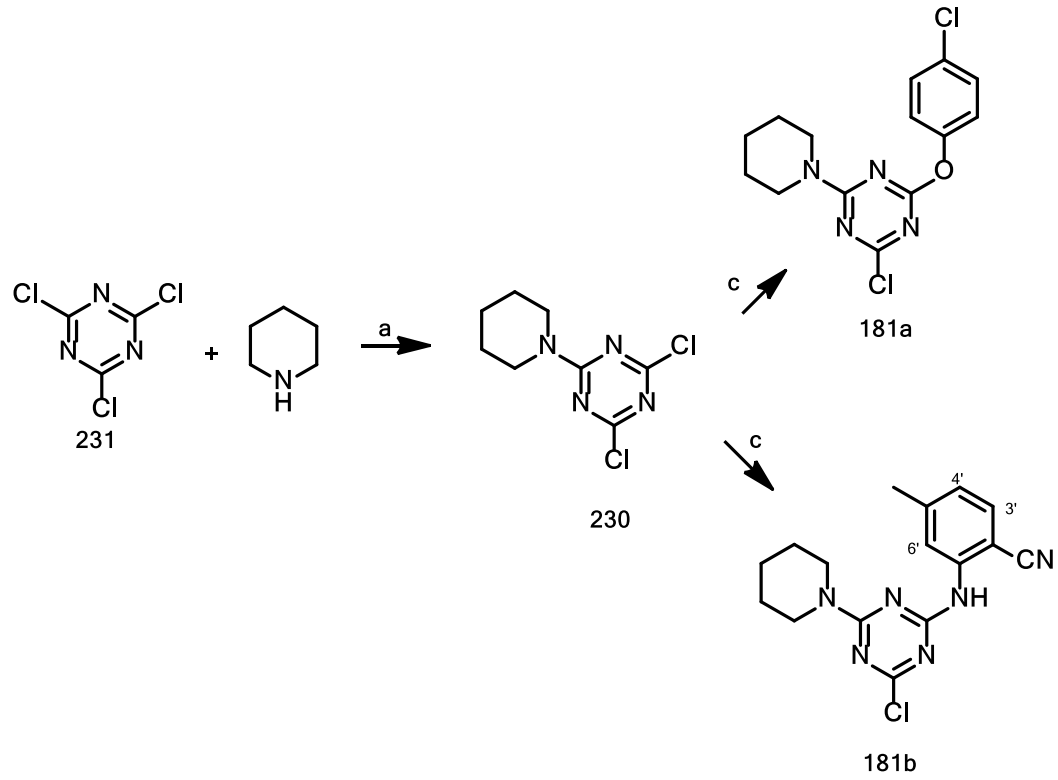

Scheme 3.45: *Reagents and conditions*; (a) acetone, **231** (2.0 mmol), piperidine (2.0 mmol), KO^{t}Bu (2.2 eq.), 0°C–RT, 4 h, 87%; (b) **230** (0.5 mmol), 4-chlorophenoxide **166a** (0.55 mmol), KO^{t}Bu (1.2 eq.), THF, 0°C–RT, 4 h, 78%; (c) **230** (0.5 mmol), 2-amino-4-methylbenzonitrile **167** (0.55 mmol), THF, KO^{t}Bu (1.2 eq.), 0°C–RT, 4 h, 65%;

The formation of 2,4-dichloro-6-(piperidin-1-yl)-1,3,5-triazine **230** was confirmed by ^{1}H NMR spectroscopy which showed the presence of the expected proton multiplet signals which integrated for ten protons in the regions 4.0–3.6 ppm (4H) and 1.72–1.48 ppm (6H). ^{13}C NMR spectroscopic analysis showed the presence of two aromatic carbon signals and five carbon signals in the aliphatic region. Successful C-N bond formation was confirmed by the presence of a deshielded C-6 signal at 170 ppm.

3.8.2 Synthesis of target molecules 181a and 181b

Intermediate scaffold **230** was further reacted with 4-chlorophenol **166** or 2-amino-4-methylbenzonitrie **167** to give target molecules **181a** and **181b** in reasonable yield (Scheme 3.45).

^{1}H NMR spectroscopic data for product **181a** integrated for the expected of four aromatic protons and ten aliphatic protons. The four aromatic protons appeared as multiplets in the regions 7.36–7.33 ppm (2H) and 7.13–7.10 (2H), whilst the ten aliphatic protons on the piperidyl motif were observed in the ranges 3.85–3.73 (2H), 3.68–3.50 (2H) and 1.70–1.49 ppm (6H). The ^{13}C NMR spectrum showed the presence of 7 aromatic carbon signals. Successful C-O coupling was confirmed by the presence of a more deshielded C-O signal at 171.23 ppm relative to the C-N signal observed at 170.37 ppm.

The ^{1}H NMR spectrum for target molecule **181b** showed the expected 3 aromatic signals and a broad amino proton singlet at 8.18 ppm, whilst thirteen protons were observed in the aliphatic region. Protons H-3', H-4' and H-6' were as a doublet at 7.47 ppm (J = 7.9 Hz), another doublet at 6.96 ppm (J = 7.9 Hz) and a singlet at 7.40 ppm, respectively.

3.9 Antiviral Assay

The novel pyrimidine-based target molecules **179**, **180a** and **180b** were screened against wild-type HIV using an already established antiviral assay protocol by Dr. A. Basson at the National Institute of Communicable Diseases, Sandringham, South Africa.

The antiviral assay results obtained for the pyridine- and pyrimidine-based targets are listed in Tables 3.1. The results display the concentrations of compounds that were required to inhibit 50% of cellular activity (IC_{50}) as well as achieve 50% cell viability (CC_{50}). The selectivity index (S.I. = CC_{50}/IC_{50}) was included as an indicator of the degree to which each tested compound was selective towards the wild-type virus. Novel lead compound **142e** and nevirapine were also included in the test against wild-type HIV to improve the robustness of the assay process.

3.9.1 Antiviral and toxicity results

The antiviral assay results for novel pyrimidine-based analogues **179**, **180a** and **180b** are listed in Table 3.4.

Table 3.4: *In vitro* anti-HIV assay for novel pyrimidine-based target compounds.

Cpd	Toxicity		Activity		S. Index
	CC_{50} (μM)	S. D.	IC_{50} (μM)	S. D.	
142e	54.25	9.76	1.07	0.03	50.7
179	37.51	10.14	62.08	0.36	0.6
180a	>100	-	>100	-	-
180b	57.91	6.90	56.11	3.76	1.0
181a	25.2	1.2	>7.2	-	-
181b	30.7	0.2	>14.0	-	-
Tox Cntrl DMSO	>1%	>1%	-	-	-
Act. Cntrl NVP	-	-	0.12	0.0	-

NB: DMSO – dimethyl sulfoxide, NVP – nevirapine.

Table 3.4 shows that the carbonitrile- **179** and cyclopropylamide-derived **180a-b** pyrimidine compounds and triazine-based analogues **181a-b** were inactive against the wild-type HI virus as previously observed from the *in vitro* assay of the chloride-derived pyrimidine analogues **207-220** (Table 3.2). However, we also noted an unusual cytotoxicity profile whereby at increased concentration the test compound(s) generally became more toxic to the pseudovirus - a phenomenon which appeared to encourage viral replication as previously explained in section 3.4.2.

3.10 Conclusion

In our second approach towards constructing potential anti-HIV-1 target molecules, molecular modelling was employed to design novel pyridine-, pyrimidine- and triazine-based analogues. These compounds were designed resembling a DAPY 'horse-shoe' type configuration on the premise that they would exhibit torsional flexibility as well as targeted interactions with key hydrophobic and hydrophilic amino acid residues surrounding the allosteric binding pocket of the 3MEG-RT crystal structure. We successfully extended our already developed Pd-catalyzed protocol[2] towards accessing a new set of di-functionalized pyridine-containing, tri-functionalized pyridine-, pyrimidine-carbonitrile and cyclopropylamide target molecules. To the best of our knowledge, no such compounds were identified in the contemporary organic chemistry literature at the time of writing of this thesis.

One of the target molecules, **172**, was accessed via the use of a biocatalytic approach as a key step towards the selective hydrolysis of a pyridyl carbonitrile group in substrate **170** to afford the desired carboxamide hit compound **172**. In this vein, an existing biocatalytic procedure[10] that utilized a nitrile hydratase enzyme was employed to access the desired target compound **172**.

Despite the favourable binding conformations elicited by the synthetic targets during the preliminary molecular modelling exercise, all the compounds were observed to be inactive against the wild type HI virus.

3.11 References

1. Lansdon, E. B.; Brendza, K. M.; Hung, M.; Wang, R.; Mukund, S.; Jin, D.; Birkus, G.; Kutty, N. and Liu, X. *J. Med. Chem*. **2010**, 53, 4295 – 4299.
2. Zhan, P.; Chen, X.; Li, D.; Fang, Z.; de Clercq, E. and Liu, X., *Med. Res. Rev*. **2013**, 33 (S1) E1 - E72.
3. Changunda, C. R. K.; Basson, A. E.; van Vuuren, S. F.; Rousseau, A. L. and Bode, M. L. *Tetrahedron*, **2017**, 73, 137 – 147.
4. Newkone, G. R. and Kawato, T. *J. Org. Chem*. **1979**, 44, 2693 – 2697.
5. a) Klein, C.; Baranoff, E.; Gratzel, M and Nazeeruddin, Md.-K, *Tetrahedron Lett*. **2011,** 52, 584 – 587; b) Arora, E.; Bhasin, K. K.; Mehta, S. K.; Sharma, N.; Bhasin, A. K. K.; Jacob, C.; Felix, V. AND Neogi, S. *Polyhedron*, **2014**, 316 – 322; c) Gershon, H. *J. Org. Chem.* **1962**, 27, 3507 – 3510; d) Davies, G. D.-Jnr; Baiocchi, F.; Roland, K. and Cheng, C. C. *J. Org. Chem*. **1961**, 26, 2755 – 2763; e) Wojciechoski, J. Patent No PL 71235 A5 19740430.
6. Bach, P.; Marczynke, M. and Giordanetto, F. *Eur. J. Org. Chem.* **2012**, 6940 – 6952.
7. Deacon, P. R.; Mahon, M. F.; Molly, K.C. and Waterfield, P. C. *J. Chem. Soc. Dalton Trans.* **1997**, 3705 – 3712.
8. Mckendry, L. H. *J. Label. Compd. Radiopharm* **1984**, 517 – 523.
9. Henegar, K. E.; Ashford, S. W.; Baughman, T. A.; Sih, J. C. and Gu, R.-L. *J. Org. Chem*. **1997**, 62, 6588 – 6597.
10. a) Schade, M. A.; Manolikakes, G. and Knochel, P. *Org. Lett.* **2010**, 12, 3648 – 3650; b) Liskey, C. W.; Liao, X. and Hartwig, J. F. *J. Am. Chem. Soc.* **2010**, 132, 11389 – 11391.
11. Klingesmith, L. M.; Strieter, E. R.; Timothy E. Barder, T. E. and Buchwald, S. L. *Organometallics*, **2006**, 25, 82 – 91.
12. Birkholz, M.-N.; Freixa, Z. and Piet W. N. M. van Leeuwen, P. W. N. M. *Chem. Soc. Rev.*, **2009**, 38, 1099 –1118.
13. Nicolaou, K. C. and Webber, S. E. *J. Am. Chem. Soc*. **1984**, 106, 5734 – 5736.
14. Delia, T. J. and Nagarajan, A. *J. Heterocyclic Chem.*, **1998**, 35, 269 – 273.
15. Chhiba, V.; Bode, M. L.; Mathiba, K.; Kwezi, W. and Brady, D. *J. Mol. Catalysis B: Enzymatic* **2012**, 76, 68 – 74.
16. Chen, K.-Y. and Huang, C.-T. *Int. J. Appl. Sci. Eng*. **2004**, 2, 286 – 294.

CHAPTER FOUR – ANTIMICROBIAL ASSAY

4.0 Introduction

Synthetic organic chemistry research has contributed immensely towards the development and discovery of novel compounds that are potent against microbial infections which afflict humanity globally. Viruses, bacteria and fungi are some of the tenacious disease-causing microorganisms whose survival depends on the invasion and exploitation of human host cell machinery. The human body, with its ideal temperature conditions and nutrients, provides an attractive incubation vessel for microbial growth and proliferation. Despite the successful research and development of potent antimicrobials over the years, microorganisms have progressively adapted themselves by evolving into drug-resistant strains[1] which pose a public health challenge. As such, microbial diseases continue to account for loss of lives across the globe. Thus, there is an ever growing need for continuous research into novel antimicrobial agents as alternative platforms for the development of potent antimicrobials to combat these drug-resistant illnesses.

Whilst our main objective in the first part of this research project was to design and develop novel pyridine-based compounds that could display NNRTI activity as already explained in Chapter 2, we also decided to screen such compounds against the common disease-causing microbes. Microbial organisms that were investigated include gram-positive bacteria *Bacillus cereus*, *Enterococcus faecalis* and *Staphylococcus aureus*; and gram-negative bacteria *Klebsiella pneumoniae* and *Pseudomonas aeruginosa* as well as the fungal microbe *Candida albicans*.

As such, this chapter is dedicated towards describing the assessment of antimicrobial activity of novel pyridyl-benzamides, -benzylamines, -sulfonamides, selected oxygen- and sulfur-coupled target molecules of general structures **142**, **143**, **144**, **151**, **157** and **160**, respectively (Fig. 4.1), which were accessed via synthetic methodologies[2] already discussed in Chapter 2.

The antimicrobial assays were carried out under the guidance of Professor Sandy van Vuuren, Department of Pharmacy and Pharmacology, University of the Witwatersrand.

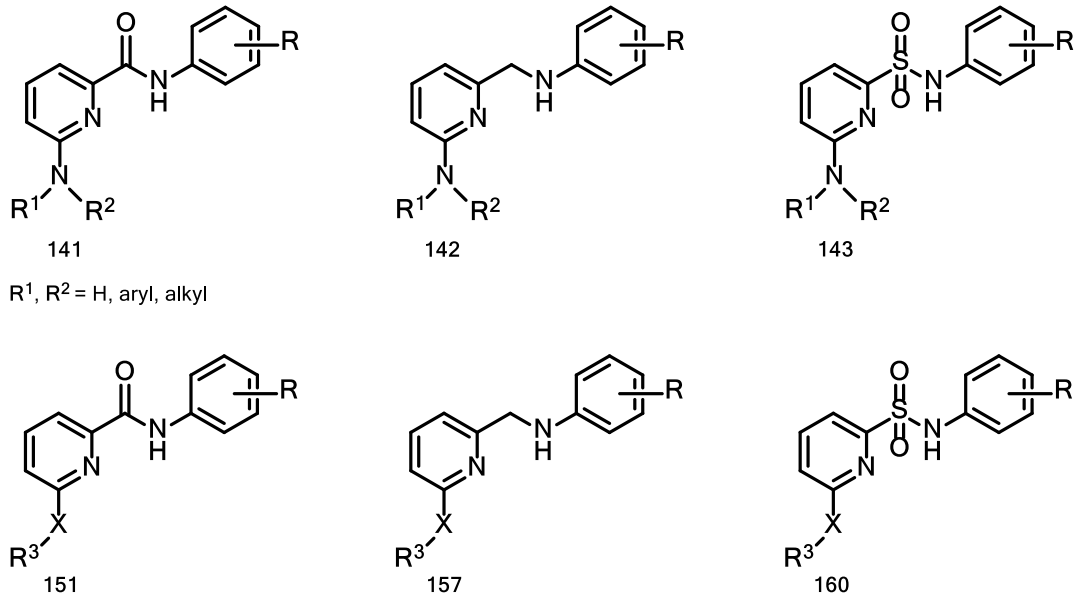

Figure 4.1: General structures of novel pyridyl-benzamide **142**, -benzylamine **143** and -sulfonamide **144** analogues as well as O- and S-coupled targets **151**, **157** and **160**.

4.1 Antimicrobial Assay

Antimicrobial activity of pyridyl-benzamides **142a-l**, **147a-f** and**151a-e**; pyridyl-benzylamines **143a-e**, **152** and **157a-e** and pyridyl-sulfonamides **144a-h**, **159a-b** and **160a-e** were evaluated using the microdilution method. The target compounds were dissolved in an appropriate amount of solvent to give a 5 mg/ml stock solution so that an initial concentration of 2.5 mg/ml was obtained in the first set of wells. The minimum inhibitory concentration (MIC) assay methodology developed by Leboho *et al.*[2] was used to ascertain the susceptibility of bacterial and yeast inoculum towards the pyridyl-benzamide, -benzylamine and -sulfonamide analogues.

Under sterile conditions, Tryptone Soya broth (100 µl) was placed in all wells of a 96 well microtitre plate. Samples (100 µl) in duplicate were serially diluted and an inoculum of approximately 1 × 10^6 colony forming units (CFU)/ml added. Bacterial cultures *(B. cereus* ATCC 11778, *S. aureus* ATCC 25923, *E. faecalis* ATCC 29212, *P. aeruginosa* ATCC 27858 and *K. pneumoniae* ATCC 13883) were incubated with serial dilutions at 37°C for 24 h with ciprofloxacin (0.01 mg/ml) as the control drug.

The fungal microbe *C. albicans* ATCC 10231 was incubated with serial dilutions at 37°C for 48 h with amphotericin (0.1 mg/ml) as the control drug. After incubation, 40 µl of the colour indicator, *p*-iodonitrotetrazolium violet (0.4 mg/ml) was added to each well, which turned purple-pink in the

presence of microbial growth. The end point MIC value was therefore taken as the first clear well within a column, which represented the lowest concentration of test sample that inhibited microbial growth.

4.2 Antimicrobial activity results

Antimicrobial activity results for the pyridyl-benzamide; -benzylamine and -sulfonamide test compounds are listed in Tables 4.1, 4.2 and 4.3, respectively. As a guide, we considered antimicrobial activity values that fell below a 100 µg/ml threshold as being significant.

As shown in Table 4.1, target compounds **142e** and **142i** (Fig. 4.2) showed reasonable antimicrobial activity of 39 µg/ml against the gram-positive bacterium *S. aureus* ATCC 25923. Another pyridyl-benzamide compound, **147i**, also displayed excellent antimicrobial activity (39 µg/ml) against another gram-positive bacterium, *B. cereus* (Fig. 4.2; Table 4.1). It was quite interesting to note that the 2-chloro- and 4-chloro-substituted analogues **142e** and **142i**, respectively, displayed meaningful antimicrobial activity (39 µg/ml) against *S. aureus* as opposed to the unsubstituted- (**142g** and **147b**) and 3-chloro-derivatives (**142h**) which were found to be inactive (Fig. 4.3). These observations possibly support the hypothesis that chlorine substitutions at the *ortho*- and *para*- positions are important contributing factors towards conferring reasonable antimicrobial activity in pyridyl-benzamide target compounds **142e** and **142i**.

Another gram-positive bacterium (*B. cereus* ATCC 11778) was observed to be highly susceptible (39 µg/ml) towards 4-cyanopyridyl-benzamide analogue **147e**, contrastingly; a corresponding analogue bearing an unsubstituted phenyl ring **147b** (Fig. 4.3) exhibited no antimicrobial activity against the gram-positive bacterial strains under study.

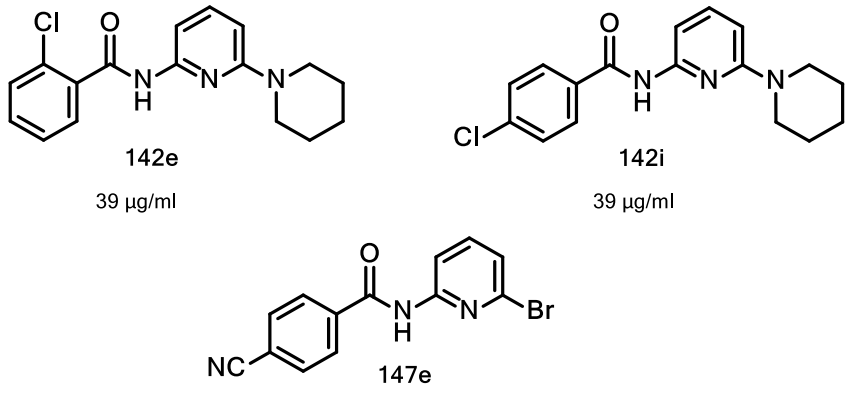

Figure 4.2: Pyridyl-benzamide compounds that were active against *S. aureus* (**142e**, **142i** and *B. cereus* (**147e**).

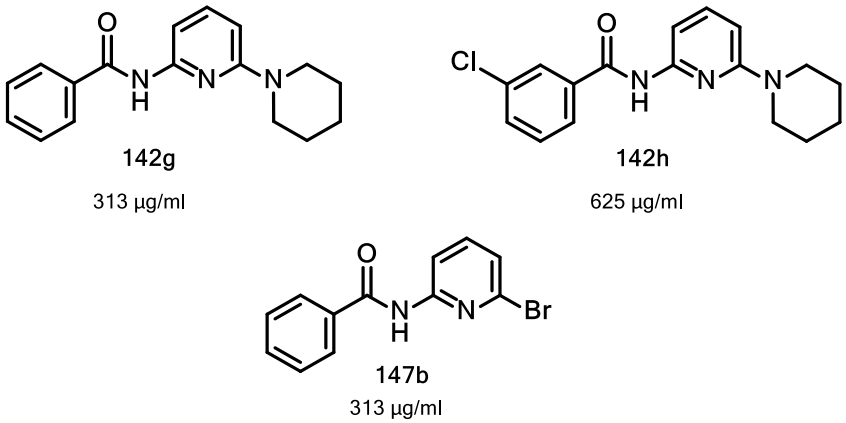

Figure 4.3: Inactive pyridyl-benzamide analogues **142g-h** and **147b**

Table 4.1: MIC results for novel pyridyl-benzamide compounds **142a-l**, **147a-f** and **151a-e**

Compound	*B. cereus* µg/ml	*S. aureus* µg/ml	*P. aeruginosa* µg/ml	*K. pneumoniae* µg/ml	*C. albicans* µg/ml	*E. faecalis* µg/ml
142a	>1,250	>1,250	156	156	156	625
142b	625	288	156	313	313	625
142c	625	625	156	625	313	625
142d	313	313	117	156	313	469
142e	625	**39**	117	391	313	625
142f	235	313	156	313	313	625
142g	313	>1,250	156	313	235	625
142h	625	625	156	313	235	625
142i	469	**39**	938	625	1,250	>1,250
142j	313	625	156	235	313	>1,250
142l	313	>1,250	156	>1,250	313	>1,250
151a	156	313	156	313	>1,250	>1,250
151b	938	>1,250	313	>1,250	>1,250	>1,250
151c	313	156	156	313	>1,250	>1,250
151d	313	117	156	313	>1,250	>1,250
151e	313	313	156	313	>1,250	>1,250
147a	313	313	235	>1,250	>1,250	>1,250
147b	313	156	156	521	>1,250	625
147c	313	>1,250	156	156	156	625
147d	>1,250	625	156	156	156	625
147e	**39**	>1,250	104	625	>1,250	>1,250
147f	313	>1,250	104	703	313	>1,250
+ Control[A]			0.039	0.039	12.50	0.313
- Control[S]	>1,250	>1,250	313	313	>1,250	>1,250
Culture control	>1,250	>1,250	>1,250	>1,250	>1,250	>1,250

A = antibiotic used as a control drug (**amphotericin** for *C. albicans* ATCC 10231; **ciprofloxacin** for the other five microbes); **S** = solvent.

Table 4.2 shows that only one pyridyl-benzylamine analogue **143e** (Fig. 4.3) displayed moderate antimicrobial activity (78 µg/ml) against *B. cereus* ATCC 11778, whilst the remaining analogues were inactive against the microbial cultures under study. It was quite interesting to note that whilst the pyridyl-benzamide compound **142e** showed reasonable antimicrobial activity against *S. aureus* as already highlighted above, its reduced analogue **143e** lost activity against the same bacterial species but showed moderate activity (78 µg/ml) towards another gram-positive bacterium *B. cereus* (Fig. 4.4).

In general, the observed loss of meaningful antimicrobial activity when crossing from pyridyl-benzamides to pyridyl-benzylamines could be indicative of the significant role played by the

amide carbonyl functionality towards enhancing antimicrobial activity as witnessed for the three pyridyl-benzamide analogues **142e**, **142i** and **147e.**

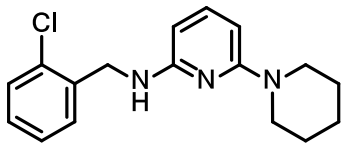

143e

78 µg/ml

Figure 4.4: Active Pyridyl-benzylamine **143e**

Table 4.2: MIC results for novel pyridyl-benzylamine analogues **143a-e**, **152** and **157a-e**

Compound	*B. cereus* µg/ml	*S. aureus* µg/ml	*P. aeruginosa* µg/ml	*K. pneumoniae* µg/ml	*C. albicans* µg/ml	*E. faecalis* µg/ml
143a	156	313	156	156	156	313
143b	156	625	156	156	156	625
143c	474	861	156	156	156	625
143d	625	>1,250	156	625	156	833
143e	**78**	117	**39**	1250	235	469
157a	>1,250	>1,250	156	313	156	>1,250
157b	313	313	156	156	-	>1,250
157c	625	>1,250	156	-	156	1,250
157d	625	>1,250	156	>1,250	>1,250	>1,250
157e	>1,250	625	235	>1,250	>1,250	>1,250
152	313	>1,250	156	156	156	625
+ Control			0.039	0.039	12.5	0.313
- Control	>1,250	>1,250	313	313	>1,250	>1,250
Culture control	>1,250	>1,250	>1,250	>1,250	>1,250	>1,250

As listed in Table 4.3, *B. cereus* ATCC 11778 displayed reasonable susceptibility (39 µg/ml) to **160e** as well as moderate susceptibility (78 µg/ml) to four other pyridyl-sulfonamide analogues **144a**, **160a**, **160c** and **160f**. Surprisingly, compound **160e** was the only sulfonamide derivative which displayed moderate to excellent antimicrobial activity against two gram-positive bacteria, *S. aureus* (78 µg/ml) and *B. cereus* (39 µg/ml), respectively. As per trend, the other members of the series, **159b** and **160b** were moderately active (78 µg/ml) against only one genetic species of the gram-positive bacteria, *S. aureus* (Figure 4.5). In general, we also observed that most of

the compounds bearing the sulfonamide moiety were found to show moderate to reasonable antimicrobial activity irrespective of the range of nucleophilic substitution (Fig. 4.5). This was not surprising given the fact that sulfonamides have historically been associated with good antimicrobial activity.

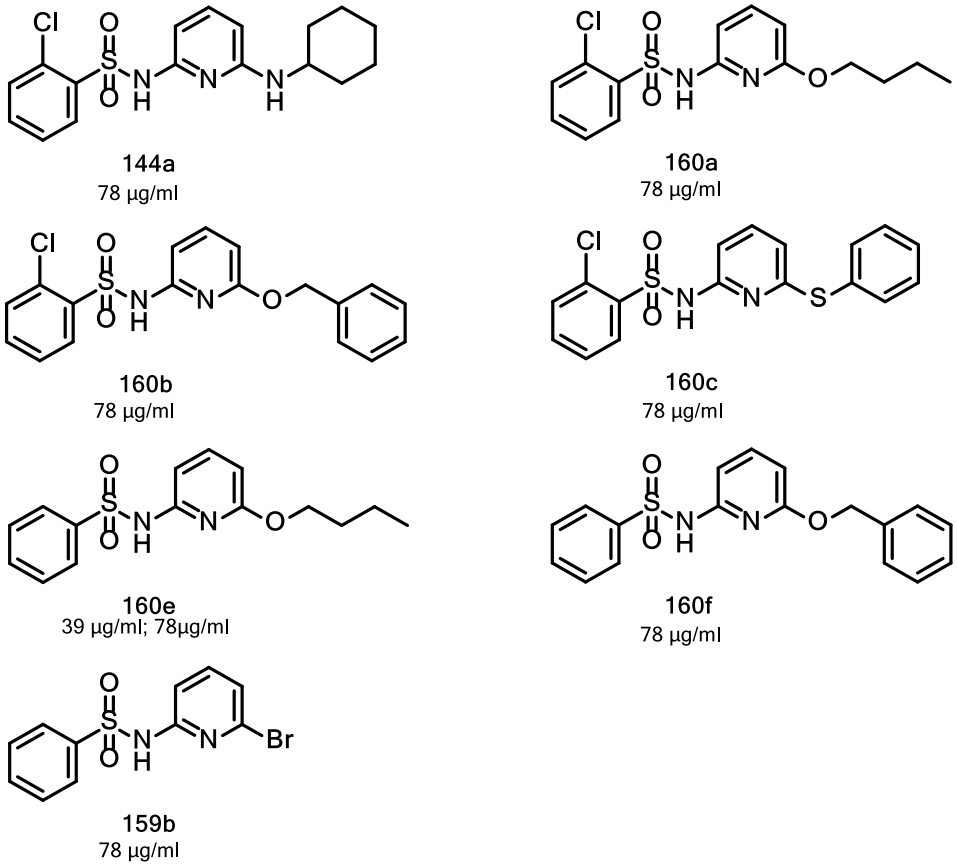

Figure 4.5: Pyridyl-sulfonamide analogues **144a**, **160a**-**c**, **160e**-**f** and **159b** showing activity in the assay

Table 4.3: MIC results for novel pyridyl-sulfonamide analogues **144a-h**, **159a-b** and **160a-f**

Compound	*B. cereus* µg/ml	*S. aureus* µg/ml	*P. aeruginosa* µg/ml	*K. pneumoniae* µg/ml	*C. albicans* µg/ml	*E. faecalis* µg/ml
144a	**78**	156	156	313	313	625
144b	>1,250	>1,250	156	313	313	625
144c	>1,250	156	156	313	469	625
144d	625	>1,250	156	313	313	625
144e	625	625	156	313	313	625
144f	313	313	235	>1,250	313	>1,250
144g	625	625	156	>1250	>1250	833
144h	625	625	156	938	>1250	833
160a	**78**	156	104	521	313	521
160b	156	**78**	156	>1,250	235	625
160c	**78**	156	156	>1,250	156	313
160d	156	>120	235	>1,250	156	625
160e	**39**	**78**	156	>1,250	938	625
160f	**78**	>1,250	156	>1,250	156	625
159a	117	156	156	469	313	625
159b	313	**78**	156	156	235	313
+ Control			0.039	0.039	12.5	313
- Control	>1,250	>1,250	313	313	>1,250	>1,250
Culture control	>1,250	>1,250	>1,250	>1,250	>1,250	>1,250

4.3 Conclusion

Three pyridyl-benzamide analogues **142e**, **142i** and **147e** (Fig. 4.2) including one pyridyl-sulfonamide target **160e** (Fig. 4.5), displayed meaningful antimicrobial activity against gram-positive bacterial strains *S. aureus* and *B. cereus*. Only one pyridyl-benzylamine compound **143e** and three sulfonamide derivatives **144a**, **160a** and **160c** showed moderate activity against *B. cereus* (39 µg/ml), whilst *S. aureus* displayed moderate susceptibility to other sulfonamide compounds **159b** and **160b**. The reasonable antimicrobial activity profiles (39 µg/ml) displayed by these pyridyl-benzamides and –sulfonamide analogues could be indicative of the biological significance of the carboxamide and sulfonamide functionalities in conferring antimicrobial activity against gram-positive bacterial strains investigated in this research project. Surprisingly, the gram-negative bacteria (*K. pneumoniae* & *P. aeruginosa*) and the fungal microbe (*C. albicans*) were resistant to all the novel test compounds that were used in the antimicrobial assay.

4.4 References

1. Eloff, J. N. *Planta Medica*, **1998**, 64, 711 – 713.

2. Changunda, C. R. K.; Rousseau, A. L.; Basson, A.; van Vuuren, S. F. and Bode, M. L. *Tetrahedron*, **2017**, 73, 137 – 147.

2. Leboho, T. C.; van Vuuren, S. F.; Michael, J. P. and de Koning, C. B. *Org. Biomol. Chem*. **2014**, 12, 307 – 315.

CHAPTER FIVE – CONCLUSION

5.1 Summary

In this research project, two approaches were employed to access novel compounds that could show good NNRTI activity. The first scaffold-hopping approach involved a virtual disconnection or "ring-opening" of the central core of an imidazo[1,2-*a*]pyridine[1] hit compound **141** previously identified in our laboratory to generate three scaffolds; a pyridyl-benzamide **142**, -benzylamine **143** and –sulfonamide **144** (Fig. 5.1). Using a Pd/*rac*-BINAP catalyzed synthetic methodology that was developed during the course of this research work, an original small set of *N*-coupled novel target molecules of general structures **141**, **142** and **143** (Fig 5.1) were synthesized and tested for antiviral activity. The Pd/*rac*-BINAP catalyzed protocol was also successfully extended towards cross-coupling of pyridyl halide substrates **147**, **155** and **159** with selected O- and S-containing nucleophiles to obtain novel targets of general structures **151**, **157** and **160**, respectively, as an additional library of compounds that were also tested against the wild-type HI virus (Scheme 5.1).

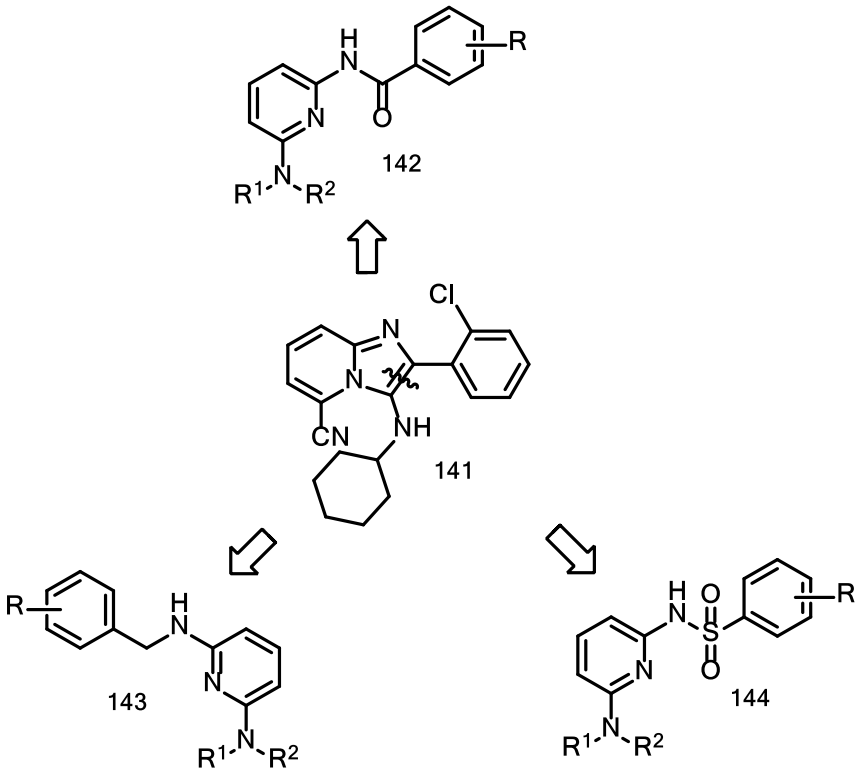

Figure 5.1: Virtual ring-opening of the imidazo[1,2-*a*]pyridine **141** to generate *N*-coupled (a) Pyridyl-benzamide **142**, (b) Pyridyl-benzylamine **143** and (c) Pyridyl-sulfonamide **144** scaffolds.

This scaffold-hopping approach proved to be successful as one pyridyl-benzamide compound **142e** (Fig. 5.2) with excellent antiviral activity (IC_{50} = 0.7μM) was identified from whole-cell antiviral screening. To the best of our knowledge, the *N*-substituted pyridyl benzamides have not previously been identified as anti-HIV compounds and represent a new compound class displaying NNRTI activity. We have recently published the scaffold-hopping approach to identify novel NNRTI in the journal, *Tetrahedron*.[2]

During the course of this work, we also observed the unanticipated displacement of fluorine, instead of bromine, by piperidine when substrate **147f** was subjected to the cross-coupling protocol to give unintended product **142g** (Scheme 5.2). This extremely facile displacement of fluorine was completely selective and no competing bromine-displacement product was observed. As expected, the reaction proceeded smoothly in the presence of base only, without any palladium catalyst. We believe this complete selectivity for displacement of fluorine, followed by the possibility of subsequently displacing bromine under palladium catalyzed conditions, makes compound **142g** a versatile intermediate for the construction of complex scaffolds. The bromine in compound **142g** was subsequently displaced with piperidine using palladium-mediated conditions to give novel product **142l** (Scheme 5.2).

Interestingly, antibacterial screening of the compound libraries also identifies compound **142e** as an antibacterial compound, displaying reasonable activity against the gram-positive *S. aureus*. Compound **142e** as well as other novel pyridyl-benzamides and -sulfonamides also displayed reasonable antimicrobial activity against the gram-positive bacteria, *S. aureus* and *B. cereus*.

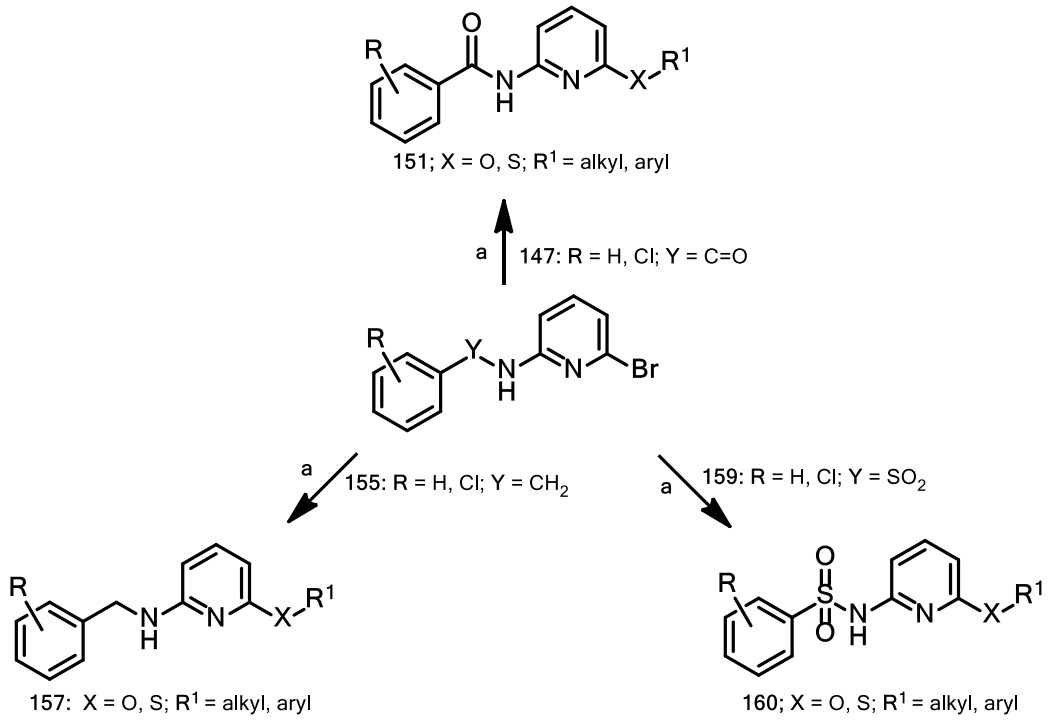

Scheme 5.1: General synthetic approach used to access novel O- and S-coupled derivatives of general structures **151**, **157** and **160**.

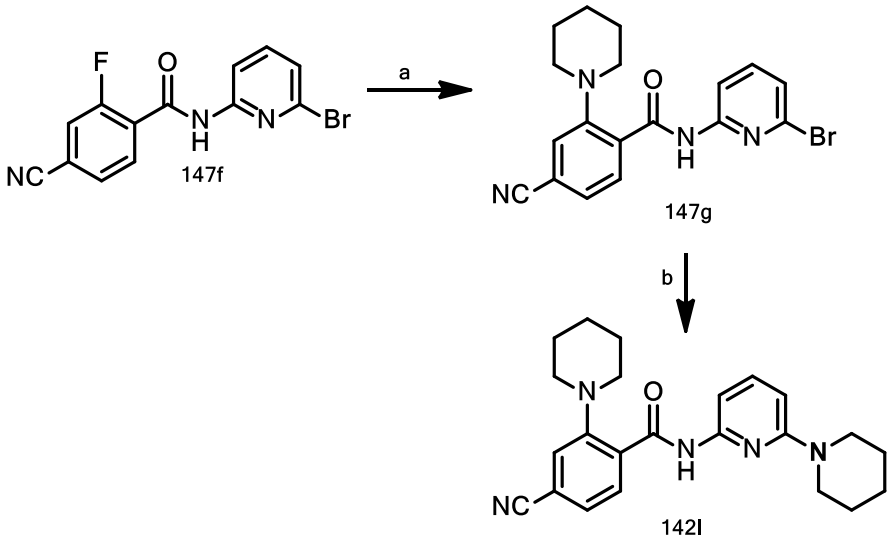

Scheme 5.2: Facile fluorine displacement reactions in the presence of (a) piperidine, KHMDS, 100-110°C, 24 h or (b) Pd catalysis, piperidine, KOtBu, 1,4-dioxane, 100-110°C, 24 h.

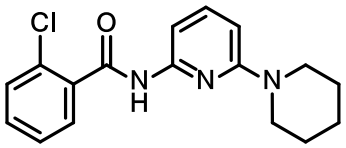

142e

IC_{50} = 0.7 μM]

Figure 5.2: Lead compound, 2-chloro-*N*-(6-(piperidin-1-yl)pyridin-2-yl)benzamide **142e**

In the second general approach towards constructing potential NNRTIs, molecular modelling was used to design novel pyridine-, pyrimidine- and triazine-based analogues possessing a 'horse-shoe' DAPY NNRTI framework typified by the rilpivirine conformation (Fig. 5.3), the concept of which was developed by Janssen and co-workers.[3-4]

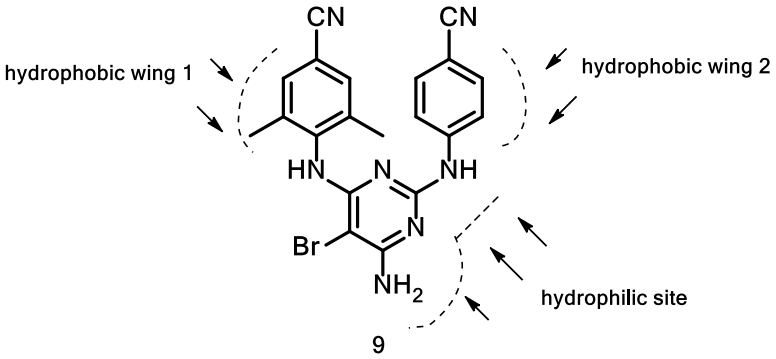

9

Figure 5.3: Etravirine **9** horse-shoe conformation

We used the pyridine, pyrimidine and triazine nuclei as central cores for constructing virtual di- and tri-functionalized derivatives which were *in silico*-docked into the allosteric site of the prepared 3MEG RT[5] crystal structure and provided di-functionalized pyridine-based as well as tri-functionalized (pyridine-, pyrimidine- and triazine-based) modelling hits as candidates for synthesis (Fig. 5.4).

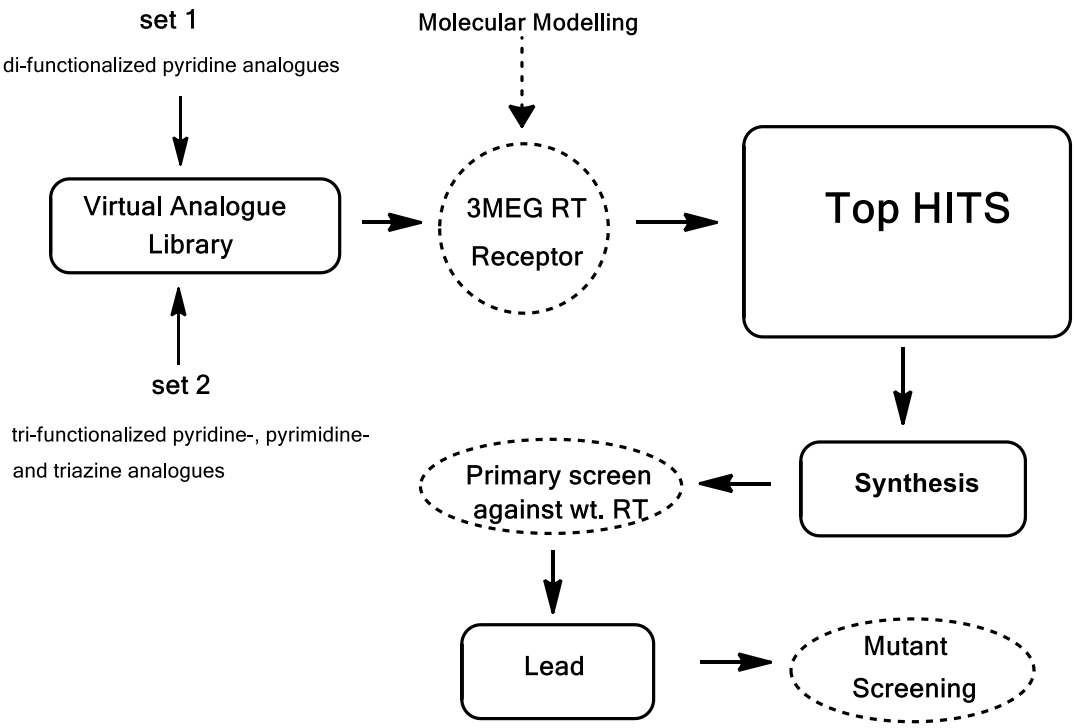

Figure 5.4: Flow diagram used for developing pyridine-, pyrimidine- and triazine-based anti-HIV target molecules

Once again, we successfully extended our already developed palladium-catalyzed protocol to the synthesis of di-functionalized pyridine-containing as well as tri-functionalized pyridine- and pyrimidine-carbonitrile and cyclopropylamide derived target molecules of general structure **182** (Fig. 5.5).

One key step in our synthesis required the selective conversion of one of the two carbonitrile groups to the corresponding amide. We were able to develop a novel a bio-catalytic approach that utilized nitrile hydratase enzyme for the selective hydrolysis of the pyridyl carbonitrile group in substrate **170**, leaving the amino phenyl nitrile moiety intact, to afford the top modelling hit carboxamide target **172** in excellent yield (Scheme 5.3)

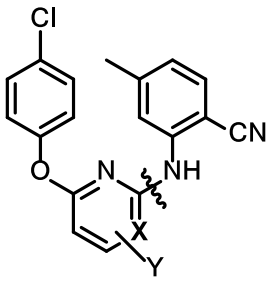

182

Difunctionalized pyridines : X= C, Y = H
Tri-functionalized pyridines : X= C, Y = CN, Amide
Tri-functionalized pyrimidines : X= N, Y = CN, Amide

Fig. 5.5: General structures for di- and tri-functionalized pyridines, and tri-functionalized pyrimidines

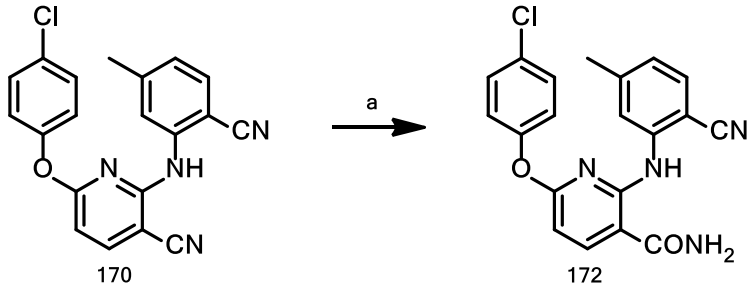

170 172

Scheme 5.3: Selective nitrile hydrolysis of substrate **170** to afford target molecule **172**

Of the two approaches, the scaffold-hopping approach was a more rewarding strategy as we managed to identify a novel pyridyl-benzamide compound **142e** with excellent activity against the wild-type virus, and moderate activity against one clinically significant mutation - **V106M** – despite an 8.9 fold loss in original activity against the wild-type RT.

5.2 Future Work

The excellent antiviral activity displayed by the pyridyl-benzamide compound **142e** against the wild-type RT positions this novel pharmacophore as a potential platform for the future development of compounds that could have better antiviral activity. Moreover, literature shows that compound **142e** closely resembles another series of novel pyridyl-benzamides that were observed to display good activity against *Trypanosoma brucei* - a human pathogen which is transmitted by the tsetse fly and causes sleeping sickness that afflicts almost one quarter of a

million people annually, in Africa.[6] Thus, the pharmacophore similarities between compound **142e** and the already identified 4-bromo-2-methyl-*N*-(pyridin-2-yl)benzamide hit compound[6] (Fig. 5.6) could place **142e** as a promising candidate for developing alternative analogues that target sleeping sickness.

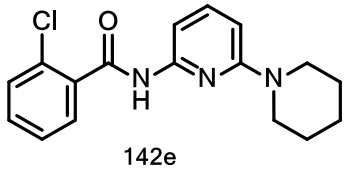

142e

2-chloro-*N*-(6-(piperidin-1-yl)pyridin-2-yl)benzamide

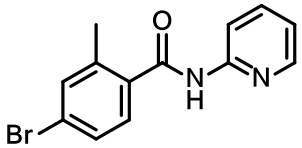

4-bromo-2-methyl-*N*-(pyridin-2-yl)benzamide

IC_{50} : *T.b. rhodiesiense*: 0.045 µM

Figure 5.6: Structures for novel pyridyl-benzamide **142e** and 4-bromo-2-methyl-*N*-(pyridin-2-yl)benzamide

Although the tri-functionalized derivatives that were accessed using the molecular modelling approach were not active against wild-type HIV, the ease of synthesis and favourable cytotoxic profiles displayed, especially by the halogen-functionalized pyrimidine derivatives **207** – **220**, provides a starting point for modifying such compounds in the quest for alternative anti-HIV leads.

Interestingly, organic chemistry literature shows that a 3,5-disubstituted pyridine[7] compound, **5b-2** exhibited excellent antiviral activity profiles against the wild-type virus in sharp contrast with the lack of activity observed from screening our 2,6-disubstituted pyridine derivative **172** (Fig. 5.7). As such, we are of the opinion that more research should be channelled towards the identification of anti-HIV leads that contain pyridine central cores.

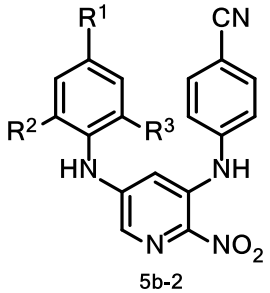

5b-2

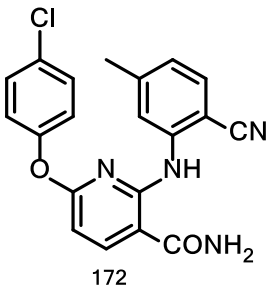

172

Figure 5.7: Structures for latest 3,5-disubstitued anti-HIV lead **5b-2** and a 2,6-disubstituted pyridine modelling hit **172**.

5.3 References

1. Bode, M. L.; Gravestock, D.; Moleele, S. S., van der Westhuyzen, C. W.; Pelly, S. C.; Steenkamp, P. A.; Hoppe, H. C.; Khan, T. and Nkabinde, L. A., *Bioorg. Med. Chem*. **2011**, 19, 4227 – 4237.
2. Changunda, C. R. K.; Rousseau, A. L.; Basson, A.; van Vuuren, S. F. and Bode, M. L. *Tetrahedron*, **2017**, 73, 137 – 147.
3. Zhan, P.; Chen, X.; Li, D.; Fang, Z.; de Clercq, E. and Liu, X., *Med. Res. Rev*. **2013**, 33 (S1) E1 - E72.
4. Janssen, P. A.; Lewi, P. J.; Arnold, E.; Daeyaert, F.; de Jonge, M.; Heeres, J.; Koymans, L.; Vinkers, M.; Guillemont, J.; Pasquier, E.; Kukla M.; Ludovici, D.; Andries, K.; de Béthune, M.P.; Pauwels, R.; Das, K.; Clark, A. D. Jr.; Frenkel, Y. V.; Hughes, S. H.; Medaer, B.; De Knaep, F.; Bohets, H.; De Clerck, F.; Lampo, A.; Williams, P. and Stoffels, P. *J. Med. Chem*. **2005**, 48, 1901 – 1909.
5. Landson, E. B.; Brendza, K. M.; Hung, M.; Wang, R.; Mukund, S.; Jin, D.; Birkus, G.; Kutty, N. and Liu, X. *J. Med. Chem*. **2009**, 17, 5744.
6. Ferrins, L.; Gazdik, M.; Rahmani, R.; Varghese, S.; Sykes, M. L.; Jones, A. J.; Avery, V. M.; White, K. L.; Ryan, E.; Charman, S. A.; Kaiser, M.; Bergostrom, C. A. S. and Baell, J. B. *J. Med. Chem*. **2014**, 57, 6393 – 6402.
7. Z. Liu, Z.; Tian, Y.; Liu, J.; Huang, B.; Kang, D.; De Clercq, E.; Daelemans, D. Pannecouque, C.; Zhan, P. and Liu, X. *Eur. J. Med. Chem.* **2017**, doi:10.1016/j.ejmech.2017.07.012.

CHAPTER SIX – EXPERIMENTAL SECTION

6.1 General

All solvents and amines were freshly distilled prior to use. Other reagents were used as purchased from Sigma-Aldrich. All infrared spectra were recorded neat using a Bruker TENSOR 27 single channel infrared spectrometer. All melting points are uncorrected and were performed using open capillary tubes on a Stuart SMP 10 melting point apparatus. ^{1}H and ^{13}C NMR spectra were recorded using either a Bruker AVANCE 111 300 or 500 MHz spectrometer in deuterated chloroform ($CDCl_3$) with trimethylsilane (TMS) as internal standard ($\delta = 0$) for ^{1}H NMR, and $CDCl_3$ ($\delta = 77.0$ ppm) for ^{13}C NMR. The chemical shift (δ) is reported in ppm and the coupling constants (*J*) in Hz. High resolution mass spectral data was collected on a Waters Synapt G2 using an ESI positive source and a cone voltage of 15 V. TLC was performed on aluminium-backed Merck silica gel 60 F_{254} plates. The purification of compounds by column chromatography was performed using gravity (particle size 0.063-0.200 mm) or flash (particle size 0.040-0.063 mm) silica gel 60 purchased from Merck. Where the word 'dioxane' is used, it should to be taken to mean '1.4-dioxane'.

6.2 Synthetic Methods for Chapter 2

Carbonyldiimidazole (CDI) carboxylic activation: Method A

Carbonyldiimidazole **148** (362 mg, 2.24 mmol) was slowly added to a 25 ml round bottomed flask containing 2-chlorobenzoic acid **146a** (250 mg, 1.60 mmol) dissolved in 1.4-dioxane (5 ml) at room temperature. The formation of the imidazolide intermediate occurred rapidly and was accompanied by the evolution of CO_2. After the organic acid had been quantitatively consumed as observed by TLC (20 min), Montmorillonite K-10 clay (362 mg), 2-amino-6-bromopyridine **145** (258 mg, 1.49 mmol) were added and the sealed reaction heated in an oil bath at 120 °C for 24 h. The cooled reaction was diluted with ethyl acetate (15 ml), washed successively with saturated brine solution (2 x 10 ml) and water (10 ml) and dried over Na_2SO_4. The organic filtrate was concentrated *in vacuo* to leave a crude mixture that was purified by flash silica column chromatography and eluting with 3–5% EtOAc/Hex to give the pyridyl-benzamide **147**.

Thionyl chloride activation: Method B

To an appropriately substituted benzoic acid (10.0 mmol) in a round-bottomed flask was added excess thionyl chloride (15 ml). The mixture was gently stirred and refluxed at 80°C in an oil bath for 24 h. After cooling the reaction mixture to room temperature, excess thionyl chloride was evaporated leaving a pale yellow benzoyl chloride residue which was dissolved in distilled acetonitrile (5 ml) and cautiously added to an ice-cold mixture of 2-amino-6-bromo-pyridine (1.6 g, 9.2 mmol) and pyridine (3 ml) in acetonitrile (15 ml). The mixture was stirred at 0°C for 30

min, warmed to room temperature and stirred for 4 h. Solvent was removed under reduced pressure and the residue was dissolved in dichloromethane (20 ml) and washed successively with aqueous saturated $NaHCO_3$ (2 x 10 ml), saturated brine solution (10 ml) and distilled water (2 x 10 ml) and then dried over anhydrous $MgSO_4$ or Na_2SO_4. The solvent was removed *in vacuo* and the crude mixture purified by flash silica gel column chromatography, eluting with 3–5% EtOAc/Hexane to give the desired product.

6.2.1 *N*-(6-bromopyridin-2-yl)-2-chlorobenzamide **147a**

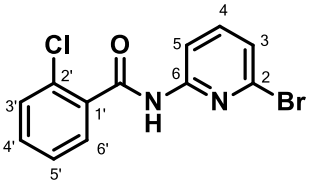

Product **147a** was prepared from method A (90 mg, 29%) or B (267 mg, 86%) and isolated as a white crystalline product. Mp: 103-104°C; IR (cm^{-1}): 3177 (NH), 1683 (C=O), 1592 (C=N), 1564 (NH bend), 1428 (C=C); ^1H NMR (300 MHz, $CDCl_3$) δ 8.58 (s, 1H, NH), 8.34 (d, *J* = 8.2 Hz, 1H, H-5), 7.74–7.67 (m, 1H, H-3'), 7.63 (t, *J* = 8.0 Hz, 1H, H-4), 7.50–7.34 (m, 3H, H-4', H-5', H-6'), 7.27 (d, *J* = 7.5 Hz, 1H, H-3, partly obscured by $CDCl_3$); ^{13}C NMR (75 MHz, $CDCl_3$) δ 164.8 (C=O), 151.1 (C-6), 140.7 (C-4), 139.4 (C-2), 134.4 (C-2'), 132.2 (Ar-C), 130.9 (C-1'), 130.6 (Ar-C), 129.9 (Ar-C), 127.3 (Ar-C), 124.1 (C-3), 112.6 (C-5); HRMS (ES^+) Calculated for $C_{12}H_9BrClN_2O$ $[M+H]^+$: 310.9587, found: 310.9576.

6.2.2 *N*-(6-bromopyridin-2-yl)benzamide **147b**

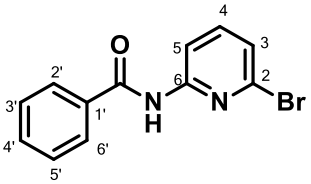

Product **147b** (254 mg, 92%) was prepared using method B and isolated as a white solid. Mp: 86-87°C; IR (cm^{-1}): 3254 (NH str.), 3083 (CH str.), 1658 (C=O str.), 1581 (C=N str.), 1558 (NH bend), 1423 (C=C); ^1H NMR (300 MHz, $CDCl_3$) δ 8.61 (br s, 1H, NH), 8.36 (d, *J* = 8.1 Hz, 1H, H-5), 7.99–7.88 (m, 2H, H-2', H-6'), 7.63–7.55 (m, 2H, H-4, H-4'), 7.50 (t, *J* = 8.4 Hz, 2H, H-3', H-5'), 7.24 (d, *J* = 7.7 Hz, 1H, H-3); ^{13}C NMR (75 MHz, $CDCl_3$) δ 165.6 (C=O), 151.6 (C-6), 140.7 (C-4), 139.3 (C-2), 133.7 (C-1'), 132.5 (C-4'), 128.9 (C-3'), 127.2 (C-2'), 123.7 (C-3), 112.5 (C-5); HRMS (ES^+) Calculated for $C_{12}H_{10}BrN_2O$ $[M+H]^+$: 276.9977, found: 276.9974.

6.2.3 *N*-(6-bromopyridin-2-yl)-3-chlorobenzamide **147c**

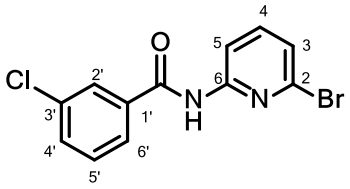

Product **147c** (295 mg, 95%) was prepared using method B and isolated as white crystals. Mp: 119-120°C; IR (cm^{-1}): 3278 (NH str.), 1669 (C=O), 1600 (C=N str.), 1561 (NH bend), 1431 (C=C); ^{1}H NMR (500 MHz, $CDCl_3$) δ 8.69 (s, 1H, NH), 8.31 (d, *J* = 8.1 Hz, 1H, H-5), 7.88 (t, *J* = 1.9 Hz, 1H, H-2') 7.75 (dt, *J* = 7.8, 1.3 Hz, 1H, H-4'), 7.59 (t, *J* = 7.9 Hz, 1H, H-4), 7.54–7.50 (m, 1H), 7.41 (t, *J* = 7.9 Hz, 1H, H-5'), 7.24 (d, *J* = 7.6 Hz, 1H, H-3); ^{13}C NMR (125 MHz, $CDCl_3$) δ 164.3 (C=O), 151.3 (C-6), 140.7 (C-4), 139.3 (C-2), 135.4 (C-3'), 135.1 (C-1'), 132.5 (C-4'), 130.1 (C-5'), 127.7 (C-2'), 125.2 (C-6'), 124.0 (C-3), 112.6 (C-5); HRMS (ES^+) Calculated for $C_{12}H_9BrClN_2O$ $[M+H]^+$: 310.9587, found: 310.9582.

6.2.4 *N*-(6-bromopyridin-2-yl)-4-chlorobenzamide **147d**

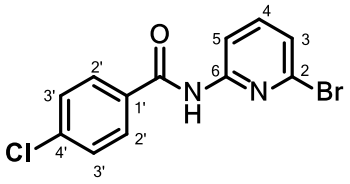

Product **147d** (304 mg, 98%) was prepared using method B and isolated as white crystals. Mp: 128-129°C; IR (cm^{-1}): 3277 (NH str.), 1669 (C=O), 1589 (C=N str.), 1561 (NH bend), 1430 (C=C); ^{1}H NMR (300 MHz, $CDCl_3$) δ 8.55 (s, 1H, N**H**), 8.32 (dd, *J* = 8.2, 0.6 Hz, 1H, H-5), 7.91–7.80 (m, 2H, H-2'), 7.61 (t, *J* = 7.8 Hz, 1H, H-4), 7.51–7.44 (m, 2H, H-3'), 7.26 (dd, *J* = 8.2, 0.6 Hz, 1H, H-3); ^{13}C NMR (75 MHz, $CDCl_3$) δ 164.5 (C=O), 151.4 (C-6), 140.7 C-4), 139.4 (C-2), 139.0 (C-4'), 132.1 (C-1'), 129.2 (C-2'), 128.7 (C-3'), 123.9 (C-3), 112.5 (C-5); HRMS (ES^+) Calculated for $C_{12}H_9BrClN_2O$ $[M+H]^+$: 310.9587, found: 310.9584.

6.2.5 *N*-(6-bromopyridin-2-yl)-4-cyanobenzamide **147e**

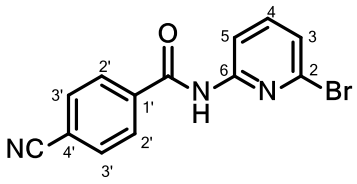

Product **147e** (283 mg, 94%) was prepared from method B and isolated as white crystals. Mp: 197-198°C; IR (cm^{-1}): 3436 and 3303 (NH str.), 2237 (CN str.), 1685 (C=O), 1584 (C=N str.), 1569 (NH bend), 1434 (C=C); ^{1}H NMR (500MHz, $CDCl_3$) δ 8.61 (s, 1H, NH), 8.32 (dd, *J* = 8.2, 0.7 Hz, 1H, H-5), 8.10–7.96 (m, 2H, H-2'), 7.89–7.77 (m, 2H, H-3'), 7.65 (t, *J* = 8.0 Hz, 1H, H-4), 7.30 (dd, *J* = 7.8, 0.7 Hz, 1H, H-3); ^{13}C NMR (75MHz, $CDCl_3$) δ

163.7 (C=O), 151.0 (C-6), 140.9 (C-4), 139.5 (C-2), 137.5 (C-1), 132.8 (C-4'), 127.9 (C-2'), 124.4 (C-3), 117.7 (C=N), 116.2 (C-4'), 112.6 (C-5); HRMS (ES$^+$) Calculated for $C_{13}H_9BrN_3O$ $[M+H]^+$: 301.9929, found: 301.9927.

6.2.6 *N*-(6-(bromopyridin-2-yl)-4-cyano-2-fluorobenzamide **147f**

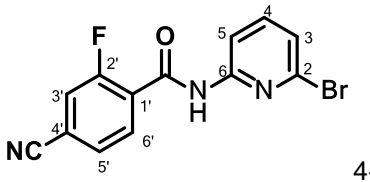

4-Cyano-2-fluorobenzoic acid (0.5 g, 3.0 mmol) was quantitatively converted to a reactive acyl chloride which was further reacted with 2-amino-6-bromopyridine **146** (0.52 g, 3.0 mmol), using method B to give compound **147f** as a white crystalline solid (1.012 g, 97%). Mp: 210–211°C; IR (cm^{-1}): 3436 (NH str.), 3097 and 2923 (CH str.), 2238 (CN), 1686 (C=O), 1621 (C=N), 1565 (NH bend), 1437 (C=C); ^{1}H NMR ($CDCl_3$, 500 MHz) δ 9.00 (d, *J* = 12.2 Hz, 1H, N**H**), 8.38 (d, *J* = 2.1 Hz, 1H, H-3'), 8.31–8.24 (m, 2H, H-5, H-6'), 7.88 (dd, *J* = 8.8, 2.4 Hz, 1H, H-5'), 7.64 (dd, *J* = 8.1, 1.5 Hz, 1H, H-4), 7.54 (dd, *J* = 11.0, 1.4 Hz, 1H, Ar-H); ^{13}C NMR (126 MHz, $CDCl_3$) δ 160.620 (d, $J_{C\text{-}F}$ = 250 Hz), 159.617 (d, $J_{C\text{-}F}$ = 3 Hz), 149.4 (Ar-C), 149.1 (C-2), 141.0 (C-4), 133.3 (d, $J_{C\text{-}F}$ = 2 Hz), 128.8 (d, $J_{C\text{-}F}$ = 4 Hz), 125.3 (d, $J_{C\text{-}F}$ = 12 Hz), 125.2 (Ar-C), 120.4 (d, $J_{C\text{-}F}$ = 28 Hz), 117.5 (d, $J_{C\text{-}F}$ = 10 Hz), 116.4 (Ar-C), 115.9 (Ar-C), 115.8 (Ar-C); HRMS (ES$^+$) Calculated for $C_{13}H_8BrFN_3O$ $[M+H]^+$: 319.9835, found: 319.9831.

General procedures for transition metal-catalyzed preparation of compounds **142**

Copper (1) Iodide-catalyzed procedure for the preparation of compounds **142** – Method C

Copper (I) iodide (9.5 mg, 5 mol %), *N*-(6-bromopyridin-2-yl)-2-chlorobenzamide **147a** (311 mg, 1.0 mmol), dioxane (3 ml, degassed) and a magnetic stirrer were added to an oven-dried 10ml round bottomed flask containing dioxane (3 ml) under nitrogen purge. The flask was sealed and heated with stirring at 80°C in an oil bath (5 min). Ethylene glycol (2 eq.), amine (1.3 mmol) and K_3PO_4 (510 mg, 2.4 mmol) were added and the sealed reaction was heated at 120°C -135°C for 24 h. The reaction mixture was cooled to room temperature, diluted with chloroform/dichloromethane (15 ml) and filtered through Celite. The filtrate was washed successively with saturated aqueous $NaHCO_3$ (10 ml) and distilled water (2 x10 ml). After drying over $MgSO_4$, the solvent was removed under reduced pressure and the crude brown mixture was purified by silica gel column chromatography, eluting the desired compound with 2 – 5% EtOAc/Hexane.

Palladium/rac-BINAP-catalyzed procedure for the preparation of compounds **142** - Method D

Tris-(dibenzylideneacetone)-di-palladium (0) [Pd_2dba_3], (19 mg, 2 mol %), *rac*-BINAP (38 mg, 6 mol %), dioxane (3–5 ml, degassed) and a magnetic stirrer were added to an oven-dried 10 ml round bottomed flask and purged with nitrogen. The flask was sealed and heated with stirring at 80°C in an oil bath (5 min). An *N*-(6-bromopyridin-2-yl)benzamide **147a-e** (1.0 mmol), an amine (1.3–3.0 mmol) and potassium *tert*-butoxide (2.4 mmol) were added and the sealed reaction was heated at 120–130°C for 24 h. The reaction mixture was cooled to room temperature, diluted with chloroform (15 ml) and filtered. The filtrate was washed successively with saturated aqueous $NaHCO_3$ (10 ml) and distilled water (2x10 ml). After drying over $MgSO_4$, the solvent was removed *in vacuo* and the crude brown mixture was purified by silica gel flash column chromatography, eluting the title compound with 2–5% EtOAc/Hexane.

6.2.3.1 2-Chloro-*N*-(6-(cyclohexylamino)-pyridin-2-yl)-benzamide **142a**

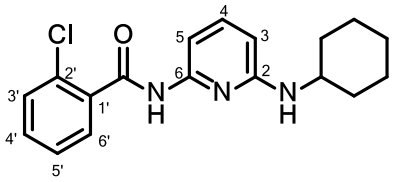

Reaction of *N*-(6-bromopyridin-2-yl)-2-chlorobenzamide **147a** (311 mg, 1.0 mmol) with freshly distilled cyclohexylamine (130 mg, 1.3 mmol) using method C gave rise to product **142a** (261 mg, 79%) as a golden yellow oil. Use of method D also gave rise to product **142a** (247 mg, 75%); IR (cm^{-1}) 3388 (NH str.), 2927 and 2852 (CH str.), 1681 (C=O), 1611 (C=N), 1430 (C=C); ^{1}H NMR (300 MHz, $CDCl_3$) δ 8.27 (s, 1H, Amide N**H**), 7.66 (dd, *J* = 7.4, 1.6 Hz, 1H, H-3'), 7.56 (d, *J* = 7.7 Hz, 1H, H-5), 7.51–7.29 (m, 4H, H-4 overlaps with 4', H-5' and H-6'), 6.15 (d, *J* = 8.1 Hz, 1H, H-3), 4.35 (d, *J* = 6.9 Hz, 1H, NH), 3.60–3.33 (m, 1H, cyclohexyl), 2.18–1.92 (m, 2H, cyclohexyl), 1.81–1.56 (m, 3H, cyclohexyl), 1.45–0.78 (m, 5H, cyclohexyl); ^{13}C NMR (75 MHz, $CDCl_3$) δ 164.5 (C=O), 157.0 (C-2), 149.6 (C-6), 139.7 (C-4), 135.4 (C-2'), 131.5 (Ar-C), 130.9 (C-1'), 130.4 (Ar-C), 129.8 (Ar-C), 127.1 (Ar-C), 103.2 (C-3), 102.0 (C-5), 50.2 (cyclohexyl), 33.3 (cyclohexyl), 25.8 (cyclohexyl), 24.9 (cyclohexyl); HRMS (ES^+) Calculated for $C_{18}H_{21}ClN_3O$ $[M+H]^+$: 330.1373, found: 330.1374.

6.2.3.2 *N*-(6-(benzylamino)-pyridin-2-yl)-2-chlorobenzamide **142b**

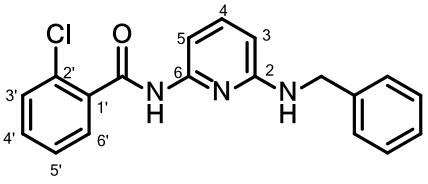

Reaction of *N*-(6-bromopyridin-2-yl)-2-chlorobenzamide **147a** (311 mg, 1.0 mmol) with freshly distilled benzylamine (139.2 mg, 1.3 eq.) using method C gave product **142b** (85 mg, 25%) as a pale yellow oil. Use of method D also gave **142b** (209 mg, 62%). IR (cm^{-1}) 3379 (NH str.), 3028 (CH str.), 1670 (C=O), 1608 (C=N), 1432 (C=C); ^{1}H NMR (300 MHz, $CDCl_3$) δ 8.29 (s, 1H, Amide N**H**), 7.68 (dd, *J* = 7.1, 2.0 Hz, 1H, H-3'), 7.63 (d, *J* = 7.0 Hz, 1H, H-5), 7.50–7.26 (m, 9H, Ar-H), 6.18 (d, *J* = 8.1 Hz, 1H, H-3), 4.76 (t, *J* = 5.8 Hz, 1H, N**H**), 4.45 (d, *J* = 5.8 Hz, 2H, PhC**H**$_2$-); ^{13}C NMR (75 MHz, $CDCl_3$) δ 164.5 (C=O), 157.4 (C-2), 149.5 (C-6), 139.8 (C-4), 139.2 (Ar-C), 135.3 (C-2'), 131.6 (Ar-C), 130.9 (C-1'), 130.4 (Ar-C), 129.9 (Ar-C), 128.6 (Ar-C), 127.4 (Ar-C), 127.3 (Ar-C), 127.1 (Ar-C), 103.4 (C-3), 102.7 (C-5), 46.1 (Bn**C**H$_2$-; HRMS (ES^+) Calculated for $C_{19}H_{17}ClN_3O$ $[M+H]^+$: 338.1060, found: 338.1064.

6.2.3.3 2-Chloro-*N*-(6-(phenylamino)-pyridin-2-yl)benzamide **142c**

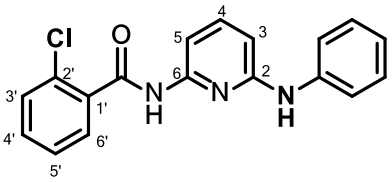

Reaction of *N*-(6-bromopyridin-2-yl)-2-chlorobenzamide **147a** (311 mg, 1.0 mmol) with freshly distilled aniline (121 mg, 1.3 eq.) using method C gave product **142c** (139 mg, 43%) as a pale yellow oil. Use of method D also gave **142c** (210 mg, 65%); IR (cm^{-1}) 3301 (NH str.), 3043 (CH str.), 1654 (C=O), 1590 (C=N), 1561 (NH bend), 1494 (C=C); ^{1}H NMR (300 MHz, $CDCl_3$) δ 9.30 (s, 1H, N**H**), 8.56 (s, 1H, N**H**), 8.27 (d, *J* = 8.2 Hz, 1H, Ar-H), 7.63–7.54 (m, 2H, Ar-H), 7.39–7.26 (m, 4H, Ar-H), 7.25–7.20 (m, 3H, Ar-H), 7.05 (t, *J* = 7.3, 1H, H-4), 6.80 (ddd, *J* = 8.0, 6.0, 2.3 Hz, 1H); ^{13}C NMR (75 MHz, $CDCl_3$) δ 167.7 (C=O), 151.6 (C-2), 146.7 (C-6), 141.0 (Ar-C), 140.5 (C-4), 139.4 (C-2'), 133.4 (Ar-C), 129.4 (Ar-C), 127.7 (Ar-C), 123.6 (Ar-C), 123.2 (Ar-C), 121.7 (Ar-C), 118.0 (Ar-C), 116.5 (Ar-C), 115.7 (C-3), 112.4 (C-5); HRMS (ES^+) Calculated for $C_{18}H_{15}ClN_3O$ $[M+H]^+$: 324.0904, found: 324.0893.

6.2.3.4 2-Chloro-*N*-(6-morpholinopyridin-2-yl)benzamide **142d**

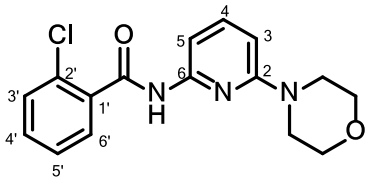

Reaction of *N*-(6-bromopyridin-2-yl)-2-chlorobenzamide **147a** (311 mg, 1.0 mmol) with freshly distilled morpholine (113.2 mg, 1.3 eq.) using method D gave product **142d** (178 mg, 56%) as a pale yellow oil. IR (cm^{-1}): 3396 and 3251 (NH str.), 2962 and 2852 (CH str.), 1676 (C=O), 1600 (C=N), 1566 (NH bend), 1436 (C=C); ^{1}H NMR (300 MHz, $CDCl_3$) δ 8.37 (s, 1H, N**H**), 7.76–7.63 (m, 2H, Ar-H), 7.57 (t, *J* = 8.0 Hz, 1H, H-4), 7.47–7.28 (m, 3H, Ar-H), 6.39 (d, *J* = 6.6 Hz, 1H, H-3), 3.85–3.71 (m, 4H, morpholinyl), 3.52–3.33 (m, 4H, morpholinyl); ^{13}C NMR (75 MHz, $CDCl_3$) δ 164.6 (C=O), 158.3 (C-2), 149.4 (C-6), 140.0 (C-4), 135.4 (C-2'), 131.6 (Ar-C), 130.8 (C-1'), 130.4 (Ar-C), 129.8 (Ar-C), 127.1 (Ar-C), 103.3 (C-3), 103.1 (C-5), 66.7 (morpholinyl), 45.4 (morpholinyl); HRMS (ES^+) Calculated for $C_{16}H_{17}ClN_3O_2$ $[M+H]^+$: 318.1009, found: 318.1006.

6.2.3.5 2-Chloro-*N*-(6-(piperidin-1-yl)-pyridin-2-yl)benzamide **142e**

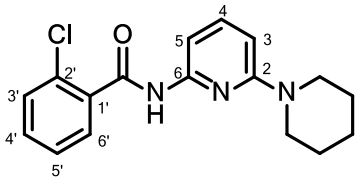

Reaction of *N*-(6-bromopyridin-2-yl)-2-chlorobenzamide **147a** (311 mg, 1.0 mmol) with freshly distilled piperidine (1.3 eq.) using method D gave compound **142e** (214 mg, 68%) as a light yellow oil which solidified on drying. Mp: 111-113°C. IR (cm^{-1}) 3190 (NH str.), 2929 and 2851 (CH str.), 1683 (C=O), 1605 (C=N), 1561 (NH bend), 1440 (C=C); ^{1}H NMR (300 MHz, $CDCl_3$) δ 8.65 (s, 1H, N**H**), 7.70–7.42 (m, 3H, Ar-H), 7.41–7.28 (m, 2H, Ar-H), 7.28–7.17 (m, 1H, Ar-H), 6.33 (d, *J* = 8.3 Hz, 1H, H-3), 3.54–3.27 (m, 4H, piperidyl), 1.67–1.45 (m, 6H, piperidyl); ^{13}C NMR (75 MHz, $CDCl_3$) δ 164.8 (C=O), 158.2 (C-2), 149.5 (C-6), 139.8 (C-4), 135.6 (C-2'), 131.2 (Ar-C), 130.8 (Ar-C), 130.2 (Ar-C), 129.4 (Ar-C), 127.0 (Ar-C), 103.2 (C-3), 101.8 (C-5), 46.0 (piperidyl), 25.4 (piperidyl), 24.7 (piperidyl); HRMS (ES^+) Calculated for $C_{17}H_{19}ClN_3O$ $[M+H]^+$: 316.1217, found: 316.1206.

6.2.4.6 *N*-(6-(piperidin-1-yl)-pyridin-2-yl)benzamide **142g**

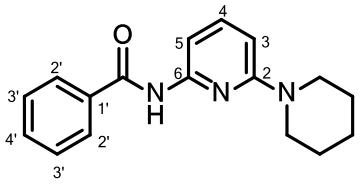

Reaction of *N*-(6-bromopyridin-2-yl)benzamide **147b** (278 mg, 1.0 mmol) with piperidine (25 mg, 3.0 eq.) using method D gave compound **142f** (155 mg, 55%) as a pale brown oil. IR (cm^{-1}) 3290 (NH str.), 2931 and 2852 (CH str.), 1670 (C=O), 1604 (C=N), 1440 (C=C); ^{1}H NMR (300 MHz, $CDCl_3$) δ 8.3 (s, 1H, N**H**), 7.96–7.85 (m, 2H, Ar-H), 7.66–7.44 (m, 5H, Ar-H), 6.42 (d, *J* = 8.2 Hz, 1H, H-3), 3.57–3.42 (m, 4H, (piperidyl), 1.69–1.60 (m, 6H, (piperidyl); ^{13}C NMR (75 MHz, $CDCl_3$) δ 165.4 (C=O), 158.4 (C-2), 149.7 (C-6), 139.8 (C-4), 134.9 (C-1'), 131.9 (C-4'), 128.7 (C-2'), 127.1 (C-3') , 103.0 (C-3), 101.9 (C-5), 46.2 (piperidyl), 25.5 (piperidyl), 24.8 (piperidyl); HRMS (ES^+) Calculated for $C_{17}H_{20}N_3O$ $[M+H]^+$: 282.1606, found: 282.1603.

6.2.4.7 3-Chloro-*N*-(6-(piperidin-1-yl)-pyridin-2-yl)benzamide **142h**

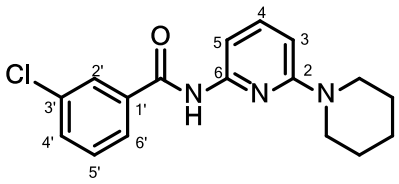

Reaction of *N*-(6-bromopyridin-2-yl)-3-chlorobenzamide **147c** (311 mg, 1.0 mmol) with piperidine (255 mg, 3.0 eq.) using method D gave product **142g** (164 mg, 52%) as a pale yellow oil which solidified on drying. Mp: 94-96°C; IR (cm^{-1}) 3289 (NH str.), 2928 and 2849 (CH str.), 1655 (C=O), 1604 (C=N), 1440 (C=C); ^{1}H NMR (500 MHz, $CDCl_3$) δ 8.24 (s, 1H, NH), 7.91–7.86 (m, 1H, Ar-H), 7.75 (d, *J* = 7.7 Hz, 1H, Ar-H), 7.58–7.48 (m, 3H, Ar-H), 7.40 (t, *J* = 8.2, 1H, H-4), 6.42 (d, *J* = 8.1 Hz, 1H, H-3), 3.53–3.46 (m, 4H, piperidyl), 1.67–1.57 (m, 6H, piperidyl); ^{13}C NMR (125 MHz, $CDCl_3$) δ 164.1 (C=O), 158.4 (C-2), 149.4 (C-6), 139.8 (C-4), 136.7 (Ar-H), 134.9 (Ar-H), 131.9 (Ar-H), 130.0 (Ar-H), 127.5 (Ar-H), 125.2 (Ar-H), 103.3 (C-3), 101.8 (C-5), 46.2 (piperidyl), 25.5 (piperidyl), 24.7 (piperidyl); HRMS (ES^+) Calculated for $C_{17}H_{19}ClN_3O$ $[M+H]^+$: 316.1217, found: 316.1206.

6.2.4.8 4-Chloro-*N*-(6-(piperidin-1-yl)-pyridin-2-yl)benzamide **142i**

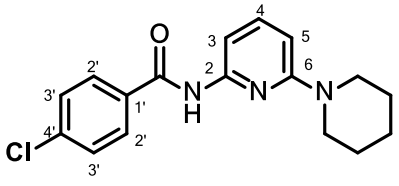

Reaction of *N*-(6-bromopyridin-2-yl)-4-chlorobenzamide **147d** (311 mg, 1.0 mmol) with piperidine (255 mg, 3.0 eq.) using method D gave product **142h** (202

mg, 64%) as off-white crystals. Mp: 140-142°C; IR (cm^{-1}) 3273 (NH str.), 2932 and 2845 (CH str.), 1658 (C=O), 1603 (C=N), 1425 (C=C); ^{1}H NMR (500 MHz, $CDCl_3$) δ 8.30 (s, 1H, NH), 7.85–7.77 (m, 2H, Ar-H), 7.62–7.48 (m, 2H, Ar-H), 7.48–7.39 (m, 2H, Ar-H), 6.42 (d, *J* = 7.9, 1H, H-3), 3.55–3.43 (m, 4H, piperidyl), 1.67–1.56 (m, 6H, piperidyl); ^{13}C NMR (125 MHz, $CDCl_3$) δ 164.4 (C=O), 158.4 (C-2), 149.5 (C-6), 139.8 (C-4), 138.1 (C-4'), 133.2 (C-1'), 128.9 (C-3'), 128.6 (C-2'), 103.2 (C-3), 101.9 (C-5), 46.2 (piperidyl), 25.5 (piperidyl), 24.7 (piperidyl); HRMS (ES^+) Calculated for $C_{17}H_{19}ClN_3O$ $[M+H]^+$: 316.1217, found: 316.1205.

6.2.4.9 4-Cyano-*N*-(6-(piperidin-1-yl)-pyridin-2-yl)benzamide **142j**

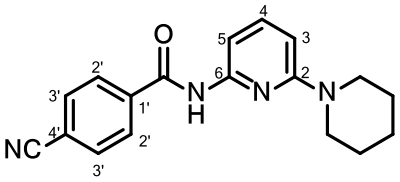

Reaction of *N*-(6-bromopyridin-2-yl)-4-cyanobenzamide **147e** (319 mg, 1.0 mmol) with piperidine (255 mg, 3.0 eq.) using method D gave product **142i** (149 mg, 48%) as pale yellow crystals. Mp: 127-128°C; IR (cm^{-1}): 3344 (NH str.), 2934 and 2855 (CH str.), 2230 (CN), 1667 (C=O), 1601 (C=N), 1443 (C=C); ^{1}H NMR (300 MHz, $CDCl_3$) ^{1}H NMR (300 MHz, $CDCl_3$) δ 8.20 (br s, 1H, NH), 8.02–7.97 (m, 2H, Ar-H), 7.83–7.74 (m, 2H, Ar-H), 7.58–7.49 (m, 2H, Ar-H), 6.45 (dd, *J* = 6.2, 2.8 Hz, 1H, Ar-H), 3.51 (m, 4H, piperidyl), 1.68–1.58 (m, 6H, piperidyl); ^{13}C NMR (75 MHz, $CDCl_3$) δ 163.6 (C=O), 158.4 (C-2), 149.1 (C-6), 139.9 (C-4), 138.7 (Ar-C), 132.6 (C-1'), 130.9 (Ar-C), 128.8 (Ar-C), 127.9 (Ar-C), 127.8 (Ar-C), 117.9 (CN), 115.4 (C-4'), 103.6 (C-3), 101.9 (C-5), 46.1 (piperidyl), 25.5 (piperidyl), 24.7 (piperidyl); HRMS (ES^+) Calculated for $C_{18}H_{19}N_4O$ $[M+H]^+$: 307.1559, found: 307.1554.

6.2.5 *N*-(6-(bromopyridin-2-yl)-4-cyano-2-(piperidin-1-yl)benzamide **147g**

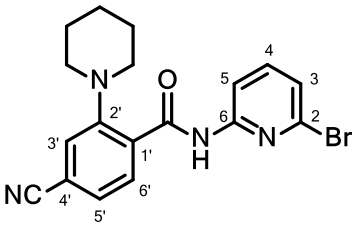

Reaction of compound **147f** (319 mg, 1.0 mmol) with piperidine (1.3 eq), as described for compounds **142a**-**i**, gave compound **147g** (327 mg, 85%) as yellow crystals. Mp: 164-165°C; IR (cm^{-1}): 3430 (NH str.), 2937 and 2856 (CH str.), 2228 (CN str.), 1677 (C=O), 1605 (C=N), 1557 (NH bend), 1422 (C=C); ^{1}H NMR (300 MHz, $CDCl_3$) δ 12.92 (s, 1H, NH), 8.30 (t, *J* = 8.0 Hz, 2H, Ar-H), 7.60–7.53 (m, 3H, Ar-H), 7.22 (d, *J* = 7.6 Hz, 1H, H-5), 3.04–2.97 (m, 4H, 2 x C*H*$_2$ - piperidyl), 1.99–1.91 (m, 4H, 2 x C*H*$_2$ - piperidyl), 1.72–1.60 (m, 2H, C*H*$_2$ - piperidyl); ^{13}C NMR (125 MHz, $CDCl_3$) δ 162.7 (C=O), 153.1 (C-6), 151.7 (C-2'), 140.4 (C-

4), 139.6 (C-2), 132.5 (Ar-C), 131.1, 128.1, 125.1, 123.5 (C-3), 117.8 (CN), 116.2 (C-4'), 112.9 (C-5), 55.2 (piperidyl), 25.6 (piperidyl), 23.7 (piperidyl); HRMS (ES$^+$) Calculated for $C_{18}H_{18}BrN_4O$ $[M+H]^+$: 385.0664, found: 385.0655.

6.2.5.1 Alternative procedure for preparation of compound **147g**

N-(6-(bromopyridin-2-yl)-4-cyano-2-fluorobenzamide **147f** (319 mg, 1.0 mmol), 1,4-dioxane (10 ml, degassed), piperidine (128 mg, 1.5 eq.) and a magnetic stirrer were added to an oven-dried 10 ml round-bottomed flask under nitrogen purge. The mixture was stirred at 60°C in an oil bath (5 min). A base, KHMDS (2.5 ml of 0.5 M solution in hexane) or KO^{t}Bu (269 mg, 2.4 eq.), was added in small portions and the reaction heated at 110°C for 3 h. After cooling to room temperature, the reaction mixture was diluted with dichloromethane or chloroform (15 ml) and filtered. The filtrate was washed successively with saturated aqueous $NaHCO_3$ (10 ml) and distilled water (2 x 10 ml), dried over anhydrous Na_2SO_4 and the solvent removed *in vacuo* to give a pale yellow solid **147g** (385 mg, 99%).

6.2.6 2-(benzyloxy)-*N*-(6-bromopyridin-2-yl)-4-cyanobenzamide (**147i**)

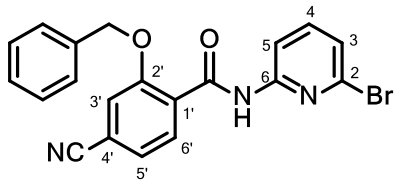

N-(6-(bromopyridin-2-yl)-4-cyano-2-fluorobenzamide **147f** (319 mg, 1.0 mmol), THF (10 ml) degassed), benzyl alcohol (162 mg, 1.5 mmol) and a magnetic stirrer were added to an oven-dried 10 ml round-bottomed flask under nitrogen purge. The sealed reaction mixture was stirred at 60°C in an oil bath (5 min). A base, KHMDS (2.5 ml of 0.5 M solution in hexane) (2.0 eq.), was added in small portions and the sealed reaction heated at 110°C for 24 h. After cooling to room temperature, THF was removed *in vacuo* and the crude brown residue was re-dissolved in dichloromethane or chloroform (15 ml) and filtered. The filtrate was washed successively with saturated aqueous $NaHCO_3$ (10 ml) and distilled water (2 x 10 ml), dried over anhydrous Na_2SO_4 and the solvent removed *in vacuo* to give a pale yellow residue. The crude yellow residue was purified using flash column chromatography as described for compounds **142a-i** to give a white solid **147i** (245 mg, 64%).

^{1}H NMR (500 MHz, $CDCl_3$) δ 8.37 (d, *J* = 8.1Hz, 1H), 8.31 (dd, *J* = 8.2, 0.7 Hz, 1H), 7.60–7.42 (m, 6H, Ar-H), 7.45 (d, *J* = 1.4 Hz, 1H), 7.46–7.42 (m, 2H, Ar-H), 7.40 (d, *J* = 1.4 Hz, 1H, H-3'), 7.22 (dd, *J* = 7.7, 0.7 Hz, 1H, Ar-H), 5.35 (s, 2H, PhC**H**$_2$); ^{13}C NMR (126 MHz, $CDCl_3$) δ 161.7 (C=O), 158.1 (C-2'), 156.5 (C-6), 151.3 (Ar-C), 140.4 (C-2), 133.8 (Ar-C), 133.6 (Ar-C), 129.3

(Ar-C), 129.2 (Ar-C), 127.8 (Ar-C), 125.6 (Ar-C), 125.3 (Ar-C), 124.0 (C-3), 116.5 (C-4'), 113.0 (C-5), 72.4 (-*C*H_2-); HRMS (ES$^+$) Calculated for $C_{20}H_{14}BrN_3O_2$ [M]$^+$: 408.0348, found: 408.0289

6.2.7 4-Cyano-2-(piperidin-1-yl)-N-(6-(-piperidin-1-yl)pyridin-2-yl)benzamide **142l**

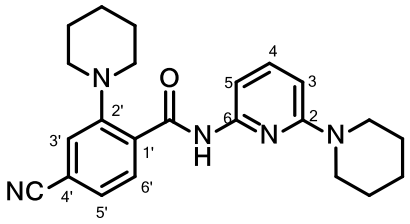

Reaction of compound **147g** (385 mg, 1.0 mmol) with piperidine (111 mg, 1.3 mmol), as described for compounds **142a-i**, gave compound **142l** (331 mg, 85%) as pale yellow crystals. Mp: 171-173°C; IR (cm^{-1}): 3130 (NH str.), 2927 and 2833 (CH str.), 2229 (CN str.), 1668 (C=O), 1599 (C=N), 1566 (NH bend), 1440 (C=C); ^{1}H NMR (300 MHz, $CDCl_3$) δ 12.31 (br s, 1H, NH), 8.34 (d, *J* = 8.4 Hz, 1H, H-5), 7.62 (d, *J* = 7.8 Hz, 1H. H-6'), 7.56–7.47 (m, 3H, Ar-H), 6.44 (d, *J* = 8.2 Hz, 1H, H-3), 3.60–3.50 (m, 4H, piperidyl), 3.07–2.95 (m, 4H, piperidyl), 2.05–1.90 (m, 4H, piperidyl), 1.71–1.55 (m, 8H, piperidyl); ^{13}C NMR (75 MHz, $CDCl_3$) δ 162.4 (C=O), 158.1 (C-2'), 153.0 (C-6), 149.9 (C-2), 139.6 (C-4), 132.6 (Ar-C), 132.0 (Ar-C), 127.9 (Ar-C), 124.6, 118.1 (CN), 115.6 (C-4'), 103.0 (C-3), 102.5 (C-5), 55.1 (piperidyl), 46.1 (piperidyl), 25.7 (piperidyl), 25.4 (piperidyl), 24.9 (piperidyl), 23.7 (piperidyl); HRMS (ES$^+$) Calculated for $C_{23}H_{28}N_5O$ [M+H]$^+$: 390.2294, found: 390.2296.

6.2.8 General procedure for preparing compounds **151**

A similar palladium-catalyzed protocol as applied in the preparation of novel targets **142a-i** was used with the sealed reaction being heated at 130-140°C for 24 h.

6.2.8.1 *N*-(6-butoxypyridin-2-yl)-2-chlorobenzamide **151a**

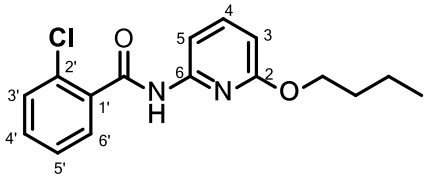

Reaction of compound **147a** (310 mg, 1.0 mmol) with *n*-butanol (89 mg, 1.2 mmol) yielded compound **151a** (138 mg, 45%) as a colourless oil. IR (cm^{-1}): 3275 (NH br str.), 2958 and 2872 (CH str.), 1676 (C=O str.), 1591 (C=N), 1575 (NH bend), 1523 (C=C); ^{1}H NMR (300 MHz, $CDCl_3$) δ 8.30 (s, 1H, NH), 7.89 (d, *J* = 7.7 Hz, 1H), 7.71 (dd, *J* = 7.4, 1.7 Hz, 1H, Ar-H), 7.64 (t, *J* = 8.0 Hz, 1H, H-4), 7.48–7.32 (m, 3H, Ar-H), 6.52 (dd, *J* = 8.1, 0.6 Hz, 1H, H-3), 4.18 (t, *J* = 6.6 Hz, 2H, -OC**H**$_2$C$_3$H$_7$), 1.77–1.67 (m, 2H, -OCH$_2$C**H**$_2$C$_2$H$_5$), 1.53–

1.37 (m, 2H, -O(CH_2)$_2$C**H**$_2$$CH_3$), 0.96 (t, *J* = 7.4 Hz, 3H, -C**H**$_3$); ^{13}C NMR (75 MHz, $CDCl_3$) δ 164.6 (C=O), 162.9 (C-2), 148.7 (C-6), 140.9 (C-4), 132.1 (Ar-C), 131.8 (Ar-C), 130.9 (Ar-C), 130.5 (Ar-C), 130.0 (Ar-C), 127.2 (Ar-C), 106.6 (C-3), 105.7 (C-5), 65.9 (butoxy), 31.1 (butoxy), 19.3 (butoxy), 13.9 (butoxy); HRMS (ES$^+$) Calculated for $C_{16}H_{18}ClN_2O_2$ [M+H]$^+$: 305.1057, found: 305.1047.

6.2.8.2 2-Chloro-*N*-(6-phenoxypyridin-2-yl)benzamide **151b**

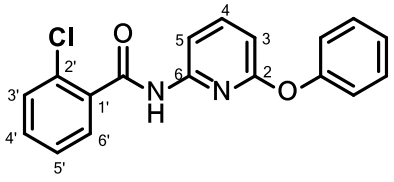

Reaction of compound **147a** (310 mg, 1.0 mmol) with phenol (123 mg, 1.3 mmol) yielded compound **151b** (231 mg, 70%) as a pale brown oil. IR (cm^{-1}): 3176 (NH str.), 3075 (CH str.), 1684 (C=O), 1563 (NH bend), 1426 (C=C); ^{1}H NMR (300 MHz, $CDCl_3$) δ 8.60 (s, 1H, NH), 8.34 (d, *J* = 8.2 Hz, 1H, H-5), 7.73–7.66 (m, 1H, Ar-H), 7.62 (t, *J* = 8.0 Hz, 1H, H-4), 7.49–7.42 (m, 2H, Ar-H), 7.42–7.33 (m, 2H, Ar-H), 7.31–7.17 (m, 2H, Ar-H), 6.95–6.87 (m, 1H, Ar-H), 6.86–6.79 (m, 2H, Ar-H); ^{13}C NMR (75 MHz, $CDCl_3$) δ 164.9 (C=O), 155.6 (C-2), 151.0 (C-6), 140.8 (Ar-C), 139.4 (Ar-C), 134.3 (Ar-C), 132.2 (Ar-C), 131.0 (Ar-C), 130.6 (Ar-C), 129.9 (Ar-C), 129.6 (Ar-C), 127.3 (Ar-C), 124.2 (Ar-C), 120.6 (Ar-C), 115.3 (Ar-C), 112.69 (Ar-C); HRMS (ES$^+$) Calculated for $C_{18}H_{14}ClN_2O_2$ [M+H]$^+$: 325.0744, found: 325.0744.

6.2.8.3 *N*-(6-(benzyloxy)-pyridin-2-yl)-2-chlorobenzamide **151c**

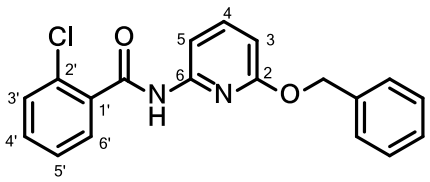

Reaction of compound **147a** (310 mg, 1.0 mmol) with benzyl alcohol (141 mg, 1.3 mmol) yielded compound **151c** (169 mg, 52%) as a brown oil. IR (cm^{-1}): 3411 (NH str.), 3060 and 2947 (CH str.), 1669 (C=O), 1605 (C=N), 1574 (NH bend), 1430 (C=C); ^{1}H NMR (500 MHz, $CDCl_3$) δ 8.29 (s, 1H, NH), 7.96–7.90 (m, 2H, Ar-H), 7.67 (t, *J* = 8.0 Hz, 1H, H-4), 7.60–7.55 (m, 1H, Ar-H), 7.53–7.47 (m, 1H, Ar-H), 7.46–7.41 (m, 1H, Ar-H), 7.40–7.36 (m, 1H, Ar-H), 7.35–7.30 (m, 1H, Ar-H), 6.62–6.58 (m, 1H, Ar-H),), 5.33–5.27 (m, 2H, PhC**H**$_2$); ^{13}C NMR (125 MHz, $CDCl_3$) δ 165.4 (C=O), 162.4 (C-2), 149.1 (C-6), 141.1 (C-4), 137.1 (Ar-C), 134.5 (Ar-C), 132.2 (Ar-C), 128.9 (Ar-C), 128.5 (Ar-C), 127.9 (Ar-C), 127.9 (Ar-C), 127.8 (Ar-C), 127.1 (Ar-C), 106.6 (C-3), 106.0 (C-5), 67.8, PhC**H**$_2$-; HRMS (ES$^+$) Calculated for $C_{19}H_{16}ClN_2O_2$ [M+H]$^+$: 339.0900, found: 339.0892.

6.2.8.4 2-Chloro-*N*-(6-phenylthio)-pyridin-2-yl)benzamide **151d**

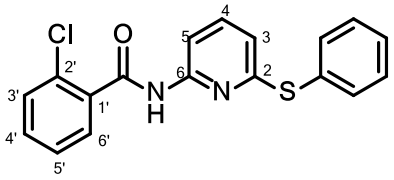

Reaction of compound **147a** (310 mg, 1.0 mmol) with thiophenol (143 mg, 1.3 mmol) yielded compound **151d** (237 mg, 63%) as a pale brown oil. IR (cm^{-1}): 3225 (NH str.), 3058 and 2936 (CH str.), 1649 (C=O), 1563 (NH bend), 1429 (C=C); ^{1}H NMR (300 MHz, $CDCl_3$) δ 8.49 (s, 1H, NH), 8.07 (d, *J* = 8.1 Hz, 1H, H-5), 7.68 (dd, *J* = 7.6, 1.6 Hz, 1H, Ar-H), 7.62–7.56 (m, 2H, Ar-H), 7.53 (t, *J* = 8.0 Hz, 1H, H-4), 7.48–7.28 (m, 6H, Ar-H), 6.64 (d, *J* = 7.8 Hz, 1H, H-3); ^{13}C NMR (75 MHz, $CDCl_3$) δ 164.8 (C=O), 159.8 (C-2), 150.6 (C-6), 139.1 (C-4), 135.0 (Ar-C), 134.8 (Ar-C), 131.9 (Ar-C), 131.0 (Ar-C), 130.6 (Ar-C), 130.5 (Ar-C), 129.9 (Ar-C), 129.6 (Ar-C), 129.2 (Ar-C), 127.2 (Ar-C), 117.6 (C-3), 110.1 (C-5); HRMS (ES^+) Calculated for $C_{18}H_{14}ClN_2OS$ $[M+H]^+$: 341.0515, found: 341.0506.

6.2.8.5 *N*-(6-benzylthio)-pyridin-2-yl)-2-chlorobenzamide **151e**

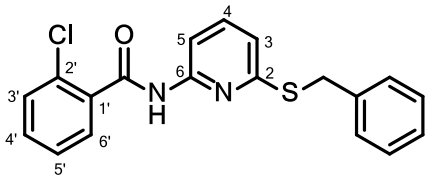

Reaction of compound **147a** (310 mg, 1.0 mmol) with benzylthiol (161 mg, 1.3 mmol) yielded compound **151e** (203 mg, 52%) as a pale brown oil. IR (cm^{-1}): 3406 (NH str.), 3062 (CH str.), 1683 (C=O), 1587 (C=N), 1561 (NH bend), 1429 (C=C); ^{1}H NMR (300 MHz, $CDCl_3$) δ 8.51 (s, 1H, NH), 8.05 (d, *J* = 8.1 Hz, 1H, H-5), 7.74 (dd, *J* = 7.3, 1.8 Hz, 1H, Ar-H), 7.55 (t, *J* = 7.9 Hz, 1H, H-4), 7.47–7.33 (m, 5H, Ar-C), 7.32–7.19 (m, 3H, Ar-H), 6.95 (d, *J* = 7.7, 1H, H-3), 4.34 (s, 2H, PhC**H**$_2$S-); ^{13}C NMR (75 MHz, $CDCl_3$) δ 164.5 (C=O), 157.3 (C-2), 150.6 (C-6), 138.5 (C-4), 137.8 (Ar-C), 134.7 (Ar-C), 132.0 (Ar-C), 130.8 (Ar-C), 130.5 (Ar-C), 130.3 (Ar-C), 128.9 (Ar-C), 128.5 (Ar-C), 127.3 (Ar-C), 127.2 (Ar-C), 118.4 (C-3), 109.6 (C-5), 34.5 (Ph**C**H_2S-); HRMS (ES^+) Calculated for $C_{19}H_{16}ClN_2OS$ $[M+H]^+$: 355.0672, found: 355.0660.

6.2.9 General procedure for the preparation of compounds **152** and **155**

6.2.9.1 6-Bromo-*N*-(2-chlorobenzyl)pyridin-2-amine **152**

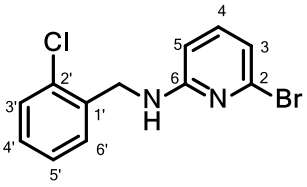

2-Chlorobenzaldehyde **148** (1.47 g, 10 mmol), 2-amino-6-bromo-pyridine **146** (1.55 g, 9.0 mmol) and 4Å molecular sieves were placed into a 100 ml round bottomed flask containing dry acetonitrile (25 ml). The pH was adjusted to pH 5–6 by dropwise addition of conc. HCl, with bromocresol green as indicator. The reaction mixture was stirred under reflux until the reactants were quantitatively converted to the imine intermediate. Sodium cyanoborohydride (0.9 g, 15.0 mmol) was added portion-wise over 2 h while maintaining the pH of the reaction mixture between 5 and 6. After 24 h, the reaction mixture was cooled, filtered and the solvent removed under reduced pressure to leave an off-white residue which was purified by silica gel column chromatography, eluting with 5–10% EtOAc/Hexane, to give **152** (2.35 g, 88%) as off-white crystals. Mp: 77-78°C; IR (cm^{-1}): 3261 (NH str.), 3085 (CH str.), 1600 and 1590 (C=N str.), 1560 (NH bend), 1427 (C=C); ^{1}H NMR (300 MHz, $CDCl_3$) δ 7.48–7.34 (m, 2H, Ar-H), 7.29–7.16 (m, 3H, Ar-H), 6.74 (dd, *J* = 7.4, 0.6 Hz, 1H, Ar-H), 6.25 (d, *J* = 8.1 Hz, 1H, H-3), 5.28–5.14 (m, 1H, NH), 4.57 (d, *J* = 6.2 Hz, 2H, ClPhC**H**$_2$-); ^{13}C NMR (75 MHz, $CDCl_3$) δ 158.5 (C-6), 140.3 (C-2), 139.6 (C-4), 135.8 (C-2'), 133.5 (C-1'), 129.6 (Ar-C), 129.4 (Ar-C), 128.7 (Ar-C), 127.0 (Ar-C), 116.4 (C-3), 104.7 (C-5), 44.0 (ClPh**C**H_2-); HRMS (ES^+) Calculated for $C_{12}H_{11}BrClN_2$ $[M+H]^+$: 296.9794, found: 296.9792.

6.2.9.1 *tert*-Butyl (6-bromopyridin-2-yl)(2-chlorobenzyl)carbamate **155**

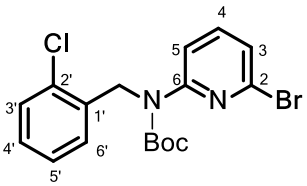

Dimethylaminopyridine (DMAP, 0.2 g, 1.6 mmol) and di-*tert*-butyl dicarbonate (3.27 g, 15.0 mmol) were added to a 50 ml round bottomed flask containing 6-bromo-*N*-(2-chlorobenzyl)-pyridin-2-amine **152** (2.96 g, 10.0 mmol) dissolved in dry acetonitrile (20 ml). The reaction mixture was stirred slowly at room temperature (5 min) before heating the mixture at 40°C for 24 h. After cooling to room temperature, the solvent was removed under reduced pressure and the crude mixture was dissolved in dichloromethane (20 ml), washed twice with distilled water (2 x 15 ml) and dried over anhydrous $MgSO_4$. The organic solvent was removed *in vacuo* to leave a pale yellow crude product which was purified by silica gel column chromatography, eluting with 10% EtOAc/Hexane to give **155** (4.19 g, 98%) as an off-white oily

product which solidified on drying. ^{1}H NMR ($CDCl_3$, 500 MHz) δ 7.80 (d, *J* = 8.2 Hz, 1H, H-5), 7.50–7.45 (m, 1H, Ar-H), 7.35–7.32 (m, 1H, Ar-H), 7.22–7.18 (m, 1H, Ar-H), 7.17–7.13 (m, 3H, Ar-H), 5.28 (s, 2H, ClPhC**H**$_2$N-), 1.38 (s, 9H, Boc); ^{13}C NMR (125 MHz, $CDCl_3$) δ 154.2 (C-6), 153.6 (Boc carbonyl), 139.2 (C-2'), 138.9 (C-1'), 136.5 (Ar-C), 132.7 (Ar-C), 129.2 (Ar-C), 128.0 (Ar-C), 127.9 (Ar-C), 126.6 (Ar-C), 123.2 (C-3), 117.3 (C-5), 82.1 (-O**C**$(CH_3)_3$ Boc), 47.7 (ClPh**C**H_2N-), 28.0 (–C(**C**$H_3)_3$, Boc); HRMS (ES^+) Calculated for $C_{17}H_{20}ClN_2O_2$ $[M+H]^+$: 319.1213, found: 319.1221.

6.2.10 General procedure for the preparation of compounds **143**

Tris-(dibenzylideneacetone)-di-palladium (0) [Pd_2dba_3], (19 mg, 2mol %), *rac*-BINAP (38 mg, 6mol %), dioxane (3–5 ml, degassed) and a magnetic stirrer were added to an oven-dried 10 ml round bottomed flask under nitrogen purge. The flask was sealed and heated with stirring at 80°C in an oil bath for 5 min. *tert*-Butyl (6-bromopyridin-2-yl)(2-chlorobenzyl)carbamate **155** (420 mg, 1.0 mmol), an amine (1.3–3.0 eq.) and cesium carbonate (782 mg, 2.4 mmol) were added and the sealed reaction was heated at 120°C for 24 h. The reaction mixture was cooled to room temperature, diluted with dichloromethane/chloroform (15 ml) and filtered. The filtrate was washed successively with saturated aqueous $NaHCO_3$ (10 ml) and distilled water (2 x 10 ml). After drying over anhydrous Na_2SO_4, the solvent was removed under reduced pressure and the crude mixture was purified by silica gel flash column chromatography, eluting the desired Boc-protected compound with 2–5% EtOAc/Hexane. The Boc-protected compound was dissolved in chloroform (10 ml) containing hydrochloric acid (3 ml) and warmed at 30°C for 2 h. The mixture was cautiously neutralized with sodium bicarbonate, washed with distilled water (2 x 10 ml) and dried over anhydrous Na_2SO_4. The solvent was removed *in vacuo* to give the desired compounds **143a**-**e**.

6.2.10.1 *N*^{2}-(2-chlorobenzyl)-*N*^{6}-cyclohexylaminopyridine-2, 6-diamine **143a**

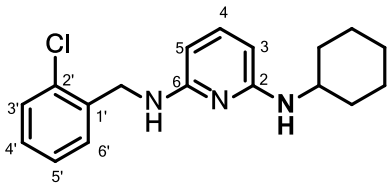

Reaction of **155** with cyclohexylamine (1129 mg, 1.5 mmol) gave compound **143a** (189 mg, 60%) as a pale yellow oil. IR (cm^{-1}) 3417 (NH str.), 2926 and 2851 (CH str.), 1588 and 1570 (NH bend), 1420 (C=C); ^{1}H NMR (300 MHz, $CDCl_3$) δ 7.81–7.71 (m, 1H, Ar-H), 7.44–7.30 (m, 4H, Ar-H), 7.28–7.20 (m, 2H, Ar-H), 5.80 (d, *J* = 8.5 Hz, 1H, H-5), 5.58 (d, *J* = 8.3 Hz, 1H, H-3), 4.51 (d, *J* = 5.9 Hz, 2H, ClPhC**H**$_2$N-), 3.33–3.19 (m, 1H,

cyclohexyl), 2.03–1.92 (m, 2H, cyclohexyl), 1.86–1.73 (m, 2H, cyclohexyl), 1.67–1.58 (m, 1H, cyclohexyl), 1.43–1.22 (m, 5H, cyclohexyl); ^{13}C NMR (75 MHz, $CDCl_3$) δ 152.3 (C-2), 151.6 (C-6), 144.9 (C-4), 134.0 (Ar-C), 132.8 (Ar-C), 129.7 (Ar-C), 128.9 (Ar-C), 128.0 (Ar-C), 127.2 (Ar-C), 93.7 (C-3), 92.0 (C-5), 51.5 (ClPh**C**H_2N-), 43.7 (cyclohexyl), 32.3 (cyclohexyl), 25.2 (cyclohexyl), 24.6 (cyclohexyl); HRMS (ES$^+$) Calculated for $C_{18}H_{23}ClN_3$ [M+H]$^+$: 316.1581, found: 316.1599.

6.2.10.2 *N*^{2}-benzyl-*N*^{6}-(2-chlorobenzyl)-pyridine-2,6-diamine **143b**

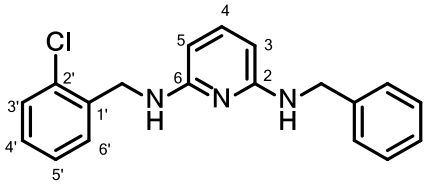

Reaction of **155** with benzylamine (161 mg, 1.5 mmol) gave compound **143b** (184 mg, 57%) as a pale yellow oil. IR (cm^{-1}) 3417 (NH str.), 2926 and 2851 (CH str.), 1588 and 1570 (NH bend), 1420 (C=C); ^{1}H NMR (300 MHz, $CDCl_3$) δ 7.44–7.13 (m, 10H, Ar-H), 5.73 (d, *J* = 6.0 Hz, 1H, H-5), 5.70 (d, *J* = 6.0 Hz, 1H, H-3), 4.82–4.70 (m, 1H, NH), 4.69–4.59 (m, 1H, NH), 4.53 (d, *J* = 6.2 Hz, 2H, -C**H**$_2$-), 4.43 (d, *J* = 5.8 Hz, 2H, -C**H**$_2$-); ^{13}C NMR (75 MHz, $CDCl_3$) δ 158.0 (C-2), 157.8 (C-6), 139.8 (C-4), 139.1 (Ar-C), 137.2 (Ar-C), 133.2 (Ar-C), 129.4 (Ar-C), 129.2 (Ar-C), 128.5 (Ar-C), 128.2 (Ar-C), 127.4 (Ar-C), 127.0 (Ar-C), 126.8 (Ar-C), 95.4 (C-3), 95.3 (C-5), 46.3 (–**C**H_2-), 43.9 (–**C**H_2-); HRMS (ES$^+$) Calculated for $C_{19}H_{19}ClN_3$ [M+H]$^+$: 324.1268, found: 324.1267.

6.2.10.3 *N*^{2}-(2-chlorobenzyl)-*N*^{6}-phenylpyridine-2, 6-diamine **143c**

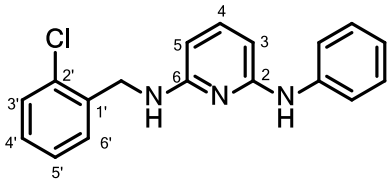

Reaction of **155** with aniline (140 mg, 1.5 mmol) gave compound **143c** (158 mg, 51%) as a pale brown oil. IR (cm^{-1}) 3400 (NH str.), 2958 and 2920 (CH str.), 1578 (NH bend), 1432 (C=C); ^{1}H NMR (300 MHz, $CDCl_3$) δ 7.48–7.13 (m, 9H, Ar-H), 7.02–6.92 (m, 1H, Ar-H), 6.32 (s, 1H, NH), 6.16 (dd, *J* = 7.9, 0.6 Hz, 1H, H-5), 5.85 (dd, *J* = 8.0, 0.6 Hz, H-3), 4.92–4.79 (m, 1H, NH), 4.58 (d, *J* = 6.2 Hz, 2H, -C**H**$_2$-); ^{13}C NMR (75 MHz, $CDCl_3$) δ 157.8 (C-6), 154.9 (C-2), 140.9 (C-2'), 139.2 (C-4), 137.0 (C-1'), 133.3 (Ar-C), 129.4 (Ar-C), 129.0 (Ar-C), 128.3 (Ar-C), 126.9 (Ar-C), 122.0 (Ar-C), 119.9 (Ar-C), 97.4 (C-3), 97.2 (C-5), 43.9 (-C**H**$_2$-); HRMS (ES$^+$) Calculated for $C_{18}H_{17}ClN_3$ [M+H]$^+$: 310.1111, found: 310.1109.

6.2.10.4 *N*-(2-chlorobenzyl)-6-morpholinopyridine-2-amine **143d**

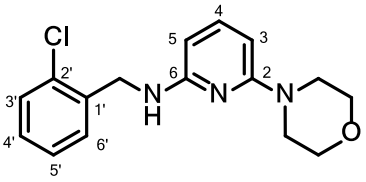

Reaction of **155** with morpholine (131 mg, 1.5 mmol) gave compound **143d** (133 mg, 44%) as a pale brown oil. IR (cm^{-1}) 3369 (NH str.), 2959 and 2852 (CH str.), 1581 (NH bend), 1433 (C=C); ^{1}H NMR (300 MHz, $CDCl_3$) δ 7.48–7.31 (m, 2H, Ar-H), 7.29–7.13 (m, 3H, Ar-H), 5.93 (d, *J* = 8.4 Hz, 1H, H-5), 5.79 (d, *J* = 8.4 Hz, 1H, H-3) 4.79 (br s, 1H, NH), 4.57 (d, *J* = 5.9 Hz, 2H, -C**H**$_2$-), 3.89–3.72 (m, 4H, morpholinyl), 3.55–3.35 (m, 4H, morpholinyl); ^{13}C NMR (75 MHz, $CDCl_3$) δ 158.8 (C-2), 157.3 (C-6), 139.1 (C-4), 137.2 (C-2'), 133.2 (C-1'), 129.4 (Ar-C), 129.2 (Ar-C), 128.2 (Ar-C), 126.8 (Ar-C), 96.4 (C-3), 95.5 (C-5), 66.8 (morpholinyl), 45.7 (morpholinyl), 43.8 (morpholinyl). HRMS (ES^+) Calculated for $C_{16}H_{19}ClN_3O$ $[M+H]^+$: 304.1217, found: 304.1211.

6.2.10.5 *N*-(2-chlorobenzyl)-6-(piperidin-1-yl)-pyridine-2-amine **143e**

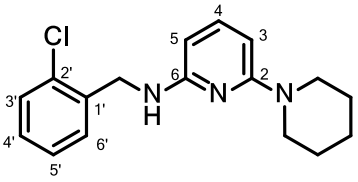

Reaction of **155** with piperidine (128 mg, 1.5 mmol) gave compound **143e** (160 mg, 53%) as a light yellow oil. IR (cm^{-1}): 3247 (NH str.), 2877 (CH str.), 1602 and 1579 (NH bend), 1441 (C=C); ^{1}H NMR (300 MHz, $CDCl_3$) δ 7.50–7.39 (m, 1H, Ar-H), 7.39–7.30 (m, 1H, Ar-H), 7.28–7.13 (m, 3H, Ar-H), 5.96 (d, *J* = 8.1 Hz, 1H, H-5), 5.69 (d, *J* = 7.8 Hz, 1H, H-3), 4.87–4.63 (m, 1H, NH) , 4.56 (d, *J* = 6.0 Hz, 2H, -C**H**$_2$-), 3.56–3.34 (m, 4H, piperidyl), 1.69–1.50 (m, 6H, piperidyl); ^{13}C NMR (75 MHz, $CDCl_3$) δ 158.9 (C-2), 157.3 (C-6), 139.0 (Ar-C'), 137.4 (Ar-C), 133.2 (Ar-C), 129.3 (Ar-C), 129.2 (Ar-C), 128.1 (Ar-C), 126.8 (Ar-C), 95.7 (C-3), 94.8 (C-5), 46.3 (piperidyl), 43.9 (piperidyl), 25.5 (piperidyl), 24.9 (piperidyl); HRMS (ES^+) Calculated for $C_{17}H_{21}ClN_3$ $[M+H]^+$: 302.1424, found: 302.1420.

6.2.11 General procedure for preparation of novel compounds **157a**–**157e**

A similar palladium-catalyzed protocol as applied in the preparation of novel targets **143a-i** was used with the sealed reaction being heated at 130-140°C for 24 h.

6.2.11.1 6-Butoxy-*N*-(2-chlorobenzyl)pyridin-2-amine **157a**

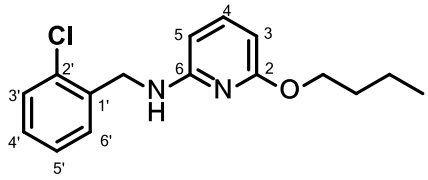

Reaction of compound **155** (427 mg, 1.0 mmol) with *n*-butanol (111 mg, 1.5 mmol) gave compound **157a** (190 mg, 65%) as a pale yellow oil. IR (cm^{-1}): 2959 and 2873 (CH str.), 1580 (C=N), 1442 (C=C); ^{1}H NMR (300 MHz, $CDCl_3$) δ 7.46–7.27 (m, 3H, Ar-H), 7.24–7.12 (m, 2H, Ar-H), 6.02 (d, *J* = 7.9 Hz, 1H, H-5), 5.91 (d, *J* = 7.9 Hz, 1H, H-3), 4.84 (t, *J* = 5.5 Hz, 1H, NH), 4.58 (d, *J* = 6.2 Hz, 2H, -C**H**$_2$-), 4.17 (t, *J* = 6.7, 6.7 Hz, 2H, butoxy), 1.78–1.63 (m, 2H, butoxy), 1.45–1.39 (m, 2H, butoxy), 0.94 (t, *J* = 7.3, 7.3 Hz, 3H, butoxy); ^{13}C NMR (75 MHz, $CDCl_3$) δ 163.5 (C-2), 157.3 (C-6), 140.0 (C-4), 136.9 (Ar-C), 133.3 (Ar-C), 129.4 (Ar-C), 129.1 (Ar-C), 128.3 (Ar-C), 126.8 (Ar-C), 98.1 (C-3), 97.8 (C-5), 65.5 (butoxy), 44.0 (-**C**H_2-), 31.3 (butoxy), 19.3 (butoxy), 13.9 (butoxy); HRMS (ES^+) Calculated for $C_{16}H_{20}ClN_2O$ $[M+H]^+$: 291.1264, found: 291.1264.

6.2.11.2 *N*-(2-chlorobenzyl)-6-phenoxypyridin-2-amine **157b**

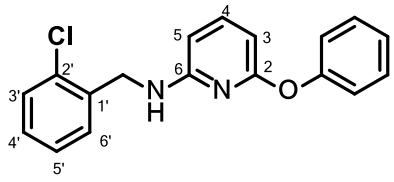

Reaction of compound **155** (427 mg, 1.0 mmol) with phenol (141 mg, 1.5 mmol) gave compound **157b** (189 mg, 61%) as a pale yellow oil. IR (cm^{-1}): 3267 (NH str.), 3065 (CH str.), 1590 and 1560 (C=N), 1428 (C=C); ^{1}H NMR (300 MHz, $CDCl_3$) δ 7.55–7.06 (m, 10H, Ar-H), 6.75 (d, *J* = 7.5 Hz, 1H, H-5), 6.25 (d, *J* = 8.2 Hz, 1H, H-3), 5.16 (t, *J* = 6.3 Hz, 1H, NH), 4.57 (d, *J* = 6.2 Hz, 2H, -C**H**$_2$-); ^{13}C NMR (75 MHz, $CDCl_3$) δ 160.8 (C-2), 158.5 (C-6), 155.1 (Ar-C), 140.3 (C-4), 139.6 (Ar-C), 135.8 (Ar-C), 133.5 (Ar-C), 129.6 (Ar-C), 129.4 (Ar-C), 129.0 (Ar-C), 128.7 (Ar-C), 128.4 (Ar-C), 127.0 (Ar-C), 116.4 (C-3), 104.8 (C-5), 44.0 (-**C**H_2-); HRMS (ES^+) Calculated for $C_{18}H_{16}ClN_2O$ $[M+H]^+$: 311.0951, found: 311.0949.

6.2.11.3 6-Benzyloxy-*N*-(2-chlorobenzyl)pyridin-2-amine **157c**

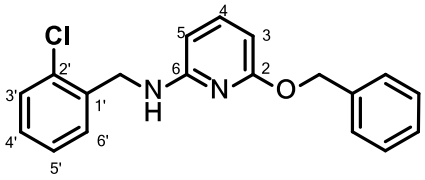

Reaction of compound **155** (427 mg, 1.0 mmol) with benzyl alcohol (141 mg, 1.3 mmol) gave compound **157c** (205 mg, 63%) as a pale brown oil. IR (cm^{-1}): 3329, 3064, 2926, 1593, 1566, 1418, 1215; ^{1}H NMR ($CDCl_3$, 500 MHz) δ 7.40–7.25 (m, 8H, Ar-H), 7.20–7.15 (m, 2H, Ar-H), 6.11–6.09 (dd, *J* = 8.0, 5.0 Hz, 1H, Ar-H), 5.93 (dd, *J* = 7.5, 5.0 Hz, 1H, Ar-H), 5.28 (s, 2H, -C**H**$_2$-), 4.87–4.81 (m, 1H, NH), 4.58 (d, *J* = 5.3 Hz, 2H, -C**H**$_2$-); ^{13}C NMR (125 MHz, $CDCl_3$) δ 163.0 (C-6), 157.1 (C-2), 140.1 (C-4), 137.9 (Ar-C), 136.9 (Ar-C), 133.3 (Ar-C), 129.4 (Ar-C), 129.1 (Ar-C), 128.4 (Ar-C), 128.3 (Ar-C), 127.8 (Ar-C), 127.5 (Ar-C), 126.8 (Ar-C), 98.6 (C-3), 98.4 (C-5), 67.1 (–**C**H$_2$-), 43.9 (-**C**H$_2$-); HRMS (ES^+) Calculated for $C_{19}H_{18}ClN_2O$ $[M+H]^+$: 325.1108, found: 325.1121.

6.2.11.4 *N*-(2-chloro-benzyl)-6-(phenylthio)pyridin-2-amine **157d**

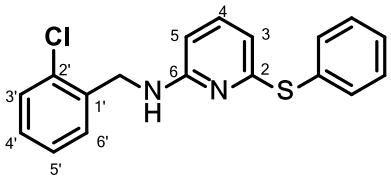

Reaction of compound **155** (427 mg, 1.0 mmol) with thiophenol (143 mg, 1.3 mmol) gave compound **157d** (228 mg, 70%) as a pale brown oil. IR (cm^{-1}): 3261 (NH str.), 3066 (CH str.), 1591 and 1560 (C=N), 1428 (C=C); ^{1}H NMR (300 MHz, $CDCl_3$) δ 7.55–7.05 (m, 10H, Ar-H), 6.73 (d, *J* = 7.5 Hz, 1H, H-5), 6.23 (d, *J* = 8.2 Hz, 1H, H-3), 5.35 (t, *J* = 6.3 Hz, 1H, NH), 4.57 (d, *J* = 6.3 Hz, 2H, -C**H**$_2$-); ^{13}C NMR (75 MHz, $CDCl_3$) δ 158.5 (C-6), 140.2 (C-2), 139.6 (C-4), 135.8 (Ar-C), 133.4 (Ar-C), 132.8 (Ar-C), 129.5 (Ar-C), 129.3 (Ar-C), 128.8 (Ar-C), 128.7 (Ar-C), 128.4 (Ar-C), 127.5 (Ar-C), 127.0 (Ar-C), 116.3 (C-3), 104.7 (C-5), 44.0 (-**C**H$_2$-); HRMS (ES^+) Calculated for $C_{18}H_{16}ClN_2S$ $[M+H]^+$: 327.0723, found: 327.0721.

6.2.11.5 6-Benzylthio-*N*-(2-chlorobenzyl)-pyridin-2-amine **157e**

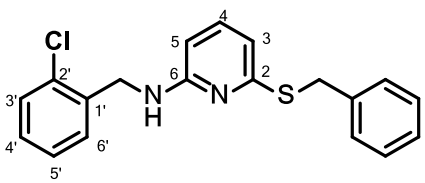

Reaction of compound **155** (427 mg, 1.0 mmol) with benzylthiol (161 mg, 1.3 mmol) gave compound **157e** (299 mg, 88%) as a pale yellow oil. IR

(cm^{-1}): 3422 (NH str.), 3060 and 3027 (CH str.), 1583 (C=N), 1567 (NH bend), 1441 (C=C); ^{1}H NMR (300 MHz, $CDCl_3$) δ 7.43–7.12 (m, 10H, Ar-H), 6.48 (dd, *J* = 7.5, 0.6 Hz, 1H. H-5), 6.06 (dd, *J* = 8.1, 0.6 Hz, 1H, H-3), 4.95 (t, *J* = 5.9 Hz, 1H, NH), 4.61 (d, *J* = 6.2 Hz, 2H, -C**H**$_2$-), 4.32 (s, 2H, -C**H**$_2$-); ^{13}C NMR (75 MHz, $CDCl_3$) δ 157.9 (C-6), 156.6 (C-2), 138.5 (C-4), 137.6 (Ar-C), 136.7 (Ar-C), 133.2 (Ar-C), 129.4 (Ar-C), 129.03 (Ar-C), 128.8 (Ar-C), 128.4 (Ar-C), 128.3 (Ar-C), 126.9 (Ar-C), 126.8 (Ar-C), 110.9 (C-3), 102.7 (C-5), 43.7 (-**C**H$_2$-), 34.2 (-**C**H$_2$); HRMS (ES^+) Calculated for $C_{19}H_{18}ClN_2S$ $[M+H]^+$: 341.0879, found: 341.0874.

6.2.12 General procedure for the preparation of compounds **159**

The appropriately substituted benzenesulfonyl chloride (10.0 mmol) was added dropwise to a stirred ice-cold solution of 2-amino-6-bromopyridine **146** (1.62 g, 9.36 mmol) in acetonitrile (20 ml) and stirred at 0°C for 20 min. The temperature was allowed to warm gradually to room temperature and the reaction was stirred for a further 4 h. After removing the solvent under reduced pressure, the crude product was dissolved in dichloromethane (20 ml) and washed consecutively with saturated $NaHCO_3$ solution (2 x 15 ml) and distilled water (2 x 15 ml). After drying the organic layer over anhydrous Na_2SO_4, the solvent was removed *in vacuo* and the crude product purified by flash silica gel column chromatography, eluting with 5 – 10% EtOAc/Hexane.

6.2.12.1 *N*-(6-bromopyridin-2-yl)-2-chlorobenzenesulfonamide **159a**

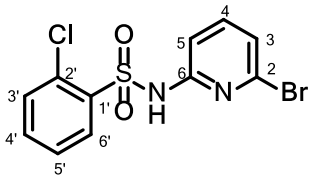

Reaction of 2-chloro-benzenesulfonyl chloride **156a** (2.10 g, 10.0 mmol) gave compound **159a** (3.391 g, 98%) as a white crystalline compound. Mp: 168-169°C; IR (cm^{-1}): 3431 and 3235 (NH stretch), 2924 (CH str.), 1631 (C=N), 1571 (NH bend), 1437 (C=C); ^{1}H NMR (300 MHz, $CDCl_3$) δ 8.21–8.16 (m, 1H, Ar-H), 7.82 (s, 1H, NH), 7.56–7.49 (m, 2H, Ar-H), 7.46–7.37 (m, 2H, Ar-H), 7.20 (dd, *J* = 8.1, 0.6 Hz, 1H, H-5), 7.14 (dd, *J* = 7.7, 0.6 Hz, 1H, H-3); ^{13}C NMR (75 MHz, $CDCl_3$) δ 149.8 (C-6), 140.4 (C-2), 140.2 (Ar-C), 136.2 (Ar-C), 134.6 (Ar-C), 132.1 (Ar-C), 132.0 (Ar-C), 131.9 (Ar-C), 127.1 (Ar-C), 123.7 (C-3), 109.76 (C-5); HRMS (ES^+) Calculated for $C_{11}H_9BrClN_2O_2S$ $[M+H]^+$: 346.9257, found: 346.9246.

6.2.12.2 *N*-(6-bromopyridin-2-yl)-benzenesulfonamide **159b**

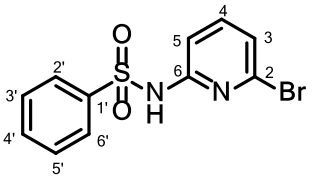

Reaction of benzenesulfonyl chloride **156b** (1.766 g, 10.0 mmol) gave compound **159b** (3.091 g, 96%) as a white crystalline compound. Mp: 111-113°C; IR (cm^{-1}): 3315 (NH str.), 3071 (CH str.), 1584 (C=N), 1568 (NH bend), 1438 (C=C); ^{1}H NMR (300 MHz, $CDCl_3$) δ 7.99–7.90 (m, 2H, Ar-H), 7.71 (br s, 1H, NH), 7.63–7.55 (m, 1H, Ar-H), 7.55–7.43 (m, 3H, Ar-H), 7.31 (dd, *J* = 8.1, 0.6 Hz, 1H, H-5), 7.15 (dd, *J* = 7.7, 0.8 Hz, 1H, H-3); ^{13}C NMR (75 Hz, $CDCl_3$) δ 150.4 (C-6), 140.5 (C-2), 140.1 (Ar-C), 139.0 (Ar-C), 133.6 (Ar-C), 129.3 (Ar-C), 127.4 (Ar-C), 123.5 (C-3), 110.1 (C-5). HRMS (ES^+) Calculated for $C_{11}H_{10}BrN_2O_2S$ $[M+H]^+$: 312.9646, found: 312.9639.

6.2.13 General procedure for the preparation of compounds **144a-h**

Tris-(dibenzylideneacetone)-di-palladium (0) [Pd_2dba_3], (19 mg, 2 mol %), *rac*-BINAP (38 mg, 6 mol %), dioxane (3 – 5 ml, degassed) and a magnetic stirrer were added to an oven-dried 10 ml round bottomed flask under nitrogen purge. The flask was sealed and heated with stirring at 80°C in an oil bath (5 min). An appropriate sulfonamide **159a** or **b** (1.0 mmol), an amine (1.3–3.0 mmol) and potassium *tert*-butoxide (2.4 mmol) were added and the sealed reaction was heated at 120–135°C for 24 h. The reaction mixture was cooled to room temperature, diluted with chloroform (15 ml) and filtered. The filtrate was washed successively with saturated aqueous $NaHCO_3$ (10 ml) and distilled water (2 x 10 ml). After drying over Na_2SO_4, the solvent was removed *in vacuo* and the crude mixture was purified by silica gel flash column chromatography, eluting the desired compound with 5–10% EtOAc/Hexane.

6.2.13.1 2-Chloro-*N*-(6-(cyclohexylamino)-pyridin-2-yl)benzenesulfonamide **144a**

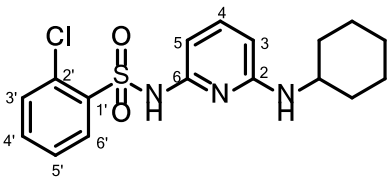

Reaction of **159a** (348 mg, 1.0 mmol) with cyclohexylamine (198 mg, 2.0 eq.) gave compound **144a** (234 mg, 64%) as a pale yellow oil. IR (cm^{-1}): 3349 and 3244 (NH str.), 3064 (CH str.), 1612 and 1593 (CN bend str.), 1452 (C=C str.); ^{1}H NMR (500 MHz, $CDCl_3$) δ 8.14 (dd, *J* = 8.1, 0.9 Hz, 1H, Ar-H), 7.43–7.28 (m, 5H, Ar-H), 6.62 (d, *J* = 8.0 Hz,

1H, H-5), 5.85 (d, *J* = 8.3 Hz, 1H, H-3), 3.25–3.17 (m, 1H, cyclohexyl), 1.99–1.90 (m, 2H, cyclohexyl), 1.81–1.73 (m, 2H, cyclohexyl), 1.60–1.56 (m, 1H, cyclohexyl), 1.34–1.19 (m, 5H, cyclohexyl); ^{13}C NMR (125 MHz, $CDCl_3$) δ 153.5 (C-6), 152.3 (C-2), 143.3 (Ar-C), 139.8 (Ar-C), 132.4 (Ar-C), 132.4 (Ar-C), 131.7 (Ar-C), 130.8 (Ar-C), 126.3 (Ar-C), 100.0 (C-3), 96.2 (C-5), 51.6 (cyclohexyl), 32.3 (cyclohexyl), 25.4 (cyclohexyl), 24.9 (cyclohexyl); HRMS (ES$^+$) Calculated for $C_{17}H_{21}ClN_3O_2S$ [M+H]$^+$: 366.1043, found: 366.1042.

6.2.13.2 *N*-(6-(benzylamino)-pyridin-2-yl)-2-chlorobenzenesulfonamide **144b**

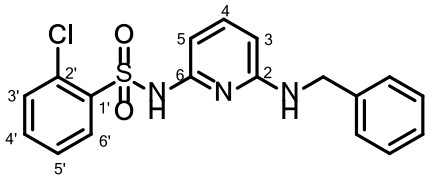

Reaction of **159a** (348 mg, 1.0 mmol) with benzylamine (140 mg, 1.5 mmol) gave compound **144b** (187 mg, 50%) as a pale brown oil. IR (cm^{-1}): 3257 (NH str.), 3106 and 2928 (CH str.), 1602 (NH bend), 1428 (C=C str.); ^{1}H NMR (300 MHz, $CDCl_3$) δ 8.14 (d, *J* = 7.2, 1.2 Hz, 1H, Ar-H), 7.70 (s, 1H, NH), 7.44–7.38 (m, 2H, Ar-H), 7.34–7.22 (m, 8H, Ar-H), 6.69 (d, *J* = 8.4 Hz, 1H, H-5), 5.81 (d, *J* = 8.4 Hz, 1H, H-3), 4.39 (d, *J* = 5.4 Hz, 2H, PhC**H**$_2$N-); ^{13}C NMR (75 MHz, $CDCl_3$) δ 153.8 (C-2), 152.9 (C-6), 143.1 (Ar-C), 139.3 (Ar-C), 137.4 (Ar-C), 132.7 (Ar-C), 132.2 (Ar-C), 131.7 (Ar-C), 130.9 (Ar-C), 128.7 (Ar-C), 127.4 (Ar-C), 127.1 (Ar-C), 126.5 (Ar-C), 101.0 (C-3), 97.4 (C-5), 46.2 (Ph**C**H$_2$N-); HRMS (ES$^+$) Calculated for $C_{18}H_{17}ClN_3O_2S$ [M+H]$^+$: 374.0730, found: 374.0726.

6.2.13.3 2-Chloro-*N*-(6-(phenylamino)-pyridin-2-yl)benzenesulfonamide **144c**

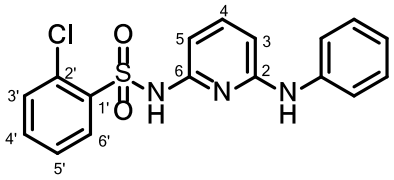

Reaction of **159a** (348 mg, 1.0 mmol) with aniline (140 mg, 1.5 mmol) gave compound **144c** (208 mg, 58%) as a pale yellow solid. Mp: 107-109°C; IR (cm^{-1}): 3350 and 3245 (NH str.), 3065 (CH str.), 1612, 1592 and 1538 (NH bend), 1452 and 1404 (C=C str.); ^{1}H NMR (300 MHz, $CDCl_3$) δ 9.01 (s, 1H, NH), 8.22–8.12 (m, 1H, Ar-H), 7.53–7.20 (m, 9H, Ar-H), 7.16–7.07 (m, 1H, Ar-H), 6.89–6.81 (m, 1H, Ar-H), 6.41–6.34 (m, 1H, Ar-H); ^{13}C NMR (75 MHz, $CDCl_3$) δ 152.8 (C-2), 152.1 (C-6), 143.0 (Ar-C), 138.9 (Ar-C), 138.3 (Ar-C), 133.0 (Ar-C), 132.2 (Ar-C), 131.8 (Ar-C), 131.0 (Ar-C), 129.4 (Ar-C), 126.6 (Ar-C), 124.6 (Ar-C), 122.2 (Ar-C),

102.8 (C-3), 99.4 (C-5); HRMS (ES+) Calculated for $C_{17}H_{15}ClN_3O_2S$ [M+H]+: 360.0574, found: 360.0572.

6.2.13.4 2-Chloro-*N*-(6-morpholinopyridin-2-yl)benzenesulfonamide **144d**

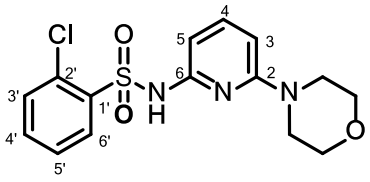

Reaction of **159a** (348 mg, 1.0 mmol) with morpholine (261 mg, 3.0 mmol) gave compound **144d** (279 mg, 79%) as a pale brown oil which solidified on drying. Mp: 178-180°C; IR (cm^{-1}): 3154 (NH str.), 3093, 2873 and 2845 (CH str.), 1596 (C=N), 1573 (NH bend), 1430 (C=C str.); ^{1}H NMR (300 MHz, $CDCl_3$) δ 8.22–8.12 (m, 1H, Ar-H), 7.63–7.50 (m, 1H, Ar-H), 7.49–7.44 (m, 2H, Ar-H), 7.42–7.31 (m, 2H, Ar-H), 6.47 (d, *J* = 7.8 Hz, 1H, H-5), 6.24 (d, *J* = 8.3 Hz, 1H, H-3), 3.80–3.68 (m, 4H, morpholinyl), 3.41–3.30 (m, 4H, morpholinyl); ^{13}C NMR (75 MHz, $CDCl_3$) δ 158.3 (C-2), 148.4 (C-6), 139.8 (Ar-C), 137.0 (Ar-C), 134.0 (Ar-C), 1319 (Ar-C), 131.8 (Ar-C), 131.7 (Ar-C), 126.9 (Ar-C), 102.1 (C-3), 100.6 (C-5), 66.5 (morpholinyl), 45.2 (morpholinyl); HRMS (ES+) Calculated for $C_{15}H_{17}ClN_3O_3S$ [M+H]+: 354.0679, found: 354.0677.

6.2.13.5 2-Chloro-*N*-(6-(piperidin-1-yl)-pyridin-2-yl)benzenesulfonamide **144e**

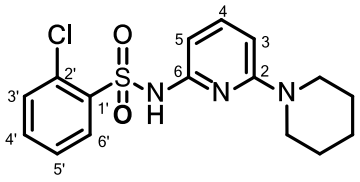

Reaction of **159a** (348 mg, 1.0 mmol) with piperidine (255 mg, 3.0 mmol) gave compound **144e** (200 mg, 57%) as a pale yellow solid. Mp: 126-128°C; IR (cm^{-1}): 3229 (NH str.), 2930 and 2852 (CH str.), 1598 (C=N), 1569 (NH bend), 1437 (C=C str.); ^{1}H NMR (300 MHz, $CDCl_3$) δ8.19–8.14 (m, 1H, Ar-H), 7.76–7.22 (m, 5H, Ar-H), 6.32 (d, *J* = 7.2 Hz, 1H, H-5), 6.22 (d, *J* = 7.4 Hz, 1H, H-3), 3.47–3.29 (m, 4H, cyclohexyl), 1.71–1.50 (m, 6H, cyclohexyl); ^{13}C NMR (75 MHz, $CDCl_3$) δ 157.6 (C-2), 148.8 (C-6), 139.9 (Ar-C), 137.5 (Ar-C), 133.7 (Ar-C), 131.7 (Ar-C), 131.6 (Ar-C), 128.9 (Ar-C), 126.8 (Ar-C), 101.6 (C-3), 99.7 (C-5), 46.1 (cyclohexyl), 25.3 (cyclohexyl), 24.6 (cyclohexyl). HRMS (ES+) Calculated for $C_{16}H_{19}ClN_3O_2S$ [M+H]+: 352.0887, found: 352.0885.

6.2.13.6 *N*-(6-(cyclohexylamino)-pyridin-2-yl)benzenesulfonamide **144f**

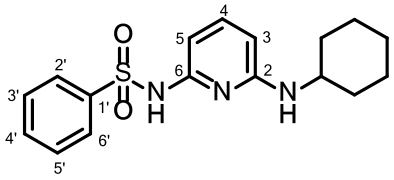

Reaction of **159b** (313 mg, 1.0 mmol) with cyclohexylamine (198 mg, 2.0 mmol) gave compound **144f** (216 mg, 65%) as a pale yellow oil. IR (cm^{-1}): 3251 (NH str.), 3103, 2930 and 2854 (CH str.), 1600 (C=N), 1540 (NH bend), 1445 (C=C str.), ^{1}H NMR (500 MHz, $CDCl_3$) δ 8.98–7.91 (m, 2H, Ar-H), 7.56–7.39 (m, 4H, Ar-H), 7.34 (t, *J* = 8.4 Hz, 1H, H-4), 6.59 (d, *J* = 8.1 Hz, 1H, H-5), 5.83 (d, *J* = 8.3 Hz, 1H, H-3), 3.19 (s, 1H, cyclohexyl), 1.99–1.88 (m, 2H, cyclohexyl), 1.80–1.70 (m, 2H, cyclohexyl), 1.61–1.52 (m, 1H, cyclohexyl), 1.35–1.18 (m, 5H, cyclohexyl); ^{13}C NMR (75 MHz, $CDCl_3$) δ 154.4 (C-2), 151.9 (C-6), 143.9 (Ar-C), 142.7 (Ar-C), 131.6 (Ar-C), 128.6 (Ar-C), 126.9 (Ar-C), 100.2 (C-3), 95.5 (C-5), 51.6 (cyclohexyl), 32.2 (cyclohexyl), 25.3 (cyclohexyl), 24.7 (cyclohexyl); HRMS (ES^+) Calculated for $C_{17}H_{22}N_3O_2S$ $[M+H]^+$: 332.1433, found: 332.1426.

6.2.13.7 *N*-(6-morpholinopyridin-2-yl)benzenesulfonamide **144g**

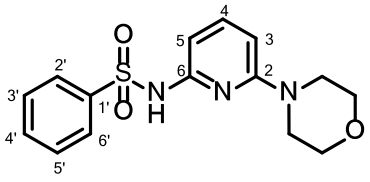

Reaction of **159b** (313 mg, 1.0 mmol) with morpholine (1.5 eq.) gave compound **144g** (179 mg, 56%) as a pale yellow oil. IR (cm^{-1}): 3212 (NH str.), 2918, 2891and 2857 (CH str.), 1601 (C=N), 1571 (NH bend), 1435 (C=C str.); ^{1}H NMR (300 MHz, $CDCl_3$) δ 7.98–7.90 (m, 2H, Ar-H), 7.73–7.35 (m, 5H, Ar-H), 6.57 (d, *J* = 7.8 Hz, 1H, H-5), 6.25 (d, *J* = 8.3 Hz, 1H, H-3), 3.79–3.68 (m, 4H, morpholinyl), 3.41–3.30 (m, 4H, morpholinyl); ^{13}C NMR (75 MHz, $CDCl_3$) δ 158.4 (C-2), 149.0 (C-6), 140.8 (Ar-C), 139.9 (Ar-C), 133.0 (Ar-C), 129.0 (Ar-C), 127.3 (Ar-C), 101.9 (C-3), 100.3 (C-5), 66.6 (morpholinyl), 45.3 (morpholinyl); HRMS (ES^+) Calculated for $C_{15}H_{18}N_3O_3S$ $[M+H]^+$: 320.1069, found: 320.1069.

6.2.13.8 *N*-(6-(piperidin-1-yl)-pyridin-2-yl)benzenesulfonamide **144h**

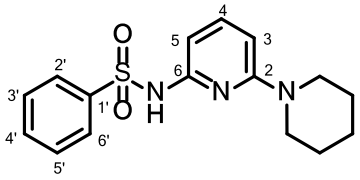

Reaction of **159b** (313 mg, 1.0 mmol) with piperidine (128 mg, 1.5 mmol) gave compound **144h** (194 mg, 61%) as a pale yellow solid. Mp: 133-135°C; IR (cm^{-1}): 3236 (NH str.), 2935 and 2854 (CH str.), 1599 (C=N), 1565 (NH bend), 1440 (C=C str.); ^1H NMR (300 MHz, $CDCl_3$) δ 8.03–7.83 (m, 2H, Ar-H), 7.60–7.39 (m, 4H, Ar-H), 7.32 (t, *J* = 8.4 Hz, 1H, H-4), 6.43 (d, *J* = 7.7 Hz, 1H, H-5), 6.32 (d, *J* = 8.4 Hz, 1H, H-3), 3.51–3.30 (m, 4H, piperidyl), 1.65–1.49 (m, 6H, piperidyl); ^{13}C NMR (75 MHz, $CDCl_3$) δ 158.1 (C-2), 148.9 (C-6), 140.2 (Ar-C), 139.7 (Ar-C), 132.8 (Ar-C), 128.9 (Ar-C), 127.3 (Ar-C), 101.7 (C-3), 99.1 (C-5), 46.0 (morpholinyl), 25.3 (morpholinyl), 24.6 (morpholinyl); HRMS (ES^+) Calculated for $C_{16}H_{20}N_3O_2S$ $[M+H]^+$: 318.1276, found: 318.1277.

6.2.14 General procedure for the preparation of compounds **160a-f**

The same method was used as for the preparation of compounds **144a-h** except that the sealed reaction was heated at 135-140°C for 24 h.

6.2.14.1 *N*-(6-butoxypyridin-2yl)-2-chloro-benzenesulfonamide **160a**

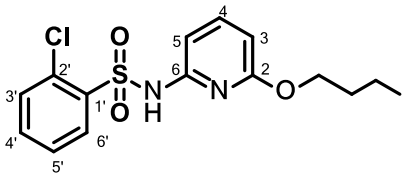

Reaction of compound **159a** (347 mg, 1.0 mmol) with *n*-butanol (148 mg, 2.0 mmol) gave compound **160a** (211 mg, 62%) as a pale yellow oil. IR (cm^{-1}): 3243 (NH str.), 2960 and 2931 (CH str.), 1594 (NH bend), 1441 (C=C); ^1H NMR (500 MHz, $CDCl_3$) δ 8.19–8.14 (m, 1H, Ar-H), 7.59–7.51 (m, 1H, Ar-H), 7.50–7.34 (m, 4H, Ar-H), 6.69 (d, *J* = 7.7 Hz, 1H, H-5), 6.36 (d, *J* = 8.2 Hz, 1H, H-3) 4.07 (t, *J* = 6.6 Hz, 2H, butoxy), 1.69–1.62 (m, 2H, butoxy), 1.47–1.33 (m, 2H, butoxy), 0.94 (t, *J* = 7.3 Hz, 3H, butoxy); ^{13}C NMR (125 MHz, $CDCl_3$) δ 163.2 (C-2), 147.7 (C-6), 140.6 (Ar-C), 136.7 (Ar-C), 134.1 (Ar-C), 132.0 (Ar-C), 131.9 (Ar-C), 131.8 (Ar-C), 126.9 (Ar-C), 106.3 (C-3), 103.3 (C-5), 66.0 (butoxy), 30.9 (butoxy), 19.2 (butoxy), 13.9 (butoxy); HRMS (ES^+) Calculated for $C_{15}H_{18}ClN_2O_3S$ $[M+H]^+$: 341.0727, found: 341.00719.

6.2.14.2 *N*-(6-(benzyloxy)-pyridin-2-yl)-2-chloro-benzenesulfonamide **160b**

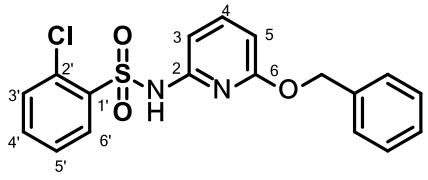

Reaction of compound **159a** (347 mg, 1.0 mmol) with benzyl alcohol (216 mg, 2.0 mml) gave compound **160b** (300 mg, 80%) as a brown solid. Mp: 121-123°C; IR (cm^{-1}): 3247 (NH str.), 2877 (CH str.), 1602 (C=N), 1579 (NH bend), 1441 (C=C); ^{1}H NMR (500 MHz, $CDCl_3$) δ 8.16 (dt, *J* = 7.9, 1.0 Hz, 1H, Ar-H), 7.50–7.42 (m, 4H, Ar-H), 7.39–7.29 (m, 6H), 6.74 (d, *J* = 7.8Hz, 1H, H-5), 6.44 (d, *J* = 8.1 Hz, 1H, H-3), 5.15 (s, 2H, PhC**H**$_2$S-); ^{13}C NMR (125 MHz, $CDCl_3$) δ 162.7 (C-2), 147.6 (C-6), 140.8 (Ar-C), 136.9 (Ar-C), 136.6 (Ar-C), 134.2 (Ar-C), 132.0 (Ar-C), 131.8 (Ar-C), 131.8 (Ar-C), 128.6 (Ar-C), 128.5 (Ar-C), 128.0 (Ar-C), 127.9 (Ar-C), 127.0 (Ar-C), 106.7 (C-3), 103.7 (C-5), 67.8 (Ph**C**H$_2$S-; HRMS (ES^+) Calculated for $C_{18}H_{16}ClN_2O_3S$ $[M+H]^+$: 375.0570, found: 375.0568.

6.2.14.3 2-Chloro-*N*-(6-(phenylthio)-pyridin-2-yl)benzenesulfonamide **160c**

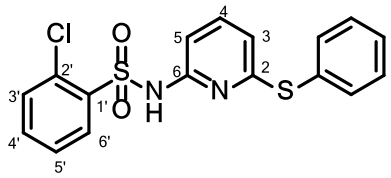

Reaction of compound **159a** (347 mg, 1.0 mmol) with thiophenol (330 mg, 3.0 mmol) gave compound **160c** (312 mg, 83%) as a brown solid. Mp: 129-131°C; IR (cm^{-1}): 3231 (NH str.), 2924 (CH str.), 1570 (C=N), 1435 (C=C); ^{1}H NMR (500 MHz, $CDCl_3$) δ 8.11–8.08 (m, 1H, Ar-H), 7.58 (br s, 1H, NH), 7.54–7.46 (m, 4H, Ar-H), 7.43–7.35 (m, 4H, Ar-H), 7.31 (t, *J* = 7.5 Hz, 1H, H-4), 6.92 (d, *J* = 8.1 Hz, 1H, H-5), 6.54 (d, *J* = 7.8 Hz, 1H, H-3); ^{13}C NMR (75 MHz, $CDCl_3$) ^{13}C NMR (126 MHz, $CDCl_3$) δ 149.7 (C-6), 138.9 (C-2), 135.1 (Ar-C), 134.6 (Ar-C), 134.2 (Ar-C), 132.0 (Ar-C), 131.9 (Ar-C), 131.7 (Ar-C), 130.0 (Ar-C), 129.6 (Ar-C), 129.4 (Ar-C), 127.0 (Ar-C), 123.7 (Ar-C), 116.8 (C-3), 107.6 (C-5); HRMS (ES^+) Calculated for $C_{17}H_{14}ClN_2O_2S_2$ $[M+H]^+$: 377.0185, found: 377.0177.

6.2.14.4 *N*-(6-(benzylthio)-pyridin-2-yl)-2-chlorobenzenesulfonamide **160d**

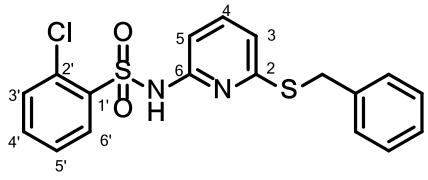

Reaction of compound **159a** (347 mg, 1.0 mmol) with benzylthiol (372 mg, 3.0 mmol) gave compound **160d** (281 mg, 72%) as a pale brown solid. Mp: 122-123°C; IR (cm^{-1}): 3256 (NH str.), 2929 (CH str.), 1565 (NH bend), 1430 (C=C); ^{1}H NMR (500 MHz, $CDCl_3$) δ 8.16–8.14 (m, 1H, Ar-H), 7.80–7.57 (br m, 1H, NH), 7.54–7.18 (m, 9H, Ar-H), 6.91 (d, *J* = 8.0 Hz, 1H, H-5), 6.80 (d, *J* = 7.8 Hz, 1H, H-3), 4.29–4.19 (m, 2H, PhC**H**$_2$S-); ^{13}C NMR (126 MHz, $CDCl_3$) δ 149.4 (C-6), 138.3 (C-4), 137.7 (C-2), 136.5 (Ar-C), 134.3 (Ar-C), 131.9 (Ar-C), 131.8 (Ar-C), 129.1 (Ar-C), 128.8 (Ar-C), 128.6 (Ar-C), 128.5 (Ar-C), 127.2 (Ar-C), 127.1 (Ar-C), 118.0 (C-3), 107.3 (C-5), 34.3 (Ph**C**H$_2$S-); HRMS (ES^+) Calculated for $C_{18}H_{16}ClN_2O_2S_2$ $[M+H]^+$: 391.0342, found: 391.0339.

6.2.14.5 *N*-(6-butoxypyridin-2-yl)-benzenesulfonamide **160e**

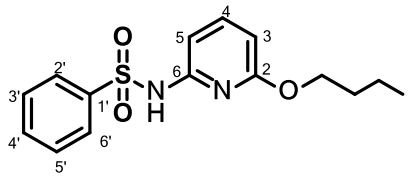

Reaction of compound **159b** (347 mg, 1.0 mmol) with *n*-butanol (222 mg, 3.0 mmol) gave compound **160e** (162 mg, 53%) as a pale brown solid. Mp: 94-96°C; IR (cm^{-1}): 3237 (NH str.), 2962 and 2931 (CH str.), 1613 (C=N), 1574 (NH bend), 1441 (C=C); ^{1}H NMR (300 MHz, $CDCl_3$) δ 7.99–7.91 (m, 2H, Ar-H), 7.61–7.52 (m, 1H, Ar-H), 7.51–7.41 (m, 3H, Ar-H), 7.31 (br s, 1H, NH), 6.77 (d, *J* = 7.7 Hz, 1H, H-5), 6.37 (d, *J* = 8.1 Hz, 1H, H-3), 4.05 (t, *J* = 6.6 Hz, 2H, butoxy), 1.70–1.58 (m, 2H, butoxy), 1.45–1.31 (m, 2H, butoxy), 0.92 (t, *J* = 7.4 Hz, 3H, butoxy); ^{13}C NMR (75 MHz, $CDCl_3$) δ 163.3 (C-2), 148.2 (C-6), 140.6 (Ar-C), 139.7 (Ar-C), 133.1 (Ar-C), 129.0 (Ar-C), 127.3 (Ar-C), 105.9 (C-3), 103.2 (C-5), 66.0 (butoxy), 30.9 (butoxy), 19.2 (butoxy), 13.8 (butoxy); HRMS (ES^+) Calculated for $C_{15}H_{19}N_2O_3S$ $[M+H]^+$: 307.1116, found: 307.1114.

6.2.14.6 *N*-(6-(benzyloxy)-pyridin-2-yl)-benzenesulfonamide **160f**

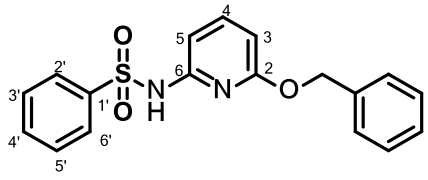

Reaction of compound **159b** (347 mg, 1.0 mmol) with benzyl alcohol (141 mg, 1.3 mmol) gave compound **160f** (218 mg, 64%) as a pale brown solid. Mp: 133-135°C; IR (cm^{-1}): 3246 (NH str.), 2877 (CH str.), 1603 (C=N), 1580 (NH bend), 1441 (C=C); ^{1}H NMR (300 MHz, $CDCl_3$) δ 7.97–7.91 (m, 2H, Ar-H), 7.62–7.40 (m, 5H, Ar-H), 7.39–7.23 (m, 5H, Ar-H), 6.78 (dd, *J* = 7.8, 0.7 Hz, 1H, H-5), 6.43 (dd, *J* = 8.1, 0.6 Hz, 1H, H-3), 5.12 (s, 2H, PhC**H**$_2$O-); ^{13}C NMR (75 MHz, $CDCl_3$) δ 162.7 (C-2), 148.2 (C-6), 140.8 (Ar-C), 139.7 (Ar-C), 136.9 (Ar-C), 133.1 (Ar-C), 129.0 (Ar-C), 128.4 (Ar-C), 127.9 (Ar-C), 127.9 (Ar-C), 127.3 (Ar-C), 106.2 (C-3), 103.6 (C-5), 67.8 (-**C**H_2O-); HRMS (ES^+) Calculated for $C_{18}H_{17}N_2O_3S$ $[M+H]^+$: 341.0960, found: 341.0954.

6.2.15 *In vitro* assessment of antiviral activity and toxicity

Pyridyl-benzamide (**142a–l**, **147a–i** and **151a-e**), -benzylamine (**143a–e**, **152** and **157a–e**) and –sulfonamide (**144a–h**, **159a–b** and **160a–f**) test compounds were dissolved in dimethyl sulfoxide (DMSO) and serial dilutions were prepared in cell culture medium in the wells of 96-well culture plates. A standardized amount of pseudoviruses, sufficient to produce a fluorescent signal of approximately 1 x 10^5 relative light units (RLU) in the media control after 48 hours of incubation, were combined with HEK293T cells. For cell toxicity screens, the pseudoviruses were excluded. The cells and pseudoviruses were added to the drug dilutions in the culture plate and incubated for 48 hours at 37°C under 5% CO_2 in a humidified atmosphere. A medium control, which contained no inhibitor, was included to represent full (100%) cell viability or viral activity. For cell viability assessment, the CellTiter 96® AQueous One Solution Cell Proliferation Assay (Promega, Madison, WI, USA) was used. The tetrazolium compound 3-(4,5-dimethylthiazol 2-yl)-5-(3-carboxymethoxyphenyl)-2-(4-sulfophenyl)-2H-tetrazolium (MTS) and the phenazine ethosulfate (PES) electron coupling reagent were added and bio-reduced by viable cells into a coloured formazan product which was quantified at 490 nm on a VERSAmax microplate reader (Molecular Devices, Sunnyvale, CA, USA). The degree of compound toxicity was assessed by reference to the absorbance of the medium (no drug) control.

For the quantification of viral infection, the Bright-Glo™ Luciferase Assay System (Promega, Madison, WI, USA) was used. Infection by the pseudoviruses permitted the HEK293T cells to express firefly luciferase, and a direct correlation exists between the amount of luciferase

expression and degree of viral infection. The presence of reverse transcriptase inhibitors prevents the expression of luciferase. After the addition of the luciferase substrate to the wells of the culture plates, the contents of the wells were mixed and transferred to black 96-well plates. Luminescence was then measured on a Victor3 luminometer (PerkinElmer, Waltham, MA, USA). The amount of HIV-1 inhibition was assessed by reference to the luminescence of the medium (no drug) control.

6.3 Synthetic Methods for Chapter 3

6.3.1 Preparation of di-functionalized pyridine-based derivatives **161-163**

Palladium/rac-BINAP-catalyzed procedure for the preparation of compounds **161-163**: Method E

Tris-(dibenzylideneacetone)-di-palladium (0) [Pd_2dba_3], (19 mg, 2 mol %), *rac*-BINAP (38 mg, 6 mol %), DMF (3–5 ml, degassed) and a magnetic stirrer were added to an oven-dried 10 ml round bottomed flask and purged with nitrogen. The flask was sealed and heated with stirring at 80°C in an oil bath (5 min). Approximately 237 mg (1.0 mmol) of 2,6-dibromopyridine **168**, 4-chlorophenol (130 mg, 1.0 mmol) and potassium *tert*-butoxide (2.4 mmol) were added and the sealed reaction was heated at 130-140°C for 24 h. The reaction mixture was cooled to room temperature, diluted with dichloromethane (15 ml) and filtered. The filtrate was washed successively with saturated aqueous $NaHCO_3$ (10 ml) and distilled water (2 x 10 ml). After drying over $MgSO_4$, the solvent was removed *in vacuo* and the crude brown mixture was purified by silica gel flash column chromatography, eluting the title compound with hexane – 3% EtOAc/Hexane.

6.3.1.1 2-Bromo-6-(piperidin-1-yl)pyridine **165**

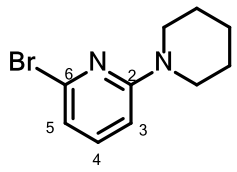

2.6-Dibromopyridine **168** (237 mg, 1.0 mmol) was reacted with freshly distilled piperidine (111 mg, 1.3 eq.) using method E to generate intermediate product **165** (215 mg, 89%) as a yellow oil. ^{1}H NMR (500 MHz, $CDCl_3$) δ 7.23 (dd, *J* = 8.4, 7.4 Hz,1H, H-4), 6.66 (d, *J* = 7.4 Hz, 1H, H-3), 6.49 (d, *J* = 8.4 Hz, 1H, H-5), 3.52–3.42 (m, 4H), 1.64–1.59 (m, 6H); ^{13}C NMR (126 MHz, $CDCl_3$) δ 159.3, 140.2, 139.3, 114.9, 104.7, 46.0, 25.4, 24.6.

6.3.1.2 2-(4-chlorophenoxy)-6-(piperidin-1-yl)pyridine **161**

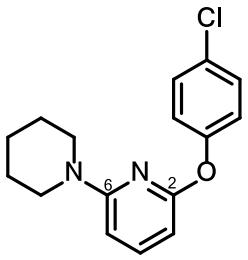

2-Bromo-6-(piperidin-1-yl)pyridine **165** (121 mg, 0.5 mmol) was reacted with 4-chlorophenoxide **166** (77 mg, 0.6 mmol) using method E to afford product **161** (93.85 mg, 65%) as a brown oil. ^{1}H NMR (500 MHz, $CDCl_3$) δ 7.40 (t, *J* = 8.0 Hz, 1H), 7.30–7.27 (m, 2H), 7.09–7.05 (m, 2H), 6.29 (d, *J* = 8.2 Hz, 1H), 6.01 (d, *J* = 7.7 Hz, 1H), 3.43–3.38 (m, 4H), 1.62–1.53 (m, 6H); ^{13}C NMR (126 MHz, $CDCl_3$) δ 162.1, 158.4, 153.2, 141.3, 140.5, 129.2, 122.5, 100.7, 97.3, 46.0, 25.3, 24.7; HRMS (ES^+) Calculated for $C_{16}H_{18}ClN_2O$ $[M+H]^+$: 289.1108, found: 289.1104.

6.3.1.3 4-Methyl-2-((6-(piperidin-1-yl)pyridin-2-yl)amino)benzonitrile **162**

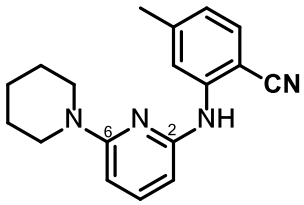

Reaction of 2-bromo-6-(piperidin-1-yl)pyridine **165** (121 mg, 0.5 mmol) with 2-amino-4-methylbenzonitrile **167** (79 mg, 0.6 mmol) using method E gave product **162** (115.49 mg, 65%) as a brown oil. ^{1}H NMR (300 MHz, $CDCl_3$) δ 8.14 (s, 1H), 7.42–7.35 (m, 2H), 6.76–6.71 (m, 2H), 6.22 (d, *J* = 8.3 Hz, 1H), 6.14 (d, *J* = 7.7 Hz, 1H), 3.63–3.50 (m, 6H), 2.35 (s, 3H), 1.68–160 (m, 4H); ^{13}C NMR (75 MHz, $CDCl_3$) δ 158.5, 152.5, 144.5, 139.2, 137.9, 132.2, 121.4, 118.8, 117.8, 99.4, 98.7, 97.0, 46.4, 25.5, 24.8, 22.3; HRMS (ES^+) Calculated for $C_{18}H_{15}ClN_3O$ $[M+H]^+$: 293.1766, found: 293.1759.

6.3.1.4 2-((6-Bromopyridin-2-yl)amino)-4-methylbenzonitrile **169**

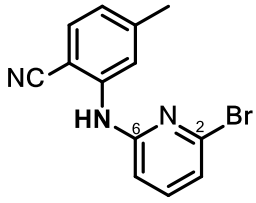

Exactly 237 mg (1.0 mmol) of 2.6-dibromopyridine **168** was reacted with 2-amino-4-methylbenzonitrile (172 mg, 1.3 mmol) at a temperature of 135-140 ℃ using method E to generate intermediate product **169** (233 mg, 81%) as a brown solid. ^{1}H NMR (500 MHz,

$CDCl_3$) δ 7.98 (s, 1H), 7.46 (d, *J* = 8.0 Hz, 1H), 7.43 (t, *J* = 7.7 Hz, 1H), 7.05 (dd, *J* = 8.5 Hz, 1H), 6.94 (s, 1H), 6.90–6.87 (m, 1H), 6.81 (d, *J* = 8.1 Hz, 1H), 2.42 (s, 3H); ^{13}C NMR (126 MHz, $CDCl_3$) δ 154.0, 145.3, 142.7, 140.0, 139.9, 132.6, 123.4, 120.2, 119.5, 117.2, 108.9, 98.9, 22.4.

6.3.1.5 2-((6-(4-Chlorophenoxy)pyridin-2-yl)amino)-4-methylbenzonitrile **163**

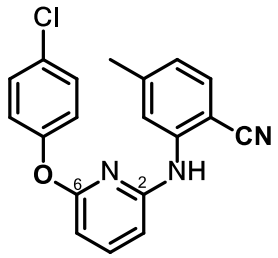

Reaction of 2-((6-bromopyridin-2-yl)amino)-4-methylbenzonitrile **169** (150 mg, 0.52 mmol) with 4-chlorophenol **166** (87 mg, 0.65 mmol) using method E gave product **163** (113 mg, 75%) as a brown oil. IR (cm^{-1}): 2962 and 2852 (CH str.), 2179 (CN), 1600 (C=N), 1436 (C=C); ^{1}H NMR (500 MHz, $CDCl_3$) δ 7.77 (s, 1H), 7.60 (t, *J* = 7.9 Hz, 1H), 7.38–7.35 (m, 2H), 7.19–7.16 (m, 1H), 7.14–7.11 (m, 2H), 6.86 (s, 1H), 6.73 (d, *J* = 7.9 Hz, 1H), 6.50 (t, *J* = 7.8, 2H), 2.12 (s, 3H); ^{13}C NMR (126 MHz, $CDCl_3$) δ 162.4, 152.7, 145.3, 143.0, 141.1, 132.1, 129.9, 129.6, 123.3, 122.3, 118.9, 117.6, 116.7, 104.9, 102.5, 97.0, 22.2; HRMS (ES^+) Calculated for $C_{16}H_{17}ClN_3O_2$ $[M+H]^+$: 336.0904, found: 336.0898.

6.3.2 Preparation of 2,6-dichloroisonicotinic acid **187b**[9]

6.2.3.1 Preparation of citric trimethyl ester **195**[7]

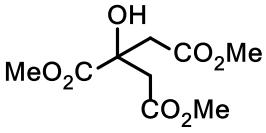

195

Citric acid powder **193** (63.0 g, 305 mmol) was added to a 250 ml round bottomed flask containing methyl alcohol (30 ml). The flask was immersed in an ice bath and stirred until the acid was dissolved. Thionyl chloride (25 ml) was added dropwise to the ice-cold mixture with gentle stirring for 2 h. The reaction was stirred under ice-cold conditions for another 2 h. After removing the ice bath, the reaction was allowed to warm to room temperature and stirred overnight. Excess solvent was removed *in vacuo* to give the trimethyl ester **195** (86.7 g, 99%) as an off white solid. ^{1}H NMR (300MHz, $CDCl_3$): δ 3.77 (s, 6H), 3.67 (s, 9H).

6.2.3.2 Preparation of 2.6-dihydroisonicotinic acid **192**[8]

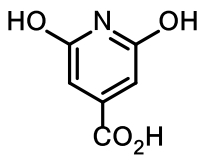

192

Citric acid trimethyl ester **195** (87 g, 300 mmol) and biuret **194** (30 g, 500 mmol) were thoroughly mixed and added to a 600 ml beaker with a mounted thermometer and heated on a hot plate temperature of 160-170° C. As the reaction temperature approached 120℃, the mixture melted to a golden brown slurry with the evolution of ammonia. At 130℃, another charge of biuret (30g, 500 mmol) was added to the reaction and the mixture triturated (10 min). The mixture was heated at 140° C until no gas evolution was evident (1 h) whilst the reaction turned caramel brown. After cooling the reaction to 80℃, hot water was added and the mixture stirred at 80°C for 30 min. Sodium hydroxide pellets were cautiously added to the mixture until an alkaline pH (9.0–9.5) was achieved.

After filtering the mixture through a sintered glass crucible to remove insoluble matter, the golden brown filtrate was acidified (pH 2–3) using concentrated hydrochloric acid (15–20 ml). The reaction mixture was chilled overnight and filtered to give a pale brown solid which was recrystallized from methanol to yield **192** (46.5 g, 73%) as a tan solid. IR (cm^{-1}) 3402 and 3289 (OH str.), 3093 and 2891 (CH str.), 1693 (C=O str.), 1593 (C=N str.), 1502 (C=C str.); ^{1}H NMR (300MHz, DMSO-*d*$_6$) δ 7.92 (br s, 1H), 7.45 (br s, 1H), 6.18 (s, 2H), ^{13}C NMR (126MHz, DMSO-*d*$_6$) δ 166.8, 161.4, 148.9, 96.6.

6.2.3.3 Synthesis of 2,6-dichloroisonicotinic acid **187b**[5]

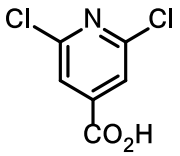

187b

2.6-Dihyroxyisonicotinic acid **192** (9.7 g, 62.5 mmol) and tetraethyl ammonium chloride (12.4 g, 93.8 mmol) were slowly added to an ice cold 250 ml round bottomed flask containing phosphoryl trichloride (10 ml). After attaching a condenser, the reaction mixture was gently heated to 120℃ in an oil bath, and the evolved acidic fumes trapped in a beaker containing 25% aqueous sodium hydroxide. The brown mixture was heated at 130–140℃ for 24 h. After

cooling to room temperature, crushed ice (75 g) was cautiously added and the mixture stirred for 4 h. The product was extracted with EtOAc (6 x 100 ml), washed with saturated ammonium chloride and dried over anhydrous Na_2SO_4 to give product **187b** (10.57 g, 88 %) as a light brown solid. ^{1}H NMR (500MHz, DMSO-*d*$_6$) δ 13.5 (br s, 1H), 7.86 (s, 2H); ^{13}C NMR (126MHz, DMSO-*d*$_6$) δ 164.2, 150.6, 145.1, 123.4.

6.3.3 *General procedure for the preparation of acid chlorides, amides and carbonitriles* – Method F

a) Preparation of acid chlorides

An appropriate aromatic carboxylic acid **187a** or **187b** (382 mg, 2.0 mmol) and a magnetic stirrer were placed into a 50 ml round bottomed flask containing thionyl chloride (10 ml). The mixture was gently stirred and refluxed in an oil bath at 80℃ for 24 h. After cooling the reaction mixture to room temperature, excess thionyl chloride was evaporated *in vacuo* to leave a crude residue of the acid chloride. The highly reactive acid was subsequently used without further purification.

b) Preparation of amides **186a**[3,4] and **186b**[3,10a]

A solution of an appropriate acid chloride (2.0 mmol) in dichloromethane (5 ml) was cautiously added to an ice-cold mixture of excess 25% aqueous ammonia (5 ml) or cyclopropylamine) (2.1 mmol) and pyridine (1 ml) in dichloromethane (15 ml). The mixture was stirred at 0°C (30 min) and then allowed to warm to room temperature for 4 h. The reaction was washed successively with aqueous saturated $NaHCO_3$ (2 x 10 ml), saturated brine solution (10 ml), distilled water (2 x 10 ml) and finally dried over anhydrous Na_2SO_4. After evaporating the solvent, the crude mixture was purified by silica gel flash column chromatography, eluting the title compound **185** with 5–10% EtOAc/hexane.

b) Preparation of carbonitriles **185a**[5a,6] and **185b**[10a-b]

To prepare a corresponding (iso)nicotinonitrile (**185**) from an appropriate carboxamide **186a** or **186b** (189 mg, 1.0 mmol) obtained from above, catalytic amounts of tetraethylammonium chloride (5% w/w) and a magnetic stirrer were added to a 50 ml round bottomed flask chilled in an ice bath. Operating in a well-ventilated area, thionyl chloride (10 ml) or $POCl_3$ (5 ml) was cautiously added (dropwise) into the reaction mixture. After attaching a *findenser*, the reaction

was heated with stirring at 80℃ in an oil bath for 24 h. After cooling to room temperature, excess thionyl chloride or $POCl_3$ was removed *in vacuo* to leave a crude residue which was re-dissolved in dichloromethane (10 ml) and filtered. The filtrate was washed successively with saturated aqueous K_2CO_3 (2 x 5 ml) and distilled water (5 ml). After drying over anhydrous Na_2SO_4, the solvent was evaporated to yield a carbonitrile which was sufficiently pure for use in the next reaction.

2,6-dichloronicotinitrile **185a**

Reaction of 2,6-dichloronicotinoyl chloride (411 mg, 2 mmol) with excess 25% aqueous ammonia (5 ml) gave 2,6-dichloronicotinamde **186a** (380 mg, 99%) as a pale yellow solid. ^{1}H NMR (500 MHz, $CDCl_3$) δ 8.23 (d, *J* = 7.9 Hz, 1H), 7.40 (d, *J* = 7.9 Hz, 1H), 6.67 (s, 1H, NH), 6.24 (s, 1H, NH); ^{13}C NMR (126 MHz, $CDCl_3$) δ 165.0, 152.4, 146.5, 142.8, 128.5, 123.7. Dehydration of **186a** with $POCl_3$ at 80℃ for 24 h afforded 2,6-dichloronicotinonitrile **185a** as an off-white solid. ^{1}H NMR (300 MHz, $CDCl_3$) δ 7.95 (d, *J* = 8.1 Hz, 1H), 7.43 (d, *J* = 8.1 Hz, 1H).

2,6-dichloroisonicotinonitrile **185b**

$POCl_3$-mediated dehydration of the intermediate compound 2,6-dichloronisocotinamide **186b** prepared using Method F above gave 2,6-dichloronisonicotinonitrile **185b** as a white solid. ^{1}H NMR (500 MHz, DMSO) δ 8.23 (s, 2H); ^{13}C NMR (126 MHz, DMSO) δ 150.7, 126.5, 125.3, 115.2.

c) Preparation of cyclopropylamides **188a** and **188b**

A solution of an appropriate acid chloride (2.0 mmol) in dichloromethane (5 ml) was cautiously added to an ice-cold mixture of cyclopropylamine (120 mg, 2.1 mmol) and pyridine (1 ml) in dichloromethane (15 ml). The mixture was stirred at 0°C (30 min) and then allowed to warm to room temperature for 4 h. The reaction was washed successively with aqueous saturated $NaHCO_3$ (2 x 10 ml), saturated brine solution (10 ml), distilled water (2 x 10 ml) and finally dried over anhydrous Na_2SO_4. After evaporating the solvent, the crude mixture was purified by silica gel flash column chromatography, eluting the title compound **188** with 5–10% EtOAc/hexane.

i. 2,6-dichloro-*N*-cyclopropylnicotinamide **188a**

Reaction of 2,6-dichloronicotinoyl chloride (411 mg, 2 mmol) with excess 25% aqueous ammonia (5 ml) gave 2,6-dichloro-N-cyclopropylnicotinamide **188a** (380 mg, 99%) as a pale yellow solid. ^{1}H NMR (500 MHz, CDCl3) δ 8.23 (d, *J* = 7.9 Hz, 1H), 7.40 (d, *J* = 7.9 Hz, 1H),

6.67 (s, 1H), 6.24 (s, 1H); ^{13}C NMR (126 MHz, CDCl3) δ 165.0, 152.4, 146.5, 142.8, 128.5, 123.7.

ii. 2,6-dichloro-*N*-cyclopropylisonicotinamide **188b**

Reaction of 2,6-dichloroisonicotinoyl chloride (411 mg, 2 mmol) with cyclopropylamine (120 mg, 2.1 mmol) gave 2,6-dichloro-*N*-cyclopropylisonicotinamide **188b** (380 mg, 99%) as a pale yellow solid. ^{1}H NMR (300 MHz, $CDCl_3$) δ 7.55 (s, 2H), 6.43 (s, 1H, NH), 2.96–2.84 (m, 1H), 0.96–0.87 (m, 2H), 0.69–0.62 (m, 2H); ^{13}C NMR (75 MHz, $CDCl_3$) δ 164.4, 151.5, 146.8, 124.6, 120.6, 23.5, 6.8.

6.3.4 General procedure for the preparation of compounds **170**, **171a-b**, **175** and **176a-b** and **190**, **191**, **196** and **197**

Tris-(dibenzylideneacetone)-di-palladium (0) [Pd_2dba_3] (28 mg, 3 mol %), *rac*-BINAP (38 mg, 6 mol %), 1,4-dioxane (3–5 ml) and a magnetic stirrer were added to an oven-dried 10 ml round bottomed flask and purged with nitrogen. The flask was sealed and heated with stirring at 80°C in an oil bath for 5 min. Thereafter, the appropriate carbonitrile substrate **185** (1.0 mmol), or cyclopropylamide substrate **188** (232 mg, 1.0 mmol), 4-chlorophenol (64 mg, 0.5 mmol) and sodium *tert*-butoxide (1.5 mmol) were added and the sealed reaction heated at 110–120°C for 24 h. The cooled reaction mixture was filtered and the excess solvent removed *in vacuo* to leave a crude mixture which was re-dissolved in dichloromethane and filtered. The filtrate was washed successively with aqueous saturated $NaHCO_3$ (10 ml), and distilled water (2 x 10 ml). After drying over anhydrous Na_2SO_4 and evaporating excess solvent, the crude mixture was purified by silica gel flash column chromatography, eluting the target with 0–3% EtOAc/hexane.

6.3.4.1 (a) 2-Chloro-6-(4-chlorophenoxy)nicotinonitrile **190 and 191**

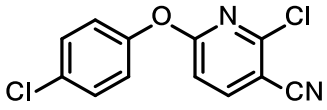

190

Reaction of 2,6-dichloronicotinonitrile **185a** (346 mg, 2.0 mmol) with 4-chlorophenol **166** (128 mg, 1.0 mmol) gave product **190** (257 mg, 87%) with respect to **166**, respectively, as a white oil. ^{1}H NMR (300MHz, $CDCl_3$): δ 7.94 (d, J = 8.3 Hz, 1H), 6.63 (d, J = 8.3 Hz, 1H), 7.26–7.21 (m, 2H), 6.98–6.94 (m, 1H), 6.91–6.86 (m, 1H); ^{13}C NMR (75 MHz, $CDCl_3$) δ 163.0, 150.9, 145.9, 144.8, 131.1, 129.2, 122.9, 114.8, 110.1, 104.8.

6.3.4.1 (b) 2,6-Bis(4-chlorophenoxy)nicotinonitrile **191**

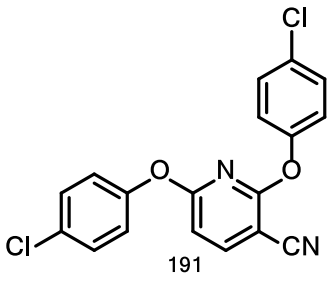

191

Reaction of 2,6-dichloronicotinonitrile **185a** (173 mg, 1.0 mmol) with 4-chlorophenol **166** (128 mg, 2.0 mmol) gave product **191** (363 mg, 78%) with respect to **166**, as a white oil. IR (cm^{-1}): 3043 (CH str.), 2218 (CN), 1553 (C=N str.), 1457 (C=C); ^{1}H NMR (300 MHz, $CDCl_3$) δ 7.94 (d, *J* = 8.3 Hz, 1H), 7.25–7.22 (m, 4H), 6.98–6.93 (m, 2H), 6.91–6.87 (m, 2H), 6.63 (d, *J* = 8.3 Hz, 1H); ^{13}C NMR (75 MHz, $CDCl_3$) δ 164.1, 161.1, 150.8, 145.9, 132.1, 131.1, 129.4, 123.0, 114.8, 104.8; HRMS (ES^+) Calculated for $C_{18}H_{11}Cl_2N_2O_2$ $[M+H]^+$: 357.0179, found: 357.0183.

6.3.4.2 (a) 2-Chloro-6-(4-chlorophenoxy)isonicotinonitrile **196**

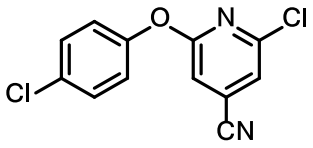

196

Reaction of 2,6-dichloroisonicotinonitrile **185b** (346 mg, 2.0 mmol) with 4-chlorophenol **166** (128 mg, 1.0 mmol) gave product **196** (265 mg, 99%), respectively, as a white oil. ^{1}H NMR (300 MHz, $CDCl_3$) δ 7.43–7.38 (m, 2H), 7.25 (d, *J* = 1.0 Hz, 1H, H-3), 7.11–7.07 (m, 2H), 7.06 (d, *J* = 1.0 Hz, 1H, H-5).

6.3.4.2 (b) 2,6-bis-(4-chlorophenoxy)isonicotinonitrile **197**

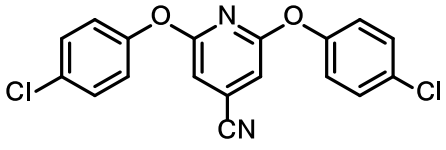

197

Reaction of 2,6-dichloronicotinonitrile **185b** (173 mg, 1.0 mmol) with 4-chlorophenol **166** (128 mg, 2.0 mmol) gave product **197** (354 mg, 99%) with respect to **166**, as a white oil. IR (cm^{-1}): 3001 (CH str.), 2213 (CN), 1566 (C=N str.), 1470 (C=C); ^{1}H NMR (300 MHz, $CDCl_3$) δ 7.94 (d, *J* = 8.3 Hz, 1H), 7.25–7.22 (m, 2H), 6.98–6.93 (m, 2H), 6.91–6.87 (m, 2H), 6.63 (d, *J* = 8.3 Hz, 1H); ^{13}C NMR (75 MHz, $CDCl_3$) δ 162.9, 151.1,

129.6, 122.8, 122.6, 119.9, 115.0, 112.1, 106.6; HRMS (ES+) Calculated for $C_{18}H_{11}Cl_2N_2O_2$ $[M+H]^+$: 357.0198, found: 357.0181.

6.3.4.3 6-(4-Chlorophenoxy)-2-((2-cyano-5-methylphenyl)amino)nicotinonitrile **170**

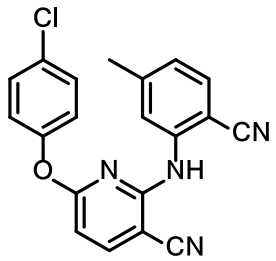

170

Reaction of 6-(4-chlorophenoxy)nicotinonitrile **190** (133 mg, 0.5 mmol) with 2-amino-4-methylbenzonitrile **167** (80 mg, 0.6 mmol) gave product **170** (133 mg, 87%) as a yellow oil. ^{1}H NMR (300MHz, $CDCl_3$): δ 7.94 (d, *J* = 8.3 Hz, 1H), 6.63 (d, *J* = 8.3 Hz, 1H), 7.26–7.21 (m, 2H), 6.98–6.94 (m, 1H), 6.91–6.86 (m, 1H); ^{13}C NMR (75 MHz, $CDCl_3$) δ 160.1 (C-6), 154.9 (C-2), 151.2 (C-1"), 145.2 (C-1'), 143.9 (C-4), 141.7 (Ar-C), 132.2 (Ar-C), 131.2 (C-3'), 129.8 (Ar-C), 127.9 (Ar-C), 123.8 (C-4'), 123.6, 120.1, 117.2 (CN), 115.4 (CN), 106.0 (C-5), 98.9 (C-3), 22.2; HRMS (ES)+ $C_{20}H_{13}ClN_4O$ for HRMS[M+H]+: found: 361.0977.

6.3.4.4 2-(4-Chlorophenoxy)-6-((2-cyano-5-methylphenyl)amino)isonicotinonitrile **175**

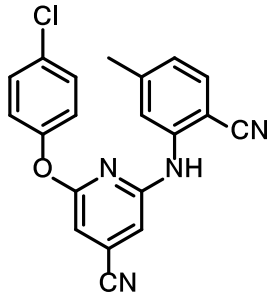

175

Reaction of 6-(4-chlorophenoxy)isonicotinonitrile **196** (133 mg, 0.5 mmol) with 2-amino-4-methylbenzonitrile **167** (80 mg, 0.6 mmol) gave product **175** (181 mg, 99%) as a pale yellow solid. ^{1}H NMR (300MHz, $CDCl_3$) δ 8.14 (d, *J* = 1.0 Hz, 1H), 7.86 (d, *J* = 1.0 Hz, 1H), 7.76 (s, 1H), 7.67 (d, *J* = 8.4 Hz, 1H), 7.41–7.35 (m, 4H), 7.17–7.11 (m, 2H), 2.55 (s, 3H); ^{13}C NMR (75MHz, $CDCl_3$) 154.7, 150.4, 146.3, 145.5, 142.1, 132.6, 132.1, 129.6, 124.1, 123.3, 120.6, 119.4, 117.2, 115.4, 113.1, 106.7, 99.6, 22.4; HRMS (ES+) Calculated for $C_{20}H_{14}ClN_4O$ $[M+H]^+$: 361.0856, found: 361.0837.

6.3.5 General procedure for the preparation of compounds **171** and **176**

Palladium-catalyzed cross-coupling procedure for the preparation of compounds **171** *and* **176** – Method G

Tris-(dibenzylideneacetone)-di-palladium (0) [Pd_2dba_3] (28 mg, 3 mol %), *rac*-BINAP (38 mg, 6 mol %) or Xantphos (35 mg, 3 mol %), THF (5 ml) and a magnetic stirrer were added to an oven-dried 10 ml round bottomed flask and purged with nitrogen. The flask was sealed and heated with stirring at 80 ℃ in an oil bath for 5 min. Thereafter, the appropriate cyclopropylamide substrate **188a** or **188b** (1.0 mmol), 4-chlorophenol (64 mg, 0.5 mmol) and sodium *tert*-butoxide (2.4 mmol) were added and the sealed reaction heated at 135–140℃ for 24 h. The cooled reaction mixture was filtered and the excess solvent removed *in vacuo* to leave a crude mixture which was re-dissolved in dichloromethane and filtered. The filtrate was washed successively with aqueous saturated $NaHCO_3$ (10 ml), and distilled water (2 x 10 ml). After drying over anhydrous Na_2SO_4 and evaporating excess solvent, the crude mixture was purified by silica gel flash column chromatography, eluting the target compound with 10–25% EtOAc/hexane.

6.3.5.1 2-Chloro-6-(4-chlorophenoxy)-*N*-cyclopropylnicotinamide **198a**

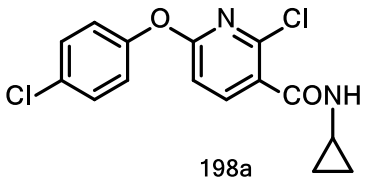

198a

2,6-Dichloro-*N*-cyclopropylnicotinamide **188a** (232 mg, 1.0 mmol) was reacted with 4-chlorophenol (153 mg, 1.2 mmol) using method G to give product **198a** (220 mg, 68%) as a white solid. ^{1}H NMR (500 MHz, $CDCl_3$) δ 8.56 (d, *J* = 8.0 Hz, 1H), 7.68 (s, 1H), 7.41 (d, *J* = 8.3 Hz, 2H), 7.16 (d, *J* = 8.0 Hz, 1H), 7.10 (d, *J* = 8.4 Hz, 2H), 2.98–2.91 (m, 1H), 0.88 (q, *J* = 5.9, 5.9, 5.5 Hz, 2H), 0.63–0.58 (m, 2H); ^{13}C NMR (126 MHz, $CDCl_3$) δ 163.7, 158.8, 151.0, 150.5, 144.7, 131.4, 129.9, 123.1, 119.9, 115.3, 23.2, 6.9.

6.3.5.2 2-Chloro-6-(4-chlorophenoxy)-*N*-cyclopropylnicotinamide **198b**

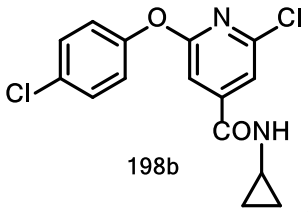

198b

2,6-Dichloro-*N*-cyclopropylisonicotinamide **188b** (232 mg, 1.0 mmol) was reacted with 4-chlorophenol (153 mg, 1.2 mmol) using method G to give product **198b** (230 mg, 71%) as a white solid. ^{1}H NMR (500 MHz, $CDCl_3$) δ 7.39–7.34 (m, 2H), 7.29–7.24 (m, 2H), 7.09–7.06 (m, 2H), 6.29 (d, *J* = 31.2 Hz, 1H), 2.94–2.86 (m, 1H), 0.93–0.88 (m, 2H), 0.67–0.62 (m, 2H); ^{13}C NMR (126 MHz, $CDCl_3$) δ 165.2, 163.2, 151.7, 149.9, 147.8, 130.7, 129.8, 122.5, 120.6, 116.1, 107.5, 23.4, 6.9.

6.3.5.3 2-(4-chlorophenoxy)-*N*-cyclopropyl-6-(piperidin-1-yl)isonicotinamide **171a**

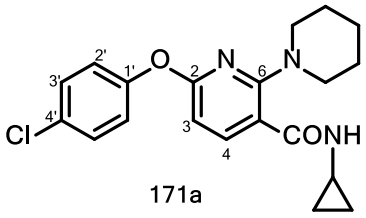

171a

Reaction of 2-chloro-6-(4-chlorophenoxy)-*N*-cyclopropylnicotinamide **198a** (162 mg, 0.5 mmol) with piperidine (51 mg, 0.6 mmol) with Xantphos (18 mg, 1.5 mol%) as supporting ligand using method F gave title compound **171a** (99 mg, 54%) as pale yellow oil. IR (cm^{-1}): 3438 (NH str.), 3020 (CH str.), 1680 (C=O), 1572 (C-N); 1452 (C=C); ^{1}H NMR (500 MHz, $CDCl_3$) δ 8.32 (d, *J* = 8.7 Hz, 1H, H-4), 7.58 (s, 1H, NH), 7.35 (d, *J* = 8.8 Hz, 2H, Ar-H), 7.07 (d, *J* = 8.8 Hz, 2H, Ar-H), 6.34 (d, *J* = 8.8 Hz, 1H, Ar-H), 3.38–3.31 (m, 4H), 2.94–2.88 (m, 1H), 1.62–1.56 (m, 2H), 1.50–1.44 (m, 4H), 0.82 (m, 2H), 0.59–0.53 (m, 2H); ^{13}C NMR (126 MHz, $CDCl_3$) δ 165.7 (C=O), 159.2 (C-2), 158.2 (C-6), 151.4 (C-1'), 143.3 (Ar-C), 130.2 (Ar-C), 129.2 (Ar-C), 123.6 (Ar-C), 102.9 (Ar-C), 100.9 (Ar-C), 45.8, 25.3, 24.69, 22.8, 6.9; HRMS (ES^+) Calculated for $C_{20}H_{23}ClN_3O_2$ $[M+H]^+$: 372.1471, found: 372.1457.

6.3.5.4 6-(4-Chlorophenoxy)-2-((2-cyano-5-methylphenyl)amino)-*N*-cyclopropylnicotinamide **171b**

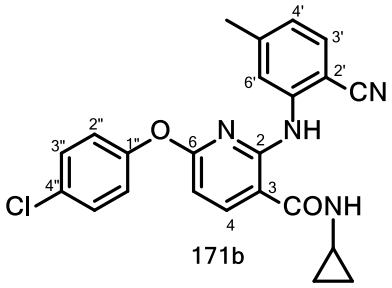

171b

Reaction of 2-chloro-6-(4-chlorophenoxy)-*N*-cyclopropylnicotinamide **198a** (162 mg, 0.5 mmol) with 2-amino-4-methylbenzonitrile **167** (80 mg, 0.6 mmol) gave product **171b** (24 mg, 11%; *rac*-BINAP) or (142 mg, 63%; Xantphos as a pale yellow oil. IR (cm^{-1}): 3321 (NH str.) 3029, 2972 (CH str.), 2231 (CN), 1683 (C=O str.); ^{1}H NMR (500 MHz, $CDCl_3$) δ 8.51 (d, *J* = 8.4 Hz, 1H, H-4), 7.64 (s, 1H, H-6'), 7.57 (s, 1H, NH), 7.43–7.40 (m, 2H, Ar-H), 7.37 (d, *J* = 7.9 Hz, 1H, H-3'), 7.16–7.13 (m, 2H), 7.00 (s, 1H, NH), 6.78 (d, *J* = 8.6 Hz, 1H, H-4'), 6.59 (d, *J* = 8.4 Hz, 1H, H-3), 2.97–2.92 (m, 1H), 2.08 (s, 3H), 0.89–0.84 (m, 2H), 0.63–0.58 (m, 2H); ^{13}C NMR (126 MHz, $CDCl_3$) δ 164.8 (C=O), 159.6 (C-6), 154.0 (C-2), 151.2 (C-1"), 145.3, 143.8, 141.9, 132.1, 131.2, 129.9, 123.8, 123.3, 119.5, 117.2 (CN), 107.9, 106.0, 98.1 (C-2'), 23.0, 22.2, 6.9; HRMS (ES^+) Calculated for $C_{23}H_{20}ClN_4O_2$ $[M+H]^+$: 417.1118, found: 417.1090.

6.3.5.5 6-(4-Chlorophenoxy)-*N*-cyclopropyl-2-(piperidin-1-yl)isonicotinamide **176a**

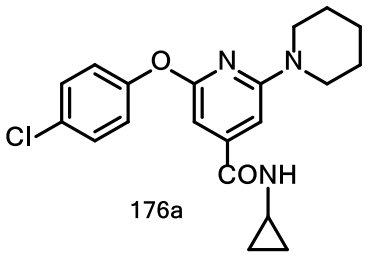

176a

Reaction of 2-chloro-6-(4-chlorophenoxy)-*N*-cyclopropylisonicotinamide **198b** (162 mg, 0.5 mmol) with piperidine (128 mg, 1.5 mmol) with *rac*-BINAP (28 mg, 3 mol%) or Xantphos (18 mg, 2 mol%) as supporting ligand gave title compound **176a** (99 mg, 53%) or (125 mg, 67%) as a yellow oil, respectively. ^{1}H NMR ($CDCl_3$, 300 MHz) δ 7.39–7.28 (m, 2H), 7.11–7.03 (m, 2H), 6.88–6.77 (m, 1H), 6.67–6.59 (m, 1H), 6.25–6.10 (m, 1H), 3.70–3.26 (m, 4H), 2.95–2.78 (m, 1H), 1.70–1.52 (m, 6H), 0.96–0.81 (m, 2H), 0.70–0.52 (m, 2H); ^{13}C NMR (126 MHz, $CDCl_3$) δ 167.9 (C=O), 162.7 (C-6), 159.3 (C-2), 158.6 (C-1'), 152.8 (C-4), 146.9, 129.3, 122.6, 107.2, 102.9, 98.9 (C-3), 94.0 (C-5), 46.0, 25.4, 24.6, 23.2, 6.8; HRMS (ES^+) Calculated for $C_{20}H_{23}ClN_3O_2$ $[M+H]^+$: 372.1479, found: 372.1424.

6.3.5.6 2-(4-Chlorophenoxy)-6-((2-cyano-5-methylphenyl)amino)-*N*-cyclopropylisonicotinamide **176b**

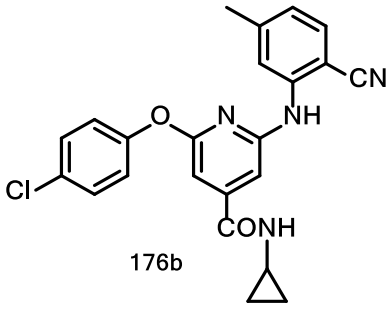

176b

Reaction of 2-chloro-6-(4-chlorophenoxy)-*N*-cyclopropylisonicotinamide **198b** (162 mg, 0.5 mmol) with 2-amino-4-methylbenzonitrile **167** (80 mg, 0.6 mmol) with *rac*-BINAP or Xantphos as supporting ligand using method F gave title compound **176b** (122 mg, 53%) or (157 mg, 75%) as a brown solid. ^{1}H NMR (500 MHz, $CDCl_3$) δ 7.94 (s, 1H), 7.46 (d, *J* = 7.9 Hz, 1H), 7.38–7.33 (m, 1H), 7.17–7.04 (m, 3H), 6.92 (d, *J* = 7.9 Hz, 1H), 6.83–6.69 (m, 1H), 6.46 (d, *J* = 37.1 Hz, 1H), 2.96–2.83 (m, 1H), 2.41 (s, 3H), 0.89 (dd, *J* = 14.2, 6.6 Hz, 2H), 0.66 (p, *J* = 6.7, 6.7, 6.7, 6.7 Hz, 2H); ^{13}C NMR (126 MHz, $CDCl_3$) δ 165.8, 154.7, 150.4, 146.3, 145.5, 142.1, 132.6, 132.1, 129.6, 124.1, 123.3, 120.6, 119.4, 117.2, 113.1, 106.7, 99.6, 23.4, 22.4, 22.2, 6.7; HRMS (ES$^+$) Calculated for $C_{23}H_{20}ClN_4O_2$ $[M+H]^+$: 419.1275, found: 419.1240.

6.3.6 Biocatalysis as a key step in the synthesis of **172** and **200**

Enzyme-based nitrile hydrolysis procedure – Method G

The nitrile hydrolysis protocol was based on the procedure developed by Chhiba *et al*. An appropriate carbonitrile substrate (20 mg) was dissolved in methanol (1 ml). After addition of Tris buffer to pH 9.0, *Rhodochrous* nitrilase enzyme extract (20 mg) was added and the reaction mixture was equilibrated at 37°C with agitation for 24–72 h whilst samples were collected at 12 h intervals to monitor the reaction progress.

6.3.6.1 6-Bis(4-chlorophenoxy)isonicotinamide **200**

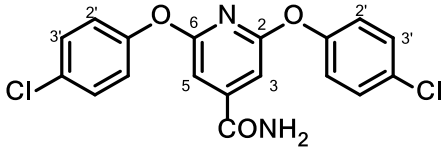

200

Enzyme-catalyzed hydrolysis of 2,6-bis(4-chlorophenoxy)isonicotinonitrile **197** gave compound **200** (17 mg, 73%) as a yellow oil. IR (cm^{-}

^{1}): 3580 and 3435 (NH str.), 2987 (CH str.), 1674 (C=O), 1561 (C=N), 1444 (C=C) ;^{1}H NMR (500 MHz, DMSO) δ 9.63 (br s, 2H, NH_2), 7.88 (s, 2H, H-3 and H-5), 7.17 (d, J = 8.4 Hz, 4H, Ar-H), 6.75 (d, J = 8.3 Hz, 4H, Ar-H); ^{13}C NMR (126 MHz, DMSO) δ 162.8 (C=O), 156.8 (C-2 and C-6), 150.7 (C-1'), 143.8 (C-4), 129.6 (C-4'), 123.2 (C-3'), 122.8 (C-2'), 117.4 (C-3 and C-5); HRMS (ES)+ $C_{18}H_{12}Cl_2N_2O_3$ Calculated for HRMS[M]+: 375.2029, Found: 375.2022

6.3.6.2 6-(4-Chlorophenoxy)-2-((2-cyano-5-methylphenyl)amino)nicotinamide **172**

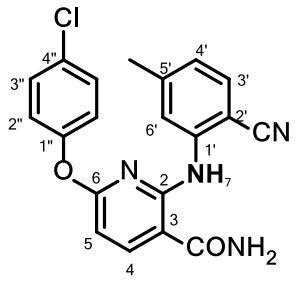

172

Enzyme-catalyzed hydrolysis of 6-(4-chlorophenoxy)-2-((2-cyano-5-methylphenyl)amino)nicotinonitrile **170** afforded target product **172** (64%) as a light yellow solid. Mp: 204–205℃; IR (cm^{-1}): 3633 and 3480 and 3380 (NH str.), 3010 (CH str.), 2216 (CN), 1662 (C=O), 1587 (C=N), 1518 (NH bend), 1483 (C=C); (^{1}H NMR (500 MHz, DMSO) δ 9.40 (br s, 1H, NH), 8.18 (d, J = 8.4 Hz, H-4,), 7.51–7.45 (m, 3H, H-3', NH_2), 7.43–7.40 (m, 2H, H-2"), 7.31 (s, 1H, H-6'), 7.26–7.21 (m, 2H, H-3"), 6.91 (d, J = 7.9 Hz, H-4'), 6.77 (d, J = 8.4 Hz, 1H, H-5), 2.12 (s, 3H); ^{13}C NMR (126 MHz, DMSO) δ 165.2 (C=O), 159.5 (C-6), 155.6 (C-2), 152.2 (C-1"), 144.4 (C-1'), 143.1 (C-4), 142.1 (Ar-C), 142.3 (Ar-C), 133.2 (C-3'), 129.7 (Ar-C), 129.5 (Ar-C), 124.7 (C-4'), 124.5, 123.4, 117.9 (CN), 107.9 (Ar-C), 105.8 (C-5), 101.8 (C-2'), 21.8; HRMS (ES)$^{+}$ $C_{20}H_{16}ClN_4O_2$ for HRMS[M+H]+: found: 379.0952.

6.3.7 General - Synthesis of pyrimidine derivatives

Synthesis of 2,4,6-trichloropyrimidine-based analogues **207–220**

As a first step, commercially available barbituric acid was converted to a more reactive 2,4,6-trichloropyrimidine **204**[5,9] substrate using the method developed by Henegar[9] contained in literature. The second step employed the Dehlia[15] methodology to effect a base-promoted nucleophilic displacement reaction of chlorine at the C-6 position of substrate **204** with substituted phenolate nucleophiles to generate a 2,4-dichloro-6-(chlorophenoxy)-substituted pyrimidine intermediate **222**. The diaryl ether intermediate **222** was eventually aminated using selected amines **167a-e** to afford novel target molecules **207–220**.

Preparation of 2,4,6-trichloropyrimidine **204**[9] – Method G

Barbituric acid (5.07 g, 44.5 mmol) and tetraethyl ammonium chloride (6.10 g, 44.5 mmol) were added to a 100ml 3-necked round-bottomed flask chilled in ice. After thoroughly mixing the reagents, a reflux condenser was attached onto the middle neck the top end connected to a tubing (rubber) dipped at one end in 50% aqueous NaOH for trapping HCl fumes during the reaction. After inserting a thermometer into the other side neck, $POCl_3$ (15 ml) was cautiously added via a separating funnel (30 mins). The reaction mixture was heated in an oil bath to maintain the reaction temperature at 130–140 ℃ for 24 h. After cooling the reaction to room temperature and removing of excess $POCl_3$ *in vacuo*, crushed ice (75 g) to the brown mixture. The mixture was stirred and allowed to warm to room temperature over 4 h. The mixture was extracted with ethyl acetate (7 x 100 ml), dried Na_2SO_4 and the organic solvent evaporated to give **204** (6.5 g, 80%) as a yellow oil. The crude product was purified in a flash silica column using 3–5% EtOAc/Hex and gave **204** (6.33 g, 78%) as a pale yellow oil. ^{1}H NMR (500 MHz, $CDCl_3$) δ 7.39 (s, 1 H); ^{13}C NMR (126 MHz, $CDCl_3$) δ 163.1, 160.4, 120.1.

Preparation of 2,4-dichloro-6-(chlorophenoxy)-substituted pyrimidine intermediate **222**[15] – Method H

Exactly 183 mg (1.0 mmol) of 2,4,6-trichloropyrimidine **204**[5b](183 mg, 1.0 mmol) dissolved in acetone (5 ml) was placed in a 25 ml round bottomed flask chilled in ice (0-5℃). A solution of the appropriate substituted phenoxide (1.0 mmol) made by mixing the phenol **166** (1.10 mmol) and NaOH (1.10 mmol) in water (5 ml) was slowly added with stirring. The reaction was stirred for 1 h under the same conditions to allow quantitative formation of the product. Thereafter, the mixture was allowed to warm to room temperature while stirring for a further 4 h. After evaporating the excess solvent, the crude product was diluted with ethyl acetate (20 ml) and washed successively with saturated $NaHCO_3$ (10 ml) and water (10 ml). The organic layer was dried over Na_2SO_4 and filtered. The solvent was evaporated in vacuo to give 2,4-dichloro-6-(chlorophenoxy)-substituted pyrimidine intermediate **222** in good yield. Intermediate **222** was aminated using selected amines to afford novel targets **207**–**220**.

Amination of 2,4-dichloro-6-(chlorophenoxy)-substituted pyrimidine **222** – Method I

To a 25 ml round bottomed flask containing substrate **222** (1.0 mmol) dissolved in freshly distilled THF at room temperature was added an appropriate amine **167** (1.1 eq.). Approximately 160 mg (1.5 mmol) of KO^{t}Bu was added sparingly to the mixture over 1 h with stirring. After evaporating the solvent, the crude residue was dissolved in DCM (25 ml) and washed successively with saturated aqueous NH_4Cl (2 x 20 ml) and water. The organic phase

was dried over Na_2SO_4, filtered and evaporated to leave the crude product. The product was purified by flash column chromatography eluting with 5–15% EtOAc/Hex to give title compounds **207**–**220**.

6.3.7.1 (a) 4-Chloro-6-(4-chlorophenoxy)-*N*-(5-methylpyridin-2-yl)pyrimidin-2-amine **207**

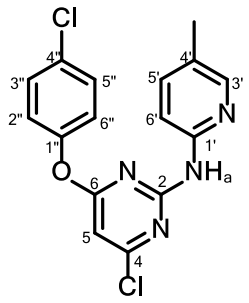

207

Reaction of 2,4,6-trichloropyrimidine **204** (551mg, 3.0 mmol) with sodium 4-chlorophenoxide **166a** (3.1 mmol) using the method H gave 2,4-dichloro-6-(4-chlorophenoxy)pyrimidine **222a** (744 mg, 90%) as a white oil.

Reaction of compound **222a** (138 mg, 0.5 mmol) with 5-methylpyridin-2-amine **167a** (60 mg, 0.55 mmol) using method I gave title compound **207** (162 mg, 93%) as an off-white solid. Mp: 230–233°C; IR cm^{-1}: 3108 and 2916 (CH str.), 1616 (CN), 1567 (NH bend), 1460 (C=C); ^1H NMR (300 MHz, $CDCl_3$) δ 8.13–8.05 (m, 2H), 7.63 (d, *J* = 8.3 Hz, 1H), 7.44–7.41 (m, 2H), 7.29–7.25 (m, 1H), 7.13–7.10 (m, 2H), 6.41 (s, 1H), 2.25 (s, 3H) ;^{13}C NMR (75 MHz, $CDCl_3$) δ 170.1, 162.5, 157.4, 156.7, 155.9, 152.3, 132.3, 130.1, 125.1, 124.5, 122.6, 119.0, 100.8, 30.9; HRMS (ES^+) Calculated for $C_{16}H_{13}Cl_2N_4O$ $[M+H]^+$: 347.0466, found: 347.0467.

6.3.7.1 (b) 2-((4-Chloro-6-(4-chlorophenoxy)pyrimidin-2-yl)amino)-4-methylbenzonitrile **208**

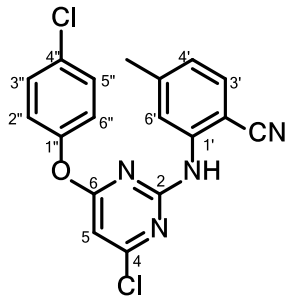

208

Reaction of compound **222a** (138 mg, 0.5 mmol) with 2-amino-4-methylbenzonitrile **167** (73 mg, 0.55 mmol) using method I gave title compound **208** (128 mg, 68%) as a white solid. IR cm^{-1}: 3095 (CH str.), 2232 (CN) 1580 (C=N str.), 1557 (NH bend), 1430 (C=C); Mp: 170-172°C, ^1H NMR (300 MHz, $CDCl_3$) δ 7.79 (br s, 1H), 7.53 (br s, 1H),

7.45–7.37 (m, 3H), 7.17–7.07 (m, 2H), 6.84 (ddd, *J* = 7.9, 1.5, 0.7 Hz, 1H), 6.52 (s, 1H), 2.18 (s, 3H); ^{13}C NMR (75 MHz, $CDCl_3$) δ 171.0, 162.2, 158.2, 150.8, 145.4, 141.0, 132.3, 131.6, 127.0, 123.9, 123.4, 120.2, 116.8, 99.5, 98.7, 22.5; HRMS (ES^+) Calculated for $C_{18}H_{13}Cl_2N_4O$ $[M+H]^+$: 371.0466, found: 371.0467.

6.3.7.1 (c) 4-Chloro-N-(3-chloro-4-methylphenyl)-6-(4-chlorophenoxy)pyrimidin-2-amine **209**

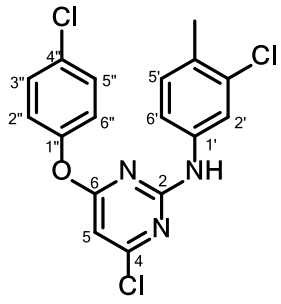

209

Reaction of compound **222a** (138 mg, 0.5 mmol) with 3-chloro-4-methylamine **167b** (78 mg, 1.10 eq.) using method I gave title compound **209** (97 mg, 51%) as a white solid. Mp:163-164℃; IR cm^{-1}: 3367 (NH str.), 3098 (CH str.), 1553 (C=N), 1517 (NH bend), 1455 (C=C); ^{1}H NMR (500 MHz, $CDCl_3$) δ 7.46–7.40 (m, 3H), 7.13–7.06 (m, 3H), 7.03–6.99 (m, 1H), 6.94–6.91 (m, 1H), 6.39 (s, 1H), 2.28 (s, 3H); ^{13}C NMR (126 MHz, $CDCl_3$) δ 170.8, 161.9, 158.5, 150.9, 137.1, 134.6, 131.6, 130.7, 130.5, 129.9, 123.2, 119.4, 117.2, 98.1, 19.32; HRMS (ES^+) Calculated for $C_{17}H_{13}Cl_3N_3O$ $[M+H]^+$: 381.0077, found: 371.0074.

6.3.7.1 (d) *N*-(4-bromo-3-methylphenyl)-4-chloro-6-(4-chlorophenoxy)pyrimidin-2-amine **210**

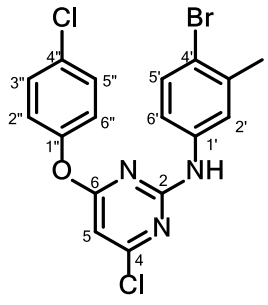

210

Reaction of compound **222a** (138 mg, 0.5 mmol) with 2-amino-4-methylbenzonitrile **167c** (102 mg, 0.55 mmol) using method I gave title compound **210** (100 mg, 47%) as a white solid. Mp:148–150℃; IR cm^{-1}: 3380 (NH str.), 3104 and 3009 (CH str.), 1568 (C=N str.), 1532 (NH bend), 1455 (C=C); ^{1}H NMR (500 MHz, $CDCl_3$) δ 7.64 (s, 1H), 7.48 (d, *J* = 8.5 Hz, 1H), 7.31–7.28 (m, 2H), 7.15–7.13 (m, 1H), 7.03–7.00 (m, 2H), 7.00–6.98 (m, 1H), 5.99 (s, 1H), 2.38–2.35 (m, 3H); ^{13}C NMR (126 MHz, $CDCl_3$) δ 170.6 (C-6), 164.1 (C-2), 159.8 (C-

1"), 150.8, 139.3, 136.5, 133.2 (2 Ar-C signals overlapping), 131.0, 129.7, 125.2, 122.6, 121.9, 85.9, 23.0; HRMS (ES$^+$) Calculated for $C_{17}H_{13}BrCl_2N_3O$ [M+H]$^+$: 423.9619, found: 423.9621.

6.3.7.2 (a) 4-Chloro-6-(2,4-dichlorophenoxy)-*N*-(5-methylpyridin-2-yl)pyrimidin-2-amine **211**

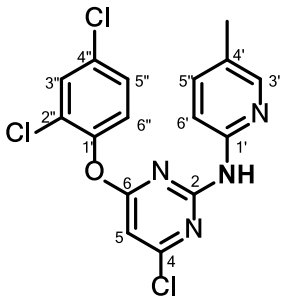

211

Reaction of 2,4,6-trichloropyrimidine **204** (367 mg, 2.0 mmol) with sodium 2,4-dichlorophenoxide **166b** (326 mg, 2.0 mmol) using the method H gave 2,4-dichloro-6-(2,4-dichlorophenoxy)pyrimidine **222b** (558 mg, 90%) as a white oil.

Reaction of compound **222b** (155 mg, 0.5 mmol) with 5-methylpyridin-2-amine **167a** (60 mg, 0.55 mmol) using method I gave title compound **211** (149 mg, 78%) as a white solid. IR cm^{-1}: 3234 (NH str.), 3095 and 3016 and 2916 (CH str.), 1614 (C=N str.), 1566 (NH bend), 1453 (C=C); Mp:200–202℃; ^{1}H NMR (500 MHz, $CDCl_3$) δ 8.15–8.11 (m, 2H), 7.55–7.47 (m, 2H), 7.50–7.47 (m, 1H), 7.34 (dd, *J* = 8.7, 2.5 Hz, 1H), 7.23 (d, *J* = 8.5 Hz, 1H), 7.17 (d, *J* = 8.6 Hz, 1H), 6.50 (s, 1H), 2.25 (s, 3H); ^{13}C NMR (126 MHz, $CDCl_3$) δ 169.7, 162.2, 157.9, 149.5, 148.0, 147.5, 138.3, 132.0, 130.3, 128.6, 128.1, 127.7, 125.0, 112.2, 98.0, 17.7; HRMS (ES$^+$) Calculated for $C_{16}H_{12}Cl_3N_4O$ [M+H]$^+$: 381.0077, found: 381.0068.

6.3.7.2 (b) 2-((4-Chloro-6-(2,4-dichlorophenoxy)pyrimidin-2-yl)amino)-4-methylbenzonitrile **212**

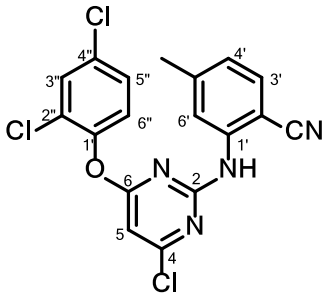

212

Reaction of compound **222b** (155 mg, 0.5 mmol) with 2-amino-4-methylbenzonitrile **167** (73 mg, 0.55 mmol) using method I gave title compound **212** (114 mg, 56%) as a white solid. IR cm^{-1}: 3392 and 3382 (NH str.), 3190 (CH str.), 2208 (CN), 1580 (C=N str.), 1526 (NH bend), 1380 (C=C); Mp:151–152℃; ^{1}H NMR (300 MHz, $CDCl_3$) δ 7.73 (br s, 1H),

7.53–7.49 (m, 2H), 7.39 (d, *J* = 7.9 Hz, 1H), 7.33 (dd, *J* = 8.7, 2.5 Hz, 1H), 7.18 (d, *J* = 8.7 Hz, 1H), 6.84 (d, *J* = 7.9 Hz, 1H), 6.59 (s, 1H), 2.19 (s, 3H); ^{13}C NMR (75 MHz, $CDCl_3$) δ 169.8 (C-6), 162.3 (C-2), 158.1 (C-1"), 147.3 (C-1'), 145.0, 140.8, 132.3, 132.2, 130.4, 128.4, 128.3, 124.9, 123.9, 120.1, 116.7, 99.4, 98.7, 22.2; HRMS (ES$^+$) Calculated for $C_{16}H_{12}Cl_3N_4O$ $[M+H]^+$: 405.0077, found: 405.0066.

6.3.7.3 4-Chloro-*N*-(5-methylpyridin-2-yl)-6-(piperidin-1-yl)pyrimidin-2-amine **213**

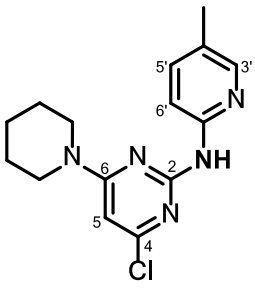

213

Reaction of compound **204** (183 mg, 1.0 mmol) with piperidine (103 mg, 1.2 mmol) using method I gave 2,4-dichloro-6-(piperidin-1-yl)pyrimidine **222c** (193 mg, 83%) as a white oil.

Reaction of compound **222c** (116 mg, 0.5 mmol) with 5-methylpyridin-2-amine **167a** (60 mg, 0.55 mmol) using method I gave title compound **213** (91 mg, 60%) as a yellow solid. IR cm^{-1}: 3237 and 3176 (NH str.), 2941 and 2854 (CH str.), 1615 (C=N str.), 1519 (C=C); Mp: 256–259 ℃; ^{1}H NMR (300 MHz, $CDCl_3$) δ 8.18–8.10 (m, 2H), 7.83 (br s, 1H), 7.48 (dd, *J* = 8.5, 2.3 Hz, 1H), 6.07 (s, 1H, H-5), 3.64–3.56 (m, 4H), 2.27 (s, 3H), 1.72–1.59 (m, 6H).; ^{13}C NMR (75 MHz, $CDCl_3$) δ 162.9, 159.9, 158.3, 150.7, 147.9, 138.3, 126.6, 112.2, 93.8, 45.6, 25.51, 24.6, 17.7; HRMS (ES$^+$) Calculated for $C_{15}H_{19}ClN_5$ $[M+H]^+$: 304.1329, found: 304.1331.

6.3.7.4 a) 4-Chloro-6-(3,5-dichlorophenoxy)-*N*-(5-methylpyridin-2-yl)pyrimidin-2-amine **214**

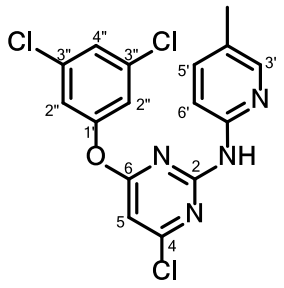

214

Reaction of 2,4,6-trichloropyrimidine **204** (367 mg, 2.0 mmol) with sodium 3,5-dichlorophenoxide **166c** (342 mg, 2.1 mmol) using method H gave 2,4-dichloro-6-(4-chlorophenoxy)pyrimidine **222d** (285 mg, 92%) as a white oil.

Reaction of compound **222d** (196 mg, 0.5 mmol) with 5-methylpyridin-2-amine **167a** (60 mg, 0.55 mmol) using method I gave title compound **214** (142 mg, 74%) as an off-white solid. Mp: 218–220℃; IR (cm^{-1}): 3083 and 2922 (CH str.), 1563 (C=N str.), 1481 (NH bend), 1402 (C=C); ^{1}H NMR (500 MHz, $CDCl_3$) ^{1}H NMR (500 MHz, $CDCl_3$) δ 8.15 (d, *J* = 2.0 Hz, 1H), 7.67 (br s, 1H), 7.49 (dd, *J* = 8.3, 2.2 Hz, 1H), 7.41 (s, 1H), 7.26 (d, *J* = 2.4 Hz, 1H, pyrimidyl proton overlaps with solvent signal), 7.10 (d, *J* = 1.8 Hz, 2H), 7.06 (d, *J* = 8.5 Hz, 1H), 2.31 (s, 3H); ^{13}C NMR (126 MHz, $CDCl_3$) δ 170.2, 161.9, 159.1, 153.3, 149.8, 147.7, 139.1, 135.4, 128.1, 126.0, 120.5, 112.6, 90.1, 17.8; HRMS (ES^+) Calculated for $C_{16}H_{12}Cl_3N_4O$ $[M+H]^+$: 381.0077, found: 381.0079.

6.3.7.4 b) 2-((4-Chloro-6-(3,5-dichlorophenoxy)pyrimidin-2-yl)amino)-4-methylbenzonitrile **215**

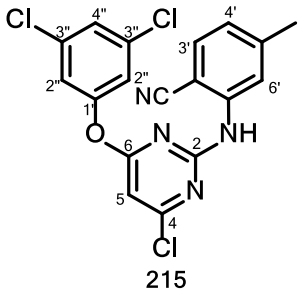

215

Reaction of compound **222d** (196 mg, 0.5 mmol) with 2-amino-4-methylbenzonitrile **167** (73 mg, 0.55 mmol) using method I gave title compound **215** (124 mg, 61%) as an off-white solid. Mp: 236–238 ℃; IR (cm^{-1}): 3295 (NH str.), 2980 (CH str.), 2227 (CN), 1573 (C=N str.), 1432 (C=C); ^{1}H NMR (500 MHz, $CDCl_3$) δ 7.79–7.72 (m, 1H), 7.57 (d, *J* = 8.0 Hz, 1H), 7.28–7.26 (m, 3H), 7.15–7.07 (m, 2H), 6.65 (s, 1H), 2.48–2.46 (m, 3H); ^{13}C NMR (126 MHz, $CDCl_3$) δ 162.0, 161.5, 160.4, 145.8, 139.5, 133.4, 133.1, 132.7, 128.8, 126.08,

123.7, 121.2, 120.5, 116.2, 103.1, 22.2; HRMS (ES$^+$) Calculated for $C_{18}H_{13}Cl_3N_4O$ [M+H]$^+$: 405.0077, found: 405.0070.

6.3.7.5 a) 4-Chloro-6-(4-fluorophenoxy)-*N*-(5-methylpyridin-2-yl)pyrimidin-2-amine **216**

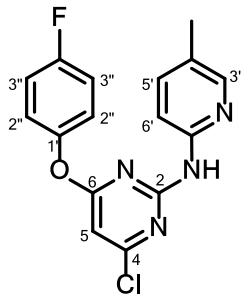

216

Reaction of 2,4,6-trichloropyrimidine **204** (367 mg, 2.0 mmol) with 4-fluorophenoxide **166d** (236 mg, 2.1 mmol) using method H gave 2,4-dichloro-6-(4-fluorophenoxy)pyrimidine **222e** (487 mg, 94%) as a white oil.

Reaction of compound **222e** (166 mg, 0.5 mmol) with 5-methylpyridin-2-amine **167a** (60 mg, 0.55 mmol) using method I gave title compound **216** (101 mg, 61%) as an off-white solid. Mp: 238–240 °C; IR (cm^{-1}): 2919 (CH str.), 1615 (C=N str.), 1568 (NH bend), 1457 (C=C); ^{1}H NMR (500 MHz, $CDCl_3$) δ 8.07 (s, 1H), 7.88 (br s, 1H), 7.66 (br s, 1H), 7.16–7.12 (m, 5H), 6.40 (s, 1H), 2.25 (s, 3H); ^{13}C NMR (126 MHz, $CDCl_3$) δ 170.9, 162.0, 160.4 (d, $J_{C\text{-}F}$ = 245 Hz), 158.0, 149.5, 148.3 (d, $J_{C\text{-}F}$ = 2.7 Hz), 148.0, 138.4, 127.6, 123.5 (d, $J_{C\text{-}F}$ = 8.5 Hz), 116.3 (d, $J_{C\text{-}F}$ = 23.5 Hz), 112.3, 98.2, 17.7; NMR DATA; HRMS (ES$^+$) Calculated for $C_{16}H_{13}ClFN_4O$ [M+H]$^+$: 331.0762, found: 331.0758.

6.3.7.5 b) 2-((4-Chloro-6-(4-fluorophenoxy)pyrimidin-2-yl)amino)-4-methylbenzonitrile **217**

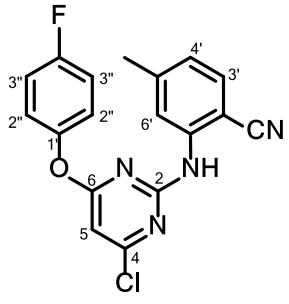

217

Reaction of compound **222e** (166 mg, 0.5 mmol) with 2-amino-4-methylbenzonitrile **167** (73 mg, 0.55 mmol) using method I gave title compound **217** (96 mg, 54%) as an off-white solid. IR (cm^{-1}): 3399 (NH str.), 3111 (CH str.), 2211 (CN), 1563 (C=N str.), 1435 (C=C); Mp: 166–168 °C; ^{1}H NMR (500 MHz, $CDCl_3$) δ 7.81 (br s, 1H), 7.51 (br s, 1H), 7.39

(d, J = 7.9 Hz, 1H), 7.14–7.11 (m, 4H), 6.84 (d, J = 7.9 Hz, 1H), 6.49 (s, 1H), 2.18 (s, 3H); ^{13}C NMR (126 MHz, $CDCl_3$) δ 170.9, 162.1, 160.4, (d, $J_{C\text{-}F}$ = 245 Hz), 158.2, 148.2 (d, $J_{C\text{-}F}$ = 3 Hz), 145.0, 142.0, 132.3, 123.8, 123.3 (d, $J_{C\text{-}F}$ = 9 Hz), 120.2, 116.8, 116.5 (d, $J_{C\text{-}F}$ = 23.5 Hz), 99.5, 98.7, 22.2; HRMS (ES$^+$) Calculated for $C_{16}H_{13}ClFN_4O$ [M+H]$^+$: 355.0762, found: 331.0768.

6.3.7.6 a) 4-Chloro-*N*-(5-methylpyrimidin-2-yl)-6-(4-(trifluoromethyl)phenoxy)pyrimidin-2-amine **218**

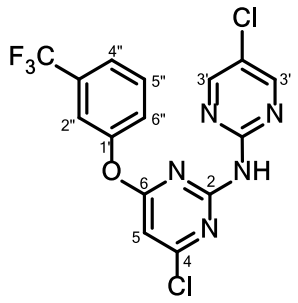

218

Reaction of 2,4,6-trichloropyrimidine **204** (367 mg, 2.0 mmol) with 3-(trifluoromethyl)phenoxide **166e** (324 mg, 2.1 mmol) using method H gave 2,4-dichloro-6-(3-(trifluoromethyl)phenoxy)pyrimidine **222e** (562 mg, 91%) as a white oil.

Reaction of compound **222e** (155 mg, 0.5 mmol) with 5-chloropyrimidine-2-amine **167f** (60 mg, 0.55 mmol) using method I gave title compound **218** (169 mg, 84%) as an off-white solid. IR (cm^{-1}): 3239 (NH str.), 3054 (CH str.), 1553 (C=N str.), 1430 (C=C); Mp: 206–207 °C; ^{1}H NMR (500 MHz, $CDCl_3$) δ 8.77 (d, J = 4.7 Hz, 1H), 8.49 (s, 2H), 8.25 (s, 1H), 7.63–7.46 (m, 3H), 6.54 (s, 1H); ^{13}C NMR (126 MHz, $CDCl_3$) δ 170.1, 162.5, 157.3, 156.6, 155.8, 152.3, 132.1 (q, $J_{C\text{-}F}$ = 33 Hz), 130.2, 125.1, 124.6, 122.6 (q, $J_{C\text{-}F}$ = 3.9 Hz), 119.0 (q, $J_{C\text{-}F}$ = 4.0 Hz), 100.8; HRMS (ES$^+$) Calculated for $C_{16}H_{13}ClFN_4O$ [M+H]$^+$: 402.0126, found: 402.0131.

6.3.7.6 b) 4-chloro-*N*-(5-methylpyridin-2-yl)-6-(3-(trifluoromethyl)phenoxy)pyrimidin-2-amine **219**

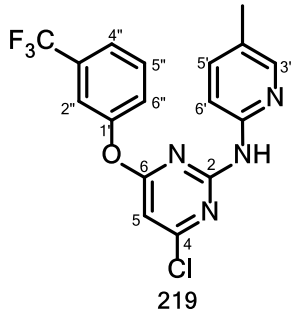

219

Reaction of compound **222e** (155 mg, 0.5 mmol) with 5-methylpyridin-2-amine **167a** (60 mg, 0.55 mmol) using method I gave title compound **219** (143 mg, 75%) as a

pale yellow solid. IR (cm^{-1}): 3210 (NH str.), 3008 (CH str.), 1610 (C=N), 1568 (NH bend), 1442 (C=C); Mp: 186–188 °C; ^{1}H NMR (500 MHz, $CDCl_3$) δ 8.60 (br s, 1H), 8.19 (s, 1H), 7.62–7.52 (m, 3H), 7.49 (s, 1H), 7.37 (d, J = 7.6 Hz, 1H), 7.19 (d, J = 7.6 Hz, 1H), 6.46 (s, 1H), 2.23 (s, 3H); ^{13}C NMR (126 MHz, $CDCl_3$) δ 170.3, 162.2, 158.0, 152.6, 149.6, 148.1, 138.3, 132.3 (q, J_{C-F} = 33 Hz), 130.3, 127.6, 125.6, 123.5 (q, J_{C-F} = 273 Hz), 122.6 (q, J_{C-F} = 3.7 Hz), 119.5 (q, J_{C-F} = 3.6 Hz), 112.3, 98.3, 17.7; HRMS (ES$^+$) Calculated for $C_{16}H_{13}ClFN_4O$ $[M+H]^+$: 381.0730, found: 381.0720.

6.3.7.6 c) 2-((4-Chloro-6-(3-(trifluoromethyl)phenoxy)pyrimidin-2-yl)amino)-4-methylbenzonitrile **220**

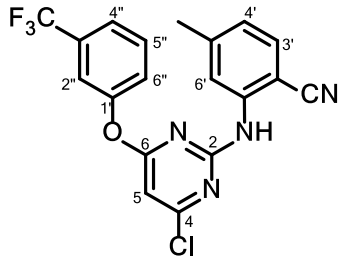

220

Reaction of compound **222e** (155 mg, 0.5 mmol) with 2-amino-4-methylbenzonitrile **167** (73 mg, 0.55 mmol) using method I gave title compound **220** (102 mg, 50%) as an off-white solid. IR (cm^{-1}): 3398 (NH str.), 3130 (CH str.), 2214 (CN), 1529 (NH bend), 1430 (C=C); Mp: 132–134 °C; ^{1}H NMR (300 MHz, $CDCl_3$) δ 7.74 (s, 1H), 7.59–7.57 (m, 2H), 7.51 (s, 1H), 7.45 (s, 1H), 7.39–7.37 (m, 2H), 6.83 (d, J = 7.9 Hz, 1H), 6.55 (s, 1H), 2.10 (s, 3H); ^{13}C NMR (75 MHz, $CDCl_3$) δ 170.4, 162.4, 158.3, 152.5, 145.0, 140.8, 132.3, 132.3, 130.3, 125.6, 124.0, 122.8 (q, J_{C-F} = 3.7 Hz), 120.4, 119.2 (q, J_{C-F} = 3.9 Hz), 116.7, 99.7, 99.0, 22.2; HRMS (ES$^+$) Calculated for $C_{19}H_{13}ClFN_4O$ $[M+H]^+$: 405.0730, found: 405.0733.

6.3.8 Synthesis of pyrimidine-based nitrile **179** and cyclopropylamide **180a-b** derivatives

The pyrimidine-based nitrile **179** and cyclopropylamide **180** derivatives were synthesized from intermediate scaffolds **223** (2,6-dichloropyrimidine-4-carbonitrile) and **224** (2,6-dichloro-*N*-cyclopropylpyrimidine-4-carboxamide), respectively. Substrate **223** and **224** were accessed from 2,6-dichloropyrimidine-4-carboxylic acid **226.**

Preparation of 2,6-dichloropyrimidine-4-carboxylic acid **226**[5c] – Method J

Orotic acid **225** (8.5g, 54.8 mmol), Et_4NCl (8.0 g) and a stirrer bar were added to an ice-chilled 100 ml round bottomed flask containing $POCl_3$ (20 ml). The reaction mixture was heated in an

oil bath at 130-145℃ for 24 h. After cooling to room temperature, crushed ice (200g) was added to the mixture and the reaction allowed to warm to room temperature over 4 h. An ethyl acetate extract (6 x 100 ml) of the reaction mixture was dried over anhydrous Na_2SO_4 and evaporated *in vacuo* to give 2,6-dichloroyrimidine-4-carboxylic acid **226**[5d] (9.3 gr, 88%) as pale yellow oil. ^{1}H NMR (300 MHz, $CDCl_3$) δ 8.11 (s, 1H).

Preparation of intermediate scaffolds 2,6-dichloropyrimidine-4-carbonitrile **223**[5e] *and 2,6-dichlorocyclopropyl-4-carboxamide* **224** – Method K

An appropriate amount of substrate **225** was reacted with thionyl chloride to generate a highly reactive 2,6-dichloropyrimidine-4-carbonyl chloride which was aminated with excess 25% aqueous ammonia or cyclopropylamine using similar reaction conditions explained in section 6.3.3 to generate 2,6-dichloropyrimidine-4-carboxamide **227**[5d] or 2,6-dichlorocyclopropyl-4-carboxamide **224**, respectively, in quantitative yield. Substrate **227** was further dehydrated with $POCl_3$ to afford 2,6-dichloropyrimidine-4-carbonitrile **223** in quantitative yield.

a) Compound **227**[5d]; Off-white solid; ^{1}H NMR (500 MHz, DMSO) δ 7.27 (s, 2H, NH_2), 6.77 (s, 1H, H-5); ^{13}C NMR (126 MHz, DMSO) δ 167.0, 166.7, 165.3, 159.9, 102.9.

b) Compound **223**[5d] (2,6-dichloropyrimidine-4-carbonitrile) ^{1}H NMR (300 MHz, DMSO) δ 9.66 (s, 1H, H-5),

c) Compound **224** (2,6-dichloro-*N*-cyclopropylpyrimidine-4-carboxamide) ^{1}H NMR (300 MHz, $CDCl_3$) δ 8.08 (s, 1H, H-5), 7.80 (s, 1H, NH).

6.3.8.1 6-(4-Chlorophenoxy)-2-((2-cyano-5-methylphenyl)amino)pyrimidine-4-carbonitrile **179**

Reaction of 2,6-dichloropyrimidine-4-carbonitrile **223** (174 mg, 1.0 mmol) with sodium 4-chlorophenoxide **166a** using similar reaction conditions detailed in method H gave 2-chloro-6-(4-chlorophenoxy)pyrimidine-4-carbonitrile **228** (253 mg, 95%) as a white oil. ^{1}H NMR (300 MHz, $CDCl_3$) δ 7.41–7.28 (m, 2H, H-2”), 7.21 (s, 1H, H-5), 7.17–7.06 (m, 2H). Intermediate **228** (133 mg, 0.5 mmol) was aminated with 2-amino-4-methylbenzonitrile **167** using an already developed palladium catalyzed protocol to generate target compound **179** (138 mg, 76%) as a yellow solid. HRMS (ES^+) Calculated for $C_{19}H_{12}ClN_5O$ $[M+H]^+$: 362.0809, found: 362.0789.

6.3.8.2 a) 6-(4-Chlorophenoxy)-2-((2-cyano-5-methylphenyl)amino)-*N*-cyclopropylpyrimidine-4-carboxamide **180a**

Reaction of 2,6-dichloro-*N*-cyclopropylpyrimidine-4-carboxamide **224** (233 mg, 1.0 mmol) with sodium 4-chlorophenoxide **166a** (1.0 eq.) using similar reaction conditions detailed in method H gave 2-chloro-6-(4-chlorophenoxy)-*N*-cyclopropylpyrimidine-4-carboxamide **229a** (289 mg, 89%) as a white oil. ^{1}H NMR (300 MHz, $CDCl_3$) δ 7.77 (s, 1H, H-5), 7.59 (s, 1H, NH), 7.43–7.38 (m, 2H), 7.13–7.07 (m, 2H, H-3"), 2.94–2.91 (m, 1H), 0.94–0.91 (m, 2H), 0.72–0.68 (m, 2H). Thereafter, palladium-catalyzed amination of **229a** with 2-amino-4-methylbenzonitrile **167** afforded the target product **180a** (269 mg, 64%). ^{1}H NMR (500 MHz, $CDCl_3$) δ 7.76–7.74 (m, 2H, H-6' overlaps with amide N*H*), 7.52 (s, 1H, NH), 7.44–7.39 (m, 3H), 7.29 (s, 1H), 7.15–7.12 (m, 2H), 6.83 (d, *J* = 8.6 Hz, 1H), 2.98–2.94 (m, 1H), 0.93–0.90 (m, 2H), 0.75–0.71 (m, 2H); ^{13}C NMR (126 MHz, $CDCl_3$) δ 171.8, 163.5, 160.0, 157.9, 151.0, 145.3, 141.4, 132.2, 131.5, 129.9, 123.5, 119.6, 117.2, 98.3, 97.9, 22.7, 22.2, 6.6; HRMS (ES$^+$) Calculated for $C_{22}H_{19}ClN_5O_2$ $[M+H]^+$: 420.1227, found: 420.1205.

6.3.8.2 b) 2-((2-cyano-5-methylphenyl)amino)-*N*-cyclopropyl-6-(3,5-dichlorophenoxy)pyrimidine-4-carboxamide **180b**

Reaction of 2,6-dichloro-*N*-cyclopropylpyrimidine-4-carboxamide **224** (233 mg, 1.0 mmol) with sodium 3.5-dichlorophenoxide **166b** using similar reaction conditions detailed in section 3.11 gave 2-chloro-6-(3,5-dichlorophenoxy)-*N*-cyclopropylpyrimidine-4-carboxamide **229b** (341 mg, 95%) as a light yellow oil. ^{1}H NMR (300 MHz, DMSO) δ 8.94 (d, *J* = 5.0 Hz, 1H, amide N*H*), 7.64 (t, *J* = 1.8, 1.8 Hz, 1H, H-4"), 7.56 (d, *J* = 1.8 Hz, 2H, H-2"), 7.53 (s, 1H, H-5), 2.94 – 2.90 (m, 1H), other cyclopropyl protons overlapped with DMSO solvent signal in the aliphatic region; ^{13}C NMR (75 MHz, DMSO) δ 170.81, 162.14, 161.80, 158.22, 152.58, 134.69, 126.44, 121.20, 105.29, 23.20, 5.61. Substrate **229b** (166 mg, 0.5 mmol) was further reacted with amine **167** using palladium-catalyzed conditions to give title compound **180b** (139 mg, 61%) as a pale yellow oil. ^{1}H NMR (300 MHz, DMSO) δ 8.47 (br s, 1H, amide N*H*), 8.27 (br s, NH), 7.62 (s, 1H, H-6"), 7.49 (d, *J* = 8.0 Hz, H-3'), 7.26 (t, *J* = 1.8 Hz, 1H, H-4"), 7.14 (d, *J* = 1.8 Hz, 2H, H-2"), 7.10 (d, *J* = 8.0 Hz, H-4'), 3.00–2.98 (m, 1H), 2.97 (s, 3H, -CH_3), 0.88–0.81 (m, 2H), 0.70–0.60 (m, 2H); HRMS (ES$^+$) Calculated for $C_{22}H_{18}Cl_2N_5O_2$ $[M+H]^+$: 454.0838, found: 454.0794.

6.3.9 Synthesis of chloride-substituted triazine derivatives **181a**-**b**

Target compounds **181a** and **181b** were synthesized via intermediate compound 2,4-dichloro-6-(piperidin-1-yl)-1,3,5-triazine **230a**, whilst novel target molecule **181c** was constructed via intermediate scaffold 2,4-dichloro-6-(4-chlorophenoxy)-1,3,5-triazine **230b**.

Preparation of 2,4-dichloro-6-(piperidin-1-yl)-1,3,5-triazine **230 –** Method L

Piperidine (172 mg, 2.0 mmol) was added dropwise to an ice-cold mixture of cyanuric acid (372 mg, 2.0 mmol) and KO^{t}Bu in acetone with stirring. A white precipitate formed rapidly as the reaction mixture was stirred for a 30 min, under ice-cold conditions. The reaction was allowed to warm to room temperature over 4 h. After evaporating the solvent, the crude residue was dissolved in dichloromethane (20 ml) and washed successively with saturated aqueous ammonium chloride (5 ml) and water (5 ml). The organic layer was dried over anhydrous Na_2SO_4 and evaporated *in vacuo* to give product **230** (406 mg, 87%) as a light yellow oil. ^{1}H NMR (500 MHz, $CDCl_3$) δ 4.00–3.60 (m, 4H), 1.97–1.39 (m, 6H); ^{13}C NMR (126 MHz, $CDCl_3$) δ 170.1, 163.8, 163.5, 45.4, 44.6, 25.7, 24.2, 24.2, 24.1.

6.3.9.1 2-Chloro-4-(4-chlorophenoxy)-6-(piperidin-1-yl)-1,3,5-triazine **181a**

Aqueous 4-chlorophenoxide (0.5 mmol) was reacted with **230** (118 mg, 0.5 mmol) using similar reaction conditions detailed in method L. The crude reaction mixture was purified on a flash silica column by eluting with 3–5% EtOAc/Hexane to give title compound **181a** (127 mg, 78%) as a yellow oil. ^{1}H NMR (500 MHz, $CDCl_3$) δ 7.45–7.31 (m, 2H), 7.19–7.04 (m, 2H), 3.85–3.73 (m, 2H), 3.68–3.50 (m, 2H), 1.70–1.49 (m, 6H). ^{13}C NMR (126 MHz, $CDCl_3$) δ 171.2, 170.4, 164.8, 150.3, 131.0, 129.4, 123.0, 45.1, 44.9, 25.7, 25.6, 24.3.

6.3.9.2 2-((4-Chloro-6-(piperidin-1-yl)-1,3,5-triazin-2-yl)amino)-4-methylbenzonitrile **181b**

2-amino-4-methylbenzonitrile **167** (70 mg, 0.5 mmol) was reacted with **230a** (118 mg, 0.5 mmol) using similar reaction conditions detailed in method L. The crude reaction mixture was purified on a flash silica column by eluting with 10–25% EtOAc/Hexane and gave compound **181a** (95 mg, 65%) as a brown oil. ^{1}H NMR (300 MHz, $CDCl_3$) δ 8.18 (s, 1H), 7.47 (d, J = 7.9 Hz, 1H), 7.40 (s, 1H), 6.96 (d, J = 7.9 Hz, 1H), 3.81–3.75 (m, 4H), 2.42 (s, 3H), 1.69–1.62 (m, 6H).

6.3.10 References

1. Lansdon, E. B.; Brendza, K. M.; Hung, M.; Wang, R.; Mukund, S.; Jin, D.; Birkus, G.; Kutty, N. and Liu, X. *J. Med. Chem*. **2010**, 53, 4295 – 4299.
2. Zhan, P.; Chen, X.; Li, D.; Fang, Z.; de Clercq, E. and Liu, X., *Med. Res. Rev*. **2013**, 33 (S1) E1 - E72.
3. Changunda, C. R. K.; Basson, A. E.; van Vuuren, S. F.; Rousseau, A. L. and Bode, M. L. *Tetrahedron*, **2017**, 73, 137 – 147.
4. Newkone, G. R. and Kawato, T. *J. Org. Chem*. **1979**, 44, 2693 – 2697.
5. a) Klein, C.; Baranoff, E.; Gratzel, M and Nazeeruddin, Md.-K, *Tetrahedron Lett*. **2011,** 52, 584 – 587; b) Arora, E.; Bhasin, K. K.; Mehta, S. K.; Sharma, N.; Bhasin, A. K. K.; Jacob, C.; Felix, V. AND Neogi, S. *Polyhedron*, **2014**, 316 – 322; c) Gershon, H. *J. Org. Chem.* **1962**, 27, 3507 – 3510; d) Davies, G. D.-Jnr; Baiocchi, F.; Roland, K. and Cheng, C. C. *J. Org. Chem*. **1961**, 26, 2755 – 2763; e) Wojciechoski, J. Patent No PL 71235 A5 19740430.
6. Bach, P.; Marczynke, M. and Giordanetto, F. *Eur. J. Org. Chem.* **2012**, 6940 – 6952.
7. Deacon, P. R.; Mahon, M. F.; Molly, K.C. and Waterfield, P. C. *J. Chem. Soc. Dalton Trans.* **1997**, 3705 – 3712.
8. Mckendry, L. H. *J. Label. Compd. Radiopharm* **1984**, 517 – 523.
9. Henegar, K. E.; Ashford, S. W.; Baughman, T. A.; Sih, J. C. and Gu, R.-L. *J. Org. Chem*. **1997**, 62, 6588 – 6597.
10. a) Schade, M. A.; Manolikakes, G. and Knochel, P. *Org. Lett.* **2010**, 12, 3648 – 3650; b) Liskey, C. W.; Liao, X. and Hartwig, J. F. *J. Am. Chem. Soc.* **2010**, 132, 11389 – 11391.
11. Klingesmith, L. M.; Strieter, E. R.; Timothy E. Barder, T. E. and Buchwald, S. L. *Organometallics*, **2006**, 25, 82 – 91.
12. Birkholz, M.-N.; Freixa, Z. and Piet W. N. M. van Leeuwen, P. W. N. M. *Chem. Soc. Rev.*, **2009**, 38, 1099 –1118.
13. Nicolaou, K. C. and Webber, S. E. *J. Am. Chem. Soc*. **1984**, 106, 5734 – 5736.
14. Delia, T. J. and Nagarajan, A. *J. Heterocyclic Chem.*, **1998**, 35, 269 – 273.
15. Chhiba, V.; Bode, M. L.; Mathiba, K.; Kwezi, W. and Brady, D. *J. Mol. Catalysis B: Enzymatic* **2012**, 76, 68 – 74.
16. Chen, K.-Y. and Huang, C.-T. *Int. J. Appl. Sci. Eng*. **2004**, 2, 286 – 294.

7.0 APPENDIX

7.1 NMR Spectra for Chapter 2 Compounds

142a

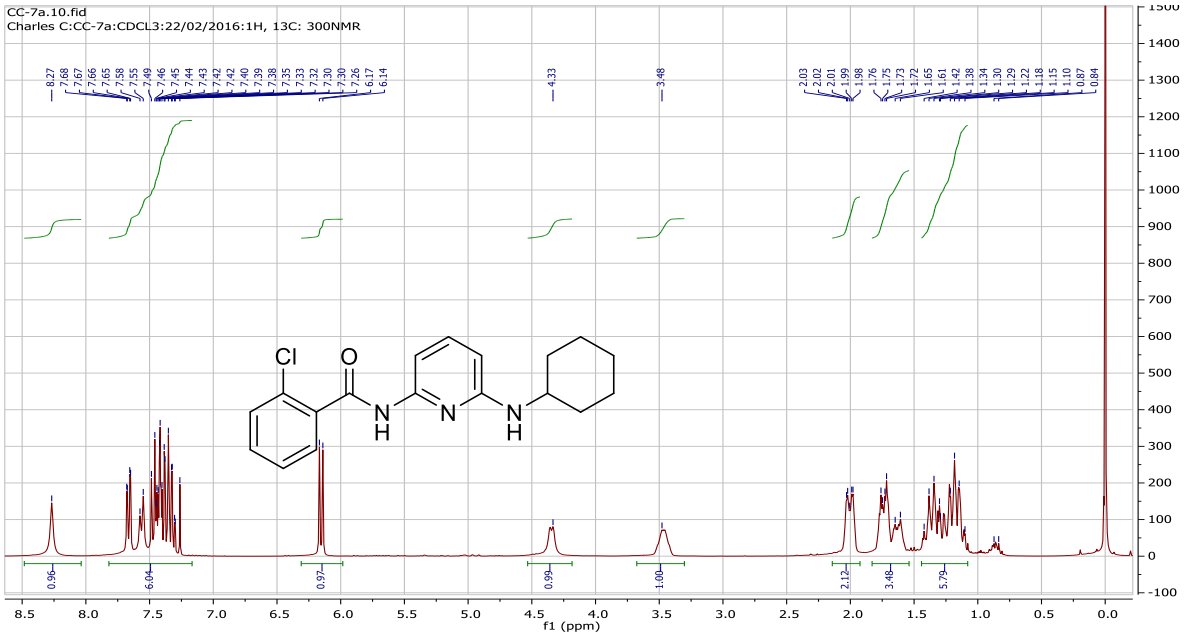

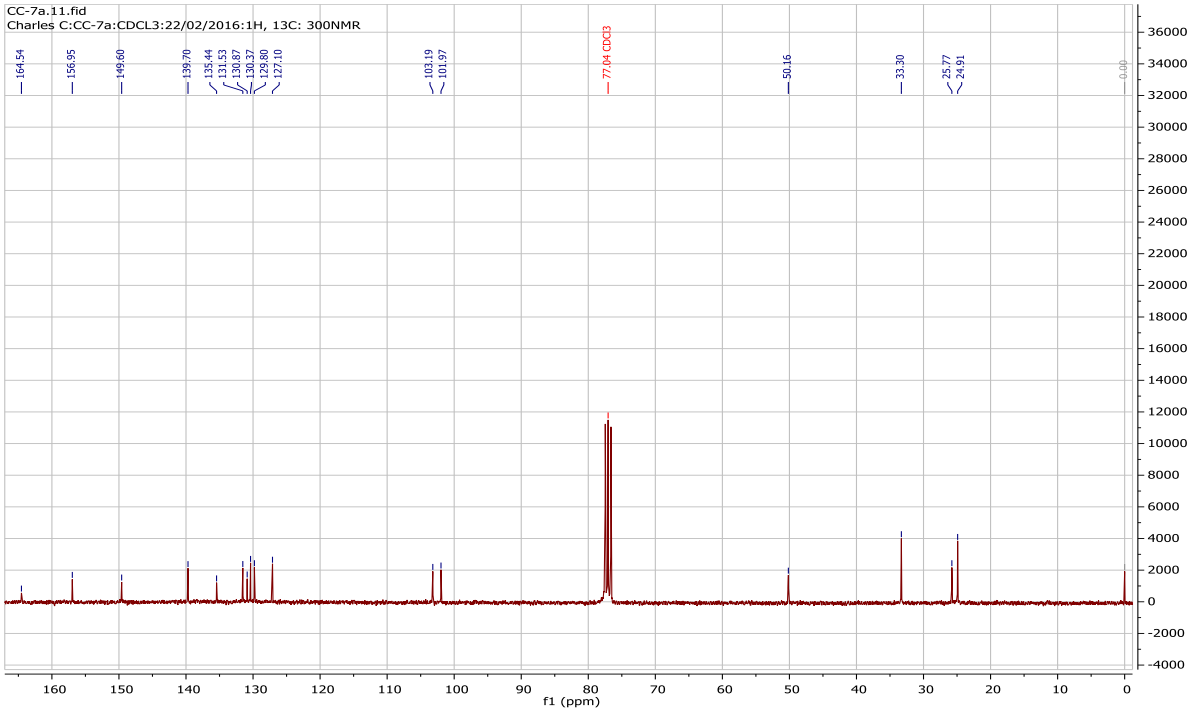

142b

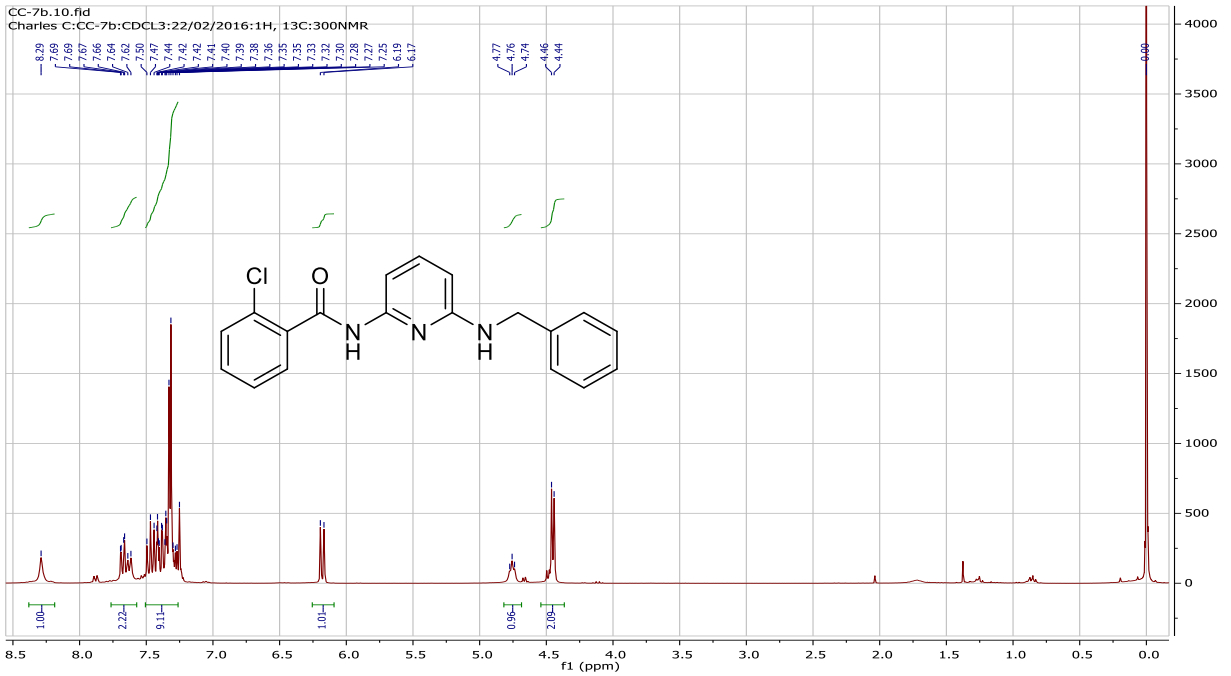
CC-7b.10.fid
Charles C:CC-7b:CDCL3:22/02/2016:1H, 13C:300NMR
Cl
O
N
H
N
N
H
f1 (ppm)

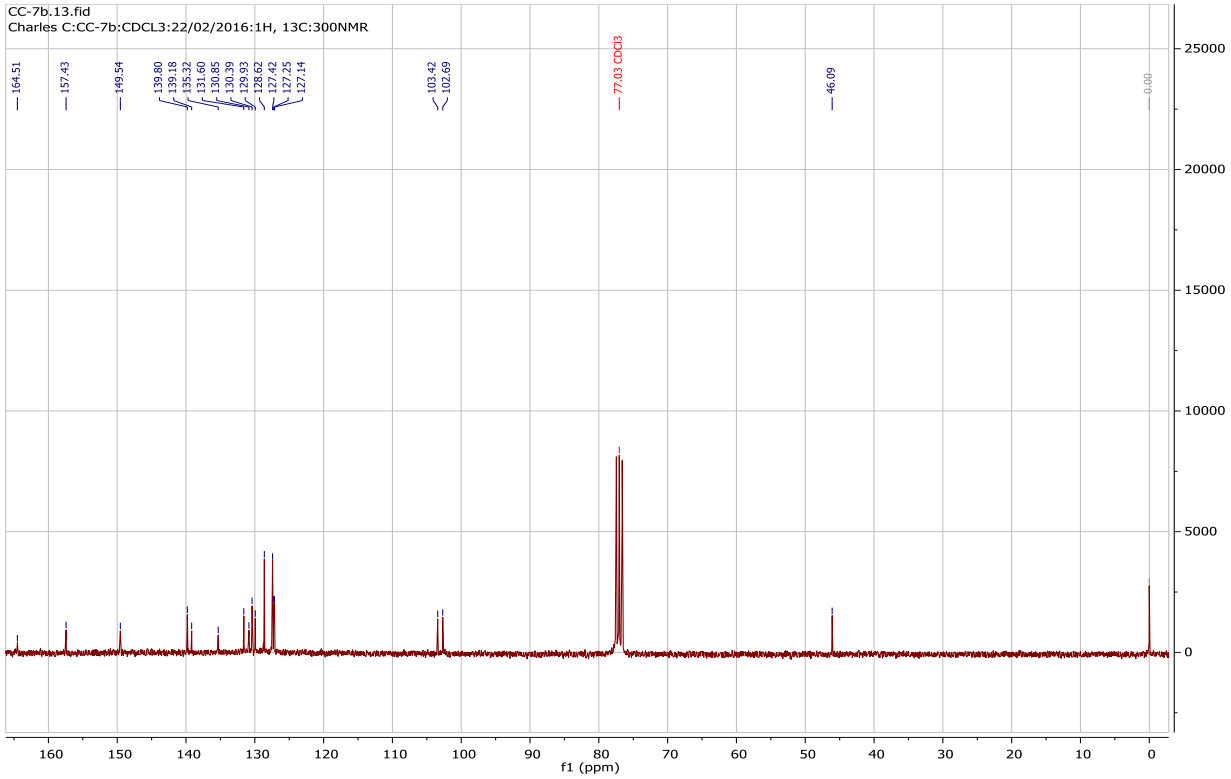
CC-7b.13.fid
Charles C:CC-7b:CDCL3:22/02/2016:1H, 13C:300NMR
77.03 CDCl3
f1 (ppm)

142c

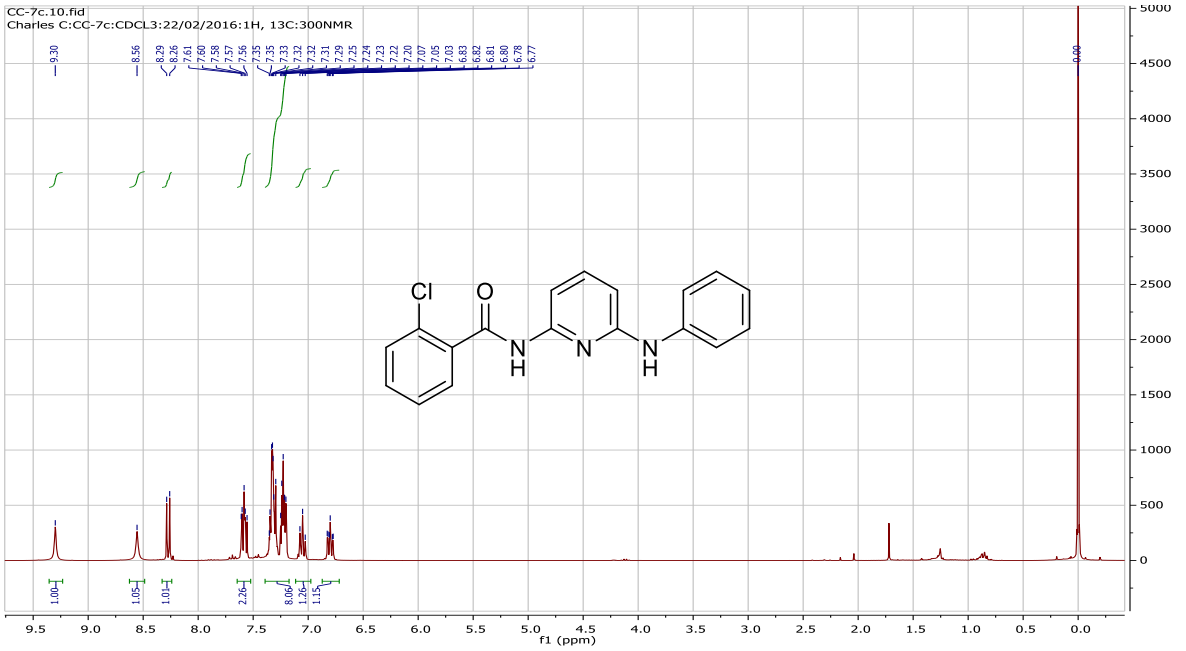
CC-7c.10.fid
Charles C:CC-7c:CDCL3:22/02/2016:1H, 13C:300NMR
Cl
O
N
H
N
N
H
f1 (ppm)

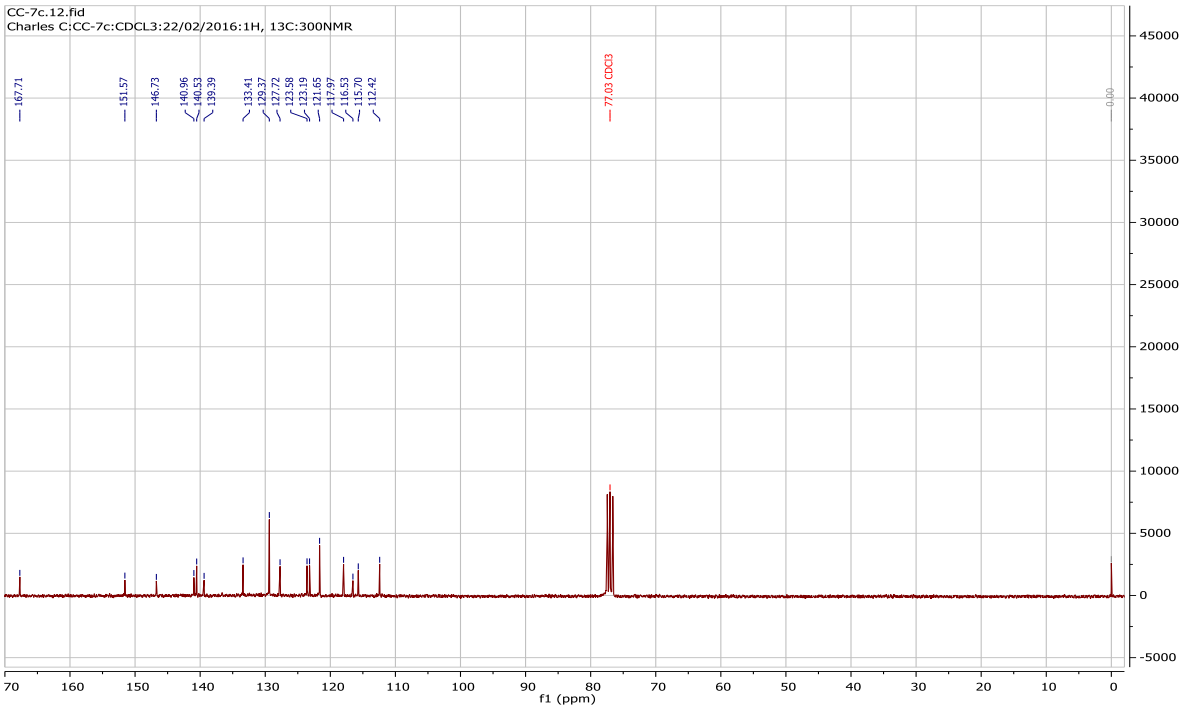
CC-7c.12.fid
Charles C:CC-7c:CDCL3:22/02/2016:1H, 13C:300NMR
167.71
151.57
146.73
140.96
140.53
139.39
133.41
129.37
127.72
123.58
123.19
121.65
117.97
116.53
115.70
112.42
77.03 CDCl3
f1 (ppm)

142d

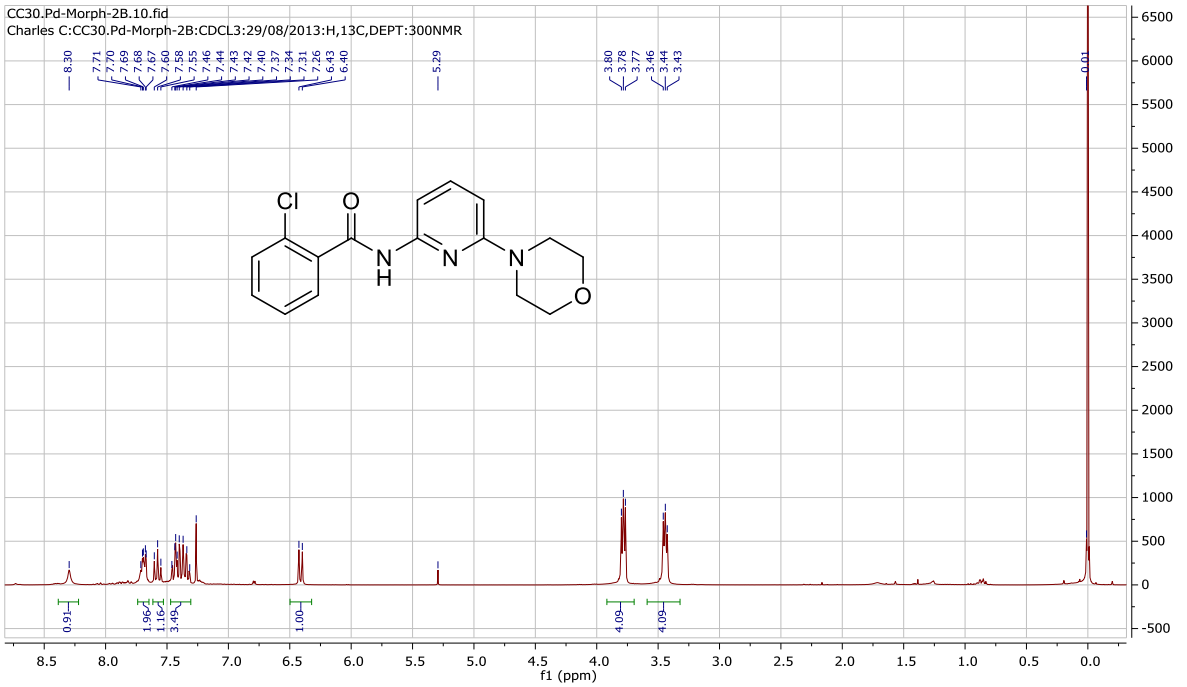
CC30.Pd-Morph-2B.10.fid
Charles C:CC30.Pd-Morph-2B:CDCL3:29/08/2013:H,13C,DEPT:300NMR
8.30
7.71
7.70
7.69
7.68
7.67
7.60
7.58
7.55
7.46
7.44
7.43
7.42
7.40
7.37
7.34
7.31
7.26
6.43
6.40
5.29
3.80
3.78
3.77
3.46
3.44
3.43
0.01
Cl
O
N
H
N
N
O
0.91
1.96
1.16
3.49
1.00
4.09
4.09
f1 (ppm)

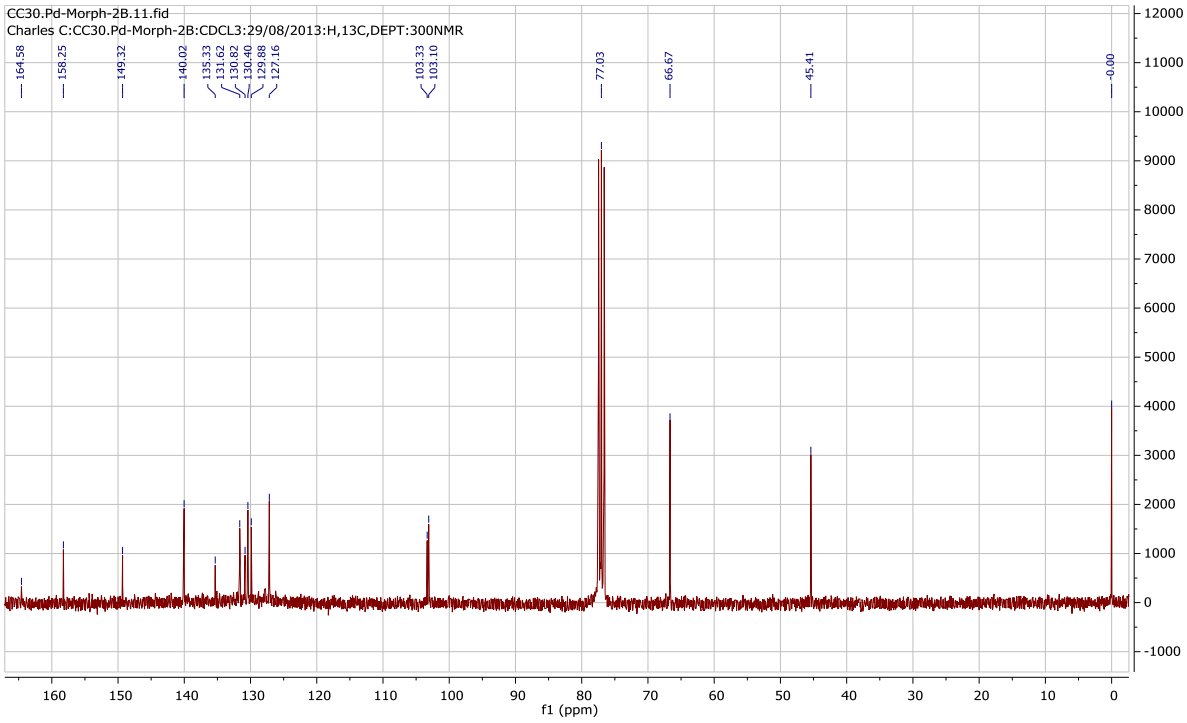
CC30.Pd-Morph-2B.11.fid
Charles C:CC30.Pd-Morph-2B:CDCL3:29/08/2013:H,13C,DEPT:300NMR
164.58
158.25
149.32
140.02
135.33
131.62
130.82
130.40
129.88
127.16
103.33
103.10
77.03
66.67
45.41
-0.00
f1 (ppm)

142e

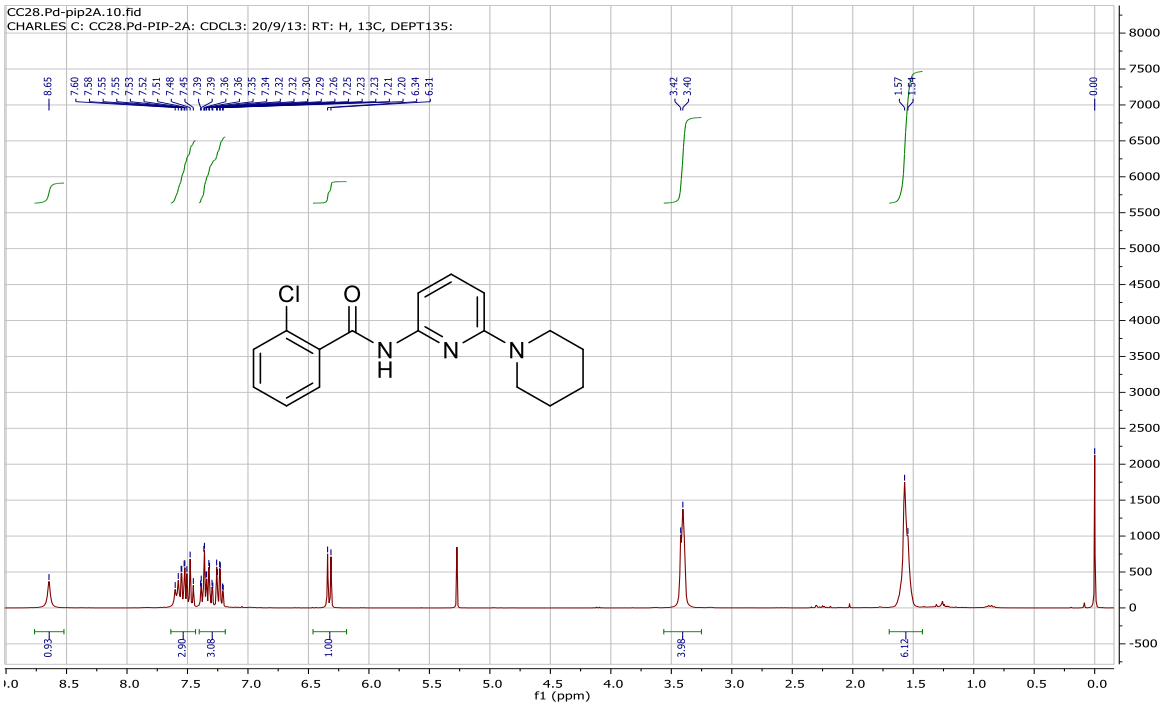
CC28.Pd-pip2A.10.fid
CHARLES C: CC28.Pd-PIP-2A: CDCL3: 20/9/13: RT: H, 13C, DEPT135:
f1 (ppm)

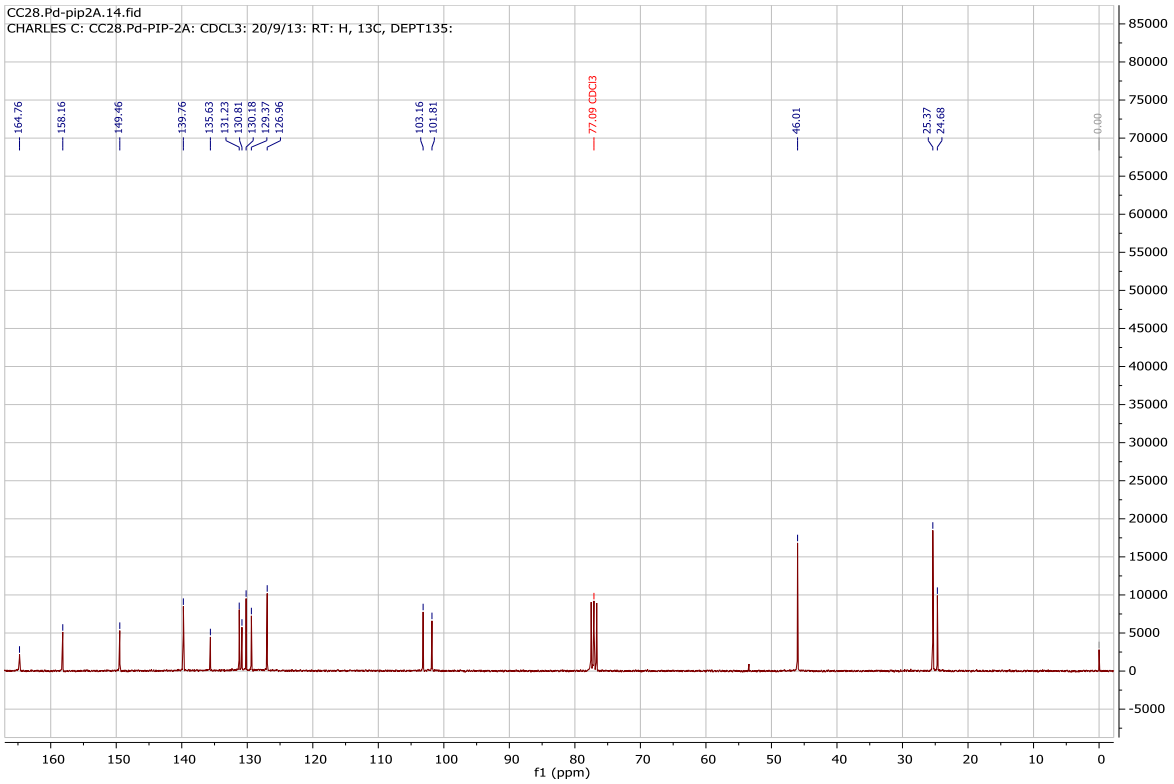
CC28.Pd-pip2A.14.fid
CHARLES C: CC28.Pd-PIP-2A: CDCL3: 20/9/13: RT: H, 13C, DEPT135:
164.76
158.16
149.46
139.76
135.63
131.23
130.81
130.18
129.37
126.96
103.16
101.81
77.09 CDCl3
46.01
25.37
24.68
f1 (ppm)

142g

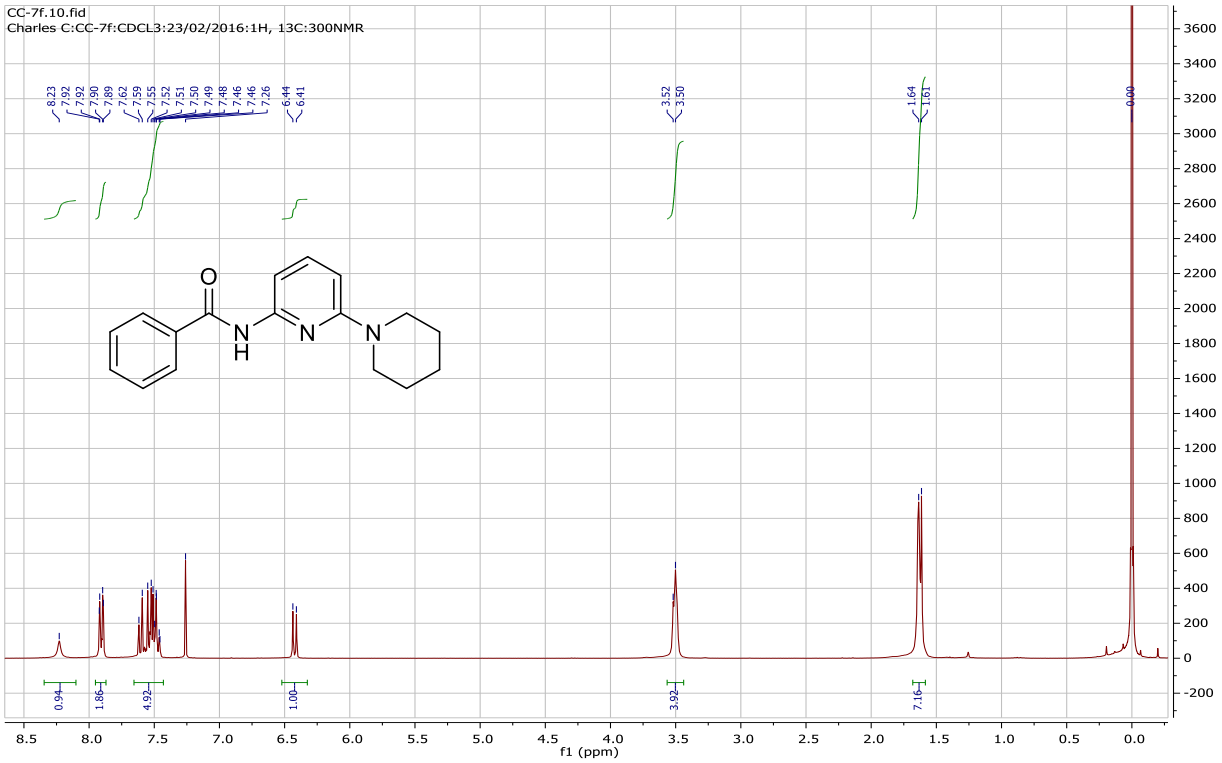
CC-7f.10.fid
Charles C:CC-7f:CDCL3:23/02/2016:1H, 13C:300NMR
8.23
7.92
7.92
7.90
7.89
7.62
7.59
7.55
7.52
7.51
7.50
7.49
7.48
7.46
7.46
7.26
6.44
6.41
3.52
3.50
1.64
1.61
0.00
O
N
H
N
N
0.94
1.86
4.92
1.00
3.92
7.16
f1 (ppm)

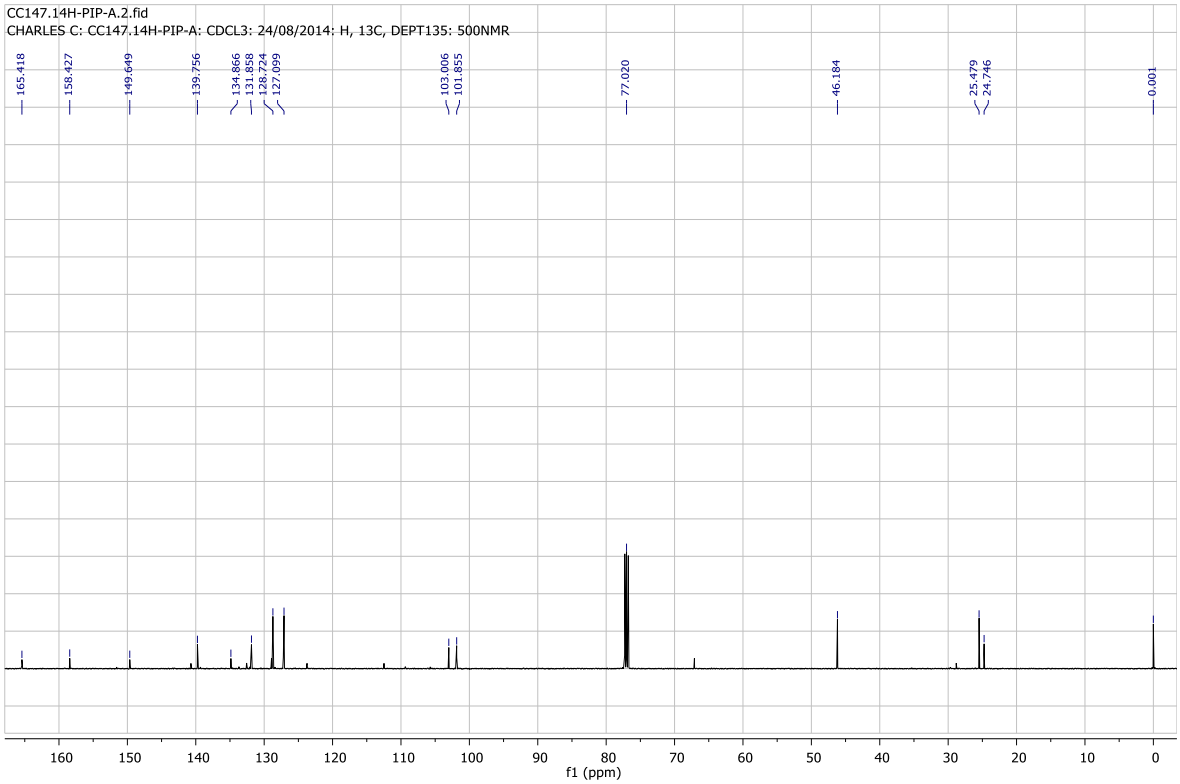
CC147.14H-PIP-A.2.fid
CHARLES C: CC147.14H-PIP-A: CDCL3: 24/08/2014: H, 13C, DEPT135: 500NMR
165.418
158.427
149.649
139.756
134.866
131.858
128.724
127.099
103.006
101.855
77.020
46.184
25.479
24.746
0.001
f1 (ppm)

142h

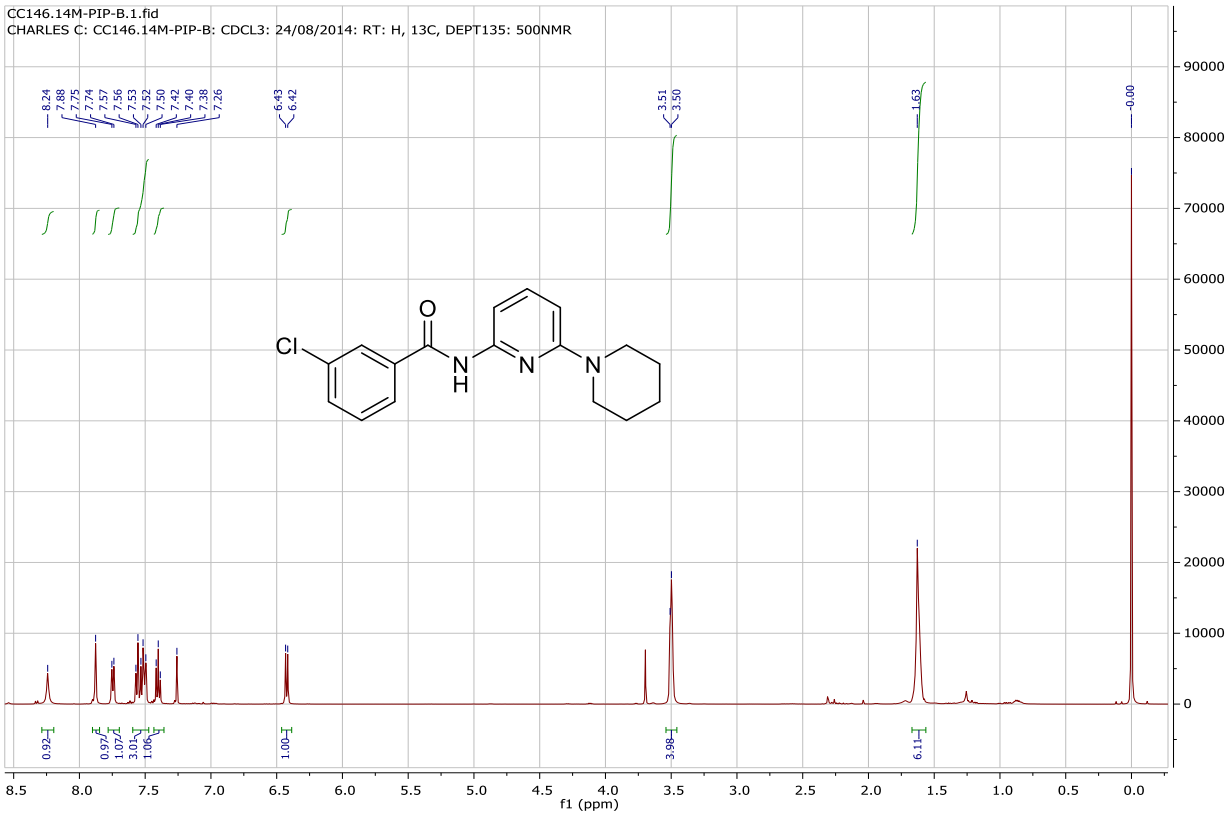
CC146.14M-PIP-B.1.fid
CHARLES C: CC146.14M-PIP-B: CDCL3: 24/08/2014: RT: H, 13C, DEPT135: 500NMR
8.24
7.88
7.75
7.74
7.57
7.56
7.53
7.52
7.50
7.42
7.40
7.38
7.26
6.43
6.42
3.51
3.50
1.63
0.00
Cl
O
N
H
N
N
0.92
0.97
1.07
3.01
1.06
1.00
3.98
6.11
f1 (ppm)

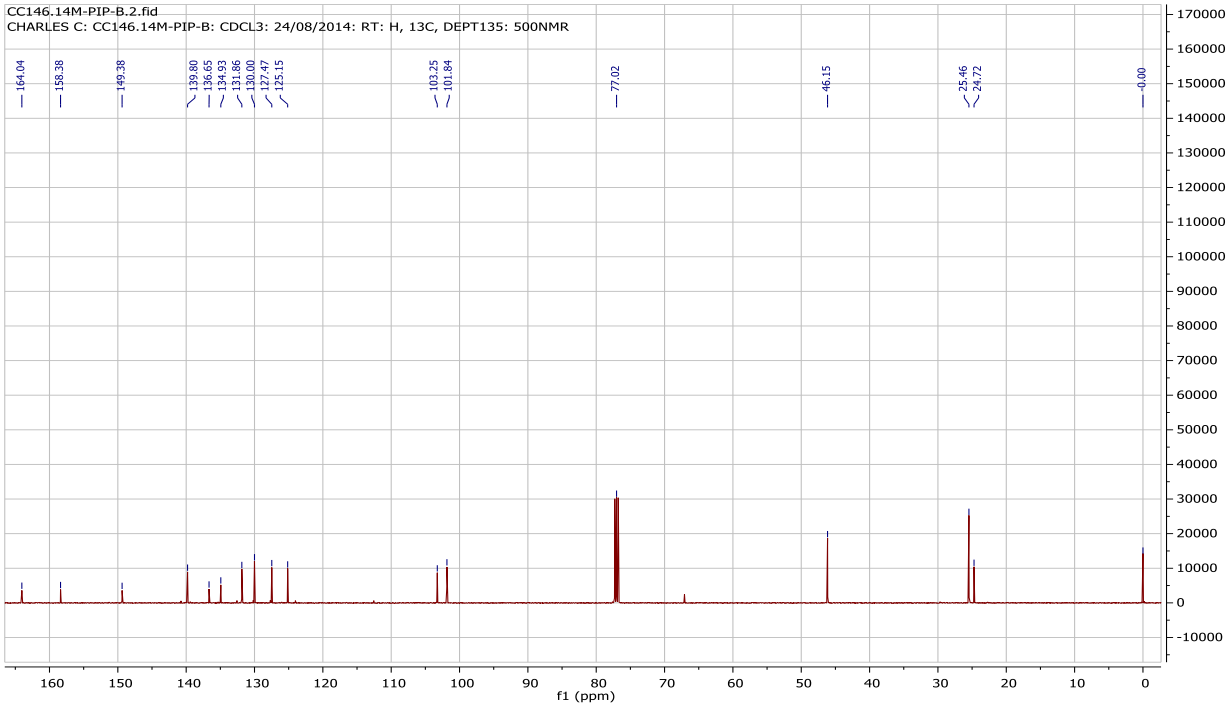
CC146.14M-PIP-B.2.fid
CHARLES C: CC146.14M-PIP-B: CDCL3: 24/08/2014: RT: H, 13C, DEPT135: 500NMR
164.04
158.38
149.38
139.80
136.65
134.93
131.86
130.00
127.47
125.15
103.25
101.84
77.02
46.15
25.46
24.72
0.00
f1 (ppm)

142i

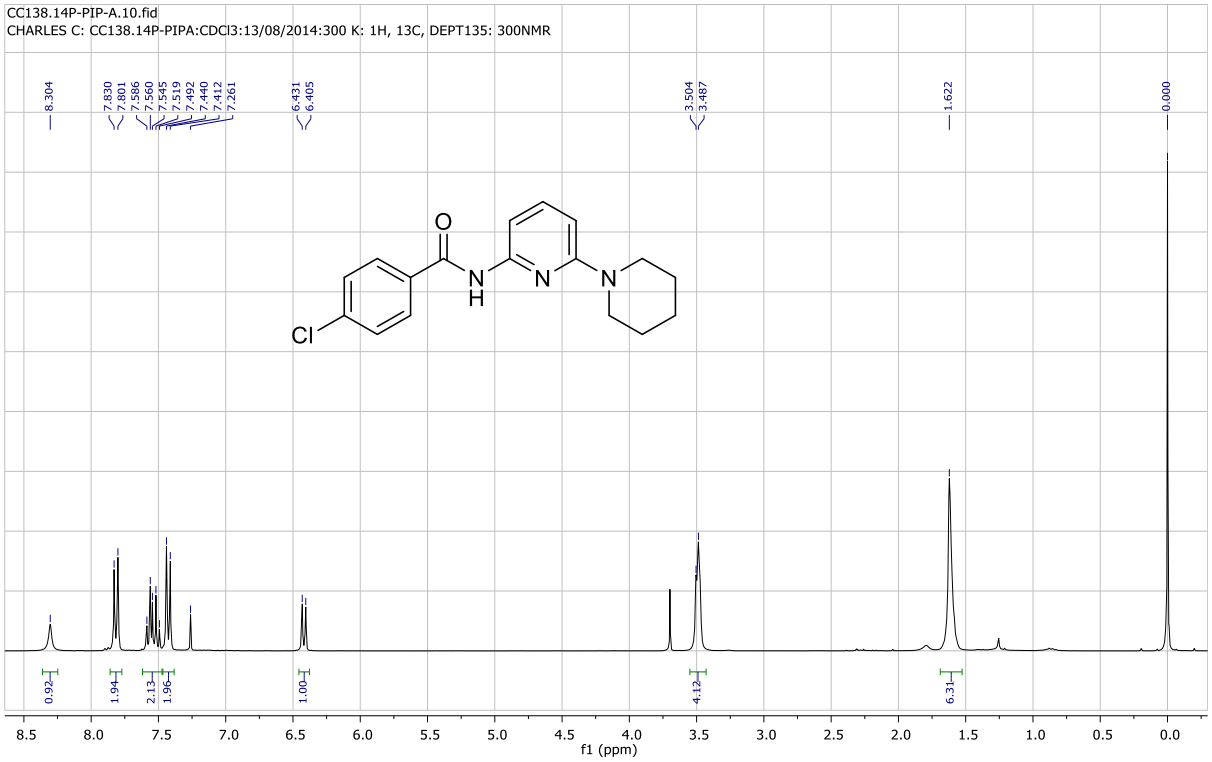
CC138.14P-PIP-A.10.fid
CHARLES C: CC138.14P-PIPA:CDCl3:13/08/2014:300 K: 1H, 13C, DEPT135: 300NMR
8.304
7.830
7.801
7.586
7.560
7.545
7.519
7.492
7.440
7.412
7.261
6.431
6.405
3.504
3.487
1.622
0.000
O
N
H
N
N
Cl
0.92
1.94
2.13
1.96
1.00
4.12
6.31
f1 (ppm)

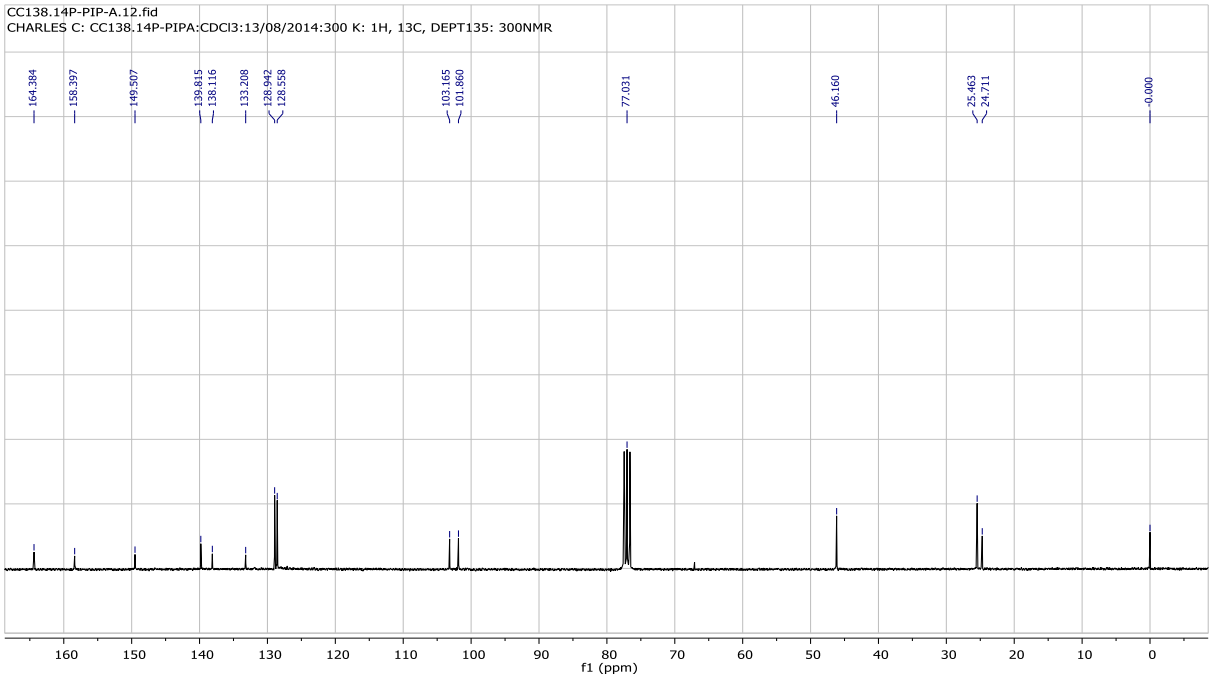
CC138.14P-PIP-A.12.fid
CHARLES C: CC138.14P-PIPA:CDCl3:13/08/2014:300 K: 1H, 13C, DEPT135: 300NMR
164.384
158.397
149.507
139.815
138.116
133.208
128.942
128.558
103.165
101.860
77.031
46.160
25.463
24.711
-0.000
f1 (ppm)

142j

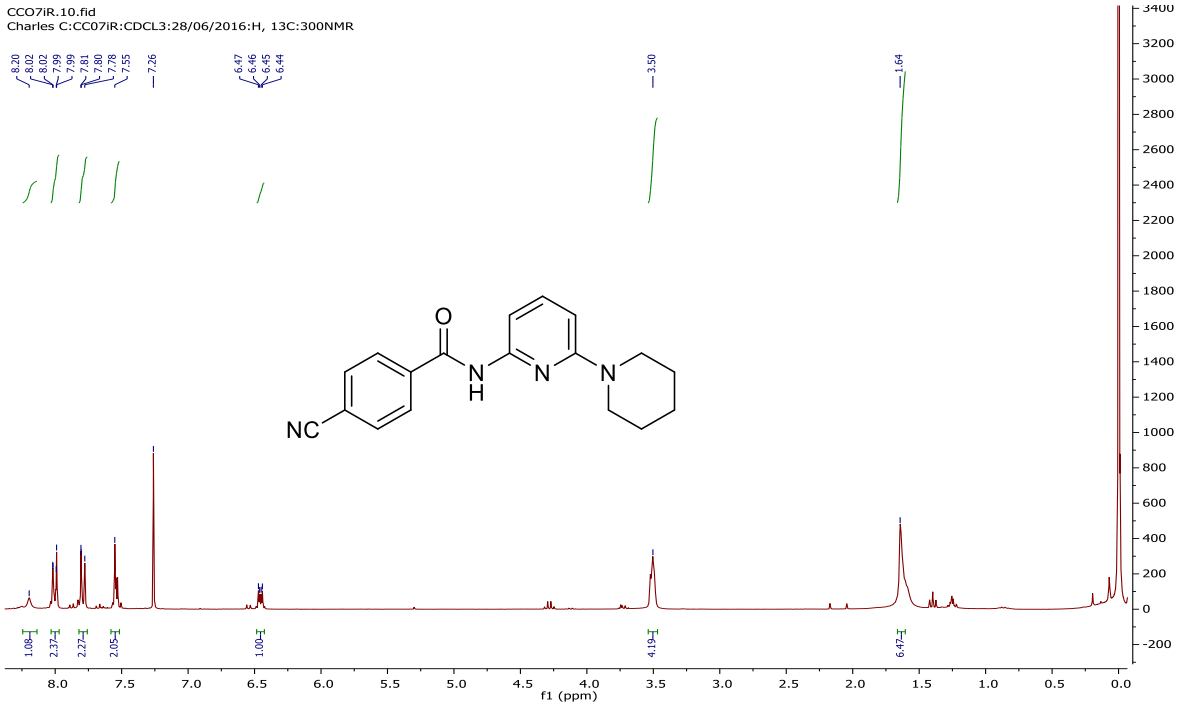
CCO7iR.10.fid
Charles C:CC07iR:CDCL3:28/06/2016:H, 13C:300NMR
8.20
8.02
8.02
7.99
7.99
7.81
7.80
7.78
7.55
7.26
6.47
6.46
6.45
6.44
3.50
1.64
O
N
H
N
N
NC
1.08
2.37
2.27
2.05
1.00
4.19
6.47
f1 (ppm)

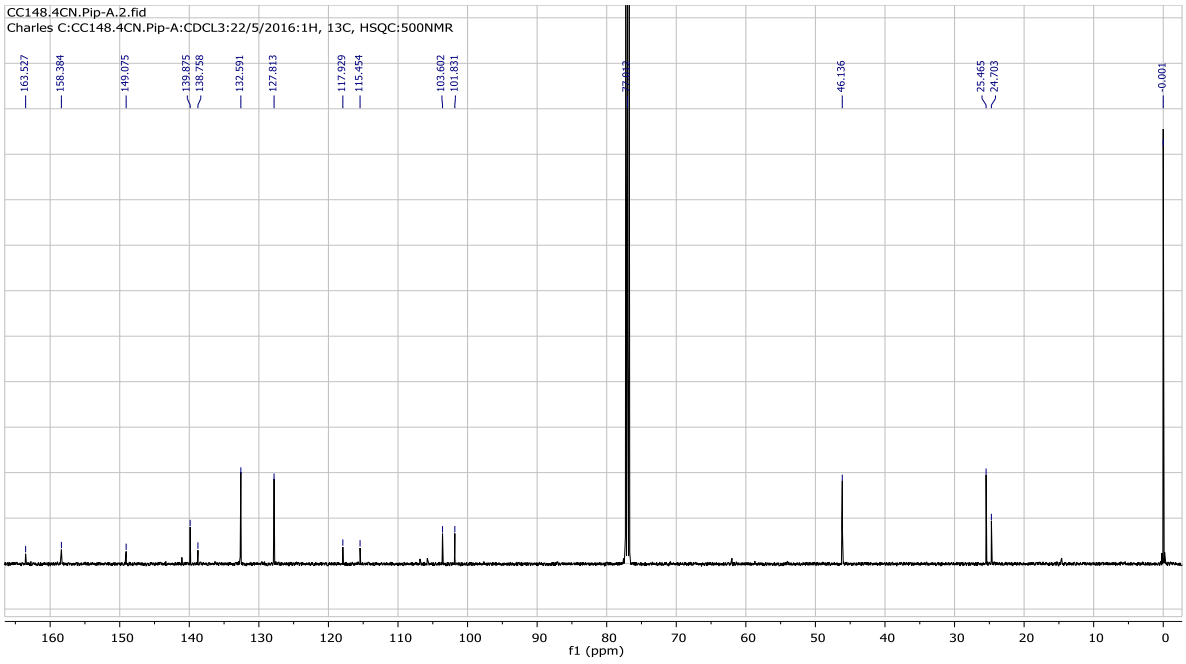
CC148.4CN.Pip-A.2.fid
Charles C:CC148.4CN.Pip-A:CDCL3:22/5/2016:1H, 13C, HSQC:500NMR
163.527
158.384
149.075
139.875
138.758
132.591
127.813
117.929
115.454
103.602
101.831
77.213
46.136
25.465
24.703
-0.001
f1 (ppm)

142l

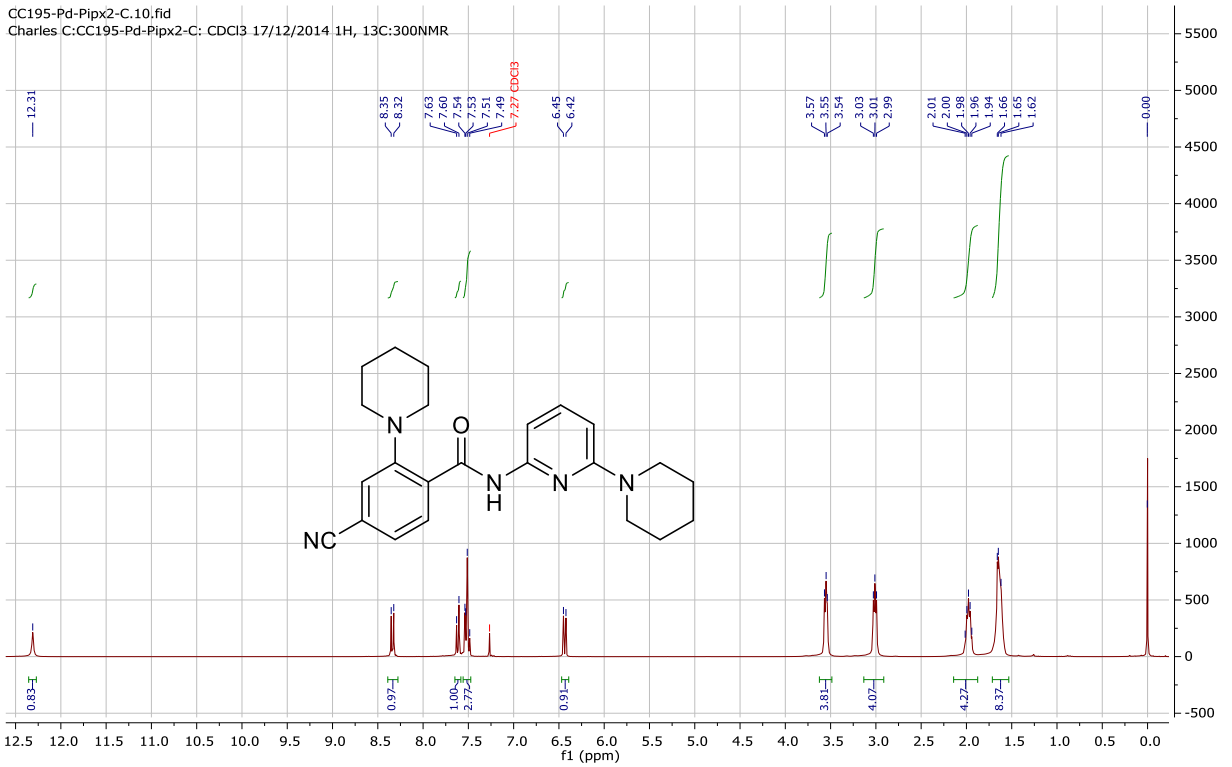
CC195-Pd-Pipx2-C.10.fid
Charles C:CC195-Pd-Pipx2-C: CDCl3 17/12/2014 1H, 13C:300NMR
12.31
8.35
8.32
7.63
7.60
7.54
7.53
7.51
7.49
7.27 CDCl3
6.45
6.42
3.57
3.55
3.54
3.03
3.01
2.99
2.01
2.00
1.98
1.96
1.94
1.66
1.65
1.62
0.00
O
N
H
N
N
N
NC
0.83
0.97
1.00
2.77
0.91
3.81
4.07
4.27
8.37
f1 (ppm)

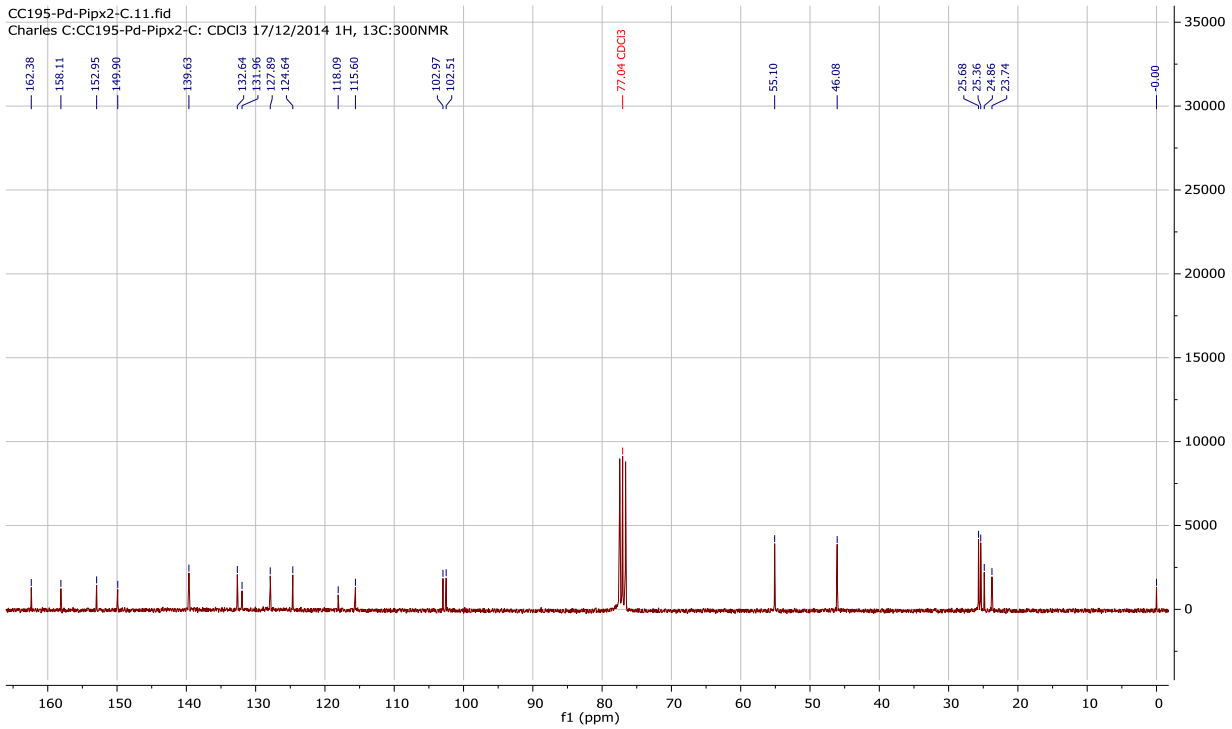
CC195-Pd-Pipx2-C.11.fid
Charles C:CC195-Pd-Pipx2-C: CDCl3 17/12/2014 1H, 13C:300NMR
162.38
158.11
152.95
149.90
139.63
132.64
131.96
127.89
124.64
118.09
115.60
102.97
102.51
77.04 CDCl3
55.10
46.08
25.68
25.36
24.86
23.74
-0.00
f1 (ppm)

143a

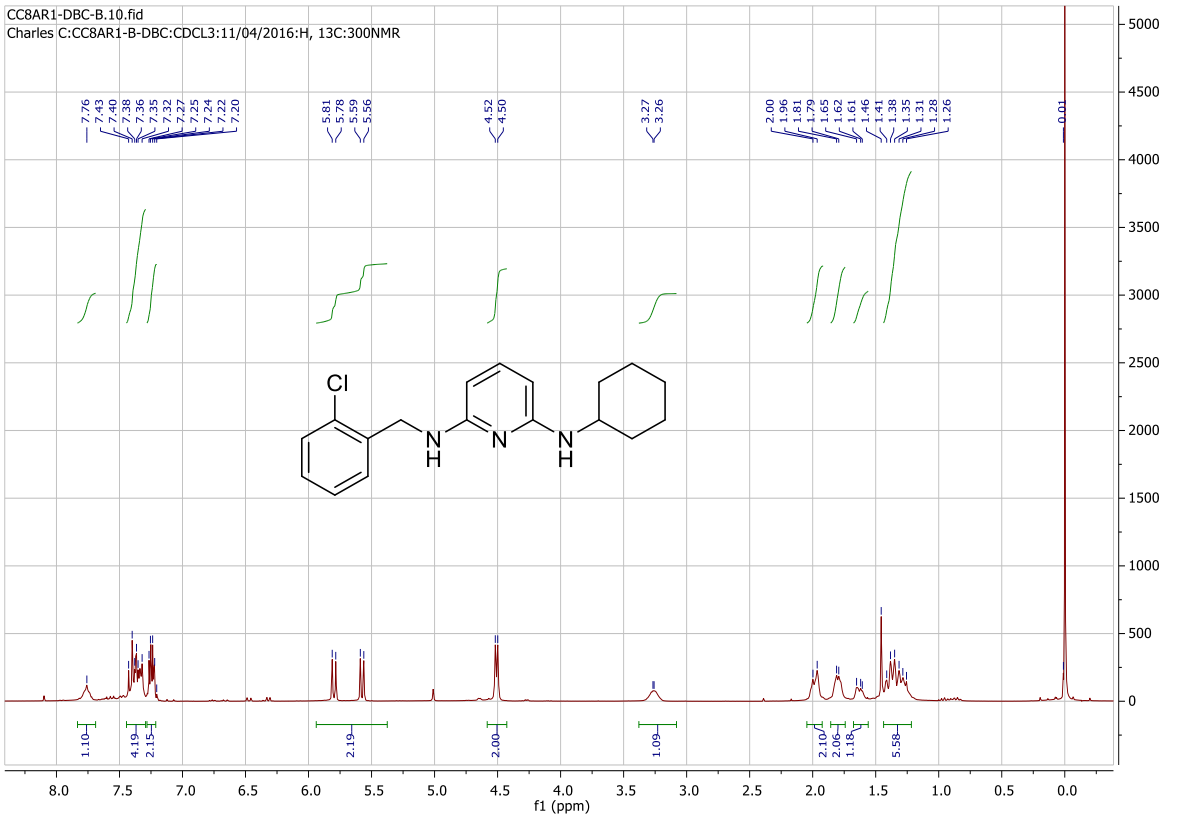
CC8AR1-DBC-B.10.fid
Charles C:CC8AR1-B-DBC:CDCL3:11/04/2016:H, 13C:300NMR
7.76
7.43
7.40
7.38
7.36
7.35
7.32
7.27
7.25
7.24
7.22
7.20
5.81
5.78
5.59
5.56
4.52
4.50
3.27
3.26
2.00
1.96
1.81
1.79
1.65
1.62
1.61
1.46
1.41
1.38
1.35
1.31
1.28
1.26
0.01
Cl
N
H
N
N
H
1.10
4.19
2.15
2.19
2.00
1.09
2.10
2.06
1.18
5.58
f1 (ppm)

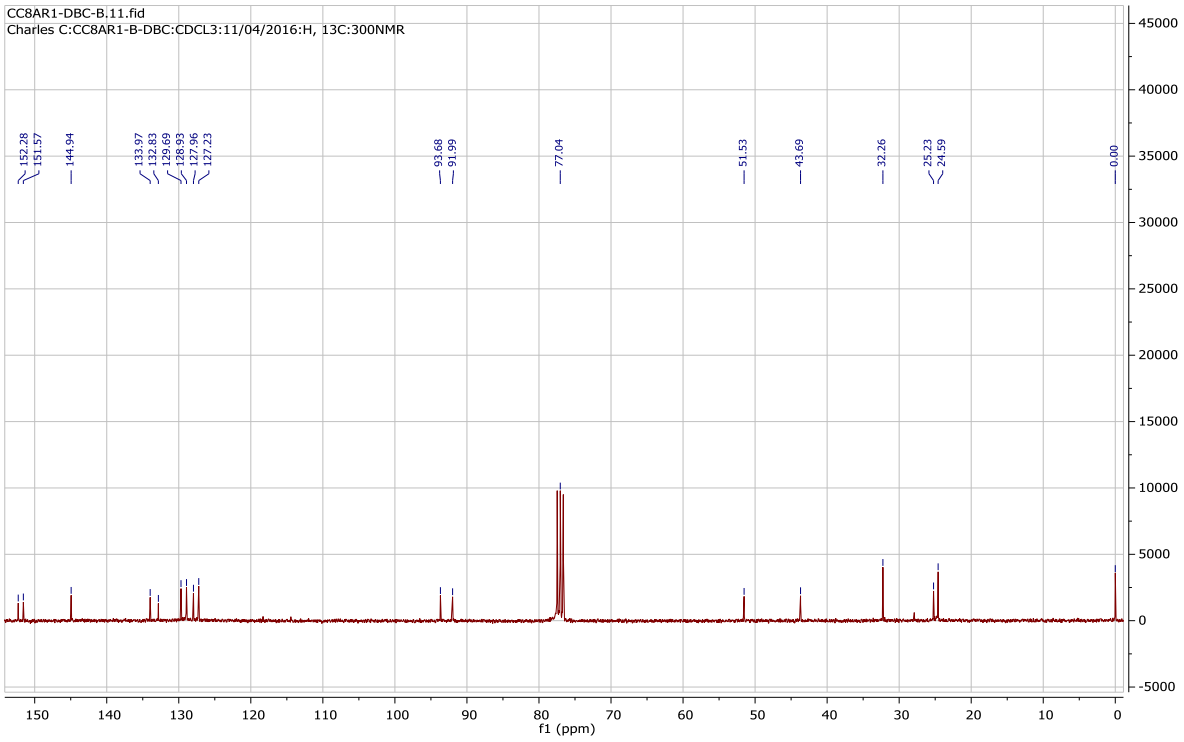
CC8AR1-DBC-B.11.fid
Charles C:CC8AR1-B-DBC:CDCL3:11/04/2016:H, 13C:300NMR
152.28
151.57
144.94
133.97
132.83
129.69
128.93
127.96
127.23
93.68
91.99
77.04
51.53
43.69
32.26
25.23
24.59
0.00
f1 (ppm)

143b

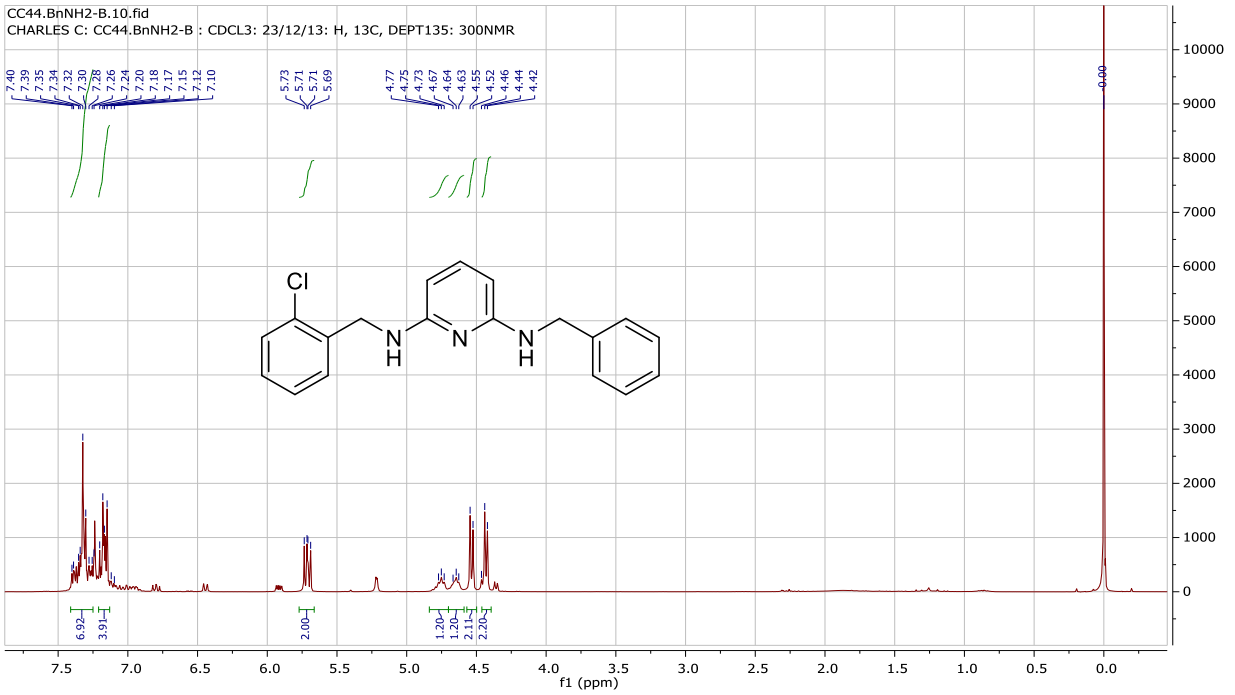
CC44.BnNH2-B.10.fid
CHARLES C: CC44.BnNH2-B : CDCL3: 23/12/13: H, 13C, DEPT135: 300NMR
7.40
7.39
7.35
7.34
7.32
7.30
7.28
7.26
7.24
7.20
7.18
7.17
7.15
7.12
7.10
5.73
5.71
5.71
5.69
4.77
4.75
4.73
4.67
4.64
4.63
4.55
4.52
4.46
4.44
4.42
0.00
Cl
N
H
N
N
H
6.92
3.91
2.00
1.20
1.20
2.11
2.20
f1 (ppm)

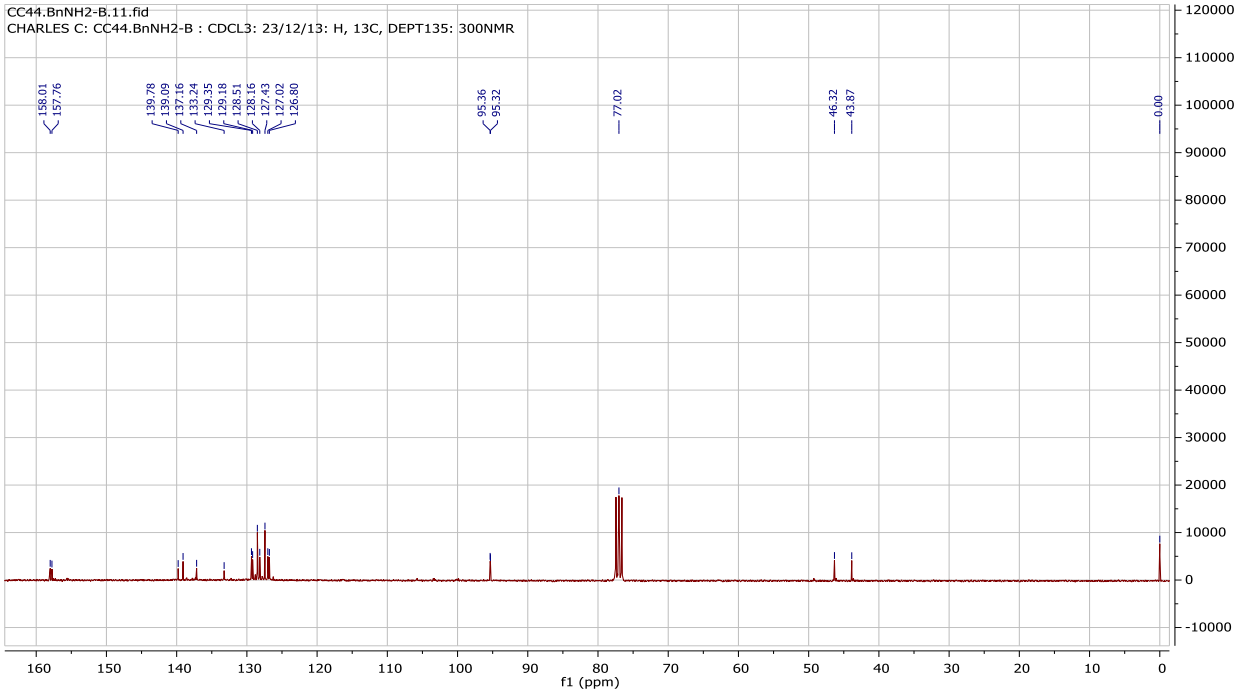
CC44.BnNH2-B.11.fid
CHARLES C: CC44.BnNH2-B : CDCL3: 23/12/13: H, 13C, DEPT135: 300NMR
158.01
157.76
139.78
139.09
137.16
133.24
129.35
129.18
128.51
128.16
127.43
127.02
126.80
95.36
95.32
77.02
46.32
43.87
0.00
f1 (ppm)

143c

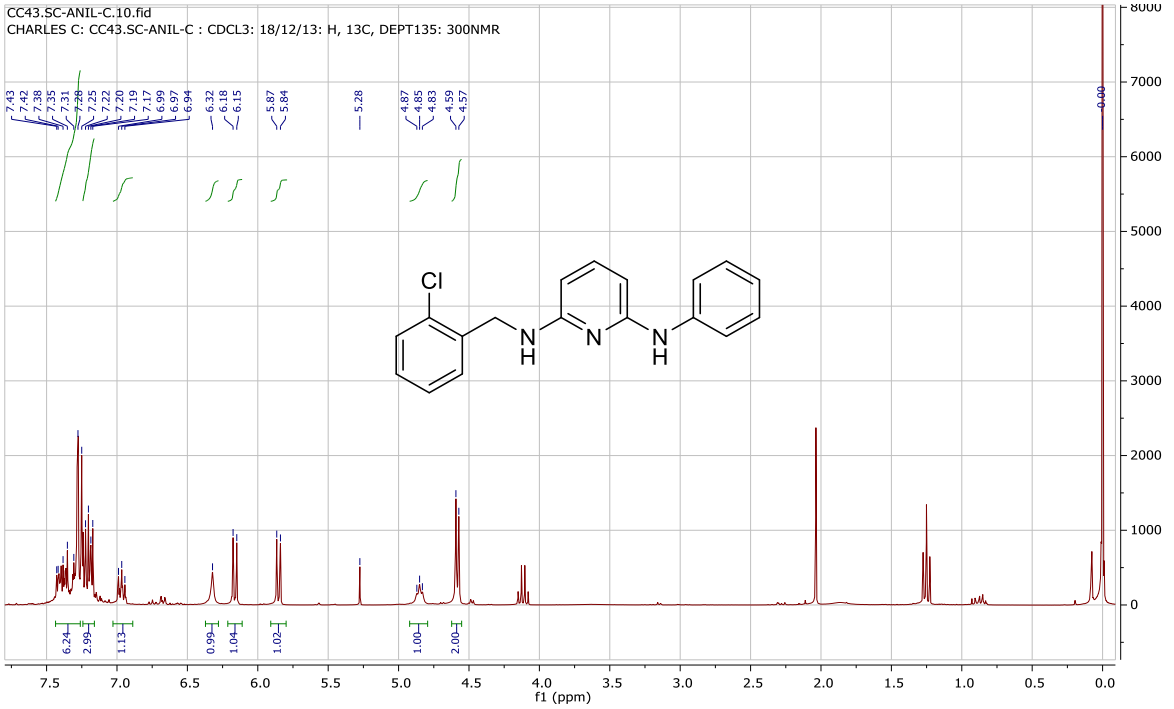
CC43.SC-ANIL-C.10.fid
CHARLES C: CC43.SC-ANIL-C : CDCL3: 18/12/13: H, 13C, DEPT135: 300NMR
7.43
7.42
7.38
7.35
7.31
7.28
7.25
7.22
7.20
7.19
7.17
6.99
6.97
6.94
6.32
6.18
6.15
5.87
5.84
5.28
4.87
4.85
4.83
4.59
4.57
0.00
Cl
N
H
N
N
H
6.24
2.99
1.13
0.99
1.04
1.02
1.00
2.00
f1 (ppm)

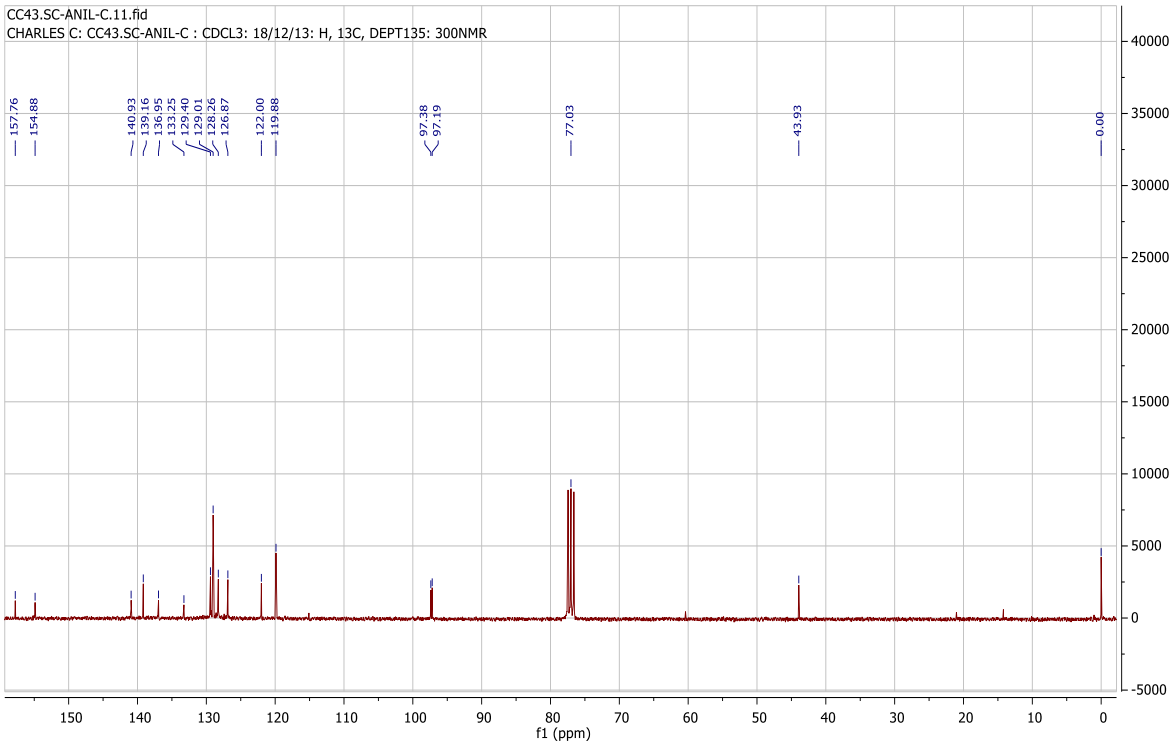
CC43.SC-ANIL-C.11.fid
CHARLES C: CC43.SC-ANIL-C : CDCL3: 18/12/13: H, 13C, DEPT135: 300NMR
157.76
154.88
140.93
139.16
136.95
133.25
129.40
129.01
128.26
126.87
122.00
119.88
97.38
97.19
77.03
43.93
0.00
f1 (ppm)

143d

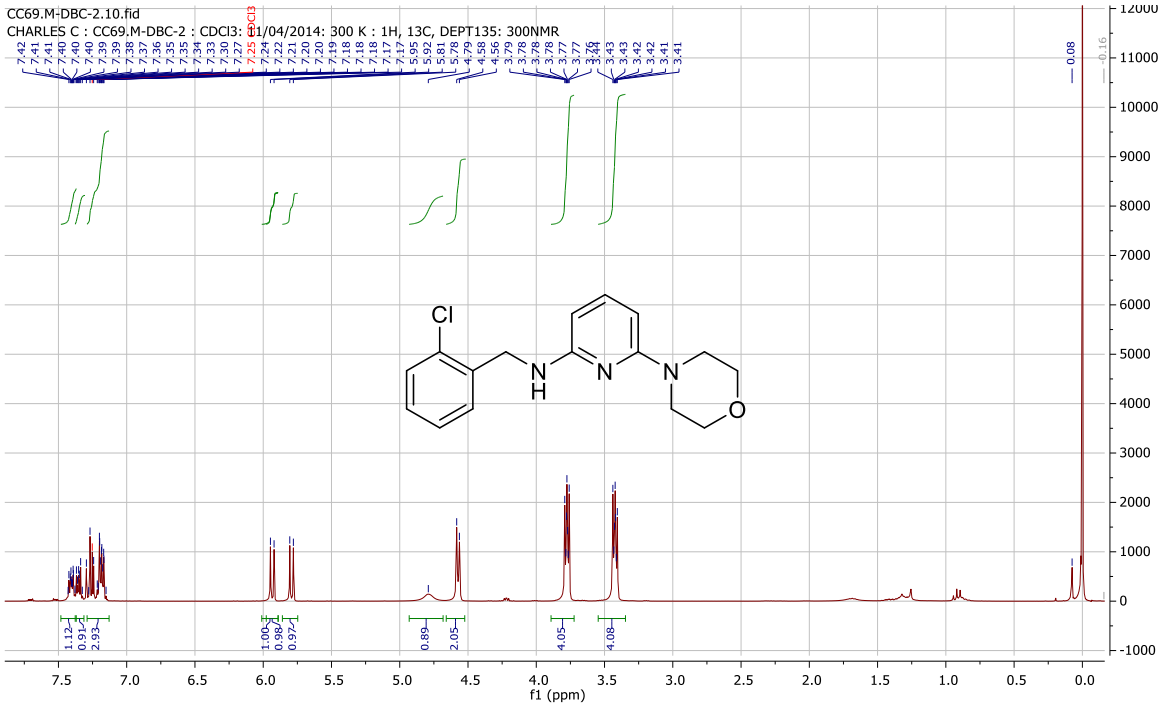
CC69.M-DBC-2.10.fid
CHARLES C : CC69.M-DBC-2 : CDCl3: 11/04/2014: 300 K : 1H, 13C, DEPT135: 300NMR
Cl
N
H
N
N
O
f1 (ppm)

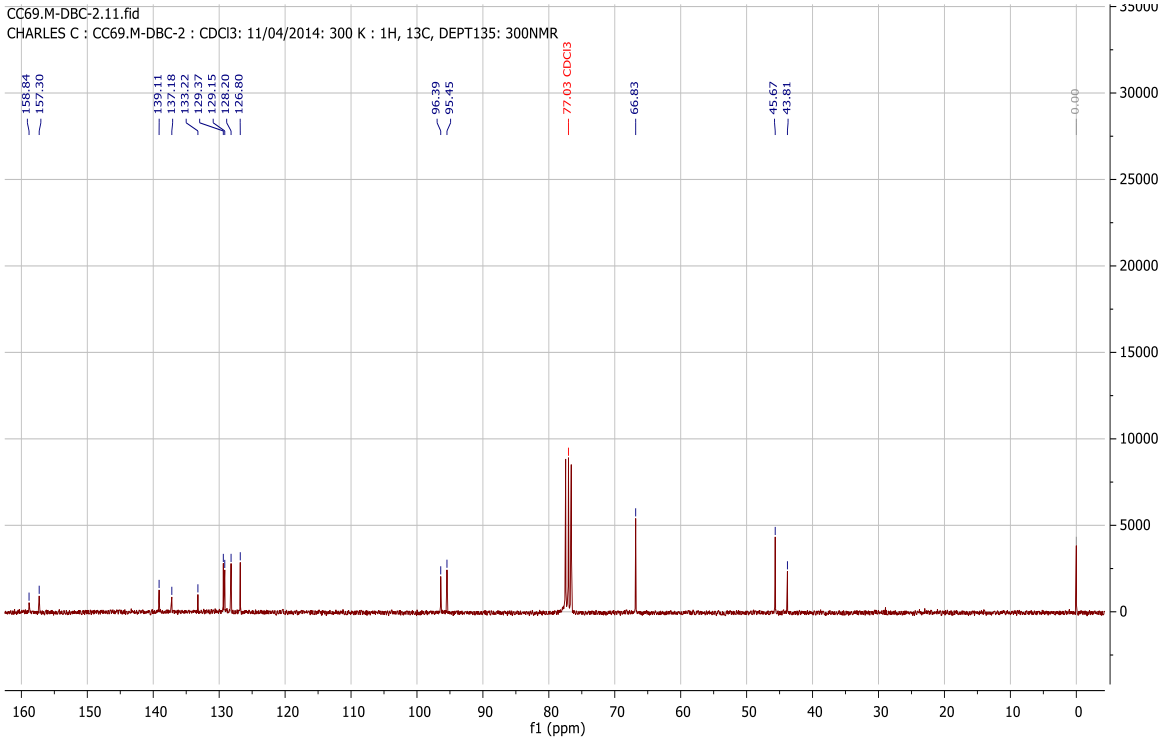
CC69.M-DBC-2.11.fid
CHARLES C : CC69.M-DBC-2 : CDCl3: 11/04/2014: 300 K : 1H, 13C, DEPT135: 300NMR
158.84
157.30
139.11
137.18
133.22
129.37
129.15
128.20
126.80
96.39
95.45
77.03 CDCl3
66.83
45.67
43.81
f1 (ppm)

143e

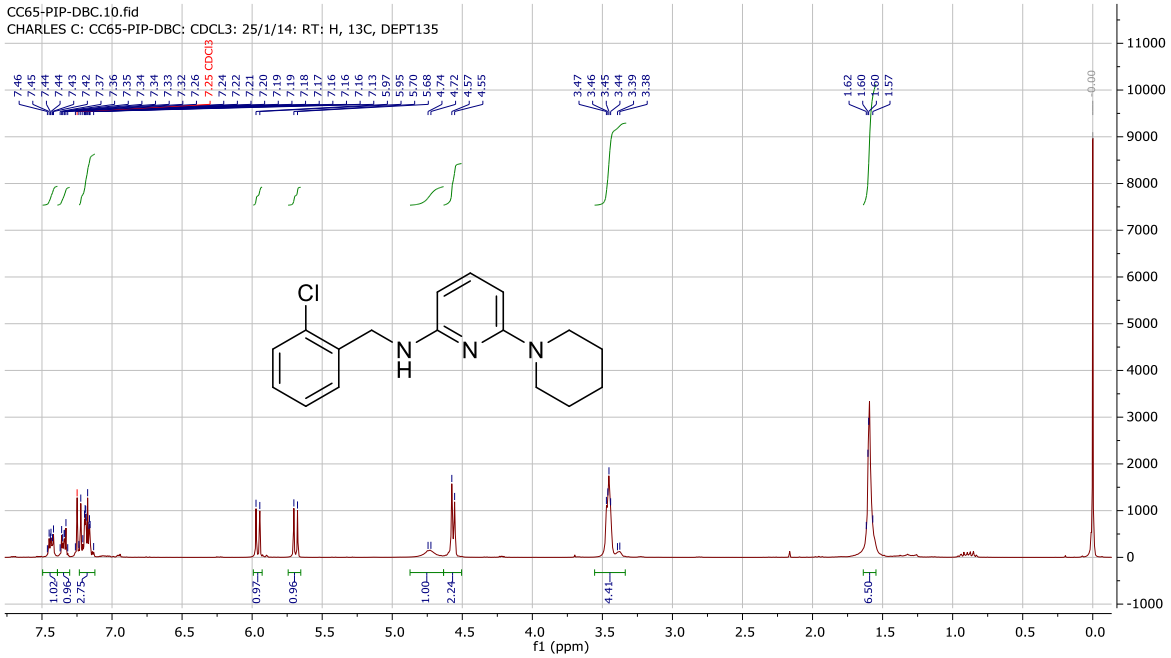
CC65-PIP-DBC.10.fid
CHARLES C: CC65-PIP-DBC: CDCL3: 25/1/14: RT: H, 13C, DEPT135
Cl
N
H
N
N
f1 (ppm)

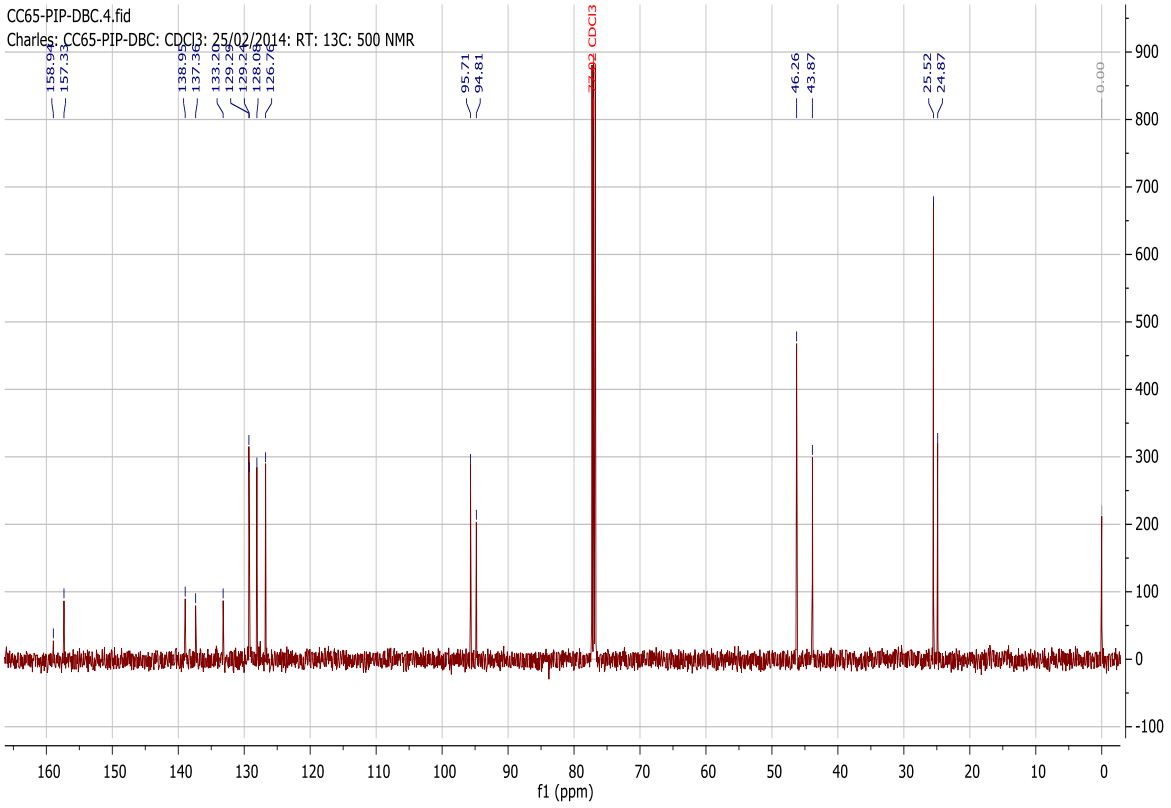
CC65-PIP-DBC.4.fid
Charles: CC65-PIP-DBC: CDCl3: 25/02/2014: RT: 13C: 500 NMR
CDCl3
f1 (ppm)

144a

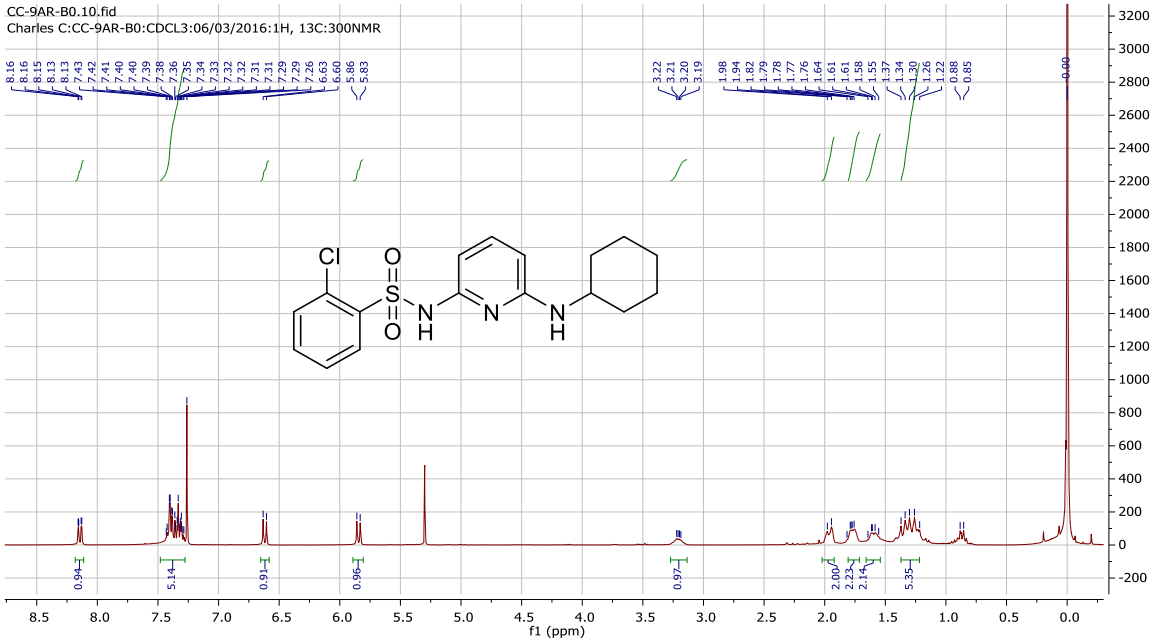
CC-9AR-B0.10.fid
Charles C:CC-9AR-B0:CDCL3:06/03/2016:1H, 13C:300NMR
Cl
O
S
O
N
H
N
N
H
f1 (ppm)

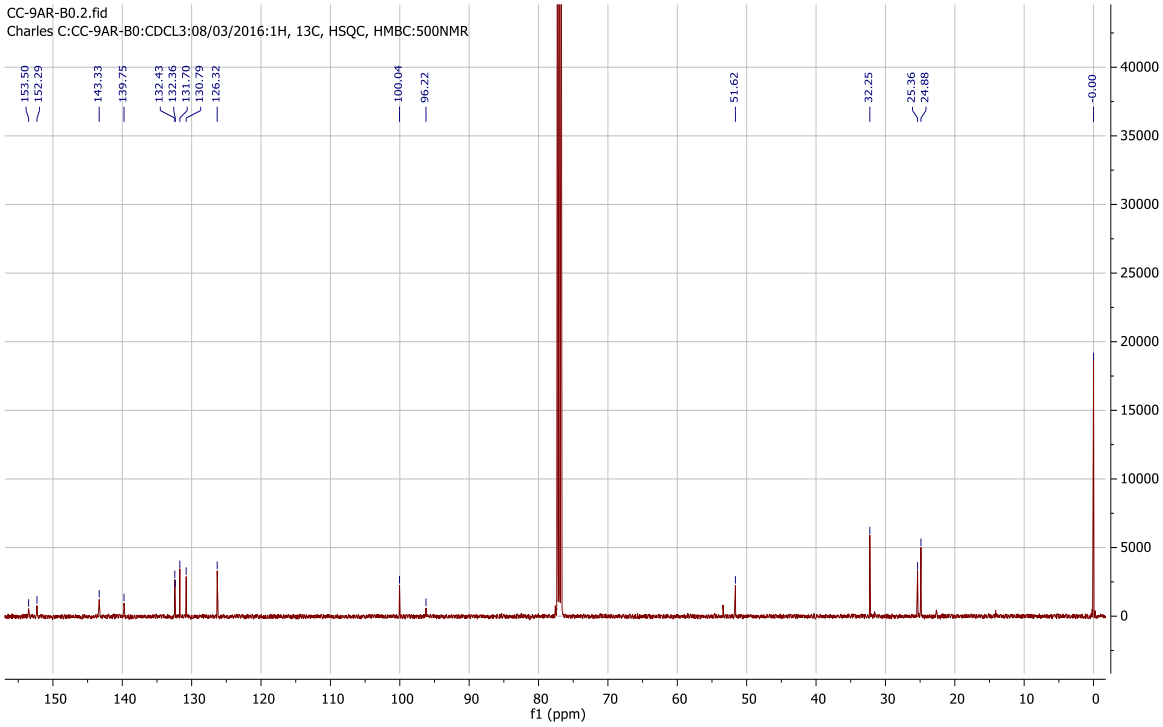
CC-9AR-B0.2.fid
Charles C:CC-9AR-B0:CDCL3:08/03/2016:1H, 13C, HSQC, HMBC:500NMR
f1 (ppm)

144b

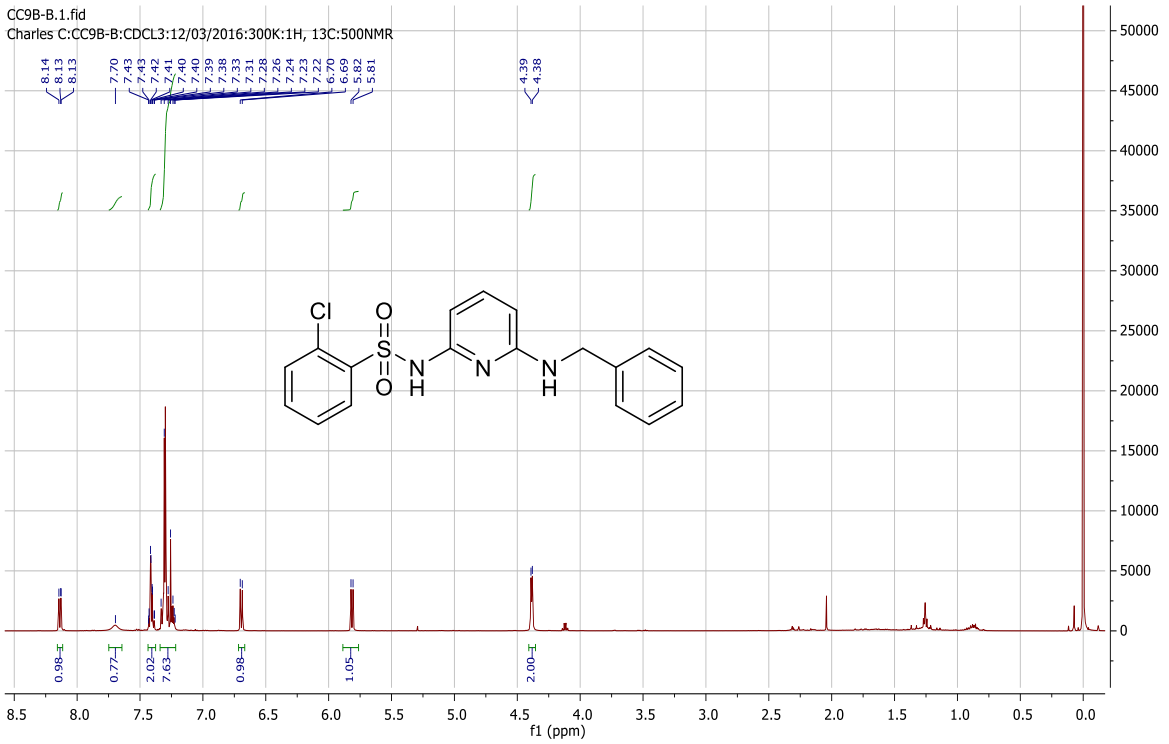
CC9B-B.1.fid
Charles C:CC9B-B:CDCL3:12/03/2016:300K:1H, 13C:500NMR
f1 (ppm)

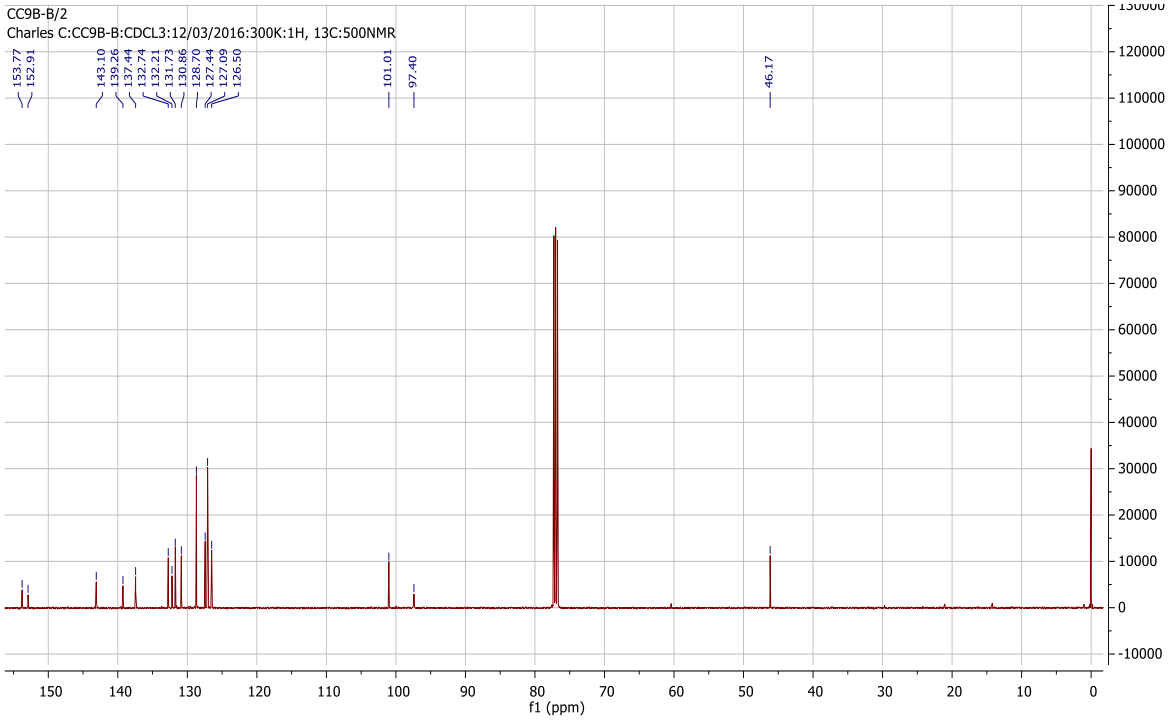
CC9B-B/2
Charles C:CC9B-B:CDCL3:12/03/2016:300K:1H, 13C:500NMR
f1 (ppm)

144c

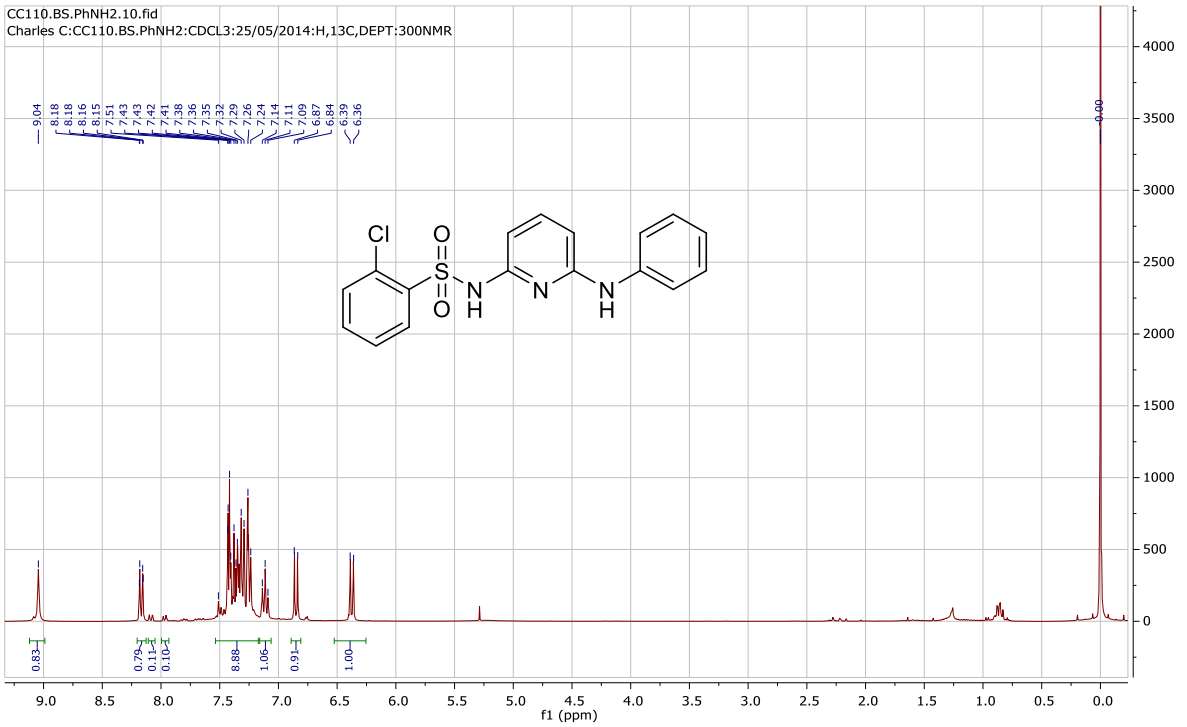
CC110.BS.PhNH2.10.fid
Charles C:CC110.BS.PhNH2:CDCL3:25/05/2014:H,13C,DEPT:300NMR
9.04
8.18
8.18
8.16
8.15
7.51
7.43
7.43
7.42
7.41
7.38
7.36
7.35
7.32
7.29
7.26
7.24
7.14
7.11
7.09
6.87
6.84
6.39
6.36
0.00
Cl
O
S
O
N
H
N
N
H
0.83
0.79
0.11
0.10
8.88
1.06
0.91
1.00
f1 (ppm)

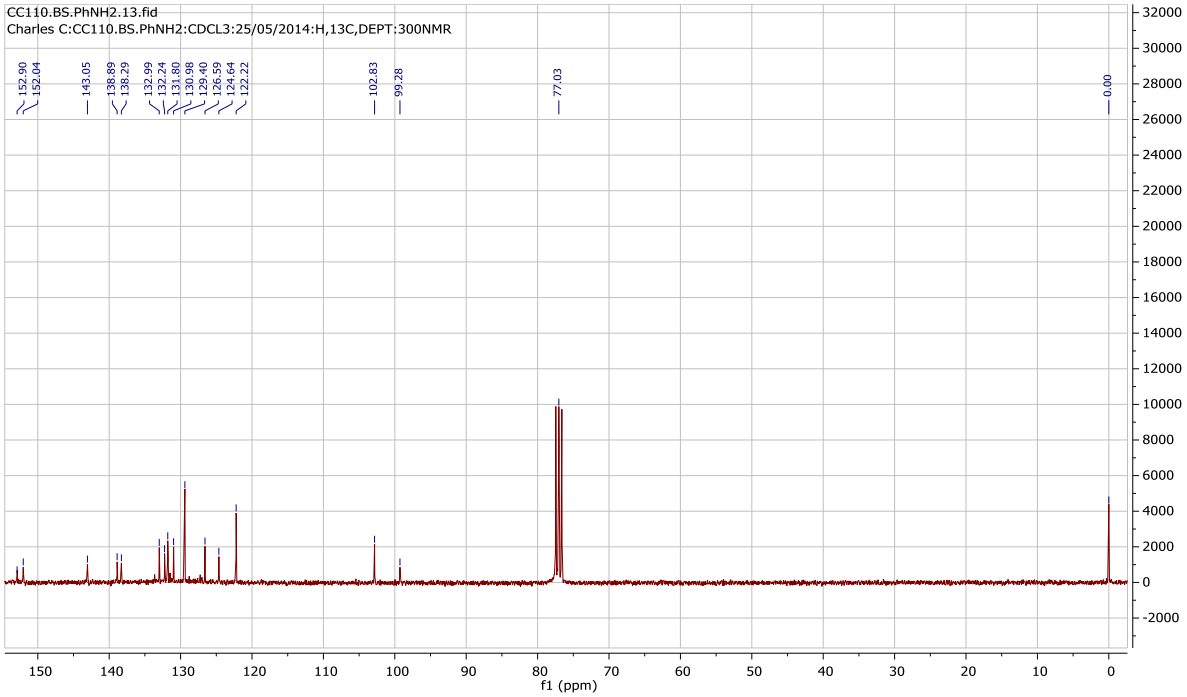
CC110.BS.PhNH2.13.fid
Charles C:CC110.BS.PhNH2:CDCL3:25/05/2014:H,13C,DEPT:300NMR
152.90
152.04
143.05
138.89
138.29
132.99
132.24
131.80
130.98
129.40
126.59
124.64
122.22
102.83
99.28
77.03
0.00
f1 (ppm)

144d

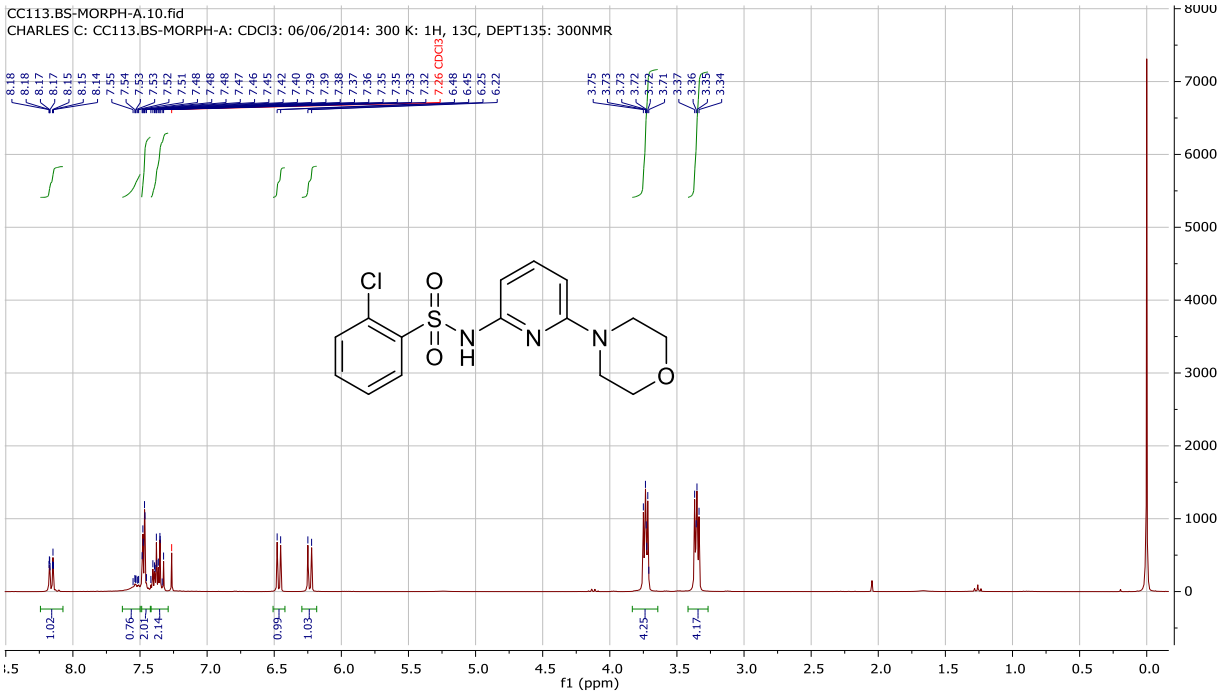
CC113.BS-MORPH-A.10.fid
CHARLES C: CC113.BS-MORPH-A: CDCl3: 06/06/2014: 300 K: 1H, 13C, DEPT135: 300NMR
f1 (ppm)

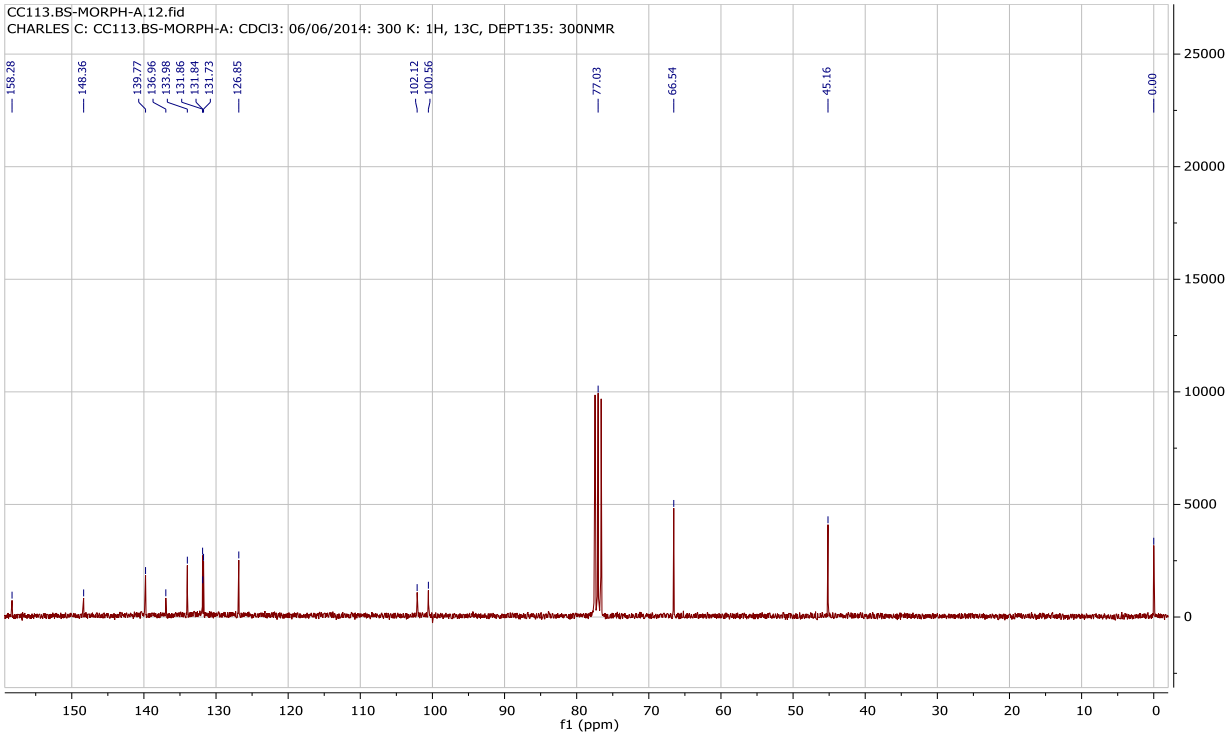
CC113.BS-MORPH-A.12.fid
CHARLES C: CC113.BS-MORPH-A: CDCl3: 06/06/2014: 300 K: 1H, 13C, DEPT135: 300NMR
f1 (ppm)

144e


CC-09E.1.fid
Charles C:CC-09E:CDCL3:28/05/2014:300K H,13C:500NMR
f1 (ppm)

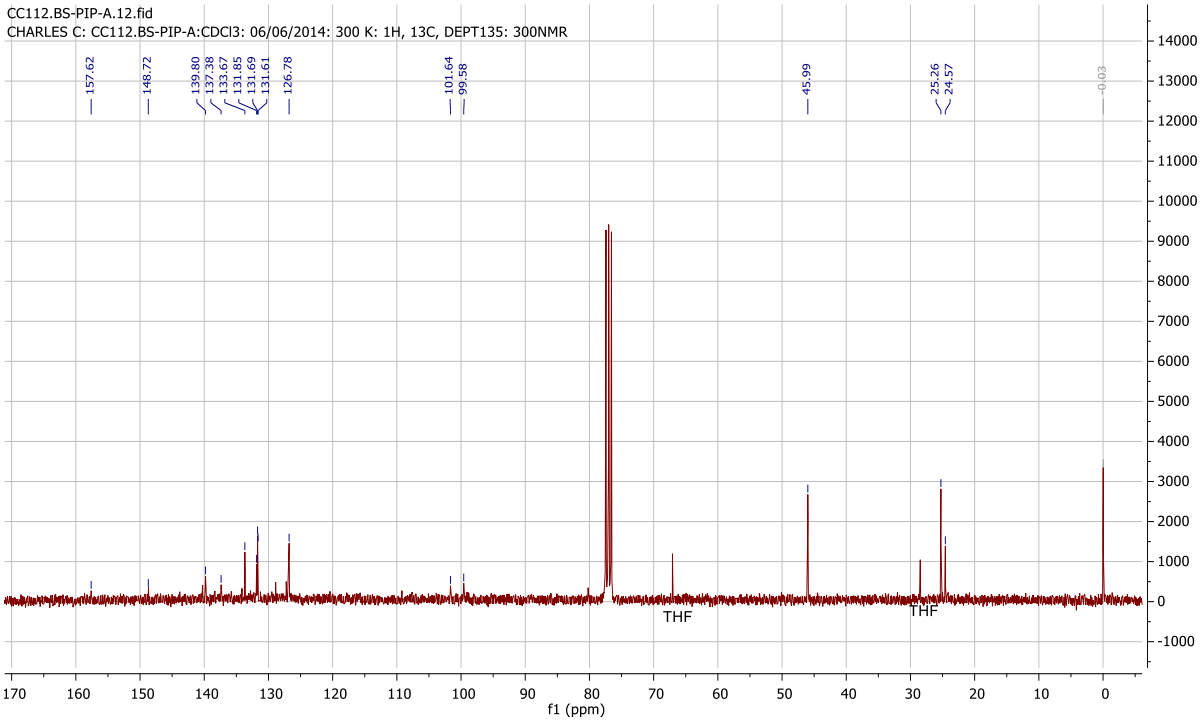
CC112.BS-PIP-A.12.fid
CHARLES C: CC112.BS-PIP-A:CDCl3: 06/06/2014: 300 K: 1H, 13C, DEPT135: 300NMR
THF
THF
f1 (ppm)

144f

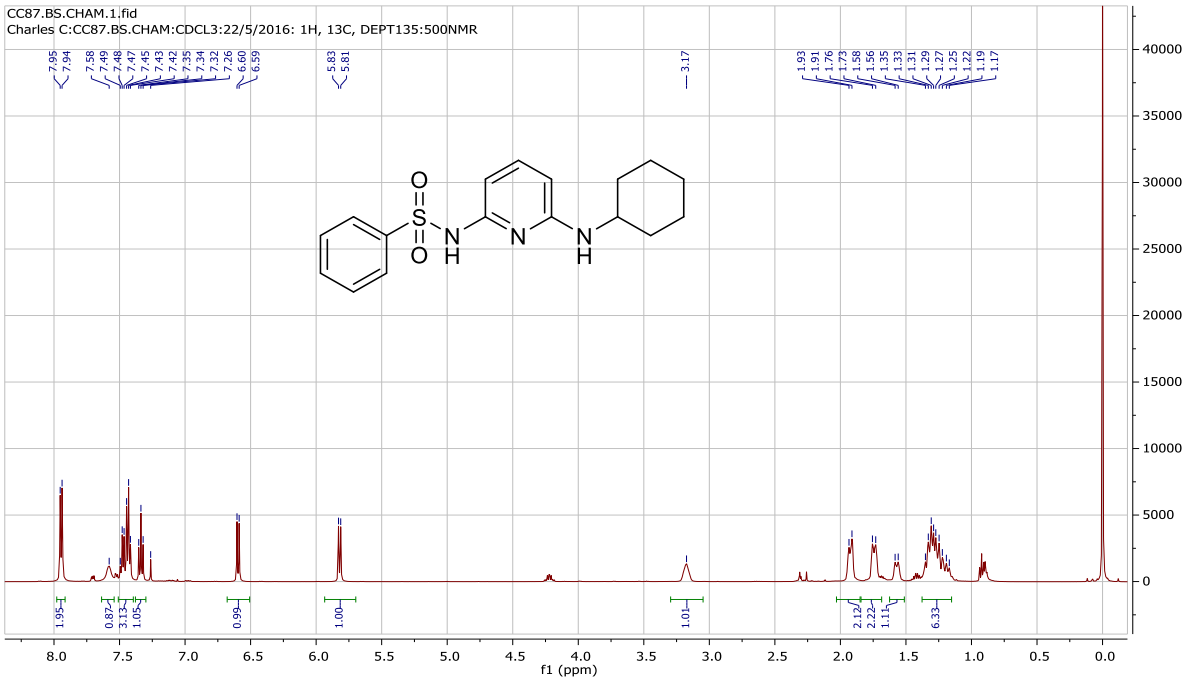
CC87.BS.CHAM.1.fid
Charles C:CC87.BS.CHAM:CDCL3:22/5/2016: 1H, 13C, DEPT135:500NMR
f1 (ppm)

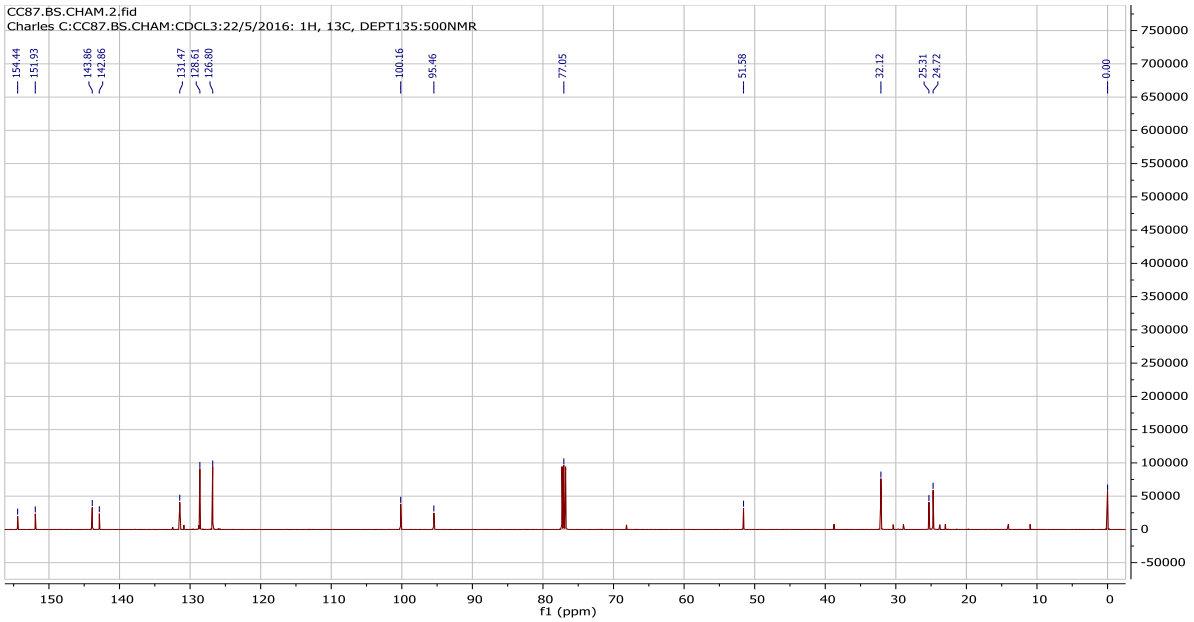
CC87.BS.CHAM.2.fid
Charles C:CC87.BS.CHAM:CDCL3:22/5/2016: 1H, 13C, DEPT135:500NMR
f1 (ppm)

144g

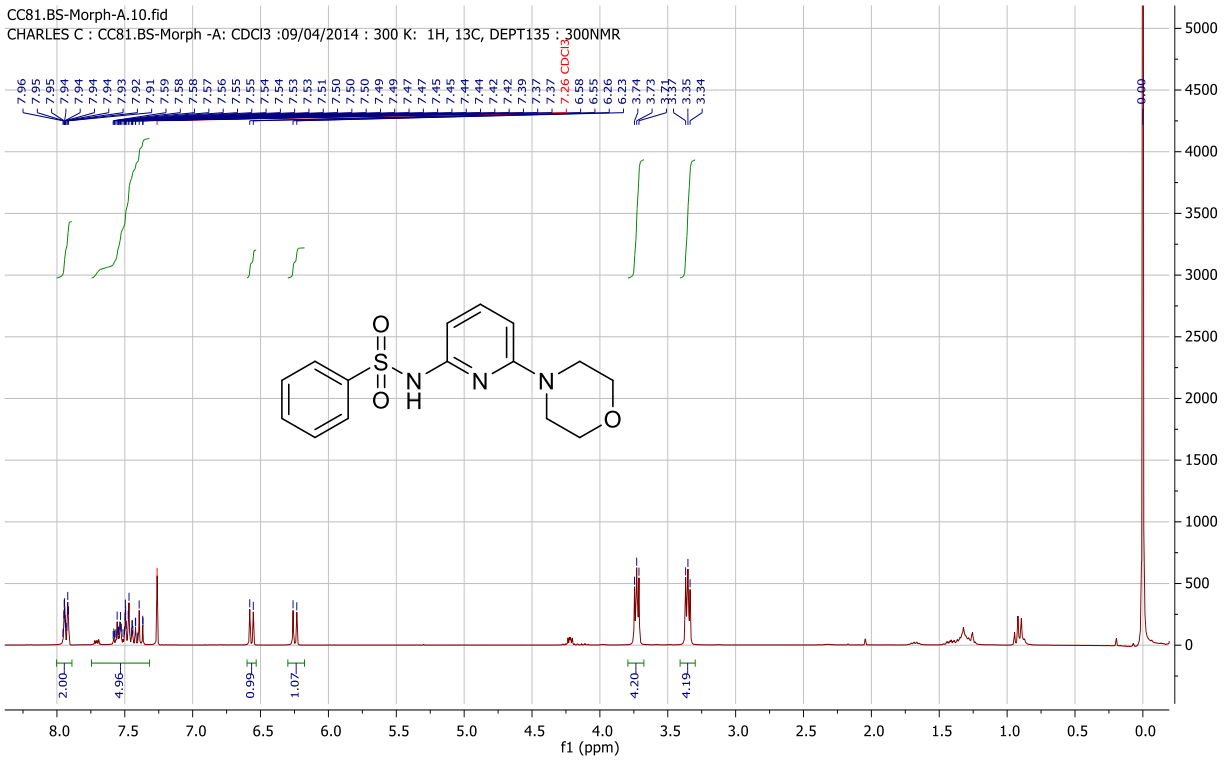
CC81.BS-Morph-A.10.fid
CHARLES C : CC81.BS-Morph -A: CDCl3 :09/04/2014 : 300 K: 1H, 13C, DEPT135 : 300NMR
f1 (ppm)

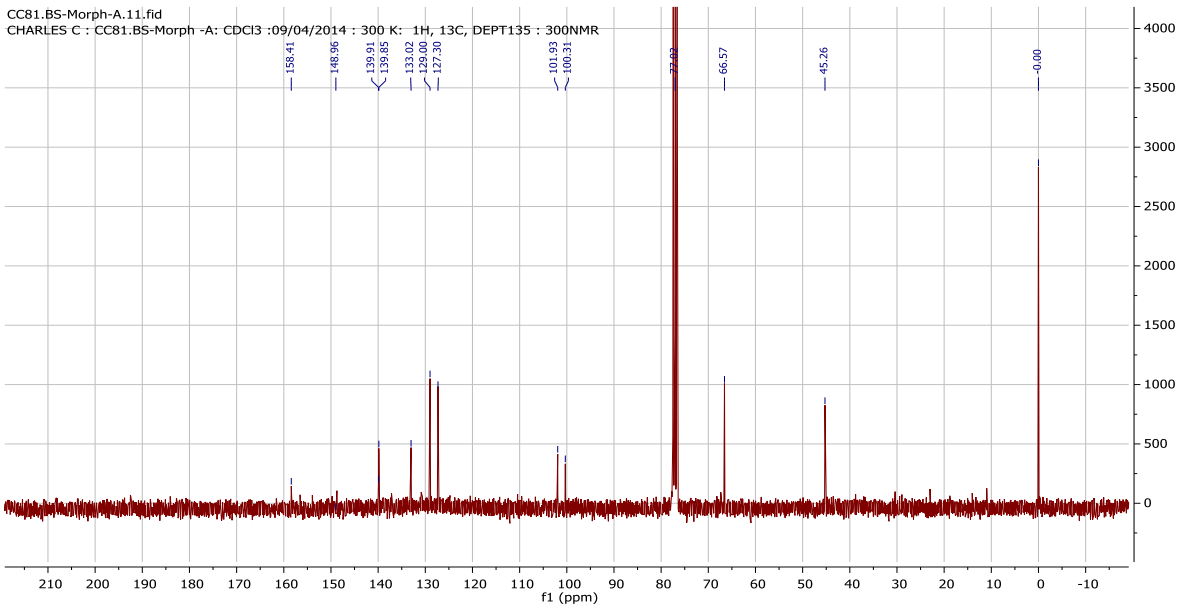
CC81.BS-Morph-A.11.fid
CHARLES C : CC81.BS-Morph -A: CDCl3 :09/04/2014 : 300 K: 1H, 13C, DEPT135 : 300NMR
f1 (ppm)

144h

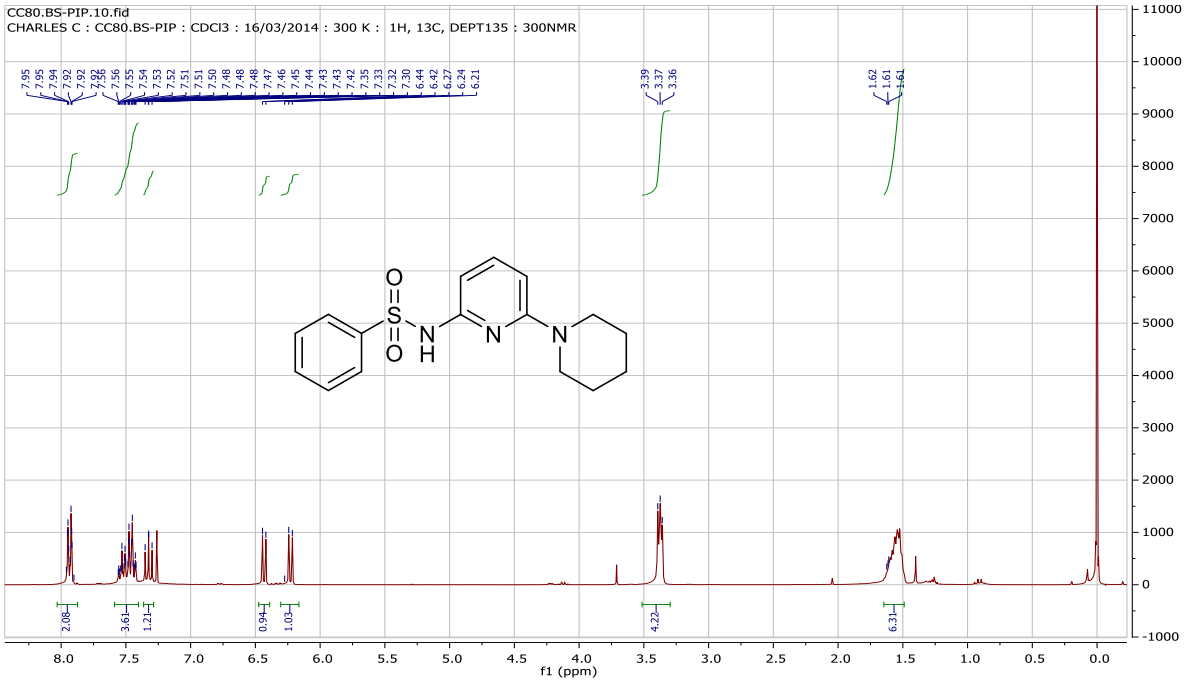
CC80.BS-PIP.10.fid
CHARLES C : CC80.BS-PIP : CDCl3 : 16/03/2014 : 300 K : 1H, 13C, DEPT135 : 300NMR
f1 (ppm)

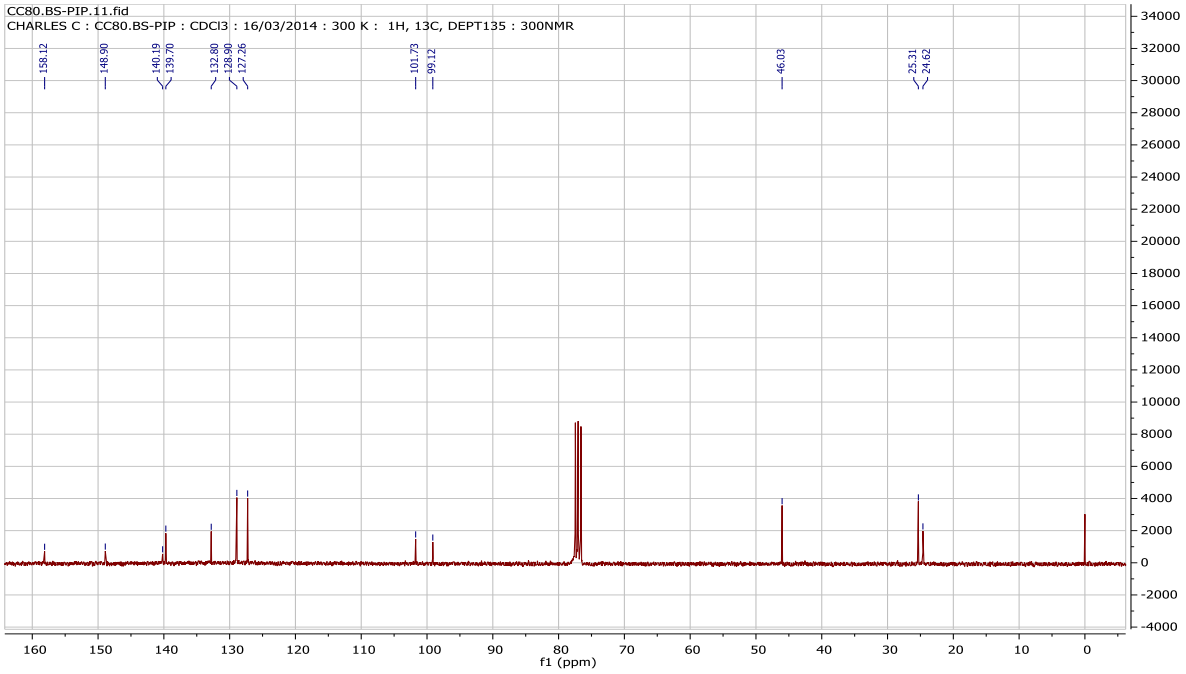
CC80.BS-PIP.11.fid
CHARLES C : CC80.BS-PIP : CDCl3 : 16/03/2014 : 300 K : 1H, 13C, DEPT135 : 300NMR
f1 (ppm)

147a

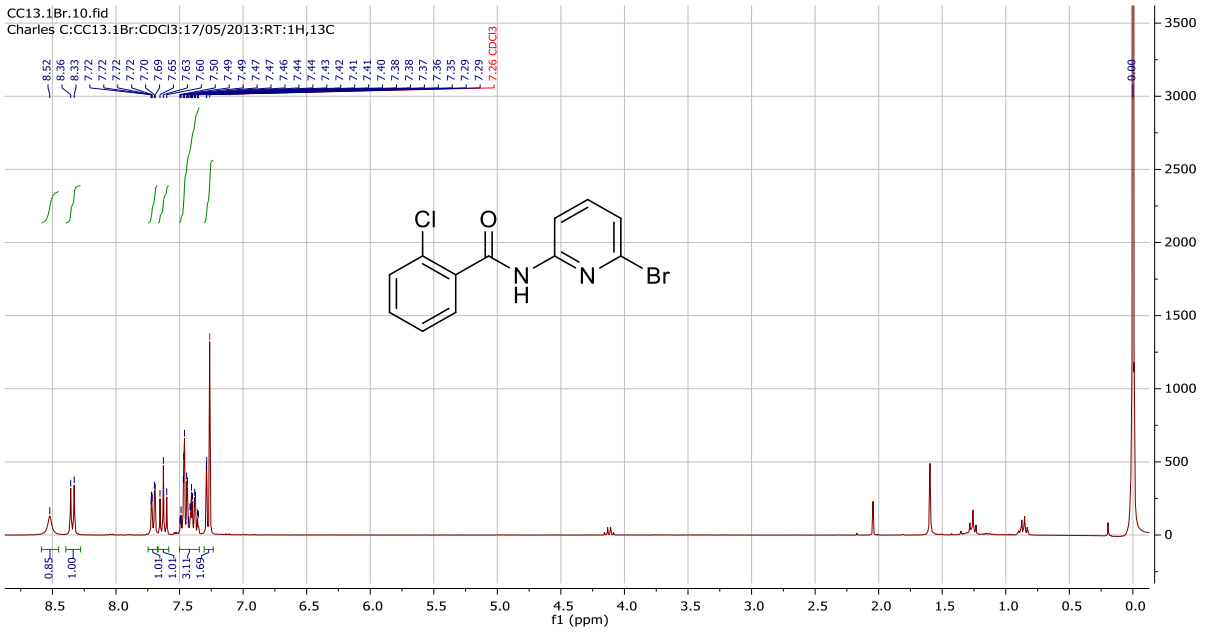
CC13.1Br.10.fid
Charles C:CC13.1Br:CDCl3:17/05/2013:RT:1H,13C
8.52
8.36
8.33
7.72
7.72
7.72
7.72
7.70
7.69
7.65
7.63
7.60
7.50
7.49
7.49
7.47
7.47
7.46
7.44
7.44
7.43
7.42
7.41
7.41
7.40
7.38
7.38
7.37
7.36
7.35
7.29
7.29
7.26 CDCl3
0.00
Cl
O
N
H
N
Br
0.85
1.00
1.01
1.01
3.11
1.68
f1 (ppm)

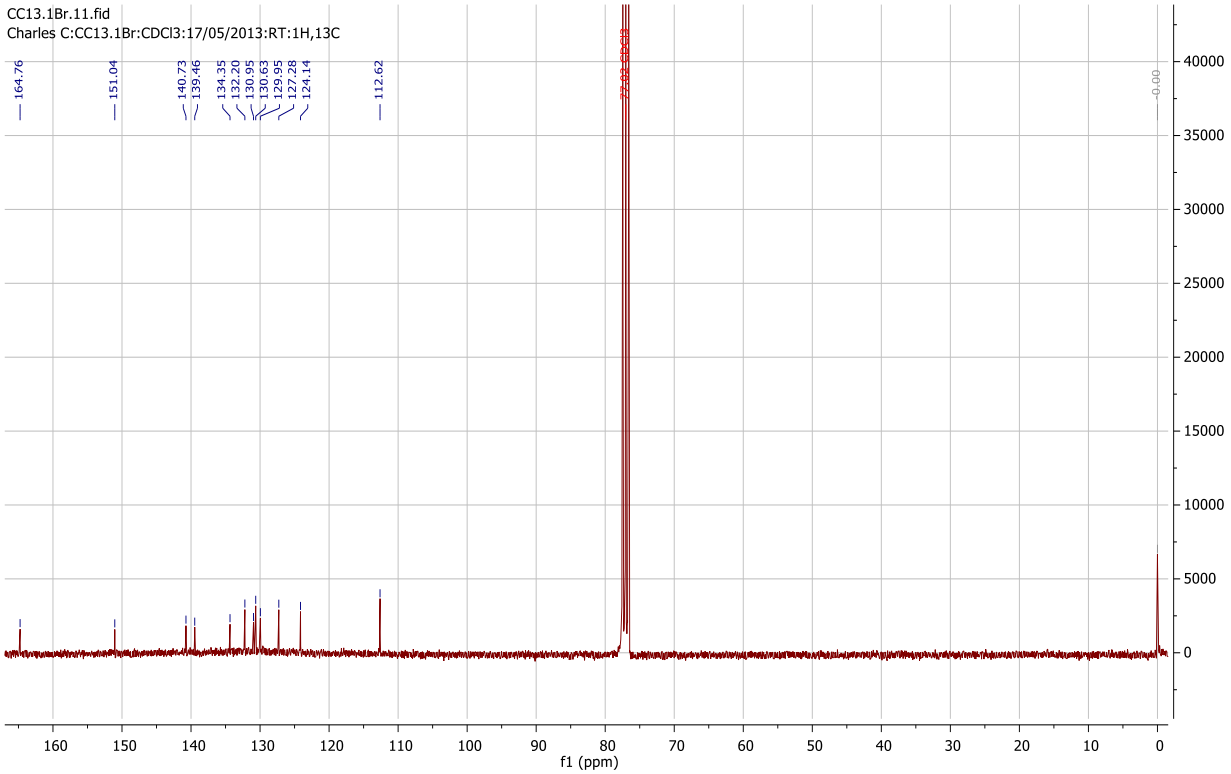
CC13.1Br.11.fid
Charles C:CC13.1Br:CDCl3:17/05/2013:RT:1H,13C
164.76
151.04
140.73
139.46
134.35
132.20
130.95
130.63
129.95
127.28
124.14
112.62
77.00 CDCl3
0.00
f1 (ppm)

147b

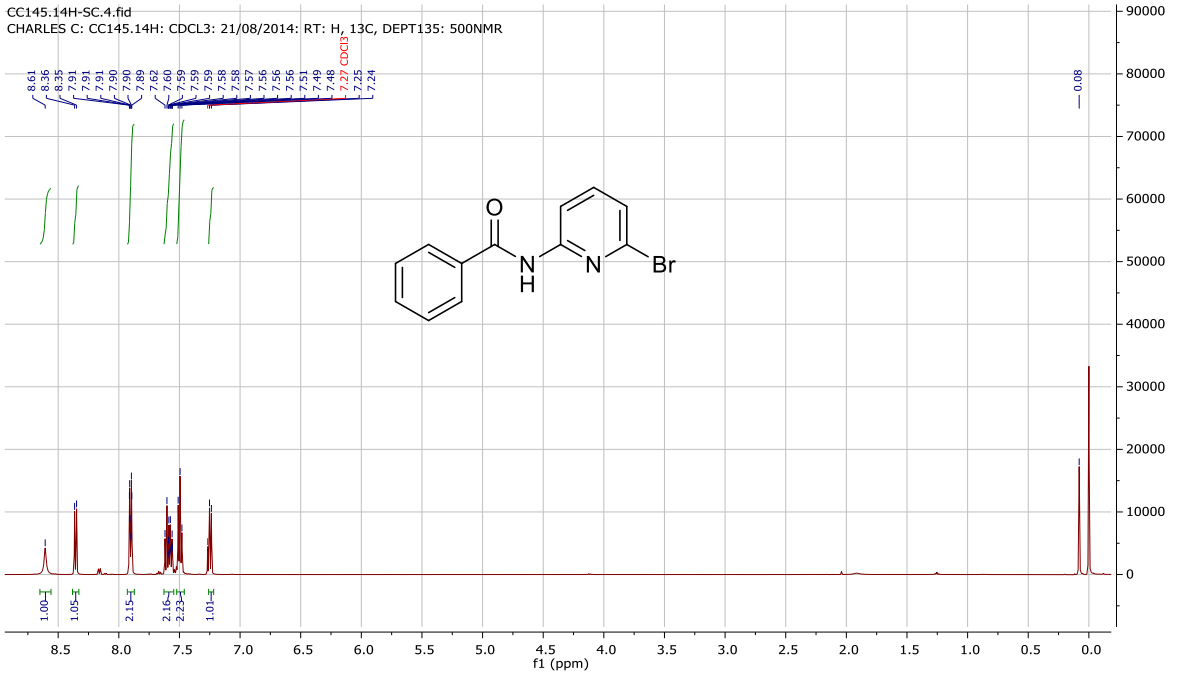
CC145.14H-SC.4.fid
CHARLES C: CC145.14H: CDCL3: 21/08/2014: RT: H, 13C, DEPT135: 500NMR
8.61
8.36
8.35
7.91
7.91
7.91
7.90
7.90
7.89
7.62
7.60
7.59
7.59
7.59
7.58
7.58
7.57
7.56
7.56
7.56
7.51
7.49
7.48
7.27 CDCl3
7.25
7.24
0.08
O
N
H
N
Br
1.00
1.05
2.15
2.16
2.23
1.01
f1 (ppm)

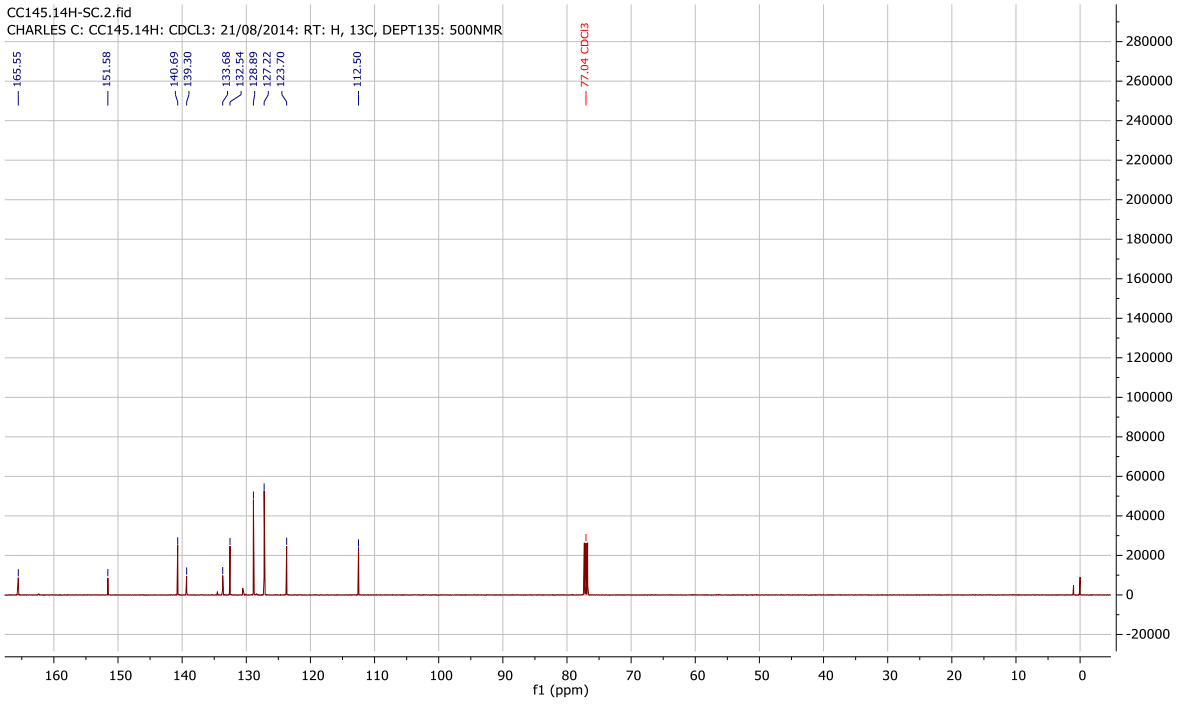
CC145.14H-SC.2.fid
CHARLES C: CC145.14H: CDCL3: 21/08/2014: RT: H, 13C, DEPT135: 500NMR
165.55
151.58
140.69
139.30
133.68
132.54
128.89
127.22
123.70
112.50
77.04 CDCl3
f1 (ppm)

147c

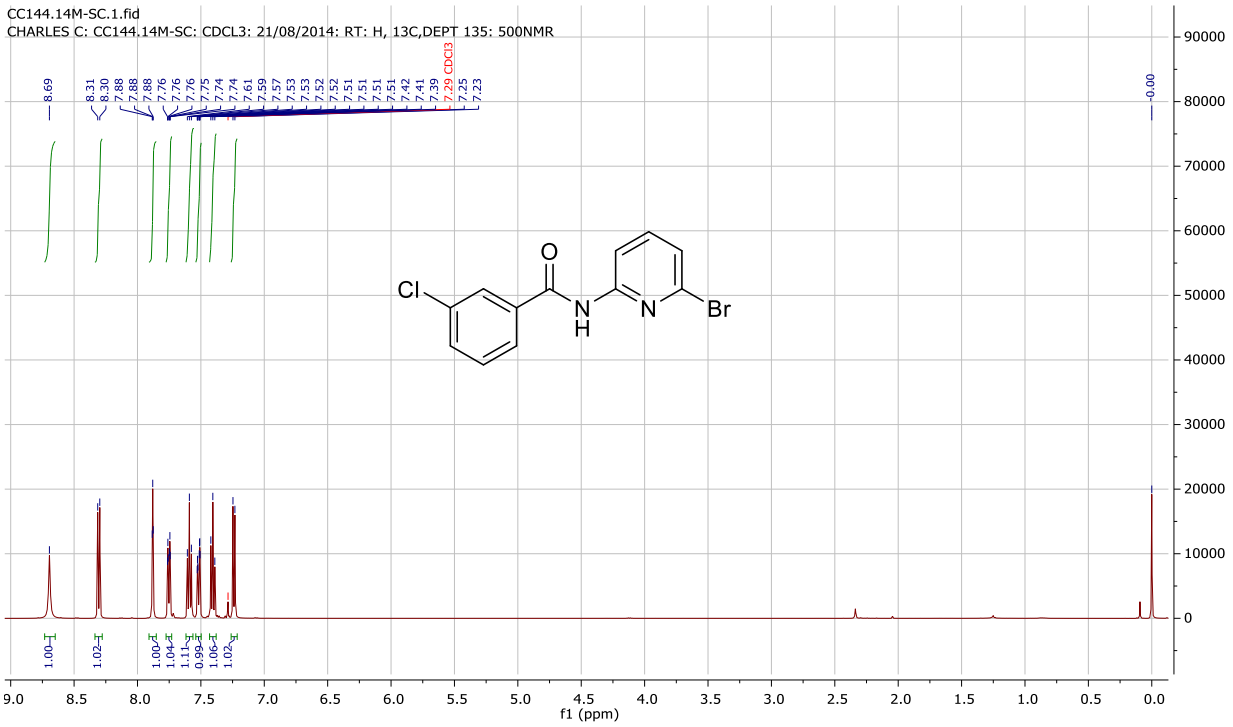
CC144.14M-SC.1.fid
CHARLES C: CC144.14M-SC: CDCL3: 21/08/2014: RT: H, 13C,DEPT 135: 500NMR
8.69
8.31
8.30
7.88
7.88
7.88
7.76
7.76
7.76
7.75
7.74
7.74
7.61
7.59
7.57
7.53
7.52
7.51
7.51
7.51
7.42
7.41
7.39
7.29 CDCl3
7.25
7.23
0.00
Cl
O
N
H
N
Br
1.00
1.02
1.00
1.04
1.11
0.99
1.06
1.02
f1 (ppm)

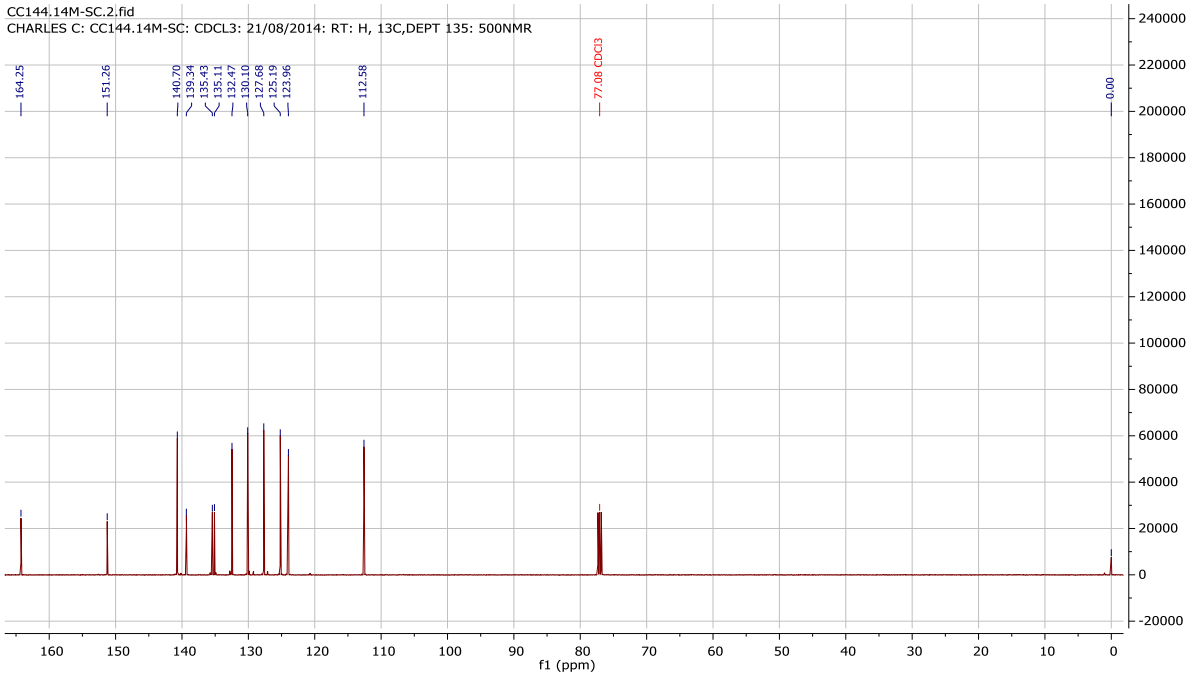
CC144.14M-SC.2.fid
CHARLES C: CC144.14M-SC: CDCL3: 21/08/2014: RT: H, 13C,DEPT 135: 500NMR
164.25
151.26
140.70
139.34
135.43
135.11
132.47
130.10
127.68
125.19
123.96
112.58
77.08 CDCl3
0.00
f1 (ppm)

147d

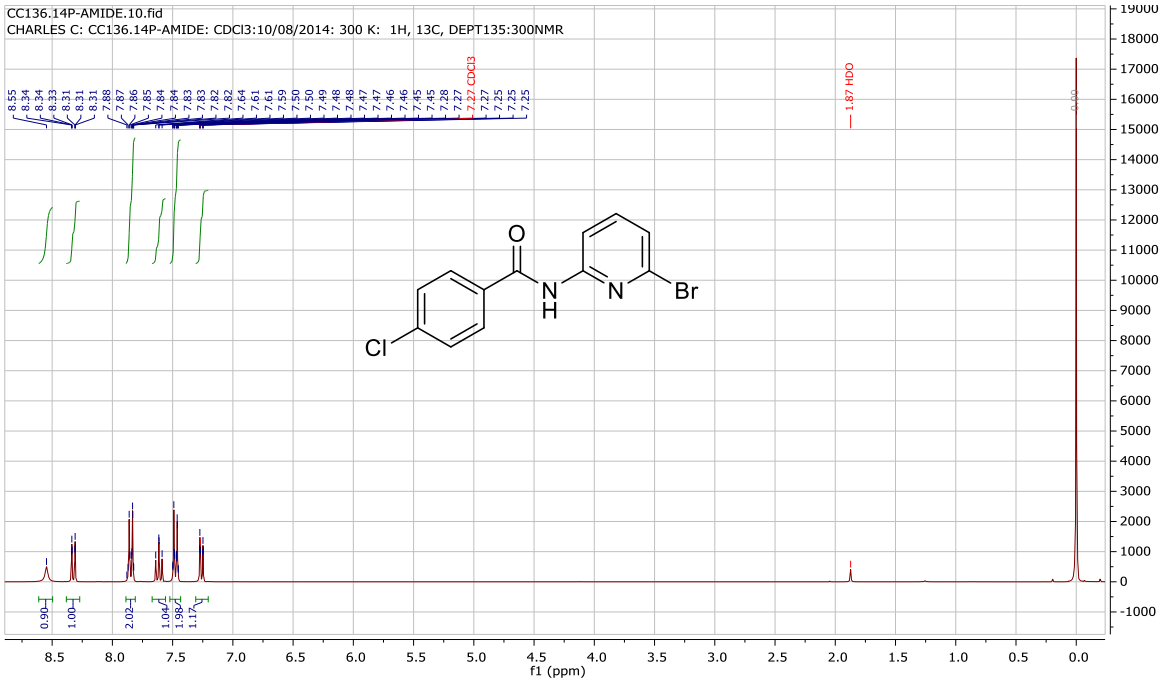
CC136.14P-AMIDE.10.fid
CHARLES C: CC136.14P-AMIDE: CDCl3:10/08/2014: 300 K: 1H, 13C, DEPT135:300NMR
CDCl3
1.87 HDO
O
N
H
N
Br
Cl
f1 (ppm)

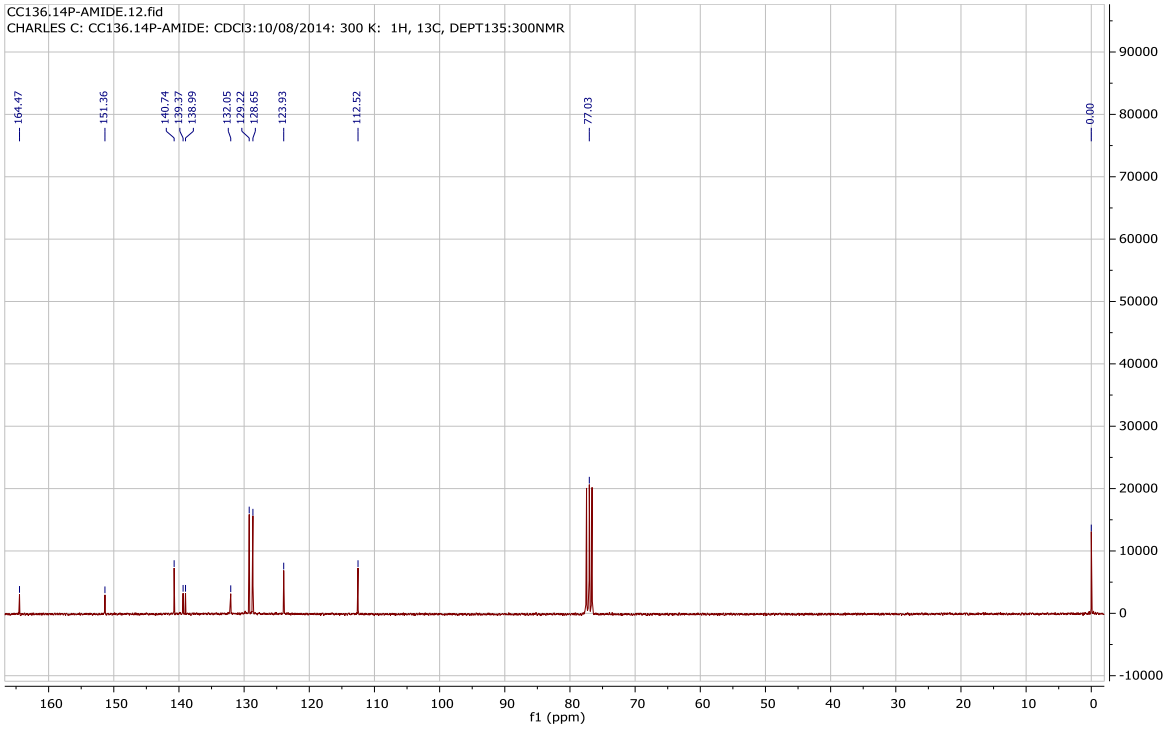
CC136.14P-AMIDE.12.fid
CHARLES C: CC136.14P-AMIDE: CDCl3:10/08/2014: 300 K: 1H, 13C, DEPT135:300NMR
164.47
151.36
140.74
139.37
138.99
132.05
129.22
128.65
123.93
112.52
77.03
0.00
f1 (ppm)

147e

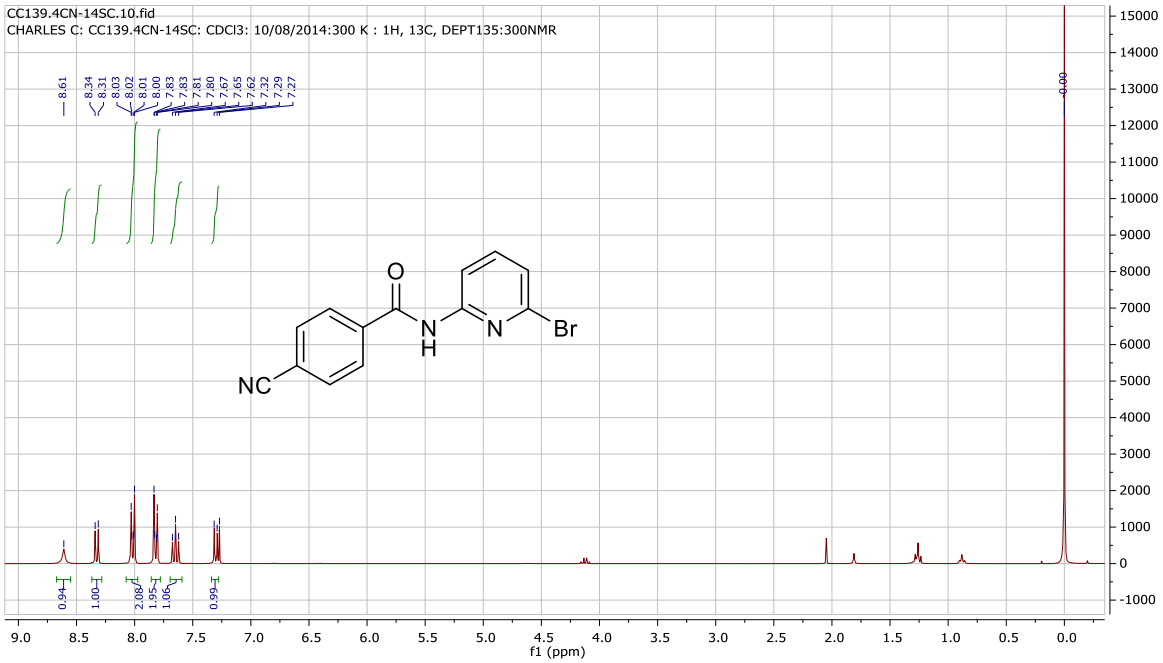
CC139.4CN-14SC.10.fid
CHARLES C: CC139.4CN-14SC: CDCl3: 10/08/2014:300 K : 1H, 13C, DEPT135:300NMR
8.61
8.34
8.31
8.03
8.02
8.01
8.00
7.83
7.83
7.81
7.80
7.67
7.65
7.62
7.32
7.29
7.27
0.00
0.94
1.00
2.08
1.95
1.06
0.99
O
N
H
N
Br
NC
f1 (ppm)

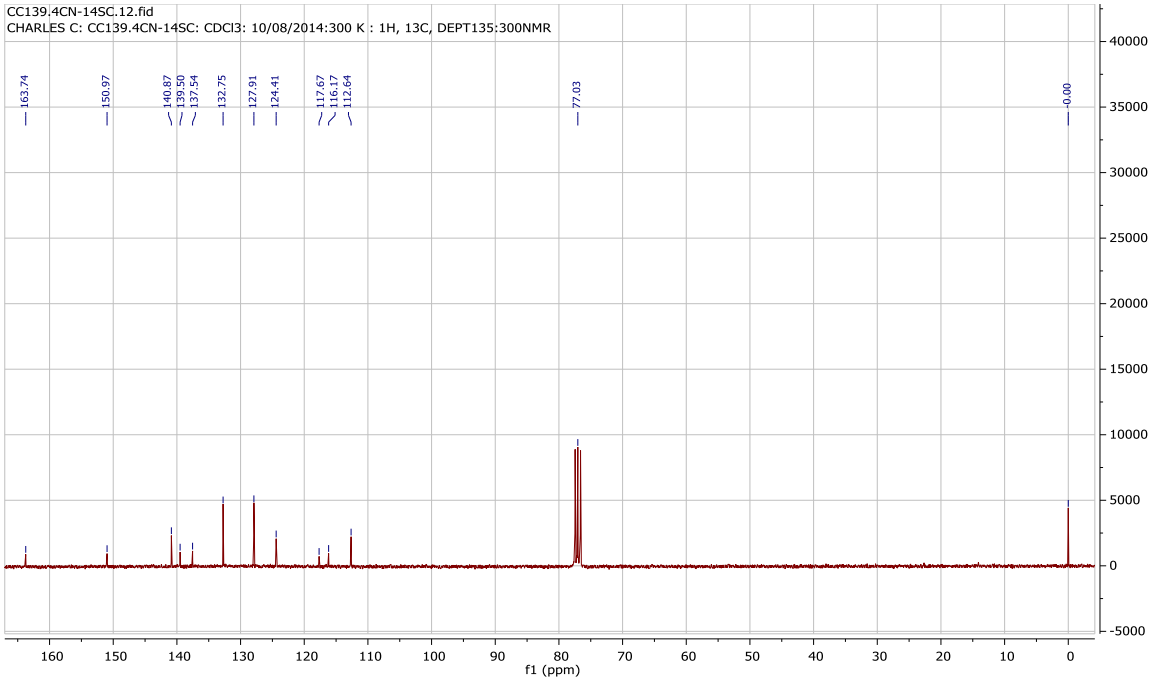
CC139.4CN-14SC.12.fid
CHARLES C: CC139.4CN-14SC: CDCl3: 10/08/2014:300 K : 1H, 13C, DEPT135:300NMR
163.74
150.97
140.87
139.50
137.54
132.75
127.91
124.41
117.67
116.17
112.64
77.03
0.00
f1 (ppm)

147f

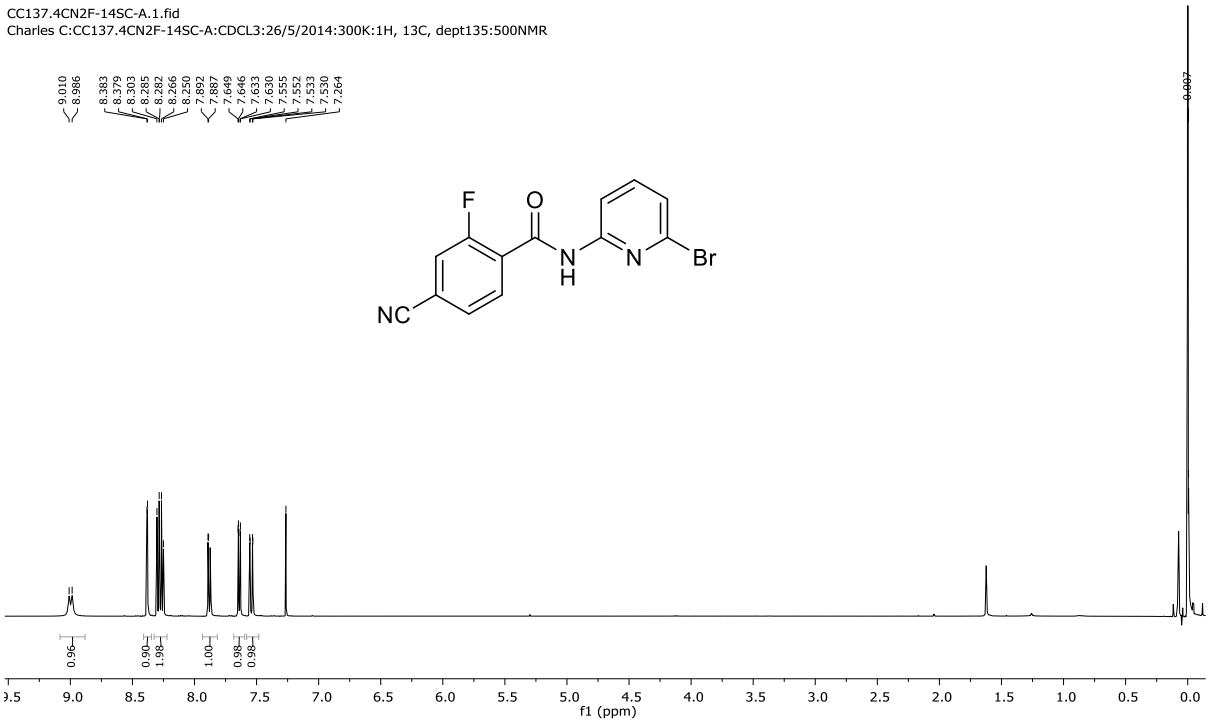
CC137.4CN2F-14SC-A.1.fid
Charles C:CC137.4CN2F-14SC-A:CDCL3:26/5/2014:300K:1H, 13C, dept135:500NMR
9.010
8.986
8.383
8.379
8.303
8.285
8.282
8.266
8.250
7.892
7.887
7.649
7.646
7.633
7.630
7.555
7.552
7.533
7.530
7.264
0.007
F
O
N
H
N
Br
NC
0.96
0.90
1.98
1.00
0.98
0.98
f1 (ppm)

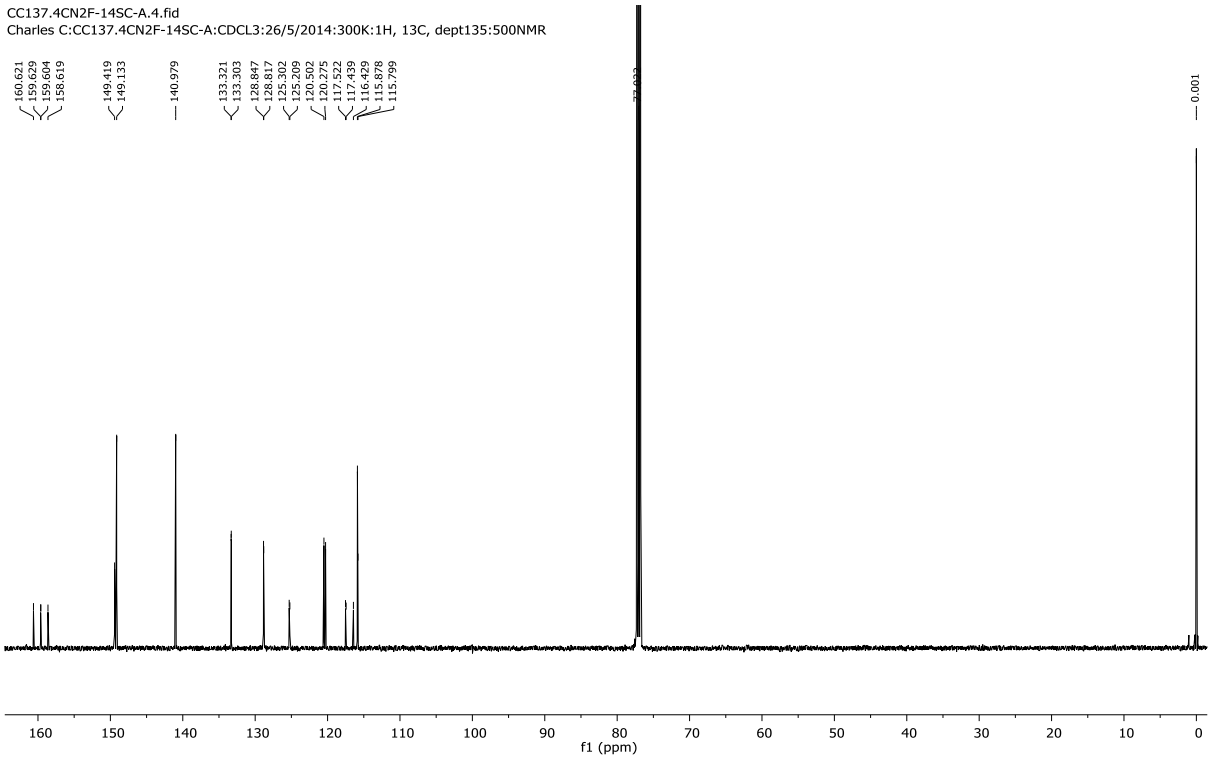
CC137.4CN2F-14SC-A.4.fid
Charles C:CC137.4CN2F-14SC-A:CDCL3:26/5/2014:300K:1H, 13C, dept135:500NMR
160.621
159.629
159.604
158.619
149.419
149.133
140.979
133.321
133.303
128.847
128.817
125.302
125.209
120.502
120.275
117.522
117.439
116.429
115.878
115.799
77.033
0.001
f1 (ppm)

147g

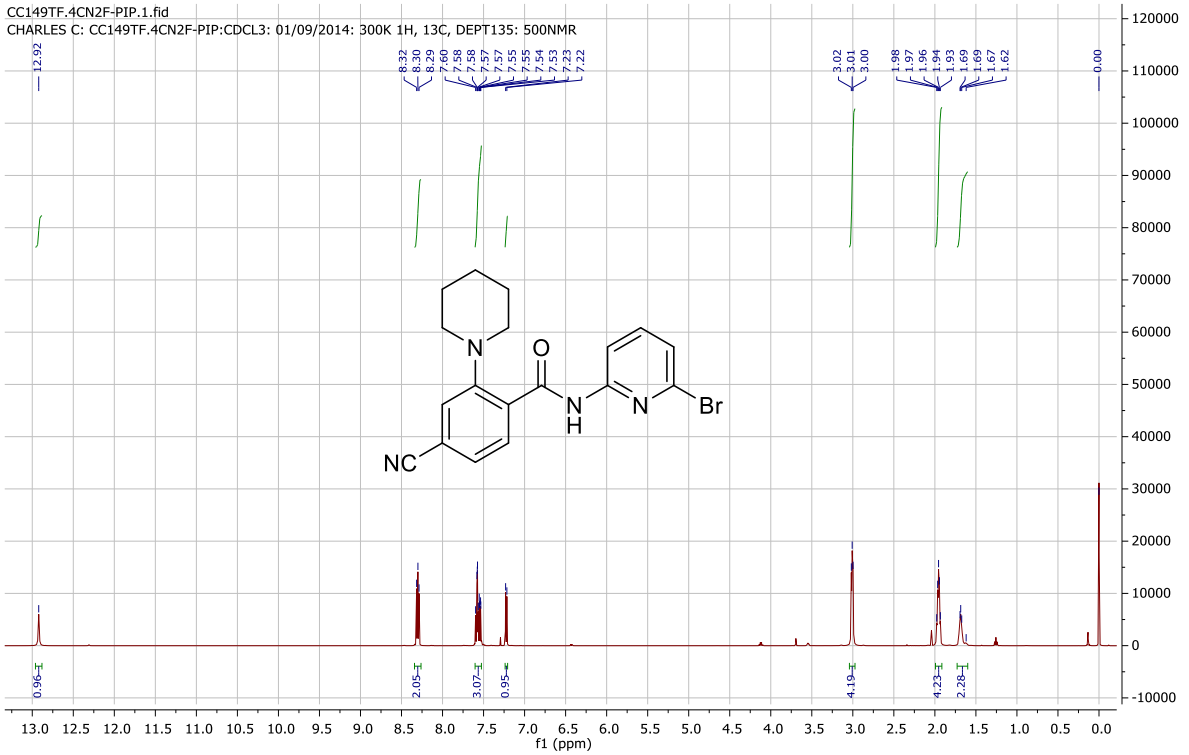
CC149TF.4CN2F-PIP.1.fid
CHARLES C: CC149TF.4CN2F-PIP:CDCL3: 01/09/2014: 300K 1H, 13C, DEPT135: 500NMR
12.92
8.32
8.30
8.29
7.60
7.58
7.58
7.57
7.57
7.55
7.55
7.54
7.54
7.53
7.23
7.22
3.02
3.01
3.00
1.98
1.97
1.96
1.94
1.93
1.69
1.69
1.67
1.62
0.00
0.96
2.05
3.07
0.95
4.19
4.23
2.28
f1 (ppm)

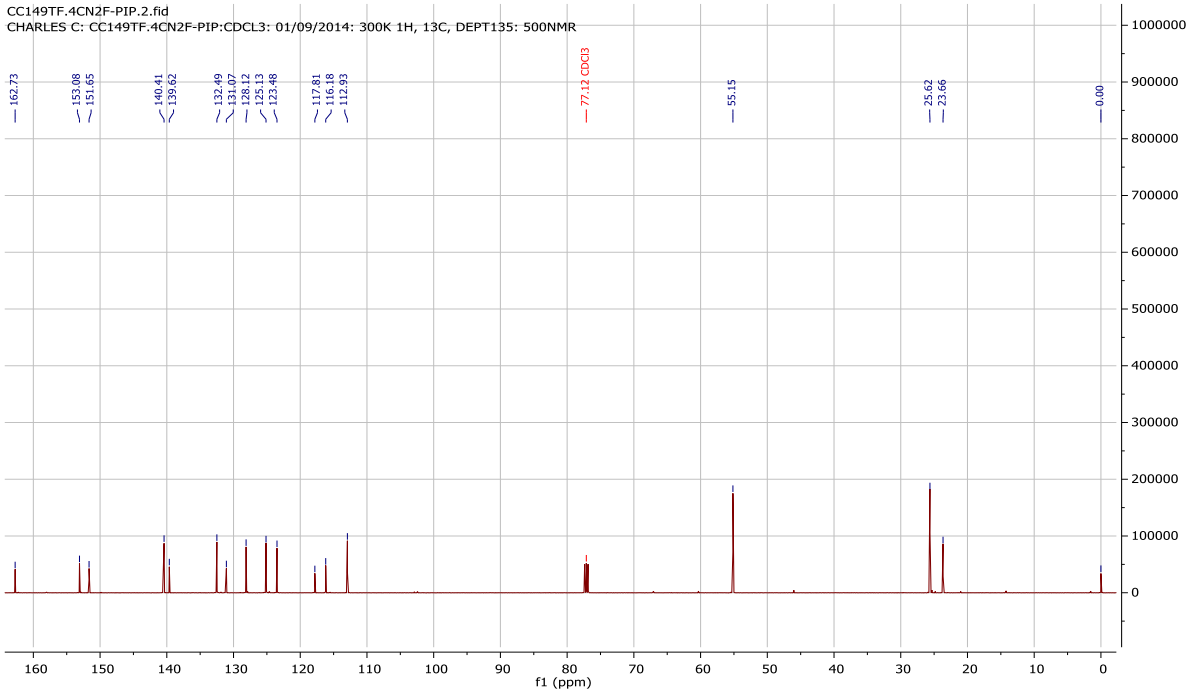
CC149TF.4CN2F-PIP.2.fid
CHARLES C: CC149TF.4CN2F-PIP:CDCL3: 01/09/2014: 300K 1H, 13C, DEPT135: 500NMR
162.73
153.08
151.65
140.41
139.62
132.49
131.07
128.12
125.13
123.48
117.81
116.18
112.93
77.12 CDCl3
55.15
25.62
23.66
0.00
f1 (ppm)

147i

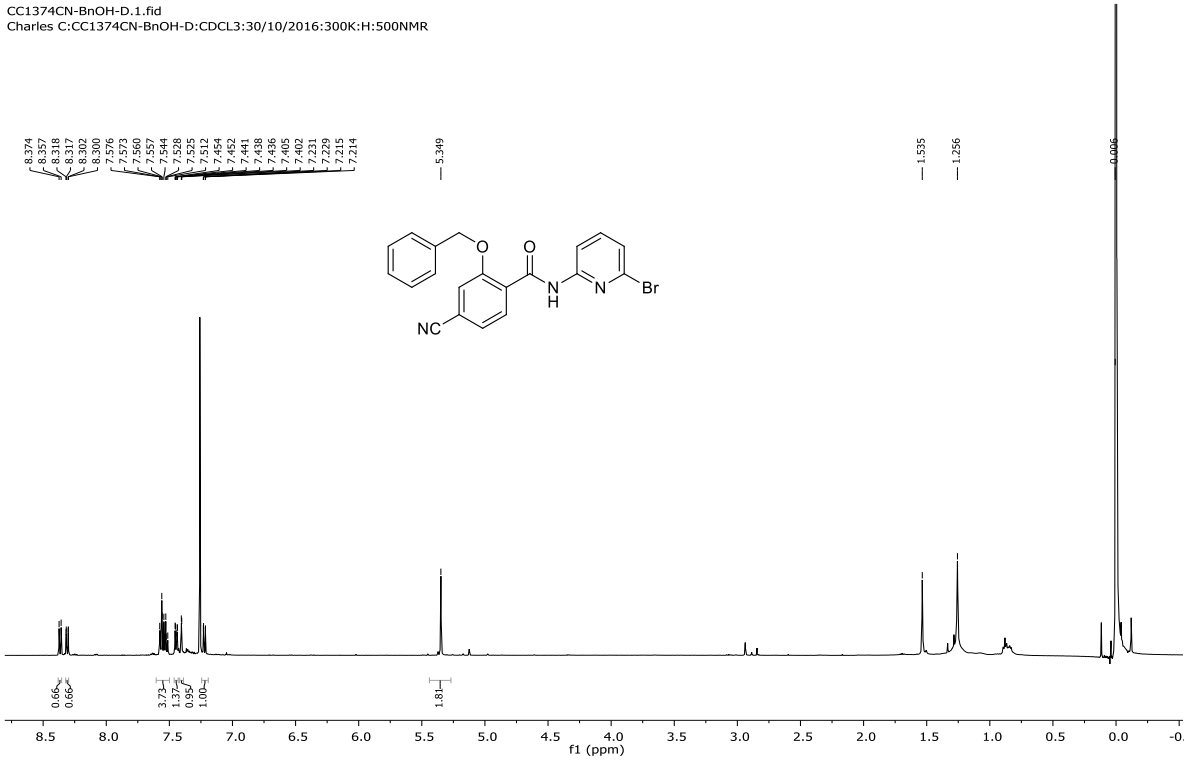
CC1374CN-BnOH-D.1.fid
Charles C:CC1374CN-BnOH-D:CDCL3:30/10/2016:300K:H:500NMR
8.374
8.357
8.318
8.317
8.302
8.300
7.576
7.573
7.560
7.557
7.544
7.528
7.525
7.512
7.454
7.452
7.441
7.438
7.436
7.405
7.402
7.231
7.229
7.215
7.214
5.349
1.535
1.256
0.006
O
O
N
H
N
Br
NC
0.66
0.66
3.73
1.37
0.95
1.00
1.81
f1 (ppm)

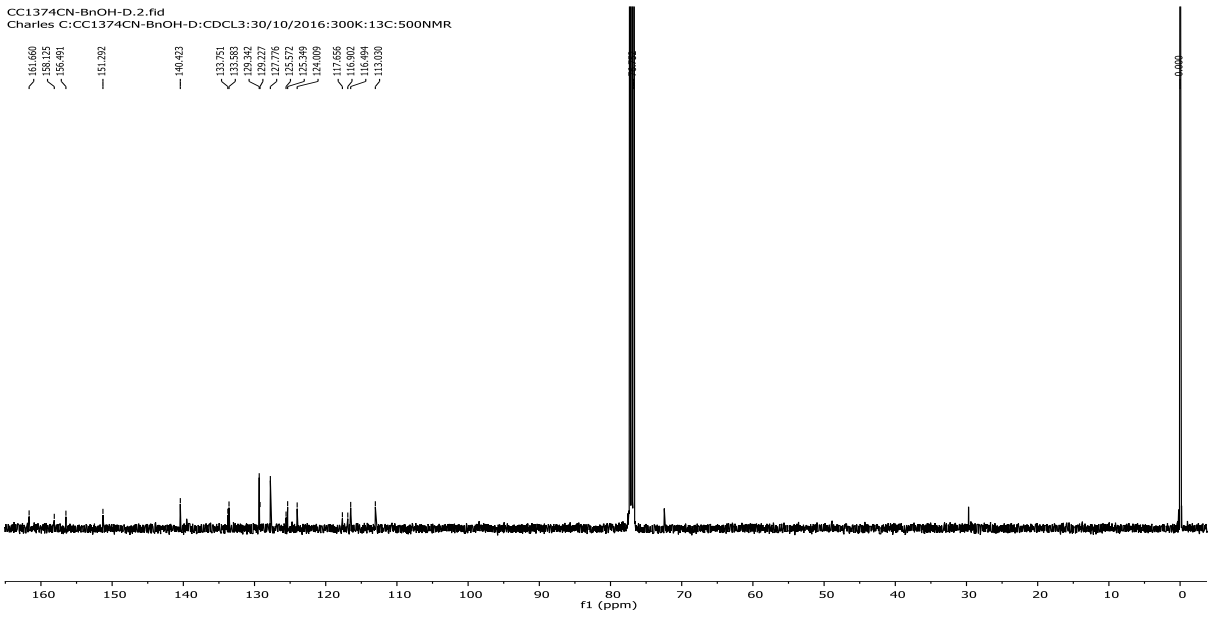
CC1374CN-BnOH-D.2.fid
Charles C:CC1374CN-BnOH-D:CDCL3:30/10/2016:300K:13C:500NMR
161.660
158.125
156.491
151.292
140.423
133.751
133.583
129.342
129.227
127.776
125.572
125.349
124.009
117.656
116.902
116.494
113.030
77.316
0.000
f1 (ppm)

151a

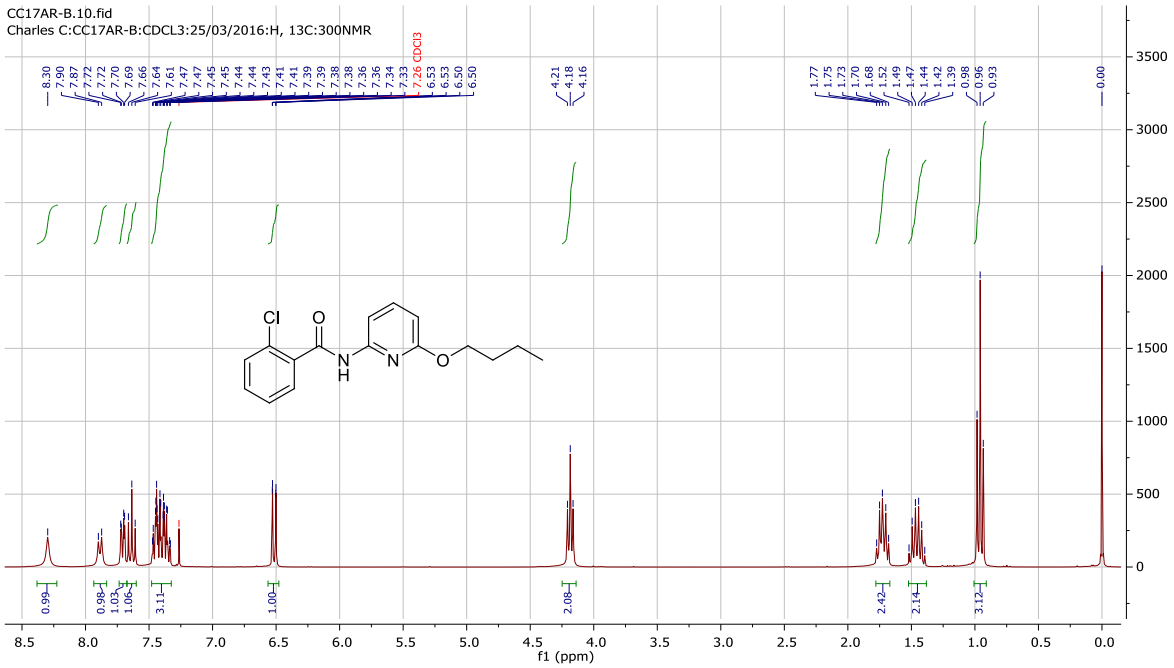
CC17AR-B.10.fid
Charles C:CC17AR-B:CDCL3:25/03/2016:H, 13C:300NMR
f1 (ppm)

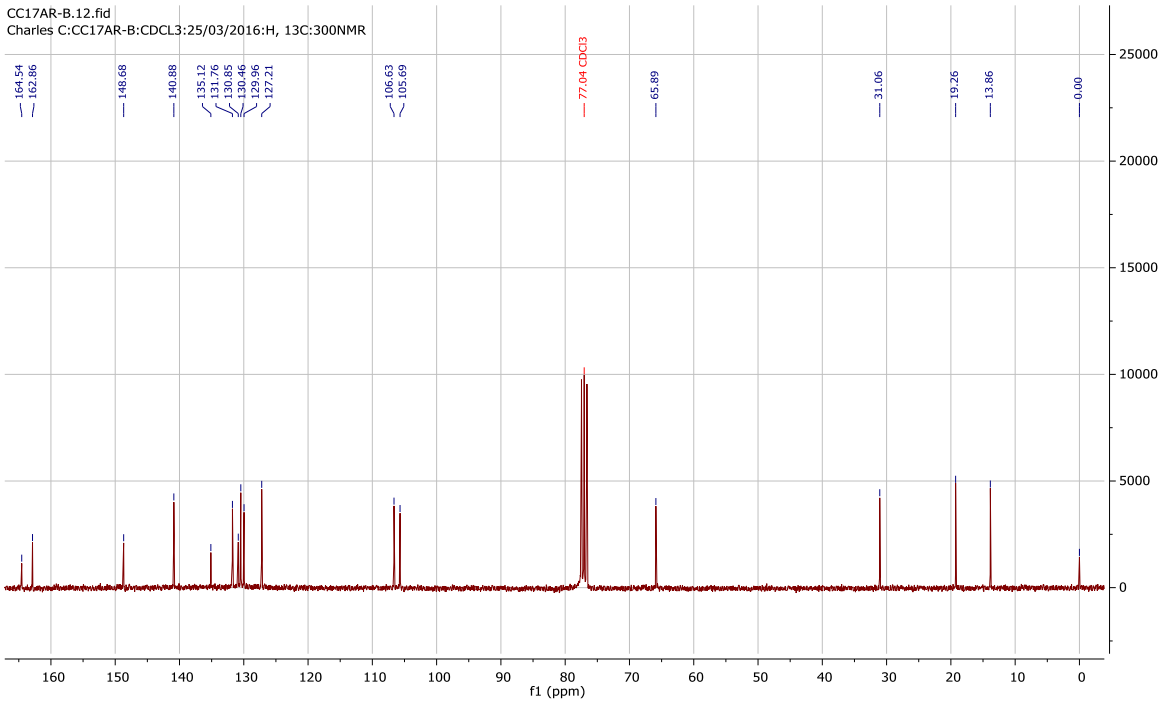
CC17AR-B.12.fid
Charles C:CC17AR-B:CDCL3:25/03/2016:H, 13C:300NMR
f1 (ppm)

151b

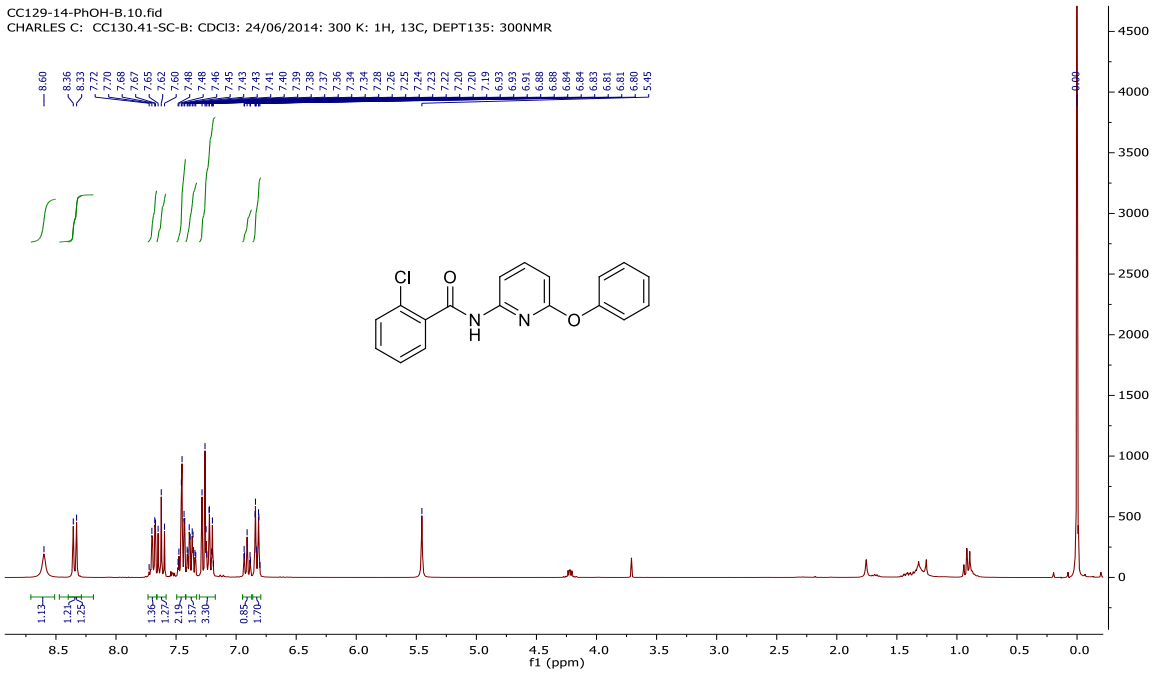
CC129-14-PhOH-B.10.fid
CHARLES C: CC130.41-SC-B: CDCl3: 24/06/2014: 300 K: 1H, 13C, DEPT135: 300NMR
Cl
O
N
H
N
O
f1 (ppm)

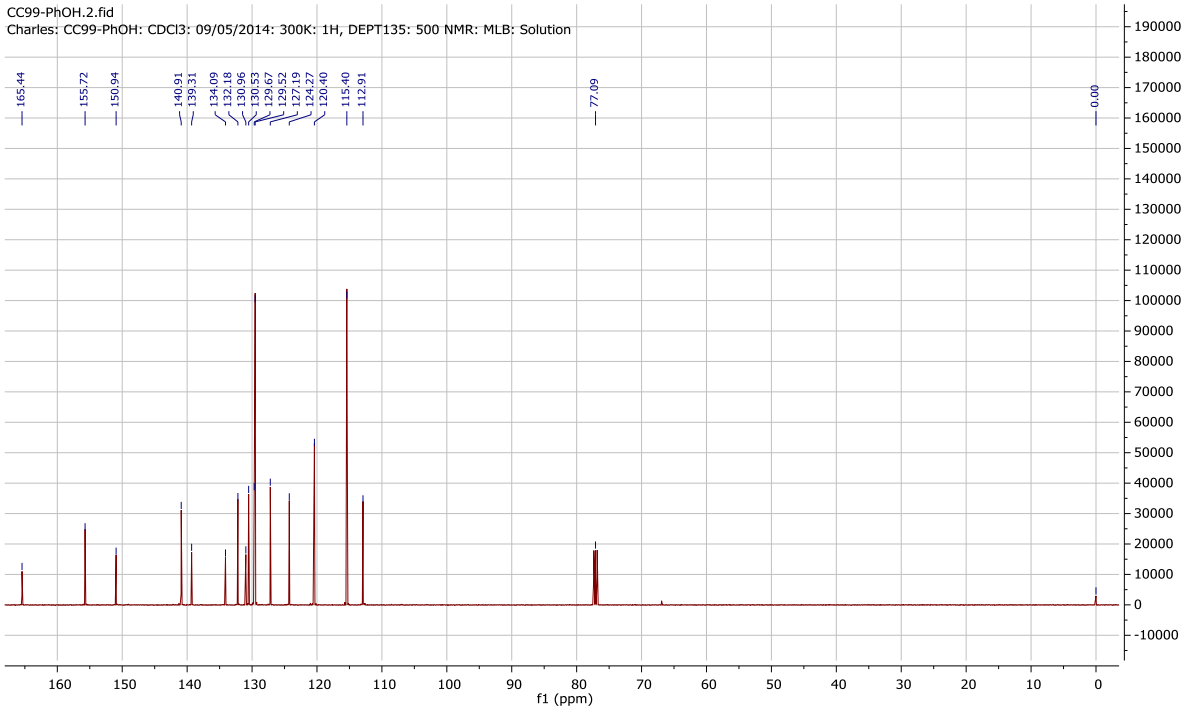
CC99-PhOH.2.fid
Charles: CC99-PhOH: CDCl3: 09/05/2014: 300K: 1H, DEPT135: 500 NMR: MLB: Solution
165.44
155.72
150.94
140.91
139.31
134.09
132.18
130.96
130.53
129.67
129.52
127.19
124.27
120.40
115.40
112.91
77.09
0.00
f1 (ppm)

151c

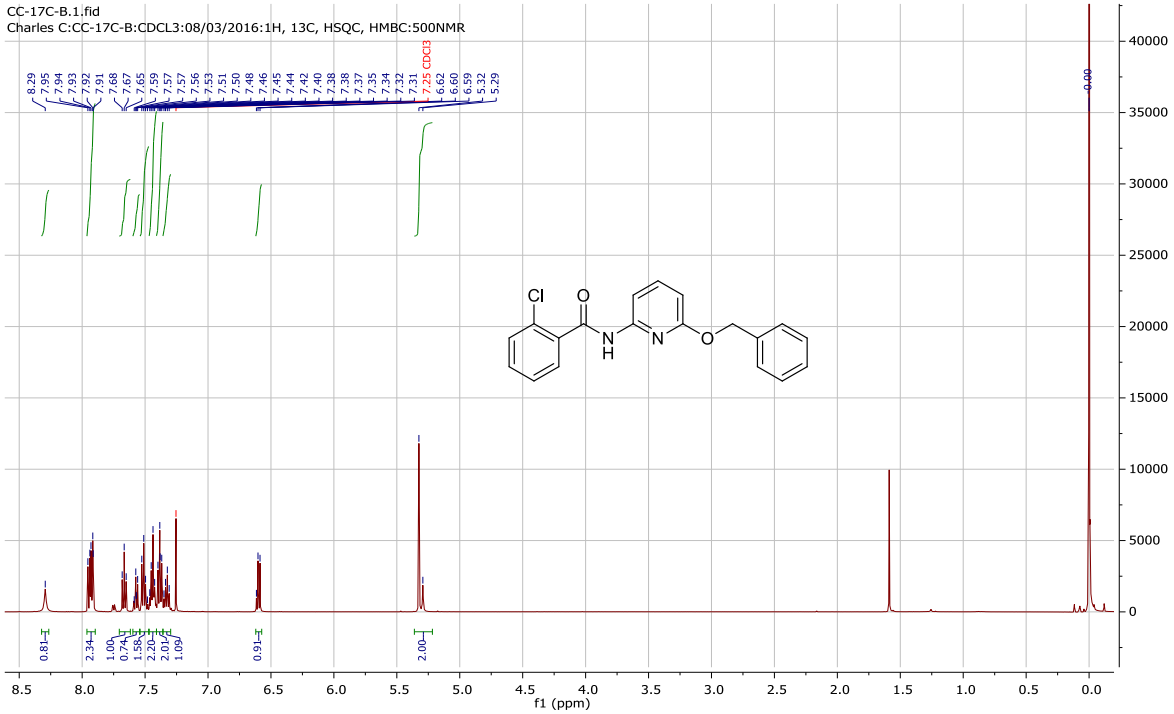
CC-17C-B.1.fid
Charles C:CC-17C-B:CDCL3:08/03/2016:1H, 13C, HSQC, HMBC:500NMR
f1 (ppm)

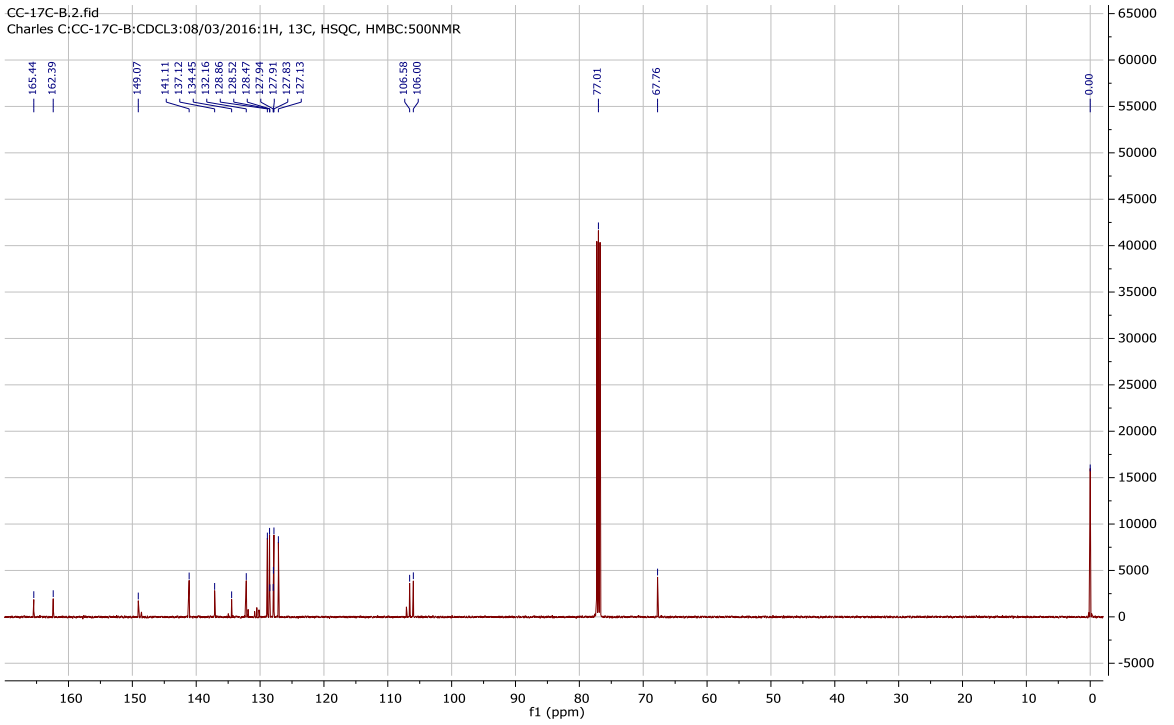
CC-17C-B.2.fid
Charles C:CC-17C-B:CDCL3:08/03/2016:1H, 13C, HSQC, HMBC:500NMR
f1 (ppm)

151d

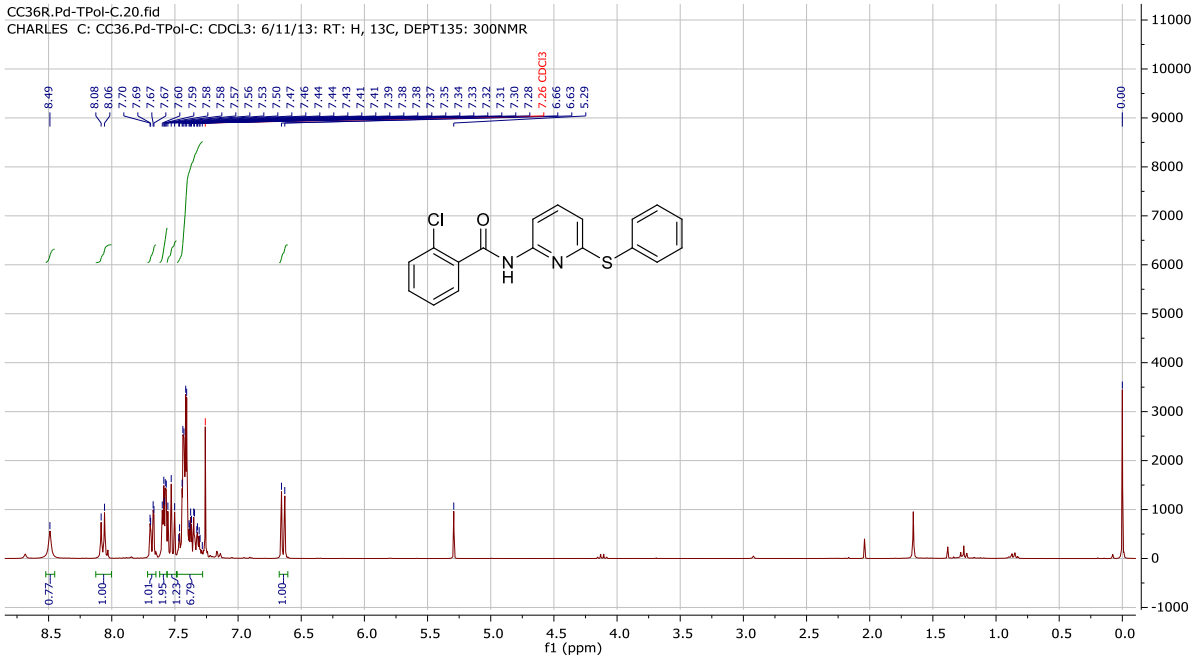
CC36R.Pd-TPol-C.20.fid
CHARLES C: CC36.Pd-TPol-C: CDCL3: 6/11/13: RT: H, 13C, DEPT135: 300NMR
8.49
8.08
8.06
7.70
7.69
7.67
7.67
7.67
7.60
7.59
7.58
7.58
7.57
7.56
7.53
7.50
7.47
7.46
7.44
7.44
7.43
7.41
7.41
7.39
7.38
7.38
7.37
7.35
7.34
7.33
7.32
7.31
7.30
7.28
7.26 CDCl3
6.66
6.63
5.29
0.00
Cl
O
N
H
N
S
0.77
1.00
1.01
1.95
1.23
6.79
1.00
f1 (ppm)

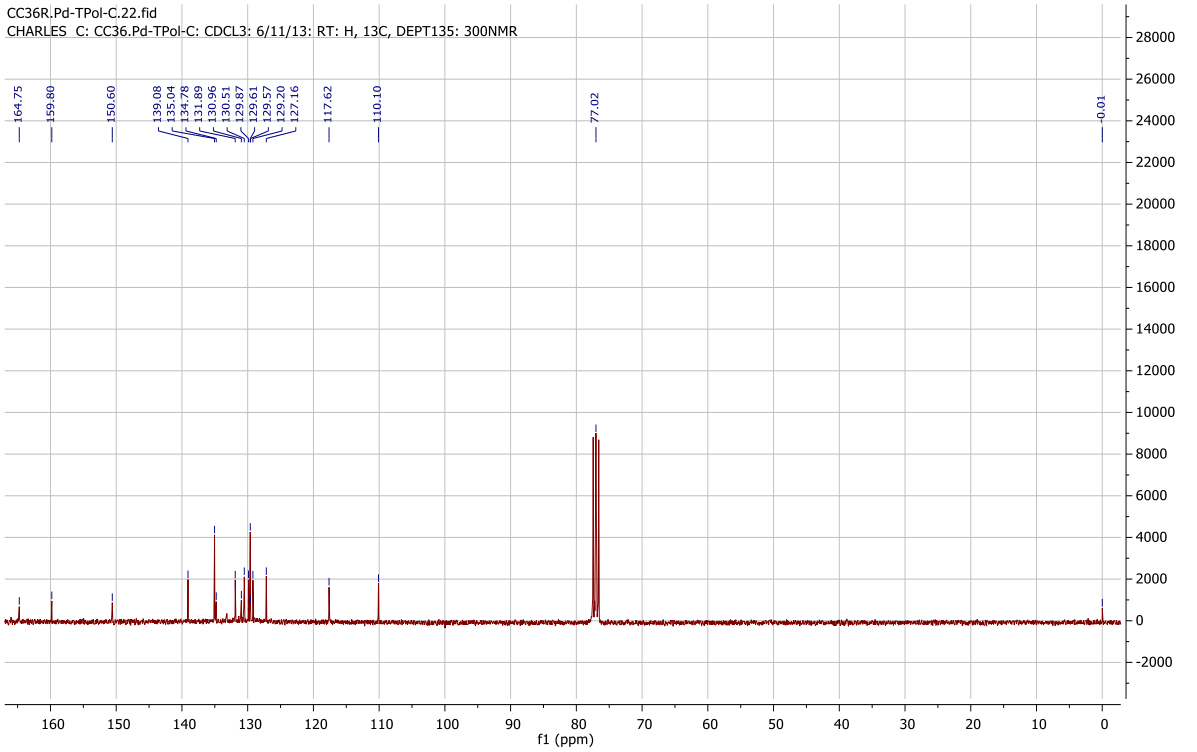
CC36R.Pd-TPol-C.22.fid
CHARLES C: CC36.Pd-TPol-C: CDCL3: 6/11/13: RT: H, 13C, DEPT135: 300NMR
164.75
159.80
150.60
139.08
135.04
134.78
131.89
130.96
130.51
129.87
129.61
129.57
129.20
127.16
117.62
110.10
77.02
0.01
f1 (ppm)

151e

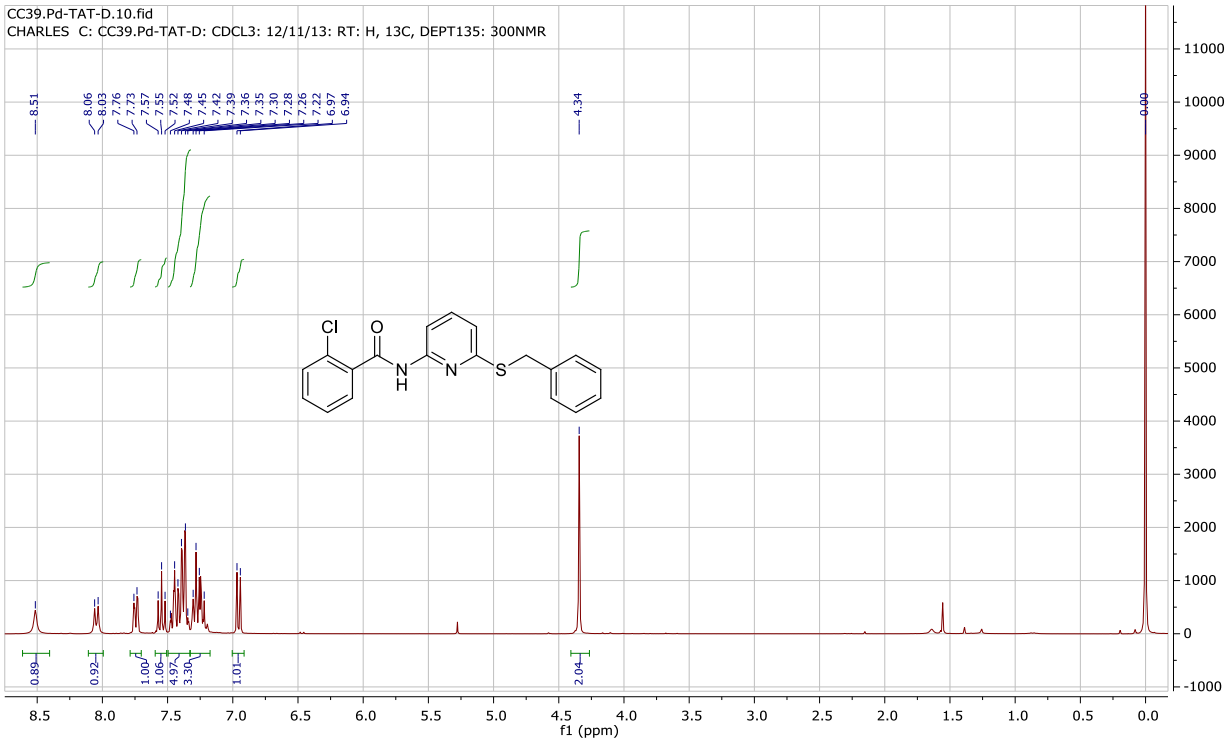
CC39.Pd-TAT-D.10.fid
CHARLES C: CC39.Pd-TAT-D: CDCL3: 12/11/13: RT: H, 13C, DEPT135: 300NMR
8.51
8.06
8.03
7.76
7.73
7.57
7.55
7.52
7.48
7.45
7.42
7.39
7.36
7.35
7.30
7.28
7.26
7.22
6.97
6.94
4.34
0.00
Cl
O
N
H
N
S
0.89
0.92
1.00
1.06
4.97
3.30
1.01
2.04
f1 (ppm)

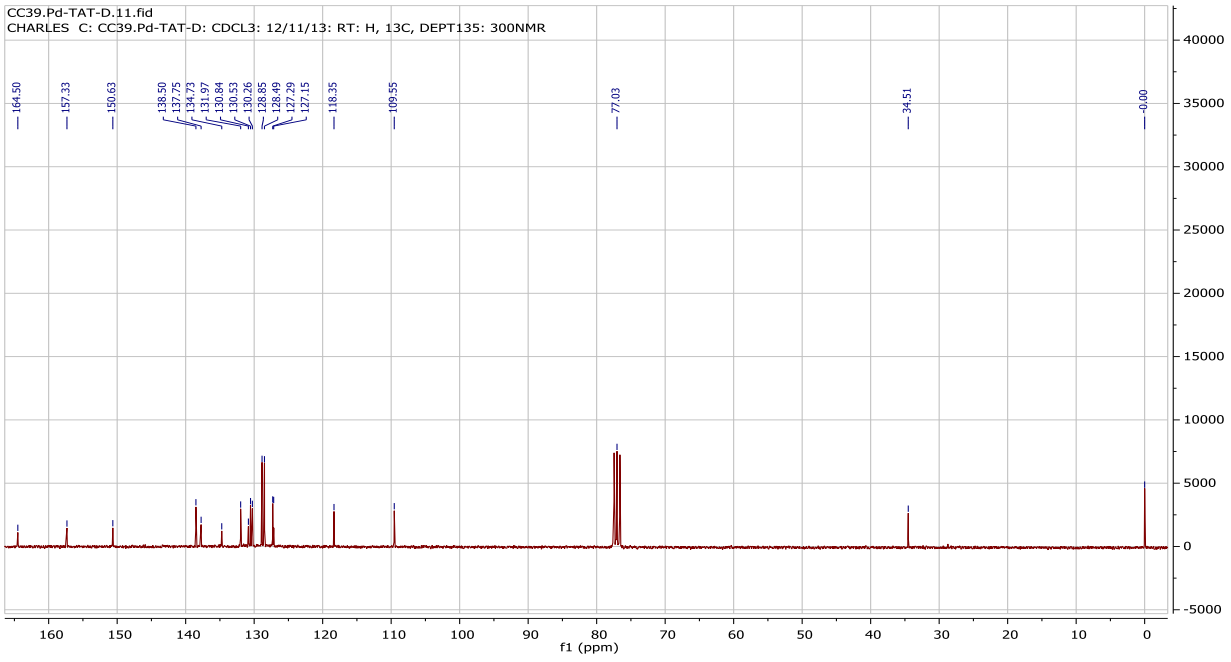
CC39.Pd-TAT-D.11.fid
CHARLES C: CC39.Pd-TAT-D: CDCL3: 12/11/13: RT: H, 13C, DEPT135: 300NMR
164.50
157.33
150.63
138.50
137.75
134.73
131.97
130.84
130.53
130.26
128.85
128.49
127.29
127.15
118.35
109.55
77.03
34.51
-0.00
f1 (ppm)

152

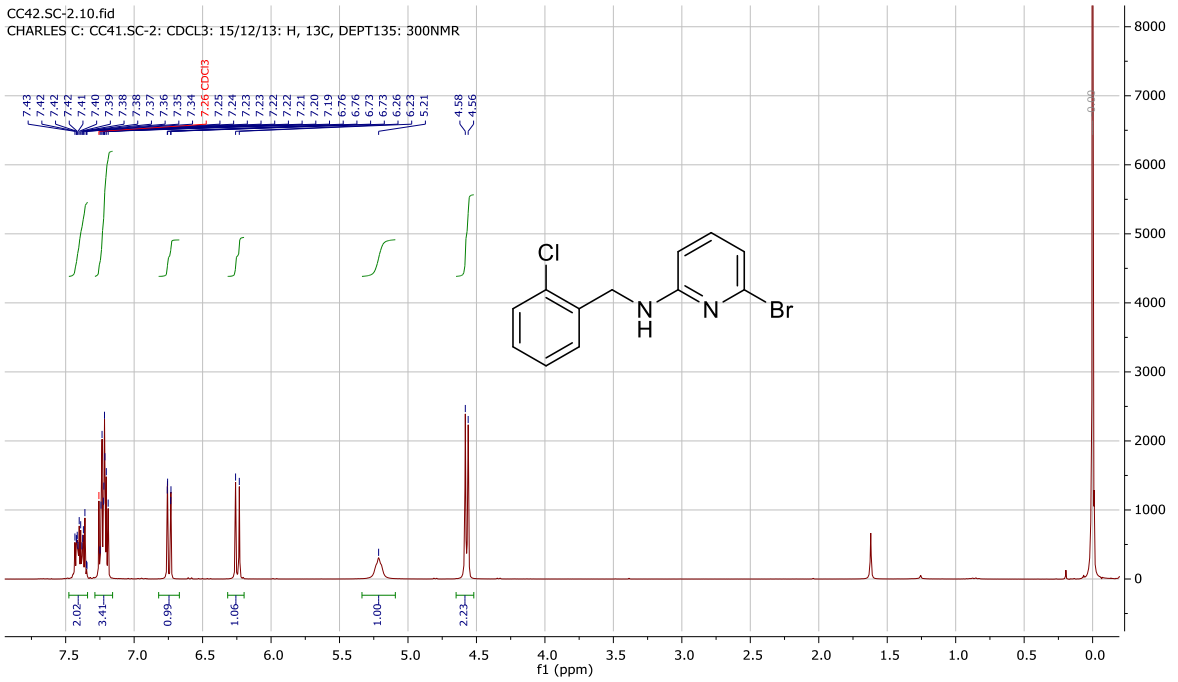
CC42.SC-2.10.fid
CHARLES C: CC41.SC-2: CDCL3: 15/12/13: H, 13C, DEPT135: 300NMR
7.43
7.42
7.42
7.42
7.41
7.40
7.39
7.38
7.38
7.37
7.36
7.35
7.34
7.26 CDCl3
7.25
7.24
7.23
7.23
7.22
7.22
7.21
7.20
7.19
6.76
6.76
6.73
6.73
6.26
6.23
5.21
4.58
4.56
0.00
Cl
N
H
N
Br
2.02
3.41
0.99
1.06
1.00
2.23
f1 (ppm)

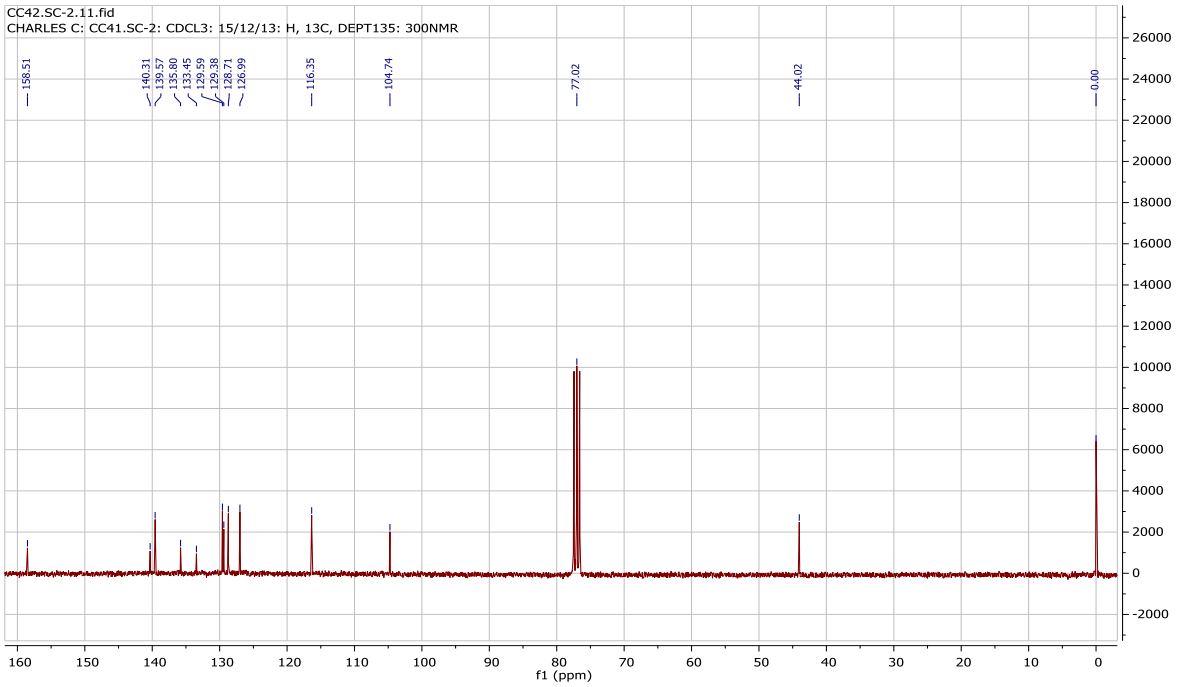
CC42.SC-2.11.fid
CHARLES C: CC41.SC-2: CDCL3: 15/12/13: H, 13C, DEPT135: 300NMR
158.51
140.31
139.57
135.80
133.45
129.59
129.38
128.71
126.99
116.35
104.74
77.02
44.02
0.00
f1 (ppm)

155

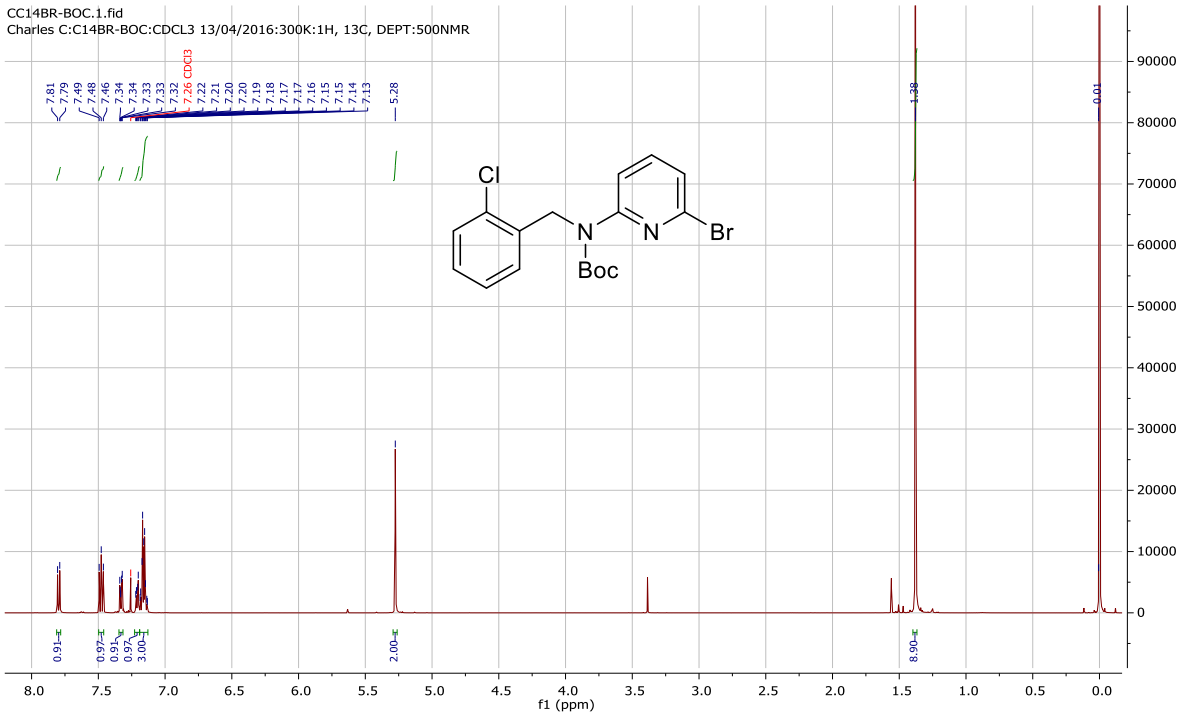
CC14BR-BOC.1.fid
Charles C:C14BR-BOC:CDCL3 13/04/2016:300K:1H, 13C, DEPT:500NMR
7.81
7.79
7.49
7.48
7.46
7.34
7.34
7.33
7.33
7.26 CDCl3
7.22
7.21
7.20
7.20
7.19
7.18
7.17
7.17
7.16
7.15
7.15
7.14
7.13
5.28
1.38
0.01
Cl
N
N
Br
Boc
0.91
0.97
0.91
0.97
3.00
2.00
8.90
f1 (ppm)

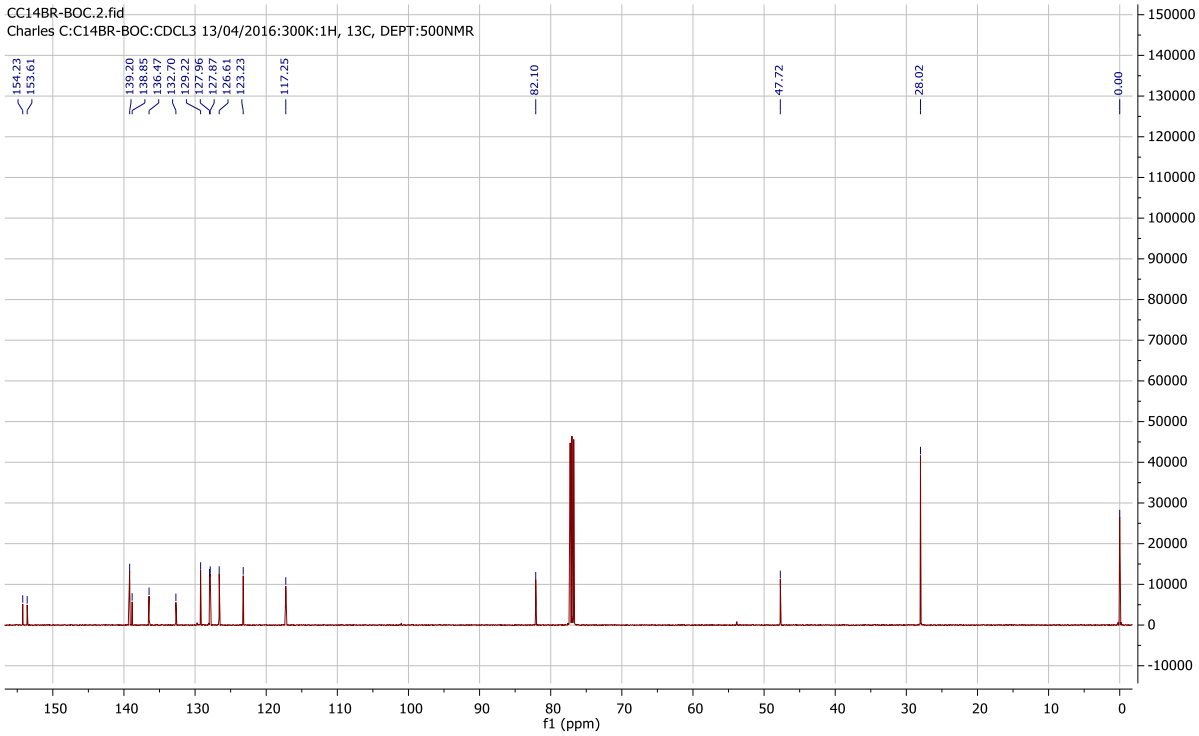
CC14BR-BOC.2.fid
Charles C:C14BR-BOC:CDCL3 13/04/2016:300K:1H, 13C, DEPT:500NMR
154.23
153.61
139.20
138.85
136.47
132.70
129.22
127.96
127.87
126.61
123.23
117.25
82.10
47.72
28.02
0.00
f1 (ppm)

157a

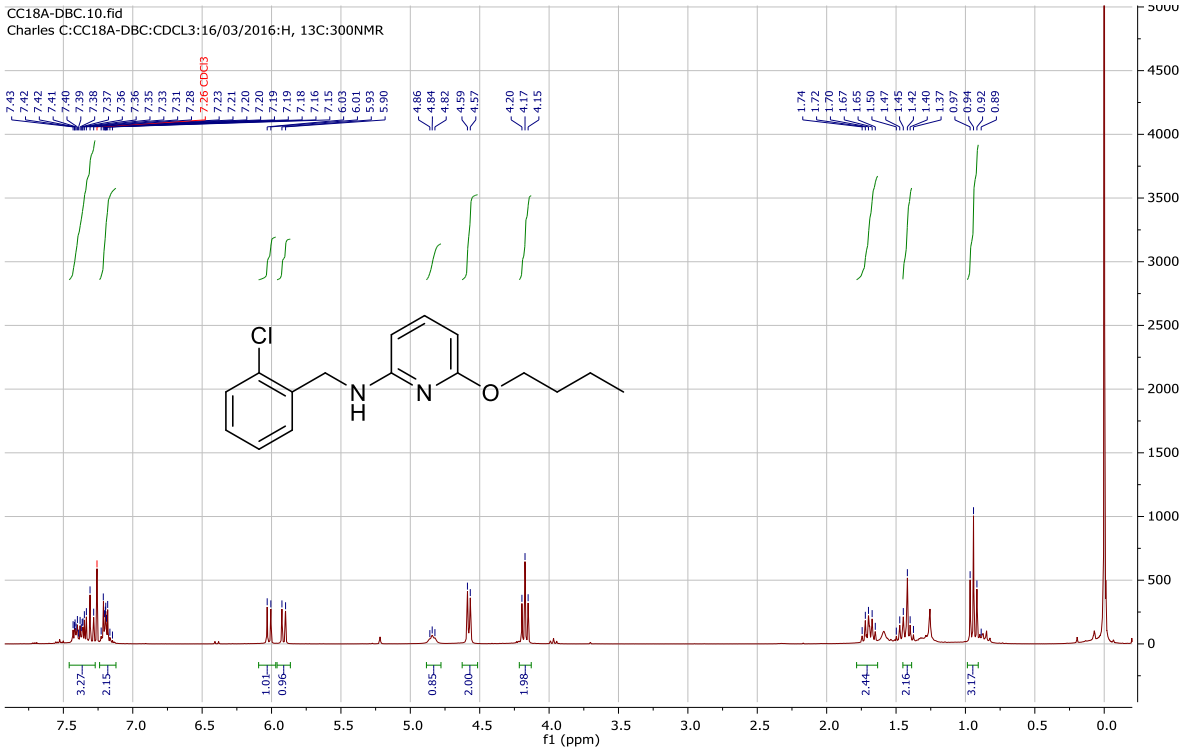
CC18A-DBC.10.fid
Charles C:CC18A-DBC:CDCL3:16/03/2016:H, 13C:300NMR
7.43 7.42 7.42 7.41 7.40 7.39 7.38 7.37 7.36 7.36 7.35 7.33 7.31 7.28 7.26 CDCl3 7.23 7.21 7.20 7.20 7.19 7.19 7.18 7.16 7.15 6.03 6.01 5.93 5.90
4.86 4.84 4.82 4.59 4.57
4.20 4.17 4.15
1.74 1.72 1.70 1.67 1.65 1.50 1.47 1.45 1.42 1.40 1.37
0.97 0.94 0.92 0.89
Cl
N
H
N
O
3.27 2.15 1.01 0.96 0.85 2.00 1.98 2.44 2.16 3.17
f1 (ppm)

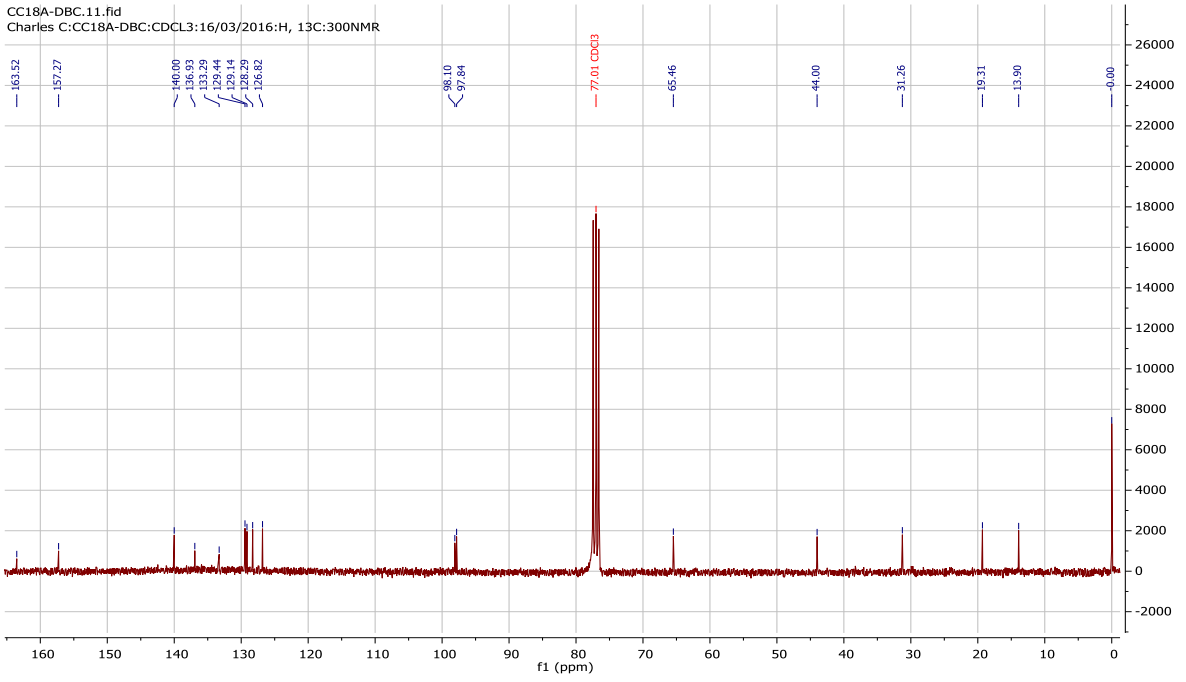
CC18A-DBC.11.fid
Charles C:CC18A-DBC:CDCL3:16/03/2016:H, 13C:300NMR
163.52 157.27 140.00 136.93 133.29 129.44 128.29 126.82 98.10 97.84 77.01 CDCl3 65.46 44.00 31.26 19.31 13.90 0.00
f1 (ppm)

157b

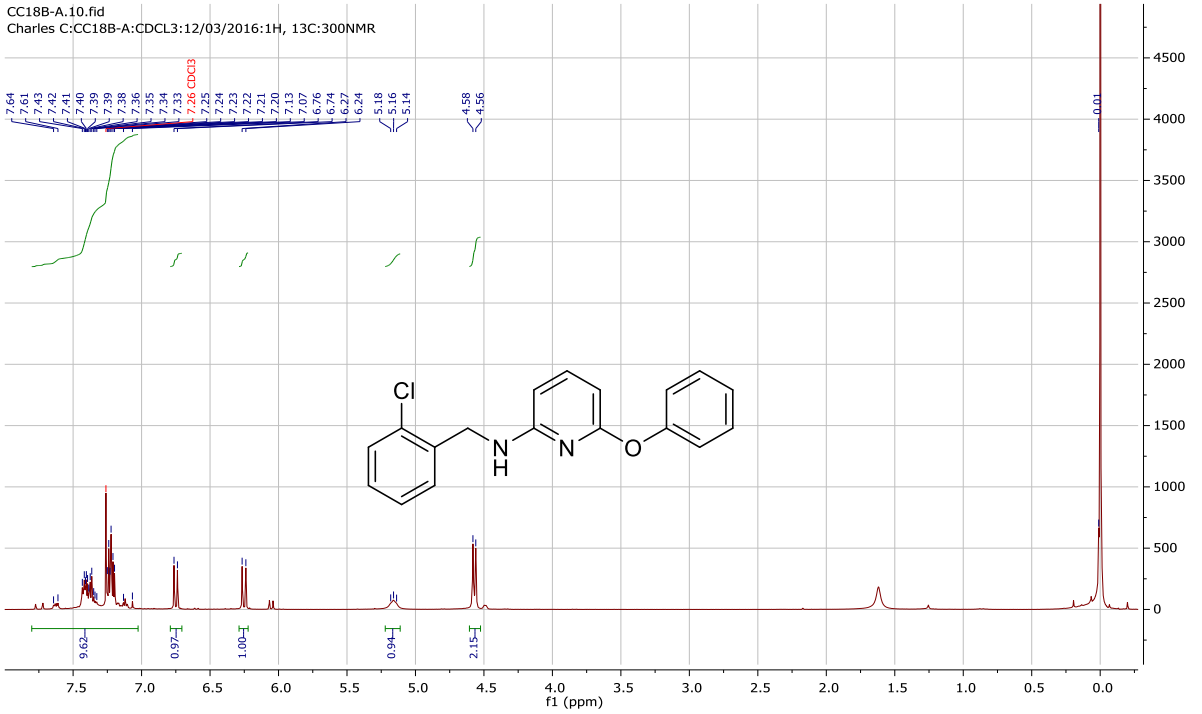
CC18B-A.10.fid
Charles C:CC18B-A:CDCL3:12/03/2016:1H, 13C:300NMR
7.64
7.61
7.43
7.42
7.41
7.40
7.39
7.39
7.38
7.36
7.35
7.34
7.33
7.26 CDCl3
7.25
7.24
7.23
7.22
7.21
7.20
7.13
7.07
6.76
6.74
6.27
6.24
5.18
5.16
5.14
4.58
4.56
0.01
Cl
N
H
N
O
9.62
0.97
1.00
0.94
2.15
f1 (ppm)

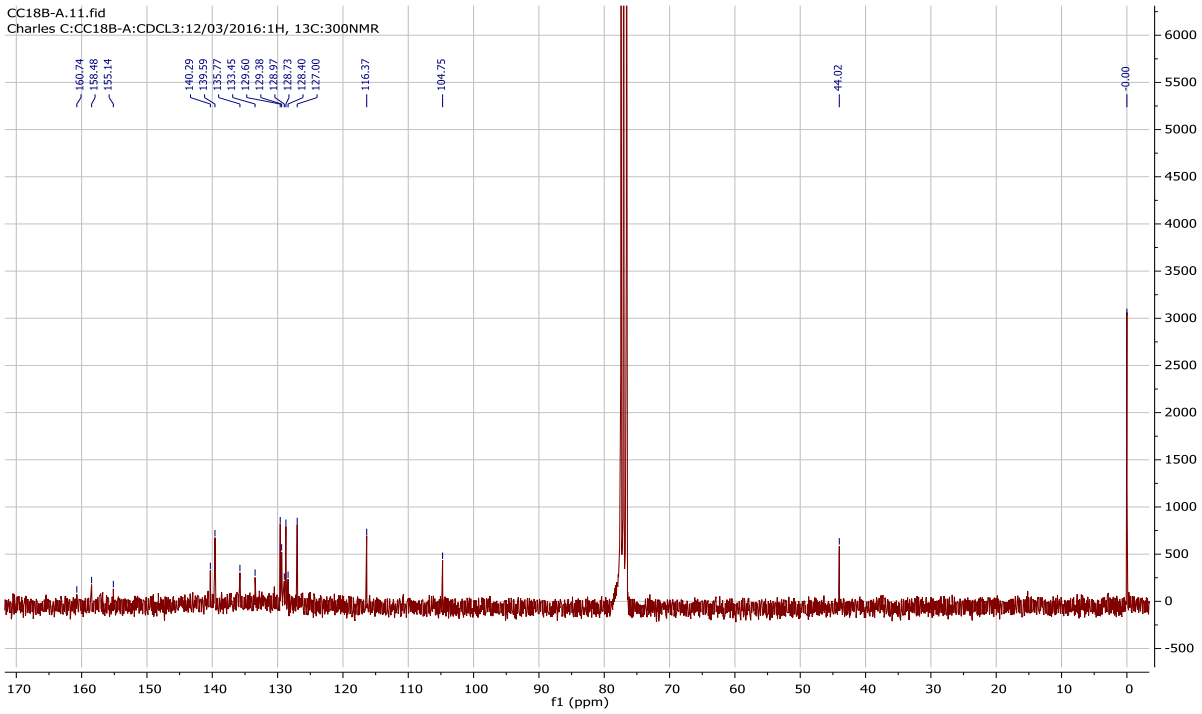
CC18B-A.11.fid
Charles C:CC18B-A:CDCL3:12/03/2016:1H, 13C:300NMR
160.74
158.48
155.14
140.29
139.59
135.77
133.45
129.60
129.38
128.97
128.73
128.40
127.00
116.37
104.75
44.02
-0.00
f1 (ppm)

157c

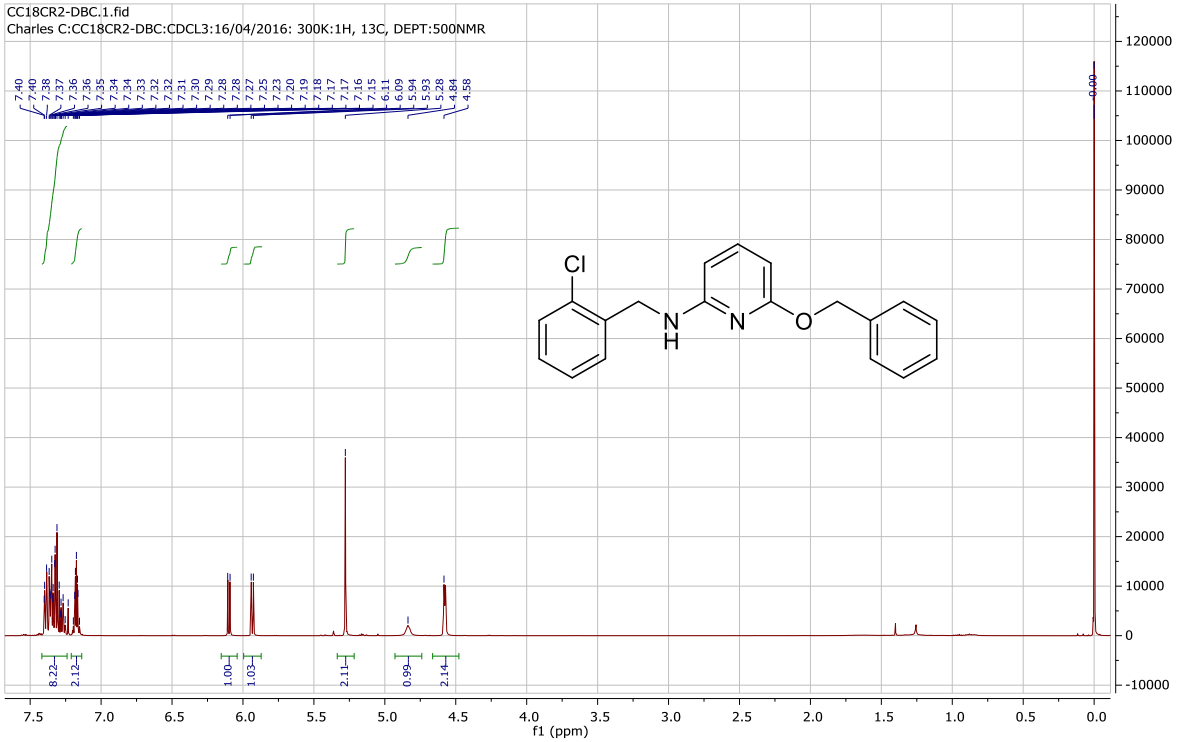
CC18CR2-DBC.1.fid
Charles C:CC18CR2-DBC:CDCL3:16/04/2016: 300K:1H, 13C, DEPT:500NMR
Cl
N
H
N
O
f1 (ppm)

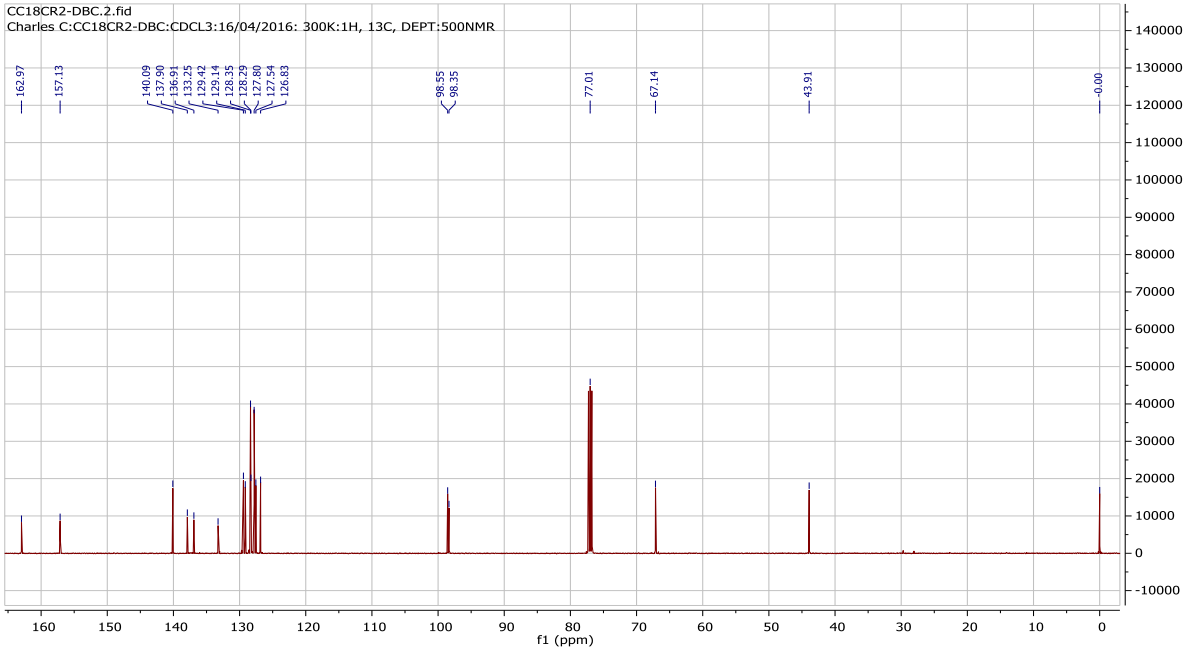
CC18CR2-DBC.2.fid
Charles C:CC18CR2-DBC:CDCL3:16/04/2016: 300K:1H, 13C, DEPT:500NMR
f1 (ppm)

157d

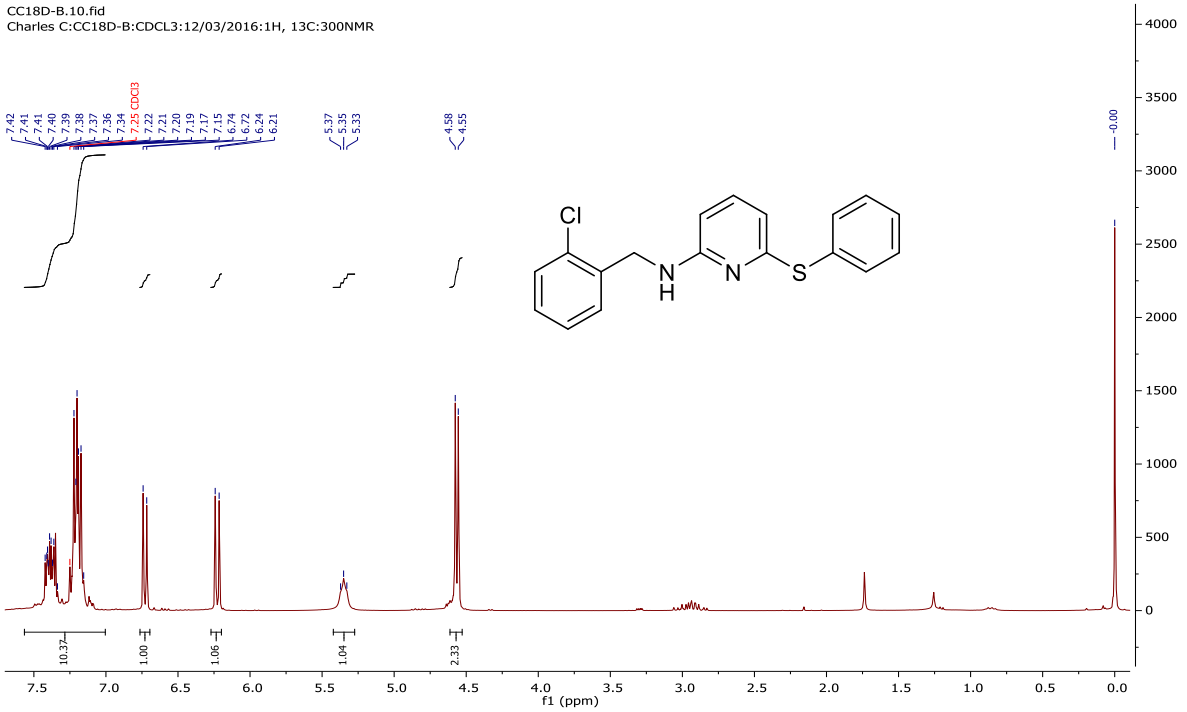
CC18D-B.10.fid
Charles C:CC18D-B:CDCL3:12/03/2016:1H, 13C:300NMR
7.42
7.41
7.41
7.40
7.39
7.38
7.37
7.36
7.34
7.25 CDCl3
7.22
7.21
7.20
7.19
7.17
7.15
6.74
6.72
6.24
6.21
5.37
5.35
5.33
4.58
4.55
-0.00
Cl
N
H
N
S
10.37
1.00
1.06
1.04
2.33
f1 (ppm)

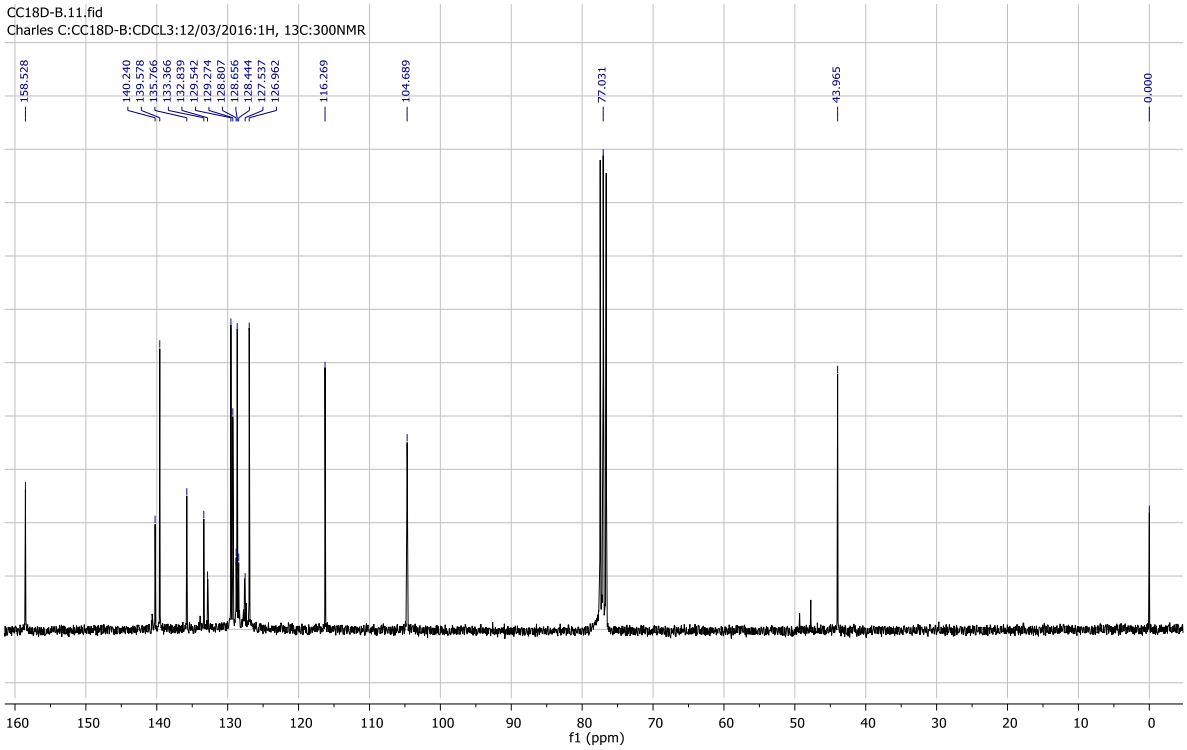
CC18D-B.11.fid
Charles C:CC18D-B:CDCL3:12/03/2016:1H, 13C:300NMR
158.528
140.240
139.578
135.766
133.366
132.839
129.542
129.274
128.807
128.656
128.444
127.537
126.962
116.269
104.689
77.031
43.965
0.000
f1 (ppm)

157e

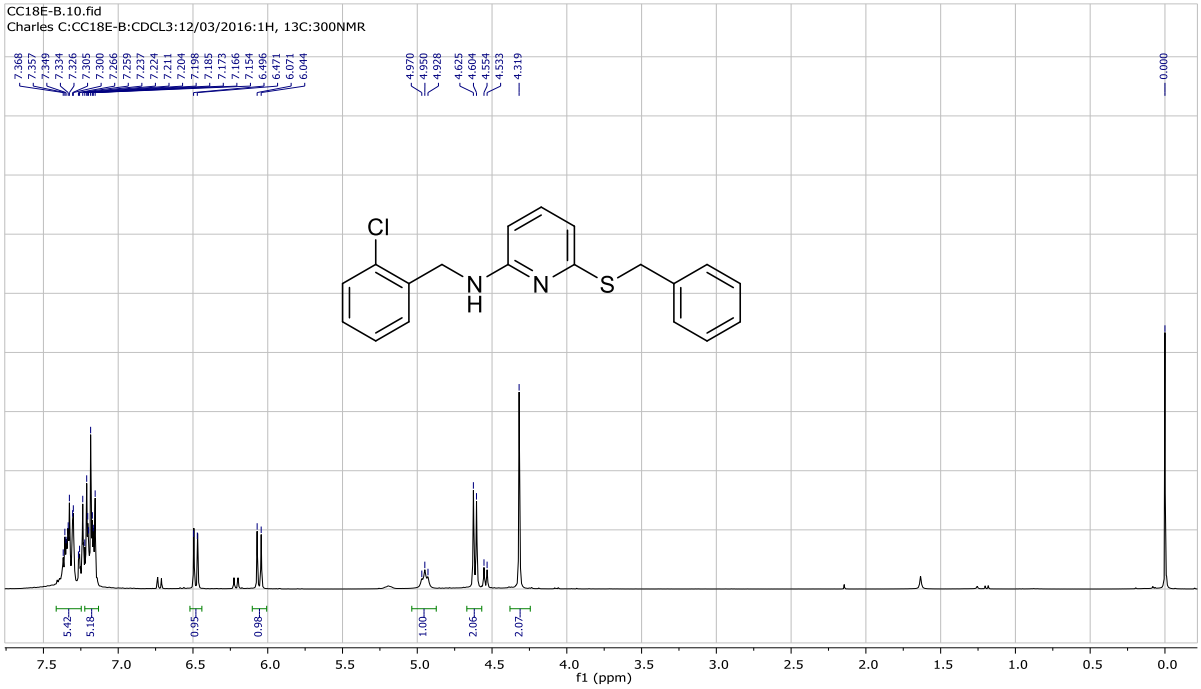
CC18E-B.10.fid
Charles C:CC18E-B:CDCL3:12/03/2016:1H, 13C:300NMR
7.368
7.357
7.349
7.334
7.326
7.305
7.300
7.266
7.259
7.237
7.224
7.211
7.204
7.198
7.185
7.173
7.166
7.154
6.496
6.471
6.071
6.044
4.970
4.950
4.928
4.625
4.604
4.554
4.533
4.319
0.000
Cl
N
H
N
S
5.42
5.18
0.95
0.98
1.00
2.06
2.07
f1 (ppm)

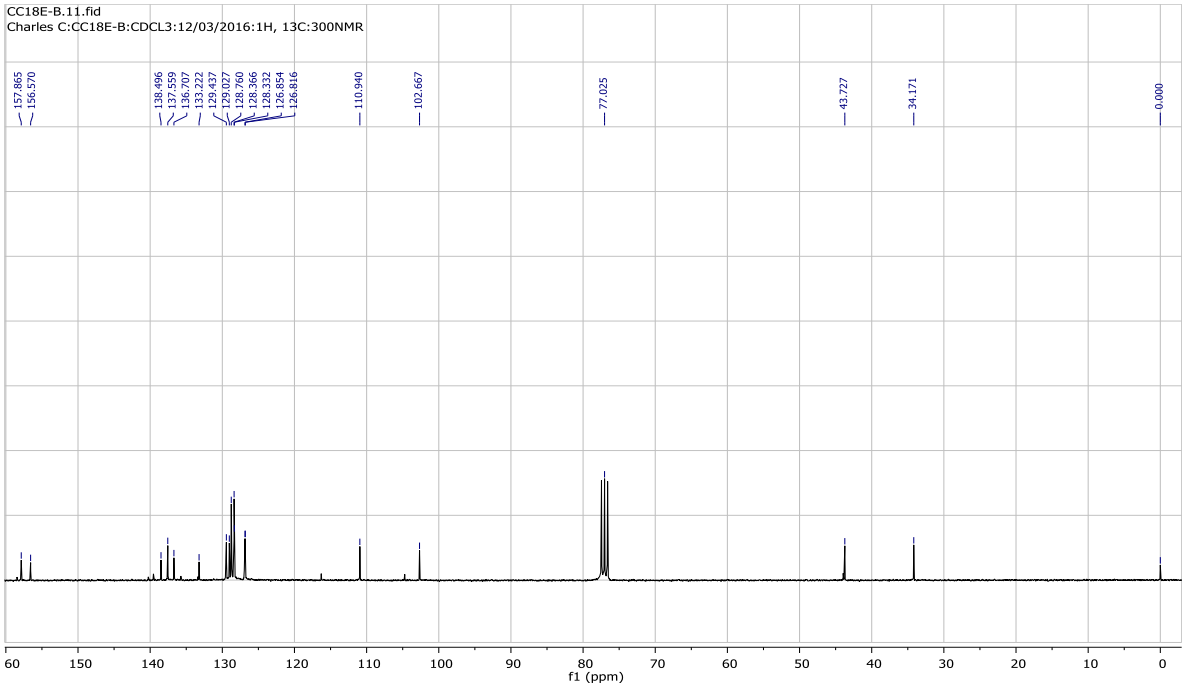
CC18E-B.11.fid
Charles C:CC18E-B:CDCL3:12/03/2016:1H, 13C:300NMR
157.865
156.570
138.496
137.559
136.707
133.222
129.437
129.027
128.760
128.366
128.332
126.854
126.816
110.940
102.667
77.025
43.727
34.171
0.000
f1 (ppm)

159a

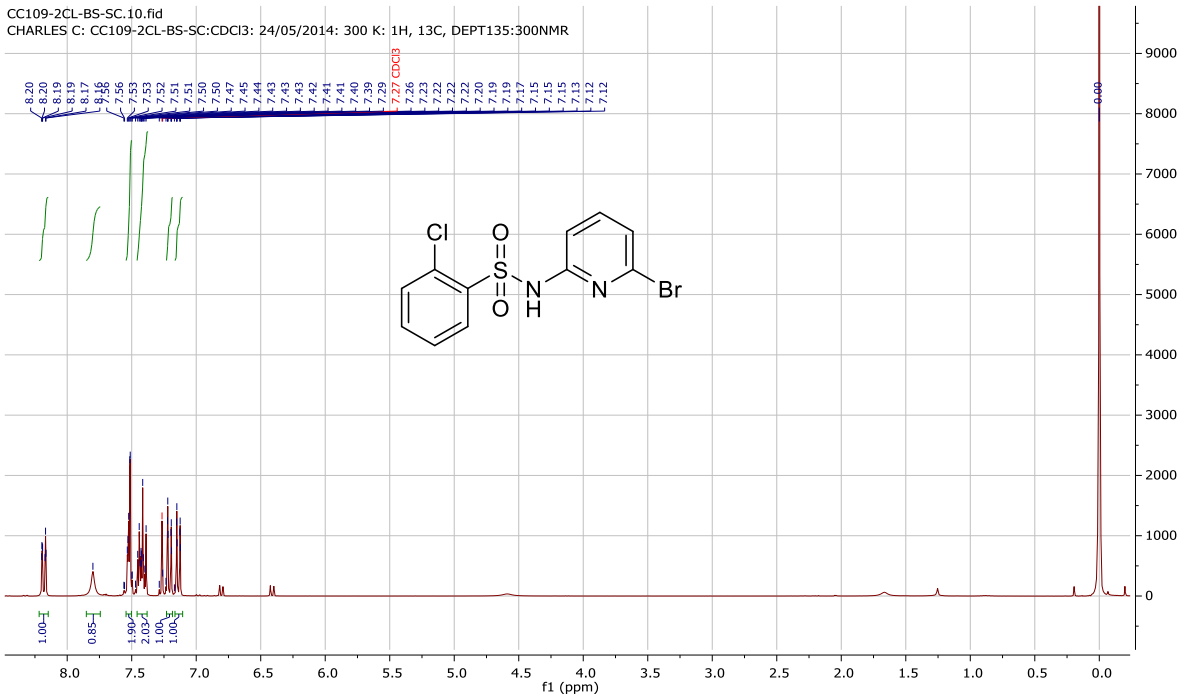
CC109-2CL-BS-SC.10.fid
CHARLES C: CC109-2CL-BS-SC:CDCl3: 24/05/2014: 300 K: 1H, 13C, DEPT135:300NMR
Cl
O
S
O
N
H
N
Br
f1 (ppm)

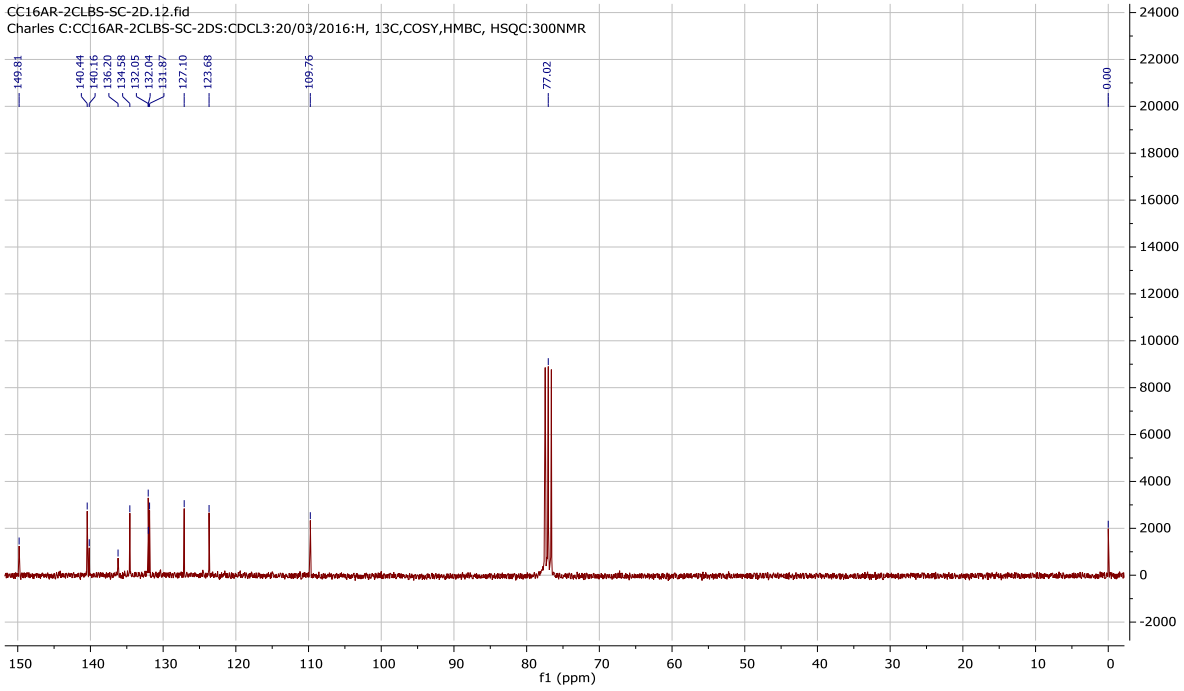
CC16AR-2CLBS-SC-2D.12.fid
Charles C:CC16AR-2CLBS-SC-2DS:CDCL3:20/03/2016:H, 13C,COSY,HMBC, HSQC:300NMR
f1 (ppm)

159b

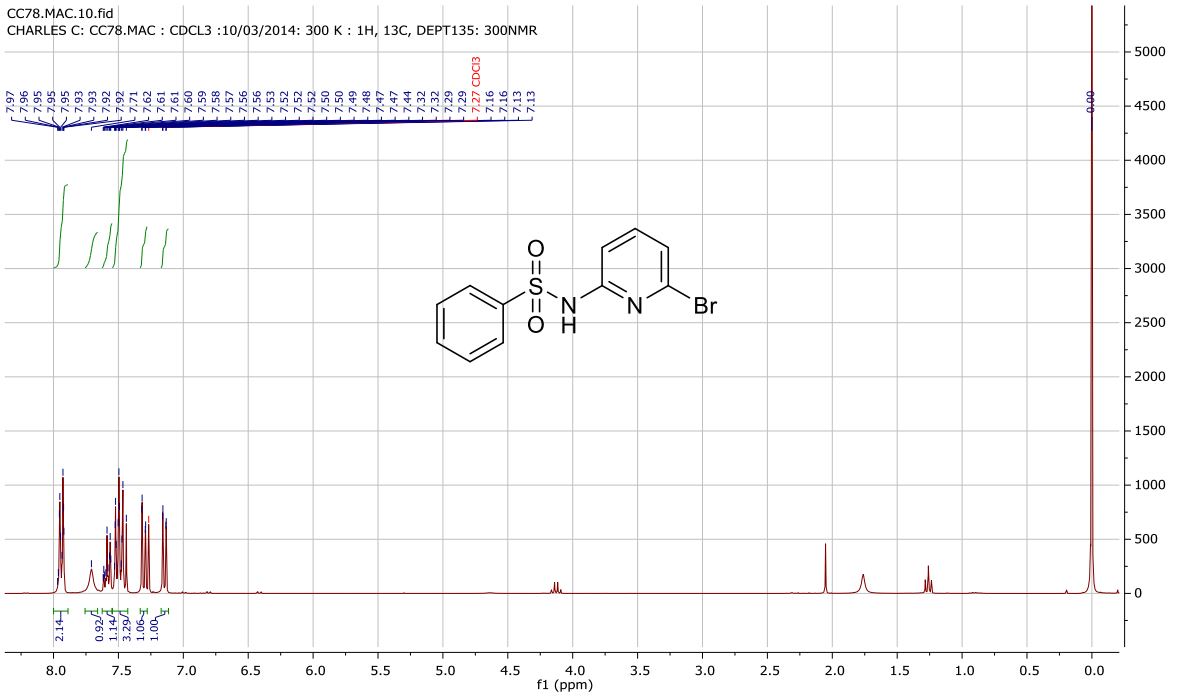
CC78.MAC.10.fid
CHARLES C: CC78.MAC : CDCL3 :10/03/2014: 300 K : 1H, 13C, DEPT135: 300NMR
7.27 CDCl3
0.00
O
S
O
N
H
N
Br
f1 (ppm)

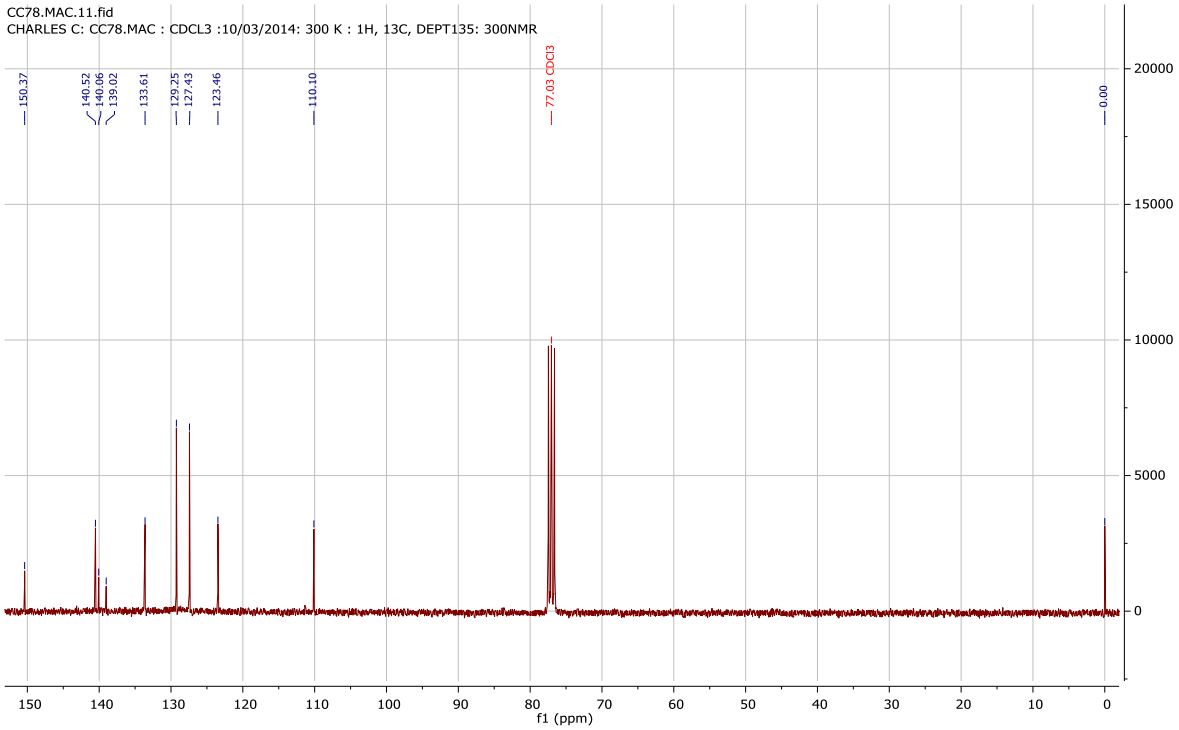
CC78.MAC.11.fid
CHARLES C: CC78.MAC : CDCL3 :10/03/2014: 300 K : 1H, 13C, DEPT135: 300NMR
150.37
140.52
140.06
139.02
133.61
129.25
127.43
123.46
110.10
77.03 CDCl3
0.00
f1 (ppm)

160a

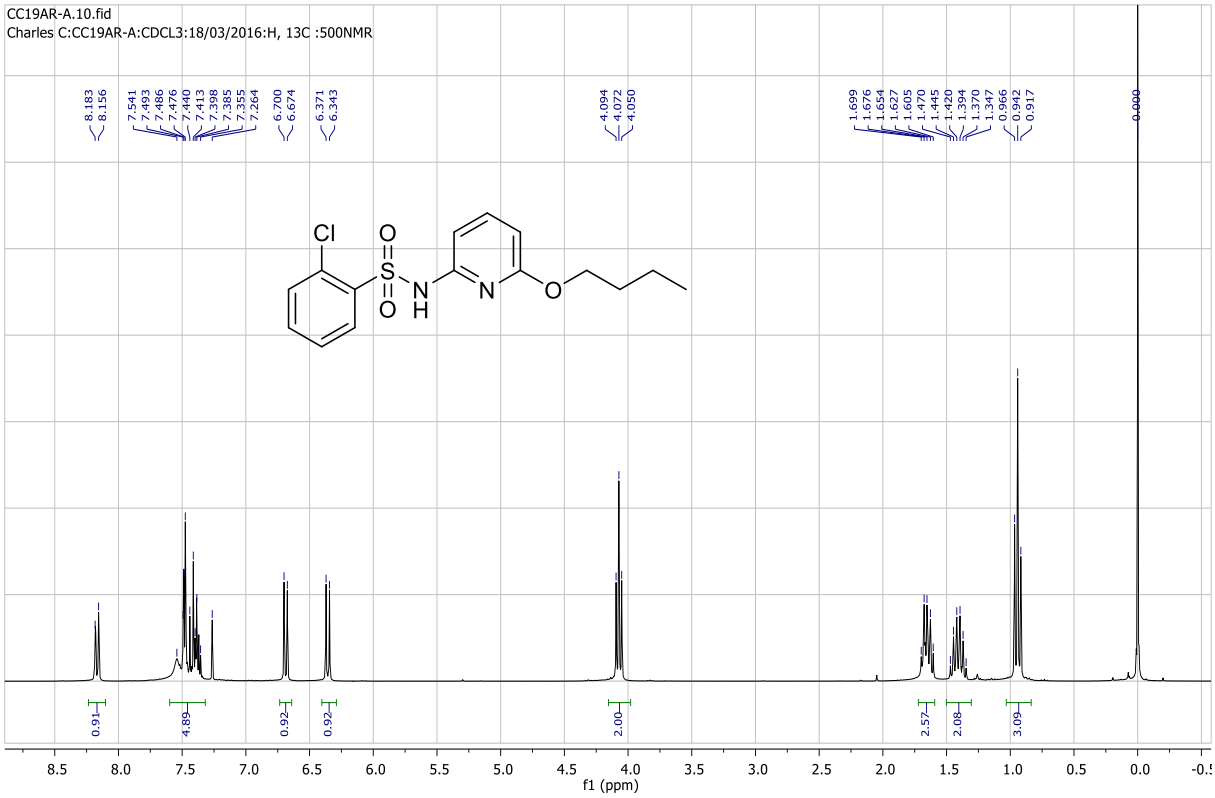
CC19AR-A.10.fid
Charles C:CC19AR-A:CDCL3:18/03/2016:H, 13C :500NMR
8.183
8.156
7.541
7.493
7.486
7.476
7.440
7.413
7.398
7.385
7.355
7.264
6.700
6.674
6.371
6.343
4.094
4.072
4.050
1.699
1.676
1.654
1.627
1.605
1.470
1.445
1.420
1.394
1.370
1.347
0.966
0.942
0.917
0.000
Cl
O
S
O
N
H
N
O
0.91
4.89
0.92
0.92
2.00
2.57
2.08
3.09
f1 (ppm)

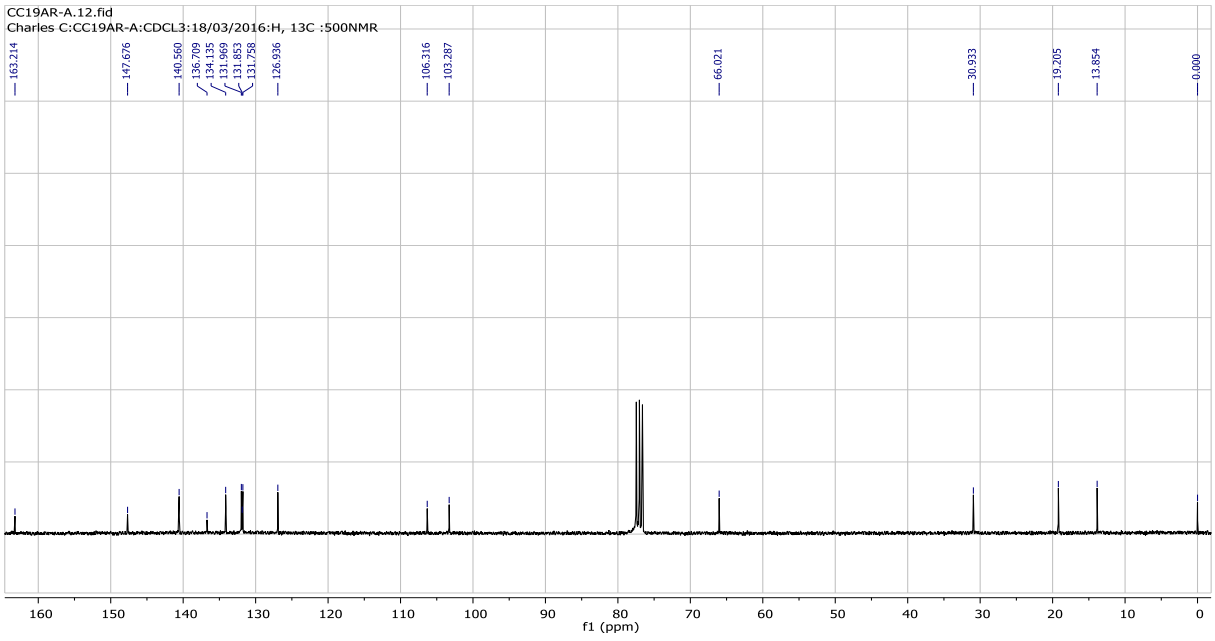
CC19AR-A.12.fid
Charles C:CC19AR-A:CDCL3:18/03/2016:H, 13C :500NMR
163.214
147.676
140.560
136.709
134.135
131.969
131.853
131.758
126.936
106.316
103.287
66.021
30.933
19.205
13.854
0.000
f1 (ppm)

160b

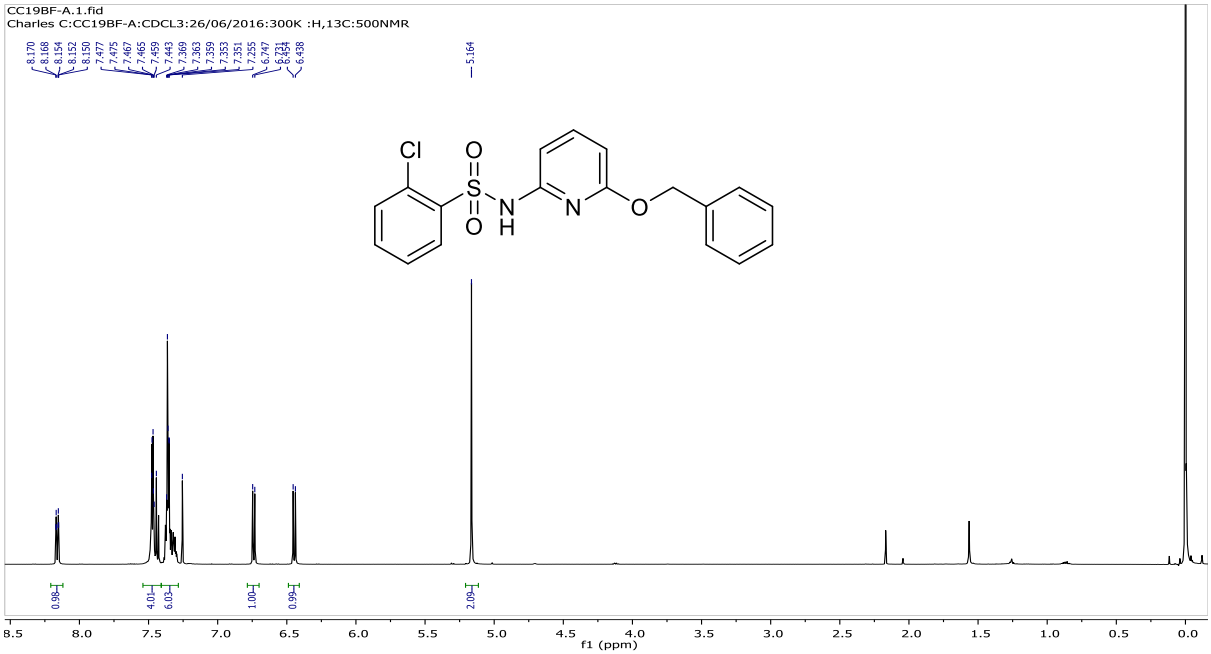
CC19BF-A.1.fid
Charles C:CC19BF-A:CDCL3:26/06/2016:300K :H,13C:500NMR
8.170
8.168
8.154
8.152
8.150
7.477
7.475
7.467
7.465
7.459
7.443
7.369
7.363
7.359
7.353
7.351
7.255
6.747
6.731
6.438
5.164
Cl
O
S
O
N
H
N
O
0.98
4.01
6.03
1.00
0.99
2.09
8.5
8.0
7.5
7.0
6.5
6.0
5.5
5.0
4.5
4.0
3.5
3.0
2.5
2.0
1.5
1.0
0.5
0.0
f1 (ppm)

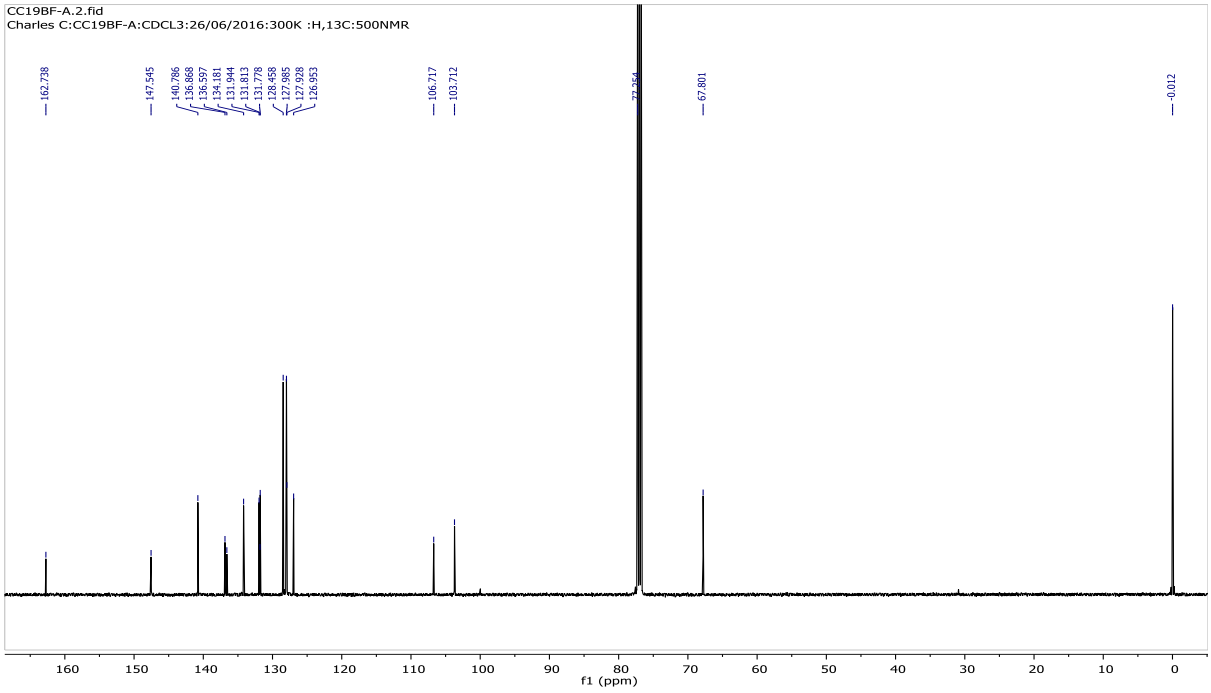
CC19BF-A.2.fid
Charles C:CC19BF-A:CDCL3:26/06/2016:300K :H,13C:500NMR
162.738
147.545
140.786
136.868
136.597
134.181
131.944
131.813
131.778
128.458
127.985
127.928
126.953
106.717
103.712
77.264
67.801
-0.012
160
150
140
130
120
110
100
90
80
70
60
50
40
30
20
10
0
f1 (ppm)

160c

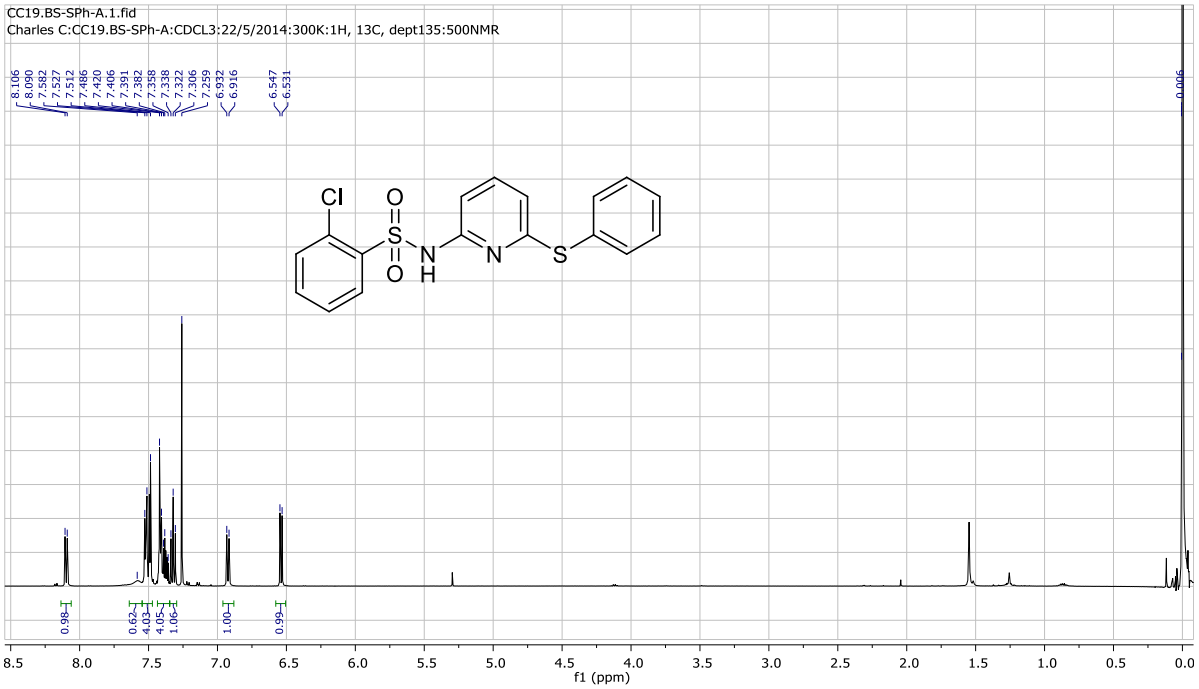
CC19.BS-SPh-A.1.fid
Charles C:CC19.BS-SPh-A:CDCL3:22/5/2014:300K:1H, 13C, dept135:500NMR
8.106
8.090
7.582
7.527
7.512
7.486
7.420
7.406
7.391
7.382
7.358
7.338
7.322
7.306
7.259
6.932
6.916
6.547
6.531
0.000
Cl
O
S
O
N
H
N
S
0.98
0.62
4.03
4.05
1.06
1.00
0.99
f1 (ppm)

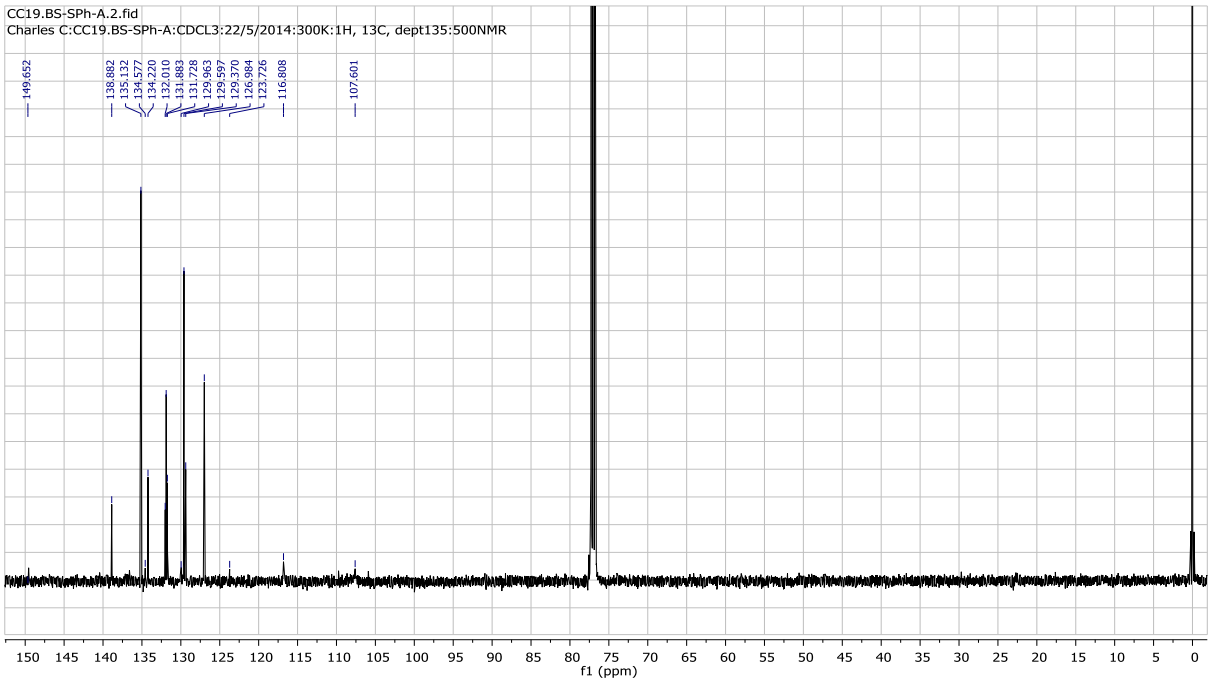
CC19.BS-SPh-A.2.fid
Charles C:CC19.BS-SPh-A:CDCL3:22/5/2014:300K:1H, 13C, dept135:500NMR
149.652
138.882
135.132
134.577
134.220
132.010
131.883
131.728
129.963
129.597
129.370
126.984
123.726
116.808
107.601
f1 (ppm)

160d

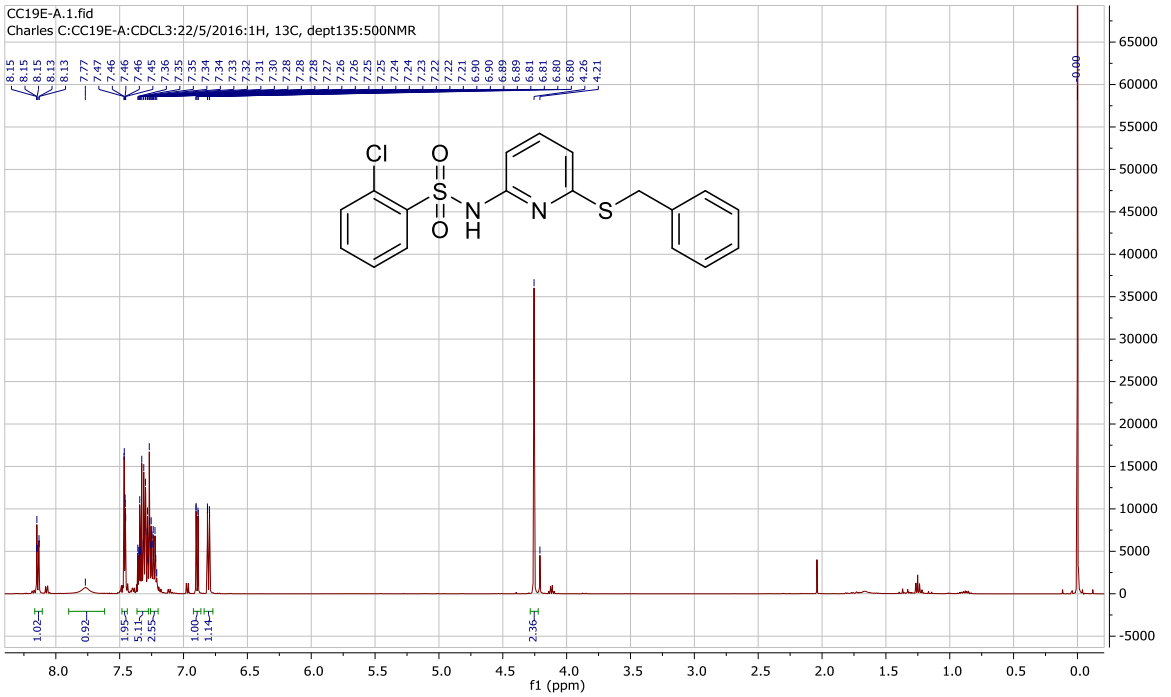
CC19E-A.1.fid
Charles C:CC19E-A:CDCL3:22/5/2016:1H, 13C, dept135:500NMR
f1 (ppm)

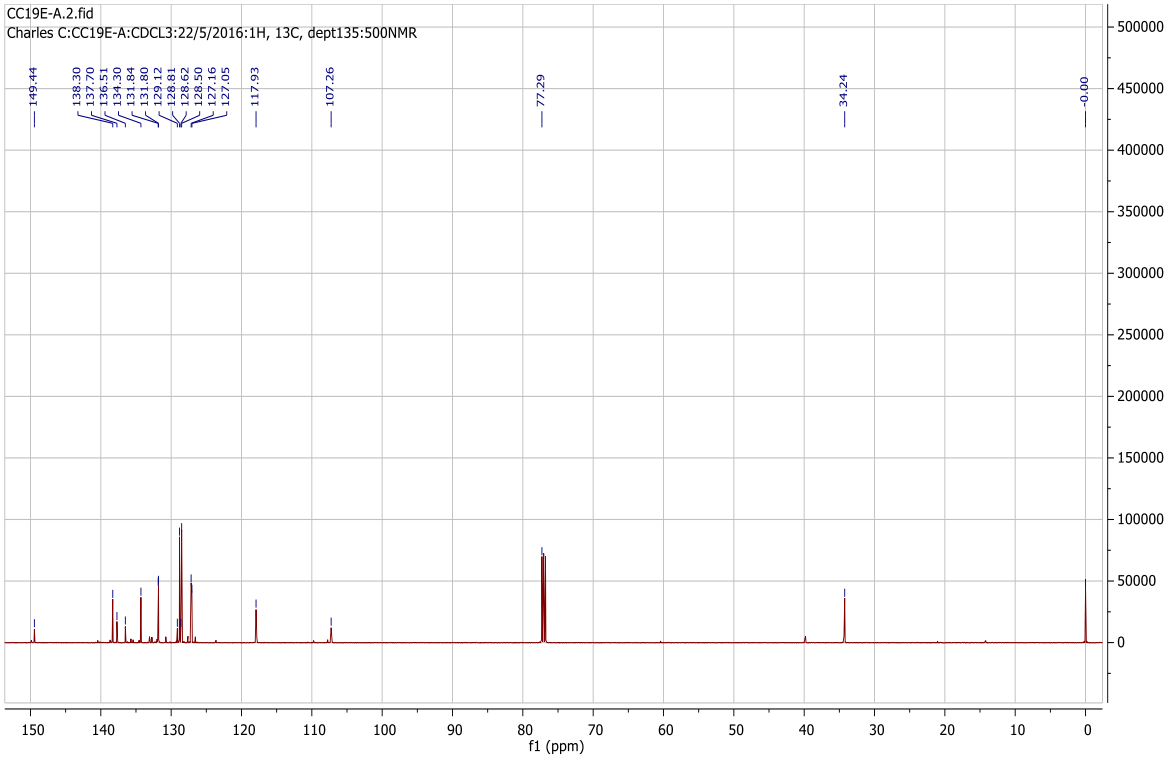
CC19E-A.2.fid
Charles C:CC19E-A:CDCL3:22/5/2016:1H, 13C, dept135:500NMR
f1 (ppm)

160e

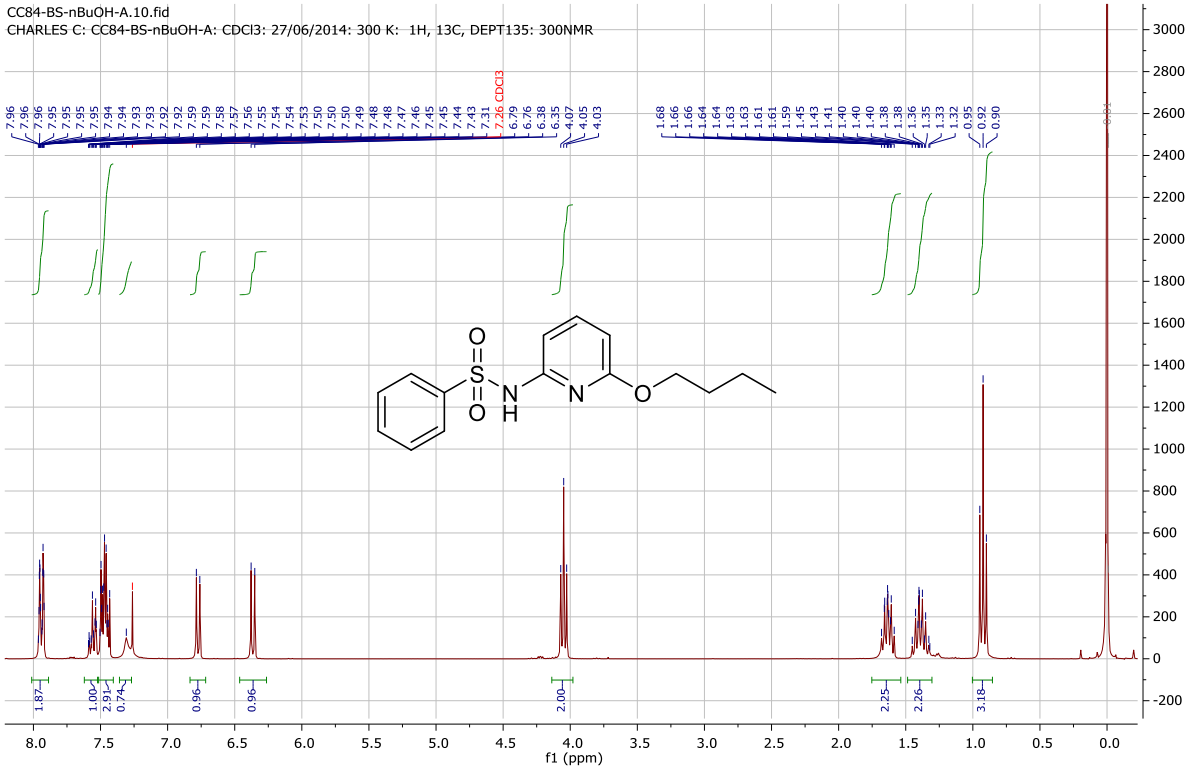
CC84-BS-nBuOH-A.10.fid
CHARLES C: CC84-BS-nBuOH-A: CDCl3: 27/06/2014: 300 K: 1H, 13C, DEPT135: 300NMR
f1 (ppm)

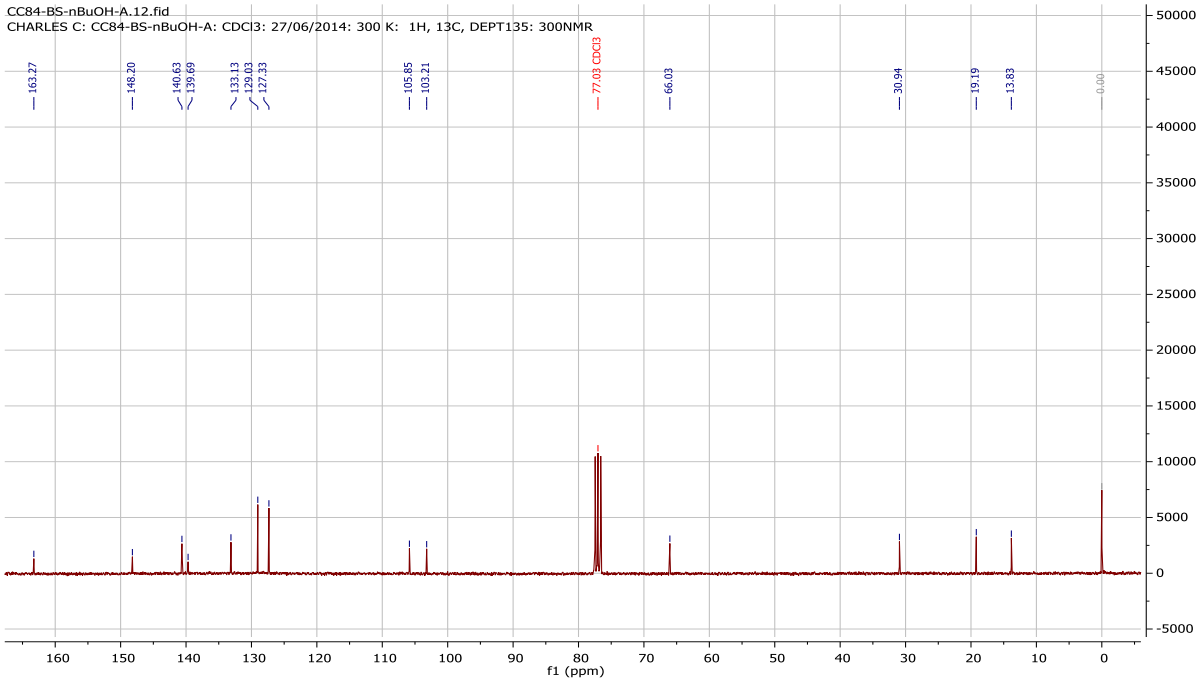
CC84-BS-nBuOH-A.12.fid
CHARLES C: CC84-BS-nBuOH-A: CDCl3: 27/06/2014: 300 K: 1H, 13C, DEPT135: 300NMR
163.27
148.20
140.63
139.69
133.13
129.03
127.33
105.85
103.21
77.03 CDCl3
66.03
30.94
19.19
13.83
f1 (ppm)

160f

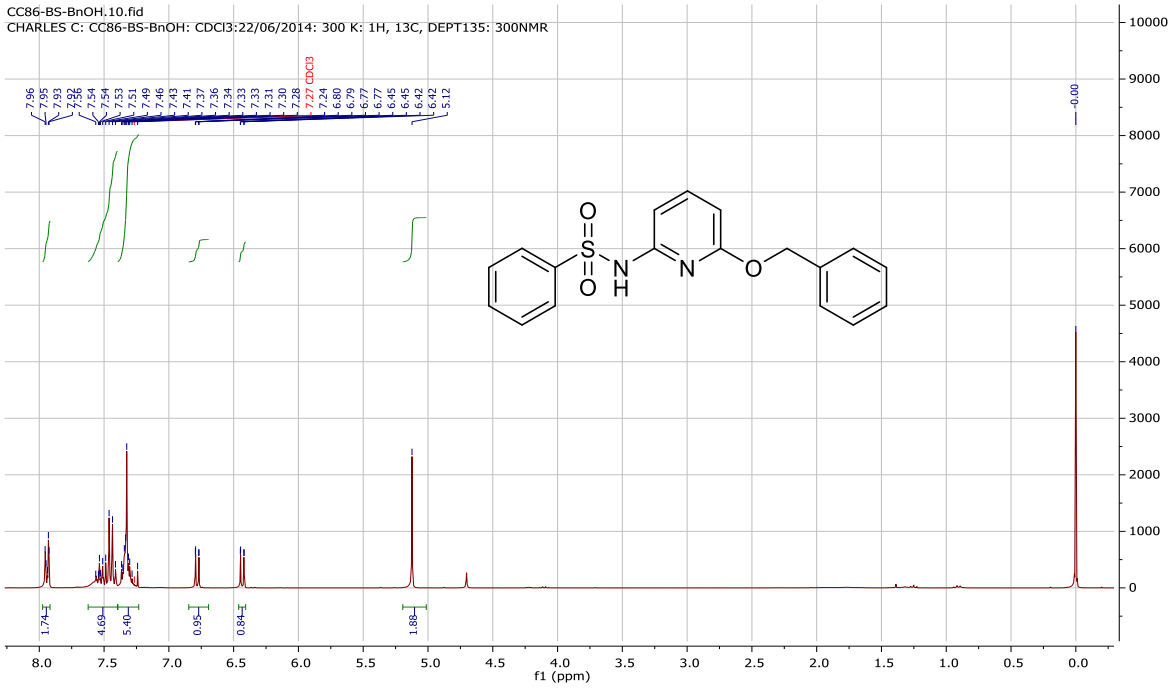
CC86-BS-BnOH.10.fid
CHARLES C: CC86-BS-BnOH: CDCl3:22/06/2014: 300 K: 1H, 13C, DEPT135: 300NMR
7.96
7.95
7.93
7.92
7.56
7.54
7.54
7.53
7.51
7.49
7.46
7.43
7.41
7.37
7.36
7.34
7.33
7.33
7.31
7.30
7.28
7.27 CDCl3
7.24
6.80
6.79
6.77
6.77
6.45
6.45
6.42
6.42
5.12
-0.00
1.74
4.69
5.40
0.95
0.84
1.88
f1 (ppm)

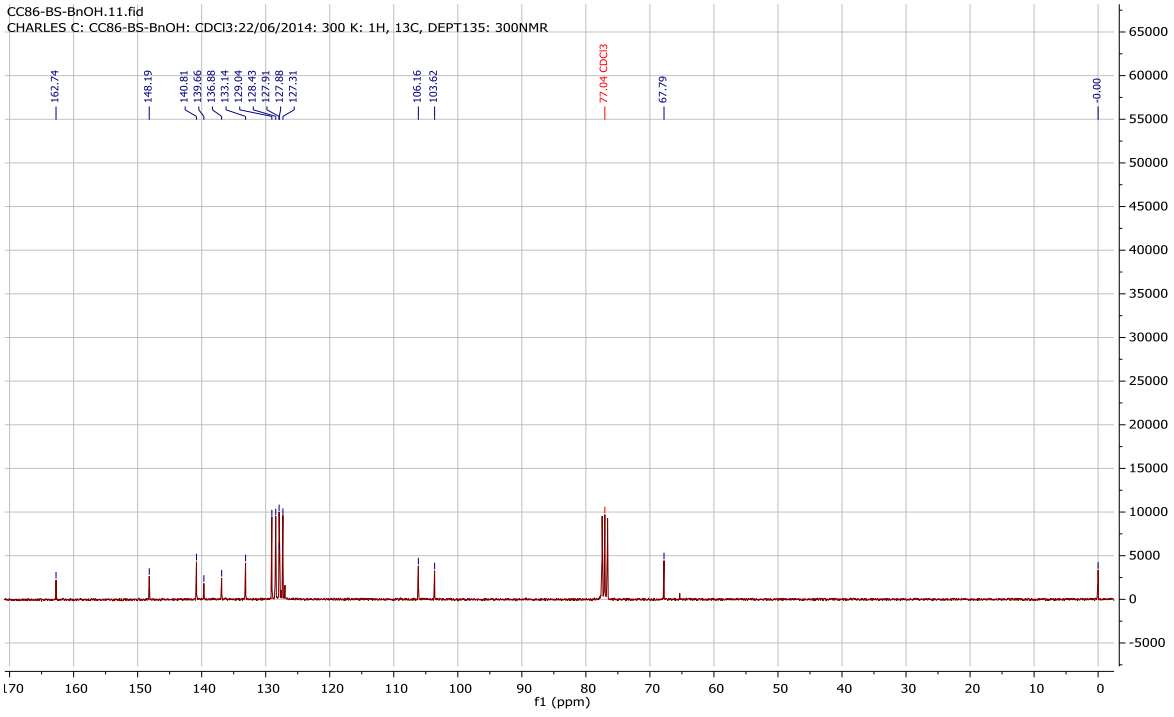
CC86-BS-BnOH.11.fid
CHARLES C: CC86-BS-BnOH: CDCl3:22/06/2014: 300 K: 1H, 13C, DEPT135: 300NMR
162.74
148.19
140.81
139.66
136.88
133.14
129.04
128.43
127.91
127.88
127.31
106.16
103.62
77.04 CDCl3
67.79
-0.00
f1 (ppm)

7.2 NMR Spectra for Chapter 3 Compounds

161

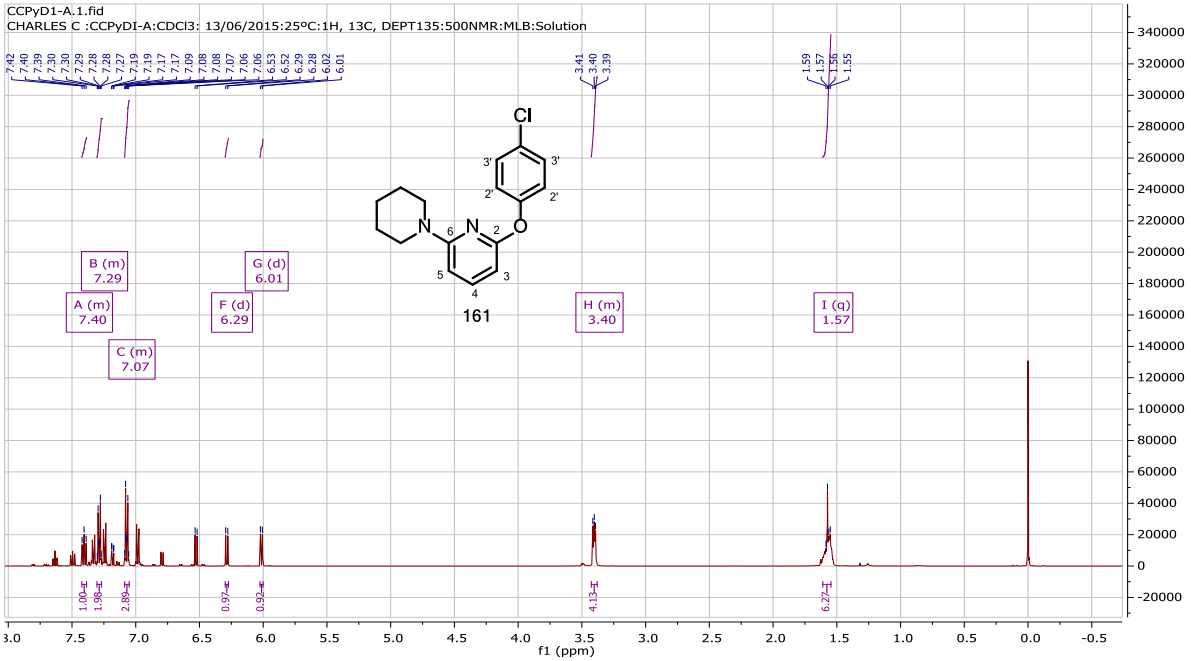

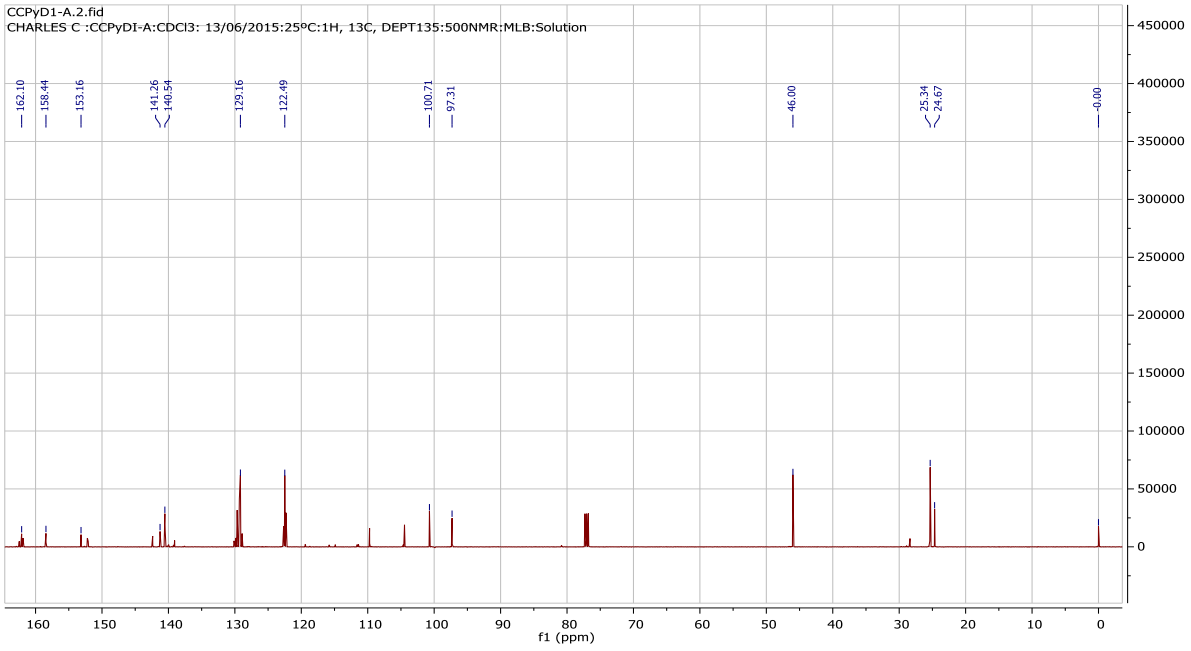

162

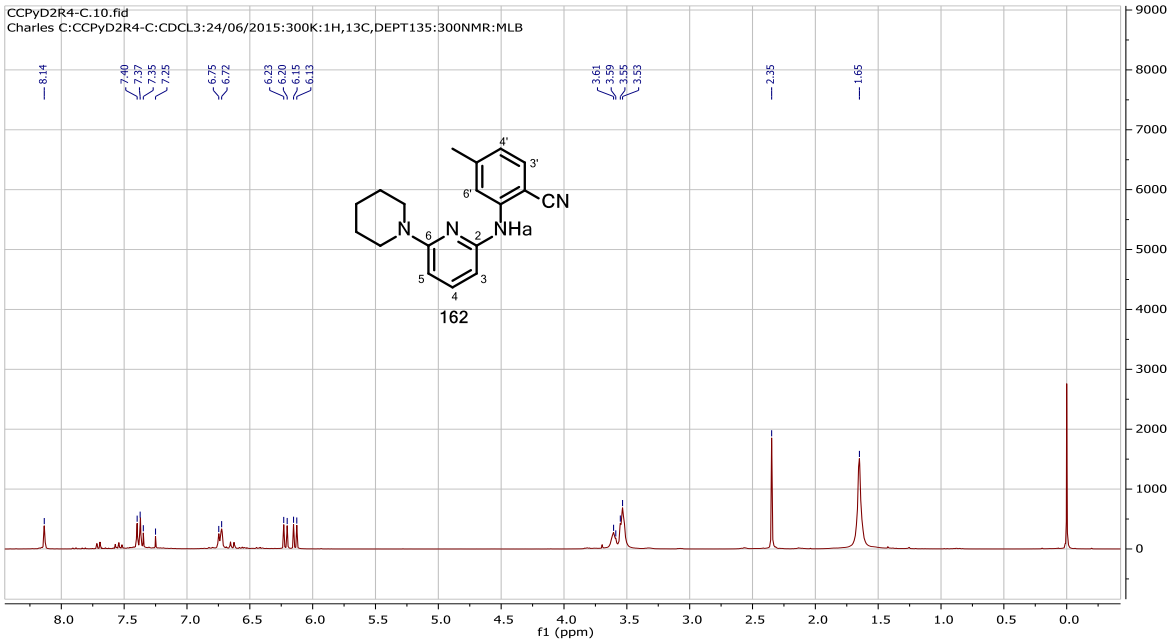
CCPyD2R4-C.10.fid
Charles C:CCPyD2R4-C:CDCL3:24/06/2015:300K:1H,13C,DEPT135:300NMR:MLB
8.14
7.40
7.37
7.35
7.25
6.75
6.72
6.23
6.20
6.15
6.13
3.61
3.59
3.55
3.53
2.35
1.65
CN
NHa
162
f1 (ppm)

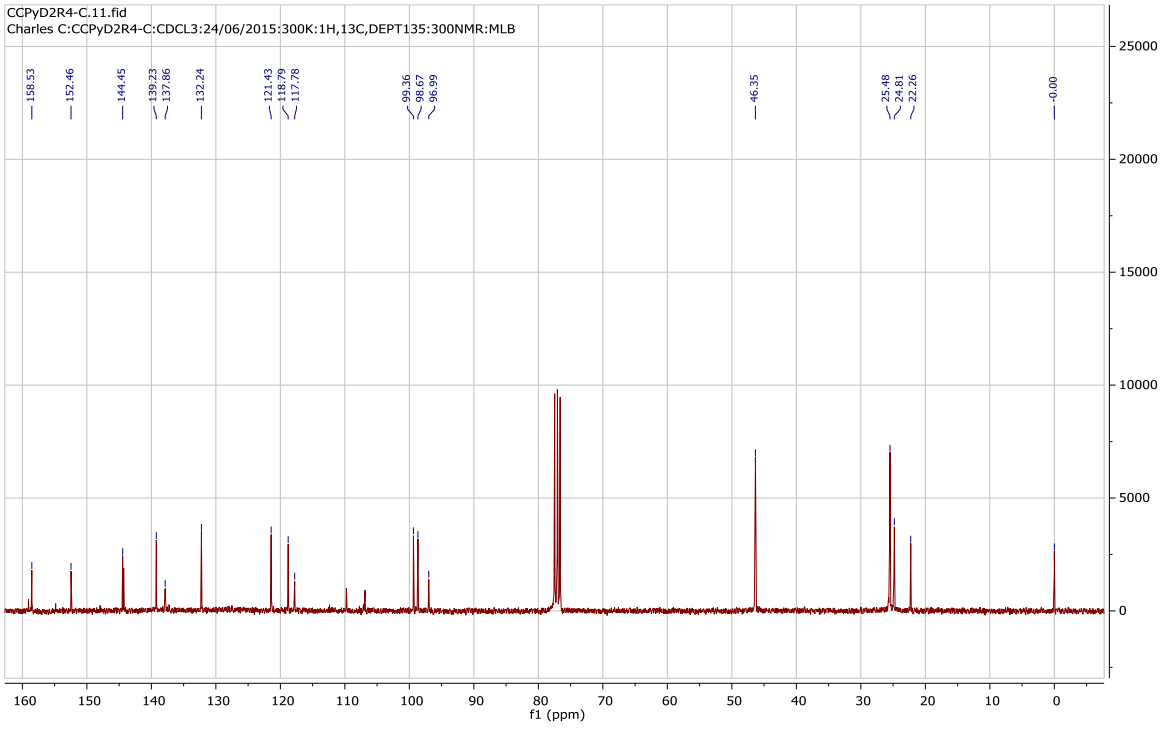
CCPyD2R4-C.11.fid
Charles C:CCPyD2R4-C:CDCL3:24/06/2015:300K:1H,13C,DEPT135:300NMR:MLB
158.53
152.46
144.45
139.23
137.86
132.24
121.43
118.79
117.78
99.36
98.67
96.99
46.35
25.48
24.81
22.26
-0.00
f1 (ppm)

163

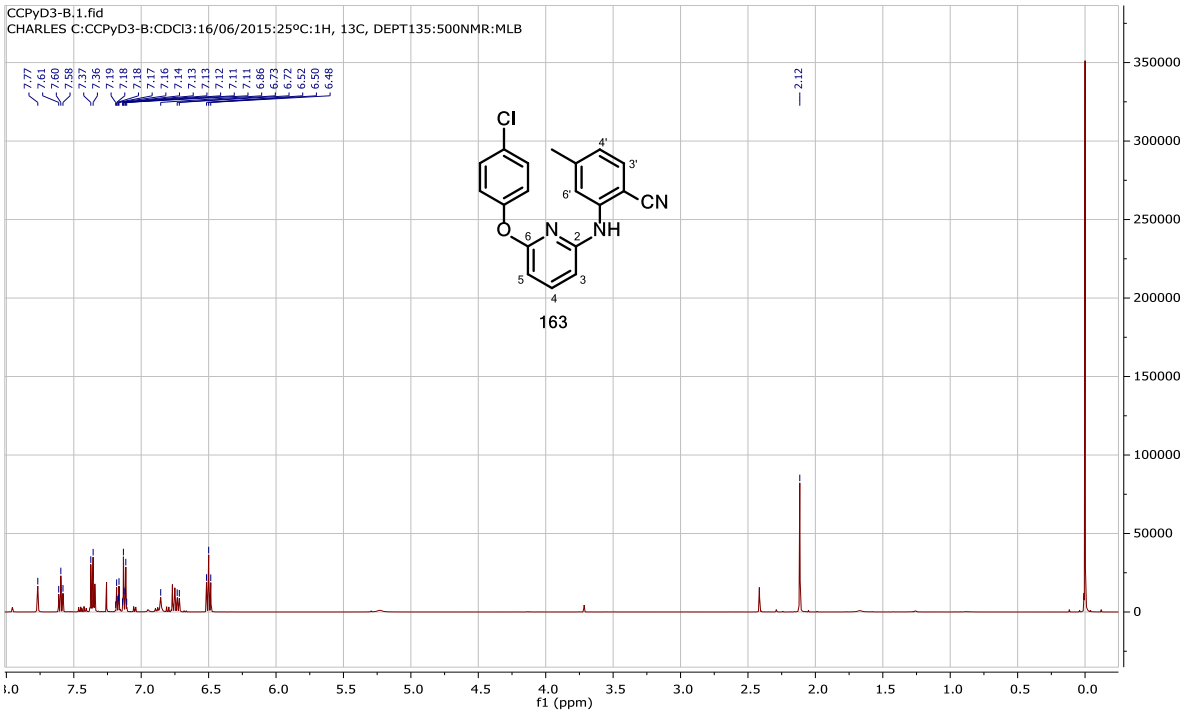
CCPyD3-B.1.fid
CHARLES C:CCPyD3-B:CDCl3:16/06/2015:25ºC:1H, 13C, DEPT135:500NMR:MLB
7.77
7.61
7.60
7.58
7.37
7.36
7.19
7.18
7.18
7.17
7.16
7.14
7.13
7.13
7.12
7.11
7.11
6.86
6.73
6.72
6.52
6.50
6.48
2.12
Cl
4'
3'
6'
CN
O
6
N
2
NH
5
3
4
163
350000
300000
250000
200000
150000
100000
50000
0
8.0
7.5
7.0
6.5
6.0
5.5
5.0
4.5
4.0
3.5
3.0
2.5
2.0
1.5
1.0
0.5
0.0
f1 (ppm)

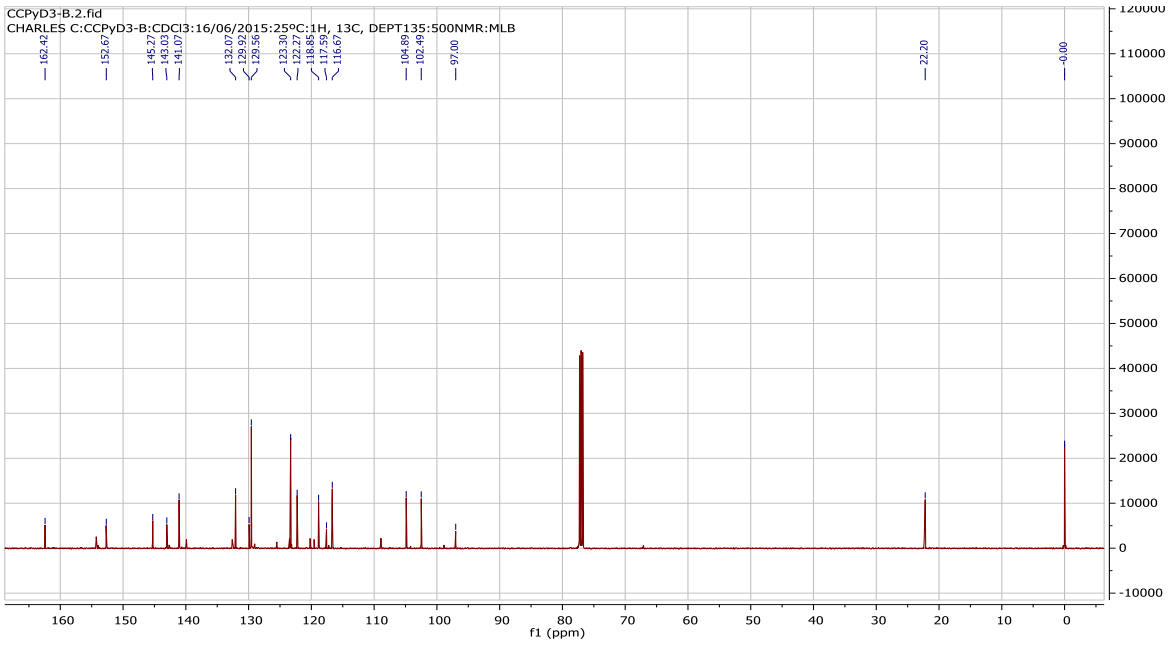
CCPyD3-B.2.fid
CHARLES C:CCPyD3-B:CDCl3:16/06/2015:25ºC:1H, 13C, DEPT135:500NMR:MLB
162.42
152.67
145.27
143.03
141.07
132.07
129.92
129.56
123.30
122.27
118.88
117.59
116.67
104.89
102.49
97.00
22.20
-0.00
120000
110000
100000
90000
80000
70000
60000
50000
40000
30000
20000
10000
0
-10000
160
150
140
130
120
110
100
90
80
70
60
50
40
30
20
10
0
f1 (ppm)

165

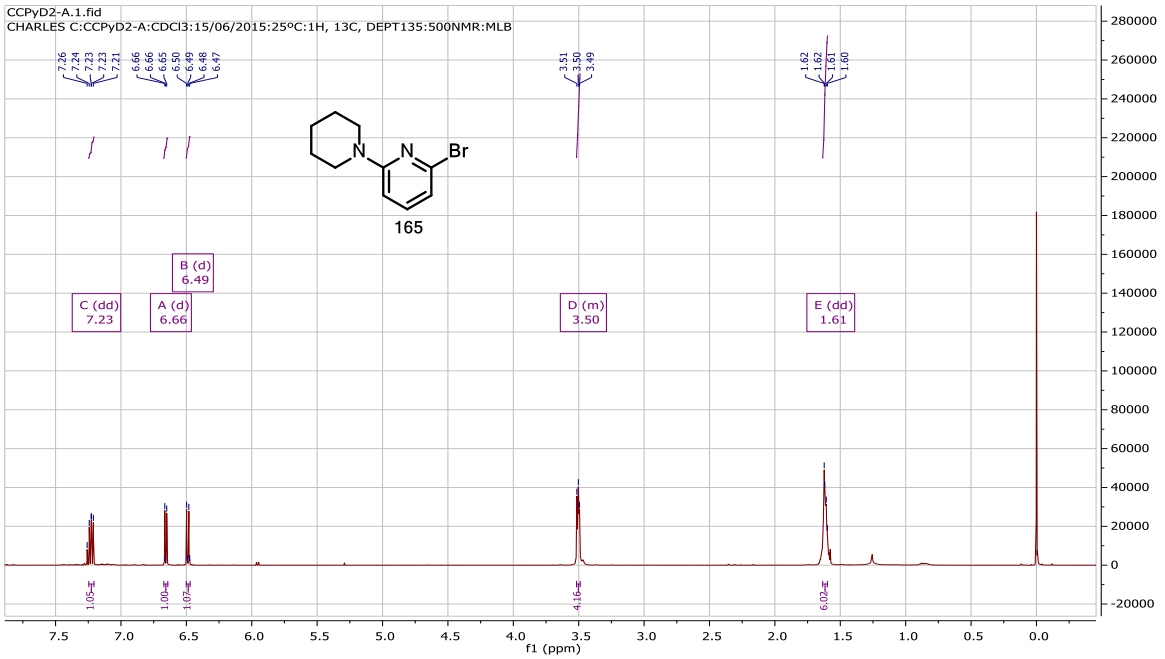
CCPyD2-A.1.fid
CHARLES C:CCPyD2-A:CDCl3:15/06/2015:25ºC:1H, 13C, DEPT135:500NMR:MLB
7.26
7.24
7.23
7.23
7.21
6.66
6.66
6.65
6.50
6.49
6.48
6.47
3.51
3.50
3.49
1.62
1.62
1.61
1.60
N
N
Br
165
B (d)
6.49
C (dd)
7.23
A (d)
6.66
D (m)
3.50
E (dd)
1.61
1.05
1.00
1.07
4.16
6.02
f1 (ppm)

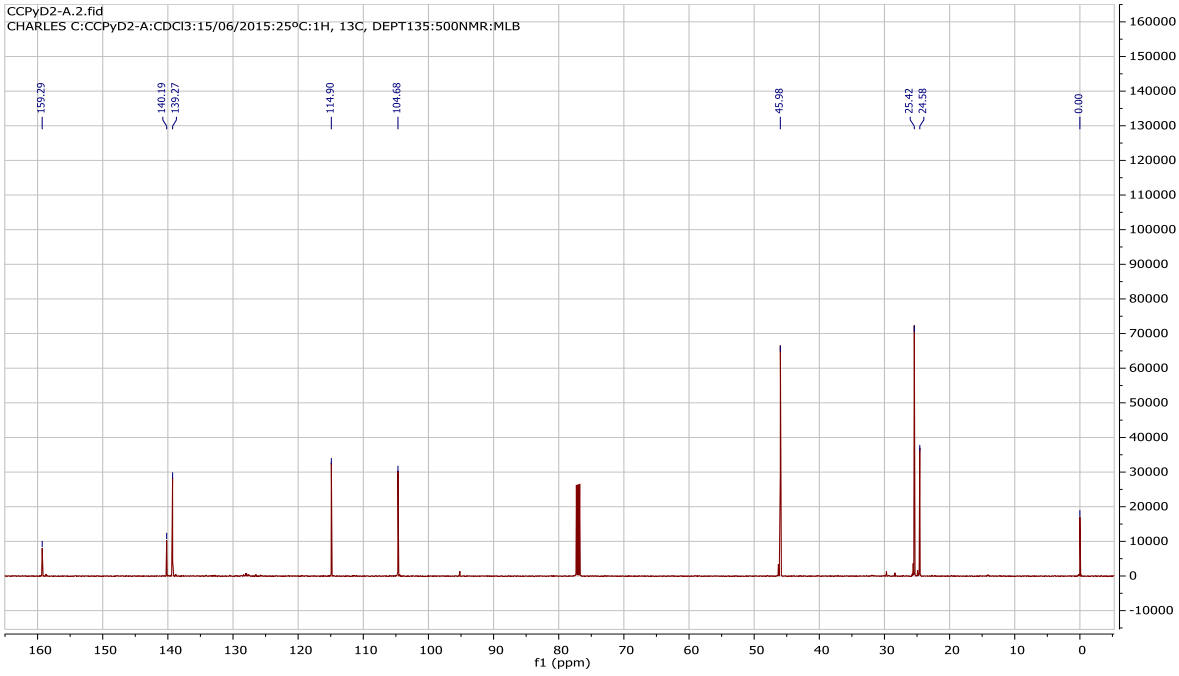
CCPyD2-A.2.fid
CHARLES C:CCPyD2-A:CDCl3:15/06/2015:25ºC:1H, 13C, DEPT135:500NMR:MLB
159.29
140.19
139.27
114.90
104.68
45.98
25.42
24.58
0.00
f1 (ppm)

169

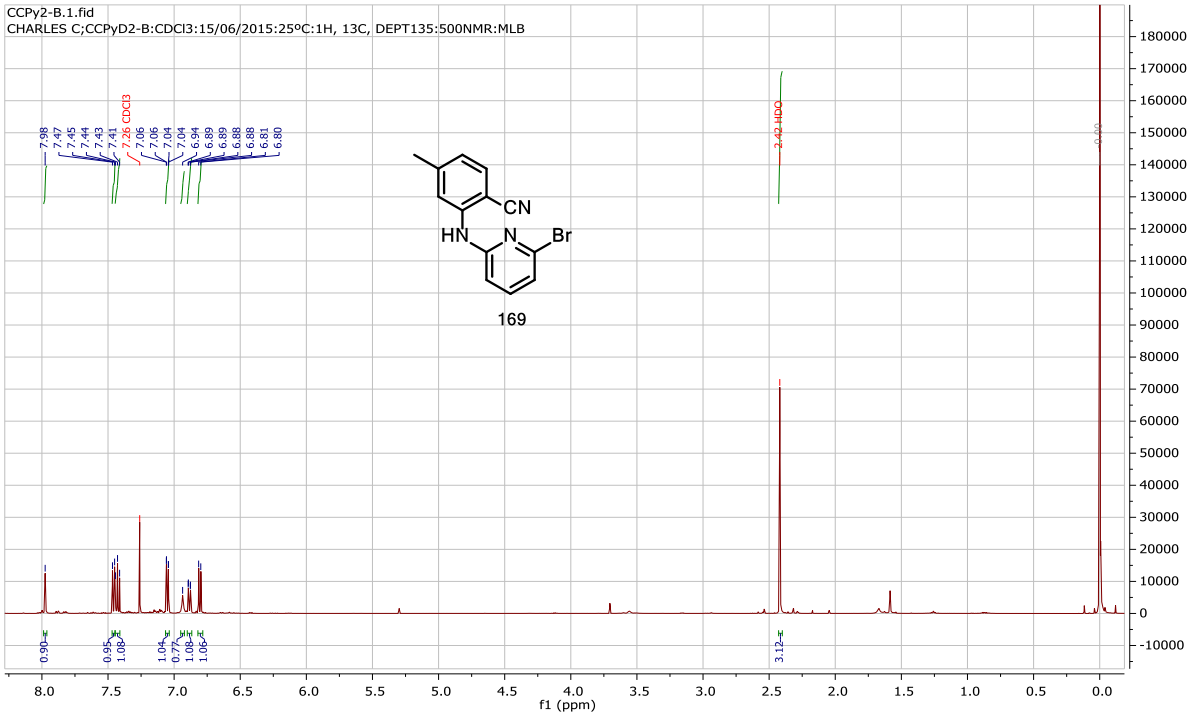
CCPy2-B.1.fid
CHARLES C;CCPyD2-B:CDCl3:15/06/2015:25ºC:1H, 13C, DEPT135:500NMR:MLB
7.98
7.47
7.45
7.44
7.43
7.41
7.26 CDCl3
7.06
7.06
7.06
7.04
7.04
6.94
6.89
6.89
6.88
6.88
6.81
6.80
2.42 HDO
-0.00
CN
HN
N
Br
169
0.90
0.95
1.08
1.04
0.77
1.08
1.06
3.12
f1 (ppm)

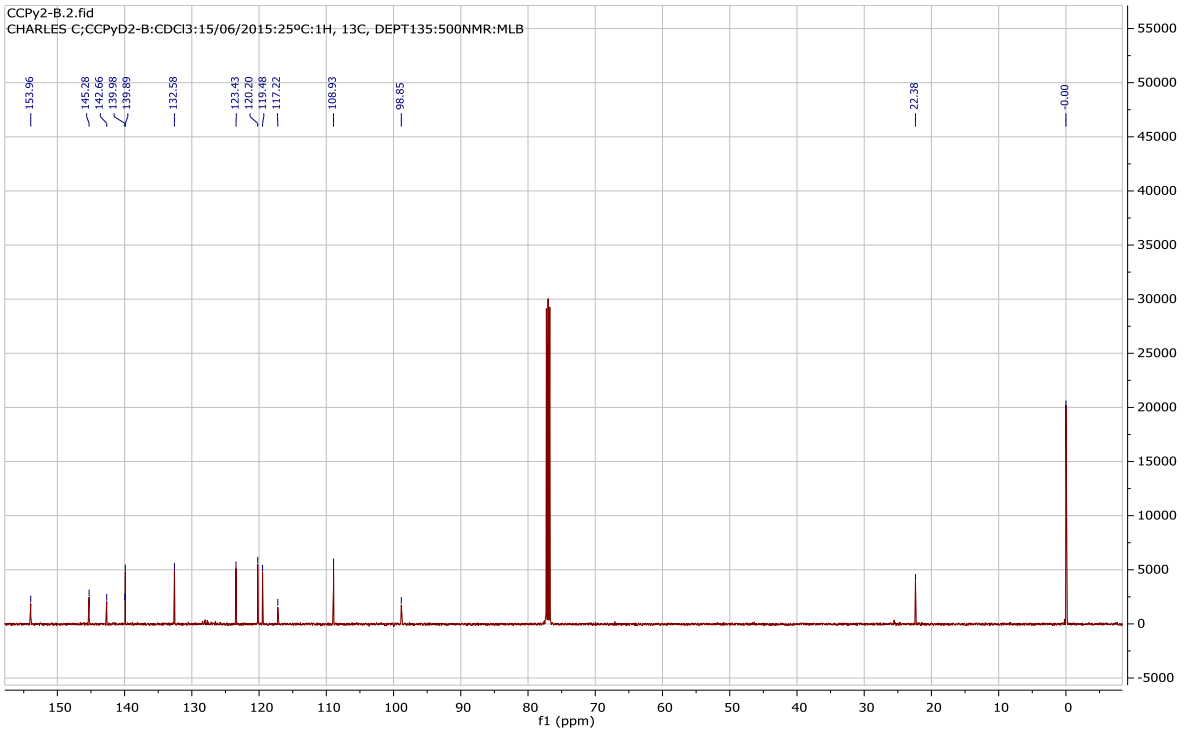
CCPy2-B.2.fid
CHARLES C;CCPyD2-B:CDCl3:15/06/2015:25ºC:1H, 13C, DEPT135:500NMR:MLB
153.96
145.28
142.66
139.98
139.89
132.58
123.43
120.20
119.48
117.22
108.93
98.85
22.38
-0.00
f1 (ppm)

171a

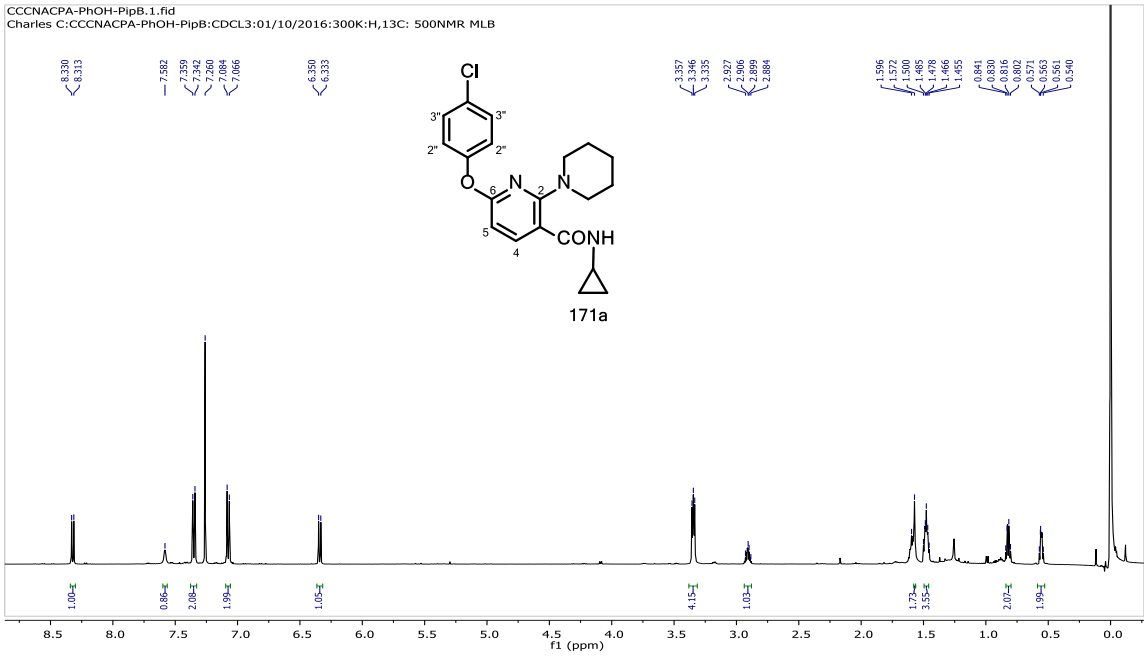
CCCNACPA-PhOH-PipB.1.fid
Charles C:CCCNACPA-PhOH-PipB:CDCL3:01/10/2016:300K:H,13C: 500NMR MLB
Cl
CONH
171a
f1 (ppm)

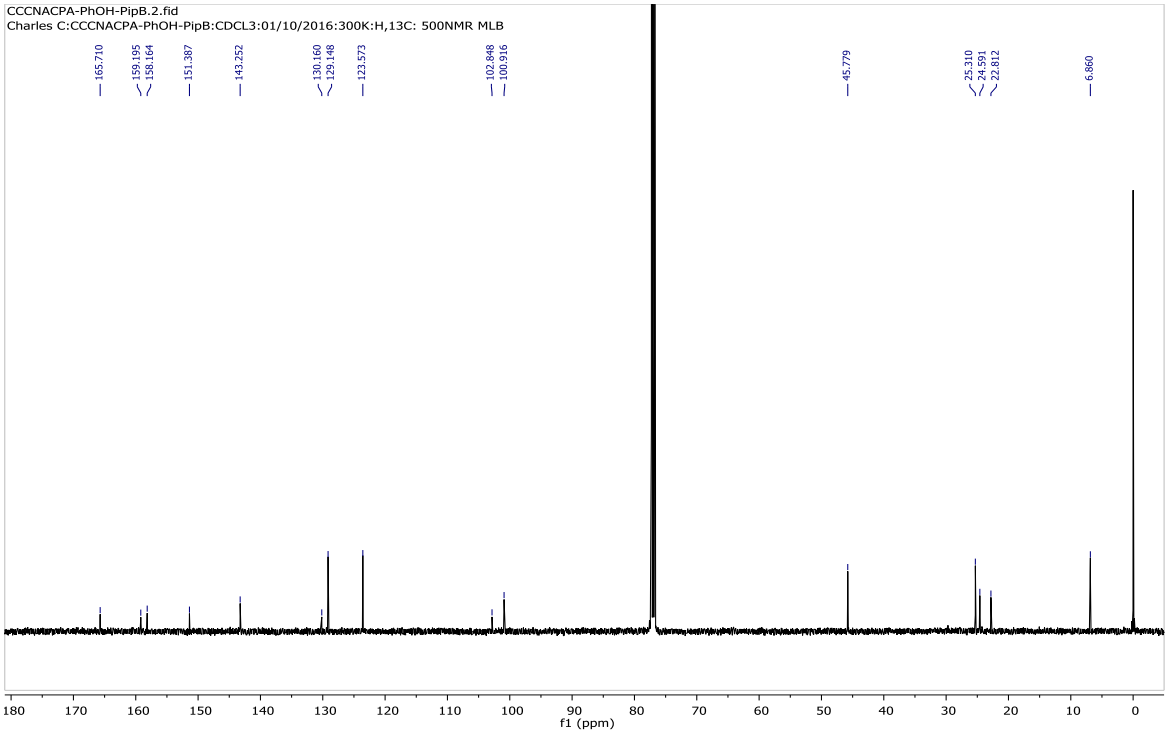
CCCNACPA-PhOH-PipB.2.fid
Charles C:CCCNACPA-PhOH-PipB:CDCL3:01/10/2016:300K:H,13C: 500NMR MLB
f1 (ppm)

171b

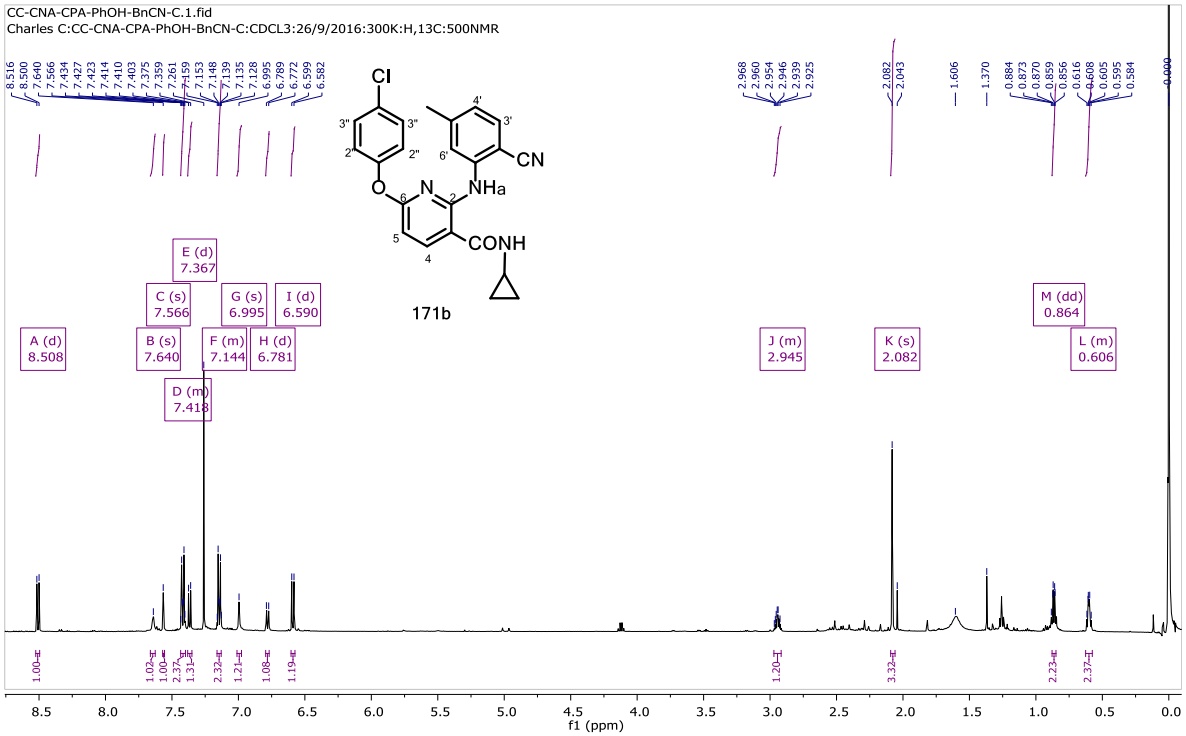
CC-CNA-CPA-PhOH-BnCN-C.1.fid
Charles C:CC-CNA-CPA-PhOH-BnCN-C:CDCL3:26/9/2016:300K:H,13C:500NMR
Cl
CN
NHa
CONH
171b
A (d) 8.508
B (s) 7.640
C (s) 7.566
D (m) 7.418
E (d) 7.367
F (m) 7.144
G (s) 6.995
H (d) 6.781
I (d) 6.590
J (m) 2.945
K (s) 2.082
L (m) 0.606
M (dd) 0.864
f1 (ppm)

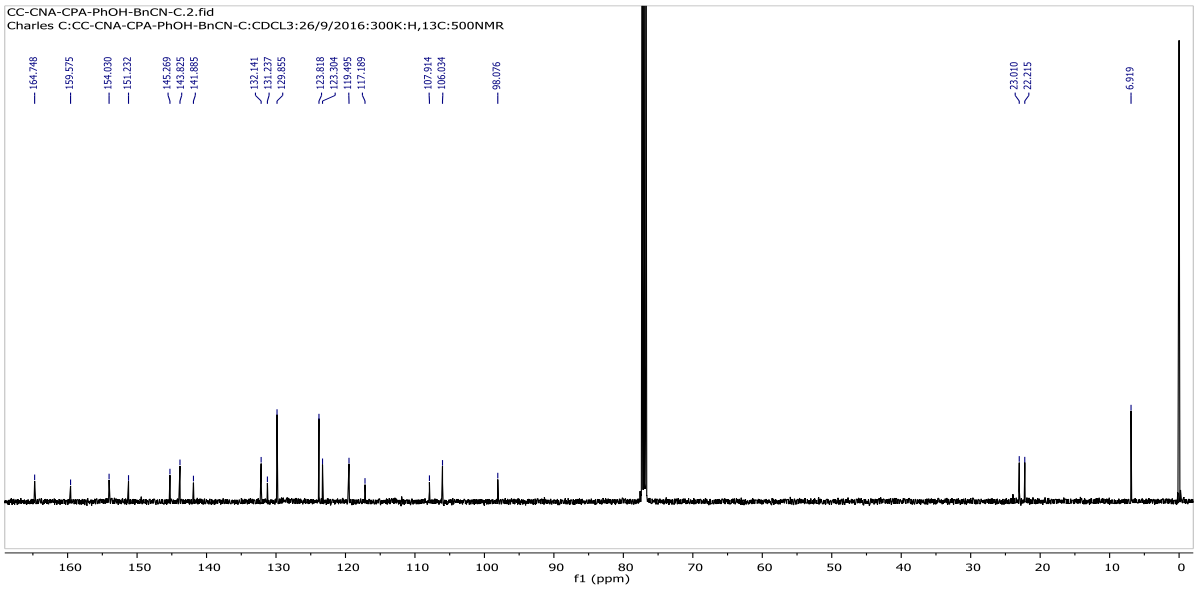
CC-CNA-CPA-PhOH-BnCN-C.2.fid
Charles C:CC-CNA-CPA-PhOH-BnCN-C:CDCL3:26/9/2016:300K:H,13C:500NMR
f1 (ppm)

172

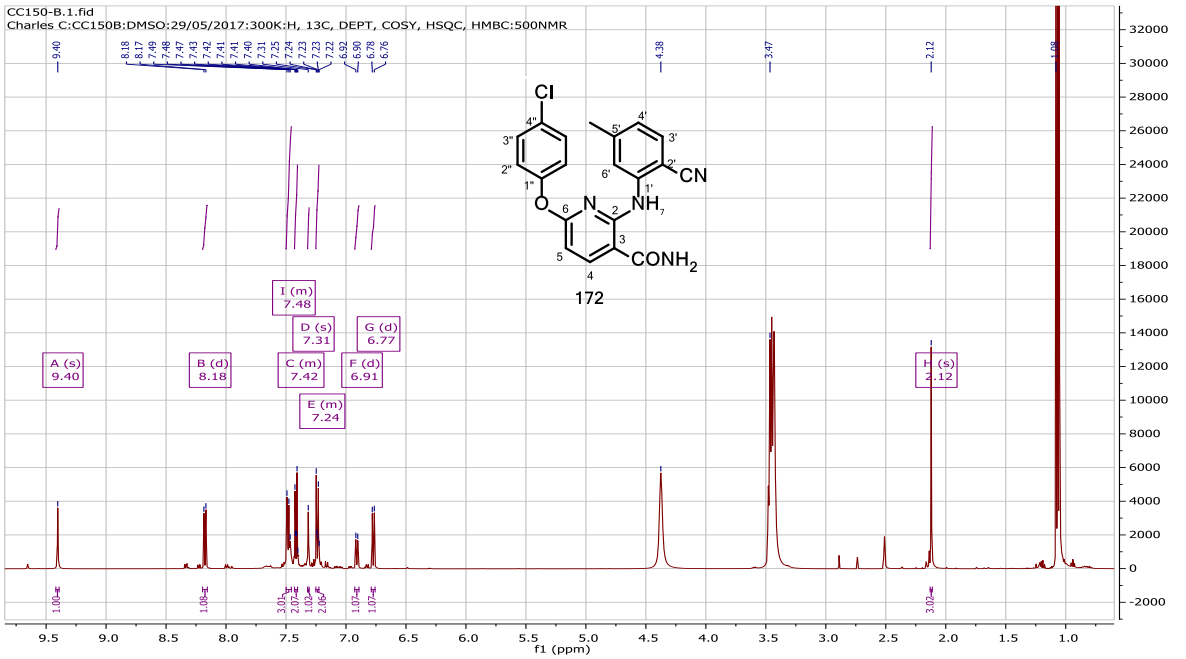
CC150-B.1.fid
Charles C:CC150B:DMSO:29/05/2017:300K:H, 13C, DEPT, COSY, HSQC, HMBC:500NMR
9.40
8.18
8.17
7.49
7.48
7.47
7.43
7.42
7.41
7.40
7.31
7.25
7.24
7.23
7.22
6.92
6.90
6.78
6.76
4.38
3.47
2.12
1.09
Cl
CN
NH
CONH2
172
A (s) 9.40
B (d) 8.18
C (m) 7.42
D (s) 7.31
E (m) 7.24
F (d) 6.91
G (d) 6.77
I (m) 7.48
H (s) 2.12
f1 (ppm)

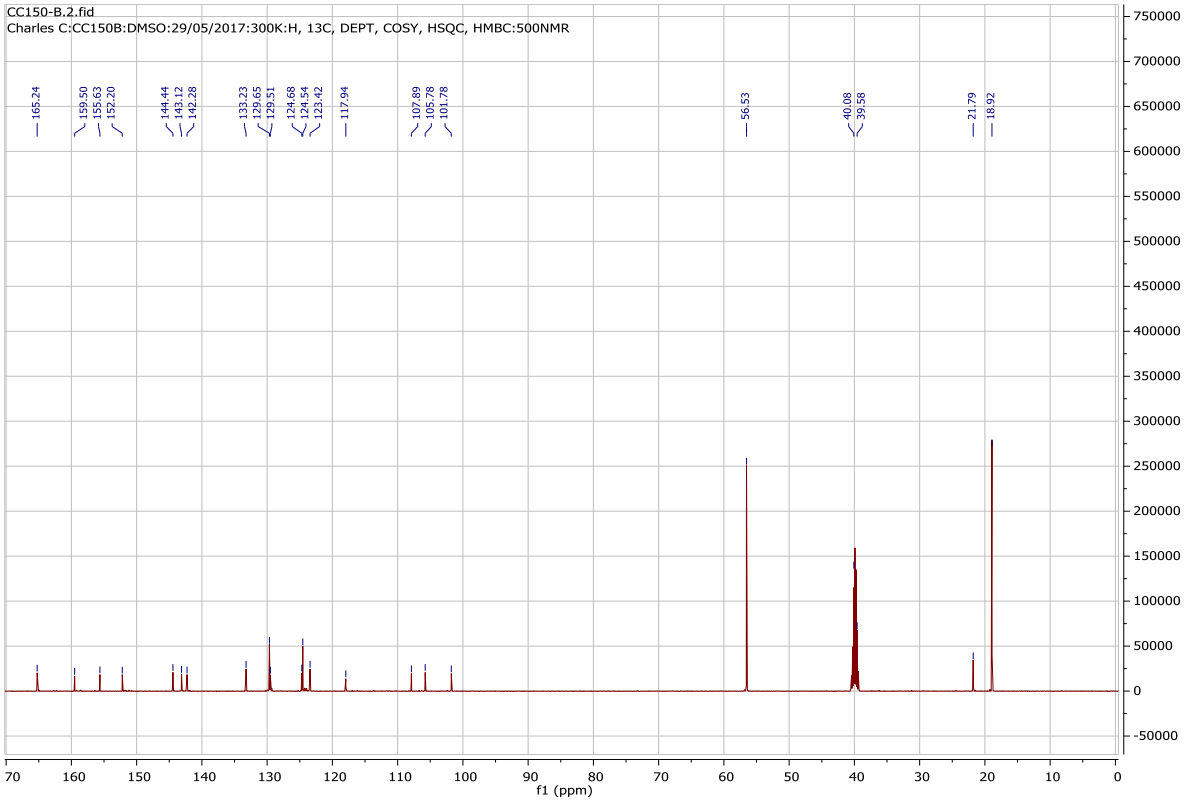
CC150-B.2.fid
Charles C:CC150B:DMSO:29/05/2017:300K:H, 13C, DEPT, COSY, HSQC, HMBC:500NMR
165.24
159.50
155.63
152.20
144.44
143.12
142.28
133.23
129.65
129.51
124.68
124.54
123.42
117.94
107.89
105.78
101.78
56.53
40.08
39.58
21.79
18.92
f1 (ppm)

176a

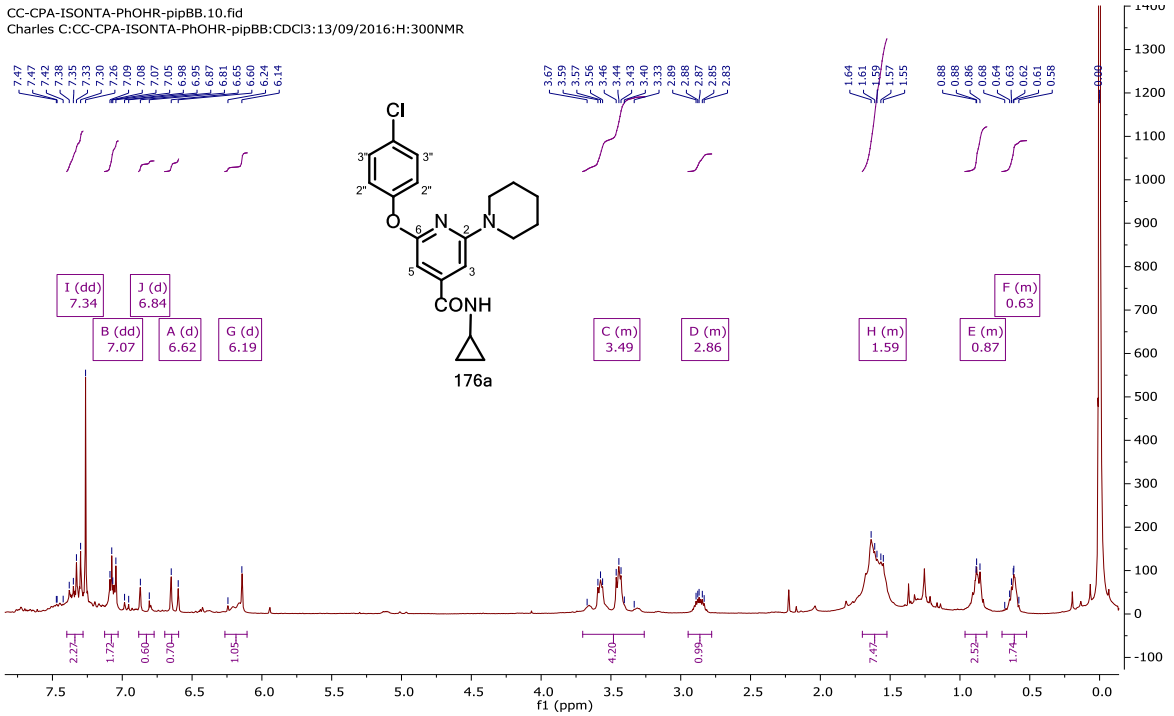
CC-CPA-ISONTA-PhOHR-pipBB.10.fid
Charles C:CC-CPA-ISONTA-PhOHR-pipBB:CDCl3:13/09/2016:H:300NMR
I (dd) 7.34
J (d) 6.84
B (dd) 7.07
A (d) 6.62
G (d) 6.19
C (m) 3.49
D (m) 2.86
H (m) 1.59
F (m) 0.63
E (m) 0.87
176a
f1 (ppm)

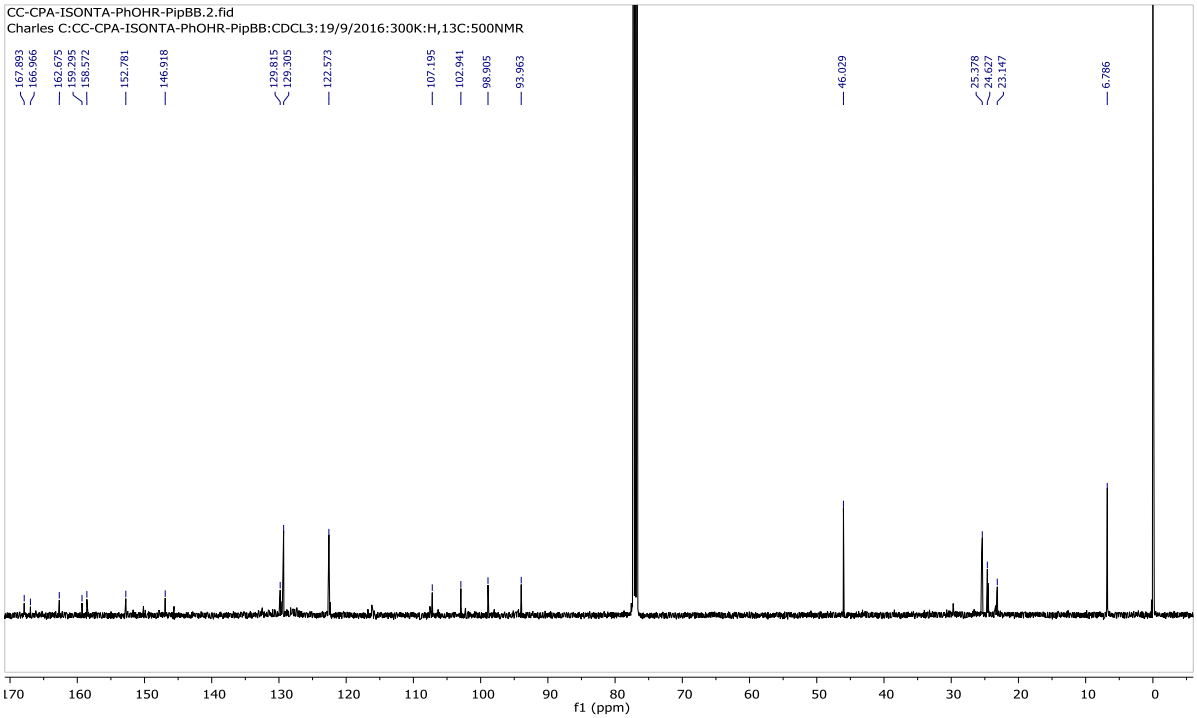
CC-CPA-ISONTA-PhOHR-PipBB.2.fid
Charles C:CC-CPA-ISONTA-PhOHR-PipBB:CDCL3:19/9/2016:300K:H,13C:500NMR
f1 (ppm)

176b

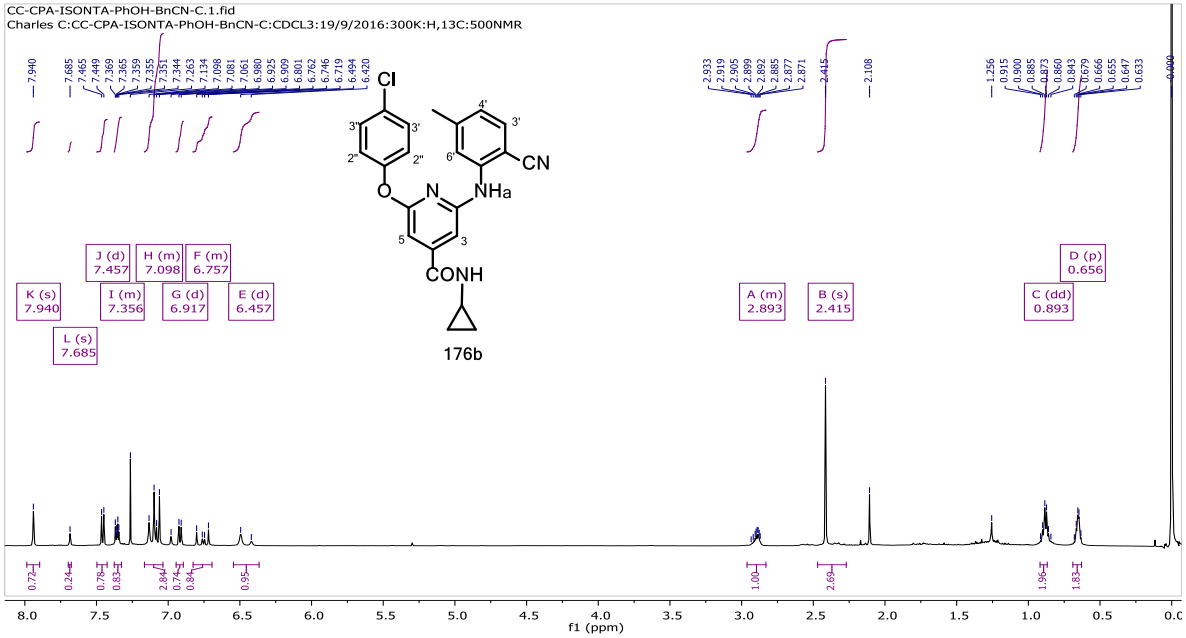
CC-CPA-ISONTA-PhOH-BnCN-C.1.fid
Charles C:CC-CPA-ISONTA-PhOH-BnCN-C:CDCL3:19/9/2016:300K:H,13C:500NMR
Cl
CN
NHa
CONH
176b
K (s) 7.940
L (s) 7.685
J (d) 7.457
I (m) 7.356
H (m) 7.098
G (d) 6.917
F (m) 6.757
E (d) 6.457
A (m) 2.893
B (s) 2.415
D (p) 0.656
C (dd) 0.893
f1 (ppm)

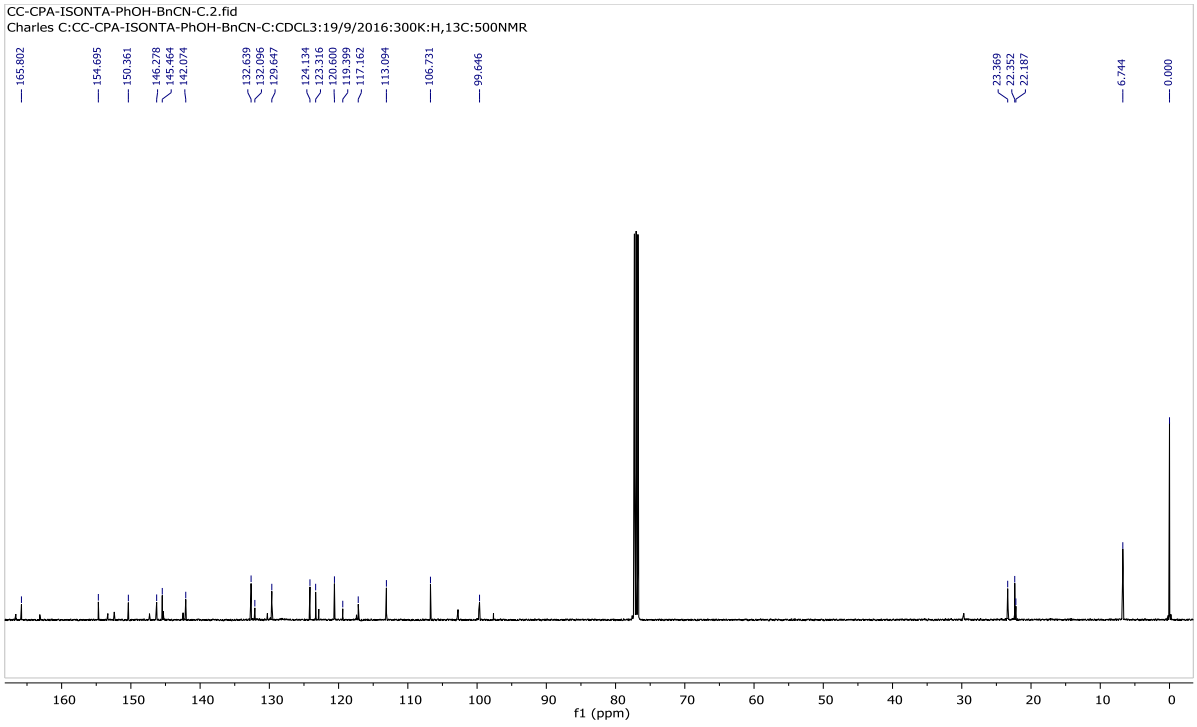
CC-CPA-ISONTA-PhOH-BnCN-C.2.fid
Charles C:CC-CPA-ISONTA-PhOH-BnCN-C:CDCL3:19/9/2016:300K:H,13C:500NMR
f1 (ppm)

180a

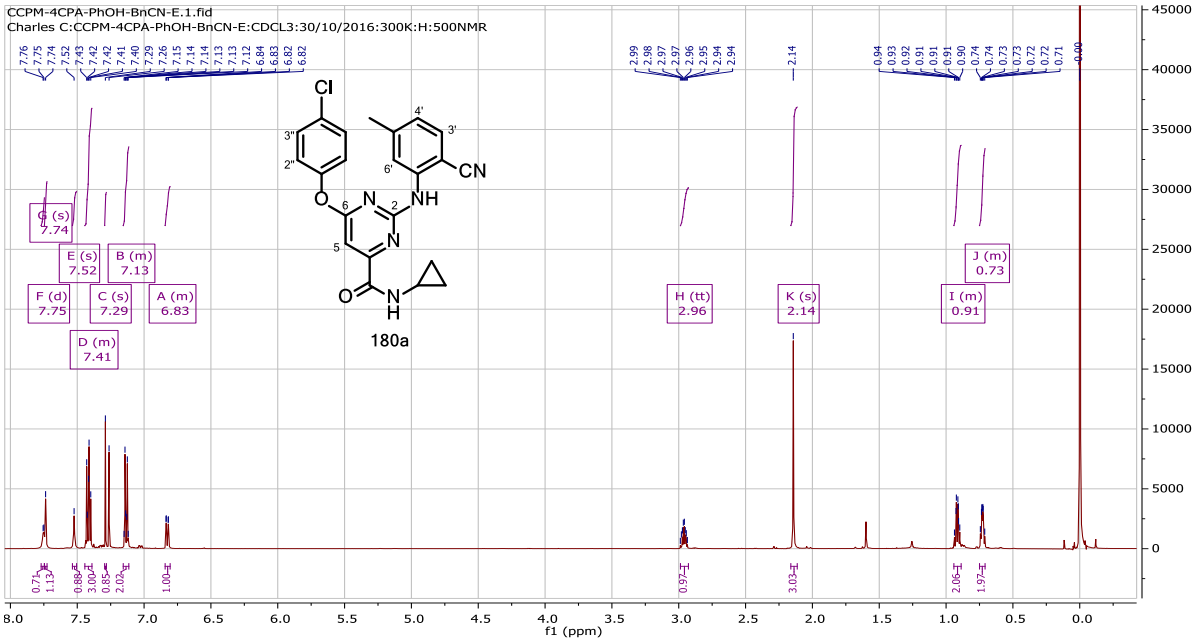
CCPM-4CPA-PhOH-BnCN-E.1.fid
Charles C:CCPM-4CPA-PhOH-BnCN-E:CDCL3:30/10/2016:300K:H:500NMR
G (s) 7.74
E (s) 7.52
B (m) 7.13
F (d) 7.75
C (s) 7.29
A (m) 6.83
D (m) 7.41
H (tt) 2.96
K (s) 2.14
J (m) 0.73
I (m) 0.91
180a
f1 (ppm)

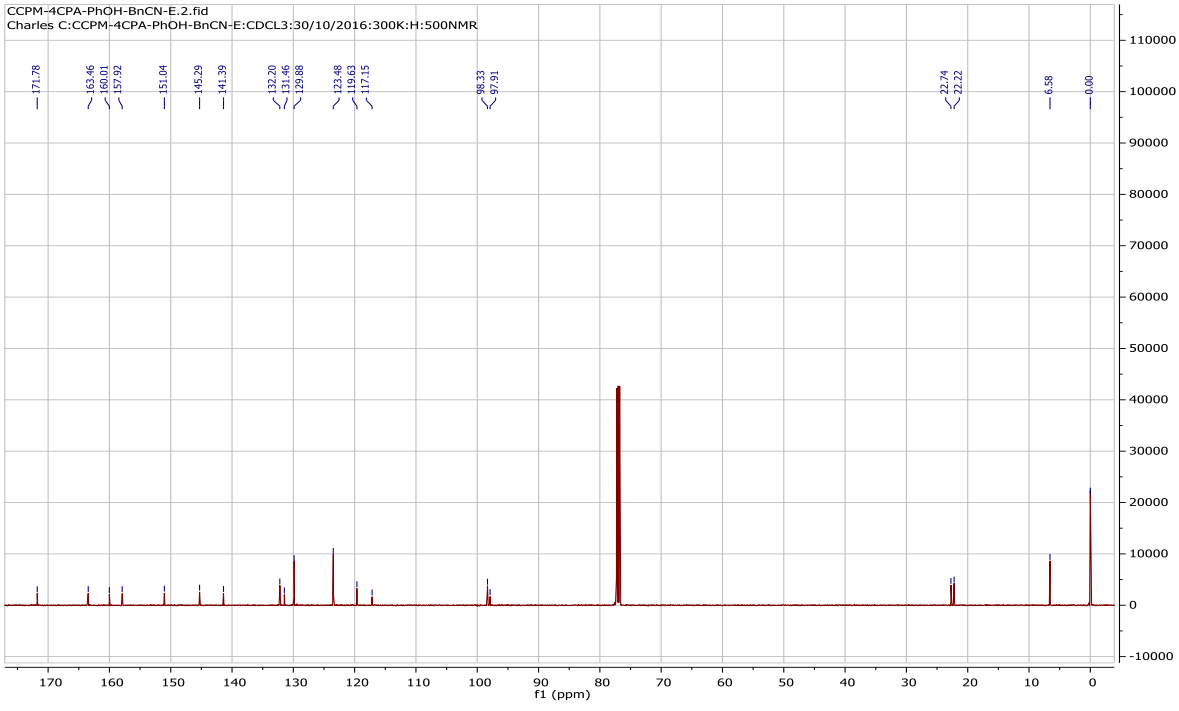
CCPM-4CPA-PhOH-BnCN-E.2.fid
Charles C:CCPM-4CPA-PhOH-BnCN-E:CDCL3:30/10/2016:300K:H:500NMR
f1 (ppm)

181a

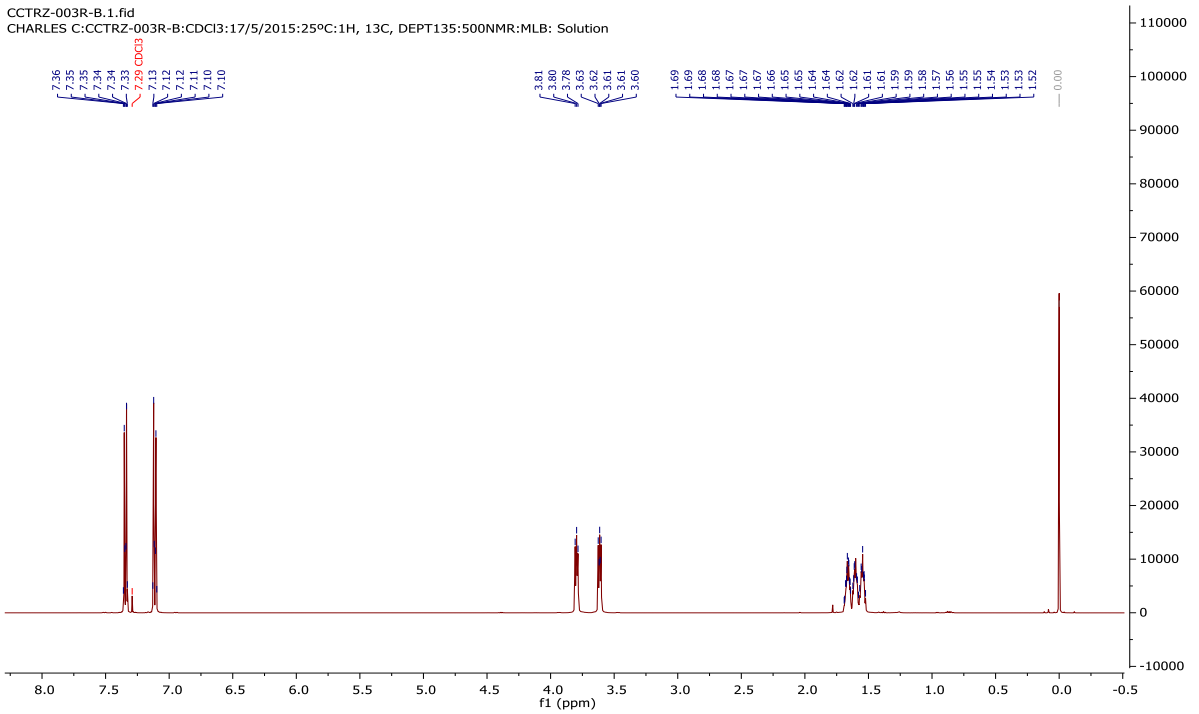
CCTRZ-003R-B.1.fid
CHARLES C:CCTRZ-003R-B:CDCl3:17/5/2015:25ºC:1H, 13C, DEPT135:500NMR:MLB: Solution
7.36
7.35
7.35
7.34
7.34
7.33
7.29 CDCl3
7.13
7.12
7.12
7.11
7.10
7.10
3.81
3.80
3.78
3.63
3.62
3.61
3.61
3.60
1.69
1.69
1.68
1.68
1.67
1.67
1.67
1.66
1.65
1.65
1.64
1.64
1.62
1.62
1.61
1.61
1.59
1.59
1.58
1.57
1.56
1.55
1.55
1.54
1.53
1.53
1.52
0.00
f1 (ppm)

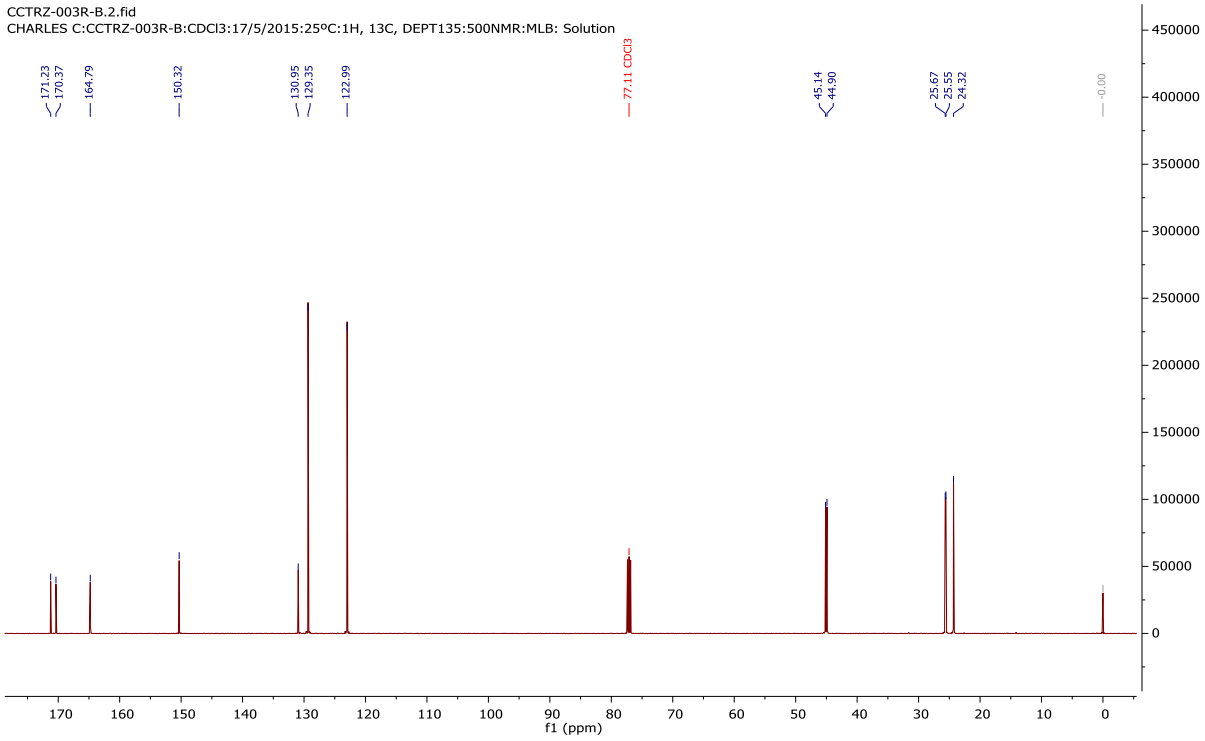
CCTRZ-003R-B.2.fid
CHARLES C:CCTRZ-003R-B:CDCl3:17/5/2015:25ºC:1H, 13C, DEPT135:500NMR:MLB: Solution
171.23
170.37
164.79
150.32
130.95
129.35
122.99
77.11 CDCl3
45.14
44.90
25.67
25.55
24.32
-0.00
f1 (ppm)

181b

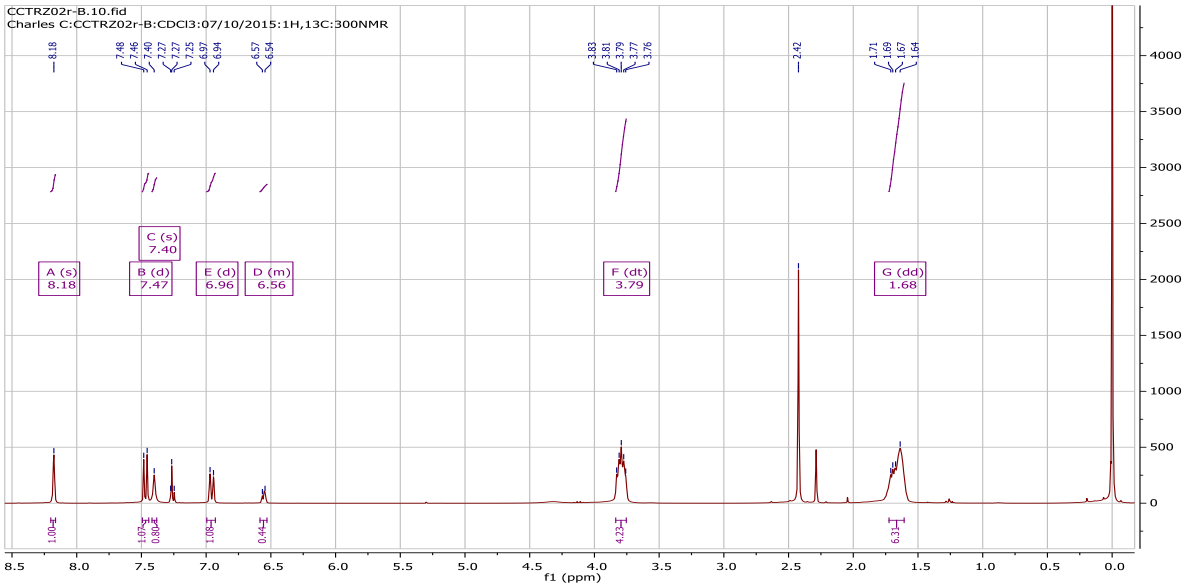
CCTRZ02r-B.10.fid
Charles C:CCTRZ02r-B:CDCl3:07/10/2015:1H,13C:300NMR
A (s) 8.18
B (d) 7.47
C (s) 7.40
E (d) 6.96
D (m) 6.56
F (dt) 3.79
G (dd) 1.68
f1 (ppm)

185b

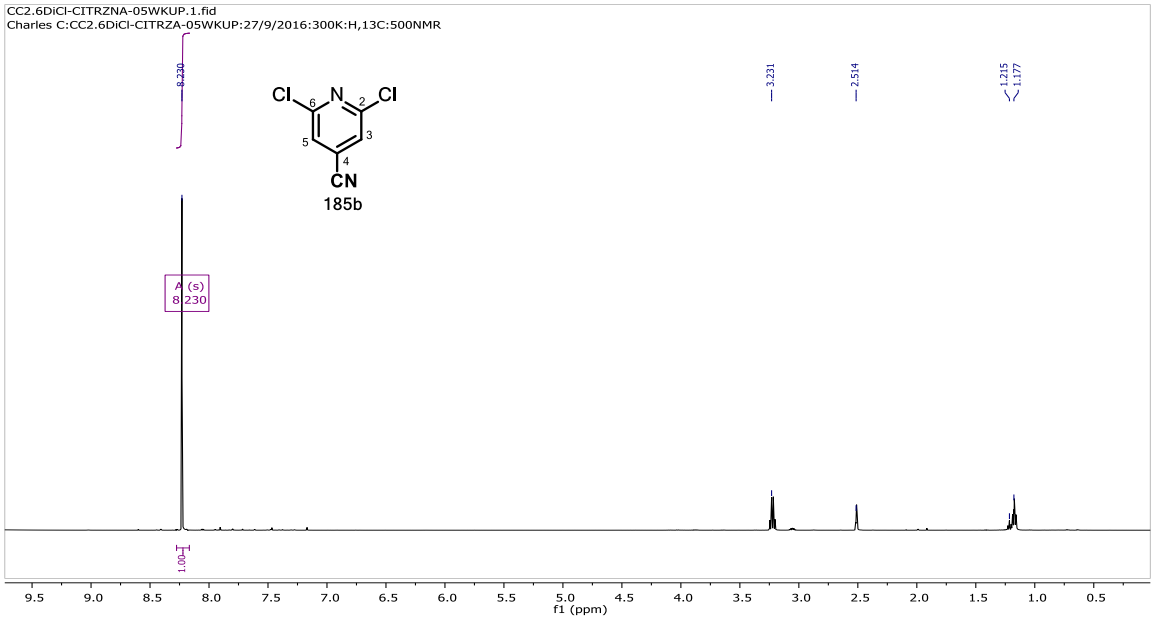
CC2.6DiCl-CITRZNA-05WKUP.1.fid
Charles C:CC2.6DiCl-CITRZA-05WKUP:27/9/2016:300K:H,13C:500NMR
8.230
3.231
2.514
1.215
1.177
Cl
N
Cl
CN
185b
A (s)
8.230
1.00
f1 (ppm)

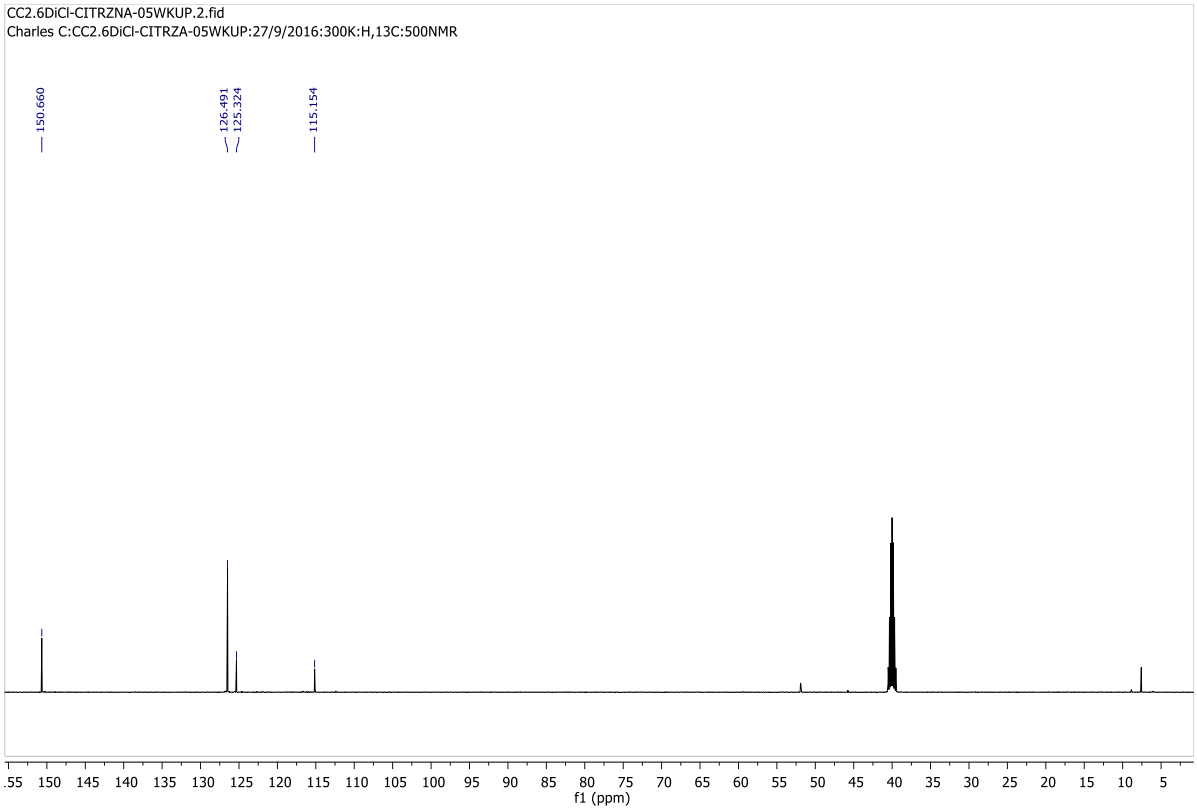
CC2.6DiCl-CITRZNA-05WKUP.2.fid
Charles C:CC2.6DiCl-CITRZA-05WKUP:27/9/2016:300K:H,13C:500NMR
150.660
126.491
125.324
115.154
f1 (ppm)

186a

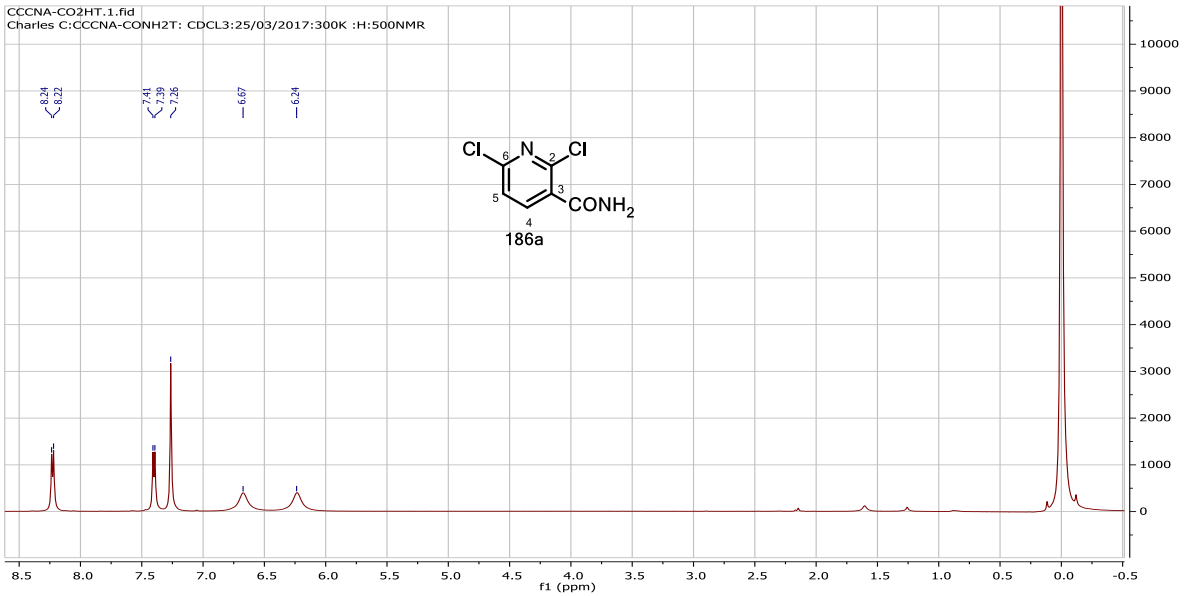
CCCNA-CO2HT.1.fid
Charles C:CCCNA-CONH2T: CDCL3:25/03/2017:300K :H:500NMR
8.24
8.22
7.41
7.39
7.26
6.67
6.24
Cl
N
Cl
CONH2
186a
f1 (ppm)

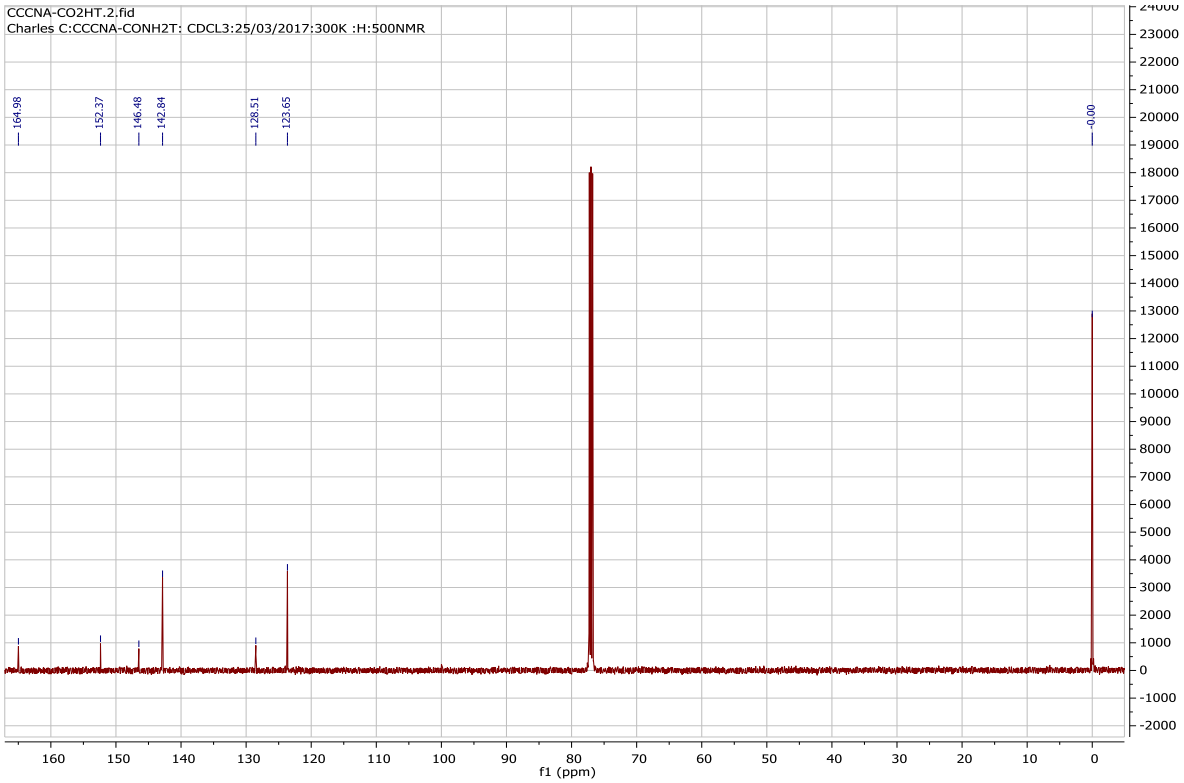
CCCNA-CO2HT.2.fid
Charles C:CCCNA-CONH2T: CDCL3:25/03/2017:300K :H:500NMR
164.98
152.37
146.48
142.84
128.51
123.65
0.00
f1 (ppm)

187b

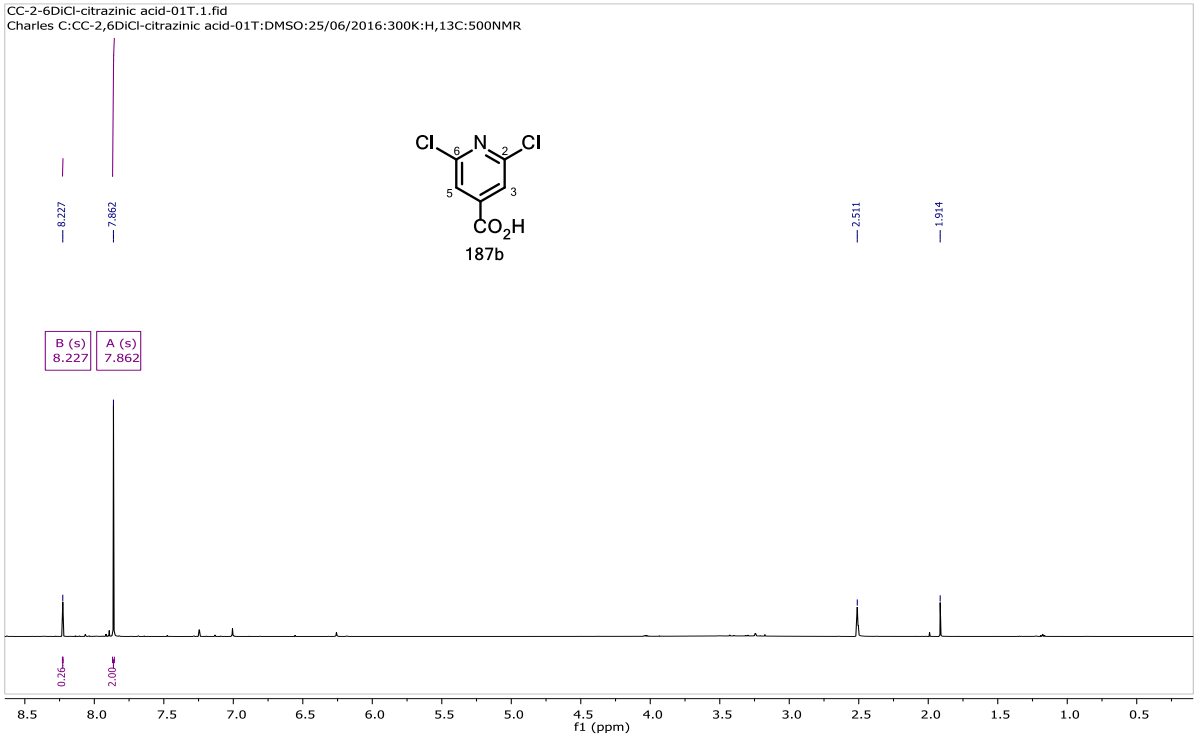
CC-2-6DiCl-citrazinic acid-01T.1.fid
Charles C:CC-2,6DiCl-citrazinic acid-01T:DMSO:25/06/2016:300K:H,13C:500NMR
8.227
7.862
2.511
1.914
Cl
N
Cl
6
2
5
3
CO2H
187b
B (s) 8.227
A (s) 7.862
0.26
2.00
f1 (ppm)

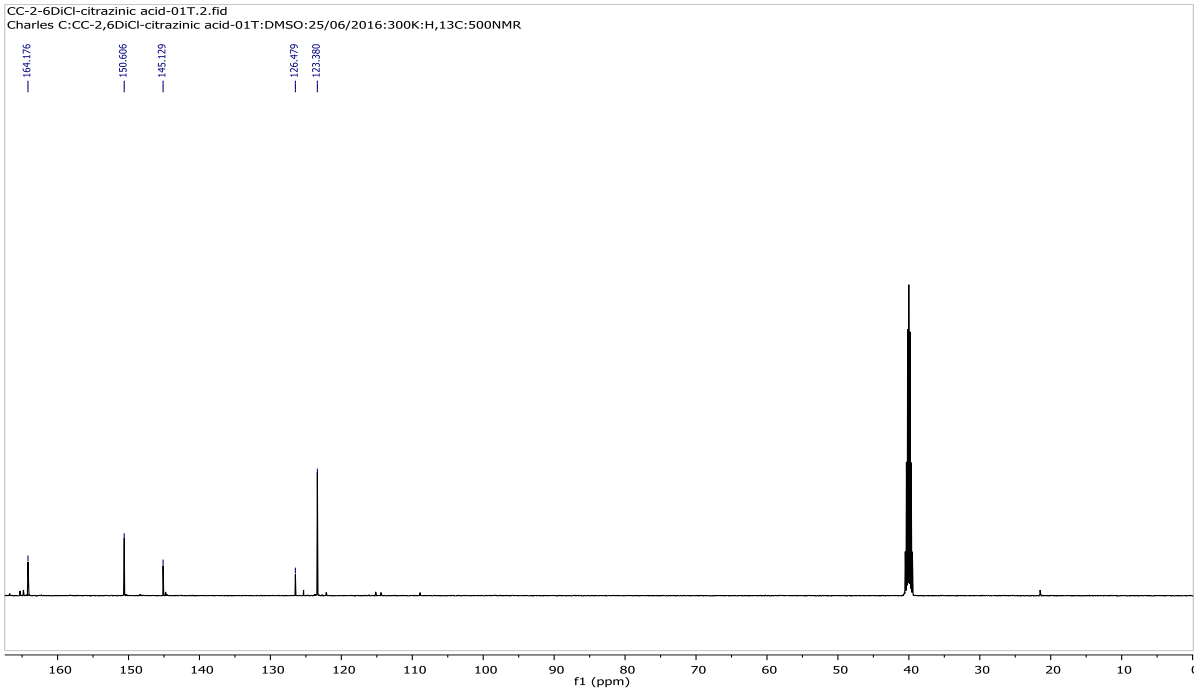
CC-2-6DiCl-citrazinic acid-01T.2.fid
Charles C:CC-2,6DiCl-citrazinic acid-01T:DMSO:25/06/2016:300K:H,13C:500NMR
164.176
150.606
145.129
126.479
123.380
f1 (ppm)

188a

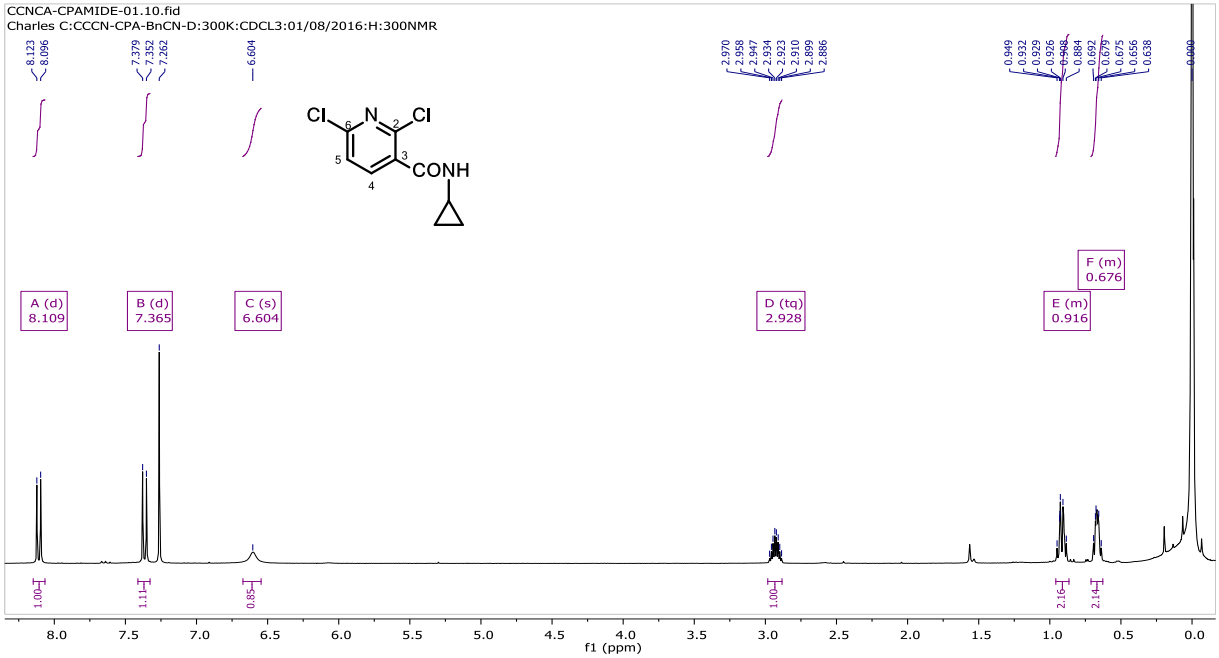
CCNCA-CPAMIDE-01.10.fid
Charles C:CCCN-CPA-BnCN-D:300K:CDCL3:01/08/2016:H:300NMR
A (d) 8.109
B (d) 7.365
C (s) 6.604
D (tq) 2.928
E (m) 0.916
F (m) 0.676
f1 (ppm)

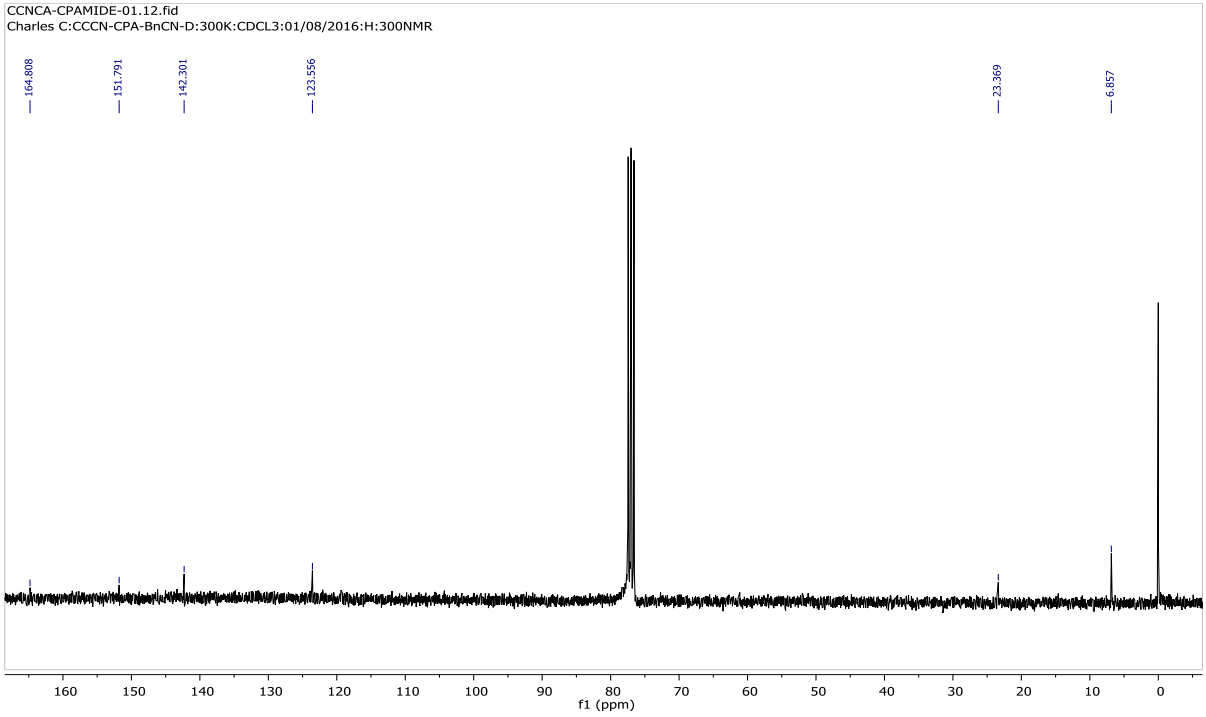
CCNCA-CPAMIDE-01.12.fid
Charles C:CCCN-CPA-BnCN-D:300K:CDCL3:01/08/2016:H:300NMR
164.808
151.791
142.301
123.556
23.369
6.857
f1 (ppm)

188b

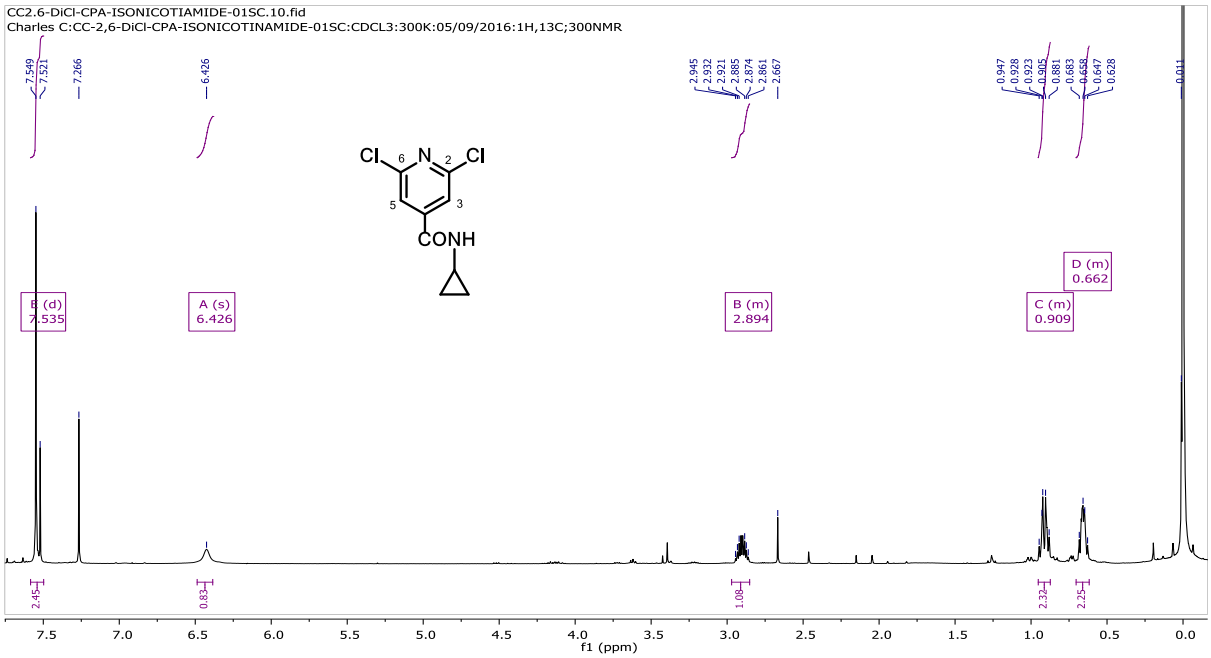
CC2.6-DiCl-CPA-ISONICOTIAMIDE-01SC.10.fid
Charles C:CC-2,6-DiCl-CPA-ISONICOTINAMIDE-01SC:CDCL3:300K:05/09/2016:1H,13C;300NMR
7.549
7.521
7.266
6.426
2.945
2.932
2.921
2.885
2.874
2.861
2.667
0.947
0.928
0.923
0.905
0.881
0.683
0.658
0.647
0.628
0.011
Cl
N
Cl
CONH
B (d)
7.535
A (s)
6.426
B (m)
2.894
D (m)
0.662
C (m)
0.909
2.45
0.83
1.08
2.32
2.25
f1 (ppm)

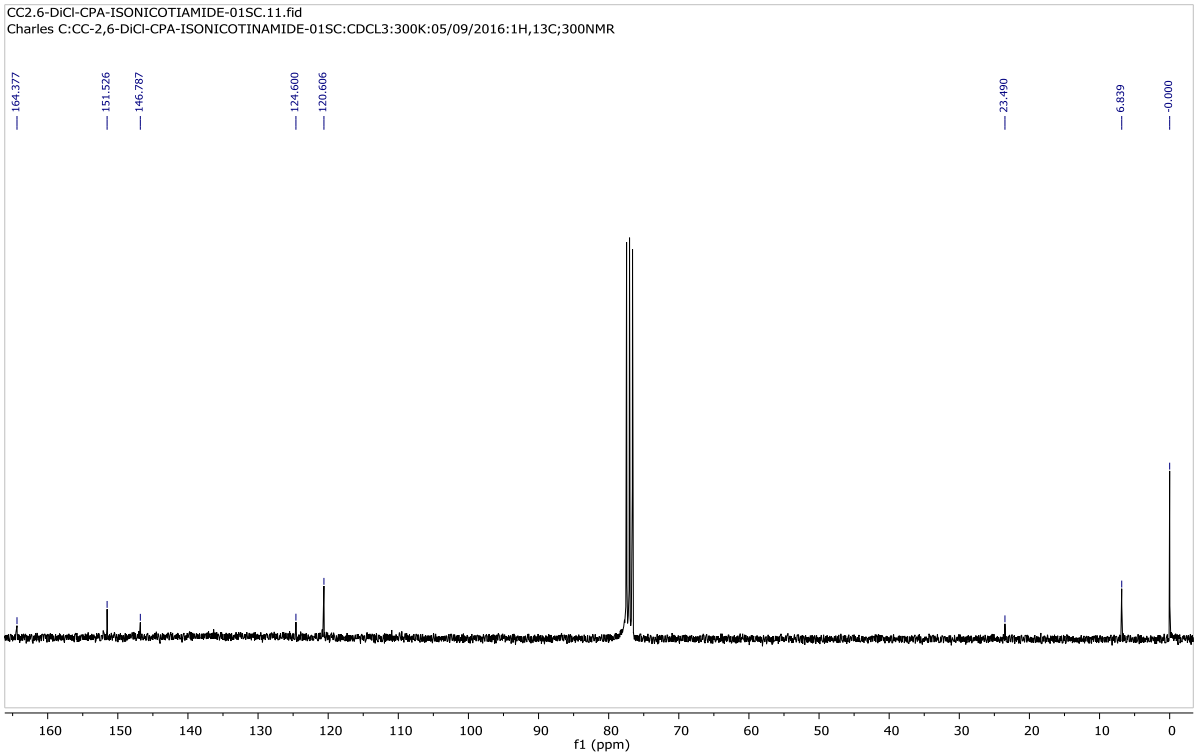
CC2.6-DiCl-CPA-ISONICOTIAMIDE-01SC.11.fid
Charles C:CC-2,6-DiCl-CPA-ISONICOTINAMIDE-01SC:CDCL3:300K:05/09/2016:1H,13C;300NMR
164.377
151.526
146.787
124.600
120.606
23.490
6.839
-0.000
f1 (ppm)

191

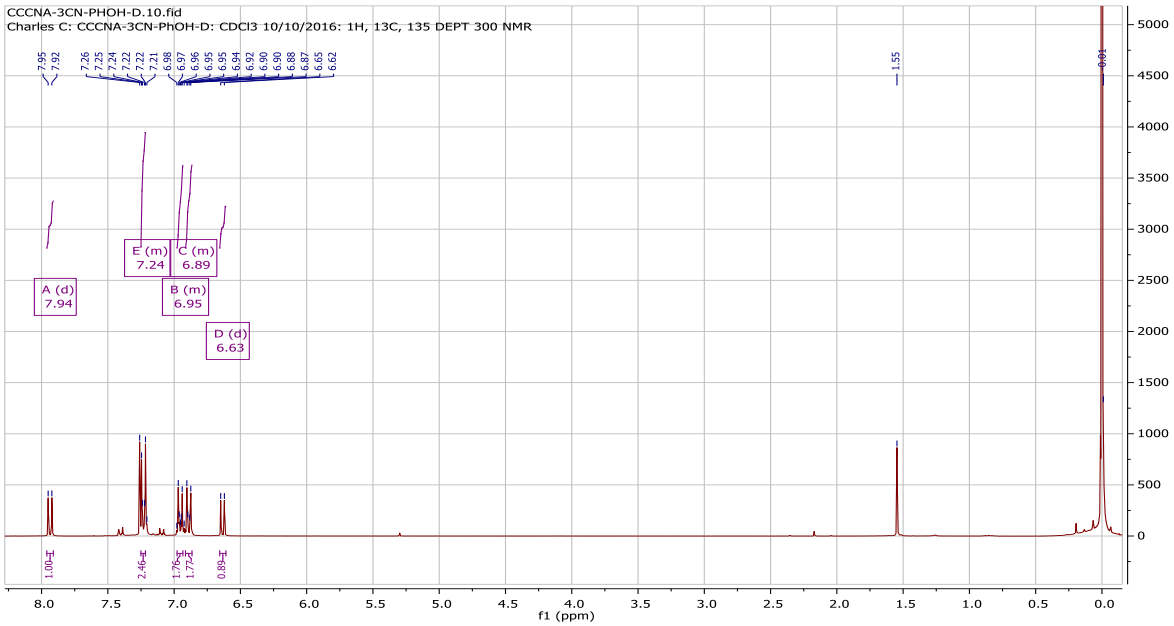
CCCNA-3CN-PHOH-D.10.fid
Charles C: CCCNA-3CN-PhOH-D: CDCl3 10/10/2016: 1H, 13C, 135 DEPT 300 NMR
A (d) 7.94
B (m) 6.95
C (m) 6.89
D (d) 6.63
E (m) 7.24
f1 (ppm)

192

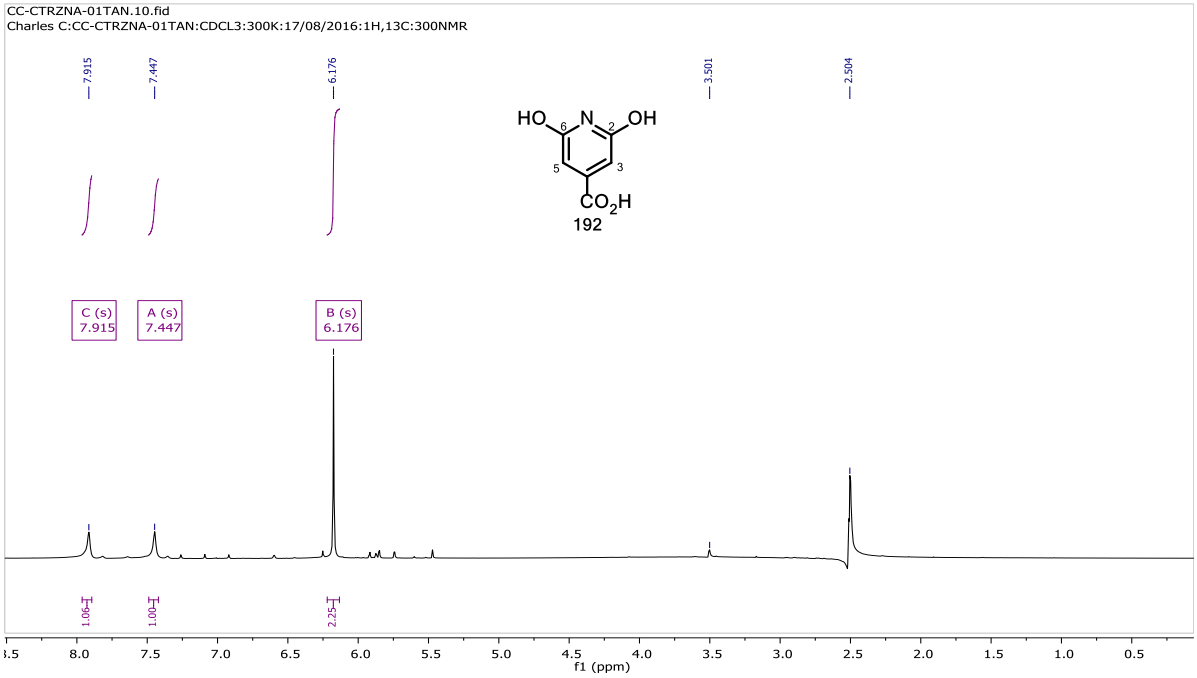
CC-CTRZNA-01TAN.10.fid
Charles C:CC-CTRZNA-01TAN:CDCL3:300K:17/08/2016:1H,13C:300NMR
7.915
7.447
6.176
3.501
2.504
HO
N
OH
CO2H
192
C (s) 7.915
A (s) 7.447
B (s) 6.176
1.06
1.00
2.25
f1 (ppm)

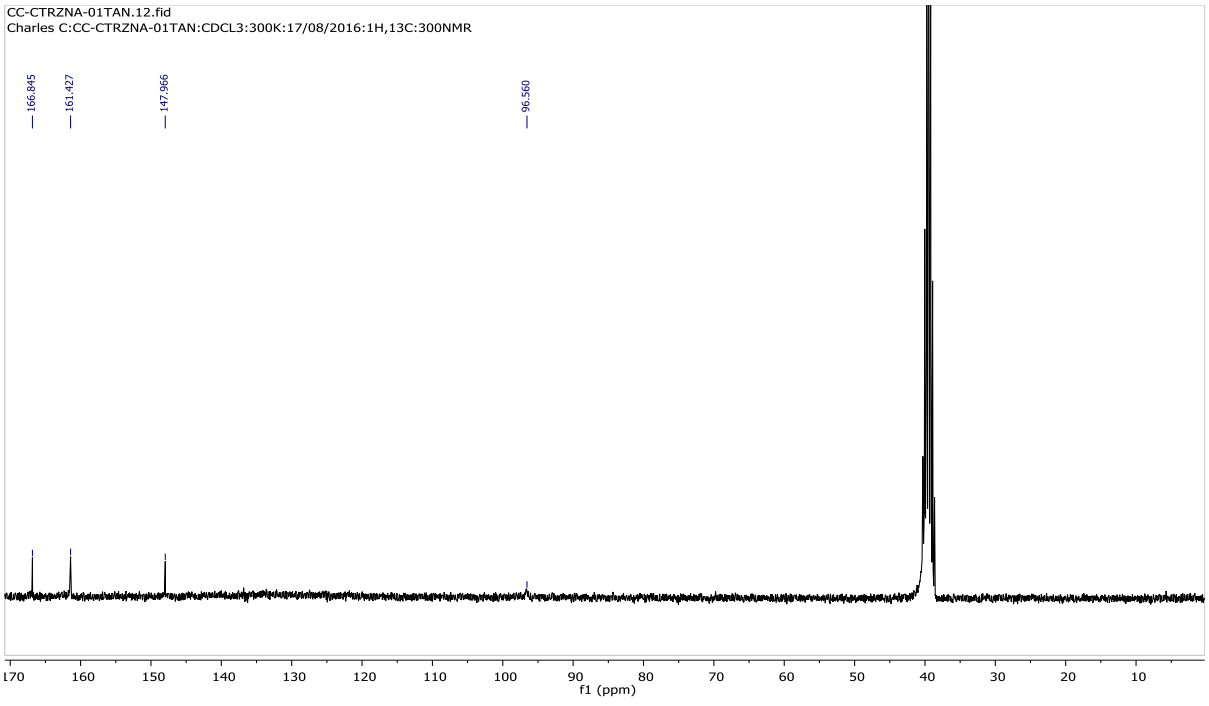
CC-CTRZNA-01TAN.12.fid
Charles C:CC-CTRZNA-01TAN:CDCL3:300K:17/08/2016:1H,13C:300NMR
166.845
161.427
147.966
96.560
f1 (ppm)

196

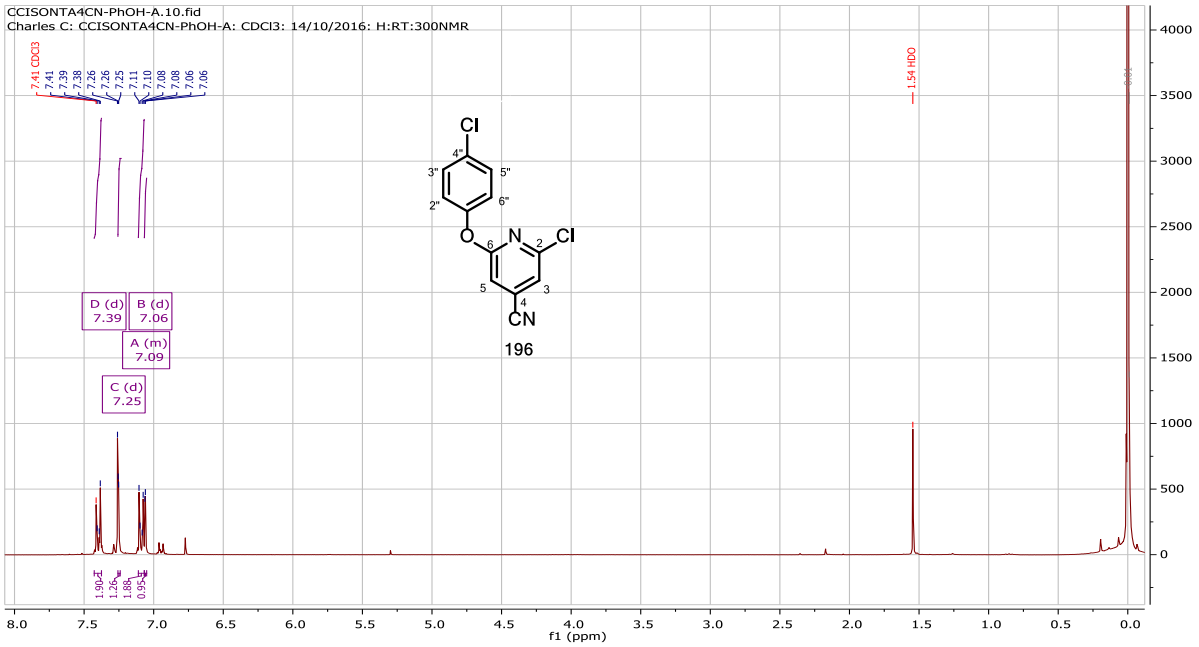
CCISONTA4CN-PhOH-A.10.fid
Charles C: CCISONTA4CN-PhOH-A: CDCl3: 14/10/2016: H:RT:300NMR
7.41 CDCl3
7.41
7.41
7.39
7.38
7.26
7.26
7.25
7.11
7.10
7.08
7.08
7.06
7.06
1.54 H2O
D (d) 7.39
B (d) 7.06
A (m) 7.09
C (d) 7.25
1.90
1.26
1.88
0.95
Cl
4"
3"
5"
2"
6"
O
6
N
2
Cl
5
3
4
CN
196
f1 (ppm)

197

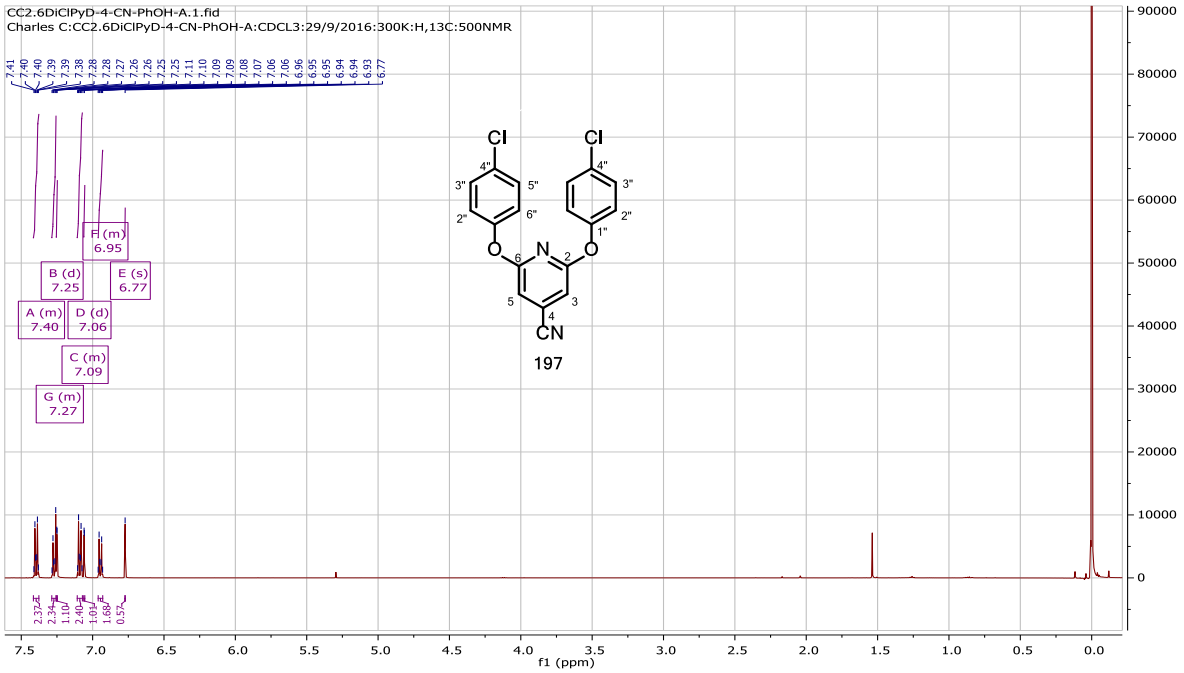
CC2.6DiClPyD-4-CN-PhOH-A.1.fid
Charles C:CC2.6DiClPyD-4-CN-PhOH-A:CDCL3:29/9/2016:300K:H,13C:500NMR
F (m) 6.95
B (d) 7.25
E (s) 6.77
A (m) 7.40
D (d) 7.06
C (m) 7.09
G (m) 7.27
Cl
Cl
CN
197
f1 (ppm)

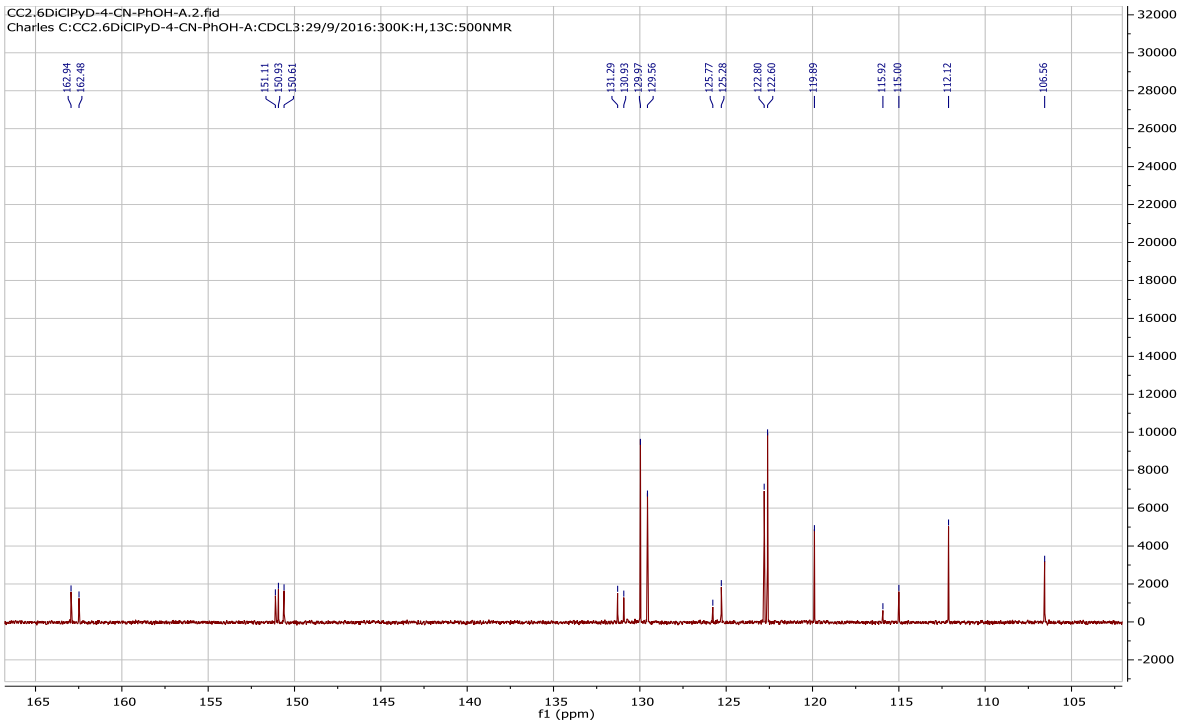
CC2.6DiClPyD-4-CN-PhOH-A.2.fid
Charles C:CC2.6DiClPyD-4-CN-PhOH-A:CDCL3:29/9/2016:300K:H,13C:500NMR
f1 (ppm)

198b

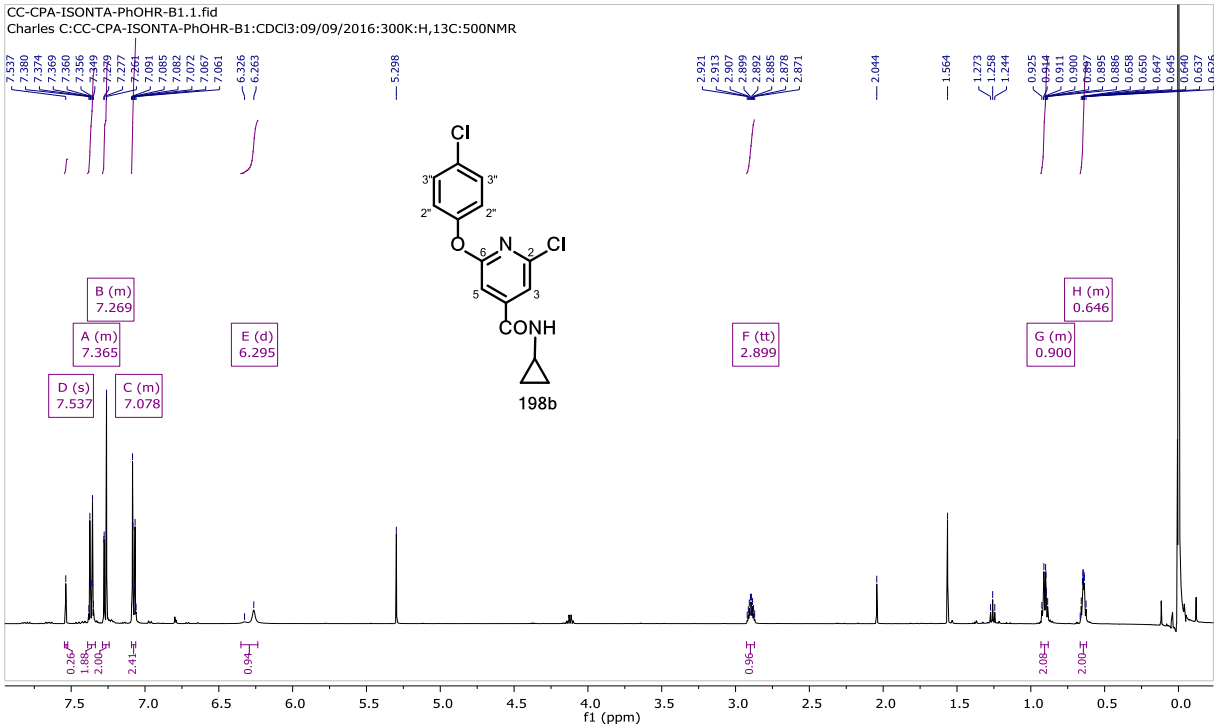
CC-CPA-ISONTA-PhOHR-B1.1.fid
Charles C:CC-CPA-ISONTA-PhOHR-B1:CDCl3:09/09/2016:300K:H,13C:500NMR
B (m) 7.269
A (m) 7.365
D (s) 7.537
C (m) 7.078
E (d) 6.295
F (tt) 2.899
H (m) 0.646
G (m) 0.900
198b
f1 (ppm)

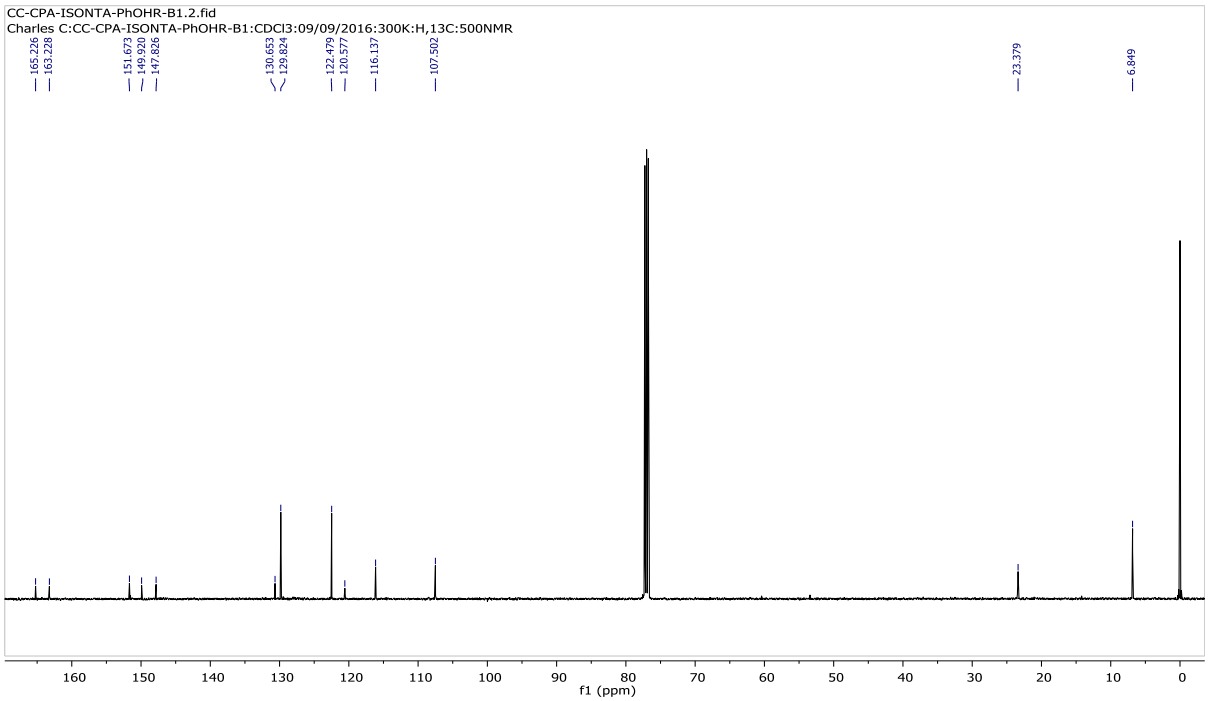
CC-CPA-ISONTA-PhOHR-B1.2.fid
Charles C:CC-CPA-ISONTA-PhOHR-B1:CDCl3:09/09/2016:300K:H,13C:500NMR
f1 (ppm)

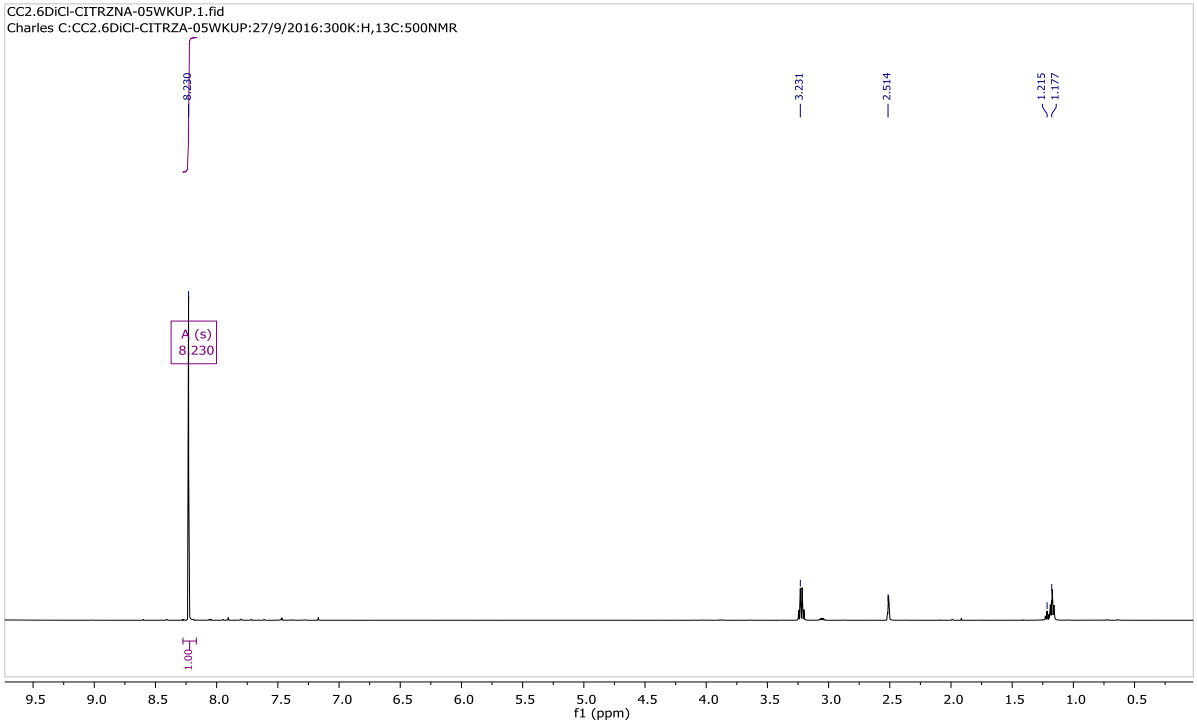
CC2.6DiCl-CITRZNA-05WKUP.1.fid
Charles C:CC2.6DiCl-CITRZA-05WKUP:27/9/2016:300K:H,13C:500NMR
8.230
3.231
2.514
1.215
1.177
A (s)
8.230
1.00
9.5 9.0 8.5 8.0 7.5 7.0 6.5 6.0 5.5 5.0 4.5 4.0 3.5 3.0 2.5 2.0 1.5 1.0 0.5
f1 (ppm)

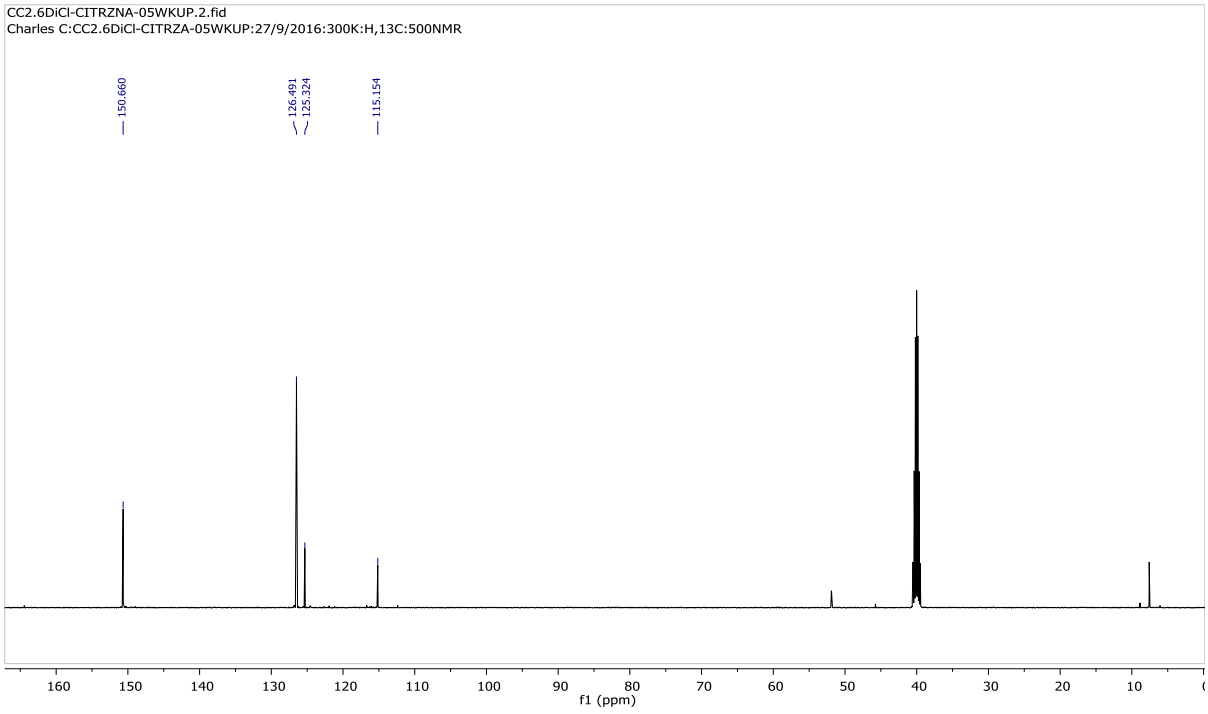
CC2.6DiCl-CITRZNA-05WKUP.2.fid
Charles C:CC2.6DiCl-CITRZA-05WKUP:27/9/2016:300K:H,13C:500NMR
150.660
126.491
125.324
115.154
160 150 140 130 120 110 100 90 80 70 60 50 40 30 20 10
f1 (ppm)

200

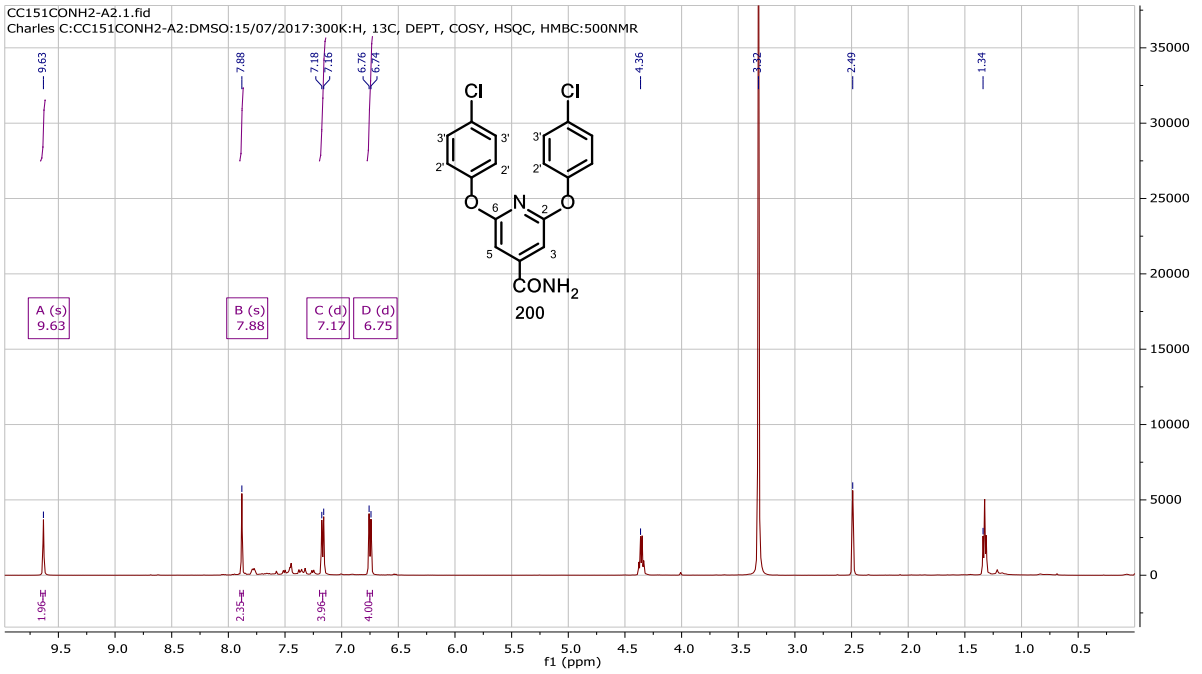

13C NMR (126 MHz, DMSO) δ 162.75, 156.77, 150.71, 143.83, 129.56, 123.21, 122.79, 117.39, 62.90, 40.52, 14.32.

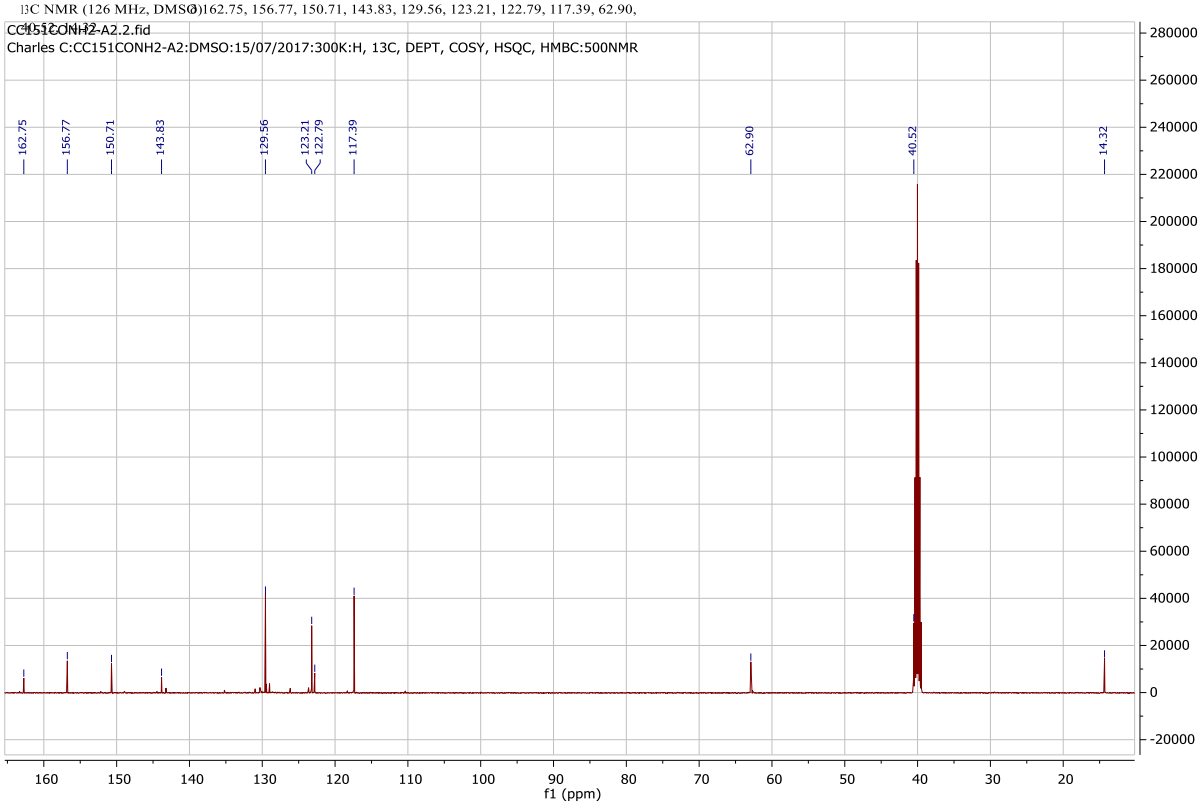

207

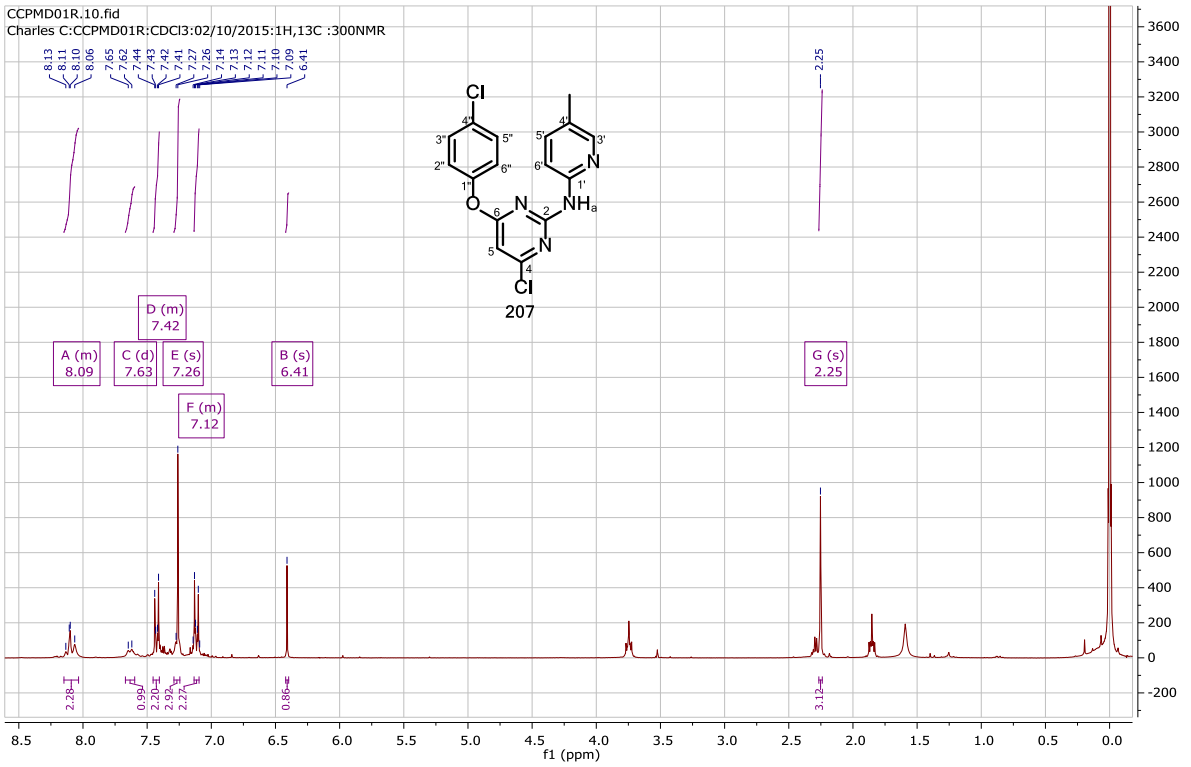
CCPMD01R.10.fid
Charles C:CCPMD01R:CDCl3:02/10/2015:1H,13C :300NMR
8.13
8.11
8.10
8.06
7.65
7.62
7.44
7.43
7.42
7.41
7.27
7.26
7.14
7.13
7.12
7.11
7.10
7.09
6.41
2.25
D (m)
7.42
A (m)
8.09
C (d)
7.63
E (s)
7.26
B (s)
6.41
F (m)
7.12
G (s)
2.25
207
2.28
0.99
2.20
2.92
2.27
0.86
3.12
f1 (ppm)

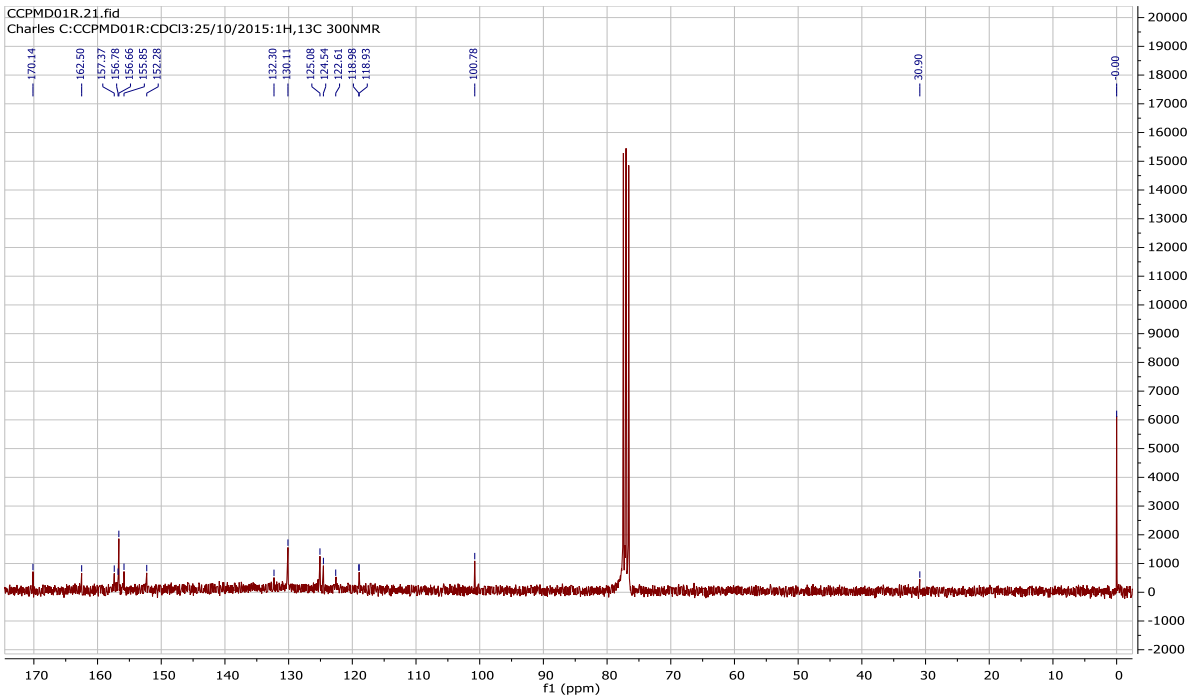
CCPMD01R.21.fid
Charles C:CCPMD01R:CDCl3:25/10/2015:1H,13C 300NMR
170.14
162.50
157.37
156.78
156.66
155.85
152.28
132.30
130.11
125.08
124.54
122.61
118.98
118.93
100.78
30.90
0.00
f1 (ppm)

208

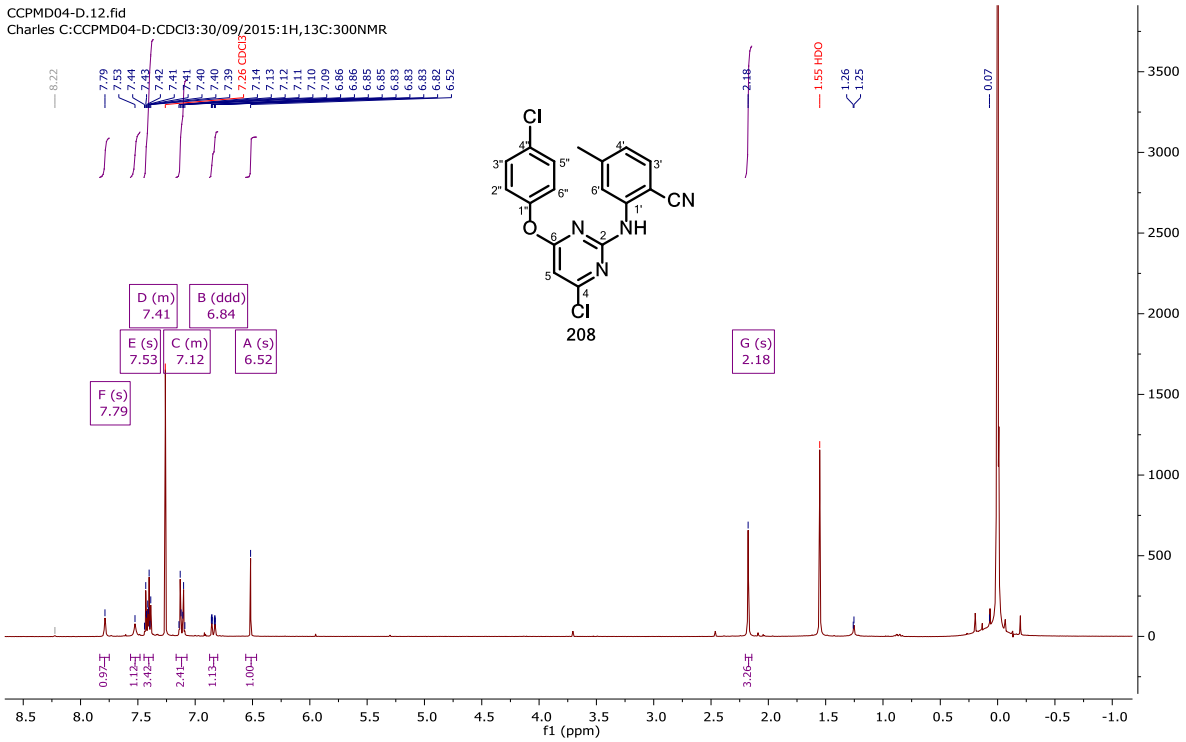
CCPMD04-D.12.fid
Charles C:CCPMD04-D:CDCl3:30/09/2015:1H,13C:300NMR
D (m) 7.41
B (ddd) 6.84
E (s) 7.53
C (m) 7.12
A (s) 6.52
F (s) 7.79
G (s) 2.18
208
f1 (ppm)

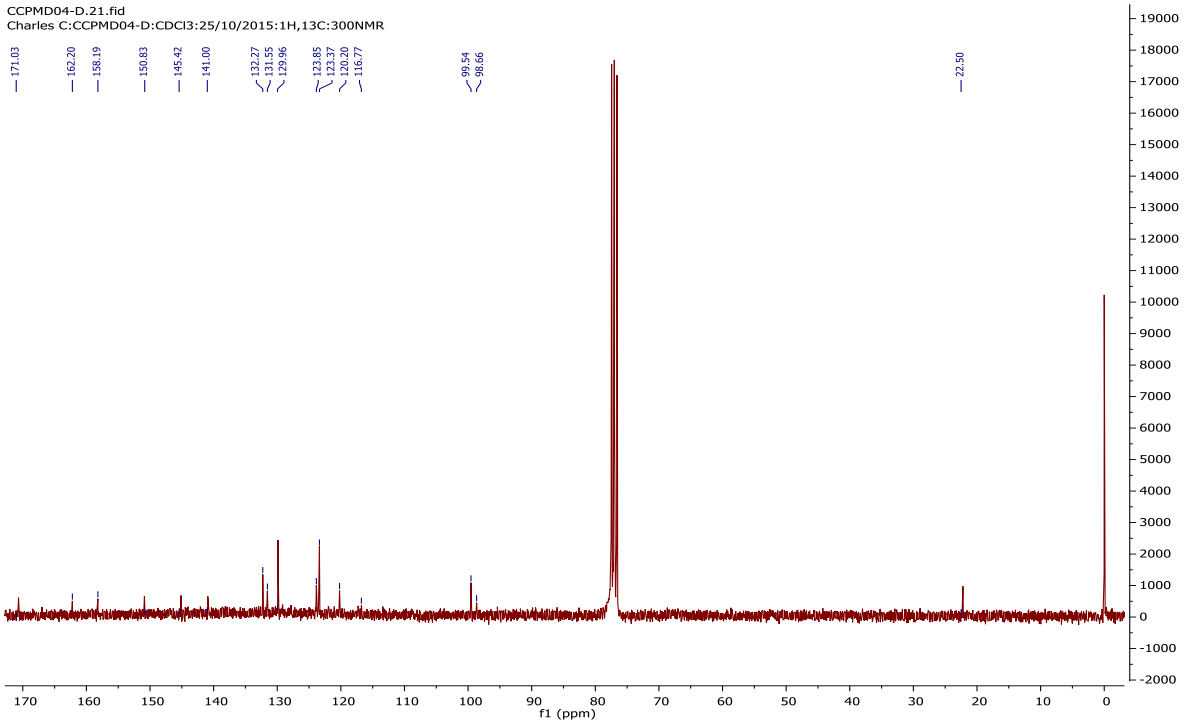
CCPMD04-D.21.fid
Charles C:CCPMD04-D:CDCl3:25/10/2015:1H,13C:300NMR
f1 (ppm)

209

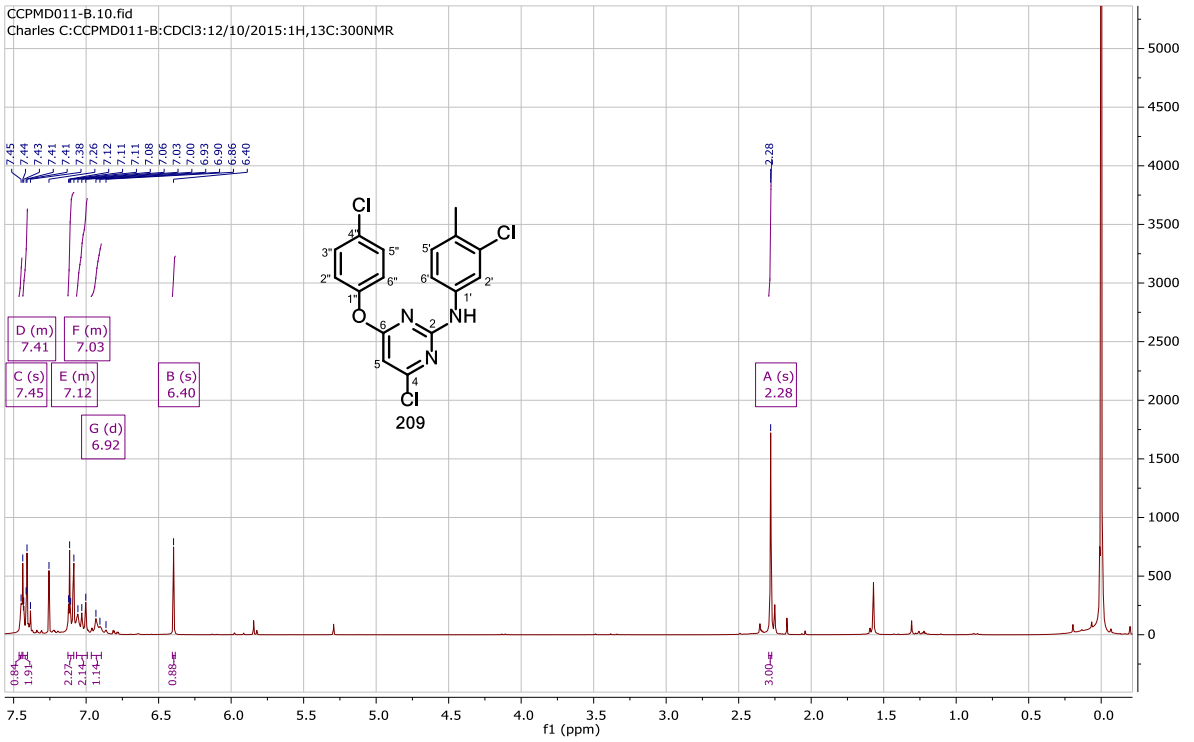
CCPMD011-B.10.fid
Charles C:CCPMD011-B:CDCl3:12/10/2015:1H,13C:300NMR
7.45
7.44
7.43
7.41
7.41
7.38
7.26
7.12
7.11
7.11
7.08
7.06
7.03
7.00
6.93
6.90
6.86
6.40
2.28
D (m) 7.41
F (m) 7.03
C (s) 7.45
E (m) 7.12
B (s) 6.40
G (d) 6.92
A (s) 2.28
0.84
1.91
2.27
2.14
1.14
0.88
3.00
Cl
Cl
NH
209
f1 (ppm)

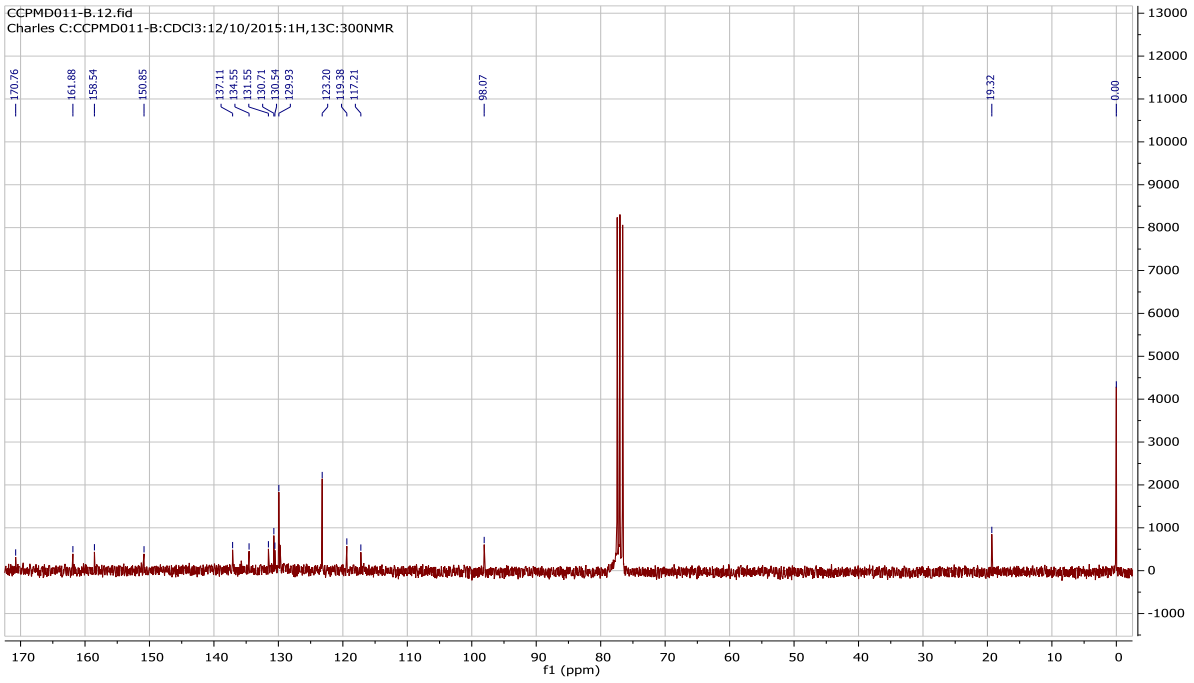
CCPMD011-B.12.fid
Charles C:CCPMD011-B:CDCl3:12/10/2015:1H,13C:300NMR
170.76
161.88
158.54
150.85
137.11
134.55
131.55
130.71
130.54
129.93
123.20
119.38
117.21
98.07
19.32
0.00
f1 (ppm)

210

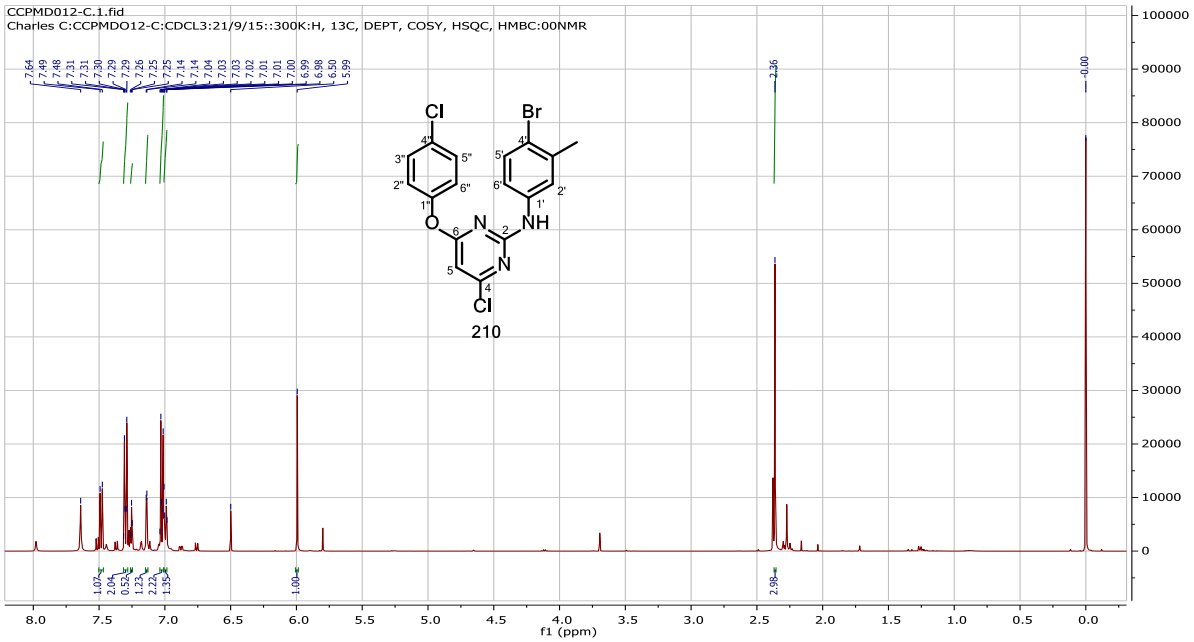
CCPMD012-C.1.fid
Charles C:CCPMDO12-C:CDCL3:21/9/15::300K:H, 13C, DEPT, COSY, HSQC, HMBC:00NMR
Cl
Br
NH
O
N
N
Cl
210
f1 (ppm)

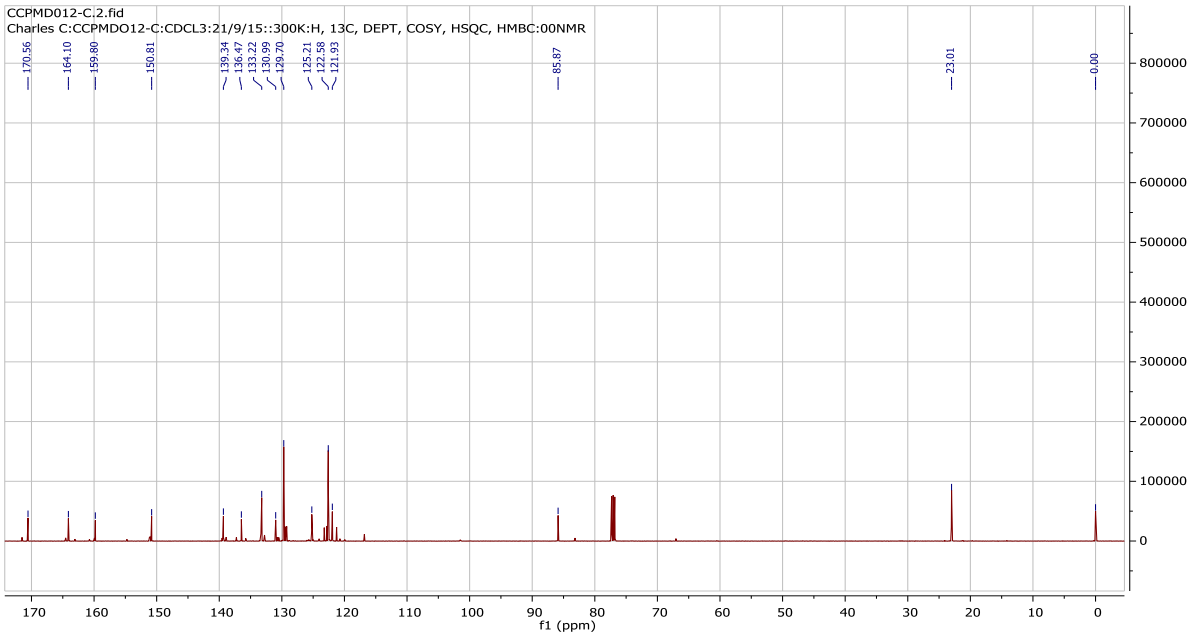
CCPMD012-C.2.fid
Charles C:CCPMDO12-C:CDCL3:21/9/15::300K:H, 13C, DEPT, COSY, HSQC, HMBC:00NMR
f1 (ppm)

211

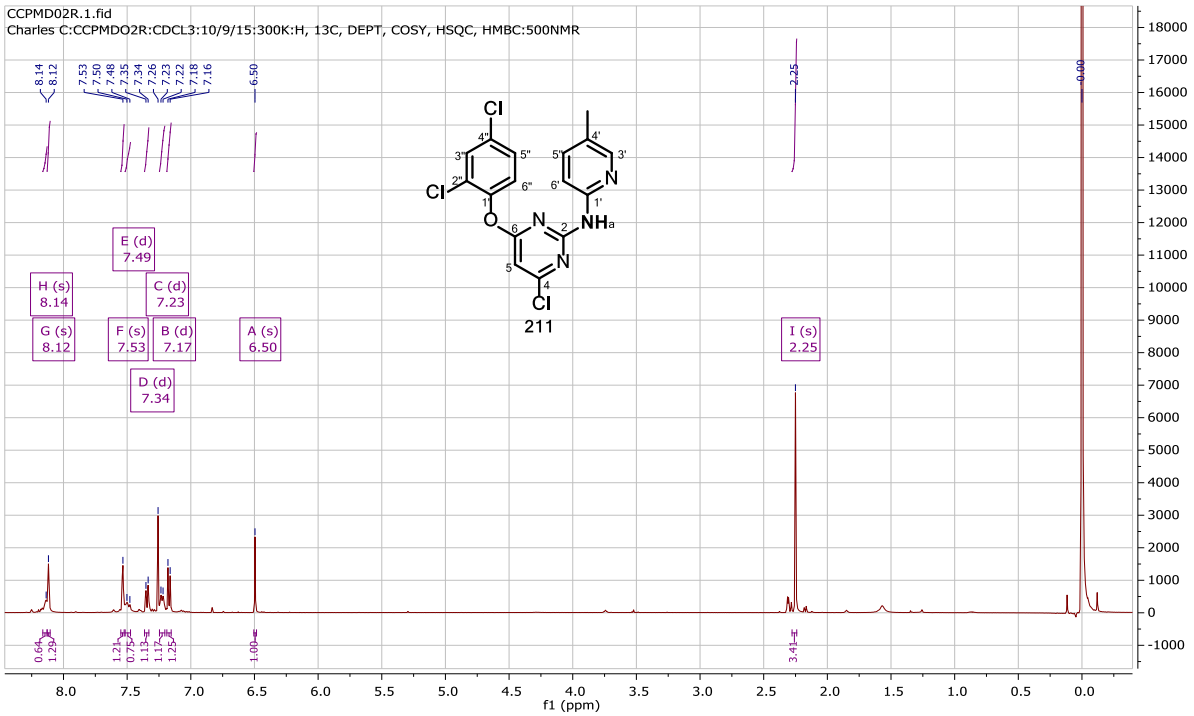
CCPMD02R.1.fid
Charles C:CCPMDO2R:CDCL3:10/9/15:300K:H, 13C, DEPT, COSY, HSQC, HMBC:500NMR
8.14
8.12
7.53
7.50
7.48
7.35
7.34
7.26
7.23
7.22
7.18
7.16
6.50
2.25
0.00
E (d)
7.49
H (s)
8.14
C (d)
7.23
G (s)
8.12
F (s)
7.53
B (d)
7.17
A (s)
6.50
D (d)
7.34
I (s)
2.25
211
f1 (ppm)

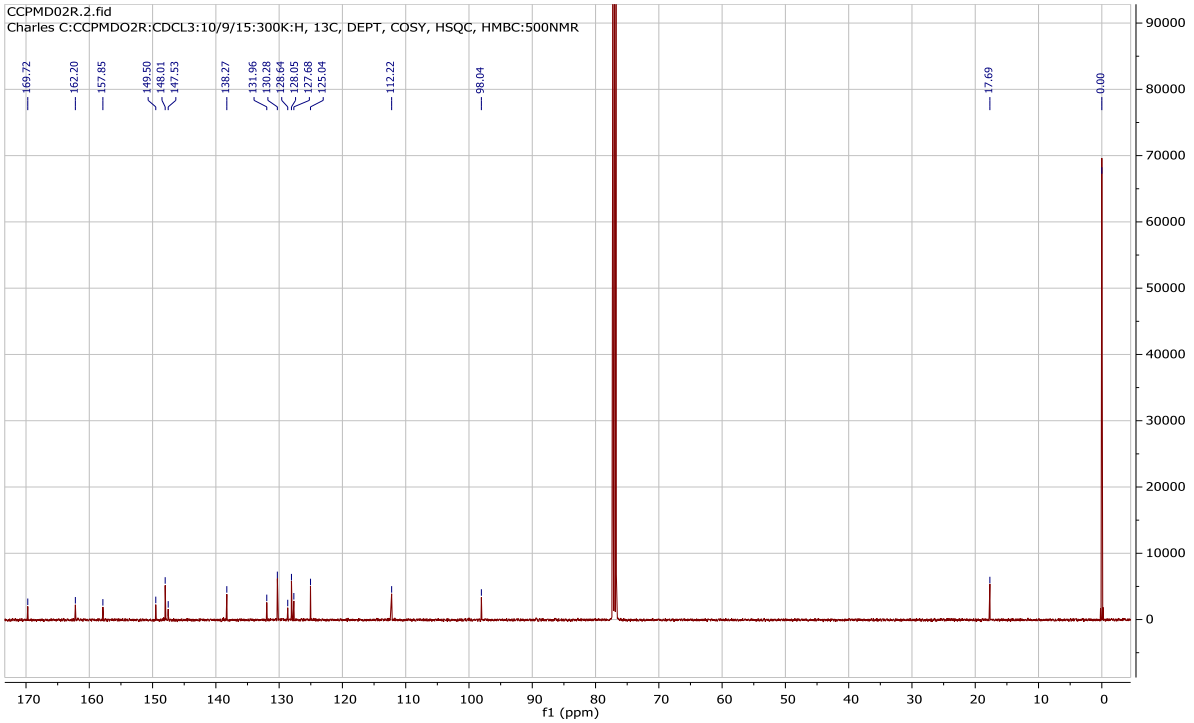
CCPMD02R.2.fid
Charles C:CCPMDO2R:CDCL3:10/9/15:300K:H, 13C, DEPT, COSY, HSQC, HMBC:500NMR
169.72
162.20
157.85
149.50
148.01
147.53
138.27
131.96
130.28
128.64
128.05
127.68
125.04
112.22
98.04
17.69
0.00
f1 (ppm)

212

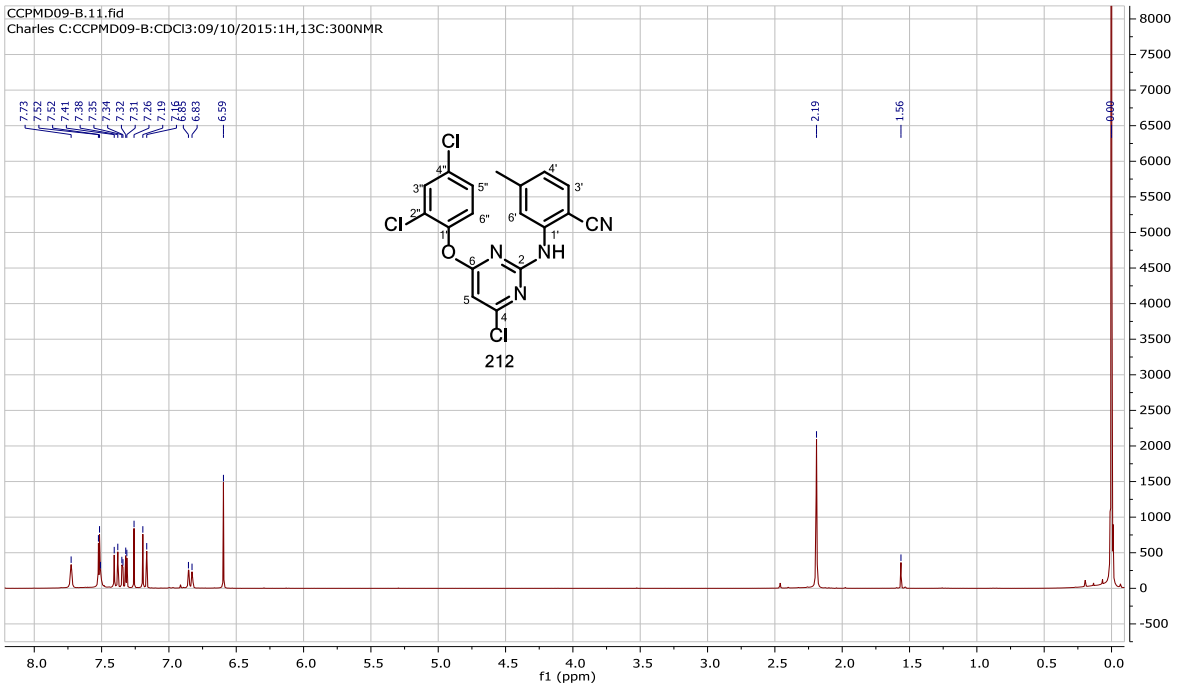
CCPMD09-B.11.fid
Charles C:CCPMD09-B:CDCl3:09/10/2015:1H,13C:300NMR
7.73
7.52
7.52
7.41
7.38
7.35
7.34
7.32
7.31
7.26
7.19
6.85
6.83
6.59
2.19
1.56
0.00
Cl
Cl
CN
NH
O
N
N
N
Cl
212
f1 (ppm)

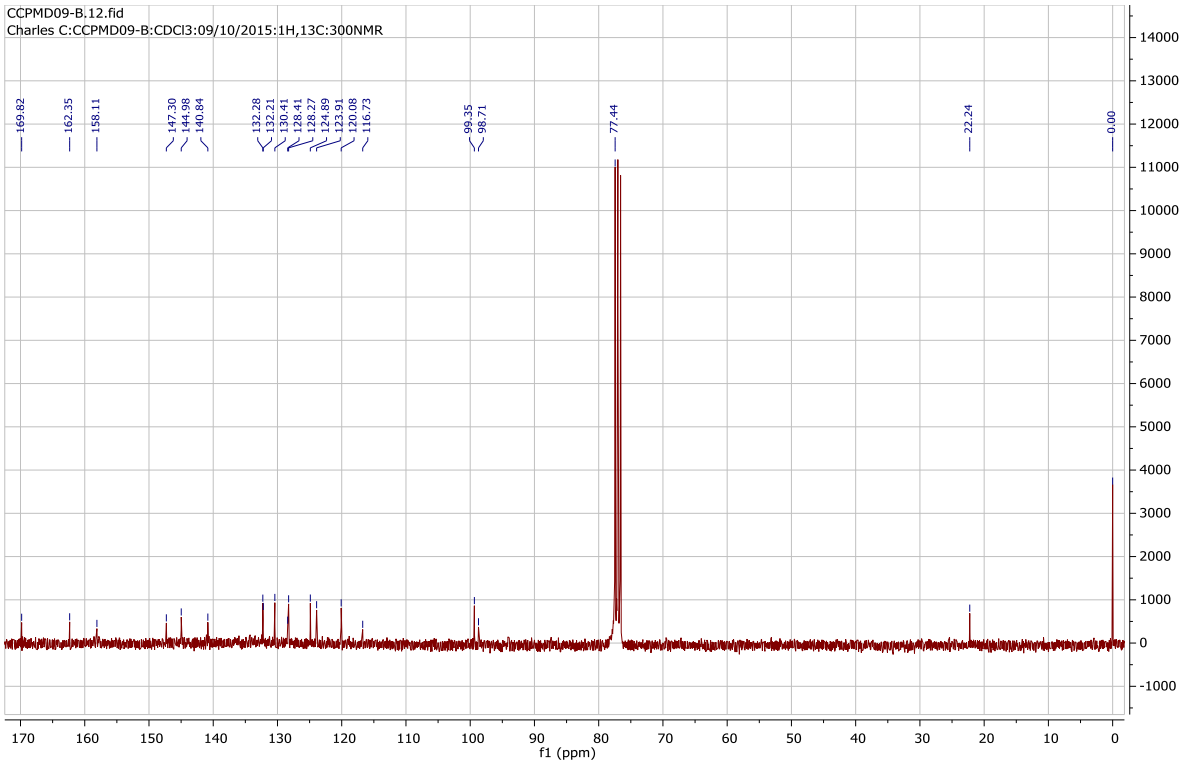
CCPMD09-B.12.fid
Charles C:CCPMD09-B:CDCl3:09/10/2015:1H,13C:300NMR
169.82
162.35
158.11
147.30
144.98
140.84
132.28
132.21
130.41
128.41
128.27
124.89
123.91
120.08
116.73
99.35
98.71
77.44
22.24
0.00
f1 (ppm)

213

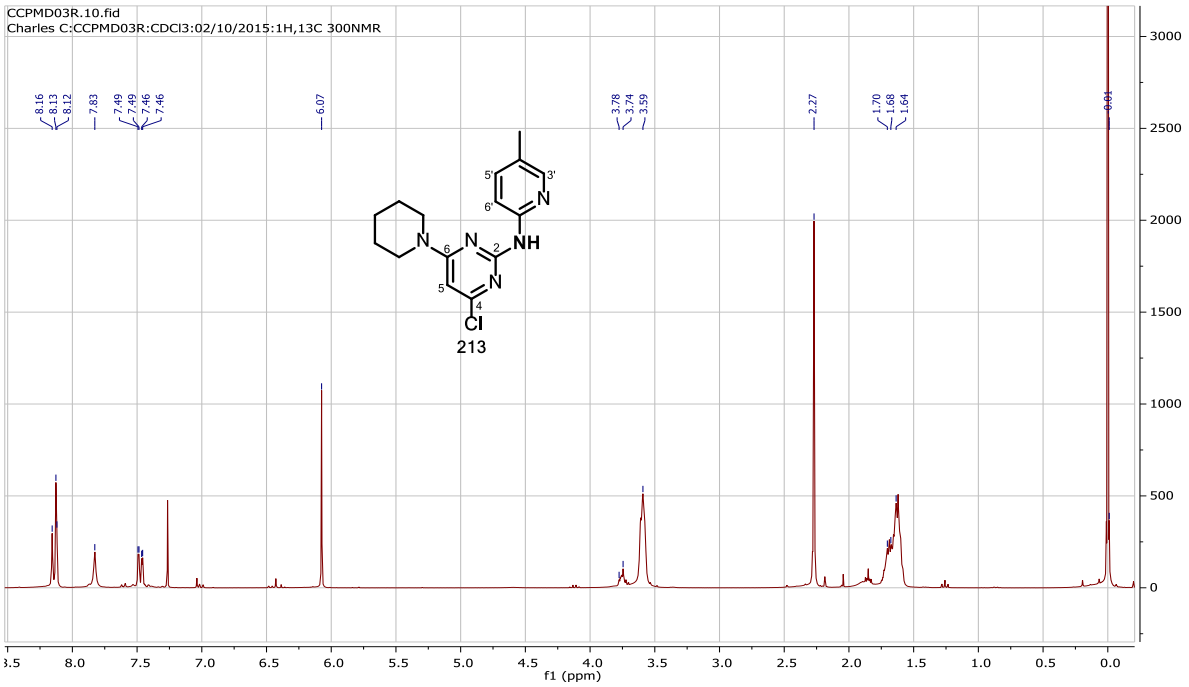
CCPMD03R.10.fid
Charles C:CCPMD03R:CDCl3:02/10/2015:1H,13C 300NMR
8.16
8.13
8.12
7.83
7.49
7.49
7.46
7.46
7.46
6.07
3.78
3.74
3.59
2.27
1.70
1.68
1.64
0.01
NH
Cl
213
f1 (ppm)

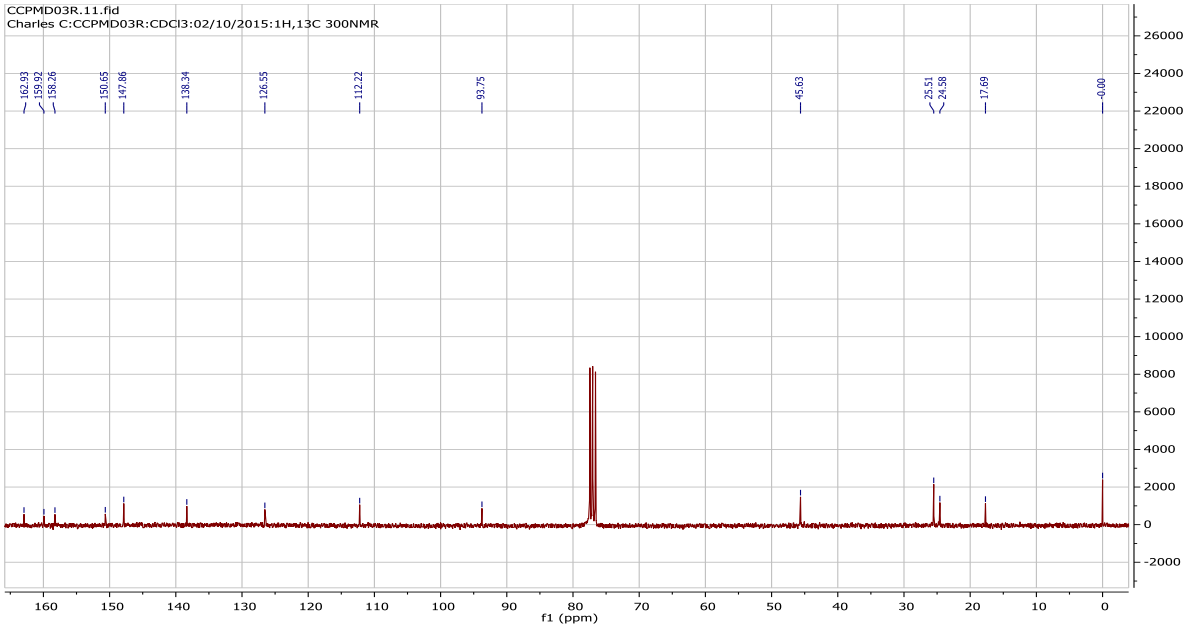
CCPMD03R.11.fid
Charles C:CCPMD03R:CDCl3:02/10/2015:1H,13C 300NMR
162.93
159.92
158.26
150.65
147.86
138.34
126.55
112.22
93.75
45.63
25.51
24.58
17.69
0.00
f1 (ppm)

214

CCPMD05R-B.1.fid
Charles C:CCPMDO5R-B:CDCL3:28/10/2015:300K:H, 13C, DEPT, COSY, HSQC, HMBC:300NMR

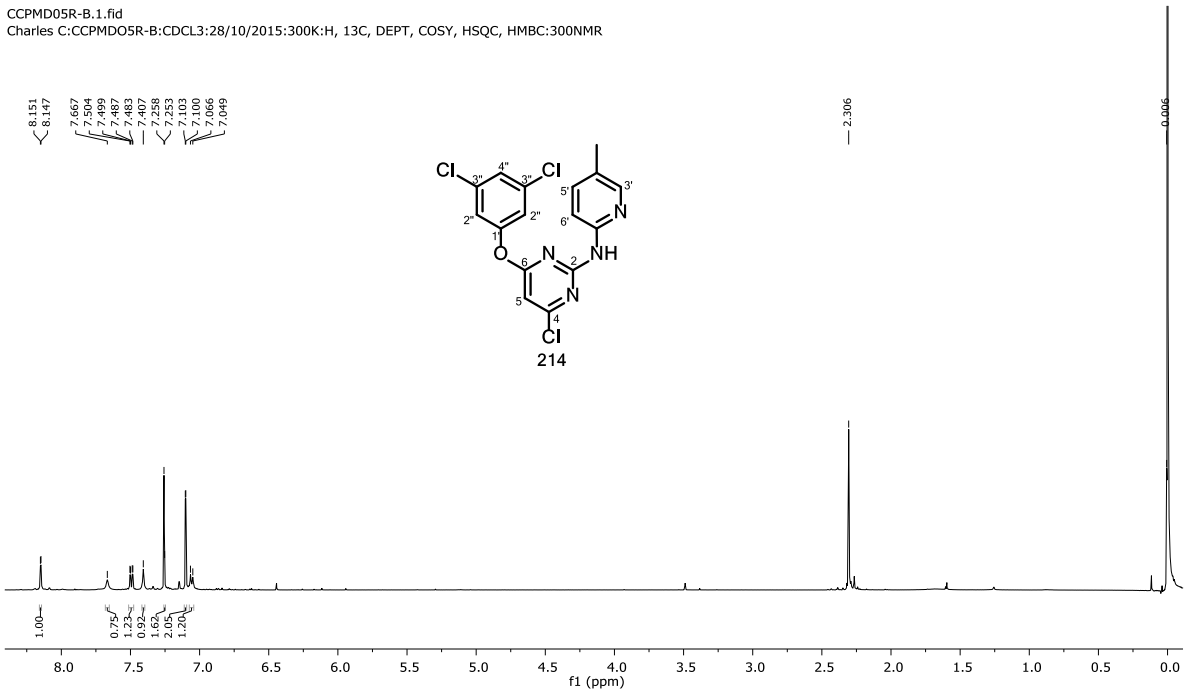

214

CCPMD05R-B.2.fid
Charles C:CCPMDO5R-B:CDCL3:28/10/2015:300K:H, 13C, DEPT, COSY, HSQC, HMBC:300NMR

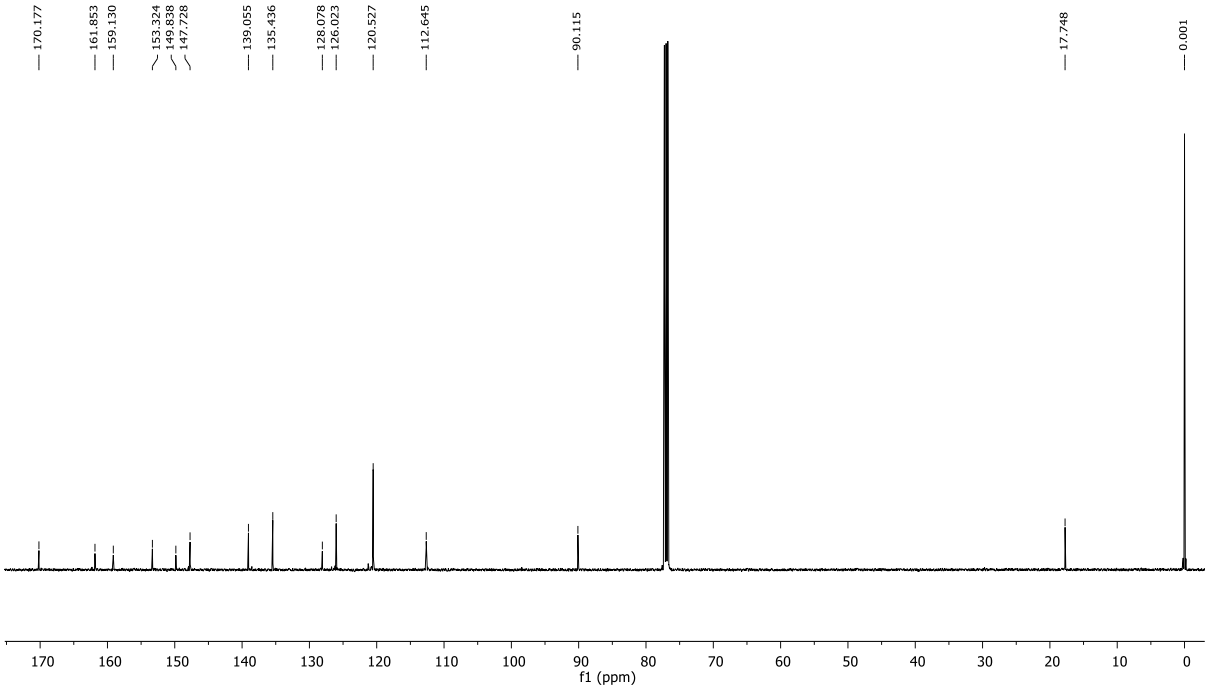

215

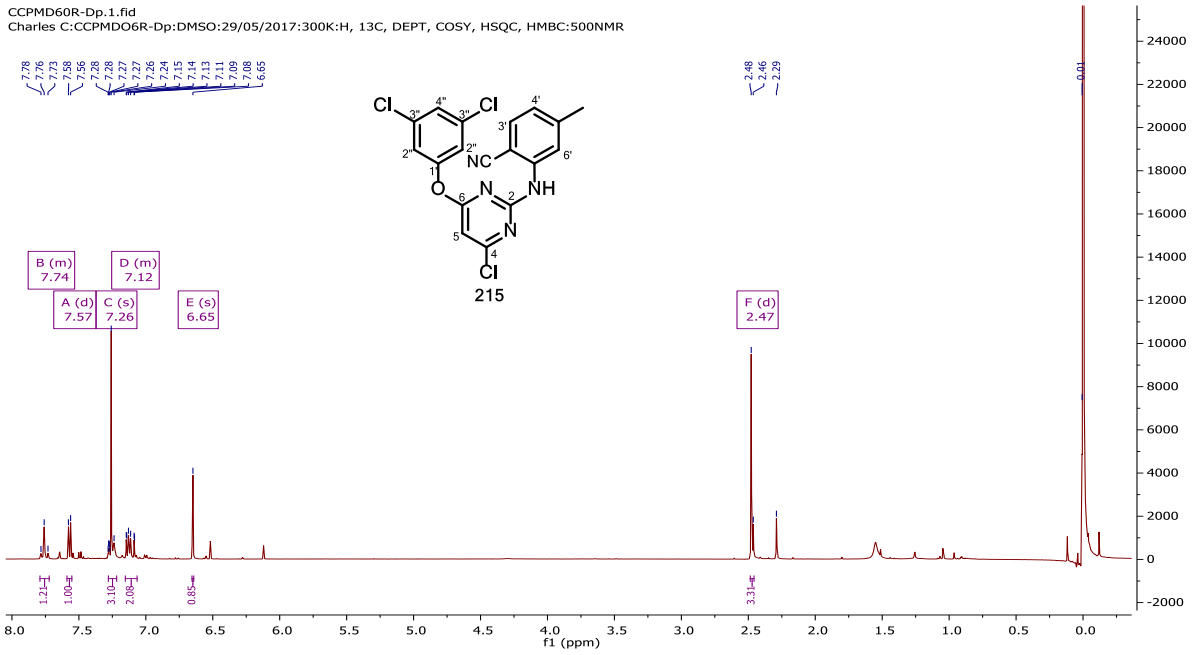
CCPMD60R-Dp.1.fid
Charles C:CCPMDO6R-Dp:DMSO:29/05/2017:300K:H, 13C, DEPT, COSY, HSQC, HMBC:500NMR
B (m) 7.74
D (m) 7.12
A (d) 7.57
C (s) 7.26
E (s) 6.65
F (d) 2.47
215
f1 (ppm)

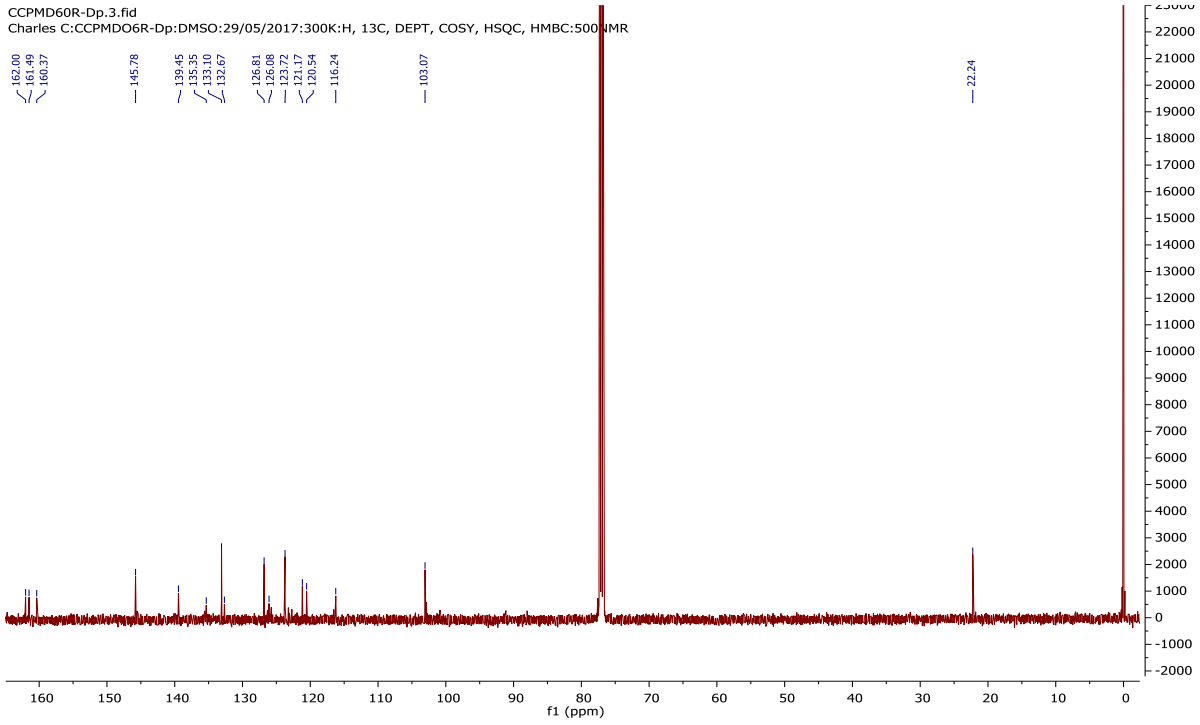
CCPMD60R-Dp.3.fid
Charles C:CCPMDO6R-Dp:DMSO:29/05/2017:300K:H, 13C, DEPT, COSY, HSQC, HMBC:500NMR
f1 (ppm)

216

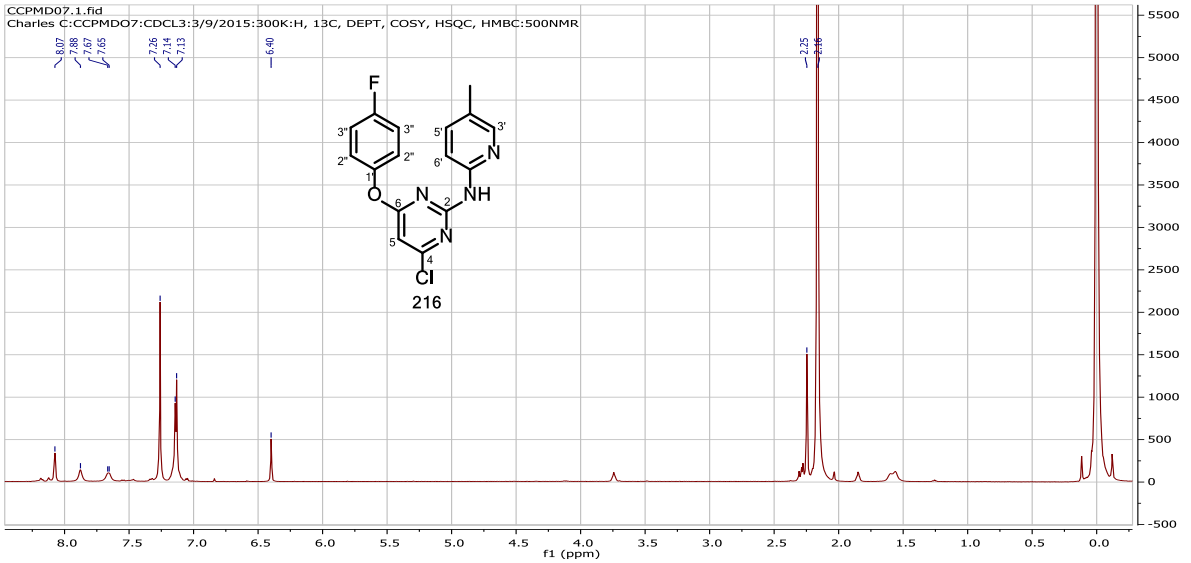
CCPMD07.1.fid
Charles C:CCPMDO7:CDCL3:3/9/2015:300K:H, 13C, DEPT, COSY, HSQC, HMBC:500NMR
8.07
7.88
7.67
7.65
7.26
7.14
7.13
6.40
2.25
2.16
F
3''
3''
2''
2''
1''
O
6
N
2
NH
5
N
4
Cl
5'
3'
6'
N
216
f1 (ppm)

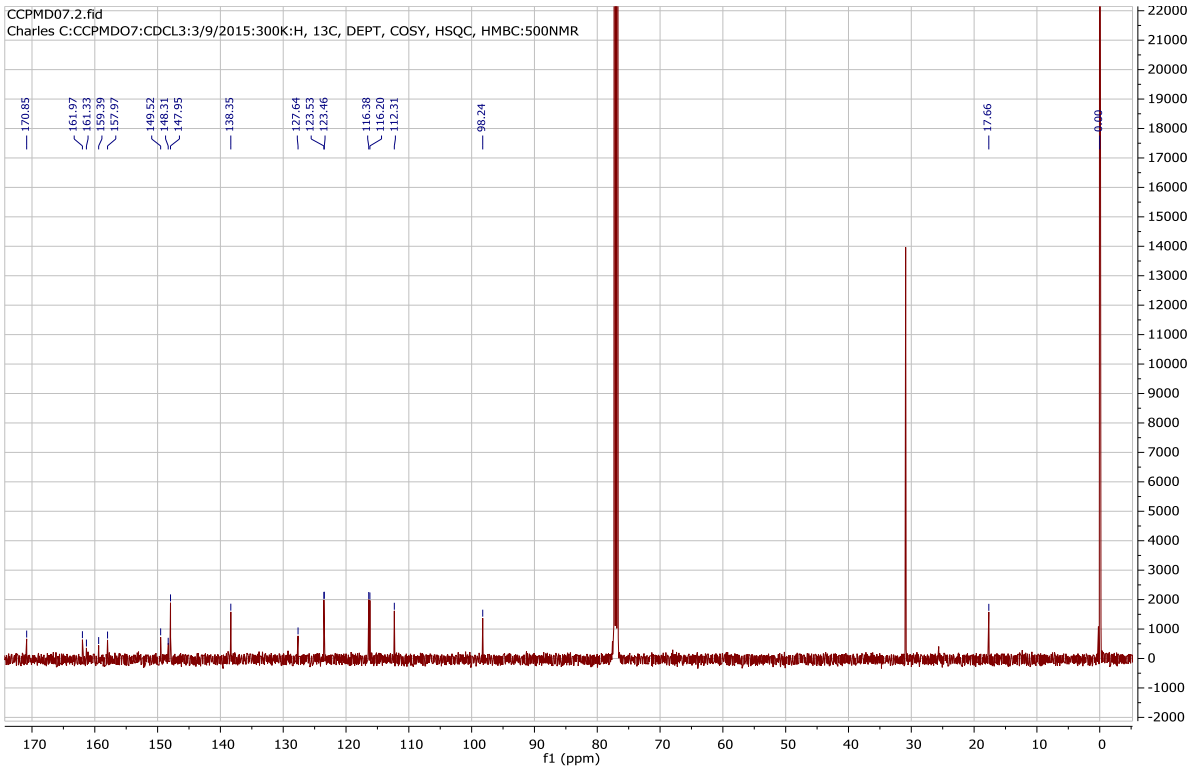
CCPMD07.2.fid
Charles C:CCPMDO7:CDCL3:3/9/2015:300K:H, 13C, DEPT, COSY, HSQC, HMBC:500NMR
170.85
161.97
161.33
159.39
157.97
149.52
148.31
147.95
138.35
127.64
123.53
123.46
116.38
116.20
112.31
98.24
17.66
0.00
f1 (ppm)

217

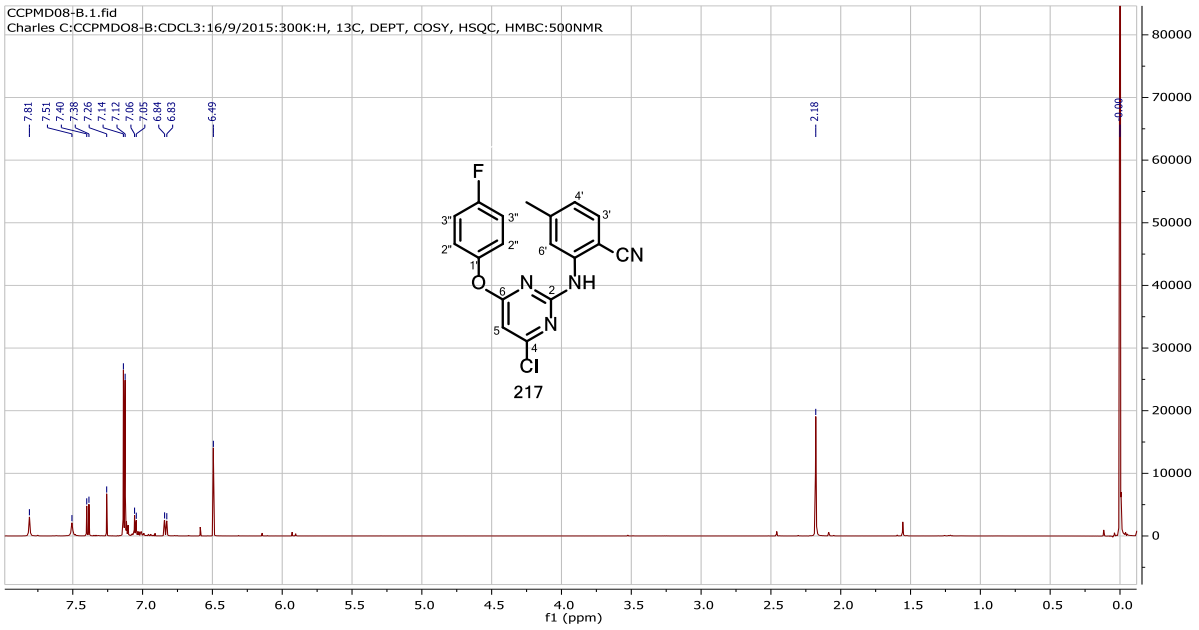
CCPMD08-B.1.fid
Charles C:CCPMDO8-B:CDCL3:16/9/2015:300K:H, 13C, DEPT, COSY, HSQC, HMBC:500NMR
7.81
7.51
7.40
7.38
7.26
7.14
7.12
7.06
7.05
6.84
6.83
6.49
2.18
0.00
F
CN
NH
N
O
Cl
f1 (ppm)

217

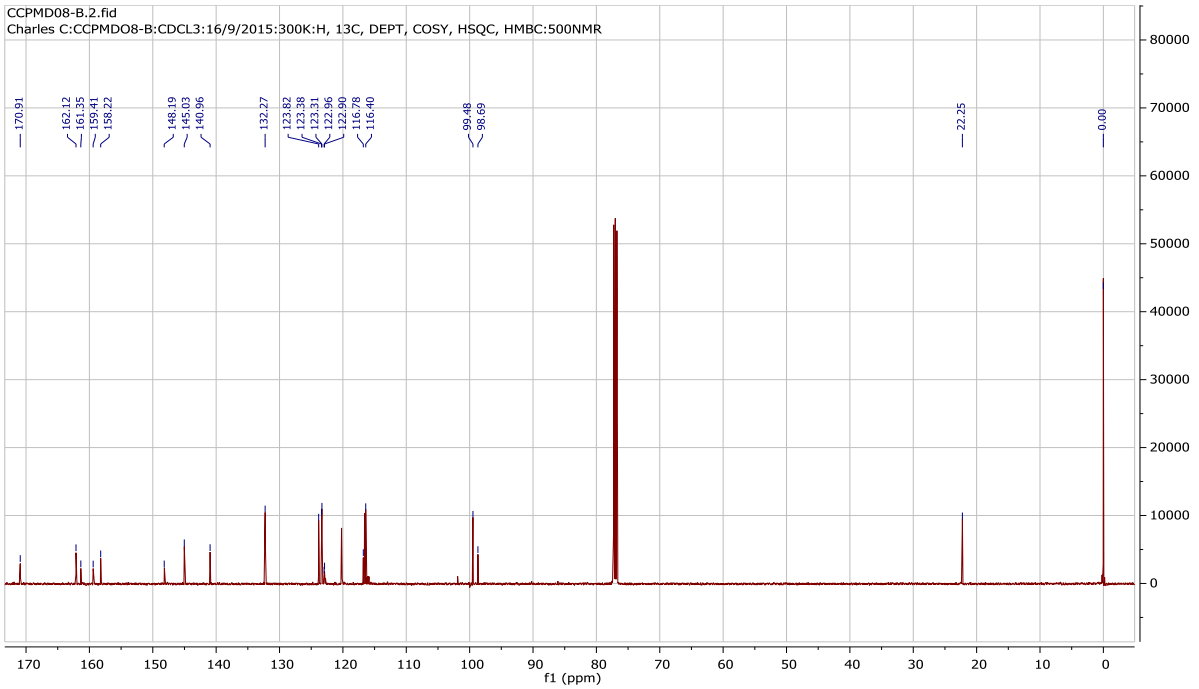
CCPMD08-B.2.fid
Charles C:CCPMDO8-B:CDCL3:16/9/2015:300K:H, 13C, DEPT, COSY, HSQC, HMBC:500NMR
170.91
162.12
161.35
159.41
158.22
148.19
145.03
140.96
132.27
123.82
123.38
123.31
122.96
122.90
116.78
116.40
98.48
98.69
22.25
0.00
f1 (ppm)

218

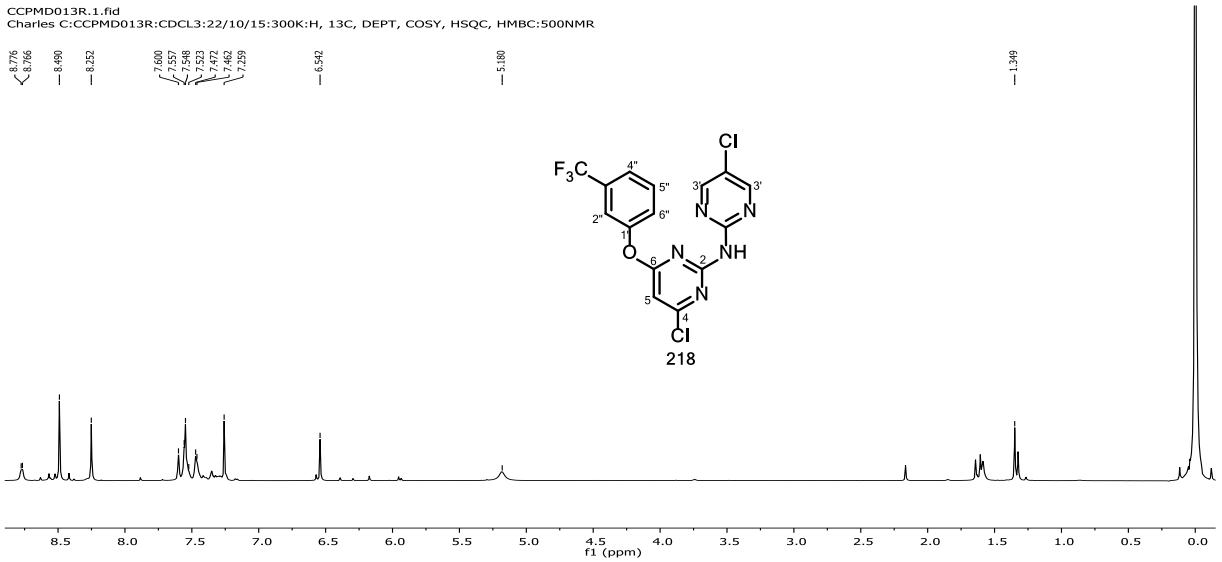
CCPMD013R.1.fid
Charles C:CCPMD013R:CDCL3:22/10/15:300K:H, 13C, DEPT, COSY, HSQC, HMBC:500NMR
8.776
8.766
8.490
8.252
7.600
7.557
7.548
7.523
7.472
7.462
7.259
6.542
5.180
1.349
Cl
F3C
4"
5"
6"
2"
1"
3'
3'
3'
N
N
O
N
2
NH
6
5
N
4
Cl
218
8.5
8.0
7.5
7.0
6.5
6.0
5.5
5.0
4.5
4.0
3.5
3.0
2.5
2.0
1.5
1.0
0.5
0.0
f1 (ppm)

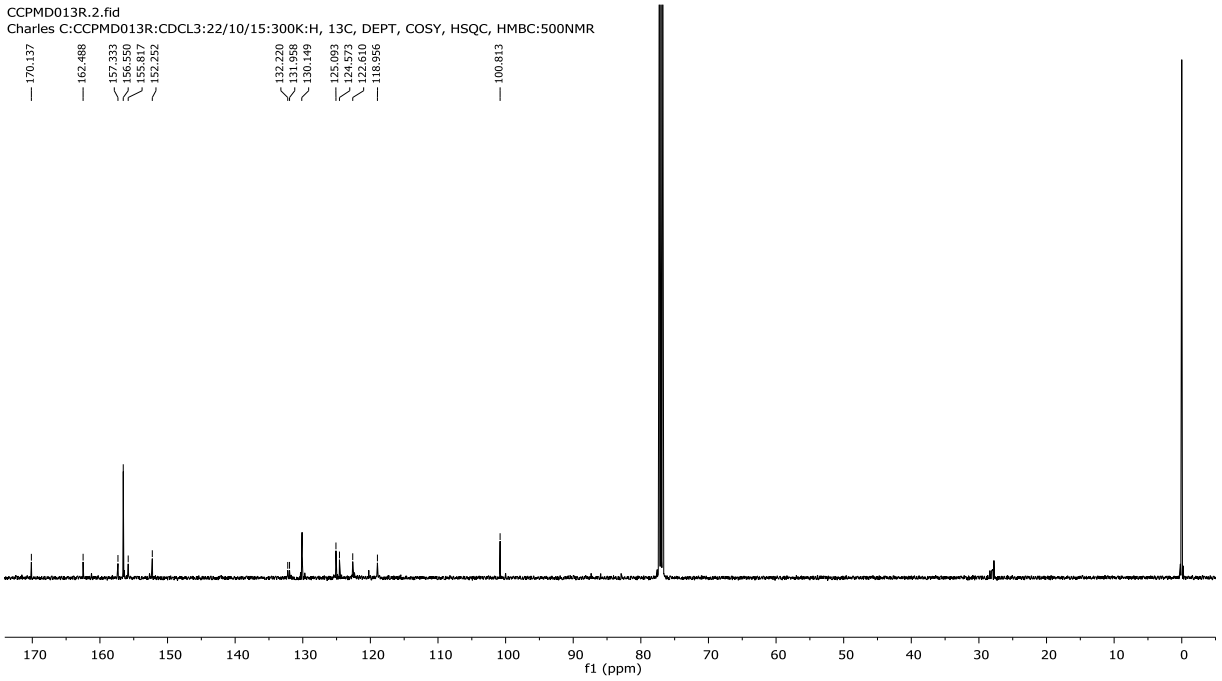
CCPMD013R.2.fid
Charles C:CCPMD013R:CDCL3:22/10/15:300K:H, 13C, DEPT, COSY, HSQC, HMBC:500NMR
170.137
162.488
157.333
156.550
155.817
152.252
132.220
131.958
130.149
125.093
124.573
122.610
118.956
100.813
170
160
150
140
130
120
110
100
90
80
70
60
50
40
30
20
10
0
f1 (ppm)

219

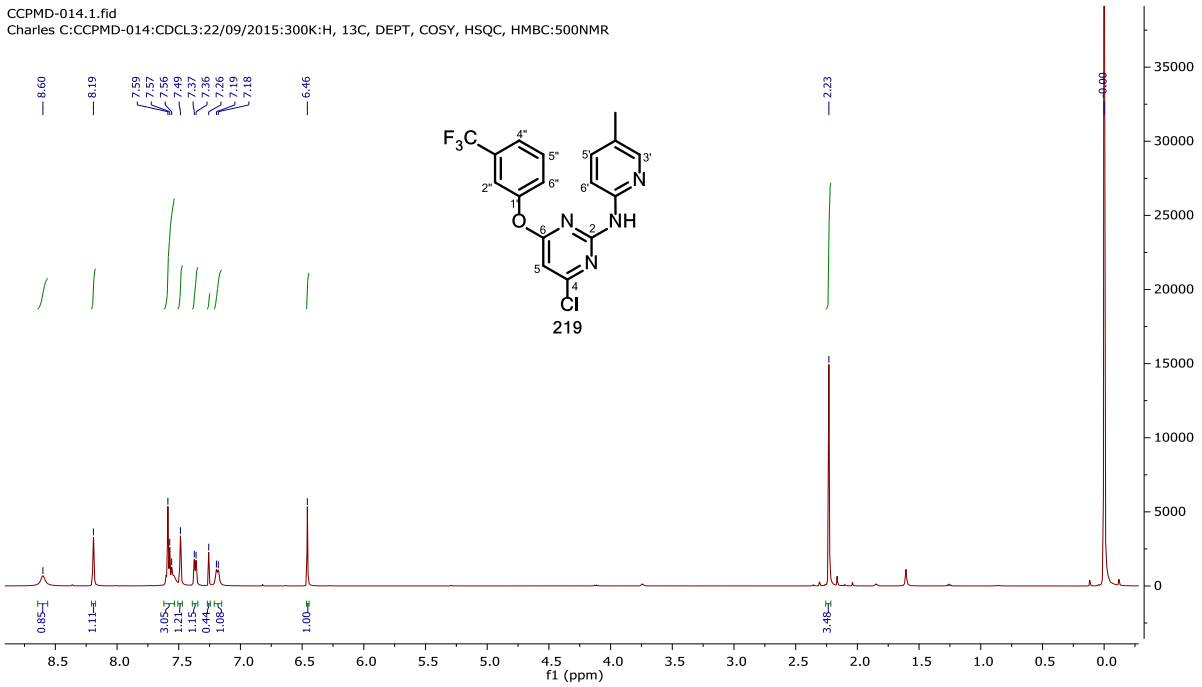
CCPMD-014.1.fid
Charles C:CCPMD-014:CDCL3:22/09/2015:300K:H, 13C, DEPT, COSY, HSQC, HMBC:500NMR
8.60
8.19
7.59
7.57
7.56
7.49
7.37
7.36
7.26
7.19
7.18
6.46
2.23
0.00
0.85
1.11
3.05
1.21
1.15
0.44
1.08
1.00
3.48
F3C
4"
5"
6"
2"
1"
5'
3'
6'
N
O
6
N
2
NH
5
N
4
Cl
219
f1 (ppm)

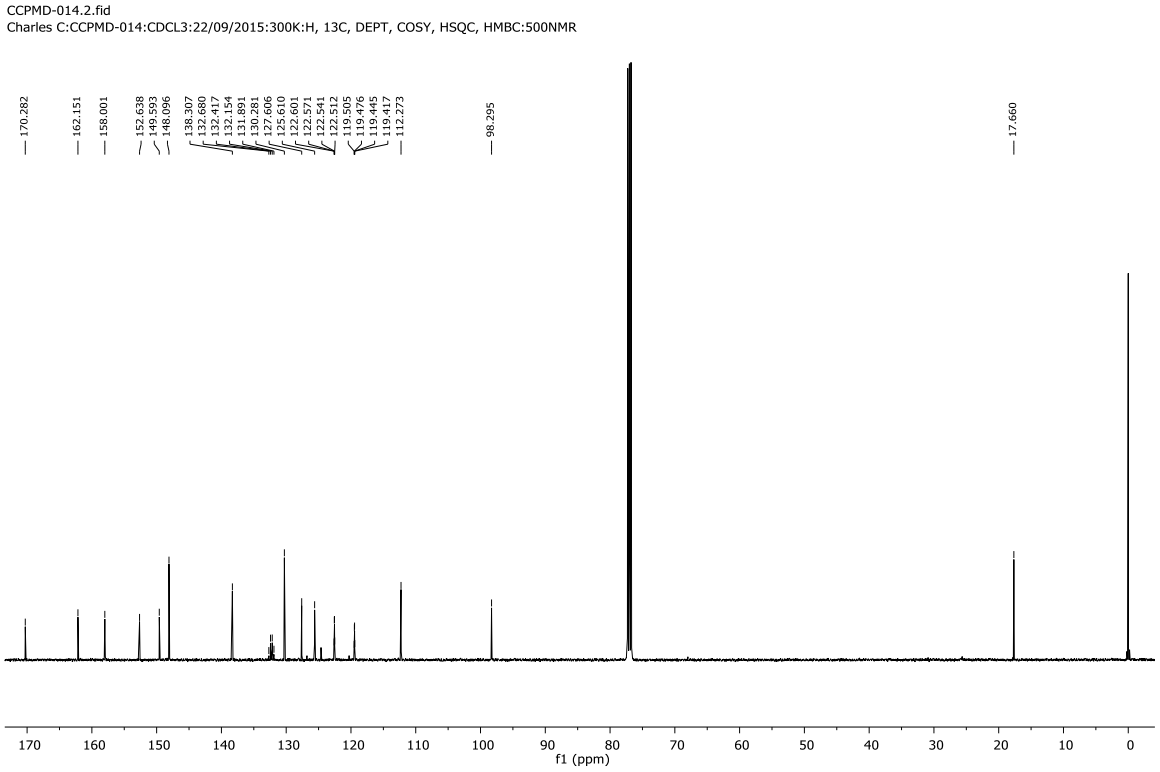
CCPMD-014.2.fid
Charles C:CCPMD-014:CDCL3:22/09/2015:300K:H, 13C, DEPT, COSY, HSQC, HMBC:500NMR
170.282
162.151
158.001
152.638
149.593
148.096
138.307
132.680
132.417
132.154
131.891
130.281
127.606
125.610
122.601
122.571
122.541
122.512
119.505
119.476
119.445
119.417
112.273
98.295
17.660
f1 (ppm)

220

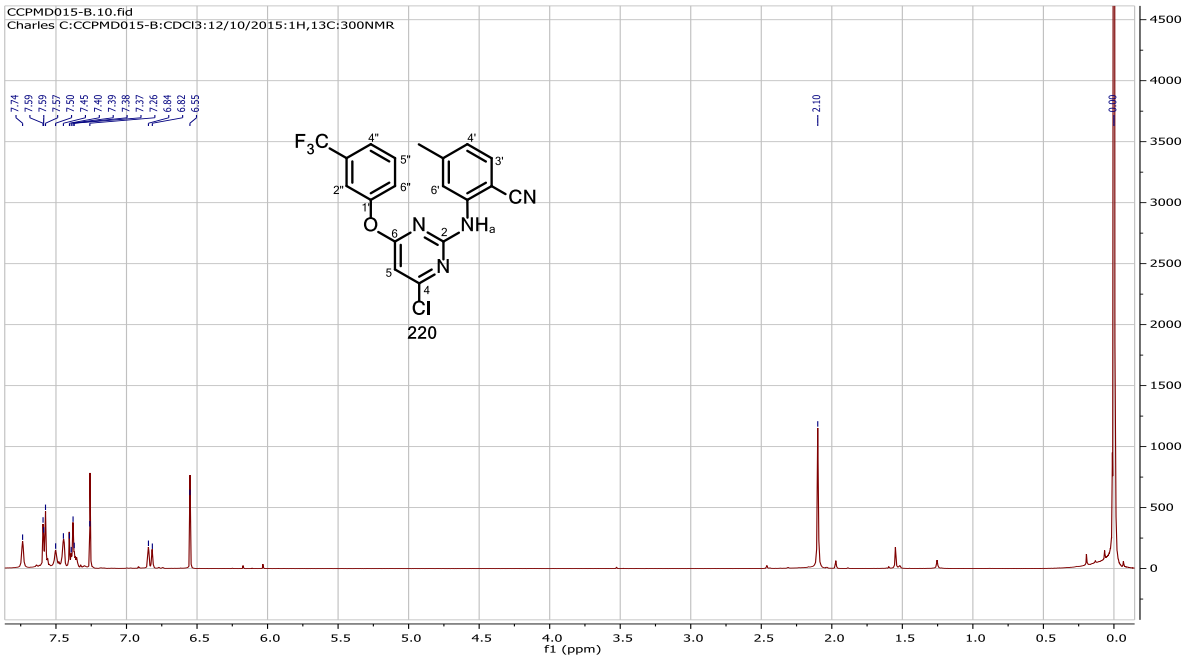
CCPMD015-B.10.fid
Charles C:CCPMD015-B:CDCl3:12/10/2015:1H,13C:300NMR
7.74
7.59
7.59
7.57
7.50
7.45
7.40
7.39
7.38
7.37
7.26
6.84
6.82
6.55
2.10
0.00
F3C
CN
NHa
Cl
220
f1 (ppm)

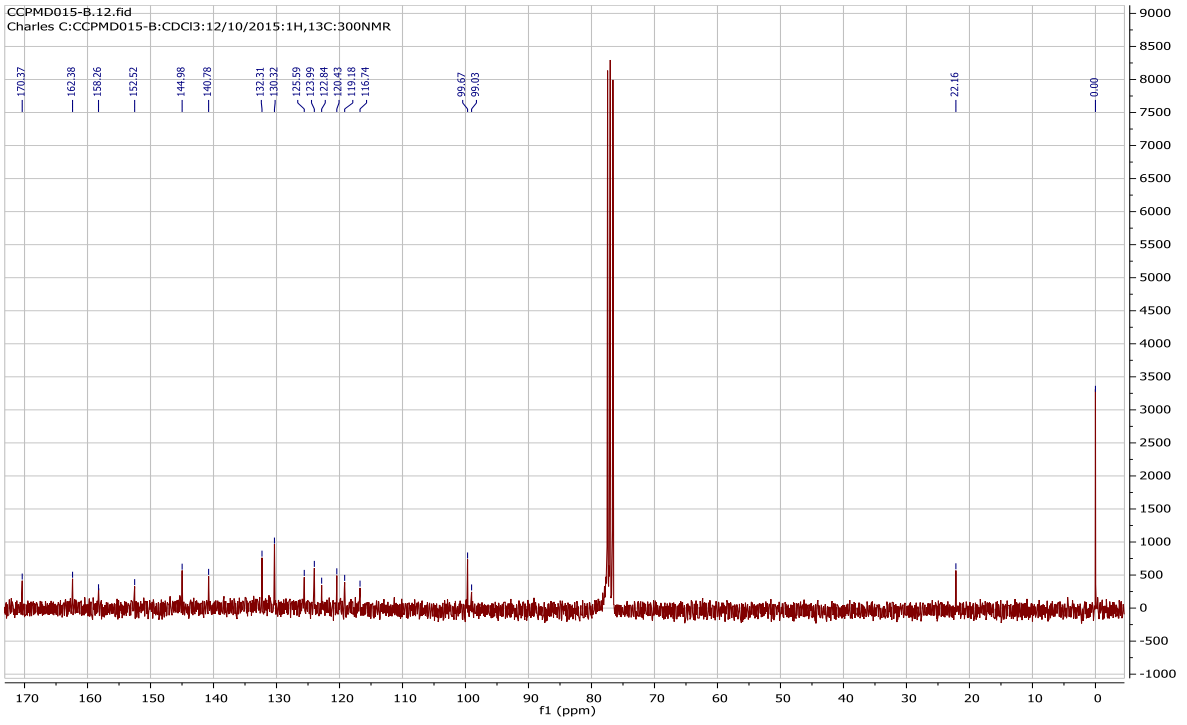
CCPMD015-B.12.fid
Charles C:CCPMD015-B:CDCl3:12/10/2015:1H,13C:300NMR
170.37
162.38
158.26
152.52
144.98
140.78
132.31
130.32
125.59
123.99
122.84
120.43
119.18
116.74
99.67
99.03
22.16
0.00
f1 (ppm)

204

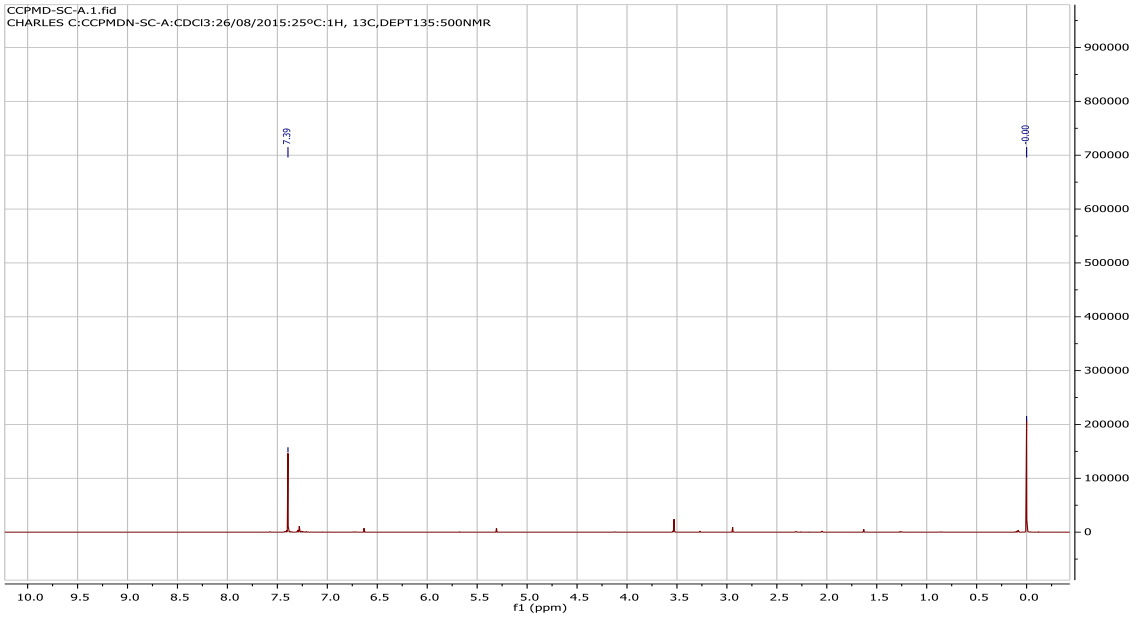
CCPMD-SC-A.1.fid
CHARLES C:CCPMDN-SC-A:CDCl3:26/08/2015:25ºC:1H, 13C,DEPT135:500NMR
7.39
0.00
900000
800000
700000
600000
500000
400000
300000
200000
100000
0
10.0 9.5 9.0 8.5 8.0 7.5 7.0 6.5 6.0 5.5 5.0 4.5 4.0 3.5 3.0 2.5 2.0 1.5 1.0 0.5 0.0
f1 (ppm)

227

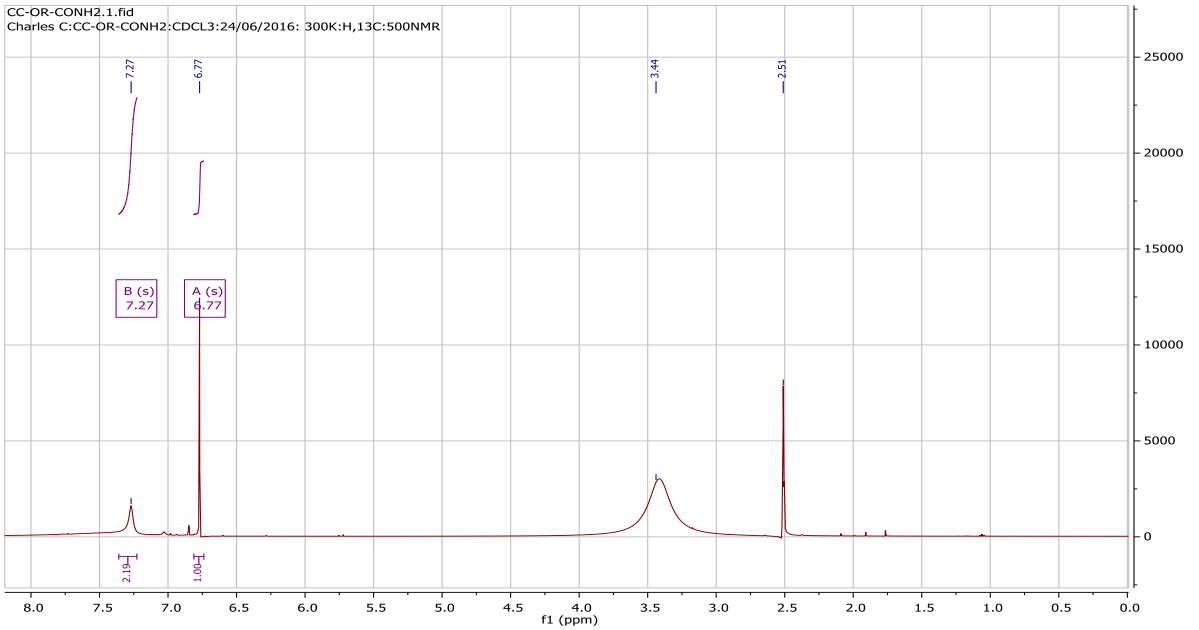
CC-OR-CONH2.1.fid
Charles C:CC-OR-CONH2:CDCL3:24/06/2016: 300K:H,13C:500NMR
7.27
6.77
3.44
2.51
B (s)
7.27
A (s)
6.77
2.19
1.00
f1 (ppm)

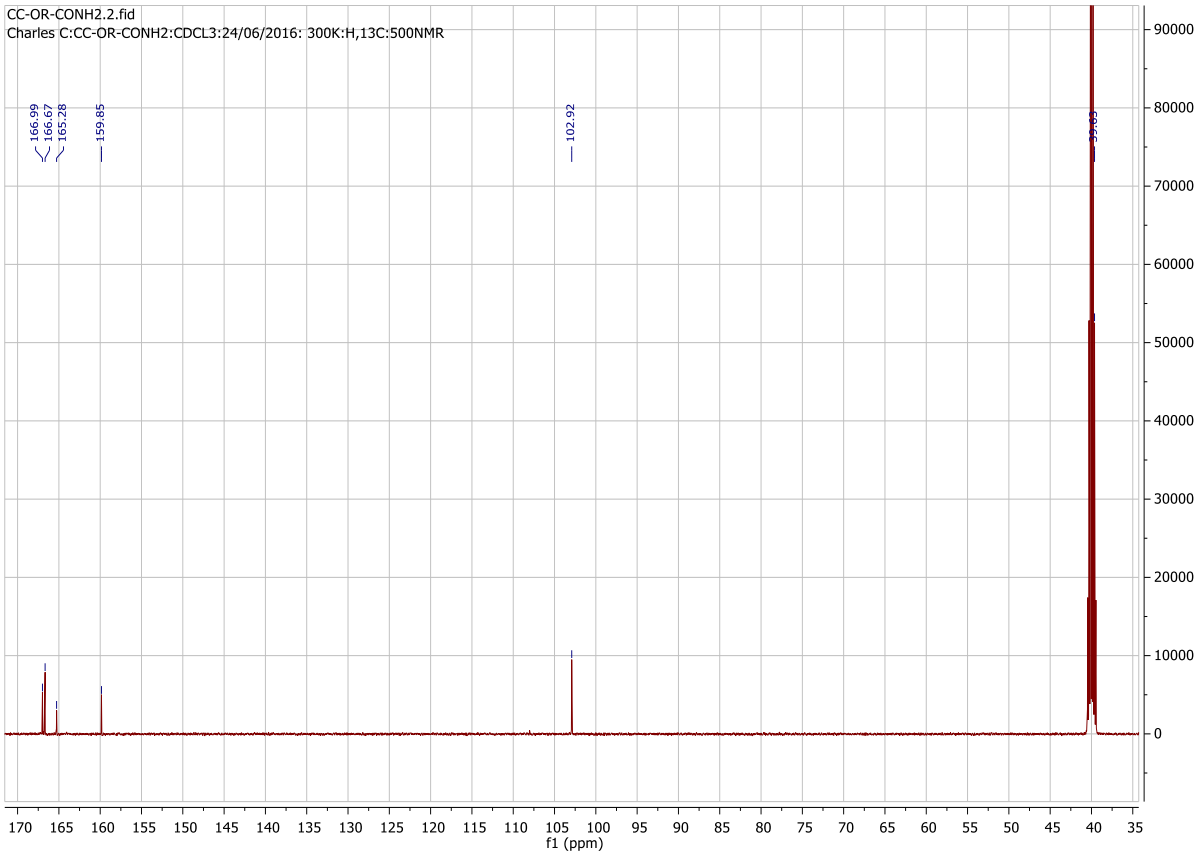
CC-OR-CONH2.2.fid
Charles C:CC-OR-CONH2:CDCL3:24/06/2016: 300K:H,13C:500NMR
166.99
166.67
165.28
159.85
102.92
39.93
f1 (ppm)

224

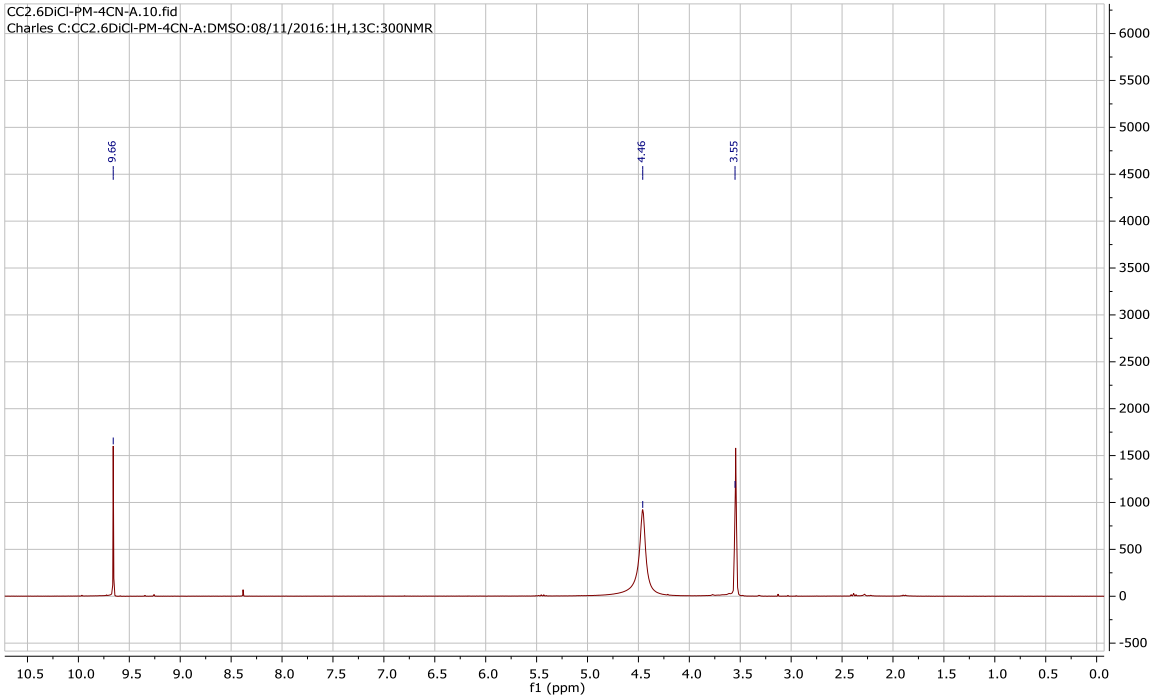
CC2.6DiCl-PM-4CN-A.10.fid
Charles C:CC2.6DiCl-PM-4CN-A:DMSO:08/11/2016:1H,13C:300NMR
9.66
4.46
3.55
f1 (ppm)

229a

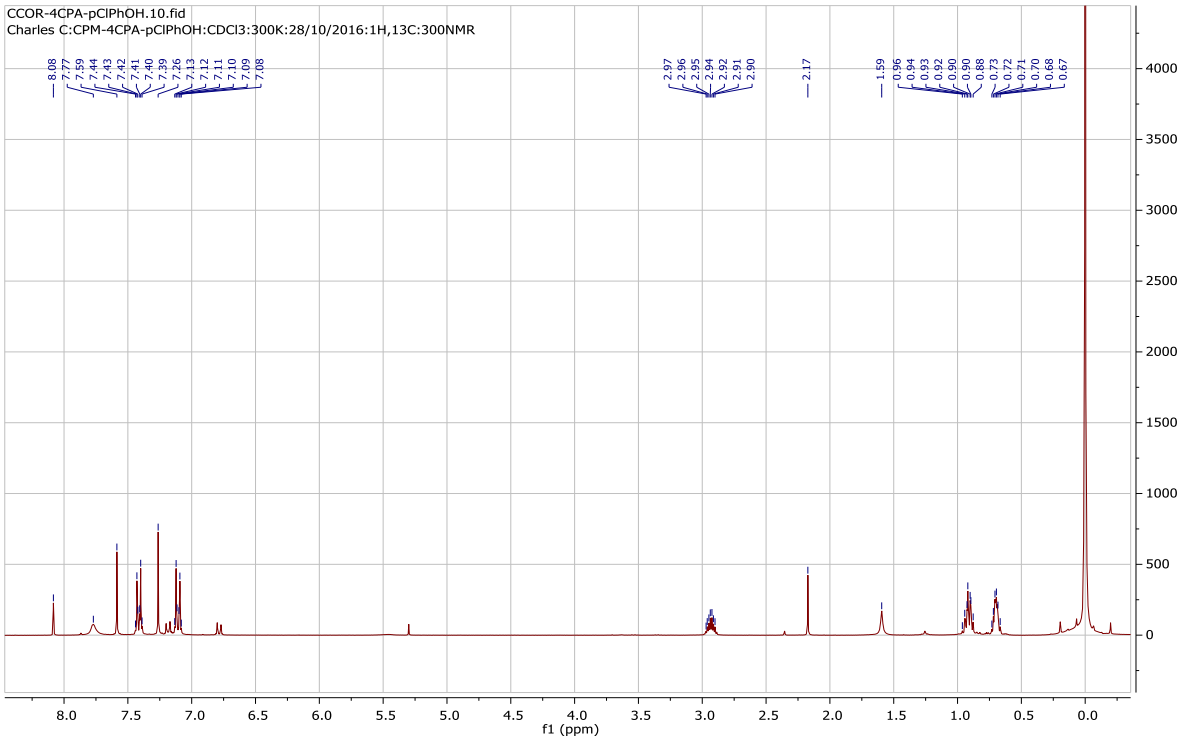
CCOR-4CPA-pClPhOH.10.fid
Charles C:CPM-4CPA-pClPhOH:CDCl3:300K:28/10/2016:1H,13C:300NMR
8.08
7.77
7.59
7.44
7.43
7.42
7.41
7.40
7.39
7.26
7.13
7.12
7.11
7.10
7.09
7.08
2.97
2.96
2.95
2.94
2.92
2.91
2.90
2.17
1.59
0.96
0.94
0.93
0.92
0.90
0.90
0.88
0.73
0.72
0.71
0.70
0.68
0.67
f1 (ppm)

180a

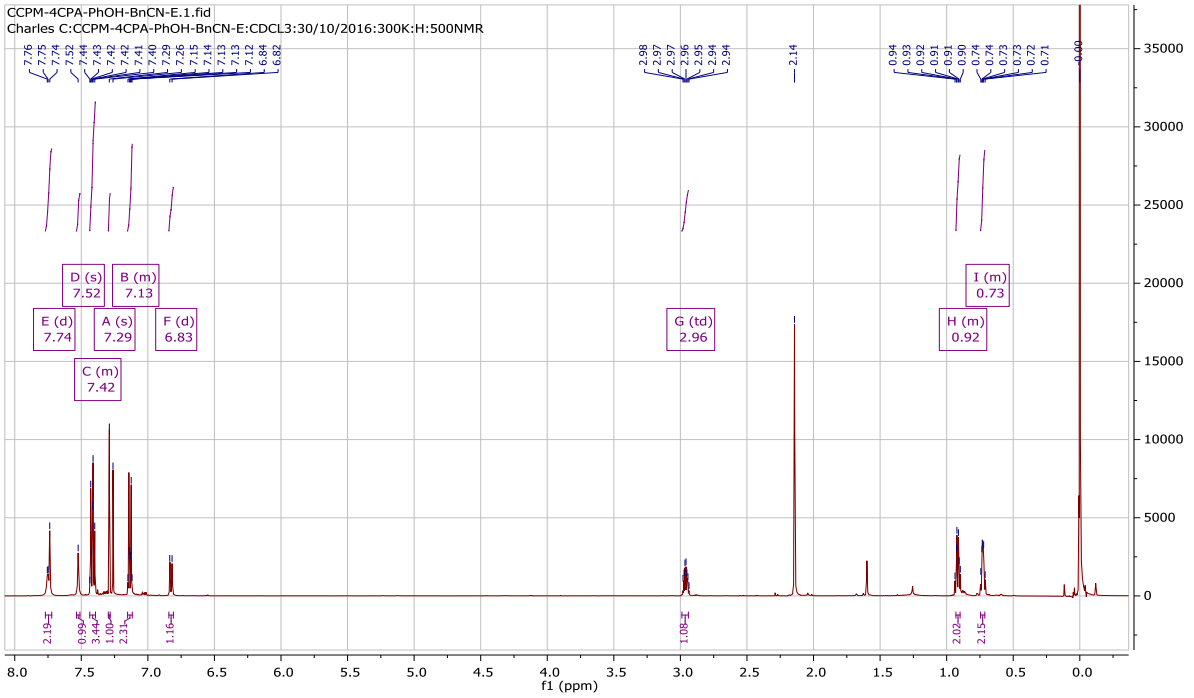
CCPM-4CPA-PhOH-BnCN-E.1.fid
Charles C:CCPM-4CPA-PhOH-BnCN-E:CDCL3:30/10/2016:300K:H:500NMR
D (s) 7.52
B (m) 7.13
E (d) 7.74
A (s) 7.29
F (d) 6.83
C (m) 7.42
G (td) 2.96
I (m) 0.73
H (m) 0.92
f1 (ppm)

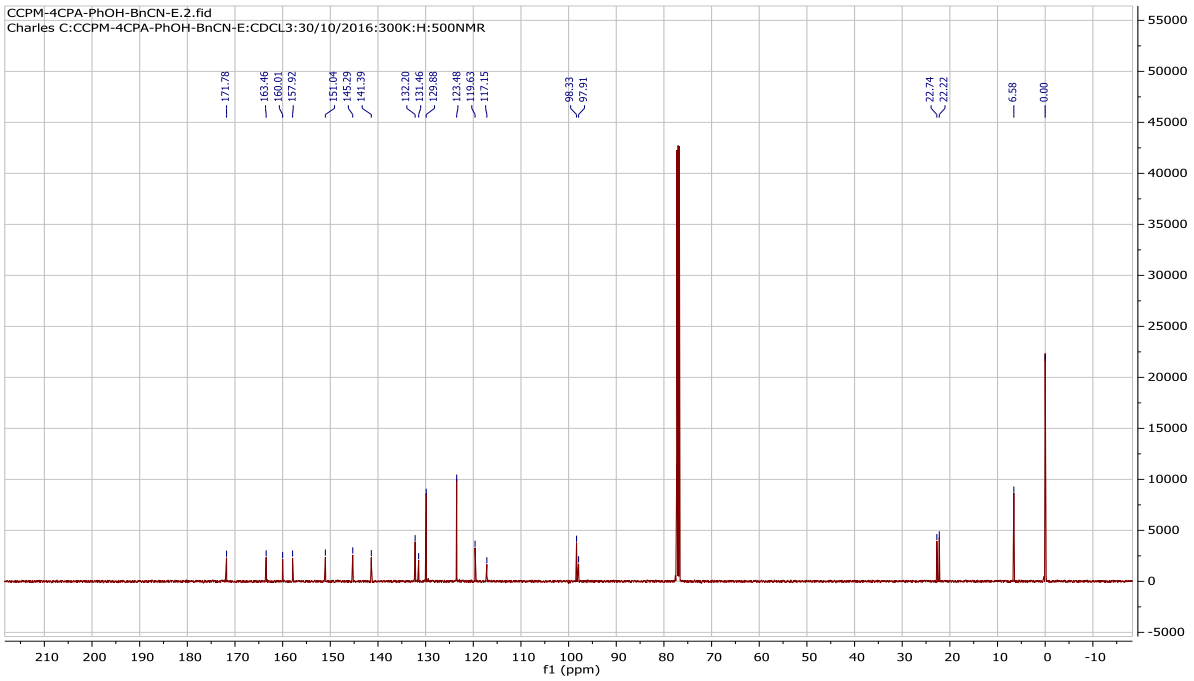
CCPM-4CPA-PhOH-BnCN-E.2.fid
Charles C:CCPM-4CPA-PhOH-BnCN-E:CDCL3:30/10/2016:300K:H:500NMR
f1 (ppm)

229b

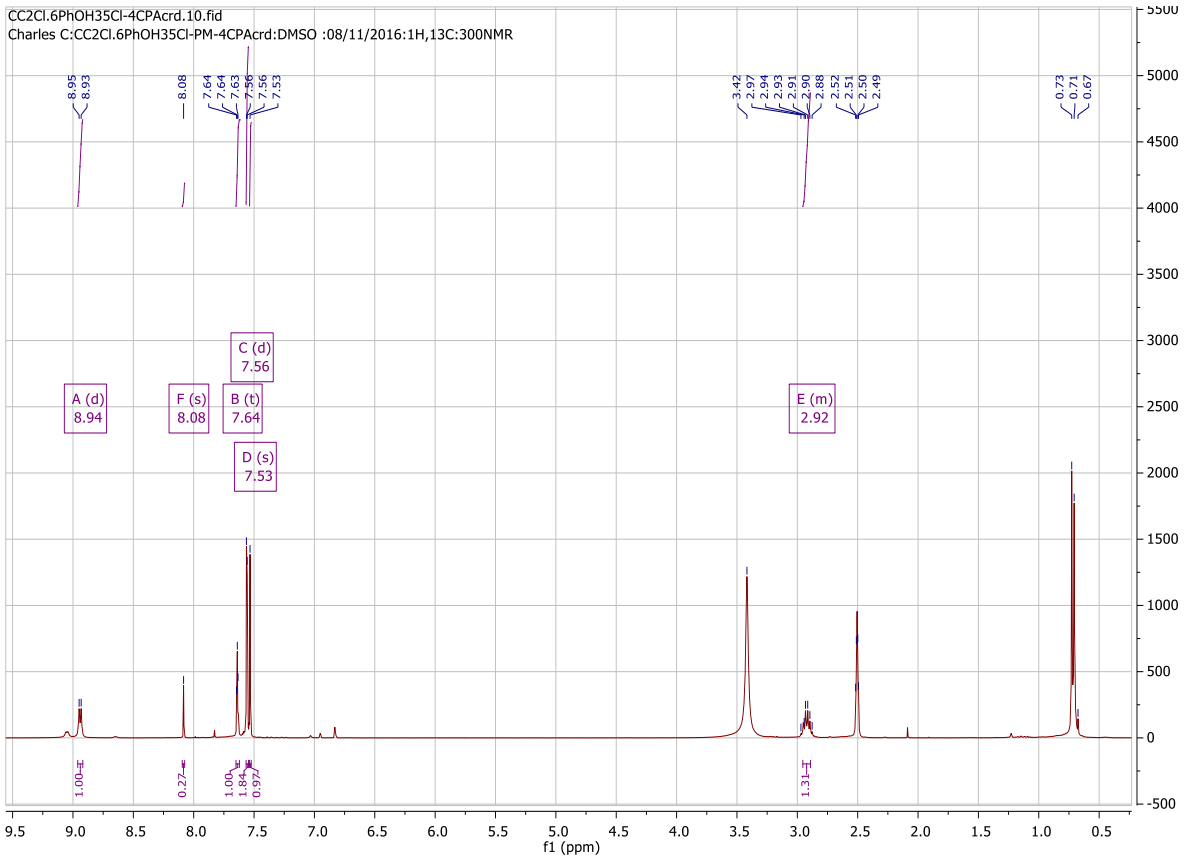
CC2Cl.6PhOH35Cl-4CPAcrd.10.fid
Charles C:CC2Cl.6PhOH35Cl-PM-4CPAcrd:DMSO :08/11/2016:1H,13C:300NMR
8.95
8.93
8.08
7.64
7.64
7.63
7.56
7.56
7.53
3.42
2.97
2.94
2.93
2.91
2.90
2.88
2.52
2.51
2.50
2.49
0.73
0.71
0.67
A (d) 8.94
F (s) 8.08
B (t) 7.64
C (d) 7.56
D (s) 7.53
E (m) 2.92
1.00
0.27
1.00
1.84
0.97
1.31
f1 (ppm)

230

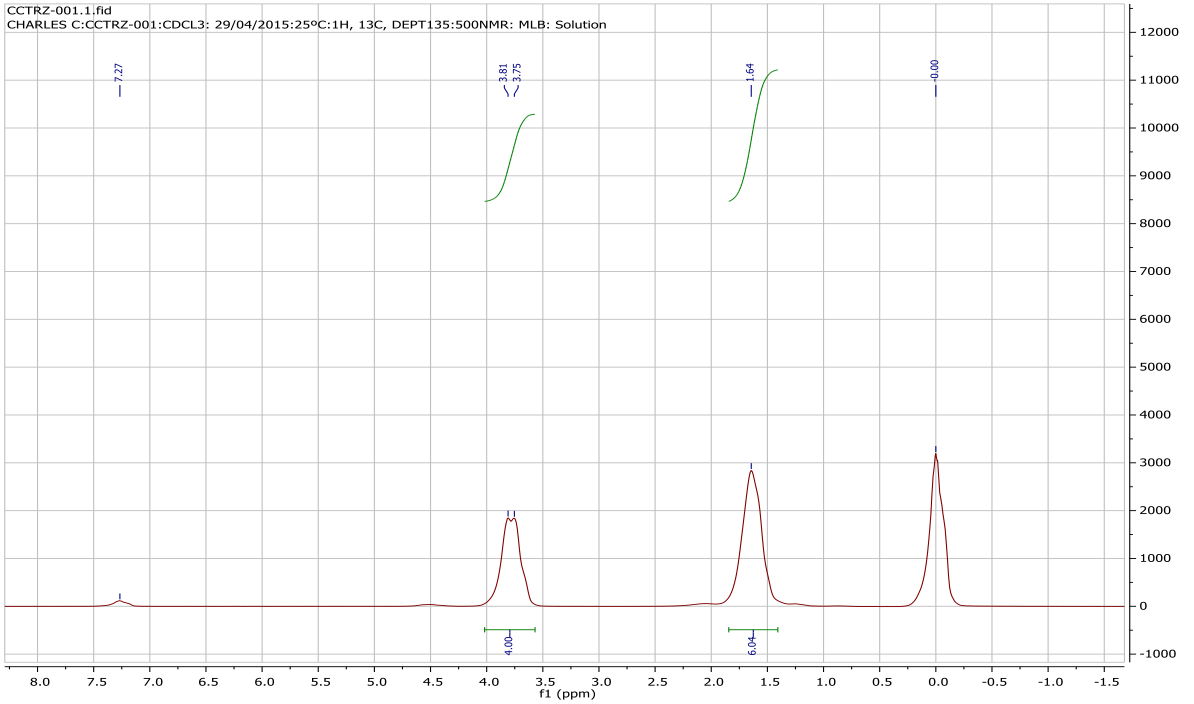
CCTRZ-001.1.fid
CHARLES C:CCTRZ-001:CDCL3: 29/04/2015:25ºC:1H, 13C, DEPT135:500NMR: MLB: Solution
7.27
3.81
3.75
1.64
0.00
4.00
6.04
f1 (ppm)

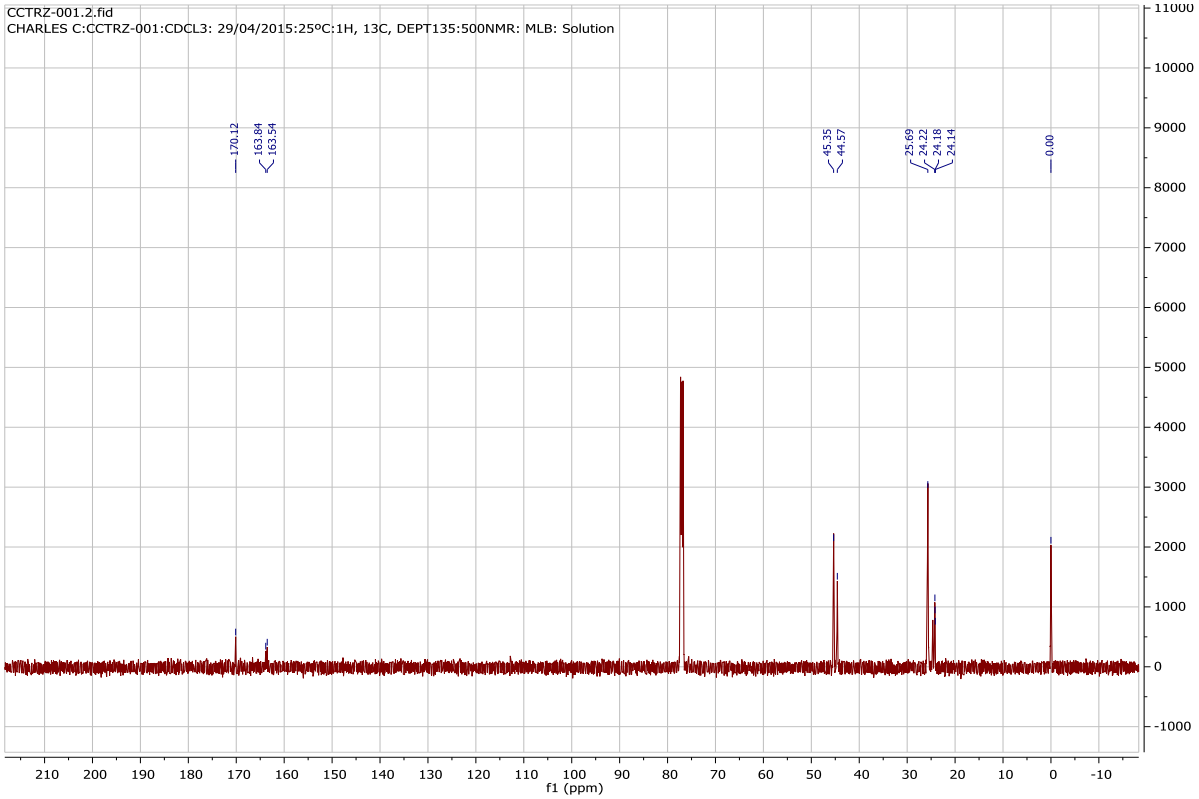
CCTRZ-001.2.fid
CHARLES C:CCTRZ-001:CDCL3: 29/04/2015:25ºC:1H, 13C, DEPT135:500NMR: MLB: Solution
170.12
163.84
163.54
45.35
44.57
25.69
24.22
24.18
24.14
0.00
f1 (ppm)